NAT'L INST. OF STAND & TECH
A11106 362183
NIST
PUBLICATIONS

NAT'L INST. OF STAND & TECH
A11106 362515
tandards
. Bldg.
MAY 14 1981
190826
QC100
.U57

NBS SPECIAL PUBLICATION 477

U.S. DEPARTMENT OF COMMERCE / National Bureau of Standards

WIND AND SEISMIC EFFECTS

Proceedings of the Eighth Joint UJNR Panel Conference

QC
100
.U57
NO.477
1977

NATIONAL BUREAU OF STANDARDS

The National Bureau of Standards[1] was established by an act of Congress March 3, 1901. The Bureau's overall goal is to strengthen and advance the Nation's science and technology and facilitate their effective application for public benefit. To this end, the Bureau conducts research and provides: (1) a basis for the Nation's physical measurement system, (2) scientific and technological services for industry and government, (3) a technical basis for equity in trade, and (4) technical services to promote public safety. The Bureau consists of the Institute for Basic Standards, the Institute for Materials Research, the Institute for Applied Technology, the Institute for Computer Sciences and Technology, the Office for Information Programs, and the Office of Experimental Technology Incentives Program.

THE INSTITUTE FOR BASIC STANDARDS provides the central basis within the United States of a complete and consistent system of physical measurement; coordinates that system with measurement systems of other nations; and furnishes essential services leading to accurate and uniform physical measurements throughout the Nation's scientific community, industry, and commerce. The Institute consists of the Office of Measurement Services, and the following center and divisions:

Applied Mathematics — Electricity — Mechanics — Heat — Optical Physics — Center for Radiation Research — Laboratory Astrophysics[2] — Cryogenics[2] — Electromagnetics[2] — Time and Frequency[2].

THE INSTITUTE FOR MATERIALS RESEARCH conducts materials research leading to improved methods of measurement, standards, and data on the properties of well-characterized materials needed by industry, commerce, educational institutions, and Government; provides advisory and research services to other Government agencies; and develops, produces, and distributes standard reference materials. The Institute consists of the Office of Standard Reference Materials, the Office of Air and Water Measurement, and the following divisions:

Analytical Chemistry — Polymers — Metallurgy — Inorganic Materials — Reactor Radiation — Physical Chemistry.

THE INSTITUTE FOR APPLIED TECHNOLOGY provides technical services developing and promoting the use of available technology; cooperates with public and private organizations in developing technological standards, codes, and test methods; and provides technical advice services, and information to Government agencies and the public. The Institute consists of the following divisions and centers:

Standards Application and Analysis — Electronic Technology — Center for Consumer Product Technology: Product Systems Analysis; Product Engineering — Center for Building Technology: Structures, Materials, and Safety; Building Environment; Technical Evaluation and Application — Center for Fire Research: Fire Science; Fire Safety Engineering.

THE INSTITUTE FOR COMPUTER SCIENCES AND TECHNOLOGY conducts research and provides technical services designed to aid Government agencies in improving cost effectiveness in the conduct of their programs through the selection, acquisition, and effective utilization of automatic data processing equipment; and serves as the principal focus wthin the executive branch for the development of Federal standards for automatic data processing equipment, techniques, and computer languages. The Institute consist of the following divisions:

Computer Services — Systems and Software — Computer Systems Engineering — Information Technology.

THE OFFICE OF EXPERIMENTAL TECHNOLOGY INCENTIVES PROGRAM seeks to affect public policy and process to facilitate technological change in the private sector by examining and experimenting with Government policies and practices in order to identify and remove Government-related barriers and to correct inherent market imperfections that impede the innovation process.

THE OFFICE FOR INFORMATION PROGRAMS promotes optimum dissemination and accessibility of scientific information generated within NBS; promotes the development of the National Standard Reference Data System and a system of information analysis centers dealing with the broader aspects of the National Measurement System; provides appropriate services to ensure that the NBS staff has optimum accessibility to the scientific information of the world. The Office consists of the following organizational units:

Office of Standard Reference Data — Office of Information Activities — Office of Technical Publications — Library — Office of International Standards — Office of International Relations.

---

[1] Headquarters and Laboratories at Gaithersburg, Maryland, unless otherwise noted; mailing address Washington, D.C. 20234.

[2] Located at Boulder, Colorado 80302.

National Bureau of Standards

MAY 26 1977

not acc.
QC
100
.U57
no. 477
1977
c. 2

WIND AND SEISMIC EFFECTS

Special publication no. 477

Proceedings of the Eighth Joint
Panel Conference of the U.S.-Japan
Cooperative Program in
Natural Resources

May 18-21, 1976
National Bureau of Standards
Gaithersburg, Md.

H.S. Lew, Editor

Center for Building Technology
Institute for Applied Technology
National Bureau of Standards
Washington, D.C. 20234

U.S. DEPARTMENT OF COMMERCE, Juanita M. Kreps, Secretary
Dr. Sidney Harman, Under Secretary

NATIONAL BUREAU OF STANDARDS, Ernest Ambler, Acting Director

Issued May 1977

Library of Congress Catalog Card Number: 77-600015

National Bureau of Standards Special Publication 477
Nat. Bur. Stand. (U.S.), Spec. Publ. 477, 626 pages (May 1977)
CODEN: XNBSAV

U.S. GOVERNMENT PRINTING OFFICE
WASHINGTON: 1977

For sale by the Superintendent of Documents, U.S. Government Printing Office, Washington, D.C. 20402
(Order by SD Catalog No. C13.10:477).
Stock No. 003-003-01772-8

PREFACE

The Eighth Joint Meeting of the U.S.-Japan Panel on Wind and Seismic Effects was held in Gaithersburg, Maryland on May 18-23, 1976. This panel is one of the eleven panels in the U.S.-Japan Cooperative Program in Natural Resources (UJNR). The UJNR was established in 1964 by the U.S.-Japan Cabinet-Level Committee on Trade and Economic Affairs. The purpose of the UJNR is to exchange scientific and technological information which will be mutually beneficial to the economics and welfare of both countries. Accordingly, the purpose of the annual joint meeting of this panel is to exchange technical information on the latest research and development activities within governmental agencies of both countries in the area of wind and seismic effects.

The proceedings include the program, the formal resolutions, and the technical papers presented at the Joint Meeting. The papers were presented in the respective language of each country. The texts of the papers, all of which were prepared in English, have been edited for obvious errors and clarity. The contents of the papers are the sole responsibility of the individual authors. The illustrations were reproduced from the working documents used at the Joint Meeting. The formal resolutions were drafted at the closing session of the Joint Meeting and adopted unanimously by the panels of both countries.

It should be noted that throughout these proceedings certain commercial equipment, instruments or materials are identified in order to specify adequately experimental procedure. In no case does such identification imply recommendation or endorsement by the National Bureau of Standards, nor does it imply that the material or equipment identified is necessarily the best available for the purpose.

Pages of the technical papers are numbered with a prefix corresponding to the theme number. The texts are consecutively numbered in each theme.

H. S. Lew, Secretary
U.S. Panel on Wind and
Seismic Effects

SI Conversion Units

In view of present accepted practice in this technological area, U.S. customary units of measurements have been used throughout this report. It should be noted that the U.S. is a signatory to the General Conference on Weights and Measures which gave official status to the metric SI system of units in 1960. Conversion factors for units in this report are:

	Customary Unit	International (SI), UNIT	Conversion Approximate
Length	inch (in)	meter (m)[a]	1 in=0.0254m*
	foot (ft)	meter (m)	1 ft=0.3048m*
Force	pound (lbf)	newton (N)	1 lbf=4.448N
	kilogram (kgf)	newton (N)	1 kgf=9.807N
Pressure Stress	pound per square inch (psi)	newton/meter^2	1 psi=6895N/m^2
	kip per square inch (ksi)	newton/meter^2	1 ksi=5895x10^{6}N/m^2
Energy	inch-pound (in-lbf)	joule (J)	1 in-lbf=0.1130 J
	foot-pound (ft-lbf)	joule (J)	1 ft-lbf=1.3558 J
Torque or Bending Moment	pound-inch	newton-meter (N-m)	1 lbf-in=0.1130 N-m
	pound-foot (lbf-ft)	newton-meter (N-m)	1 lbf-ft=1.3558 N-m
Weight	pound (lb)	kilogram (kg)	1 lb=0.4536 kg
Unit Weight	pound per cubic foot (pcf)	kilogram per cubic meter (kg/m^3)	1 pcf=16.018 kg/m^3
Velocity	foot per second (ft/sec)	meter per second (m/s)	1 fps=0.3048 m/s
Acceleration	foot per second per second (ft/sec^2)	meter per second per second (m/s^2)	1 ft/sec^2=0.3048 m/s^2

[a]Meter may be subdivided. A centimeter (cm) is 1/100 m and a millimeter (mm) is 1/1000 m.

*Exact.

ABSTRACT

The Eighth Joint Meeting of the U.S.-Japan Panel on Wind and Seismic Effects was held in Gaithersburg, Maryland on May 18-21, 1976. The proceedings of the Joint Meeting include the program, the formal resolutions, and the technical papers. The subject matter covered in the papers includes wind effects on structures and design criteria; extreme winds for structural design; earthquake ground motions and instrumentation; seismicity and earthquake risk; seismic effects on structures and design criteria; lessons learned from recent natural disasters; design of nuclear reactor facilities.

Key Words: Accelerograph; Bridges; Buildings; Codes; Disaster; Dynamic Analysis; Earthquakes; Ground Failures; Nuclear Facilities; Seismicity; Soils; Standards; Structural Response; and Winds.

CONTENTS

Preface iii
SI Conversion iv
Abstract v
Program of the Joint Meeting x
Opening Session x
List of Members xv
Photographs of Participants xix
Formal Resolutions xxi

Themes and Technical Papers I-1

Theme I: WIND EFFECTS ON STRUCTURAL AND DESIGN CRITERIA I-1

Aspects of Hurricane Winds as Recorded at an Instrumented Suspension Bridge . . I-1
R. H. Gade, R. H. Scanlan

Study on the Wind Effect on Eaves I-12
Tatsuro Murota

Measurements of Wind Loads and Tie Down Forces on Mobile Homes I-21
Richard Marshall, Robert A. Crist

On the Wind Resistant Design Specifications for the Proposed Honshu-Shikoku Bridges (1975) I-34
Tadayoshi Okubo, Nabuyuki Narita

Equivalent Static Wind Loads for Tall Building Design I-49
Emil Simiu

A Wood House Will Resist Wind Forces I-66
Billy Bohannan

Wind Loads on Low Rise Buildings I-70
Noel J. Raufaste

Theme II: EXTREME WINDS FOR STRUCTURAL DESIGN II-1

Characteristics of the High Wind at Hachijojima Island on the Occasion of Typhoon No. 7513 . . . . . II-1
Seiji Soma

High Winds in the United States-1975 . . . . . II-15
Arnold R. Hull, Thomas D. Potter, Nathaniel B. Guttman

Mean Speed Profiles of Hurricane Winds II-30
Emil Simiu, Virendra C. Patel, John F. Nash

Theme III: GROUND MOTIONS AND INSTRUMENTATION III-1

Planning and Design of Strong Motion Instrument Networks III-1
R. B. Matthiesen

Observation of Earthquake Response of Ground With Horizontal and Vertical Seismometer Arrays III-16
Satoshi Hayashi, Hajime Tsuchida, Eiichi Kurata

Building Strong Motion Earthquake Instrumentation III-26
Christopher Rojahn

Characteristics of Underground Seismic Motions at Four Sites Around Tokyo Bay III-41
Toshio Iwasaki, Susumu Wakabayashi, Fumio Tatsuoka

THEME IV: SEISMICITY AND EARTHQUAKE RISK. IV-1

Relationship Between Earthquake Damage of Existing Wooden Houses and Seismic Intensities. IV-1
Eiichi Kuribayashi, Takayuki Tazaku, Takayuki Hadate

A Method for Calculating Nonlinear Seismic Response in Two Dimensions . . IV-18
William B. Joyner

A New Scale Representing the "Quake Sensitivity" at a Certain Region. . . IV-47
Tsutomu Terashima, Tetsuo Santo

THEME V: LESSONS LEARNED FROM RECENT NATURAL DISASTERS V-1

Damage to the Civil Engineering Structures on Hachijojima Island by Typhoon 7513 . . . . . V-1
T. Okubo, N. Narita, K. Yokoyama

Cyclone Tracy V-21
Richard D. Marshall

On the Damage to Buildings in Hachijojima Caused by Typhoon No. 7513. . . V-54
Tatsuro Murota

THEME VI: SEISMIC EFFECTS ON STRUCTURES AND DESIGN CRITERIA VI-1

Seismic Response of Reinforced Concrete Highway Bridges VI-1
Joseph Penzien, W.G. Godden, M.C. Chen, D. Williams, K. Kawashima

An Evaluation Method for the Earthquake Resistant Capacity of Reinforced Concrete and Steel Reinforced Concrete Columns VI-10
Masakazu Ozaki, Yuji Ishiyama

The Earthquake Engineering Program of the National Science Foundation . . VI-28
John B. Scalzi

Large-Scale Testing Programs Related to Wind and Seismic Effects Currently Underway in Japan. VI-37
Seiichi Inaba

Earthquake Damages to Earth Structures VI-44
Kenkichi Sawada

Dynamic Test of a Circuit Breaker for Transformer Substation. VI-50
Seiichi Inaba, Shegio Kinoshita

Comprehensive Seismic Design Provisions for Buildings - A Status Report . . VI-61
Charles Culver

Retrofitting of Vulnerability in Earthquake Disaster Mitigation Problems. . VI-69
Kaoru Ichihara, Eiichi Kuribayashi, Tadayuki Tazaki

Dynamic Response Characteristics of a Model Arch Dam. VI-85
Charles D. Norman, Roger D. Crowson, Jimmy P. Balsara

The Measurement of the Dynamic k-Value in Site and Its Application To Design VI-118
Tetsuo Kunihiro, Kaname Yahagi, Michio Okahara

Laboratory Investigation of Undisturbed Sampling and Standard Penetration Tests on Fine Sands VI-141
W. F. Marcuson III, S.S. Cooper, M.A. Bieganousky

Dynamic Soil Properties with Emphasis on Comparison of Laboratory Tests and Field Measurements. VI-158
Toshio Iwasaki, Fumio Tatsuoka

Design Earthquakes VI-179
Ellis L. Krinitzsky, Frank K. Chang

Relation Between Seismic Coefficient and Ground Acceleration for Gravity Quaywall VI-192
Satoshi Hayashi, Setsuo Noda, Tatsuo Uwabe

Investigation of Earthquake Resistance of Structural (Shear) Wall Buildings Carried out at Portland Cement Association VI-199
Mark Fintel

A Philosophy for Structural Integrity of Large Panel Buildings VI-220
Mark Fintel, Donald M. Schultz

THEME VII: DESIGN OF NUCLEAR REACTOR FACILITIES VII-1

Wind and Seismic Design of U.S. Nuclear Power Plants VII-1
Lawrence C. Shao, Richard J. Stuart, Charles H. Hofmayer

Outline of Basic Philosophy and Practices of Aseismatic Design for Nuclear Facilities in Japan VII-29
Makoto Watabe, Yorihiko Ohsaki

Tornado-Borne Missiles VII-36
James F. Costello

THEME VIII: SPECIAL SESSION ON GUATEMALA EARTHQUAKE VIII-1

Structural Damage to Bridges Resulting from the Guatemala Earthquake . . . VIII-1
James D. Cooper

EIGHTH JOINT MEETING
OF THE
U.S.-JAPAN PANEL ON WIND AND SEISMIC EFFECTS
MAY 18-21, 1976
AT THE
NATIONAL BUREAU OF STANDARDS

TUESDAY-May 18

OPENING SESSION

10:00 Call to order by Dr. H.S. Lew, Secretary, U.S. Panel

Remarks by Mr. Robert S. Walleigh, Acting Deputy Director
National Bureau of Standards

Remarks by Mr. Kiichiro Nagara, Counselor, Embassy of Japan

Remarks by Dr. Edward O. Pfrang, Chairperson, U.S. Panel
National Bureau of Standards

Remarks by Dr. Kaoru Ichihara, Chairperson, Japan Panel

10:30 Introduction of U.S. Panel Members by U.S. Chairperson and
Japan Panel Members by Japan Chairperson

10:45 Election of Conference Chairperson

11:00 Adoption of Agenda

11:15 Adjourn

11:30 Group Photograph

12:00 Lunch-Dining Room "C"

SESSION II - WIND EFFECTS ON STRUCTURES AND DESIGN CRITERIA

Chairman: Dr. Edward O. Pfrang

1:30 Aspects of Hurricane Winds as Recorded at an Instrumented Suspension
Bridge -- R.H. Gade and R.H. Scanlan

2:00 Study of Wind Effects on Eaves --
Tatsuro Murota (Presented by Masakazu Ozaki)

2:30 Measurements of Wind Loads and Tie-Down Forces on Mobile Homes --
Richard Marshall and Robert A. Crist

2:40 On the Wind Resistant Design Specifications for the Proposed Shikoku
Bridges (1975) -- Tadayoshi Okubo and Nobuyuki Narita

2:50 Equivalent Static Wind Loads for Tall Buildings --
Emil Simiu (Presented by Robert A. Crist)

3:00 Break

3:20 A Wood House Will Resist Wind Forces --
Billy Bohannan

3:30 Wind Loads on Low-Rise Buildings --
Noel J. Raufaste

3:40 Discussion

4:10 Adjourn

4:15 Informal Discussion of Resolution and Task Committees

WEDNESDAY-May 19

SESSION III: EXTREME WINDS FOR STRUCTURAL DESIGN

Chairman: Dr. Kaoru Ichihara

9:00 Characteristics of the High Wind at Hachijojima Island on the Occasion of Typhoon No. 7513 -- Seiji Soma (Presented by Masakazu Ozaki)

9:30 High Winds in the United States 1975 --
Arnold R. Hull, Thomas D. Potter, Nathaniel B. Guttman

10:00 Mean Profiles of Hurricane Winds --
Emil Simiu (Presented by Robert A. Crist)

10:10 Discussion

10:30 Break

SESSION IV: EARTHQUAKE GROUND MOTIONS AND INSTRUMENTATION

Chairman: Dr. Edward O. Pfrang

10:45 Planning and Design of Strong-Motion Instrument Networks --
R.B. Matthiesen

11:15 Observation of Earthquake Response of Ground with Horizontal and Vertical Seismometer Arrays -- Satoshi Hayashi, Hajime Tsuchida and Eiichi Kurata

11:45 Building Strong-Motion Earthquake Instrumentation --
Christopher Rojahn

11:55 Characteristics of Underground Seismic Motions at Four Sites Around Tokyo Bay -- Toshio Iwasaki, Susumo Wakabayashi and Fumio Tatsuoka

12:05 Discussion

12:30 Lunch-Dining Room "C"

SESSION V: SEISMICITY AND EARTHQUAKE RISK

Chairman: Dr. Kaoru Ichihara

2:00 Relationship Between Earthquake Disaster on Existing Houses and Seismicity -- Eiichi Kuribayashi, Tadayuki Tazaki and Takayuki Hadate

2:30 A Method for Calculating Nonlinear Seismic Response in Two Dimensions -- William B. Joyner (Presented by R.B. Matthiesen)

2:40 A New Scale Representing the "Quake Sensitivity" at a Certain Region -- Tsutomu Terashima and Tetsuo Santo

2:50 Discussion

3:30 Break

SESSION VI: LESSONS LEARNED FROM RECENT NATURAL DISASTERS

Chairman: Dr. Kaoru Ichihara

3:45 Damage to the Civil Engineering Structures on Hachijojima Island by Typhoon 7513 -- Tadayoshi Okubo, Nobuyuki Norita and Koichi Yokouama (Presented by Masakazu Ozaki)

4:15 Cyclone Tracy -- Richard Marshall

4:45 The Damage to Buildings on Hachijojima Island Caused by Typhoon 7513 -- Tatsuro Murota

4:55 Discussion

5:15 Adjourn

THURSDAY-May 20

SESSION VII: SEISMIC EFFECTS ON STRUCTURES AND DESIGN CRITERIA

Chairman: Dr. Edward O. Pfrang

9:00 Seismic Response of Reinforced Concrete Highway Bridges -- J.A. Penzien, W.G. Gooden, M.C. Chen, D. Williams, and Kikawashima

9:30 An Evaluation Method for the Earthquake Resistant Capacity of Reinforced Concrete and Steel Reinforced Concrete Columns -- Masakazu Ozaki and Yuji Ishiyama

10:00 The Earthquake Engineering Program of the National Science Foundation John B. Scalzi

10:10 Large-Scale Testing Programs Related to Wind and Seismic Effects Currently Underway in Japan Seiichi Inaba (Presented by T. Kinoshita)

10:20 Earthquake Damages of Earth Structures -- Kenkichi Sawada

10:30 Break

10:40 Dynamic Tests of Circuit Breakers for Transformer Substation -- Seiichi Inaba and Shigeo Kinoshita

11:00 New U.S. Recommendations on Seismic Design Criteria -- Charles G. Culver

11:10 Discussion

12:00 Lunch-Dining Room "C"

1:30 Retrofitting of Vulnerability in Earthquake Disaster Mitigation Problems -- Kaoru Ichihara, Eiichi Kuribayoshi and Tadayuki Tazaki

2:00 Dynamic Response Characteristics of a Model Arch Dam -- C. Dean Norman, Roger D. Crowson and Jimmy P. Balsara

2:30 The Measurement of the Dynamic k-Value In Site and Its Application to Design -- Tetsuo Kunihiro, Kaname Yahagi and Michio Okahara

2:40 Laboratory Investigation of Undisturbed Sampling and Standard Penetration Tests in Fine Sands -- William F. Marcuson III, S.S. Cooper and W.A. Bieganousky

2:50 Dynamic Soil Properties with Emphasis on Comparison of Laboratory Tests and Field Measurements -- Toshio Iwasaki and Fumio Tatsuoka

3:00 Break

3:20 Design Earthquakes -- Ellis L. Krinitzsky and Frank K. Chang

3:30 Relation Between Seismic Coefficient and Ground Acceleration for Gravity Quaywall -- Satoshi Hayashi, Setsuo Noda and Tetsuo Uwabe

3:40 Investigation of Earthquake Resistance of Structural (Shear) Wall Buildings Carried Out at Portland Cement Association -- Mark Fintel

3:50 A Philosophy for Structural Integrity of Large Panel Buildings-- Mark Fintel and Donald M. Schultz

4:00 Discussion

4:45 Adjourn

FRIDAY-May 21

SESSION VIII: DESIGN OF NUCLEAR REACTOR FACILITIES

Chairman: Dr. Kaoru Ichihara

9:00 Wind and Seismic Design of U.S. Nuclear Power Plants -- Lawrence C. Shao, Richard J. Stuart and Charles H. Hofmayer

9:30 Outline of Basic Philosophy and Practice of Aseismometer Design for Nuclear Facilities in Japan -- Makoto Watabe and Yorihiko Osaki (Presented by Masakazu Ozaki)

10:00 Tornado Borne Missiles -- James F. Costello

10:10 Discussion

10:40 Break

SESSION IX: SPECIAL SESSION ON GUATEMALA EARTHQUAKE

Chairman: Dr. Kaoru Ichihara

11:00 Structural Damage to Bridges Resulting from the Guatemala Earthquake -- James D. Cooper

11:20 Informal Discussion of Guatemala Earthquake -- Panel: Masakazu Ozaki, James D. Cooper, Charles G. Culver, Mark Fintel and R.B. Matthiesen, and Eiichi Kuribayashi

12:15 Lunch-Dining Room "C"

SESSION X: TASK COMMITTEE REPORTS

Chairman: Dr. Edward O. Pfrang

1:15 Strong Motion Instrumentation Arrays and Data -- R.B. Matthiesen and Hajime Tsuchida (Represented by Satoshi Hayashi)

1:30 Large Scale Testing Program -- Charles G. Culver and Seiichi Inaba (Represented by Takeo Kinoshita)

1:45 Repair and Retrofit of Existing Structures -- John J. Healy and Kiyoshi Nakano (Represented by Masakazu Ozaki)

2:00 Structural Performance Evaluation -- John Scalzi and Masakazu Ozaki

2:15 Land Use Programs for Controlling Natural Hazard Effects -- S.T. Algermissen and Eiichi Kurbayashi

2:30 Disaster Prevention Methods for Lifeline Systems -- Charles Scheffey and Tadayoshi Okubo (Presented by Eiichi Kuribayashi)

2:45 High Speed Wind Recorded Data -- Thomas D. Potter and Seiji Soma (Presented by Masakazu Ozaki)

3:00 Discussion of Task Committee Reports

SESSION XI: CLOSING SESSION

Chairman: Dr. Edward O. Pfrang

4:00 Adoption of Formal Resolution

Closing Remarks --
Dr. Kaoru Ichihara
Dr. Edward O. Pfrang

4:30 Adjourn

U.S. Panel on Wind and Seismic Effects

Membership List

May 1976

Dr. Edward O. Pfrang
Chairman
Chief, Structures, Materials and Safety Division
Center for Building Technology, IAT
National Bureau of Standards
Room B368, Bldg. 226
Washington, D.C. 20234

Dr. S.T. Algermissen
Office of Earthquake Studies
Denver Federal Center
Branch of Earthquake Tactonics
USGS
Stop 978, Box 25046
Denver, Colorado 80225
303-234-4014

Mr. Billy Bohannan
Assistant Director
Wood Engineering Research
Forest Products Laboratory
USDA
P.O. Box 5130
Madison, Wisconsin 53705
608-257-2211

Dr. Roger D. Borcherdt
Office of Earthquake Studies
Branch of Earthquake Hazards
USGS
345 Middlefield Road
Menlo Park, California 94025
415-323-8111 (FTS 467-2755)

Dr. Charles G. Culver
Disaster Research Coordinator
National Bureau of Standards
Room B212, Bldg. 226
Washington, D.C. 20234
301-921-3126

Mr. Jerry Dodd
Bureau of Reclamation
Mail Code 230
P.O. Box 25007
Denver Federal Center
Denver, Colorado 80225

Dr. Michael P. Gaus
Head, Engineering Mechanics Section
Engineering Division
National Science Foundation
1800 G. Street, N.W.
Washington, D.C. 20550
202-632-5787

Mr. John J. Healy
Department of the Army
DAEN-RDM
Washington, D.C. 20314
202-693-7287

Dr. William B. Joyner
Office of Earthquake Studies
Branch of Earthquake Hazards
USGS
345 Middlefield Road
Menlo Park, California 94025
413-323-8111 (FTS 467-2754)

Mr. John W. Kaufman
Aerospace Environment Division
ES42-Space Science Laboratory
National Aeronautics and Space Administration
Marshall Space Flight Center, Alabama 35812, 205-453-3104

Dr. Noel E. LaSeur
Director
National Hurricane and Experimental Meteorology Laboratory
National Oceanic and Atmospheric Administration
P.O. Box 248265
Coral Gables, Florida 33134
305-350-4150

Dr. Richard D. McConnell
Office of Construction
Veterans Administration
811 Vermont Ave., N.W.
Washington, D.C. 20234
202-389-3103

Dr. Richard D. Marshall
Research Structural Engineer
National Bureau of Standards
Room B168, Bldg. 226
Washington, D.C. 20234
301-921-3475

Dr. R.B. Matthiesen
Chief, Branch of Seismic Engineering
Office of Earthquake Studies
USGS
345 Middlefield Road
Menlo Park, California 94025
415-323-8111 (FTS 467-2881)

Mr. Howard L. Metcalf
Staff Engineer
Construction Standards and Design Directorate
Office of the Assistant Secretary of Defense
Room 3E763
The Pentagon
Washington, D.C. 20301
202-695-2713

Mr. Keith O. O'Donnell
Assistant Chief, Structural Branch
Engineering Division, Civil Works Directorate
Office of The Chief of Engineers
ATTN: DAEN-CWE-D
Washington, D.C. 20314
202-693-7311

Dr. Thomas D. Potter
Director
National Climatic Center
Environmental Data Service
National Oceanic and Atmospheric Administration
Federal Building
Asheville, North Carolina 28801
704-258-2850 x236

Dr. John B. Scalzi
Program Manager, Earthquake Engineers
Division of Advanced Environmental Research and Technology
National Science Foundation
1800 G Street, N.W.
Washington, D.C. 20550
202-632-0648

Mr. Charles Scheffey
Director
Office of Research
HRS-1
Federal Highway Administration
Department of Transportation
Washington, D.C. 20590
202-426-2943

Mr. Lawrence C. Shao
Chief, Structural Engineering Branch
Nuclear Regulatory Commission
Washington, D.C. 20555
202-492-8035

Dr. Warren A. Shaw
Head, Civil Engineering Department
Civil Engineering Laboratory
Naval Construction Battalion Center
Port Hueneme, California 93043
805-982-5407

Mr. William J. Werner
Energy Building Technology and Standards
Department of Housing and Urban Development
Room 8158
451 7th Street, S.W.
Washington, D.C. 20410
202-755-0642

ALTERNATIVES

Dr. A. Gerald Brady
Physical Scientist
Office of Earthquake Studies
USGS
345 Menlo Park, California 94025
415-323-8111 (FTS-467-2881)

Dr. James D. Cooper
Structures & Applied Mechanics Division
Federal Highway Administration
Office of Research HRS-11
Washington, D.C. 20590
202-557-4315

Mr. G. Robert Fuller
Architectural and Engineering Division
Department of Housing and Urban Development
Room 6176, 451 7th Street, S.W.
Washington, D.C. 20411
202-755-5932

Dr. H.S. Lew
Secretary
Structures, Materials and Safety Division
Center for Building Technology, IAT
Washington, D.C. 20234
301-921-3851

Dr. Charles T. Thiel
Deputy Director
Division of Advanced Environmental Research and Technology
National Science Foundation
1800 G. Street, N.W.
Washington, D.C. 20550
202-632-5734

Mr. Drew A. Tiedemann
Bureau of Reclamation
Engineering and Research Center
Denver Federal Center
P.O. Box 25007
Denver, Colorado 80225
303-234-3029

Japanese Panel on Wind and Seismic Effects

Membership List

May 1976

Dr. Kaoru Ichihara, Chairman
Director
Public Works Research Institute
Ministry of Construction
28-32 Honkomagome 2-chome
Bunkyo-ku, Tokyo, 113

Dr. Satoshi Hayashi
Head, Structure Division
Port and Harbour Research Institute
Ministry of Transport
1-1 Nagase 3-chome
Yokosuka-shi, Kanagawa-ken, 239

Mr. Seiichi Inaba
Chief, Earthquake Engineering Laboratory
National Research Center for
Disaster Prevention
Science and Technology Agency
4489 Kurihara, Sakura-mura
Niihari-gun, Ibaragi-ken, 300-32

Mr. Toshio Iwasaki
Chief, Earthquake Resistant Structure Sec.
Structure and Bridge Division, Chiba Branch
Public Works Research Institute
Ministry of Construction
12-52 Anagawa 4-chome
Chiba-shi, Chiba-ken, 280

Dr. Tetsuo Kunihiro
Head, Structure and Bridge Division
Chiba Branch
Public Works Research Institute
Ministry of Construction
12-52 Anagawa 4-chome
Chiba-shi, Chiba-ken, 280

Mr. Eiichi Kuribayashi
Chief, Earthquake Engineering Section
Structure and Bridge Division, Chiba Branch
Public Words Research Institute
Ministry of Construction
12-52 Anagawa 4-chome
Chiba-shi, Chiba-ken, 280

Mr. Tatsuro Murato
Chief, Structure Section
Structure Division
Building Research Institute
Ministry of Construction
28-8 Hyakunin-cho 3-chome
Shinjuku-ku, Tokyo 160

Dr. Kiyoshi Nakano
Assistant Director
Building Research Institute
Ministry of Construction
28-8 Hyakunin-cho 3-chome
Shinjuku-ku, Tokyo, 160

Mr. Nobuyuki Narita
Chief, Structure Section
Structure and Bridge Division, Chiba Branch
Public Works Research Institute
Ministry of Construction
12-52 Anagawa 4-chome
Chiba-shi, Chiba-ken, 280

Dr. Masakazu Ozaki
Head, Structures Division
Building Research Institute
Ministry of Construction
28-8 Hyakunin-cho 3-chome
Shinjuku-ku, Tokyo, 160

Dr. Tetsuo Santo
Head, International Institute of Seismology
and Earthquake Engineering (I.I.S.E.E.)
Building Research Institute
Ministry of Construction
28-8 Hyakunin-cho 3-chome
Shinjuku-ku, Tokyo, 160

Mr.Kenkichi Sawada
Chief, Soil Dynamics Section
Construction Method and Equipment Division,
Chiba Branch
Public Works Research Institute
Ministry of Construction
12-52 Anagawa 4-chome
Chiba-shi, Chiba-ken, 280

Dr. Seiji Soma
Chief, First Research Section
Physical Meterology Laboratory
Nakano Branch
Meteorological Research Institute
Meteorological Agency
35-2 Nakota 1-chome
Nakano-ku, Tokyo, 165

Mr. Akira Suwa
Head, Seismological Laboratory
Meteorological Research Institute
Meteorological Agency
35-8 Koenji, Kita 4-chome
Suginami-ku, Tokyo, 166

Dr. Tsutomu Terashima
Chief, Seismology Section
International Institute of Seismology and
Earthquake Engineering (I.I.S.E.E.)
Building Research Institute
Ministry of Construction
28-8 Hyakunin-cho e-chome
Shinjuku, Tokuo, 160

Mr. Hajime Tsuchida
Chief, Earthquake Resistant Structures
Laboratory
Structure Division
Port and Harbour Research Institute
Ministry of Transport
1-1 Nagase 3-chome,
Yokosuka-shi, Kanagawa-ken, 239

Dr. Makoto Watabe
Chief, International Institute of
Seismology and Earthquake Engineering
(I.I.S.E.E.)
Building Research Institute
Ministry of Construction
28-2 Hyakunin-cho 3-chome
Shinjuku-ku, Tokyo, 160

Mr. Kaname Yahagi
Chief, Foundation Engineering Section
Structure and Bridge Division
Chiba Branch
Public Works Research Institute
Ministry of Construction
12-52 Anagawa 4-chome
Chiba-shi, Chiba-ken, 280

Dr. Tadayoshi Okubo
Secretary-General
Head, Planning and Research Administration
Division
Public Works Research Institute
Ministry of Construction
28-32 Honkomagome 2-chome
Bunkyo-ku, Takyo, 113

THE U.S. - JAPAN MEMBERS ATTENDING THE EIGHTH JOINT MEETING

RESOLUTIONS OF EIGHTH JOINT MEETING

U.S.-JAPAN PANEL ON WIND AND SEISMIC EFFECTS

U.J.N.R.

May 18-21, 1976

The following resolutions for future activities of this Joint Panel are hereby proposed:

1. The Eighth Joint Meeting was an extremely valuable exchange of technical information which was beneficial to both countries. Considering the importance of cooperative programs on the subjects of wind and seismic effects, the continuation of the Joint Panel Meeting is considered essential.

2. The resolutions of the Seventh Joint Panel Meeting are considered important to the continued cooperative program and are hereby incorporated as a part of these resolutions:

    a. Disseminate technical reports and state-of-the-art reports continually.

    b. Publish proceedings of each joint meeting for benefit of other organizations in each country.

    c. Solicit state-of-the-art papers on wind and seismic effects from other governmental and private technical organizations.

    d. Promote dissemination of technological information to developing countries.

    e. Promote cooperative research programs through the Task Committees including exchange of personnel and available equipment. Publish reports of these Task Committees.

    f. Incorporate SI Metric System for units of measurement.

3. Establish a new Task Committee to consider problems associated with soils such as liquefaction, landslides, subsidence, etc. An exchange of complete soils reports from areas of liquefactions should be encouraged. These should include accurate boring logs with description of soils and field and laboratory test data.

4. The date and location of the Ninth Joint Meeting on Wind and Seismic Effects will be May 1977 in Tokyo, Japan. Specific dates and itinerary of the meeting will be determined by the Japanese Panel with concurrence by the U.S. Panel.

Aspects of Hurricane Winds as Recorded at an Instrumented Suspension Bridge

by

R. H. GADE
Federal Highway Administration, McLean, Virginia

and

R. H. SCANLAN
Princeton University, Princeton, New Jersey

ABSTRACT

Velocity spectra of the winds of tropical storm Doria in its passage over the Newport, Rhode Island, Suspension Bridge is presented for four mean wind speeds. Data was acquired with five 3-component Gill propeller anomometers, spaced at approximately 350 feet (108 m) intervals along the semispan of the bridge. This paper presents final information on the wind mean angle of attack, turbulence levels, vertical and horizontal spectra of wind of various velocity levels, derived surface drag coefficients, and a comparison of results with standard spectra and other applicable data from the Japanese, United States, and Canadian wind literature.

KEY WORDS: Wind; wind velocity spectra

INTRODUCTION

In 1971 wind-speed measuring instruments were temporarily installed, under the supervision of the Federal Highway Administration, and with permission of the Rhode Island Turnpike and Toll Bridge Authority, on the Newport Bridge, Rhode Island. Figure 1 depicts the geographical location of this bridge. The instrumentation consisted of 3-component Gill windmill-type anemometer groups at each of five locations on the bridge. These locations are shown in Figure 2, with their respective elevations and span positions designated. The bridge, completed in 1969, satisfactorily withstood the winds of tropical storm Doria which

passed in the vicinity in August 1971. During this passage, peak horizontal wind gusts as high as 75 mph (33.5 m/s) were recorded by the instrumentation on the bridge. Some characteristics of the project and wind data obtained therefrom are discussed below.

INSTRUMENTATION

Three-component anemometers were placed in five locations designated by numbers 5 through 9 in Figure 2. The anemometers of the Gill windmill-type extended on booms out about 35 feet (10.7 m) from the lower wind truss at each location on the seaward side of the bridge. The distance constant of the Gill anemometer is 1.07 meters. The frequency response characteristics of the anemometer, relative to frequencies in the variable velocity signal of the wind, are not completely known. Research continues on this question.[1] However, the data from the anemometers is treated in the present paper as faithfully representing the component wind speeds.

The system used accomplished repeated sampling of the analog velocity signals at 14.3 Hz, resulting in a Nyquist data cut-off frequency of about 7 Hz, which was largely adequate for the wind variations observed. In the final processing, data compression permitted a reasonable array size. An upper frequency range of 1.8 Hz was obtained with the processed data set.

WIND DATA

Each transducer group furnished wind data representing the following time-varying quantities:

U: horizontal velocity component perpendicular to the bridge roadway centerline

V: horizontal velocity component parallel to the plane of the roadway centerline

W: vertical velocity component normal to V

Only the U and W components are discussed in this paper; i.e., velocities along the bridge span are not considered in present analyses.

[1] J. M. McMichael and P. S. Klebanoff, "The Dynamic Response of Helicoid Anemometers," National Bureau of Standards Report NBSIR 75-772 November 1975, (Available as PB 246-861 from the National Technical Information Services, Va. 22161.)

The basic wind data selected for analysis consisted of 40 time-histories of approximately 10 minutes each. The more convenient record length of 10 minutes was found to give consistent results to 20-minute records, which were also examined initially. The records were selected in nominal mean horizontal velocity ranges of 15, 30, 50, and 60 mph (6.7, 13.4, 22.4, and 26.8 m/s) from each of the U- and W-transducers at positions 5 through 9, respectively. Broadly speaking, the rotating storm passed in such a manner that the lowest recorded velocities approached the bridge from the southeast, while the highest velocities were almost directly perpendicular to the span. The actual mean wind velocity components together with associated variances σ^2 about the mean are presented in Table I.

PRELIMINARY RESULTS AND METHOD OF DATA PROCESSING

The basic W/U represents the tangent of the instantaneous angle of attack of the wind crossing the bridge deck. This was calculated for each of the transducer locations, and the results were plotted, Figure 3. It is observed that a band of values is produced which represents a steady diminution of mean-wind angle to the horizontal at transducer height on the bridge (average about 205.6 feet = 62.7 meters). This angle drops from about 20° in mild winds down to 3° or 4° in high winds. These results tend to confirm the validity of the aerodynamic testing of bridge models at angles to the wind not usually exceeding 6°.

The evidence of Figure 3 also suggests that there is probably also a decrease in turbulence level $\sigma/\overline{U}$ (where $\overline{U}$ is the mean horizontal velocity) with increasing wind speed. Figure 4 is a plot of this specific trend. Somewhat analogous data are presented in [2], though the possibility of much higher turbulence occurring at extremely high velocities over a sea fetch (~50 m/s) is suggested there also.

The basic time-history data referred to in Table I was digitally processed according to the flow chart presented in Table II. In order to smooth and reduce the digital data available at 0.07 second intervals to more manageable proportions, new samples were taken at every fourth point only; i.e., a sampling interval of 0.28 seconds. While basic time-history selections were visually made of winds with sustained characteristics, it was found

[2] M. Shiotani and H. Arai, "Lateral Structures of Gusts of High Winds," Paper 20 VHI Proc. Int'l. Res. Seminar on Wind Effects on Buildings and Structures, NRC, Ottawa, Canada, September 1967, pp 535-555, University of Toronto Press.

necessary to remove slight "ramp" trends from such selections prior to evaluating means. Standard Fourier transform techniques with taper window were employed, followed by conversion to power spectral density $S(n)$ in the "logarithmic" form $\frac{nS(n)}{\sigma^2}$, where n is frequency, which has become conventional in the presentation of wind spectra. The abscissa used for eventual display was the mean-wind wave number $n/\bar{U}$, $\bar{U}$ being taken at bridge mean elevation.

HORIZONTAL WIND SPECTRA

One ten-minute sample wind time-history from transducer 7U at nominal 60 mph (26.8 m/s), together with its derived spectrum presented in the standard form $nS_U(n)/\sigma_U^2$ versus $n/\bar{U}$, is presented in Figure 5, where $\bar{U}$ is the mean wind velocity at transducer height. Altogether, 20 spectra of this type were derived from the similar time-histories recorded at the five transducer locations 5 through 9 for the four selected nominal wind speed ranges.

Figures 6 through 9 present the combined spectral results for all transducers at each of the four nominal wind speeds, respectively. Along with each mean spectral plot is presented a comparative plot based on the following formula:[3]

$$\frac{nS_U(n)}{\kappa\bar{U}^2(10)} = \frac{4N}{(2+N^2)^{5/6}}$$

where κ is the surface drag coefficient, and $\bar{U}(10)$ is the mean velocity, both referred to 10-meter height, and $N = \frac{nL}{\bar{U}(10)}$, L being a peak wavelength "constant." This formula is converted for comparative purposes to the desired form as follows:

$$\frac{nS_U(n)}{\sigma_U^2} = \frac{4K^2\bar{U}^2(z)}{\sigma_U^2 \ln\frac{10}{z_o} \ln\frac{62.7}{z_o}} \left[\frac{L\frac{1}{\lambda(z)}}{\left[2 + \left(\frac{1}{\lambda(z)} L \frac{\ln\frac{62.7}{z_o}}{\ln\frac{10}{z_o}}\right)^2\right]^{5/6}} \right]$$

where K, Karman's constant, is taken as 0.4, $\bar{U}(z)$ is averaged mean wind velocity at bridge height (av. 62.7 m), and $1/\lambda(z) = n/\bar{U}(z)$; z_o, the surface roughness length, is related to κ by the formula:

$$\kappa = \frac{K^2}{\left(\ln\frac{10}{z_o}\right)^2}$$

[3] R. I. Harris, "The Nature of the Wind," Paper 3 Proc. CIRIA Seminar: The Modern Design of Wind-Sensitive Structures, London, England, 1971, pp 29-55.

The peaks of the sample and reference spectra were arbitrarily equated to obtain the values of K and L. The resulting relations are:

$$1.812\ K\bar{U}^2(10) = [n\ S_U(n)]_{max}\sigma_U{}^2$$

and

$$L = \frac{\sqrt{3}\ ln\ {}^{10}/_{z_o}}{\frac{1}{\lambda(z)}\ ln\ \frac{62.7}{z_o}}$$

VERTICAL WIND SPECTRA

A sample spectrum obtained from a ten-minute time-history of wind vertical velocity at transducer 9W at the nominal mean wind speed of 50 mph (22.4 m/s) is presented in Figure 10 in the form $\frac{nS_W(n)}{\sigma_W{}^2}$ versus $n/\bar{U}$ for $\bar{U}$ at transducer altitude. Altogether, 20 such spectra were developed. Figures 11 through 14 present mean combined spectra of vertical wind at each of the nominal horizontal wind speeds. On each of Figures 11 through 14 is presented, for comparative purposes, an empirical spectrum derived from the following formula:[4]

$$\frac{nS_W(n)}{K\bar{U}^2(10)} \quad \frac{6f}{(1 + 4f)^2}$$

where $f = {}^{z}/_{\bar{U}}$, z being the height of the transducer, and $\bar{U}$ being the mean horizontal velocity at that height.

This formula is converted for comparative purposes to the desired form as follows:

$$\frac{nS_W(n)}{\sigma_W{}^2} = \frac{K^2\ \bar{U}^2(z)\left(1/\lambda(z)\right)6z}{\sigma_W{}^2\left(ln\ \frac{62.7}{z_o}\right)^2\left(1 + 4z/\lambda(z)\right)^2}$$

The surface drag coefficient is similarly obtained by

$$0.375\ K\bar{U}^2(10) = [nS_W(n)]_{max}\ \sigma W^2$$

and z_o as above.

[4] H. A. Panofsky and R. A. McCormick, "The Spectrum of Vertical Velocity Near the Surface," Quart. Jnl. Royal Meteorological Soc., 1960, Vol. 86.

DISCUSSION

It was noted earlier that the wind fetches were different (see Figure 1) as the wind direction swung from the 15 mph (6.7 m/s) values over to 60 mph (26.8 m/s). Thermal effects probably were more strongly present at the lowest velocities, though some evidence (Figure 3) suggests that there was an unstratified (rising) condition during all measurements taken. It is of interest to note that horizontal spectral peaks at all wind speeds in the presently analyzed data occurred at practically the same frequency (0.06 Hz); similarly, the vertical peaks grouped around 0.13 Hz. In Figures 6 through 14, values of κ and (where applicable) L for the reference spectra are given. The κ values are reasonable with respect to published values for the expected fetches; values of L are shorter than values chosen for spectral matching elsewhere.[3] [5] Owen[6] and Simiu[7] comment that spectral peaks may be expected to shift widely in location. However, the right-hand, downward slopes of the spectral curves, Figures 6 through 14, exhibit fair agreement with the expected boundary layer energy cascade results ($N^{-5/3}$ law). The spectra exhibited show reasonable similarity to spectra published elsewhere of which [8] and [9] refer specifically to typhoons.

[5] A. G. Davenport, "The Dependence of Wind Loads Upon Meteorological Parameters," Paper 2, Proc. Int'l. Res. Seminar on Wind Effects on Buildings and Structures, Ottawa, Canada, September 1967, University of Toronto Press.

[6] P. R. Owen, "Buildings in the Wind," Quarterly Journal of the Royal Meteorological Society, Vol. 97, 1971, pp 396-413.

[7] E. Simiu, "Wind Spectra and Dynamic Alongwind Response," Jnl. Struct. Div. Proc., ASCE, Vol. 100, No. ST9, September 1974, pp 1897-1910.

[8] M. Hino, "Spectrum of Gust Wind," Proc. 3rd Int'l Conf. on Wind Effects on Buildings and Structures, Tokyo, 1971, pp 69-77.

[9] Y. Mitsuta, "Preliminary Results of Typhoon Wind Observation at Tarama Island, Okinawa," Proc. U.S.-Japan Res. Seminar on Wind Effects on Structures, Kyoto, Japan, September 1974.

TABLE I

MEAN AND VARIANCE OF WIND VELOCITIES OF THE
10-MINUTE DORIA DATA SEGMENTS USED FOR SPECTRAL ANALYSIS

NOMINAL VELOCITY		HORIZONTAL MEAN $\overline{U}$	HORIZONTAL VARIANCE σ_U^2		VERTICAL MEAN $\overline{W}$	VERTICAL VARIANCE σ_W^2
		MPH			MPH	
	9U	15.29	11.37	9W	4.36	3.68
	8U	18.41	8.47	8W	3.72	3.44
	7U	16.74	8.84	7W	4.42	4.86
15 MPH	6U	15.94	9.71	6W	4.01	3.52
(6.7 m/s)	5U	19.97	9.77	5W	3.52	3.58
	Average	17.270	9.632	Average	4.006	3.816
	9U	31.00	19.94	9W	4.25	3.93
	8U	31.85	28.29	8W	3.46	5.83
	7U	32.35	18.27	7W	4.05	5.38
30 MPH	6U	27.84	20.10	6W	4.26	4.83
(13.4 m/s)	5U	34.62	28.77	5W	3.48	4.94
	Average	31.532	23.074	Average	3.900	4.982
	9U	52.69	61.87	9W	2.91	9.23
	8U	51.70	58.02	8W	2.38	9.10
	7U	48.63	44.68	7W	3.56	9.93
50 MPH	6U	48.63	40.50	6W	4.23	7.30
(22.4 m/s)	5U	53.29	39.60	5W	2.96	7.51
	Average	50.988	48.926	Average	3.208	8.614
	9U	51.22	39.52	9W	3.12	6.93
	8U	52.37	27.34	8W	1.91	9.49
	7U	49.19	29.02	7W	3.46	9.11
60 MPH	6U	49.89	24.26	6W	4.51	5.13
(26.8 m/s)	5U	55.86	26.96	5W	2.69	7.78
	Average	51.706	29.420	Average	3.138	7.688

TABLE II

PROCESSING OF WIND DATA

Time-Series Data	(Sample interval 0.07 sec)
↓	
Data Resampling	(Sample interval 0.28 sec)
↓	
Demean & Detrend	
↓	
Apply Window Taper	(10% cosine^2)
↓	
Time-to-Frequency Transform	
↓	
Convert Amplitude Spectra to Reduced Power Density Spectra	$RPD_i = \frac{ampl_i^2 \times freq._i}{VARIANCE}$
↓	
Convert Frequency to Wave Number	(WN_i = $freq._i$/mean velocity)
↓	
Spectral Smoothing	(19 pt. averaging)

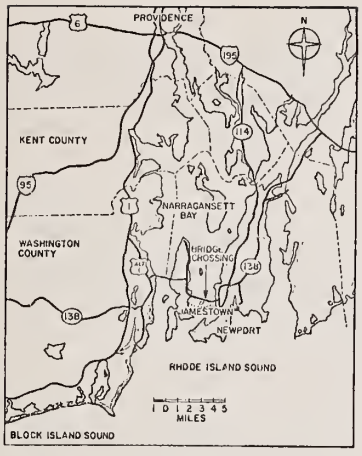

Figure 1

Site Location
Newport, R. I. Bridge

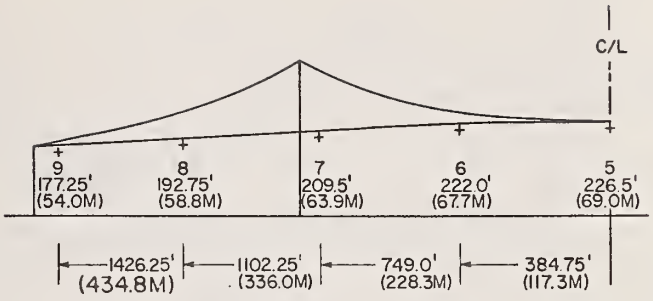

NEWPORT BRIDGE - SENSOR LOCATIONS

Figure 2

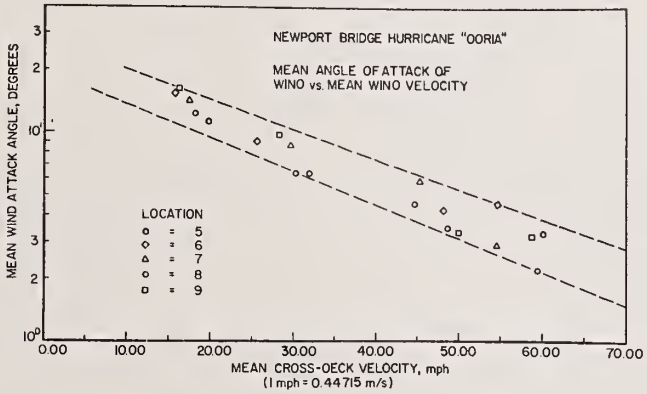

Figure 3

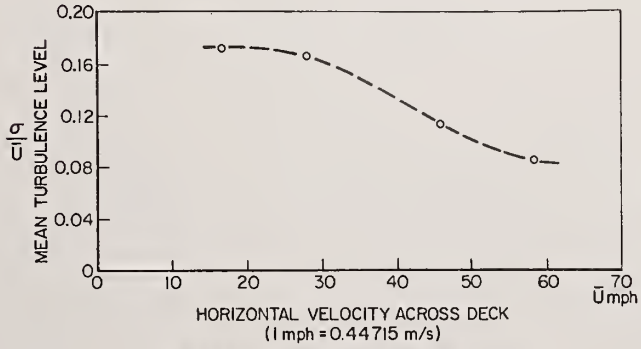

TURBULENCE LEVEL vs. MEAN WIND VELOCITY

Figure 4

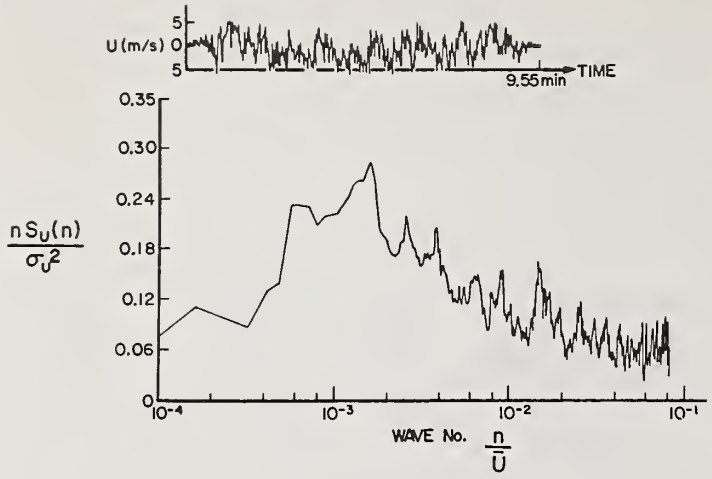

Figure 5
10-Minute Horizontal Wind Speed Record
and Velocity Spectrun (7U)

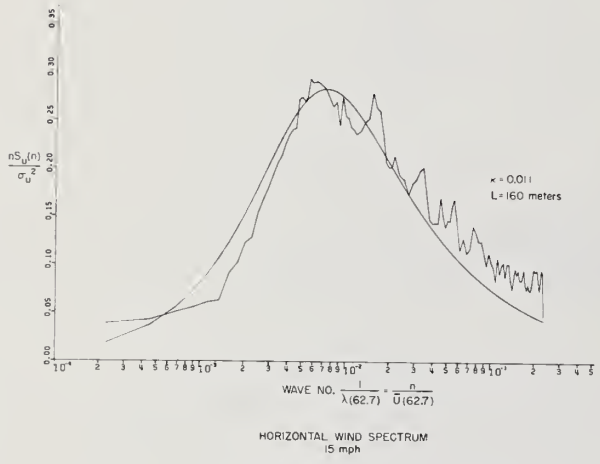

Figure 6

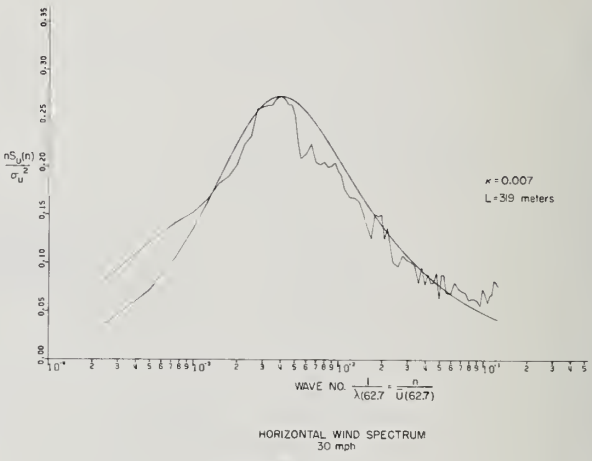

Figure 7

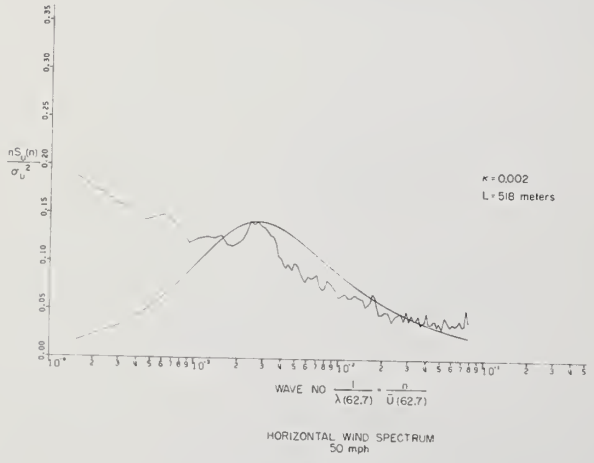

Figure 8

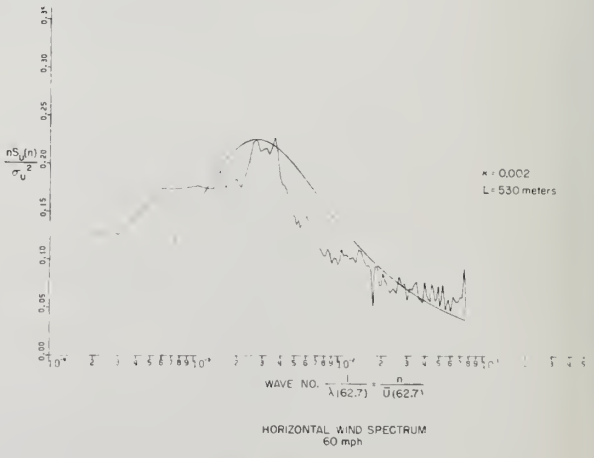

Figure 9

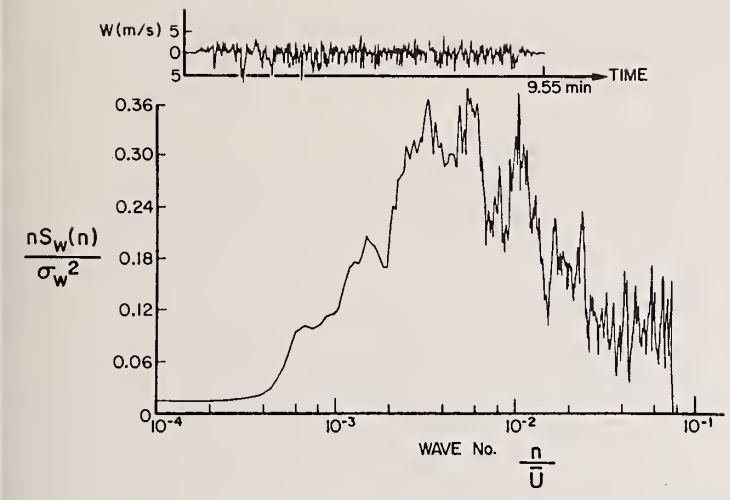

Figure 10
10-Minute Vertical Wind Speed Record
and Velocity Spectrum (9W)

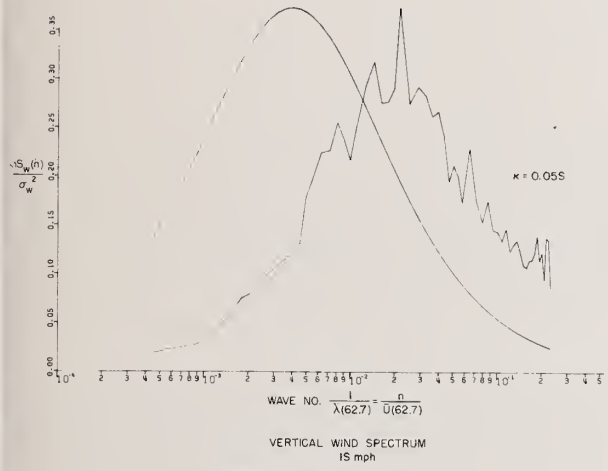

Figure 11

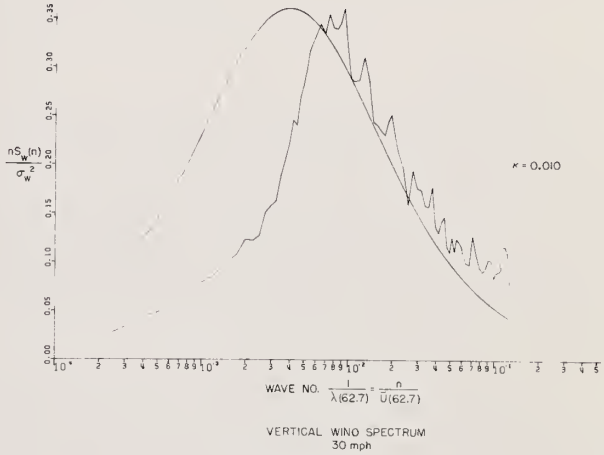

Figure 12

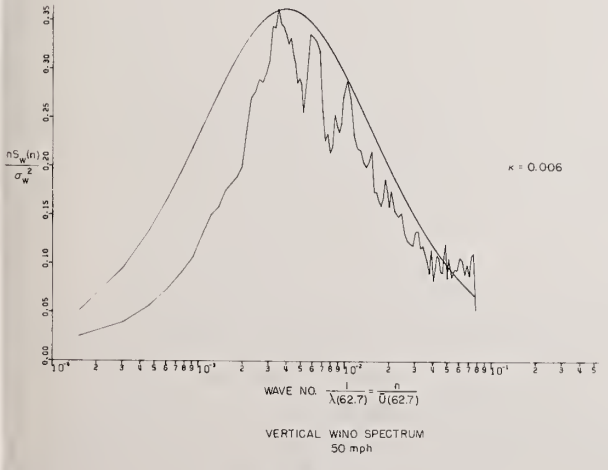

Figure 13

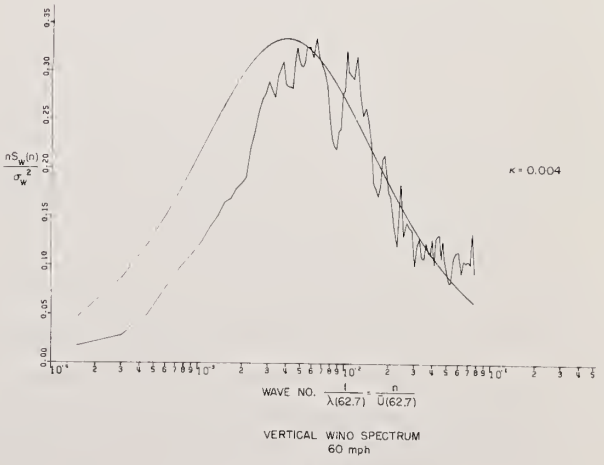

Figure 14

STUDY ON THE WIND EFFECT ON EAVES

T. MUROTA
Chief, Structure Section
Building Research Institute
Ministry of Construction
Japan

ABSTRACT

Recently in Japan damage to flat roofs of light weight roofing is increasing. The damage is often very severe to the extent that complete removal of the roofs occurs. The dynamic behavior of the eaves is related to the damage. A current research project is also described.

Key Words: Dynamics; Failure; Roofs; Wind.

1. Introduction

Eaves, and ridges of dwellings often suffer damage from severe winds. This local damage to roofs is caused by the high wind suction acting on these various parts. These local failures, however, have not caused severe damage to traditional wooden houses in Japan. This is because traditional Japanese wooden houses are constructed with heavy clay-tile roofings. When such clay-tiles are lifted away, the roof structures composed of bed boards and rafters still remain undamaged and therefore the interiors of houses are well protected from the wind and rain.

In Japan, the use of clay-tile on roofs is decreasing, and the use of light weight thin metal plate roof material is increasing. Roof structures are therefore also becoming light due to the change of the weight of the roof material. Accordingly, the damage to roofs is changing, and in some instances, these light weight roofs have shown perfect wind resistant performance. Those roofs which suffered severe damage such as complete removal of roofs, have been flat roofs or slightly pitched roofs of gentle slope. Typical damage of this type has recently been reported, in which complete removal of the roofs of about 30 prefabricated houses occurred. These houses were located in Aichi prefecture, and were subjected to an average wind of about 30 m/s as caused by Typhoon No. 7220 in 1972. The characteristics of the roofs which were damaged are as follows:

i) flat roofs
ii) long projection of eaves
iii) low flexural rigidity of the roof structures

Examination of some of the damage which occurred also indicates that one of the causes of the roof removals was vibration of the eaves.

In 1975, Typhoon No. 7513 caused similar damage to flat roofs which were constructed of light roofing material. After this storm, the Building Research Institute initiated a

research project which would study techniques to prevent damage to light weight roofs. The following will describe the ideas of this project relative to wind excited oscillations of flat roof eaves.

2. Characteristics of Wind Pressure on Eaves

It is well known from wind tunnel tests that large negative pressures develop on the wind ward edge of eaves. The values of this pressure differ according to each investigator, however, it is not unusual that a pressure coefficient of -5 be recorded near windward edge.

Shape factors for eaves have been estimated by some investigators. These factors have been determined by assuming that the pressure on eaves is static and uniformly distributed along the span. The maximum shape factor value is reported is about -3. The pressure coefficient is 0.7 to 0.8 for the under surface of eaves and the upper surface coefficient is -2.2 to -2.3. However, such large values have not been obtained in wind tunnel tests, except in the case when the eaves are very short.

The Building Code of Japan has specified a value of -0.5 prior to 1973, and after 1973 the value of -1.5 has been adopted.

In order to discuss the appropriateness of these values as a design shape factor for eaves, it is necessary to know the characteristics of the pressure fluctuation on eaves and the corresponding dynamic behavior of eaves. In the past, many investigations on the pressure fluctuation on square cylinders induced by Karman vortices, have been made. However, only the investigations which will now be described, give details on the pressure fluctuation near the edge of buildings.

In order to generate Karman vortices actively, the flow around a body has to be two-dimensional and also the cross-section of the body must not be slender in the direction of the wind. However, in case of ordinary buildings, these conditions are not satisfied. It is considered, therefore, that the turbulence induced by the separation of flow will be predominant in the pressure fluctuation generated near edges of buildings. From this point of view Ishizaki et al[1)] have measured pressure on the surface of slender square cylinders in a smooth wind tunnel flow, as shown in Fig. 1. They obtained the following results, as given in Fig. 2 and 3.

i) At points near the windward edge, high negative pressures were observed but their fluctuation was not intense.

ii) Pressure fluctuation increased on the leeward surfaces.

iii) Spectra of fluctuations showed that pressures were not composed of a single frequency component, as in case of Karman vortex excited fluctuations, but were composed of widely ranged frequency components.

iv) The reduced frequency, of the spectra of fluctuations, has a peak value 0.16, which agrees with the Strouhal number for square cylinders.

Mori[2)] has measured pressures on a flat roof model set in turbulent boundary layers as shown in Fig. 4. He obtained the following results, where h is the height of the roof model and Zo is the roughness length:

i) When h/z_o=6, the pressures contained non-convective fluctuation components of frequencies around fh/V=0.07 and also convective fluctuation components of higher frequencies (Fig. 5).

ii) When larger values of h/z_o occur, non-convective fluctuations observed near the windward edge are diffused rapidly downstream and convective fluctuations have a spectral peak at a reduced frequency of fh/V-0.2 to 0.25 which became predominant (Fig. 6 and 7).

The value of the central reduced frequency of the non-convective pressure fluctuation components, observed near the windward edge, is 0.14 where the characteristic length is taken as twice the roof height h, this value agrees with the Strouhal number for square cylinders, as in the case of the experiments of Ishizaki et al as stated before.

From the results of these two experiments, it can be concluded that the pressure fluctuation near the windward edge of flat roofs (whose lengths of the horizontal direction perpendicular to wind are large) is induced by the turbulence of flow separation at the windward edges. A spectra of these pressures have energy peaks at a reduced frequency 2fh/V, which is about the same value as the Strouhal number for square cylinders.

3. Power Spectrum of Pressure Fluctuations on Eaves

Width and/or depth of plan of ordinary houses are not large compared to their height. Therefore, air-flows round their roofs will have different properties from those of the above two experiments. It is considered, however, that pressure fluctuations on flat roof eaves are induced by turbulence of separated flow and have a random nature, which is the same for ordinary houses having flat roofs.

Then we can assume the spectra of pressure fluctuation on eaves, $S_p(f)$, as a form

$$f \cdot S_p(f) = \sigma_p^2 \cdot g(\bar{f}) \qquad (1)$$

where

$$\bar{f} = fh/V \qquad (2)$$

It is considered that the universal function g(f) can be obtained by wind tunnel experiments. This function g(f) depends on the aerodynamical shape of the houses, however, we expect the function to be constant which is applicable to flat roofs of most common sizes and shapes. In addition it will be better if pressure fluctuations under surface of eaves (this is considered to have the same nature as that on windward wall) are measured in the experiments and the effects are taken into account when determining the form of g(f).

4. Response of Eaves in Turbulent Winds

If the form of the power spectrum of pressure fluctuations on the eaves was shown in eq. (1), it is possible to obtain the statistical characteristics of the response by

applying the probabilistic theory of dynamics. This is a well-known method and the outline is as follows:

The equation of eaves is

$$\ddot{Z}(y,t) + 2\delta W_o \dot{Z}(y,t) + W_o^2(y,t) = \frac{1}{m} P(y,t) \tag{3}$$

where Z = deflection of windward edge of eave at a position y along the edge and at time t.

$W_o = (k/m)^{1/2}$, where K is spring constant of eave and m is mass per unit length in y direction.

δ = damping constant.

$P(y,t)$ = total pressure along eave span per unit length in y direction.

The solution of eq. (3), in terms of normal mode $\mu m(y)$, is

$$Z(y,t) = \Sigma\ am\ (t) \cdot \mu_m(y) \tag{4}$$

where

$$\mu_m(y) = \frac{\sin m\pi y}{\ell} \tag{5}$$

and ℓ is length of eave in the direction perpendicular to wind.

Here we need a cross spectrum of pressure fluctuation $S_p(y,y',f)$, which gives the correlation of the pressure fluctuations between two points y and y'. If this function is obtained by experiments, the spectra of the mode coefficients m is given by the equation

$$S_{am}\ (f) = |H_m(f)|^2 \cdot Jmm\ (f) \tag{6}$$

where $|H_m(f)|^2$ is the mechanical admittance function of the form

$$|H_m(f)|^2 = 1/M_m^2\ [(1-W^2/W_m^2)^4 + (2\delta W/W_m)^2] \tag{7}$$

and Jmm (f) is the joint admittance function,

$$Jmm\ (f) = \int_o^{\ell}\int_o^{\ell} S_p(y_4,y_2,t)\ \mu_m(y_1)\mu_m(y_2)dy_1dy_2 \tag{8}$$

Then the variation of a_m is obtained as follows

$$a_m = \int_o^{\ell} S_{um}(W)dw \tag{9}$$

5. Concluding Remarks

Recently in Japan damage to flat roofs of light weight roofing is increasing. The damage is often very severe such as bodily removal of roofs. The dynamic behavior of the eaves is considered to relate to this damage. In this paper is described a research project presently being conducted by the Building Research Institute concerning the problem.

Reference

1) H. Ishizaki and J. Katsura, Intensity of Fluctuating Wind Pressures on the Side Surfaces of Models with Long Rectangular Section, Transactions of A.I.J., No. 214, Dec. 1973, pp. 1-6.

2) T. Mori, Pressure Fluctuations on Steps in Turbulent Boundary Layers, M.E. Sc. Thesis, Faculty of Engineering Science, Univ. of Western Ontario, 1971.

3) Y.K. Lin, Probabilistic theory of Structural Dynamics, McGraw-Hill.

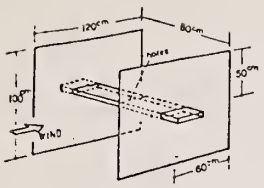

Fig. 1 Arrangement of a model[1)]

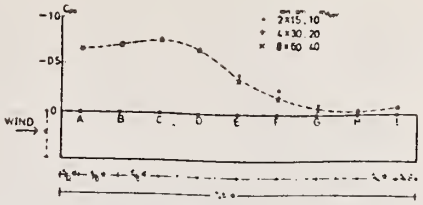

Fig. 2 Distribution of static pressure coefficient[1)]

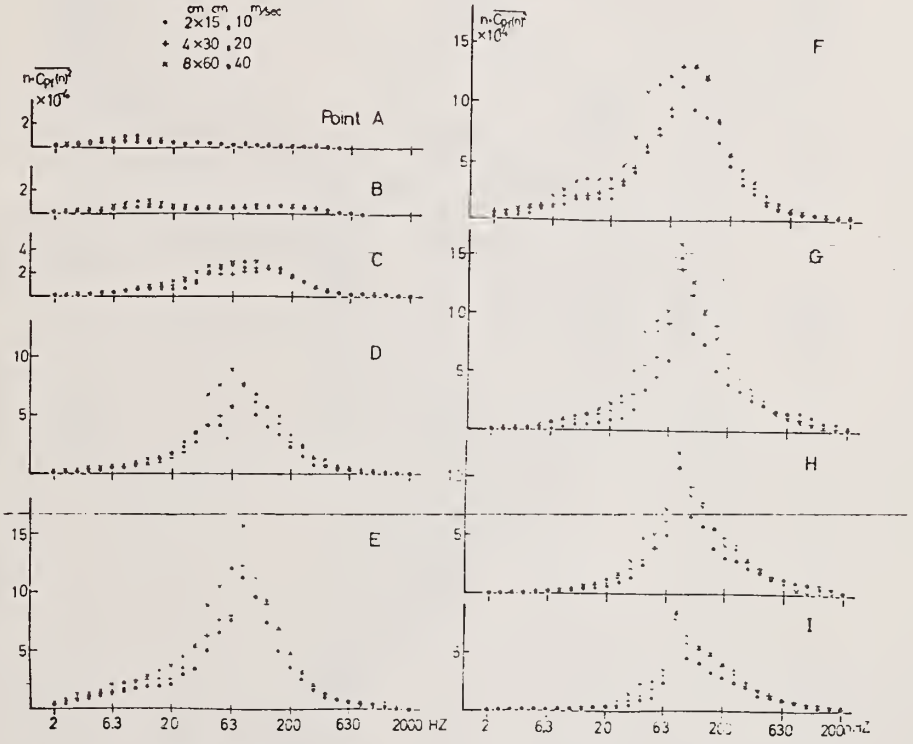

Fig. 3 Power spectra of fluctuating pressure coefficients[1)]

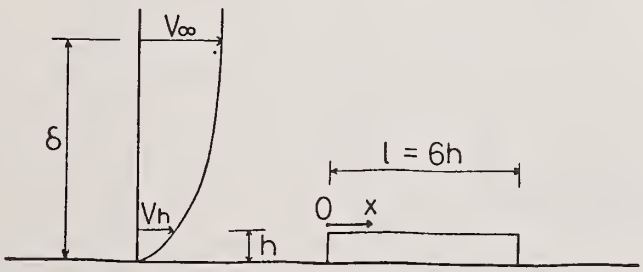

Fig. 4 Mori's wind tunnel test[2)]

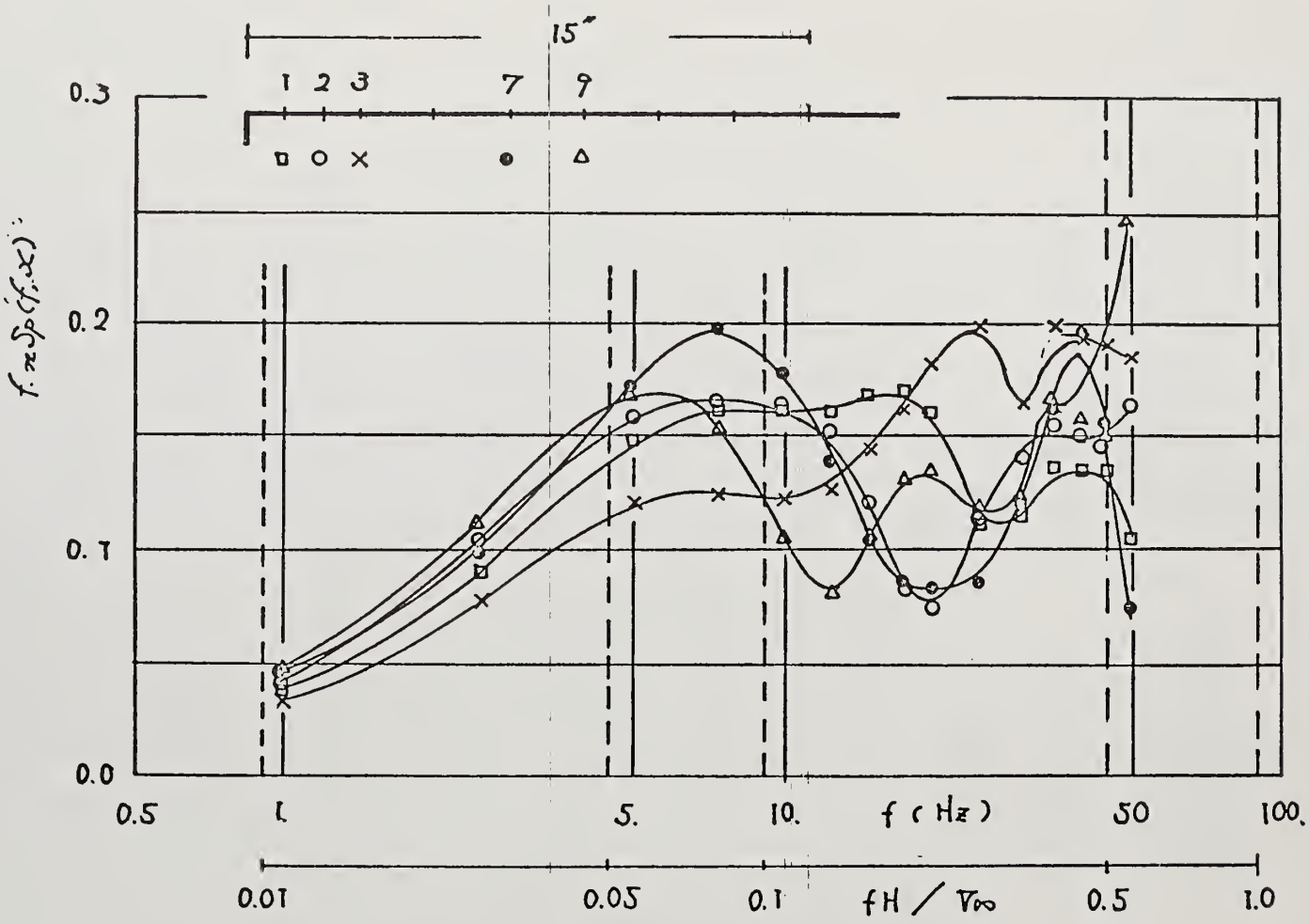

Fig.5 SPECTRA OF PRESSURE, 'B-5', H/z_0 =6, V_∞=38 FT./SEC., H/δ=0.1

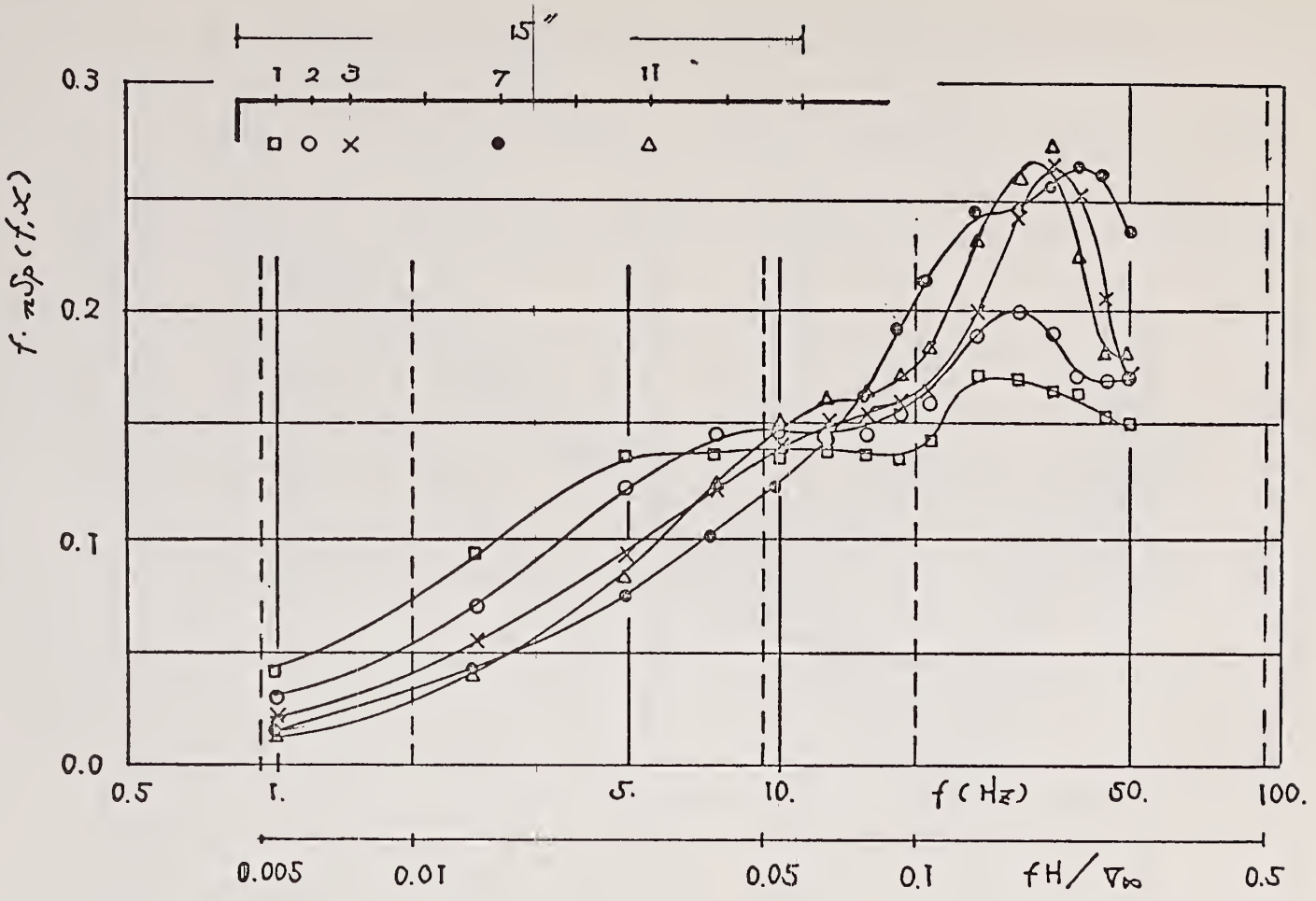

Fig.6 SPECTRA OF PRESSURE, 'C-2', H/Z_0 =50, V_∞=31 FT./SEC., H/δ=0.1

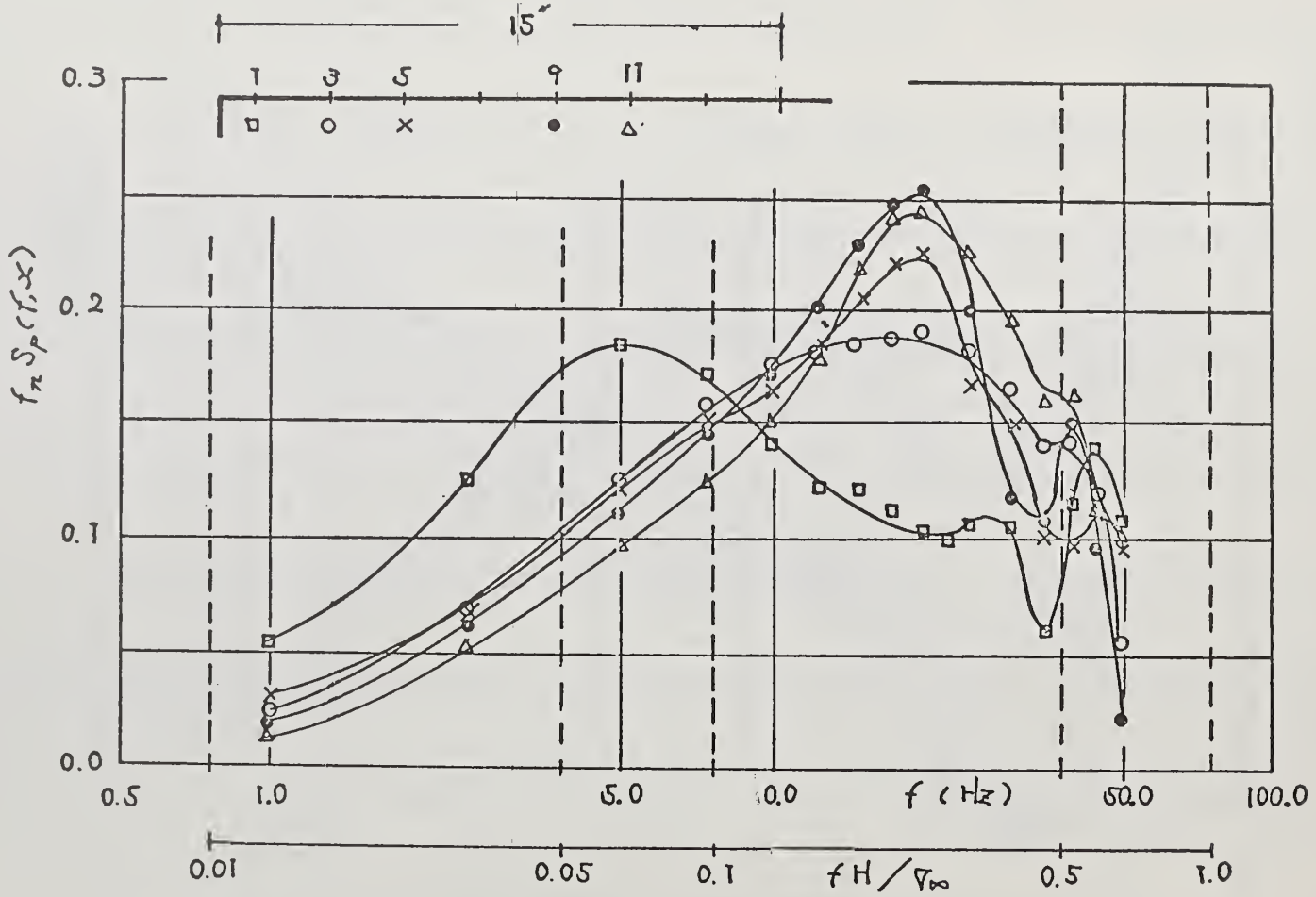

Fig.7 SPECTRA OF PRESSURE, 'C-5', H/z_0 =130, V_∞=32 FT./SEC., H/δ =0.2

MEASUREMENTS OF WIND LOADS AND TIE-DOWN FORCES ON MOBILE HOMES

RICHARD D. MARSHALL
National Bureau of Standards
Gaithersburg, Maryland

and

ROBERT A. CRIST
National Bureau of Standards
Gaithersburg, Maryland

ABSTRACT

This paper describes instrumentation, experimental techniques and progress to date on a program of research into the effects of wind on mobile homes. Direct measurements of lift and drag forces on a nominal 12 x 60 ft. (3.66 x 18.3 m) mobile home provide more reliable information on load fluctuations than is possible with the usual approach of measuring surface pressure alone. Results of spectral analysis conducted on time histories of overturning forces suggest that a simple quasi-static approach, when used with appropriate gust factors, can be employed to calculate loads for the design of mobile home anchoring systems.

Key Words: Aerodynamics; Buildings; Full-scale testing; Mobile homes; Wind loads.

1. Introduction

Although the general area of wind research has made tremendous advances over the past decade, most studies have been carried out on tall buildings and only recently have the problems associated with wind forces on low-rise buildings been given proper attention.

The purpose of the research effort described in this paper is to establish a source of data upon which to base criteria for the design of mobile homes and their anchoring systems to resist wind forces. Mobile homes account for a significant percentage of single family dwellings in the United States and, next to fire, wind is the primary cause of deaths, injuries and property damage.

The problem of wind forces on mobile homes is complicated by the fact that, near ground level, the local terrain and upwind buildings have a pronounced effect on the variation of mean wind speed and turbulence intensity with height. In addition, their limited size makes them more sensitive to wind gusts than is the case with conventional low-rise buildings where spatial averaging can substantially reduce the effectiveness of load fluctuations.

This project is being funded by the Department of Housing and Urban Development (HUD) under the Mobile Home Construction and Safety Act.

2. Description of Experiment

a) The Test Site

The field tests are being carried out on the Gaithersburg Campus of the National Bureau of Standards in an area which has a clear exposure to the prevailing winds. Strong winds in the Gaithersburg area are most frequent during the winter months from November through March and are usually associated with the passage of low pressure systems to the north. The strongest winds [50 mph (22 m/s)] generally blow from the west-northwest, although several events can be expected each winter from the southwest. The surrounding terrain is gently rolling and mean velocity profiles can best be described by a power law [$V_z = V_{30}(Z/Z_{30})^{\alpha}$] with values of α ranging from 0.16 to 0.25. This exposure corresponds approximately to Exposure C of the American National Standards Institute Standard A58.1-1972. A plan of the test site and prevailing wind directions are shown in figure 1.

b) Design and Installation of Mobile Home Support System

The test site is located on a paved parking lot which facilitated mounting the mobile home on a supporting frame and turntable so that various relative wind directions could be selected for each wind storm. This allowed an expedient method of gathering the necessary data for the forces on the mobile home during one wind season at the NBS site. Consultations were held with the project sponsor (HUD) and representatives of the mobile home manufacturing industry to determine the most representative mobile home for the research. A nominal 12 ft (3.66 m) by 60 ft (18.3 m) mobile home with a roof to ground height of 10.8 ft (3.30 m) was used. The test setup also allowed the open space between the ground and the floor level to be enclosed or open to study the effects of these two configurations on lift and drag.

The support system was designed so that the lowest first mode natural frequencies (vertical or horizontal) of the supports and the linking components were at least the $\sqrt{2}$ times the largest first mode natural frequencies of the mobile home (vertical and horizontal). This prevented resonance of the mobile home and supports and approximately uncoupled the dynamic response of the mobile home and the supports, i.e., the foundation stiffness >> mobile home stiffness. This provided a realistic simulation of the in-service foundation conditions of a mobile home. The mobile home natural frequencies were determined by temporarily mounting the home on rigid supports similar to those to be used in the experiment, exciting the home and measuring the free vibration with an accelerometer. The highest first mode natural frequencies in the place of the floor were 8 Hz vertically and 4 Hz horizontally.

The support system can best be described as three separate systems, the foundation system which consists of four beam and column assemblies, a force measurement system, and a main support frame. The four beam and column assemblies simulate an actual installation which includes diagonal and vertical tie-down cables (figure 2). The force measurement system consists of four force links to measure horizontal forces (drag) and eight force links to measure lift and overturning. All force links are connected to a main support frame with four leveling points and a turntable (figure 3). The turntable is staked to the ground through a set of wooden ties. The turntable allowed

216 degrees of rotation (figure 1) of the mobile home. A set of vertical and horizontal steel wheels on the turntable holds the home in place for rotation during windstorms as well as when it is in the stationary position. The lowest calculated first mode natural frequencies of the foundation system and main support frame are 80 Hz horizontally and 32 Hz vertically. The force link lowest calculated first mode natural frequencies are 10 Hz horizontally and 12 Hz vertically.

3. Field Measurements

a) Wind Speed

Two types of anemometers are being used to obtain wind speeds at the test site, the standard 3-cup Mod. F420C used by the National Weather Service and Mod. 27100 Gill 4-blade propeller anemometers. The Mod. F420C is mounted at the 10-meter level of an 18-meter guyed mast and provides wind speed records which can ultimately be related to extreme-mile speeds referenced in ANSI Standard A58.1-1972. Gill propeller anemometers are mounted at the 18, 10, 5, 3 and 1.5 meter levels to provide a good definition of the mean velocity profile and to allow flow characteristics at the height of the mobile home to be expressed in terms of mean wind speeds at the 10-meter level. These anemometers are conventionally used in pairs to measure the u and v components of turbulence and to establish the mean speed vector. However, the present installation uses only one anemometer at each level, the anemometers being mounted on a vertical support pipe which runs the height of the mast. The support pipe is manually adjusted prior to recording of data so that the anemometers are faced directly into the wind. A direction vane is mounted at the top of the mast.

In addition to the anemometers on the mast, two Gill anemometers are mounted on tripods which are positioned upwind of the mobile home for obtaining along-wind and cross-wind correlations. The tripods are adjustable to cover a range of heights from near ground level to the roof height. Nominal sensitivity of the anemometers is 10 mv per mph (22.4 mv per m/s).

b) Surface Pressure

Surface pressures are measured by means of differential pressure transducers of the variable reluctance type. Nominal output is $\pm$ 10 volts at the full-scale range of 0.1 psi (689 N/m^2). This allows direct recording without signal conditioning, although the transducer demodulators are provided with switch-selectible filters which are usually set at a cutoff frequency of 10 Hz. A conventional tap-tube-transducer arrangement is used, the transducers being mounted inside the mobile home and connected to the 3/8-in (95 mm) diameter pressure taps with short lengths of flexible tubing. The frequency response of this system is flat to approximately 20 Hz.

The pressure transducers are referenced to outside ambient pressure by means of an omnidirectional probe mounted on the guyed mast. Transducer offsets are measured just prior to recording of data by means of solenoid valves which shunt the active pressure line to the reference side of the transducer. The transducer and solenoid valve are

built into an assembly that can be quickly attached to a wall or ceiling tap. A total of 27 transducers are available and can be placed in various arrays, depending upon the pressure patterns being investigated. The pressure tap layout is shown in figure 4.

c) Deformation and Acceleration

Racking deformations are measured at the approximate mid-length of the mobile home with displacement transducers mounted on telescoping rods running along the diagonals of the mobile home cross-section. Recordings of horizontal acceleration have been obtained at floor level and along the bottom chord of the roof trusses for the purpose of estimating structural damping.

d) Lift and Drag Forces

The force links previously described are instrumented with strain gages in a full-bridge configuration to produce maximum sensitivity and to provide temperature compensation. Nominal sensitivity of the force links after amplification is 1 mv per lbf (225 μv per N). Bias voltages at the amplifier inputs allow the bridges to be nulled for "at rest" conditions.

e) Data Acquisition

The primary data acquisition system is a computer-controlled digital and analog system with a total capacity of 112 data channels and an effective maximum sampling rate of 13 samples per second per data channel. A programmable gain control allows the selection of five ranges for each data channel; $\pm$ 0.5, $\pm$ 1, $\pm$ 2, $\pm$ 5 and $\pm$ 10 volts. Normal operation utilizes approximately 40 data channels and the 20 kHz scan rate reduced time skew to a negligible amount for the frequencies of interest in this study. Data channels are usually sampled at the rate of 12 samples per second, but this rate is doubled for the measurement of surface pressures at points on the mobile home where large fluctuations and high frequency components are observed. Record lengths range from 500 to 1000 seconds, depending upon the sampling rate. All recordings, both digital and analog, are identified by time code.

Certain data channels are also recorded in analog form on a 14-channel recorder under control of the system computer. This allows analog analysis of selected records and digital analysis at higher sampling rates by selecting the proper ratio of record to reproduce speeds.

4. Data Reduction and Analysis

a) Methods

Because of the large amounts of data involved in this study, it is important that the data handling be as efficient and reliable as possible. An extensive package of computer software has been developed at the NBS over the past few years for the analysis of wind load data. Although the techniques used depend upon the particular variable being analyzed, the analysis generally consists of the following steps:

1. Sorting of samples by data channel.
2. Calculation of means and removal of trends.
3. Calculation of peak departures from the mean and their cumulative distributions.

4. Area integration of surface pressures.

5. Spectral analysis.

To aid in the selection of records which are to undergo detailed analysis, continuous stripchart recordings of wind speed and direction are taken during strong wind conditions and the digital recording intervals are noted on the stripcharts. A subjective assessment is then made as to the stationarity of the records and their general suitability for additional analysis.

The analog recordings provide additional information on data quality but are primarily used for spectral analysis. Auto- and crosscorrelations are obtained by use of a hybrid analyzer which accepts an analog input and computes a 400-point correlation function. By making repeated entries of the analog records, extremely stable estimates of the correlation function can be obtained. A Fourier transformation of the 400 points is then carried out. This technique has the advantage of an early look at the form of the correlation function without the expense of computer time and, if the form appears to be satisfactory, extremely reliable estimates of the spectral densities with a minimum of computational time required.

b) Typical Response Analysis

As previously described, the support system was designed to measure drag (horizontal) and overturning (lift) forces. A typical overturning force response time history is shown in figure 5 with the corresponding wind speed record from the 10-meter standard 3-cup anemometer. Refer to figure 1 for the location of the anemometer in plan. Note that the major force response correlates well in time history with the slow increases and decreases in the wind speed. To further analyze such records statistical analyses as previously discussed were performed on the force link time history of approximately 17 minutes, a portion of which is shown in figure 5. The following parameters were determined.

	mean wind speed	= 21.6 mph (9.7 m/s)
μ_{x1}	= mean force	= 119 lb (530 N)
	peak force	= 199 lb (885 N)
σ_{x1}	= standard deviation, force	= 29 lb (130 N)

This record represents relatively low magnitudes compared to others obtained in this experiment and to anticipated design wind speeds of approximately 100 mph (45 m/s). However, it can be shown that this experimental data can be scaled with confidence to the more intense wind speeds to provide data for extreme design wind speeds.

Further analysis of the time history data (figure 5) provide autocorrelation and spectral density functions. The autocorrelation function is given in general form as

$$R(\tau) = \frac{1}{T} \int_0^T x(t)x(t + \tau)dt \qquad (1)$$

and the spectral density function is the Fourier transform of the autocorrelation function or

$$S_x(f) = 4 \int_0^{\infty} R_x(\tau)\cos 2\pi f \tau d\tau \qquad (2)$$

Normalized autocorrelation and spectral density functions are given in figure 6 where

τ = time lag = 0.08 seconds

$$R(I) = \frac{R(\tau)}{\sigma_x^2}$$

and

σ_x^2 = variance of x

Also

$$NDS = \frac{fS_x(f)}{\sigma_x^2}$$

These typical records and analyses form the basis to transform the random data gathered from the experiment to forces on the mobile home in the form of design loads. It is convenient to express the wind load in terms of mean and fluctuating load components. The contribution of load fluctuations over specified frequency ranges can be determined from the spectral density function where

$$\psi_x^2 = \int^{\Delta f} S_x(f)df \qquad (3)$$

Using the spectral density functions of figure 6 for two frequency ranges $0.01 < \Delta f_1 < 10$ and $0.01 < \Delta f_2$ 1.0, values of ψ_1^2 and ψ_2^2 were obtained. The contribution to the fluctuating force by the resonant response of the mobile home is eliminated in the Δf_2 range. Note that the spectral density function shows a peak, the highest first mode natural frequency of the mobile home at 3.7 Hz which is approximately equal to that measured when the mobile home was mounted on temporary supports as previously discussed. By integration the ratio

$$\frac{\psi_{x1}^2}{\psi_{x2}^2} = 1.044 \text{ or } \frac{\psi_{x1}}{\psi_{x2}} = 1.022$$

was determined. This shows that approximately 2 percent of the fluctuating force is contributed by the resonant response of the mobile home (f > 1 Hz) and the remainder of the fluctuating force is contributed by the wind load which is considered, in this case, as a quasi-static force. In terms of the mean force, μ_{x1} = 119 lb (530N), the contribu-

tion by the resonant response of the mobile home and fluctuating wind load is 0.5 and 24 percent respectively. These observations are important in transforming the response data to design criteria through the appropriate use of parameters such as gust factors.

5. Summary and Acknowledgements

A research project has been described which is currently gathering data for the development of design criteria for mobile homes to resist wind forces. The test setup, instrumentation, data acquisition and analysis, and typical response analyses have been presented. The entire program when completed will provide data for transformation to wind load design criteria in the areas of wind profiles below 10 meters, pressure distributions on mobile homes, forces on foundation systems transferred through mobile homes, and structural response.

The assistance in the conduction of the program by Dr. Bruce Ellingwood, Mr. Charles Yancey, Mr. Randolph Williams, and Dr. James Shaver of the National Bureau of Standards is gratefully acknowledged.

NOMENCLATURE

f	Frequency
$R(\tau)$	Autocorrelation
$S(f)$	Spectral density
V	Mean wind speed
Z	Height above ground
α	Power law exponent
μ	Mean force
σ	Standard deviation of force fluctuations
τ	Lag time
ψ^2	Fraction of total variance

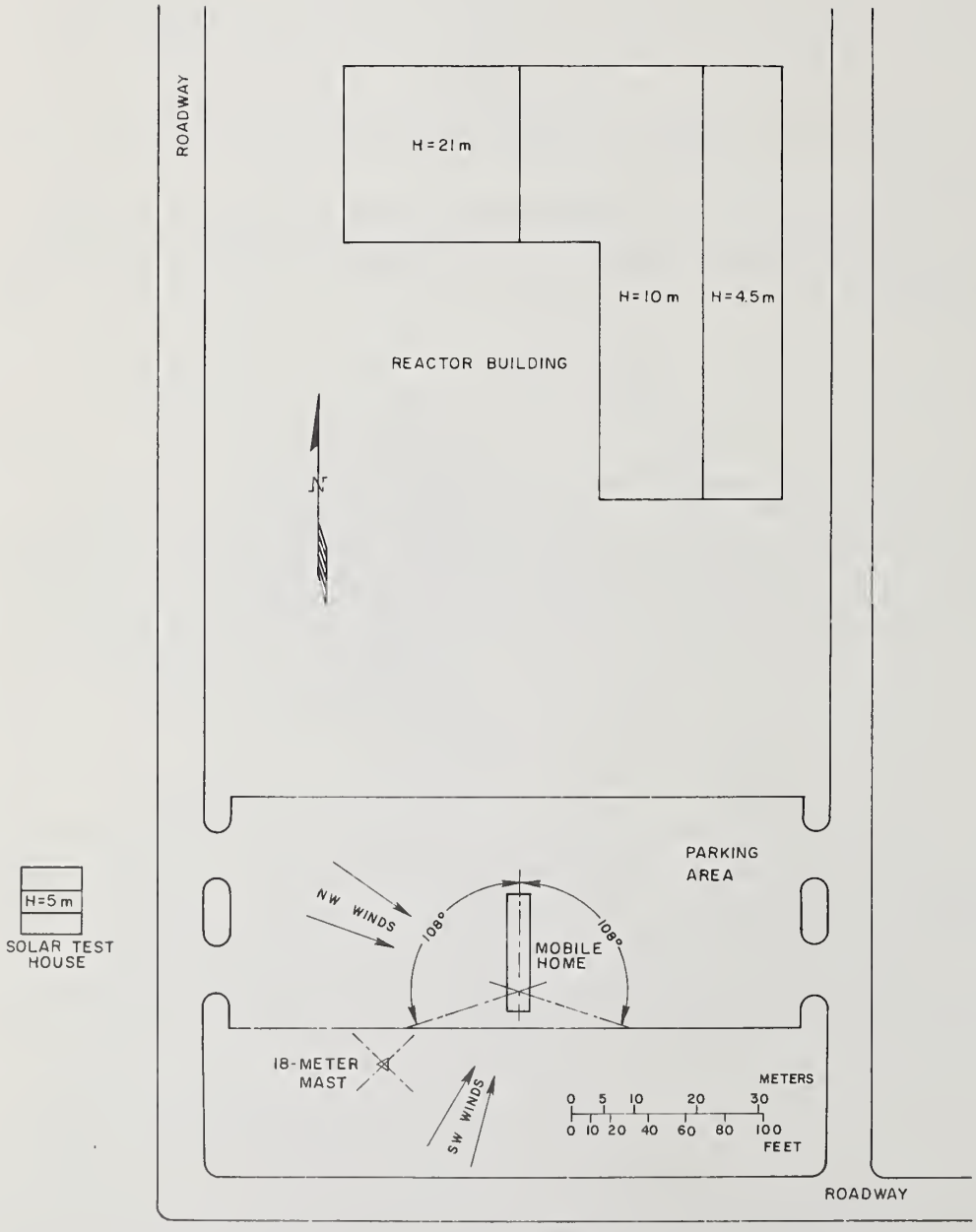

Figure 1. Test site plan

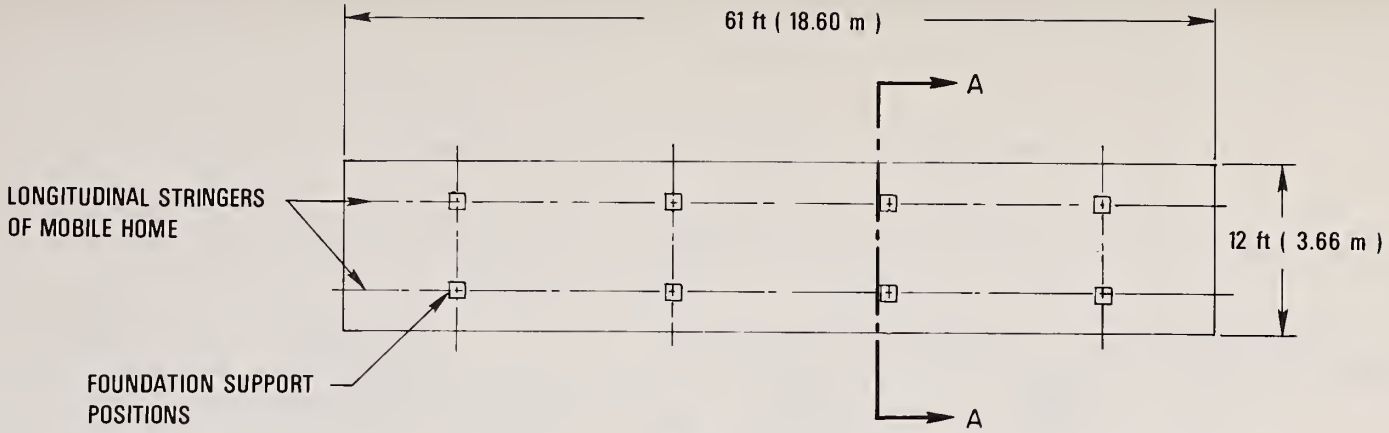

FOUNDATION SYSTEM

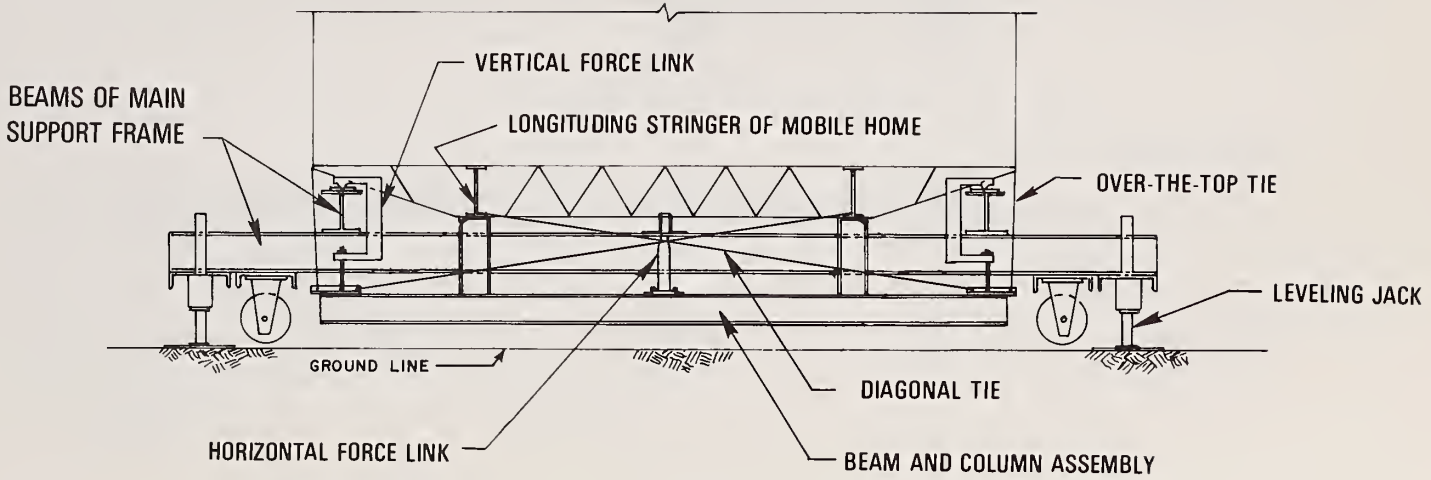

SECTION A-A (refer to figure 3 for other section details)

Figure 2. Foundation System

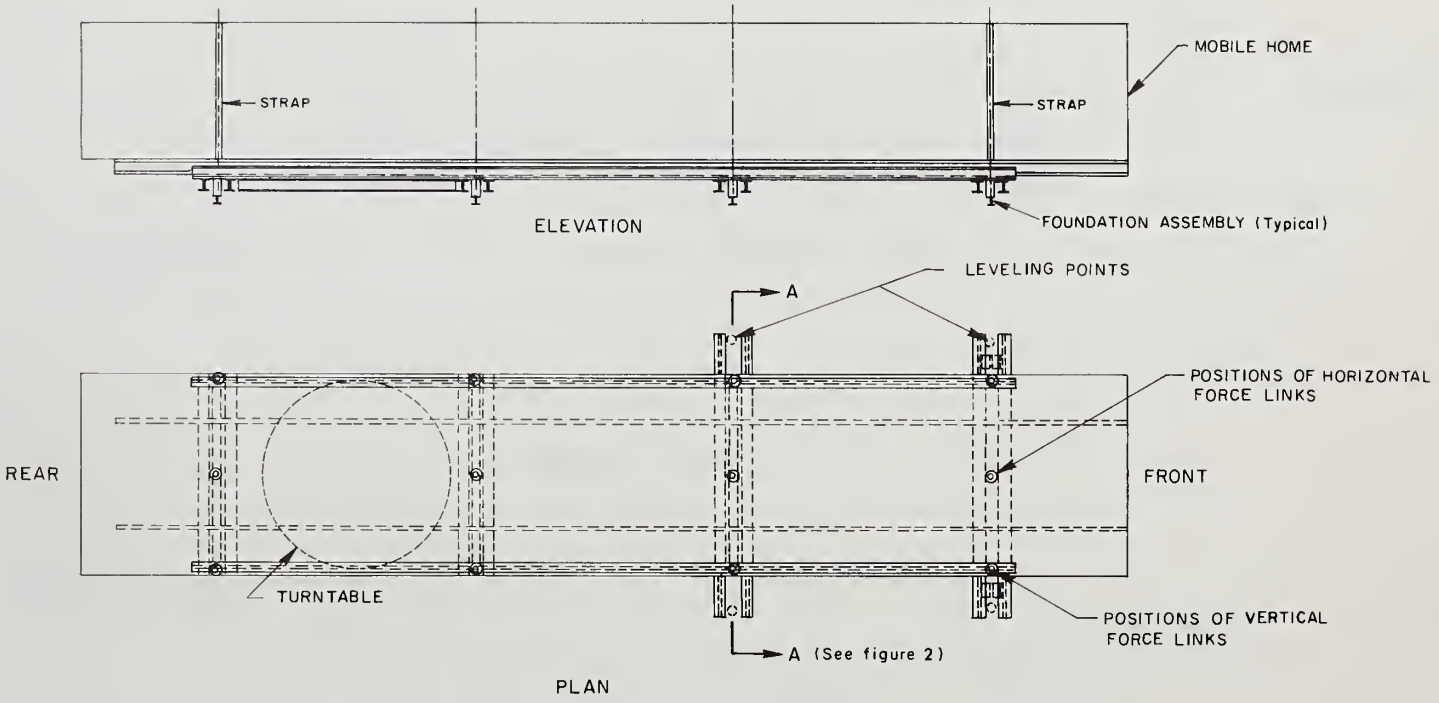

Figure 3. Layout of main support frame and turntable

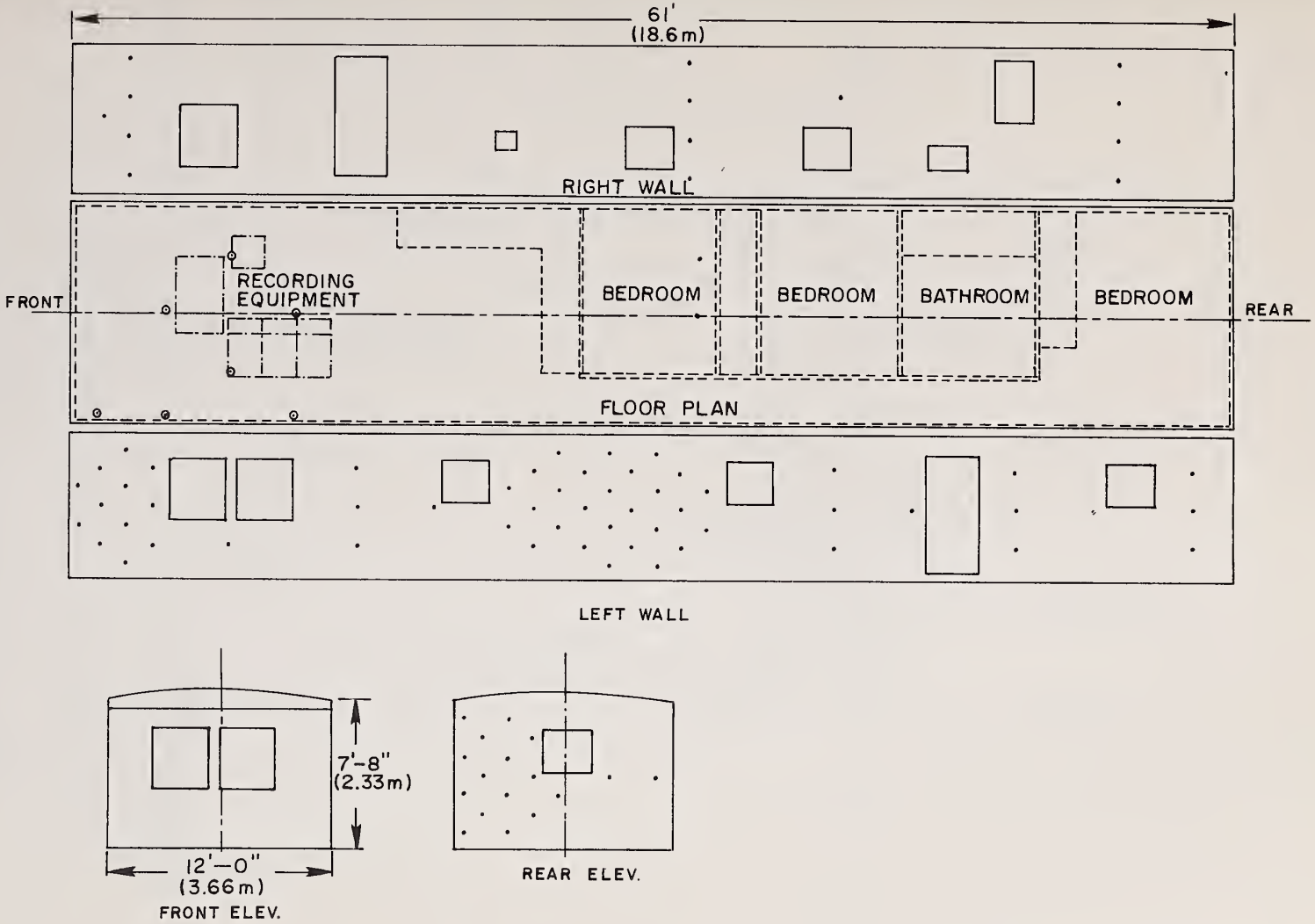

Figure 4. Layout of roof and wall pressure taps

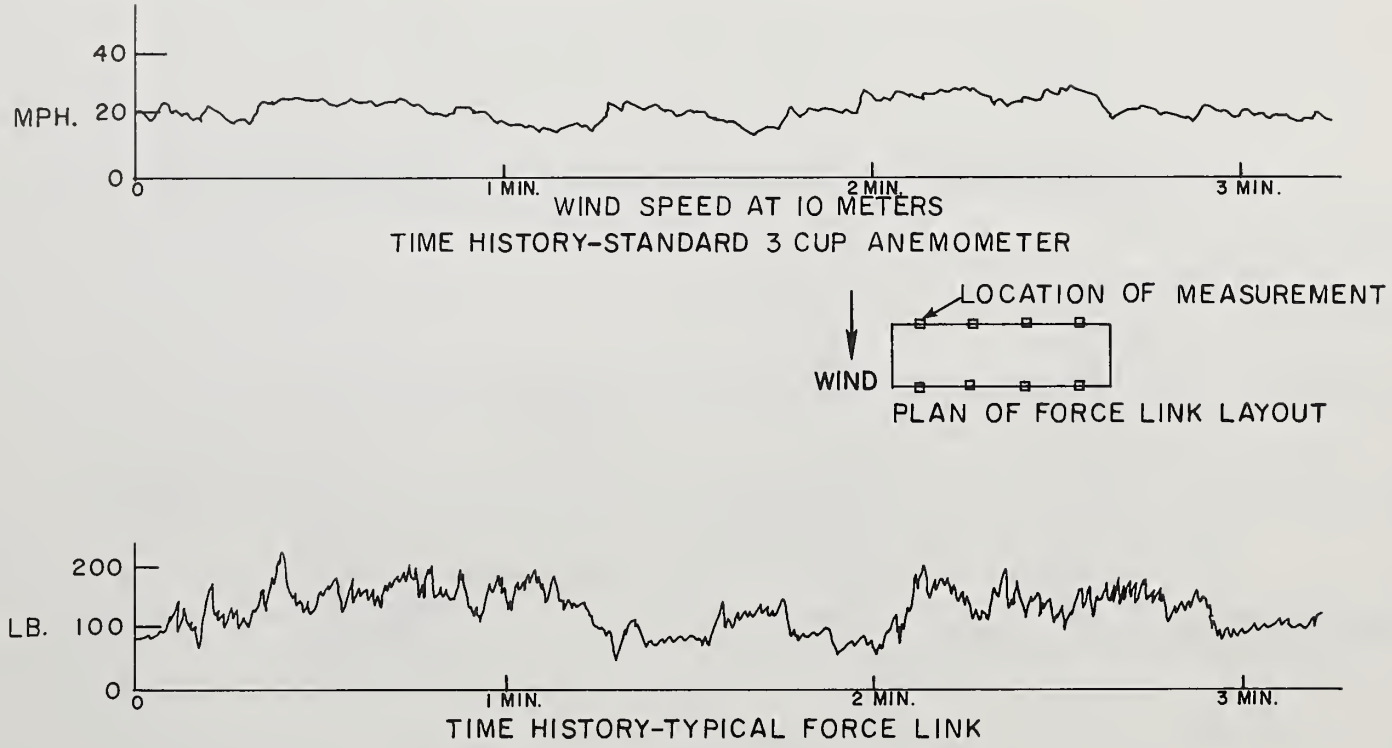

Figure 5. Typical time histories of wind speed and overturning forces

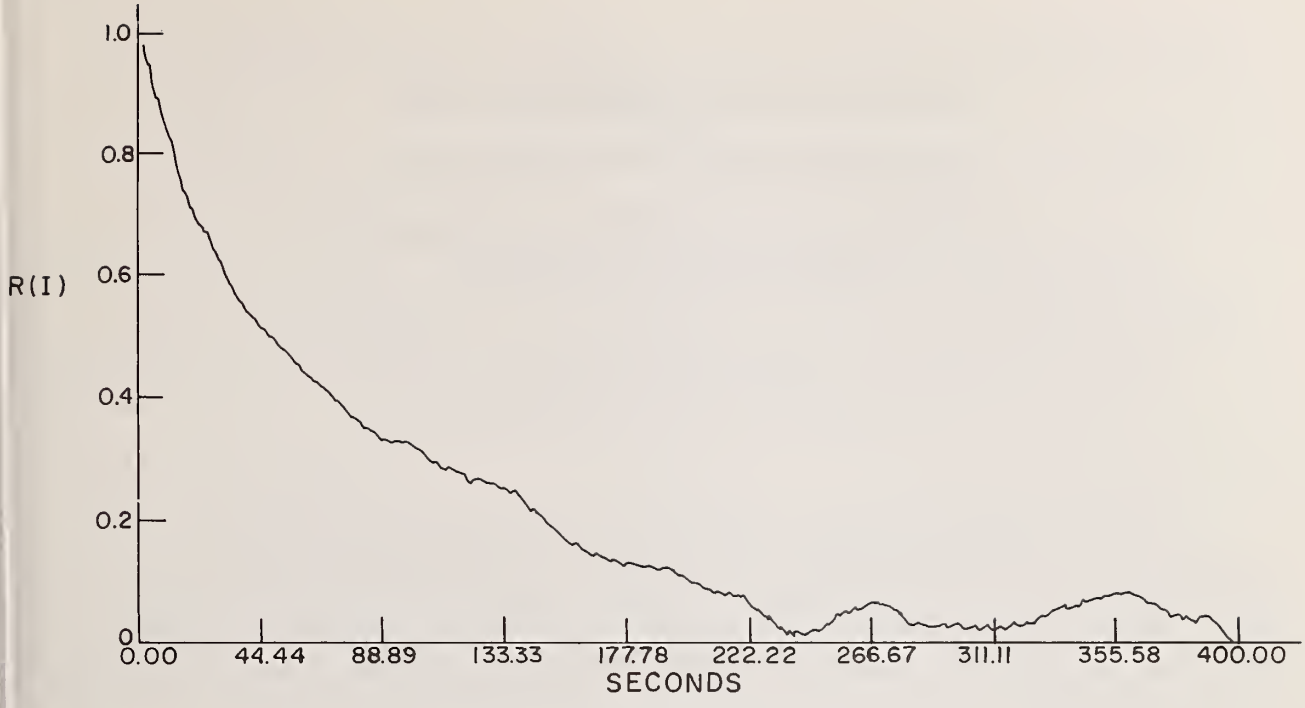

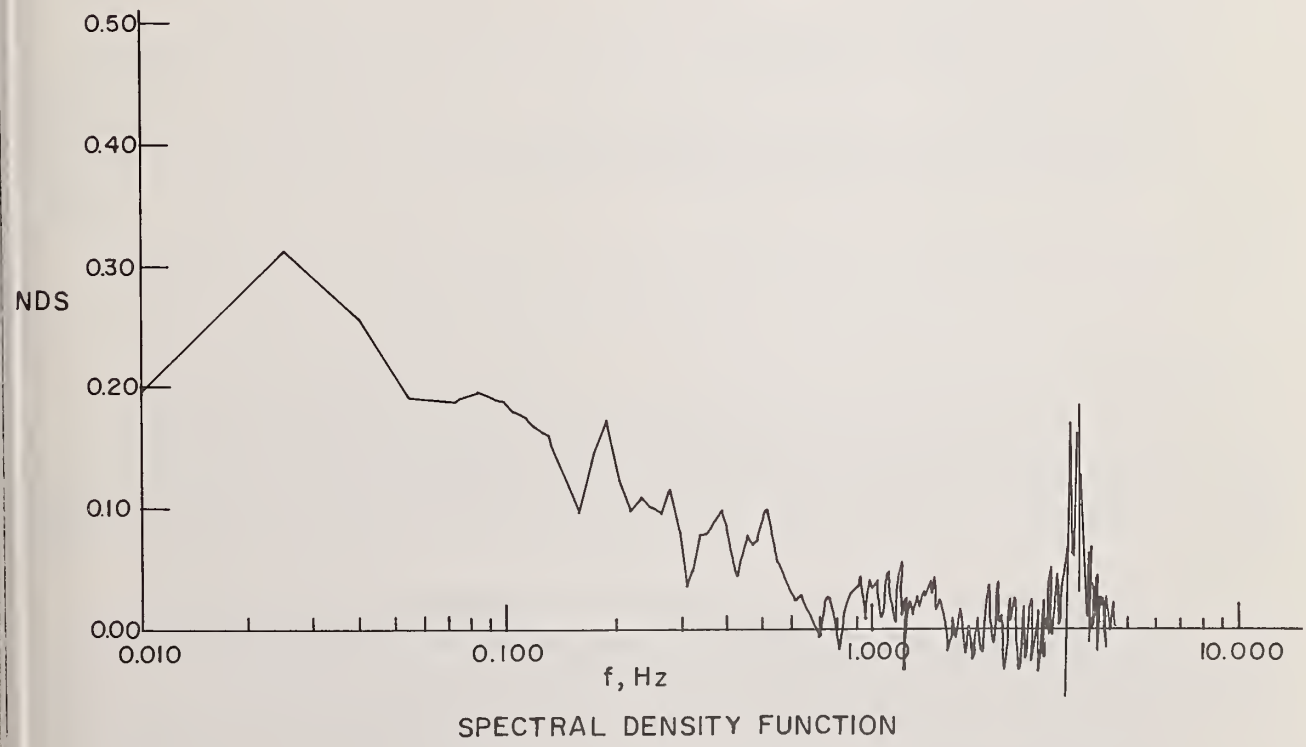

Figure 6. Typical autocorrelation and spectral density functions for force measurement

ON THE WIND RESISTANT DESIGN SPECIFICATIONS FOR THE PROPOSED HONSHU-SHIKOKU BRIDGES (1975)

T. OKUBO
Head, Planning and Research Administration Division
Public Works Research Institute
Ministry of Construction, Japan

N. NARITA
Chief, Structure Section
Structure and Bridge Division, Chiba Branch
Ministry of Construction, Japan

ABSTRACT

The newly revised specifications for the wind resistant design of the proposed Honshu-Shikoku Bridges are introduced in this paper. The previous specifications (the first edition was issued in 1964, and the second edition in 1972) have been revised by taking into account recent research activities, resulting in final edition as established in the fall of 1975.

The main subjects discussed in this paper are:

1. Scope of application
2. Basic wind and design wind speed
3. Drag coefficients
4. Gust response
5. Wind resistibility of structures under construction.

Key Words: Bridges; Specifications; Wind.

1. Introduction

The design of bridges to connect the Honshu (the mainland of Japan) with the Shikoku (the fourth largest island) was initiated after formation of the Honshu-Shikoku Bridge Authority in July 1970. The wind resistant design specifications, the first edition of which was formulated in 1964, have been revised and applied in the preliminary design of structures.

In a previous paper, the authors introduced the main features of the wind resistant design specifications for the proposed Honshu-Shikoku Bridges (1972) and related problems. The significant points that were revised are as follows;

(1) To clarify the design procedure and the constitution of articles in the specifications.

(2) To reexamine the basic wind speed in due consideration of the recent wind data in the Seto Inland Sea, and to set the basic wind speed for the respective zone or route.

(3) To determine the modification factors for converting a basic wind speed into the design wind speed, where the analytical method of the gust response was tentatively adopted.

(4) To revise the values of the drag coefficients, structural damping, and vertical wind inclination by using the data which was recently obtained.

As the design work progressed, the authority requested the formulation of design specifications which could be uniformly applied to all of the bridges in the project.

In order to meet this request the former specifications had to be extensively revised. These revisions are given in the latter part of this paper, the significant topics will now be described.

2. Expansion of Scope

The (1972) specifications were applicable to a truss stiffened suspension bridge with a span length of 500 meters or more. However, the scope of the (1975) specifications have been expanded to bridges which may be affected by strong winds in the Inland Sea. Then the boundary for the respective route, in which the specifications are applicable, is definitely stipulated. The basic wind speed, therefore, for an on-shore bridge, shall be the same as used for the off-shore bridge in an identical route.

3. Basic Wind Speed

The basic wind speed should be determined by considering the observed wind speed, durability of the structure, and the return period of the wind. The period of the wind observation in the Inland district has not been extensive enough to estimate the return values during a longer period. These wind periods have, therefore, been derived as follows;

(1) Estimation from the correlation between wind record at the construction site and that of the standard weather stations.

(2) Estimation from direct application of the Gringorten method to the observed data at the construction site.

(3) Estimation from a multi-regression method.

The estimated return wind value has not been established, and only the basic wind speed in the northern district of the Onomichi-Imabari route has been evaluated and is equal to 37 m/s.

4. Design Wind Speed - Gust Response

The effects of the statistical characteristics of the natural wind on the dynamic behavior of a structure should be taken into account on determining the design wind speed. The fundamental meterorological data, indispensable in analyzing gust responses, were collected in 1973. These data include power spectrum of the wind speed, frictional constant of the ground roughness, index of the space correlation of the wind, and other variables.

Parametric calculations of the gust response has been carried out for a series of preliminary designs with different types of bridges, spans, and rigidities. Consequently the following two types of wind speeds are defined; 1) basic wind speed, which is the ten minute averaged wind speed at a height of ten meters above sea or ground level, and 2) the design wind speed. The design wind speed can be deduced from the basic wind speed by modifying the effect to the altitude of the structure and the horizontal or vertical length of the structure. The safety factor of self-excited oscillation (flutter) may then be defined as the ratio of the flutter speed against the design wind speed. The load magnification effect due to the gust is then considered in the design wind load. In this context the consistency between the revised specifications and the design specifications for highway bridges can be preserved.

5. Drag Coefficients

a) Longitudinal Wind Load

The stiffening truss of a suspension bridge moves longitudinally due to the wind component in that direction, where its magnitude will have a great influence on the design of the expansion joints and wind shoes. It has been specified in the specifications, as indicated by wind tunnel experiments, that sixty percent of the transverse wind load shall be applied longitudinally to the stiffening truss of a suspension bridge.

b) Drag Coefficient of Solid Girder

The drag coefficient of a solid girder is given by the following empirical formula;

$$C_D = 2.1 - 0.1 \times B/D \qquad (1 \leq B/D \leq 8)$$

$$C_D = 1.3 \qquad (B/D > 8)$$

where C_D B, and D indicates the drag coefficients, width and depth of girder respectively.

6. Wind Resistibility Under Construction

How much wind load should be applied to a structure during the construction state? This is an important consideration since many accidents have occurred during the construction stage. The static and dynamic characteristics of a structure changes gradually during the progress of the construction. Therefore, the aerodynamic stability of the structure at each stage should be confirmed by a wind tunnel test using the full-model. However, if the unit construction period is assumed as two years, the return value in five years given the equivalent safety to a structure under construction as the completed structure. The intensity of the wind loading for a structure under construction is stipulated as half of the design wind load.

7. Conclusive Remarks

The following are the problems which should be examined in order to enhance the wind resistant design method of bridges;

(1) To establish a unified method for estimating the return value of the wind speed.

(2) To establish quantitative evaluation of the wind load with regard to gust effects.

(3) To improve wind tunnel techniques with regard to gusty wind.

(4) To establish a more rational factor of safety.

I. General

A. Scope of Application

The following specifications as shown in Table 1.1.1, were applied to the wind resistant design of the bridges in the Honshu-Shikoku Bridge Project.

Table 1.1.1 The district for scope of application

Route	District
Kobe-Naruto	Maiko Viaduct ∿ Akashi Straits Br. ∿ Matsuho Viaduct Tozaki Viaduct ∿ Onaruto Br. ∿ Muya Br.
Kojima-Sakaide	Shimotsuiseto Br. ∿ Bannosu Viaduct
Onomichi-Imabari	Onomichi Br. ∿ Kurushima 3rd Br. (Limited to the bridges across the straits)

B. Definitions and Symbols

1. Definitions

The following terminology is used in these specifications:

(a) Basic wind speed

Basic wind speed is the wind speed used as the basis of the wind resistant design, and is the average wind speed over a ten minute interval at a height of ten meters above the ground or water surface at the site where the bridge is to be constructed.

(b) Design wind speed

Design wind speed is the wind speed used in computing the design wind load on the structures and in establishing the wind stability of the structures against wind. The basic wind speed shall be converted to the design wind speed by multiplying appropriate

modification factors to consider the height of structure, and the horizontal linear dimension or vertical linear dimension of the structure.

(c) Critical wind speed for self-excited oscillation

Critical wind speed for self-excited oscillation is the onset wind speed of the self-excited oscillation which occurs in the structure in relation to its aeroelastic characteristics.

(d) Wind direction

Wind direction is the direction of wind in the horizontal plane.

(e) Wind inclination angle

Wind inclination angle is the angle of wind inclination measured from horizontal axis in the vertical plane, and is taken as positive when the wind blows upward.

(f) Design wind load

Design wind load is the computed air force obtained from the design wind speed, and is the mean drag component of the air forces acting in the direction of bridge axis or in the horizontal direction perpendicular to bridge axis.

(g) Circumscribed area

Circumscribed area is the average area per unit length of a structure, which is enclosed by the surrounding lines of the structural part under consideration. In computing the circumscribed area, handrail and guardfence are to be considered. However, the effect of the transverse slope of the floor deck and floor system shall be ignored.

(h) Projected area

Projected area is the average area per unit length of a structure projected to the plane which is at a right angle to the acting direction of the wind load.

(i) Solidity ratio

Solidity ratio is the ratio of the projected area to the circumscribed area.

(j) Structural damping

Structural damping is the vibration damping of a sturcture in still air, and is expressed by a logarithmic decrement.

(k) Angle of attack

Angle of attack is the angle between the direction of wind acting on the structure and the horizontal reference axis perpendicular to the bridge axis. This angle is taken as positive when the wind blows upward.

(l) Standard sea level

Standard sea level is the level for computing the elevation of the structure, where the datum of standard sea level is the mean sea level of Tokoyo Bay (T.P.).

2. Symbols

In these specifications symbols are defined as follows:

(a) V_{10}: Basic wind speed (m/s)

(b) ν_1 : Wind speed modification factor for the elevation of structure

(c) ν_2 : Wind speed modification factor for the horizontal linear dimension of structure.

(d) ν_3 : Wind speed modification factor for the vertical linear dimension of structure.

(e) ν_4 : Wind load modification factor for the horizontal line-like structure

(f) ν_5 : Wind load modification factor for the vertical line-like structure

(g) V_D : Design wind speed (m/s)

(h) Z : Elevation above ground or sea level (m)

(i) α : Power index in the power law of wind profile

(j) P_D : Mean drag force on unit length of structure (kg/m^2)

(k) C_D : Drag coefficient

(l) δ : Structural damping

(m) A_g : Circumscribed area (m^2/m)

(n) A_n : Projected area (m^2/m)

(o) ϕ : Solidity ratio

(p) ρ : Air density ($kg \cdot s^2 \cdot m^{-4}$)

II. Static Design

A. Basic Wind Speed

The following basic wind speed shall be applied to the bridge structure of the Honshu-Shikoku Bridge according to the district in which the bridge is to be constructed.

Table 2.1.1 Basic wind speed

Route	District	Basic wind speed (m/s)
Kobe-Naruto	Akashi Straits district	43
	Naruto Straits district	50
Kojima-Sakaide	Whole Route	43
Onomichi-Imabari	Kurushima Straits district	40
	Others	37

B. Design Wind Speed

The basic wind speed V_{10} shall be converted to the design wind speed V_D by multiplying by modification factors as given in the following equations:

for horizontal line-like structure: $V_D = \nu_1 \cdot \nu_2 \cdot V_{10}$

for vertical line-like structure: $V_D = \nu_1 \cdot \nu_2 \cdot V_{10}$

Modification factors ν_1, ν_2, and ν_3 shall be taken as shown in table 2.2.1, 2.2.2 and 2.2.3 respectively. When the value is not shown in the table, it shall be derived from proportional allotment and be computed to three decimal places and counting fractions of .5 and over as a whole number and disregarding the rest. In the area where the wind convergence due to special topographical conditions such as cape or peninsula is anticipated, the modification factor ν_1 may be modified by taking into account the results of field observations of the wind profiles or results from wind tunnel experiments on topographical models. The elevation and the length to be used in computing the modification factors ν_1, ν_2, and ν_3 are shown in Table 2.2.4.

Table 2.2.1 Modification factor ν_1

Elevation(m)	≤ 10	20	30	40	50	60	70	80	90	100	120	140	160	180	200
ν_1	1.00	1.10	1.17	1.22	1.26	1.29	1.32	1.35	1.37	1.39	1.43	1.46	1.49	1.51	1.53

Table 2.2.2 Modification factor ν_2

Horizontal length (m)	200	300	400	500	650	800	1,000	1,200	1,500	1,800
ν_2	1.21	1.19	1.18	1.17	1.16	1.15	1.14	1.13	1.12	1.12

Table 2.2.3 Modification factor ν_3

Vertical length (m)	80	100	120	160	200	260
ν_3	1.26	1.25	1.24	1.24	1.24	1.23

Table 2.2.4 Definition of elevation and length of structural element

Bridge type / Factor	Suspension bridge. Cable-stayed girder bridge	Others
ν_1	Suspended structure of suspension bridge and girder of cable-stayed bridge: mean elevation of center span. Cable and hanger: mean height between the elevation of the tower top and the lower surface at the mid-point of stiffening structure or bridge girder at the center span. Tower: 65 percent height of tower	The higher elevation between the mean elevation of support + [(the maximum elevation of structure) - (the mean elevation of support)] x 0.8 and the maximum elevation of designed road level.
ν_2	Center span length or maximum span length	
ν_3	Height of tower	———

C. Design Wind Load

In the static design, only the mean drag component of the air force shall be considered. The wind load shall be determined as follows:

1. Bridges with a maximum span length more than 200 meters for horizontal line-like structure:

$$P_D = \frac{1}{2}\rho V_D^2 \nu_4 C_D A_n$$

for vertical line-like structure:

$$P_D = \frac{1}{2}\rho V_D^2 \nu_5 C_D A_n$$

in which ρ, air density, shall be taken as 0-12 $kg \cdot s^2 \cdot m^{-4}$. The drag coefficient C_D and the projected area A_n shall be calculated by data given in Table 2.3.1 and 2.3.2. The modification factors ν_4 and ν_5 shall be chosen from Table 2.3.3.

Table 2.3.1 Drag Coefficient

Bridge type	Structural element		Transverse		Longitudinal	
			C_D	Remarks	C_D	Remarks
Suspension bridge	Suspended structure	Single deck	$1.1\sqrt{3/2\phi}$	Applicable to a suspended structure with solidity factor between 0.2 and 0.45 composed of two-stiffening trusses with bluff elements.	Half of C_D in transverse direction	
		Double deck	$1.2\sqrt{3/2\phi}$			
	Tower		1.8	Per one shaft of tower of rectangular cross section	1.8	Tower of rectangular cross section
	Cable	Single	0.7		-	Not considered
		Double	1.0	Center to center of cable less than 4 times of diameter		
	Hanger		0.7		-	Not considered
Others	Truss bridge		Apply correspondingly to suspended structure of suspension bridge		-	Not considered
	Solid girder		2.1-0.1 x (B/D)	$8 \geq B/D \geq 1$	-	Not considered
			1.3	$B/D > 8$	-	Not considered
Single member			See Table 2.3.1 (Supplement)		-	Not considered

Table 2.3.1 (Supplement)

Shape of cross section	Drag coefficient	Shape of cross section	Drag coefficient
circular cylinder	1.2	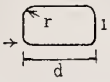 rectangular [( ): r>d/12]	1.5(1.1)
flat plate	2.2	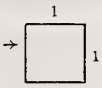 square cylinder [( ): r>d/12]	2.1(1.5)
flat plate	1.8	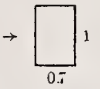 rectangular cylinder	2.7
square cylinder	1.5	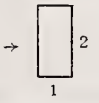 rectangular cylinder [( ): r>d/29]	2.3(2.1)

Table 2.3.2 Projected area

Bridge type	Structural element	Transverse	Longitudinal
Suspension bridge	Suspended structure	Windward side of stiffening frame, floor deck, curb and handrail	
	Tower	Windward and leeward side of tower shafts	Two tower shafts and web members
	Cable	Windward and leeward side of cable	Not considered
	Hanger	Windward and leeward side of hanger	
Bridges except suspension bridge	Truss bridge	Windward side of truss, floor deck, curb and handrail	Not considered
	Solid girder	Windward side of girder, curb and handrail	
Others		Effective cross section	

Table 2.3.3 Modification factor ν_4, ν_5

Factor \ Direction	Transverse	Longitudinal
ν_4	1.3	1.0
ν_5	1.0	1.0 free-standing tower: 1.2

Moreover, the designed sections based on the herein specified value of drag coefficients, shall be examined by wind tunnel model test as occasion demands and these drag coefficients obtained from such wind tunnel tests can then be adopted. Wind tunnel model tests shall always be carried out for the suspended structure of a suspension bridge, and when the drag coefficient to the transverse wind of zero degree angle of attack measured by wind tunnel tests differs more than 5% of herein specified value, then the structural section shall be redesigned by taking into account the measured values.

When calculating wind load together with live load, V_D shall be limited to 30 m/s.

2. Bridges with Maximum Span Length Less Than 200 m

In the case of a storm: $P_D = \left(\frac{V_D}{55}\right)^2 \cdot P_D'$

In the case of live loading: $P_D = P_D'$

where P_D' is the wind load specified in "the Specifications for Highway Bridges".

3. Wind Load Acting Upon Live Loads

When wind effects on live loads are to be considered, the following wind load perpendicular to the bridge axis shall be applied.

road deck 150 kg/m

railway deck: 450 kg/m

D. Way of Loading

The wind load is in principle to be considered as a horizontal uniform load acting in the transverse longitudinal direction of bridge axis. But, if necessary, the full and half wind loads shall be applied to the most unfavorable part and the remaining part of the structure, respectively.

The wind load shall be determined as follows:

1. Suspension bridge, cable-stayed girder bridge and the bridge with maximum span length greater than 200 m

(a) Transverse wind load

Suspended structure of a suspension bridge, deck girder of a cable-stayed bridge and truss bridge:

Full wind load shall be applied on the windward side of structure. In case of a suspension bridge, wind load acting upon hangers shall be equally divided to the stiffening girder and cables.

Cables of a suspension bridge and cable-stayed girder bridge:

In the case of a suspension bridge the wind load shall be applied to the axial line of the cable. In the case of a cable-stayed girder bridge, the wind load on the cables shall be equally divided to the girder and tower.

Tower:

The wind load shall be applied to the axis line of the windward and leeward pillar of the tower, respectively.

(b) Longitudinal Wind load

Suspended structure of a suspension bridge:

The longitudinal wind load is to be considered as a uniform load. In this case, the wind load on cables and hangers shall be ignored.

Tower:

The wind load on a tower shall be calculated using the projected area, including tower shafts and web members, and shall be considered as uniform load.

Cables, hangers, and girders of cable-stayed girder bridges;

Ignored.

2. Solid bridge with main span lengths greater than 200 m

(a) Transverse wind load

Full wind load shall be applied to the windward side of the girder.

(b) Longitudinal wind load

Ignored.

3. Bridges with main span lengths less than 200 m

The wind load shall be applied in accordance with the Specifications for Highway Bridges, except the design wind load is corrected as specified in article 2.3. However, the wind load for a railway bridge shall be applied in accordance with the Standard Specifications for Steel Railway Bridges.

E. Combination of Design Loads and Allowable Stress

Combinations of the wind load with other design loads will permit an increase in the allowable stress for each combination as given in Table 2.5.1.

Where: W : Wind load
D : Dead load
W(L) : Wind load applied together with live load
L(W) : Live load applied together with wind load W(L)
T : The effect of temperature change
B : Braking load, Starting load
LF : Rolling stock lateral load
LR : Longitudinal load of long rail

Each load shall be determined by "The design criteria of superstructures of the Proposed Honshu-Shikoku Bridges", but the maximum temperature combined with wind load can be considered as 35°C.

F. Proofing of Lateral Buckling

In the case of a suspension bridge, the lateral buckling of the suspended, structure due to wind force shall be proofed. The critical load for the lateral buckling must exceed 1.7 times of the design wind loads. The aerostatic coefficients used in the estimation of the critical load are to be obtained from wind tunnel model testing.

Table 2.5.1 Combination of loads and coefficients of increase of allowable stress

Combination of loads	Coefficients of increase of allowable stress	
	Main structure of bridge with span length more than 200 m and stiffening girder and tower of suspension bridge	Other structures
D+W+T	1.50	1.35
W	1.50	1.35
D+W(L)+L(W)+T	1.25	
B+W(L)	1.25	
LF+W(L)	1.25	
D+W(L)+L(W)+LR	1.40	
D+W(L)+L(W)+LF	1.40	
D+W(L)+L(W)+B	1.40	
D+W(L)+L(W)+B+LR	1.50	

III. Proofing of Dynamic Behavior

A. Outline

For the design of flexible structures, like suspension bridges or cable-stayed girder bridges, the investigation of the aeroelastic characteristics of the structure and the confirmation of the safety against wind action shall be performed. For this purpose, the dynamic proofing of the structural system, obtained through the static analysis, shall be conducted. The wind tunnel testing for the dynamic proof is to be based upon "the Standards of wind tunnel tests for the proposed Honshu-Shikoku Bridges (1973)".

B. Structural Damping

Relative to the vibration mode, the damping capacity of a structure can be assumed as following:

(i) for the whole system of a suspension bridge and a cable-stayed truss stiffened bridge: $\delta = 0.03$

(ii) for the whole system of a cable-stayed solid girder bridge: $\delta = 0.02$

(iii) for the free standing tower: $\delta = 0.01$

C. Vertical Inclination of Wind

The relation between the wind speed and the vertical inclination of the wind shall be assumed to lie in the domain shown as in Fig. 3.3.1. When the wind characteristics at the site where the structure is to be constructed shows a singularity, this condition shall be considered.

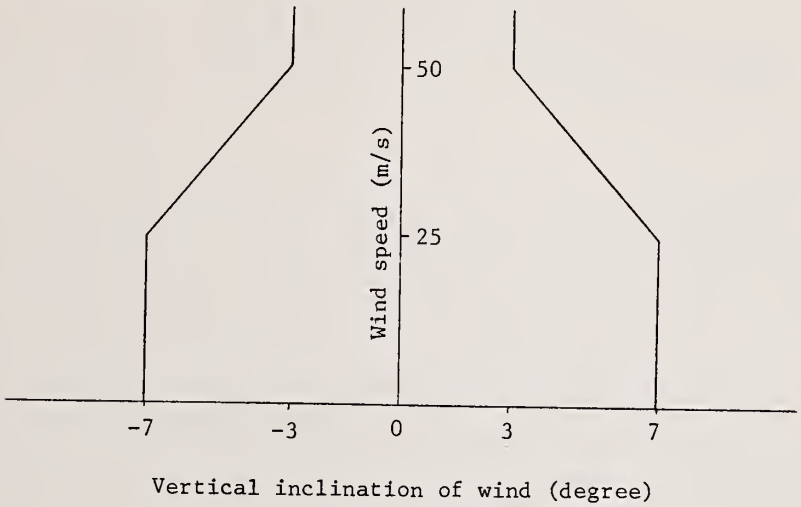

Fig. 3.3.1 Wind speed versus vertical inclination of wind

D. Critical Wind Speed for Self-excited Oscillation

The critical wind speed for a self-excited oscillation, derived from a dynamic analysis or wind tunnel test, should lie beyond the domain enclosed by the line of the wind speed of 1.2 times of design wind speed, and the lines shown in Fig. 3.3.1.

The critical wind speed shall be defined as the lowest wind speed at which the self-excited oscillation, with amplitude of one to five degrees, takes place.

E. Restricted Oscillation

When the occurrence of the restricted oscillations of the structure or elements are anticipated at the wind speed less than the design wind speed, a sufficient countermeasure relative to fatigue of the elements of disfunctioning of the structure, shall be adopted.

IV. Others

A. Examination to be taken during Construction

Enough care shall be exercised to prevent serious wind effects on the structure, not only at the time of its completion, but at each stage during construction.

Special care of free-standing towers, cables or stiffening girders during construction should be noted.

The static and dynamic safety of a structure against wind effects during each step of construction shall be confirmed through appropriate techniques such as the wind tunnel tests, and suitable countermeasures shall be taken if necessary.

Wind load during construction as a standard is to be half of design wind load.

Reference

Wind resistant design specifications (1975) for the proposed Honshu-Shikoku Bridges and its commentary: JSCE, March 1975.

EQUIVALENT STATIC WIND LOADS FOR TALL BUILDING DESIGN

EMIL SIMIU
Structural Research Engineer
Center for Building Technology
National Bureau of Standards
Washington, D.C., U.S.A.

ABSTRACT

Certain shortcomings of current procedures for computing along wind structural response have been shown to result in unrealistic estimates of tall building behavior under the action of strong winds. Differences between predictions of fluctuating response based on various such procedures have been shown to be in certain cases as high as 200%. In recent years, advances in the state of the art have been made which provide a basis for significantly improved alongwind response predictions. The purpose of the present work is to present a procedure for calculating alongwind response, including deflections and accelerations, which incorporates these advances. The meteorological and aerodynamic models on which the procedure is based are briefly described. The practical use of the procedure is illustrated in a numerical example. Estimates are provided of errors inherent in the models employed. The range of applicability of the procedure is defined, and it is indicated that for structures with unusual modal shapes or for which the influence of higher vibration modes is significant, a recently developed computer program should be employed in lieu of the procedure presented herein.

Key Words: Design; Equivalent loads; Tall Buildings; Wind loads.

1. Introduction

Several procedures for computing alongwind response have been proposed in the last decade [1, 2, 3]. The purpose of these procedures is to calculate equivalent wind loads whose effect upon the structure is the same as that of the gusty wind.

As part of an effort aimed at evaluating and improving building code provisions on design for wind loads, an analysis of current procedures for computing alongwind structural response - including the procedures described in the American National Standard A58.1 [4] and in the National Building Code of Canada [5, 6] - has been presented in ref. 7. From this analysis, the following points have emerged. First, the alongwind cross-correlation of the fluctuating pressures is represented in current procedures by models which are fundamentally inadequate [8]. It is primarily for this reason that the differences between the values of the fluctuating part of the response calculated in accordance with the A58.1 Standard, on the one hand, and the National Building Code of Canada, on the other hand, may in certain cases be as high as a few hundred percent [7]. Second, current

procedures do not take into account the dependence of the longitudinal wind velocity spectra upon height above ground. This was shown to result in significant overestimates of the components of the fluctuating velocity which produce resonant excitation in wind-sensitive structures [7, 9]. Third, current procedures do not enable the analyst to estimate the contribution of the higher vibration modes to the structural response. Fourth, existing procedures do not provide an estimate of the alongwind accelerations induced in structures by the gusty wind.

In the years following the development of the procedures described in refs. 1, 2, 3, 4 and 6, developments of significance in the context of determining structural response to wind have taken place notably in the area of boundary layer meterology. Progress has also been made in understanding and evaluating the effect of the alongwind pressure cross-correlations upon building response. Finally, effective numerical methods have been developed, from which economical computer programs, suitable for the analysis of structures subjected to wind loads, could evolve. In ref. 10, a procedure was presented for calculating alongwind response which incorporates and utilizes these advances and is thus free of the shortcomings mentioned above of the procedures currently in use. If the modal shapes of the structures analyzed are unusual or if the contribution of the higher modes to the response is significant, the procedure requires the use of a computer program. A machine-independent, Fortran version of this program is listed in Ref. 10. However, in a large number of cases of practical interest, it may be assumed that the fundamental modal shape is linear and that the response is dominated by the fundamental mode. In such cases, the procedure may be simplified, i.e., graphs can be developed which may be used for rapid-manual calculations of the alongwind deflections and accelerations.

The purpose of this paper is to present this simplified version of the procedure and to illustrate its practical use. The meteorological and aerodynamic models on which the procedure is based are briefly described. Results of numerical calculations are used to discuss some of the approximations and errors inherent in the models employed, as well as the range of applicability of the procedure presented herein.

2. Meteorological and Aerodynamic Models

a) Mean Wind Profile. In most structural engineering applications, mean wind profiles in horizontal terrain of uniform roughness over a sufficiently large fetch are currently modeled by the so-called power law, first proposed by Hellman in 1916 (11). However, as noted by Pasquill (12), the logarithmic law,

$$U(z) = 2.5\, u_* \ln \frac{z - z_d}{z_o} \qquad (1)$$

where U(z) = mean speed at height z above ground, a_d = zero plane displacement, z_o = roughness length and u_* = friction velocity, is a superior representation of mean wind profiles in the lower part of the atmospheric boundary layer. Balckadar and Tennekes (13), Tennekes (14), Carl, Tarbell and Panotsky (15), Helliwell (16) and others have shown that for high wind speeds, such as are assumed in design, the logarithmic law may be applied throughout

the height range of interest to the structural engineer.

The use of the logarithmic law in structural design is believed to be justified for the following three reasons. First, as was just mentioned, eq. (1) represents an improvement over the power law. Second, since the logarithmic law is universally employed in meteorological work, results of meteorological research may readily be used in engineering applications. Errors inherent in attempts to reformulate such results in terms of the power law are thus avoided, as is unnecessary and costly duplication of research. Third, in the logarithmic representation, the mean speed - just as the spectrum of the longitudinal velocity fluctuations (see eq. (5)) - is explicit function of u_*. Thus, if the logarithmic law is used, an internally consistent representation of the flow structure is achieved. This is not the case if the mean profiles are modeled by the power law, in which the exponent is not clearly and uniquely related to u_*. For these reasons, the logarithmic law will be employed in this work. To account for flow disturbances by the building near the ground, following common practice (6), it will be assumed that, for $0 < z < z_d + 10$ meters, $U(z) \equiv U(z_d + 10)$.

Suggested values of the roughness length z_o are given in table 1 (see refs. 16, 17, 18). For example, at Sale, Australia, for terrain described as open grassland with few trees, at Cardington, England, for open, farmland broken by a few trees and hedge rows, and at Heathrow Airport in London, $z_o = 0.08$m (16,17,19). At Cranfield, England, where the ground upwind of the anemometer is open for a distance of half a mile across the corner of an airfield, and were neighboring land is broken by small hedged fields, $z_o = 0.095$m (17,20).

3. Equivalent Static Wind Loads for Tall Building Design

The zero plane displacement may in all cases be assumed to be zero, except that in centers of large cities the smaller of the values $z_d = 20$m and $z_d = 0.73h$, where h = average height of buildings in the surrounding area, may be used (16).

In designing tall buildings it is reasonable to use mean wind speeds averaged over a period of one hour (4,6). If the mean winds U^t are averaged over periods t different from one hour, the mean winds U^h averaged over one hour may be obtained using Table 2 (21). For values of t not included in Table 2, linear interpolation is permissible. If the wind speeds are given in terms of fastest miles, the averaging period t in seconds is given by

$$t = 3600/v_f \qquad (2)$$

where v_f is the fastest mile in miles per hour.

a) Relation between Wind Speeds in Different Roughness Regimes. Consider two adjacent terrains, each of sufficiently large fetch, the roughness lengths of which are denoted z_{o1}, z_o, and over which the mean wind speeds may be described by eqs. (3) and (1), respectively:

$$U_1(z) = 2.5\, u_{*1} \ln \frac{z - z_{d1}}{z_{o1}} \qquad (3)$$

The relation between the friction velocities u_{*1}, u_* may be obtained, as a function of z_{o1}, z_o, from Fig. 1. The latter was developed in Ref. 17 on the basis of theoretical and experimental work reported by Csanady (22) and others (23).

b) Longitudinal Velocity Fluctuations. The cross-spectrum of the longitudinal fluctuating velocities at two points P_1, P_2 may be expressed in the form:

$$S_u(P_1, P_2, n) = S_u^{1/2}(P_1, n)\, S_u^{1/2}(P_2, n)\, R_u(y_1, y_2, z_1, z_2, n)\, N_u(P_1, P_2, n) \qquad (4)$$

in which y_i, z_i are the coordinates of point P_i (i=1,2) in a plane perpendicular to the direction of the mean wind and $S_u(P,n)$ is the spectral density of the longitudinal velocity fluctuations. Expressions of the spectrum $S_r(P,n)$ which take into account its dependence upon height above ground and are consistent with theoretical and experimental results of recent micrometeorological research have been presented in Ref. 9. In this work, the expression

$$\frac{nS_u(n)}{u_*^2} = \frac{200f}{(1 + 50f)^{5/3}} \qquad (5)$$

developed in Ref. 9, was used. In eq. (5), $f = n(z-z)/U(z)$. The mean square value of the fluctuations described by eq. (5) is $u^2(z) = 6u_*^2$.

The functions R_u and N_u in eq. (4) are defined as the acrosswind and the alongwind cross-correlation coefficient, respectively. By definition, if the points P_1, P_2 are in the same plane perpendicular to the mean wind direction, $N_u(P_1,P_2,n) = 1$. Otherwise, $N_u(P_1,P_2,n) < 1$; its magnitude decreases as the alongwind separation between P_1,P_2, and as the frequency n, increase. The acrosswind cross-correlation coefficient is a complex quantity, the modulus of which is known as the square root of the across-wind coherence function (24). However, its imaginary part has been determined by measurements to be negligible for wind engineering purposes (k,2,3,25). The following expression for the acrosswind cross-correlation coefficient, proposed by Davenport (3), has been used herein:

$$R_u(y_1, z_1, y_2, z_2, n) = \exp \frac{-2n\left[C_z^2(z_1 - z_2)^2 + C_y^2(y_1 - y_2)^2\right]^{1/2}}{U(z_1) + U(z_2)} \qquad (6)$$

in which $C_z = 10$, $C_y = 16$ (3).

c) Relation Between Wind Pressures and Wind Speeds. The fluctuating pressures, p_w', p_2', on the windward and leeward sides of a building are assumed to be linearly related to the velocity fluctuations u, i.e.,

$$p_w'(P) = \rho C_w U(z) u(z) \qquad (7)$$

$$p_\ell'(P) = \rho C_\ell U(z) u(z) \qquad (8)$$

in which

$$C_w = \frac{\bar{p}_w(z)}{1/2\rho U^2(z)} \qquad (9)$$

$$C_\ell = \frac{\bar{p}_\ell(z)}{1/2\rho U^2(z)} \qquad (10)$$

$\bar{p}_w$, $\bar{p}_\ell$ are the average values of the mean pressure at elevation z on the windward and the leeward faces of the building, respectively. The model represented by eqs. (7)-(10) is discussed in some detail in Ref. 10. In this work, it was assumed $C_w = 0.8$, $C_\ell = 0.5$.

It is implicit in eq. (8) that the pressure fluctuations on the leeward side are proportional to the velocity fluctuations in the upstream flow. As noted in Ref. 8, in reality the flow in the wake of the building is quite dissimilar from that in the oncoming flow. Measurements suggest that the fluctuating pressures on the leeward side are small compared to those on the windward slide and, therefore, that eq. (8) may be slightly conservative (8,26,27).

d) Cross-Spectra of Fluctuating Pressures. If eq. (7) or (8) is used,

$$S_p(P_1,P_2,n) = C_p(P_1)C_p(P_2)\rho^2 U(z_1)U(z_2) \; S_u(P_1,P_2,n) \qquad (11)$$

in which the cross-spectral density of the velocity fluctuations can be written as

$$S_u(P_1,P_2,n) = S_u^{1/2}(P_1,n)S_u^{1/2}(P_2,n)R_u(P_1,P_2,n) \; N_u(P_1,P_2,n) \qquad (12)$$

and in which $C_p(P_i) = C_w$ or C_2 according to whether $P_i(P_1,2)$ is on the windward or leeward side. Useful information regarding the magnitude of $N_u(P_1,P_2,n)$ is provided by results of measurements of cross-spectra of pressures on the windward and leeward sides of structures. Such measurements, carried out on full-scale buildings, have been reported by Lam Put (29) and by Van Koten (27) who found that except for very low frequencies, $N_u(P_{1w},P_{2\ell},n) < 0.2$ (the subscripts w, ℓ indicate that points P_1, P_2 are on the windward and leeward sides, respectively; the points P_{1w},$P_{1\ell}$ and P_{2w},$P_{2\ell}$ have coordinates y_1, z_1 and y_2, z_2, respectively). From the results of wind-tunnel measurements reported by Kao (Fig. 5.1, 5.19, 5.21 of Ref. 29) it also follows that, except for extremely low frequencies corresponding to eddies of negligible energy, $N(P_{1w},P_{2\ell},n)$ is nearly zero. It was shown in Ref. 10 that it is reasonably conservative to assume $N \equiv 1$ for $0 < n < 0.9n_1$ and $N \equiv 1$ for $0.9n_1 < n < \infty$. This assumption will be used in the present work.

4. Alongwind Deflections and Accelerations

Let B, H denote the building width and height (in meters); m, its mass per unit height (kg/m); n_1, its fundamental frequency of vibration (cycles/s); n, the damping ratio; g_a, $g_{\ddot{a}}$, the ratios of maximum probable value to r.m.s value of the fluctuating deflections and accelerations: $\overline{a'^2(z)}^{1/2}$ and $\overline{a^2(z)}$, ½r.m.s. of the alongwind deflections and accelerations (in meters); G.F., the gust response factor; a(z) and $\ddot{a}(z)$, the maximum probable alongwind deflection and acceleration, respectively (in meters). Using the assumptions stated in

this paper, and the air density being $\rho \simeq 1.25$ kg/m^3, the expressions developed in Ref. 9 can, as shown in Ref. 10, be written in the form;

$$\bar{a}(z) = 0.387 \frac{u_*^3}{n_1^2} J\left(\frac{z_o}{H}, \frac{z_d}{H}, H\right) B \frac{z}{H} \qquad (13)$$

$$\frac{\overline{a'^2}^{1/2}}{\bar{a}(z)} = 1.23 \frac{(B+R)^{1/2}}{J} \qquad (14)$$

$$g_a(z) = [2\ln 3{,}600\,\nu_a]^{1/2} + \frac{0.577}{[2\ln 3{,}600\,\nu_a]^{1/2}} \qquad (15)$$

$$\nu_a(z) = \left(\frac{R}{B+R}\right)^{1/2} n_1 \qquad (16)$$

$$G.F. = 1 + g_a \frac{\overline{a'^2(z)}^{1/2}}{\bar{a}(z)} \qquad (17)$$

$$a_{max}(z) = (G.F.)\,\bar{a}(z) \qquad (18)$$

$$\overline{\ddot{a}^2(z)}^{1/2} = 50\, n_1^2 \frac{R^{1/2}}{J} \bar{a}(z) \qquad (19)$$

$$g_{\ddot{a}}(z) = [2\ln 3{,}600 n_1]^{1/2} + \frac{0.577}{[2\ln 3{,}600 n_1]^{1/2}} \qquad (20)$$

$$\ddot{a}_{max}(z) = g_{\ddot{a}}\, \overline{\ddot{a}^2(z)}^{1/2} \qquad (21)$$

The equivalent static wind load is the product of the gust factor, G.F., by the mean wind load.

$$J\left(\frac{z_o}{H}, \frac{z_d}{H}, H\right) = \tilde{J}\left(\frac{z_o}{H}, \frac{z_d}{H}\right) + \frac{1}{H^2}(100 + 30z_d + 3z_d^2) \qquad (22)$$

$$\mathcal{B} = \left(1 - \frac{z_d}{H}\right)\tilde{\mathcal{B}} \qquad (23)$$

where all dimensions are in meters. $\tilde{J}$ can be obtained form Fig. 2 and k_1, k_2, k_3 are given in Table 3. $\tilde{\mathcal{B}}$ can be obtained from Fig. 3. For $z_d \neq 0$, eq. (23) is approximate; the approximation has been verified by numerical calculations to be of the order of 1: (10).

In eqs. (14), (15), and (17), the quantity R, associated with the resonant part f the response, may be written as

$$\mathcal{R} = \frac{C_w^2 + 2C_w C_l N_1 + C_l^2}{(C_w + C_l)^2} \frac{\pi \tilde{f}_1}{4\eta} \tilde{Y}_{11}\left(\frac{B}{H}, \frac{z_o}{H}, \frac{D}{H}, \tilde{f}_1\right) \qquad (24)$$

or, if $C_w = 0.8$, $C_L = 0.5$, $N = 0.4$,

$$\mathcal{R} = .562\, \tilde{\gamma}_1 \tilde{Y}_{11}/\eta \qquad (25)$$

in which $\tilde{f}_1 = \frac{n_1 H}{u_*}$. The values of $\tilde{Y}_{11}$ can be found in Figs. 4 thourgh 7 (linear interpolation within and between Figs. 4 through 7 is permissible). The Y_{11} curves are identified by capital Roman letters to where there correspond ratios z_o/H, z_d/H, listed in Table 4. Suggested values for the mechanical damping ratios n of steel frames and reinforced concrete frames are 0.01 and 0.02, respectively (4,6). Lower values of n may have to be used, for example in the case of welded steel stacks, of certain prestressed structures (6) or of structures of the framed tube type (33). In addition to the mechanical damping, the aerodynamic damping may, in principle be also taken into account. Aerodynamic damping is associated with changes in the relative velocity of the air with respect to the building as the latter oscillates about its mean deformed position (see Ref. 25). It appears that it may be unconservative to rely upon the effect of the aerodynamic damping; for this reason, the latter is not taken into account in Refs. 4, 6, and will also be neglected in this work.

5. Numerical Example

Consider a building for which the height H = 400m, the width B = 66m, the depth (i.e., the dimension in the alongwind direction) D = 45m, the damping ratio n = 0.01, the fundamental frequency n_1 = 0.09 cycles/s, the weight per unit volume w = 1,500 N/m^3. The basic wind speed (i.e., the fastest mile wind at 10m above ground in open terrain for which $z_{o!}$ = 0.07m) is v_f = 75mph (1 mph = 0.4474 m.s). The building is located in the center of a large city for which it may be assumed z_o = 0.65m, z_d = 20m.

The mass of building per unit height is m = w xBxD/g = 445,000 kg/m, where g = 9.81 m/s^2.

The friction velocity, u_* for the builtup terrain, is obtained as follows: Averaging time for fastest mile: t = 3600/75 = 48s (eq. (2)); ration U^t/U^n: 1.26 (Table 2); mean hourly speed at 10 m elevation in open terrain: $U_1(10) = v_f/1.26$ = 26.8 m/s; friction velocity in open terrain: $u_{*1} = U_1(10)/(2.5 \text{ in } (10/z_{o1}))$ = 2.16 m/s (eq. (3)); u_*/u_{*1} = 1.17 (Fig. 1); u_* = 1.17 x 2.16 = 2.54 m/s.

The quantities, J, $\mathcal{B}$, $\mathcal{R}$, are obtained as follows:

B/H = 0.165; $z_o/H = 1.6 \times 10^{-3}$; z_d/H = 0.05; $\tilde{f}_1 = n_1 H/u_* = 14.2$; k_1 = 111.5, k_2 = 35.25, k_3 = 3.76 (table 3); J = 17.1 (fig. 2); $\mathcal{B}$ = 8.9 (fig. 3); $\tilde{Y}_{11} = .8 \times 10^{-2}$ (table 4 and fig. 5); J = 17.1 [eq. (22)]; $\mathcal{B}$ = 8.45 [eq. (23)]; $\mathcal{R}$ = 6.4 [eq. (25)].

The quantities sought are

$$\bar{a}(z) = 0.76\ z/H \text{ (meters)} \quad \text{[eq. (13)]}$$

$$\frac{\overline{a'^2(z)}^{1/2}}{\bar{a}(z)} = 0.278 \quad \text{[eq. (14)]}$$

$$g_a = 3.46 \quad \text{[eq. (15) and (16)]}$$

$$\text{G.F.} = 1.96 \quad \text{[eq. (17)]}$$

$$a_{max}(z) = 1.49\ z/H \text{ (meters)} \quad \text{[eq. (18)]}$$

$$\overline{a'^2(z)}^{1/2} = 0.045\ z/H\ (m/s^2) \quad \text{[eq. (19)]}$$

$$g_{\bar{a}} = 3.57 \quad \text{[eq. (20)]}$$

$$\bar{a}_{max}(z) = 0.16\ m/s^2 = 0.016\ g \quad \text{[eq. (21)]}$$

a) Comparison Between Gust Response Factors Calculated Using Various Current Procedures. For the building just considered, the values of the gust response factors calculated in accordance with the procedures described in the ANSI A58.1 Standard (4), the Canadian Structural Design Manual (6) and Ref. 3 are 1.33, 2.83 and 3.38, respectively, versus 1.98 as calculated herein. As noted in Ref. 7, the gust factors calculated using Refs. 3 and 6 are overestimated, first, because the pressures on the windward and leeward sides are conservatively assumed to act in phase (i.e., to be perfectly correlated) and second, because the variation with height of the spectrum of the longitudinal velocity fluctuations is ignored. Gust factors are underestimated by the procedure of Ref. 4 because the alongwind pressure correlation coefficient, rather than being applied as a reduction factor to just the cross-spectrum of pressures acting on opposite sides of the building, is applied to the entire alongwing response, in violation of basic random vibration theory (see Ref. 3).

6. Approximations and Errors in the Estimation of the Alongwind Response

In this section, results of numerical calculations are presented on the basis of which estimates can be made of the errors associated with uncertainties regarding certain features of the models employed. The calculations were carried out for two typical buildings selected as case studies (Table 5). The wind speed at 10m elevation in open terrain ($z_o = 0.07$m) was assumed to be $v_f = 75$ mph (1 mph = 0.447 m/s), where v_f = fastest mile of wind.

a) Contribution of Higher Vibration Modes to the Response. Let n_1, n_2, n_3 denote the natural frequencies in the first three modes. For both buildings in both open and center of large city exposures, the percent contribution of the higher vibration modes to the r.m.s. of the flutuating alongwind deflections was of the order of 5-15%, if it was assumed that $n_2/n_1 = 1.2$, $n_3/n_1 = 1.5$, and about 1% if $n_2/n_1 = 2.5$, $n_3/n_1 = 5$. The contribution to the r.m.s. of the alongwind accelerations was of the order of 10-20% if $n_2/n_1 = 1.2$, $n_x/n_1 = 1.5$ and about 3-10% if $n_2/n_1 = 2.6$, $n_3/n_1 = 5$. Typical modal shapes have been used in the calculations, as indicated in Ref. 10.

b) Influence upon Calculated Response of the Deviation from a Straight Line of Fundamental Modal Shape. A convenient means for estimating the influence upon response of the shape of the fundamental mode of vibration is provided by the expression,

$$\frac{\overline{a^{12}}^{1/2}}{\bar{a}} = \frac{1 + \gamma + 2\alpha}{1 + \gamma + \alpha} Q \qquad (26)$$

derived by Vickery (3) on the bases of the assumptions that the power law holds, that the spectra of the turbulent velocity fluctuations are independent of height and that the fundamental modal shape is described as follows:

$$u_1(z) = \left(\frac{z}{H}\right)^{\gamma} \qquad (27)$$

where γ is a constant. In eq. (26), α = exponent of the power law and Q = function of geometrical, mechanical and environmental parameters, independent of γ. It may be assumed, roughly, that α can vary between 0.10 for open exposure and 0.40 for centers of large cities. It follows from eq. (26) that, for $\alpha = 0.10$, the ratios $\overline{a^{12}}^{1/2}/\bar{a}$ calculated assuming $\gamma = 0.5$ and $\gamma = 1.5$ differ by less than 1% from that calculated assuming $\gamma = 1.0$ (i.e., a linear fundamental modal shape). For $\alpha = 0.4$, the corresponding differences are about 3%. It is thus seen that deviations from a straight line of the fundamental modal shape have an insignificant effect upon the calculated ratio $\overline{a^{12}}^{1/2}/\bar{a}$.

c) Influence Upon Calculated Response of Errors in the Estimation of the Roughness Length. To estimate the magnitude of the error associated with uncertainties regarding the actual value of the roughness length, the response of buildings 1 and 2 was calculated for coastal (z_o = 0.005-0.01m), open (0.03-0.08m), suburban (z_o = 0.20-0.20m), center of town (z_o = 0.40m) and center of large city (z_o = 0.60-0.80m) exposures. The zero plane displacement was in all cases assumed to be zero. The results of the calculations are shown in Table 6.

It is seen from Table 6 that the sensitivity of the results to even large errors in the estimation of the roughness lengths is tolerably small. It is also noted that the alongwind deflections and, consequently, the design wind loads are higher by about 15% in the case of the coastal, than in the case of the open exposure.

d) Spectra in the Lower Frequency Range and Alongwind Response. It was shown in Ref. 9 that no universal relation exists that described the shape of the spectral curve in the lower frequency range and that the peak similarity coordinate appears to vary, strongly between sites and between atmosphere and laboratory. To estimate the effect of this variation, the response of buildings 1 and 2 was calculated in the cases z_o = 0.07m, z_d = 0 and a_o = 0.80 m, z_d = 20m assuming values of the peak similarity coordinate f_1 = 0.033 (eq. (5)) and f_1 = 0.01, f_1 = 0.10, f_1 = 0.19 (eqs. (11) through (13) of Ref. 9). The ratios $(a_{msx})_{f_1}/(a_{max})_{0.033}$ of the maximum probable response calculated using the values of the peak similarity coordinate f_1 and 0.33, respectively, are given in Table 7.

The results of Table 7 indicate that eq. (5) (to which there corresponds $f_1 = 0.33$) is slightly conservative. It is noted that, in view of Eq. (19), the influence of the spectral curve shape in the lower frequency range upon the value of the acceleration is negligible.

e) Acrosswind Correlation of the Pressures and Alongwind Response. In current procedures for calculating alongwind response (1,2,3,4,6) it is assumed that the values of the acrosswind cross-correlation function are nearly the same for the pressures and for the fluctuating velocities in the undisturbed flow. According to Refs. 25, 29, this assumption has been verified in the wind tunnel. However, full-scale measurements (30) suggest that if the acrosswind cross-correlation of the pressures is represented by an exponential function as in eq. (12), the values of the decay coefficients C_z, C_y are smaller than in the case of the fluctuating velocities, i.e., the acrosswind correlation of the pressures is higher than that of the velocity fluctuations which generate them. It also appears that, rather than being constants, the decay coefficients may be functions of the frequency n. For low frequencies, values as low as $C_z = 4$ have been reported (30).

It is therefore of interest to estimate the errors in the calculated alongwind response that correspond to possible errors in the values C_z, C_y. The alongwind response of buildings in open ($z_o = 0.07$m, $z_d = 0$) and large city ($z_o = 0.80$m, $z_d = 0$) exposures was therefore calculated separately for $C_z = 10$, $C_y = 16$ (case 1), for $C_z = 4$, $C_y = 6.4$ (case 6) and for four intermediate cases in which C_z, C_y were assumed either constant throughout the frequency range (case 4) or to have lower values at low frequencies and higher values near and beyond the fundamental frequency n_1, (cases 2,3,5). Graphs similar to Figs. 3 - 7, corresponding to $C_z = 6.3$, $C_v = 10$ and $C_z = 4$, $C_y = 6.4$ have been presented in Ref. 10.

The ratios $r_i = (a_{max})/(a_{max})_1$, $\ddot{r}_i = (\ddot{a}_{max})_i/(\ddot{a}_{max})_1$ in which cases 1 and i are denoted by the indices 1 and i, respectively (i = 2,3,4,5,6), are given in Table 8 for large city exposure. The values of these ratios in open exposure are of the same order of magnitude or slightly lower.

It is seen that even a considerable change in the values of C_z, C_y in the lower frequency range affects little the calculated response (cases 1,2,3). However, large decreases in these values near the fundamental frequency of the structure do increase the total response, by as much as almost 10-20% in the case of the deflection and 30-80% in the case of the acceleration.

As mentioned previously, the data available so far suggest that the acrosswind cross-correlation of the low frequency components of the pressures may be higher than was reported in Refs. 25, 29 and assumed in Refs. 1,2,3, in the ANSI A58.1 Standard and in the National Building Code of Canada. However, no persuasive evidence appears to exist to the effect that the correlation is also higher for frequency components in the range of natural frequencies of structures. Even if this were the case, it must be recalled that these components are actually attenuated to some extent (31,32); the possibly increased correlation would then, at least partly, be compensated by this attenuation.

The sensitivity of the calculated accelerations to changes in the values of exponential decay coefficients suggests that measurements of accelerations, which are relatively simple and inexpensive, might offer useful information on the actual magnitude of these coefficients.

7. Conclusions

In this paper a practical procedure for calculating alongwind deflections and accelerations has been presented, which accounts for the variation of wind spectra with height and makes allowance for the imperfect correlation in the alongwind direction of pressures acting on the windward and leeward building sides. For a specific case, a numerical example is given, and the gust response factor obtained is compared to those calculated using procedures described in current codes and standards.

The procedure presented herein may be applied to typical tall structures for which the ratios of higher to fundamental frequencies are not unusually low (e.g., for which $n_2/n_1 > 2$) and for which the fundamental modal shape may be expressed as $\mu_1(z) = (z/H)^\gamma$, where $0.5 < \gamma < 1.5$. Results of numerical calculations have been presented which show that the effect upon the response of the possible variation of the frequency, n, for which the reduced spectrum $nS(n)/\mu^2$, reaches a maximum, is small. Information is also provided on the errors in the estimation of the response associated with uncertainties regarding the actual terrain roughness and the values of the exponential decay parameters. It is noted that for structures with unusual modal shapes or for which the influence of the higher vibration modes is significant, the computer program presented in Ref. 10 should be employed in lieu of the procedure presented herein.

Acknowledgements

The writer wished to express his appreciation to E.O. Pfrang, of the Center for Building Technology, National Bureau of Standards, for his encouragement and support, and to R.D. Marshall, of the Center for Building Technology, for useful comments and suggestions offered during the preparation of this work. The capable assistance of R.L. Hocker, of the Center for Building Technology, is also gratefully acknowledged.

References

1. Davenport, A.G., Gust Loading Factors, Journal of the Structural Division, ASCE, Vol. 93, No. ST3, Proc. Paper 5255, June 1967, pp. 11-34.

2. Vellozzi, J. and Cohen, E., Gust Response Factors, Journal of the Structural Division, ASCE, Vol. 97, No. ST6, Proc. Paper 5980, June 1968, pp. 1295-1313.

3. Vickery, B.J., On the Reliability of Gust Loading Factors, Civil Engineering Transactions, April 1971, pp. 1-4.

4. American National Standards Institute, American National Standard Building Code Requirements for Minimum Design Loads In Buildings and Other Structures, New York, New York, 1972.

5. National Research Council, National Building Code of Canada, Ottawa, 1970.

6. National Research Council, Canadian Structural Design Manual, Supplement No. 4 to the National Building Code of Canada, 1970.

7. Simiu, E. and Marshall, R.D., Wind Loading and Modern Building Codes, Meeting Preprint 2268, ASCE National Structural Engineering Meeting, Cincinnati, Ohio, April 22-26, 1974.

8. Simiu, E., Gust Factors and Alongwind Pressure Correlations, Journal of the Structural Division, ASCE, Vol. 100, No. ST9, Proc. Paper 9686, April 1973, pp. 773-783.

9. Simiu E., Wind Spectra and Dynamic Alongwind.Response, Journal of the Structural Division, ASCE Vol. 100, No ST9, Proc. Paper 10815, Sept. 1974, pp. 1897-1910.

10. Simiu, E. and Lozier, D.W., The Buffeting of Tall Structures by Strong Winds, Building Science Series, Center for Building Technology, National Bureau of Standards, Washington, D.C., 1975 (to be published).

11. Hellman, G., Ueber die Bewegung der Luft in den untersten Schichten der Atmosphaere, Meteorol. Zeit., Vol 34, pp. 273, 1916.

12. Pasquill, F., Wind Structure in the Atmospheric Boundary Layer, Philosophical Transactions of the Royal Society of London, A. 269, 1971, pp. 439-456.

13. Balckadar, A.K. and Tennekes, H., Asymptotic Similarity in Neutral Baratropic Boundary Layers, Journal of the Atmospheric Sciences, Vol. 25, No., 1968, pp. 1015-1020.

14. Tennekes, H., The Logarithmic Wind Profile, Journal of the Atmospheric Sciences, Vol. 30, 1973, pp. 234-238.

15. Carl, D.M., Tarbell, T.C., and Panofsky, H.A., Profiles of Wind and Temperature from Towers over Homogeneous Terrain, Journal of the Atmospheric Sciences, Vol. 30, July 1973, pp. 788-794.

16. Hellwell, N.C., Wind Over London, Proceedings, Third International Conference of Wind Effects on Building and Structures, Tokyo, Japan, 1971.

17. Simiu, E., Logarithmic Profiles and Design Wind Speeds, Journal of the Engineering Mechanics Division, ASCE, Vol. 99, No. EMS, Proc. Paper 10100, October, 1973, pp. 1073-1983.

18. Fichtl, G., and McVehill, G., Longitudinal and Lateral Spectra of Turbulence in the Atmospheric Boundary Layer, NASA TN D-5584, Washington, D.C., 1970.

19. Deacon, E.L., Gust Variation with Height up to 150m, Quarterly Journal of the Royal Meteorological Society, Vol. 91, 1955, pp. 562-573.

20. Harris, R.I., Measurements of Wind Structure at Heights up to 598 ft above Ground Level, Proceedings, Symposium on Wind Effects on Buildings and Structures, Loughborough University of Technology, Leicestershire, England, 1968.

21. Durst, C.S., Wind Speeds over Short Periods of Time, Meteorological Magazine, Vol. 89, 1960.

22. Csanady, G.T., On the Resistance Law of a Turbulent Ekamn Layer, Journal of the Atmospheric Sciences, Vol. 24, Sept. 1967, pp. 467-471.

23. Tennekes, H. and Lumley, J.L., A First Course in Turbulence, The MIT Press, Cambridge, Mass., 1972.

24. Panofsky, H.A. and Singer, I.A., Vertical Structure of Turbulence, Quarterly Journal of the Royal Meteorological Society, Vol. 91, July, 1966, pp. 339-344.

25. Vickery, B.J. and Kao K.H., Drag of Alongwind Response of Slender Structures, Journal of the Structural Division, ASCE, Vol. 98, No. ST1, Proc Paper 8638, January 1972, pp. 21-36.

26. Dalgliesh, W.A., Statistical Treatment of Peak Gusts on Cladding, Journal of the Structural Division, ASCE, Vol. 97, No. ST9, Proc. Paper 8356, Sept. 1971, pp. 2173-2187.

27. Van Koten, H., The Fluctuating Wind Pressures on the Cladding and Inside a Building, Proceedings, Symposium on Full Scale Measurements of Wind Effects on Tall Buildings, The University of Western Ontario, June 23-29, 1974.

28. Lam Put, R., Dynamic Response of a Tall Building to Random Wind Loads, Proceedings, International Conference on Wind Effects on Buildings and Structures, Tokyo, Japan, 1971, pp. III-4.1-II.

29. Kao, K.H., Measurements of Pressure/Velocity Correlation on a Rectangular Prism in Turbulent Flow, Engineering Science Research Report BLWT-2-20, University of Western Ontario, London, Canada, 1971

30. Newberry, C.W., Eaton, K.J., and Mayne, J.R., Wind Loading on Tall Buildings - Further Results form the Royex House, Industrial Aerodynamics Abstracts 4, July-August, 1973, pp. 1-16.

31. Bearman, P.W., Some Measurements of the Distortion of Turbulence Approaching a Two-Dimensional Body, Journal of Fluid Mechanics, Vol. 53, part 3, pp. 431-467, 1972.

32. Marshall, R.D., Surface Pressure Fluctuations Near an Axisymmetric Stagnation Point, NBS Technical Note 563, National Bureau of Standards, August 1971.

33. Taoka, G.T., Hogan, M., Kahn, F.R. and Scanlan, R.H., Ambient Response Analysis of Some Tall Structures, Journal of the Structural Division, ASCE, Vol. 101, No. ST1, Proc. Paper 11051, January, 1975, pp. 49-65.

Table 1 - Suggested values of z_o for various types of exposure

Type of exposure	z_o (meters)
Coastal	0.005-0.01
Open	0.03 -0.10
Outskirts of towns, suburbs	0.20 -0.30
Centers of towns	0.40
Centers of large cities	0.60 -0.80

Table 2. Approximate ratios of probable maximum speed averaged over period t to that averaged over one hour (open terrain)

t (seconds)	2	5	10	30	60
U^t/U^h	1.53	1.47	1.42	1.28	1.24

t (seconds)	100	200	300	1000	3600
U^t/U^h	1.18	1.13	1.07	1.03	1.00

Table 3. - Value of k_1, k_2, k_3

z_o (meters)	0.01	0.07	0.20	0.40	0.60	1.00	1.20
k_1	320	225	171	135	114	90	86
k_2	-	-	-	-	36	26	22
k_3	-	-	-	-	3.95	2.65	2.25

In eqs. (14) and (16)

Table 4 - Values z_o/H, z_d/H corresponding to various γ_{11} curves

CURVE	z_o/H	z_d/H	CURVE	z_o/H	z_d/H
A	1.3×10^{-5}	0.	J'	3.4×10^{-3}	0.04
B	3.4×10^{-5}	0.	K	5.4×10^{-3}	0.
C	8.3×10^{-5}	0.	K'	5.4×10^{-3}	0.15
D	1.1×10^{-4}	0.	L	8.0×10^{-3}	0.
E	1.9×10^{-4}	0.	L'	8.0×10^{-3}	0.10
F	4.7×10^{-4}	0.	M	1.3×10^{-2}	0.
G	1.0×10^{-3}	0.	M'	1.3×10^{-2}	0.20
H	1.6×10^{-3}	0.	N	1.8×10^{-2}	0.
I	2.2×10^{-3}	0.	N'	1.8×10^{-2}	0.45
I'	2.2×10^{-3}	0.06	O	2.7×10^{-2}	0.
J	3.4×10^{-3}	0.	O'	2.7×10^{-2}	0.30

Note: If z_d/H is of the order of 0.1 or less and $z_o/H < 10^{-2}$, in determining γ_{11} it may be assumed $z_d = 0$.

Table 5 - Description of buildings selected as case studies

Building	H	B	D	n_1	η_1	w
	m			Hertz		ton/meter^2
1	365	60	45	0.10	0.01	1,200
2	150	60	45	0.20	0.01	1,500

Table 6 - Deflections and accelerations for various roughness lengths

		Exposure			
		Coastal		Open	
	z_o [a]	0.005	0.01	0.03	0.05
Building 1	$a_{max}(H)$ [c]	1.74	1.69	1.59	1.48
	$\ddot{a}_{max}(H)$ [b]	0.020	0.020	0.019	0.019
Building 2	$a_{max}(H)$ [c]	.37	.36	.33	.32
	$\ddot{a}_{max}(H)$ [b]	0.017	0.017	0.016	0.016

		Exposure		
		Suburban		
	z_o [a]	0.20	0.30	0.40
Building 1	$a_{max}(H)$ [c]	1.37	1.30	1.27
	$\ddot{a}_{max}(h)$ [b]	0.018	0.017	0.016
Building 2	$a_{max}(H)$ [c]	.27	.26	.25
	$\ddot{a}_{max}(H)$ [b]	0.014	0.013	0.012

		Exposure		
		Center of large city		
	z_o [a]	0.60	0.80	1.00
Building 1	$a_{max}(H)$ [c]	1.22	1.16	1.14
	$\ddot{a}_{max}(H)$ [b]	0.016	0.015	0.015
Building 2	$a_{max}(H)$ [c]	.23	.22	.21
	$\ddot{a}_{max}(H)$ [b]	0.011	0.011	0.010

NOTE: [a] meters; [b] units of g (g = acceleration of gravity)

Table 7 - Ratios $[a_{max}]_{f_1}/[a_{max}]_{0.035}$

	Building 1		Building 2	
Exposure	Open	Large City	Open	Large City
$f_1 = 0.01$	1.00	1.00	1.00	1.00
$f_1 = 0.10$	.93	.97	.97	.94
$f_1 = 0.19$	.97	.96	.96	.93

Table 8 - Ratios of response for various values C_x, C_y to response calculated using $C_x = 10, C_y = 16$

Case	C_x	C_y	Interval	Large City			
				Building 1		Building 2	
				r_i	$\tilde{r}_i$	r_i	$\tilde{r}_i$
1	10	16	$0<n<\infty$	1.	1.	1.	1.
2	6.3 10	10 16	$0<n<.9n_1$ $.9n_1<n<\infty$	1.01	1.	1.01	1.
3	4 10	6.4 16	$0<n<.9n_1$ $.9n_1<n<\infty$	1.02	1.	1.02	1.
4	6.3	10	$0<n<\infty$	1.06	1.3	1.05	1.4
5	4 6.3	6.4 10	$0<n<.9n_1$ $.9n_1<n<\infty$	1.07	1.3	1.08	1.4
6	4	6.4	$0<n<\infty$	1.11	1.3	1.13	1.3

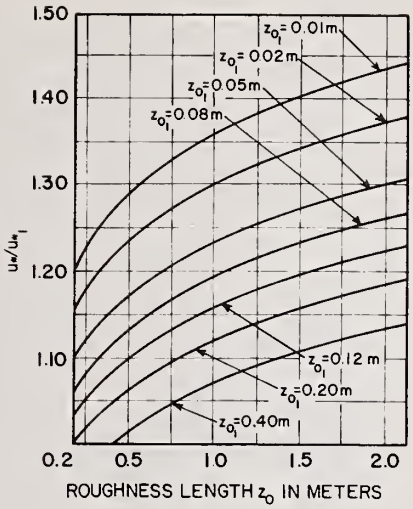

FIG. 1.—Ratios u_*/u_{*_1}

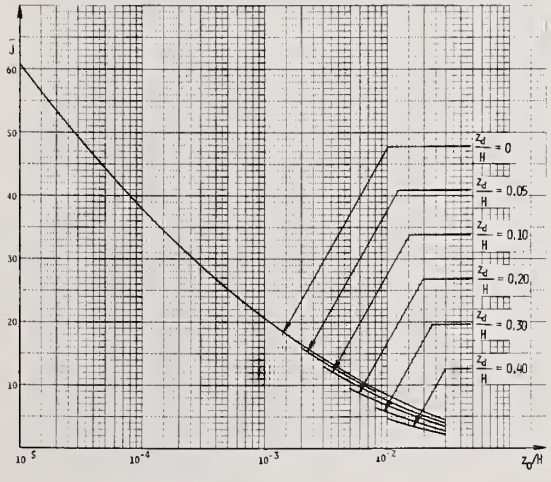

FIG. 2.—Function $\tilde{J}$

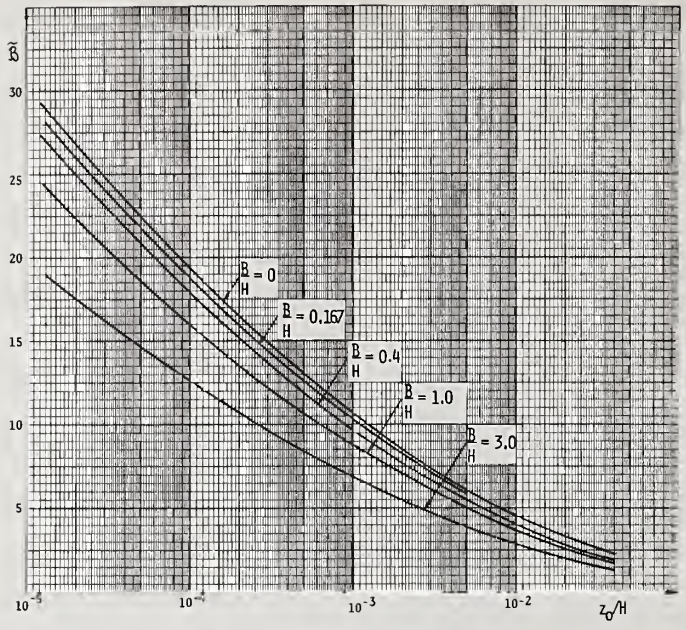

FIG. 3.—Function $\tilde{\mathcal{B}}$

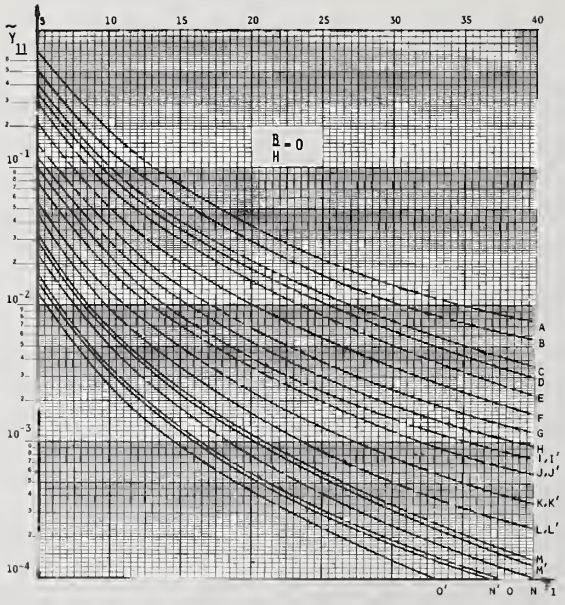

FIG. 4.—Function $\tilde{Y}_{11}$, $B/H = 0$

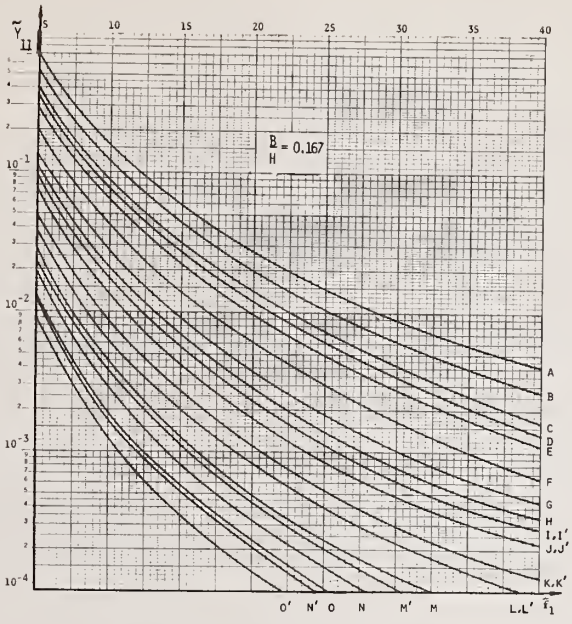

FIG. 5.—Function $\tilde{Y}_{11}$, $B/H = 0.167$

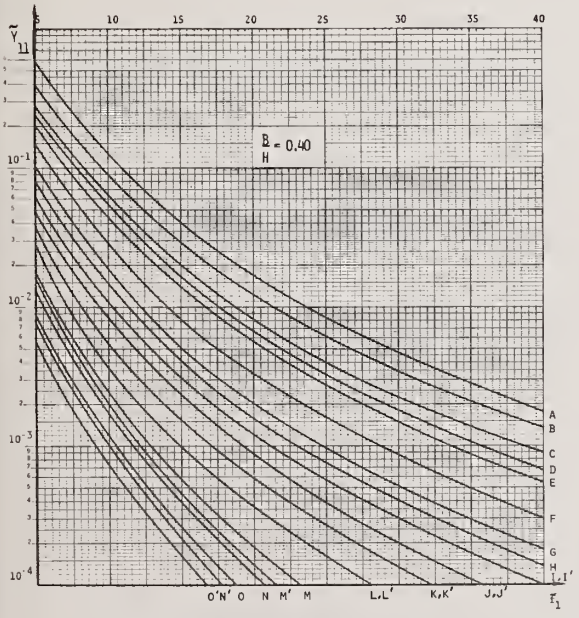

FIG. 6.—Function $\tilde{Y}_{11}$, $B/H = 0.4$

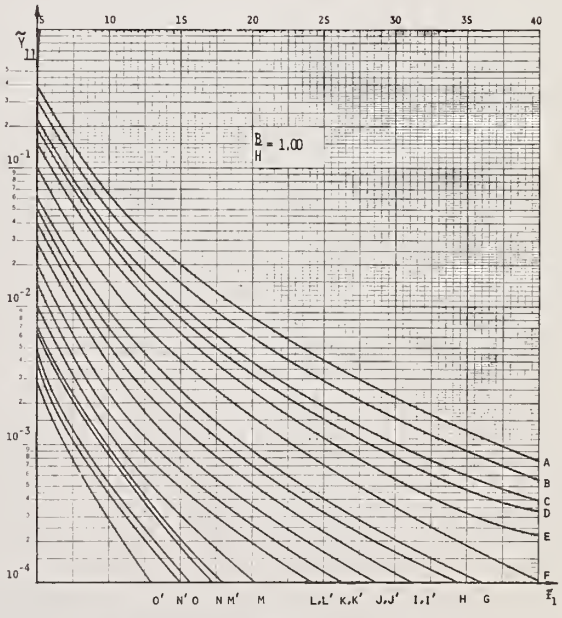

FIG. 7.—Function $\tilde{Y}_{11}$, $B/H = 1.0$

A Wood House Will Resist Wind Forces

by

Billy Bohannan

Forest Products Laboratory, Madison, Wisconsin

Experience tells us that wood-frame houses built by conventional construction practices will be long-lived structures. Why then should we be doing research on light-frame wood construction.

The answer seems simple. There are reasons to believe that the conventional wood frame systems are overbuilt in many respects. Initial evaluations have indicated that significant material savings are possible without sacrificing any of the structural integrity of wood-frame systems.

The actual structural performance of the conventional wood-frame house is not well understood. Little or no structural engineering goes into its design. While a lot of research effort has gone into defining pieces and parts of houses, much of this research has been aimed at very narrow objectives. Little attention was given to the house as a complete structural system. The interaction of components has not been evaluated.

It is assumed that the resistance to wind-caused racking or shear would be provided solely by the end-walls of a conventional wood-frame house. There are no known formulae for calculating the racking resistance of these walls. In fact, there is even some question as to how much of the total wind force actually reaches the end-walls.

KEYWORDS: Structural performance; Mode of failure; Racking resistance; Design criteria; Concentrated loads; Uniform loads.

On-going Research

One primary objective of on-going research in this area at the Forest Products Laboratory is to develop engineering criteria for the structural responses of a conventional house to simulated wind forces. Because of the many facets of the unknown character of a house, a study was broken down as follows:

1. Measure the racking resistance of walls under concentrated loads during progressive stages of construction, as the house advances from a simple wall panel to a complete 3-dimensional structure.

2. Correlate the relationship between uniform loads (wind load) and concentrated forces as they affect racking distortion.

3. Determine the ultimate state limits or weak links in the house that may lead to structural failure.

To consider these points, one full-scale house was tested under simulated wind loads. A series of six tests were conducted under horizontal forces to assess the racking properties of the house. The first five utilized concentrated loads, during progressive stages of construction, to measure stiffness of walls; the final test employed uniform loads to determine both stiffness and strength of the complete house.

The conventionally constructed wood frame house was 24 feet wide and 16 feet long. The size was limited by the dimensions of the structural test facility. The 24-foot width is fairly typical, but the 16-foot length is no more than one-half the house in length. This is, however, a reasonable distance from an end wall to a partition. The two end walls (parallel to the load) contained windows and doors.

A detailed discussion of test procedures and results is given in "Testing of a Full Scale House Under Simulated Snow and Wind Loads," USDA Forest Service Research Paper FPL-234, Forest Products Laboratory, Madison, Wisconsin.

Results

The average racking stiffness of the walls during the five progressive stages of construction are given in Table I.

Table I. Average Racking Stiffness of Two Walls During Progressive Stages of Construction.

Stage of Construction	Description	Load at 0.1-in. deflection	Relative stiffness
		Lb	Pct
No. 1	3/8-inch plywood sheathing	1,480	100.0
2	Cut-in window and door openings	910	61.5
3	Add drywall and siding	1,770	119.6
4	Add sidewalls	2,220	150.0
5	Add trussed roof system	2,760	186.5

The sequence and modes of failure in the house subjected to simulated uniform loads are given in Table II.

Table II. Sequence and Modes of Failure in House Subjected to Horizontal Uniform Loads.

Sequence of failures	Pressure p	Equivalent wind velocity 1/
	Lb/ft^2	Mi/h
1. Sole plate broke loose on loaded wall	63	157
2. Center stud on loaded wall broke in bending (estimated)	70	165
3. House slid off sill plate (foundation)	123	220

1/ From $V = 19.8 \sqrt{p}$

The first structural failure occurred along the sole plate of the loaded wall under a uniform pressure of 63 pounds per square foot. At this point it was necessary to repair the sole plate and reinforce the loaded wall to resume testing. Finally, at a pressure of 123 pounds per square foot, the connections between the floor system and the foundation failed. At this load, which equates to a wind force of approximately 220 mph, there were no visible structural failures to the end walls which were resisting racking forces. With proper anchorages to the foundation, the house would certainly have sustained a considerably larger load.

Firm conclusions cannot be derived from a single test, but observations are possible. The racking resistance of end walls were more than adequate. The wall-to-floor connection was the first weak link, but this could be easily rectified with minor design modifications. The final weak link in the resistance to wind forces was in the connection between the house and foundation. About one-fourth of the simulated wind load was transmitted to the foundation and three-eighths of the load was resisted by each end wall.

To complement the empirical evaluations of the structural performance, theoretical engineering design criteria are being developed to predict the racking strength and stiffness of walls. The theory is based on an energy approach whereby the racking force and displacement are equated to the energy absorbed by the fasteners. It considers the geometry of the sheathing panel, the number of fasteners, and the lateral resistance of fasteners in covering materials. The theoretical analyses should be published this calendar year.

Wind Loads

On

Low-Rise Buildings

Noel J. Raufaste, Jr.
National Bureau of Standards, Gaithersburg, Maryland

ABSTRACT

The National Bureau of Standards is continuing its project to develop improved design criteria for low-rise buildings in developing countries to better withstand the effects of extreme winds. This paper is an overview of the results of the project, some of which have occurred since the Seventh meeting of the U.S.-Japan Panel on Wind and Seismic Effects, that is to say, the third year of this 3 1/2 year project. To date, most data analyses have been completed and presented in several NBS published progress reports. The final report is expected to be published in the Fall of 1976.

KEYWORDS: Codes and Standards; Disaster Mitigation; Housing; Low-Rise Buildings; Socio-Economics; Structural Connections; Wind Loads.

INTRODUCTION

This paper supplements High Wind Study in the Philippines, which was presented at the 7th Joint Meeting of the U.S.-Japan Panel on Wind and Seismic Effects. It presents the results of continuing activities associated with this 3 1/2 year project to develop improved design criteria for low-rise buildings to better resist extreme winds.

The project originated in 1972 from a recognition by the Agency for International Development (AID) and the National Bureau of Standards (NBS) that additional research on wind was needed to reduce human suffering, property losses, disruptions to productive activities, and expenditures for disaster relief. This is the primary goal. The objectives are to: 1) learn more about the effects of high winds on low-rise buildings; 2) develop improved siting, design, and construction information, which would improve the resistance of buildings to extreme winds and which would be culturally acceptable to the user; 3) provide training

to local professionals and technicians in performing wind measurement and analysis of full-scale and wind-tunnel testing; and 4) provide a large-scale transfer of technology to make use of these improvements in design and construction, as well as new climatological, sociological and economic findings.

The activities and accomplishments associated with the project have produced the following benefits: 1) improved design criteria; 2) focused an awareness of the need for improved ways to design against effects of extreme winds and on the methods required to improve building designs; 3) essential documentation of new and under-used existing information; 4) excellent working relationships with public and private decision makers in several developing countries and continued excellent working relationships with building professionals in developed countries; 5) training professionals and technicians in developing countries for carrying out wind measurement and analysis procedures; and 6) methods to transfer information to users in developing countries.

The results of these efforts are significant. These activities provided the first step toward the preparation of improved wind codes and standards for developing countries. The Philippine National Building Code is currently undergoing revision that will lead to improved building practices. The project's test data including improved gust factors and mean pressure coefficients are being incorporated into Section 2.05, "Wind Pressures" of the National Structural Code for Buildings. Also, the project's test results will be made available to the subcommittee on wind loads of the American National Standards Institute, Inc. (ANSI) for possible incorporation into the American National Standard A58.1--"Minimum Design Loads for Buildings and Other Structures."

The project is scheduled for completion in September with final report printing during the Fall of 1976.

BACKGROUND

Wind loading on tall buildings has been extensively studied during the past 10 years. However, very little parallel work was devoted to buildings less than 10 meters high. Post-

disaster investigations of wind damage suggest that coefficients contained in most current codes and standards do not adequately describe the wind characteristics near the ground and the pressure distributions on low-rise buildings. Highly localized wind pressures on buildings tend to be underestimated while overall pressures tend to be overestimated. This observation was confirmed from full-scale tests during this program.

Equally important to the understanding of wind pressures on buildings, is the selection of design wind speeds in geographic areas having a high frequency of tropical storms. By taking account of local frequencies and terrain effects, it is anticipated that design speeds can be selected that will accurately reflect the risk of wind damage to buildings. It will be possible for building designers to specify more realistic design loads (from the NBS-improved pressure coefficients)[1].

Field Test Sites

Three field test sites in the Philippines were selected for recording wind load data on buildings. The sites are: Quezon City, where three houses were instrumented with wind pressure equipment; Laoag City, about 500 kilometers north of Quezon City, is the site of two test houses; and Daet, about 230 kilometers south east of Quezon City, is the location of one test house. The paper High Wind Study in the Philippines contains additional information on field test sites, wind tunnel studies, and other background information.

Wind Tunnel Studies

In addition to wind tunnel studies performed at the University of the Philippines (UP) in

---

[1] Dr. Richard D. Marshall, the project's principal investigator is responsible for the development of the test data leading to improved design pressure coefficients. This paper is based in large part on the National Bureau of Standards Interagency Report 75-790, which was authored in part by Dr. Marshall and Mr. Raufaste.

Quezon City, NBS project staff initiated a series of wind tunnel tests at the Virginia Polytechnic Institute and State University (VPI and SU). These tests used a flow simulation technique similar to that which was perfected at the University of Philippines. Since VPI and SU's wind tunnel test section was larger than that at the UP (2.14 x 2.14 meters square and 5.5 meters long) the scale ratio was increased from 1:80 to 1:70. The tests, begun in April, 1975, have been completed. They cover 32 combinations of roof slope, height-to-width ratio, length-to-width ratio and size of roof overhang. The test results are still being analyzed. Preliminary analysis suggests that additional studies should be conducted on roof slopes near 10 degrees. The wind tunnel test and the full-scale test results obtained during previous studies in the state of Montana, United States, and studies conducted by the Building Research Establishment in England and including research by NBS in the Philippines provided the basic data used in developing tentative design pressure coefficients. These and other results are discussed in more detail in the National Bureau of Standards Interagency Report (NBSIR) 75-790, FY 75 Progress Report on Design Criteria and Methodology for Construction for Low-Rise Buildings to Better Resist Typhoons and Hurricanes.

Additional wind tunnel studies are being performed by the VPI and SU. Measurements are presently being conducted at 18 locations on a scale model of a quonset shape building. These will present the characteristics of the turbulent wind flow, mean wind speed turbulence intensity at the scaled 10 meter level, and integral scale of the turbulence and typical spectra of along-wind fluctuations. Results are expected during this summer. The building being tested is a model of a low-cost house designed by CARE, Inc., Bangladesh. It is built in 1-meter modules bolted at the top and along ridges at its sides. It is about 4 meters wide and 3 meters high.

Regional Conferences

Project results were discussed at two regional conferences; one in Manila, Philippines (May 1975) and the other in Kingston, Jamaica (November 1975). These conferences provided a channel to transfer results to the building community including government agencies, private developers, design professionals, regulatory officials, and university staff from Asian and Caribbean wind-prone countries. The conference provided an opportunity for the participating

countries to comment on the design criteria and to offer suggestions for their implementation. Members from developing countries were provided an opportunity to better understand wind and building design problems common to their countries and discuss methods for solutions.

Technology Transfer

The NBS/AID high wind project results should have an impact on several key sectors of the local developing country's population--the professional community, the government policy-making sectors, and the general public--building owners and tenants. The technology developed has and is continuing to be transferred to the participating country's building community. To stimulate the general public to improve their buildings to better resist extreme winds, consumer-oriented material has been developed containing concise and graphic descriptions of technological issues, research findings, and conclusions. The use of brochures and pamphlets containing consumer-oriented material is an excellent method to transfer such information. This material consists of recommendations on siting, design, and construction, checklists of recommended construction practices, summarized technical reports prepared by NBS staff and consultants, and a selective list of resources.

A 16 mm movie, another consumer-oriented package, completed in 1975 was modified in 1976 to include information on project results. The movie summarizes the high wind research project. Starting with the destructive effects of winds on buildings, it progresses to the NBS field-testing activities and the wind tunnel-testing program and the project outputs. The movie also uses computer graphics to illustrate the effect of wind on buildings. The movie and the consumer material are two of the various ways to continue information exchanges among the users of this project and between the U.S.and other country participants. Through March 1976 over 10,000 persons--both technical and lay audiences and school children--viewed the movie.

PROJECT RESULTS

The following presents a brief description of the results of the project. The reader should reference the NBS report NBSIR 75-790 for additional information about the following project

results. NBSIR 75-790 can be obtained from the National Technical Information Service, Springfield, VA 22161 as PB 250-848.

A comprehensive review of the probablistic techniques for the analysis of extreme wind speeds was developed by Dr. Emil Simiu of NBS and published as Estimation of Extreme Wind Speeds in the Philippines. Corrections of annual extreme speeds for the type of instrumentation used, averaging time, height above ground, and type of exposure are presented so that homogeneous sets of wind records can be established. Probabilistic models are described and applied to wind records for several Philippine stations using a computer program developed at the NBS. The results are compared with design speeds presented in the National Structural Code which is part of the National Building Code of the Philippines.

Analysis of wind speed data show that design speeds currently used can be reduced in some areas of the Philippines and should be increased in other areas, including coastal plains. Similar analysis may be performed for other countries as well. The computer program is available for use by other wind-prone countries.

Simplified procedures for the calculation of wind pressures acting on building surfaces were developed. These improved design criteria provide building professionals with more accurate design loads. This information is contained in the report, A Guide to the Determination of Wind Forces, by Dr. Richard D. Marshall of NBS. The report describes the basics of wind flow around buildings and the pressures created by these flows on building surfaces. Effects of such features as roof slope, roof overhang, and building openings are discussed. It refers to material covered in Dr. Simiu's report and assumes that the basic wind speed is known or can be calculated by the designer. A procedure for determining the design speed is presented. It takes into account the general terrain roughness, local topographical features, height of building, expected life of building, and risk of failure.

Once the design speed has been obtained, the mean dynamic pressure is calculated and pressures acting on walls, roofs, and internal portions of buildings are determined by use of appropriate pressure coefficients tabulated in the report. Finally, corrections are applied to the calculated pressure to account for terrain roughness and height of building. The steps required to calculate pressures and total drag and uplift forces are summarized

and an example is presented. It is intended that these data form the basis for wind load design standards in developing countries.

Another output of the project was a set of recommendations for good construction practices and details, especially for countries experiencing extreme winds. This material is found in A Guide for Improved Masonry and Timber Connectors in Buildings by Dr. S. George Fattal of NBS and Messrs. Gerald Sherwood and Thomas Wilkenson of the Forest Products Laboratory. A survey and evaluation of some current masonry practices as used in the tropics are presented. Local practices, investigation of building products, and standards compliance are discussed and evaluated with the aid of photographs of buildings during various stages of construction. Current masonry practices in the United States are presented. Also, various types of connectors used in U.S. construction are discussed. This serves as a reference for improving building practices. The chapter addressing timber fasteners is similar in format to that for masonry connectors. It presents a general introduction to timber fasteners and a review of Philippine timber-fastener construction practices. Recommendations follow. The report also addresses suggested improvements in masonry and timber construction. The suggestions are based on a review of many masonry and timber documents, related reports, building codes, specifications, working drawings and photographs of Philippine houses and on-site post-disaster surveys of typhoon-damaged buildings.

The study also produced a method to allow a country's planners, economists, public officials, and other decision-makers to assess housing needs up to 20 years into the future. The report, The Economics of Building Needs - A Methodological Guide, by Dr. Joseph Kowalski of NBS, presents this information. The data serves as a tool to assist the decision-maker in assessing the impact of the development of buildings to better resist winds on local housing needs. The report attempts to identify those parameters that define a low-cost house. This is determined by a simple mathematical procedure based on readily available data, i.e., family income, housing expenditure, and the established regional proverty level.

The study examined cultural and socio-economic factors that affect building practices. It also shows how strong, inexpensive locally available building material can be integrated with good building design. The report, Housing in Extreme Winds, by Stephen Kliment, architectural consultant, presents this information. The report is consumer-oriented in nature and is intended for residents, owners, planners, and builders of low-cost/low-rise housing in developing countries. The report addresses the Philippines, Jamaica and Bangladesh. A general review considers socio-economic conditions prevailing in developing countries. Suggested solutions include the placement of building to exploit existing land contours and vegetation, and the design of buildings so as to conform to research recommendations concerning preferred configurations of roofs, walls, overhangs and openings. In addition, construction techniques are briefly covered. Materials that are cheap, strong and locally available are recommended, and several innovative methods of construction are mentioned. Plastics have been produced using native and imported raw materials and could serve as an excellent low-cost house once their configurations become more familiar to the population. At first, they may be used for clinics, schools and warehouses. Rural and urban components of population trends for each of the three countries are reviewed. Finally, housing characteristics peculiar to each country are summarized through text and in thumbnail sketches, in both architectural terms and in terms of occupancy characteristics. The socio-economic functions of family ties and housing needs are reviewed. The community structure, the economics of housing, the housing characteristics, and the housing programs are summarized by country.

SUMMARY

This project produced test data and information for improving current low-rise building practices. They are:

- a methodology to estimate extreme wind speeds for wind-prone countries;
- improved design criteria to determine wind forces on low-rise buildings;
- recommended good building construction practices;
- methodology to forecast housing needs; and

- cultural, architectural, and socio-economic factors that affect building practices

Thus, the study shows it is possible for wind-prone developing countries to design their low-rise buildings to better resist wind and build them at an acceptable cost.

THE FUTURE

It is anticipated that the utilization phase of this project will begin in September 1976. The purposes are: 1) continue transferring technology to participating countries; 2) provide spare parts on an as-needed basis to maintain field and laboratory equipment; 3) explore channels for expanding this technology to other developing countries subjected to extreme winds and to other professionals involved in aspects of low-rise building technology; 4) continue field and laboratory data analysis based on new information; 5) investigate further the mechanisms of information transfer at the level of the general public; and 6) assist as necessary in the incorporation of test results into codes and standards--both domestically and internationally.

CHARACTERISTICS OF THE HIGH WIND AT HACHIJOJIMA ISLAND ON THE OCCASION OF TYPHOON NO. 7513

SEIJI SOMA
Chief, Meteorological Research Institute
Meteorolocical Agency
Japan

ABSTRACT

A typhoon that attacked Hachijojima Island on October 5, 1975 brought to this island very strong winds which were beyond expectations. The value of the peak gust observed at the weather station, located at the central part of the Island, was 67.8 m/s. Moreover, in the premises of the lighthouse situated on the southeastern part of the Island, an incredible wind of 82.4 m/s was recorded. This wind was extraordinarily strong and was the third strongest recorded wind in our country. Due to this high wind, a great deal of damage was caused in various parts of the Island. Houses and buildings suffered the most from the high wind. The damage rate to houses which varied in different areas, had a high of 7.3%, which were completely destroyed, and 21% in which half of the houses were completely destroyed. Wether this strong wind was innate in the typhoon, or whether it was brought about due to the peculiar topographic features of the Island was the subject of this study. However, it was not possible to clarify these points quantitatively. Although, in certain areas, it was realized that topographic influences were apparent.

While making this survey on the typhoon's effect, it was noted that severe damage occurred to the windowpanes in tall buildings. An administrator of the building told us that these panes were broken by fragments of houses that were scattered in the high wind. This, therefore, indicates that a problem exists when tall buildings are surrounded by houses which have low wind-resistance in their vicinity. Therefore, the damage indicates that in town planning, not only a wind resistant design of individual buildings is required but also wind resistant planning of the entire environment is essential.

Key Words: Damage; Effects; Houses; Typhoon; Wind speeds.

1. Introduction

On October 5, 1975, typhoon No. 7513 passed over the northern part of Hachijojima Island and brought to this Island a wind which had a maximum speed of 67.8 m/s. This wind was the strongest ever recorded, since the weather station was established. This high wind caused a great deal of damage to houses and other structures on the Island. This typhoon was a typical wind typhoon according to newsmen, which have often attacked the Mainland of Japan in the late autumn. The amount of precipitation that was produced by the typhoon was merely 26 mm, but the wind was extremely strong. The wind speed of 67.8 m/s was only the value recorded at the weather station, and a far stronger wind of 82.4 m/s

was recorded at another part of the Island. Even in Japan, which is called one of the typhoon countries, a wind record of over 80 m/s has been experienced only twice in the past. The first was 84.5 m/s recorded at the Murotomisaki Weather Station in Shikoku Island on September 16, 1961 and the other was 85.3 m/s observed at the Miyakojima Weather Station on the Nansei Islands on September 5, 1966. The wind record of 82.4 m/s due to Typhoon No. 7513 was observed not by a station under the Japan Meteorological Agency, but at the lighthouse under the control of the Maritime Safety Agency. However, it was recorded by the same type anemometer as is used by the stations under the Japan Meteorological Agency. Therefore it is quite trustworthy.

The question concerning this strong wind, was it a natural phenomenon, or did the formation cause such an extreme wind. This is an interesting problem, which at present, still remains unsolved. I wish to describe below the characteristics of the high wind at the time of the Typhoon No. 7513. This will be achieved by referring to data of strong winds which blew on the Island in the past, and also referring to those two typhoons that were accompanied by extremely high wind, as mentioned before.

2. Topographic Features of Hachijojima Island and Wind Records in the Past

Hachijojima is a small island covering 68.3 km^2 and is situated in the Pacific Ocean 250 km south of Tokyo, and administratively belongs to the Tokyo Metropolis. Its population is 10,320. Because of its warm climate and scenic beauty, the Island is visited by a great number of tourists from the mainland. In order to accommodate these people, many high-storied hotel buildings were constructed during the past several years.

On this Island, there are two comparatively high and steep mountains in proportion to the small area, i.e., Mt. Hachijo Fuji (854 m) and Mt. Miyake (700 m) situated in the northwestern and southeastern parts of the Island, respectively. The area lying between these two mountains consists of flat land. This land is positioned in the southwestern and northeastern directions, which lead to the sea coasts. The main city area of Hachijojima is on this flat part of the land. The weather station, that recorded the wind speed of 67.8 m/s is located in the southwestern part of this flat area, which is about 1,000 m from the west coast. Due to such peculiar topographic features of the Island, the wind direction on the level area is SW-NW, and NE-ESE.

Because Hachijojima lies in the middle of the Ocean, it is prone to typhoons, and so far strong winds have been recorded on a number of occasions. Table 1 lists those recorded winds which have exceeded 50 m/s.

3. Approach of the Typhoon and the Change in Weather Elements

Photo 1 taken by radar on Mt. Fuji, 250 km north of the Island, shows the way Hachijojima was enveloped in the eye of the typhoon. Also, according to the barographic record obtained at the Hachijojima Weather Station, the funnel-shaped pressure change which is characteristic of a typhoon was noted, suggesting that the center of the typhoon was very close (Fig. 1).

From this chart, it shows that the typhoon was closest to the Island at 16.30 on the 5th, and the lowest recorded pressure was 947 mb. Wind speeds observed prior to, at and after this time are shown on Table 2.

The column on the left hand side of Table 2 shows the wind speed recorded at the Hachijojima Weather Station and the column on the right shows those values which were recorded by the lighthouse in the Sueyoshi District in the Southern part of the Island. The peak gust value in the brackets were obtained by the average gust factors, between 13.00 and 16.00 hrs. on that day, multiplied by the average wind-speed. As can be seen from this table, peak gust (or the maximum instantaneous wind speed) reached its maximum at 16.30 hrs. at both observation points. The difference between these two values, shown as the peak gust at 16.30 at the lighthouse, is due to different people who read the self-registering paper.

If one looks at the recording paper carefully, a gust of over 60 m/s wind speed was recorded five times between 16.20 and 17.00 hrs. However, the wind record obtained near the lighthouse, utilized a pen which went beyond the scale. Therefore, judgement was required in estimating the speed. It appears that a peak gust of 75 m/s occurred several times during 20 minutes initiated at 16.20.

4. Outline of Damage

The largest damage caused by the typhoon was to houses. The detailed number of damaged houses will be mentioned in the next section. Other noticeable damage included collapse of electric poles, the Loran nautical mark towers, and overturning of motor vehicles. Trees that were completely up rooted throughout the Island. Damage unique to the area was caused by the salty wind, which killed the leaves of the trees all over Mt. Hachijo Fuji, up to a height of 854 m and changed the color of the mountain to red.

According to the distribution map of the damage prepared by the weather station (Fig. 2), the most afflicted area was the flat land lying in between the two mountains. Needless to say, this is due to the fact that the principal cities and towns are located in this part of the Island. Also the southern part and the southeastern part of the Island suffered from damage. The arrows shown on the map indicate the direction in which houses and structures collapsed (Photo 2).

a) Damage Rate of Buildings and Air Current Characteristics

In order to show how the buildings suffered from the gust, it is more appropriate to show the damage rate rather than by the number damaged. The damage caused by the high wind, in various areas, was investigated resulting in the data given in Table 3. Shown is the damage ratio, which is a value calculated by dividing the number of damaged houses by the number of households.

As mentioned in Section 3, the wind direction at the peak gust time was SSW. When the wind blows in this direction, the Mitsune District should have been right behind Mt. Mihara and accordingly less windy. On the contrary, however, according to Table 3, the damage rate is higher than one would expect (51.2%).

As it happened, approximately one year before this typhoon, we had made an observation of the wind distribution on Hachijojima Island, by spreading the observation network throughout the flat area of the Island and on top of Mt. Mihara. The number of observation points at that time was nine, including the weather station.

First of all, we tried to obtain from this data what wind direction and speeds were observed at the eight other check points, where the wind at the weather station showed an SSW direction. The analytical material used at this time was restricted to the wind speed over 10 m/s. The result of the survey is shown by the diagram on Fig. 3, in which the wind direction and speed are indicated by vectors. This diagram shows that when the wind direction is SSW at the weather station (B point), it becomes 100% SW at the Mitsune District (G point). In other words, the air current that comes in from the SSW direction proceeds to the right along Mt. Mihara, keeping the strong wind speed to its back, and goes around the mountain. The diagram also shows that the wind direction on top of Mt. Mihara (A point) stands high from the S, as against the SSW at the weather station. The topographical experiments carried out by use of a wind tunnel also proved a similar air current characteristic when the SSW wind was given. Photo 3 shows an example of the experiment by the wind tunnel.

b) Wind Speed Distribution at the Time of Typhoon

At only three locations during 16.30 hrs. on the 5th, the wind speed was actually recorded; at the weather station, the upper air observation point belonging to the same station (point F), and at the lighthouse. The extent of the damage by the high wind, however, covered a very wide area and it is necessary to find out, from the viewpoint of the investigation on wind damage, what wind speed had actually blown at those respective points. Therefore, relying on past observation data, a wind speed ratio at each point as against the value observed at the Hachijojima Weather Station (in case of SSW wind) was sought, and by using this percentage ratio, values of wind speed at various points at 16.30 were estimated. These are shown on Table 4. According to this table, it is estimated that on top of Mt. Mihara (point A) the wind was 1.89 times as strong as the weather station. Therefore, the wind speed at this point at 16.30 hrs. on the 5th, is estimated to be 60.0 m/s.

The next task was to work out the peak gust at various points by reading gust factors from the past observation records on the wind recording papers and by the estimated wind speed, as shown on Table 4. These results are given in Table 5. The wind speeds and the peak gusts estimated at 16.30 hrs. are shown in Fig. 4. According to this table or the figure, the peak gust on top of Mt. Mihara at 16.30 hrs. is estimated as 77.4 m/s. The Loran nautical mark tower could not have stood against such a terrific gust. Also by this table, at point G (Mitsune District) the peak gust is estimated to have been 54.4 m/s. Considering that this district is located leeward of the mountain when an SSW wind blows, this figure seems to be extremely large. This is due to the fact that because the mountains are situated in the northwest and southeast, the level area served as a corridor between these mountains and the SSW wind blew right through to the east coast.

5. Extremely High Wind in Sueyoshi District

As mentioned before, an extremely strong peak gust of 82.4 - 85.2 m/s was recorded in the premises of the lighthouse in Sueyoshi District on the southeastern part of Hachijojima. The high rate of house destruction up to 79.1% as shown in Table 3 was due to this extreme peak gust. This gust also destroyed the lantern panes of the lighthouse, which is an unprecedented occurrence.

According to the report given by the Hachijojima Lighthouse, six sections of the lantern panes out of twelve, which sheltered the luminant components and lenses of the lighthouse, were broken, i.e. three entirely and the other three cracked. Most of the broken panes had been placed at the windward side of the lighthouse (Fig. 5).

It may have been possible that fragments of the broken glass had caused the damage to other glass on the leeward side, but the details of the situation at the moment of this destruction have not been clarified. It may be added that the lantern panes employed for this lighthouse was 7 mm thick, 1,200 mm long and 800 mm wide, reinforced against wind and curved outward as a convex lense. There have been few cases when lantern panes of lighthouses were broken by strong winds. However, in most of these cases, pebbles or other fragments blown and scattered by the wind were considered to be the immediate cause of the breakage. It is difficult to reason this situation in the Hachijojima's case when the location of the lighthouse is taken into consideration. The lighthouse is located at the windward edge of the breakwater stretched out on a cape into the sea. Consequently, it may be correct to conclude that the extremely high wind, which was the third highest wind speed in observatory history, was the exclusive factor of the destruction.

6. Records of Strong Gusts of More Than 80 m/s

Considerable lead time is needed to decide whether the record of 82.4 - 85.2 m/s in the Sueyoshi District can be attributed only to the Typhoon, or to some topographical feature which contributed to its strength. In this section, analysis will be given for reference on the situations where peak gusts of more than 80 m/s occurred.

a) The Miyakojima Typhoon II

The strongest gust ever recorded on flat ground and at a regular weather station was a maximum of 85.3 m/s. This was recorded at the Miyakojima Weather Station located on the Nansei Islands at 6:30 on September 5, 1969 during the Miyakojima Typhoon II. The direction of the wind was NE and the mean wind speed was 60.8 m/s. The distance from Miyakojima to the Typhoon was 20 km at the closest time. This was very similar to the relative distance observed in the case of Hachijojima and Typhoon No. 7513, while the Miyakojima Typhoon showed the lowest atmospheric pressure of 930 mb, which was far below that seen in Typhoon No. 7513. Miyakojima is a flat island, 108 m above sea-level at its highest point, and 2.5 times larger than the area of Hachijojima. The Miyakojima Weather Station is located on this flat island and is not influenced by the configuration of the surrounding land. Consequently, the value recorded on Miyakojima can be considered to have been brought about by the typhoon itself and not by any other influences.

Mr. Mitsuta says that the Typhoon passed slightly outward with respect to Miyakojima and consequently the island was in the proximity of the typhoon's maximum wind speed zone which produced the extremely strong winds on Miyakojima. This assumption will give some insight in the analysis of the Sueyoshi District of Hachijojima.

b) The Muroto Typhoon II

At 11:30, September 16, 1961, a maximum wind speed of 84.5 m/s (wind direction: WSW, average speed: 66.7 m/s) was recorded at Murotomisaki Weather Station. At this time, the typhoon passed rather close to the station, i.e. 7 km to the west. The lowest atmospheric pressure observed at this time was 931 mb. The extreme wind speed can be naturally attributed to the energy of this large scale powerful typhoon itself, however, some consideration should be given to the geographical characteristics of the location. Murotomisaki is shaped like a half-cylinder with its top, where the station is, 184 m above the sea. It may be natural to consider that the air current was accelerated when the wind blew in a crosswise direction over the cape. Thus, the observed value of 84.5 m/s may well include the influence of the topographic factor described above. In the case of Sueyoshi District, the site where the anemometer was set was similar to that of Murotomisaki, while the height above sea-level was 95 m, about half the height of Murotomisaki Weather Station.

c) The Factors of the Extremely High Wind Observed in Sueyoshi District

It may be misleading to determine the factors of the extremely high wind observed in the Sueyoshi District based on these two cases, but it may be worthwhile to do so at any rate, as a start of this study. Some of the important factors may be:

1. Sueyoshi District was located in the proximity of the maximum wind speed zone of Typhoon No. 7513.
2. The wind blew in a crosswise direction over the cape of the island.
3. The district is located southeast of Mt. Mihara and a corner effect of airflow may have occurred.

7. The Characteristics of Wind Damage in Hachijojima

There has not been any strong typhoons which have hit big cities for a period of sixteen years, since the Isewan Typhoon. During this period many new forms of houses and structures have been rapidly constructed and the life-style has changed significantly. Wind resistant design should have been taken into account in cases of these new houses and structures. However, we do not have experience on new types of construction, and only when they are exposed in severe condition of nature, do they show their weakness.

a) Destruction of Glass in Large Buildings

A typical example of glass damage in large buildings was seen in the case of this typhoon. This occurred in the Hachijojima Kokusai Kanko Hotel, a six-story building. The curtainwall of the large lobby facing the sea on the first floor of this hotel is 90% constructed of fixed windowpanes. The size of each windowpane is 3,000 mm long, 2,000 mm wide and 10 mm thick. The typhoon seemed to have generated a wind speed of 68 m/s, and destroyed first 13 windowpanes in the windward side of the lobby. The destruction of these windowpanes caused a strong influx of the storm's wind into the lobby. Furniture

and in the shops of the lobby were blown away and they destroyed the windowpanes on the leeward side of the lobby. The hotel personnel testified that the destruction of glass on the windward side of the lobby was not due to wind pressure, but due to objects that were blown away from the destroyed houses in the windward direction. If this is true, the damage in Hachijojima seems to imply that not only is wind resistant design for glass required for buildings, but also a more general wind resistant design, including the overall environment in the city is required.

b) Collapse of Electric Poles

This typhoon caused collapse of many electric poles; this is very common damage caused by typhoons. The number of totally torn down poles was counted at 47. 26 poles out of 47 were concrete poles and 21 were wooden, which shows that the destruction rate of concrete poles was slightly higher than that of wood. The number of poles which were half torn down or left in a leaning position reached 420. The collapse of electric poles not only crushes things under the poles, but also interrupts traffic. Moreover, the most serious effect of the destruction of electric poles is power blackouts. Power blackouts causes serious effects, not only to households, but also to the industrial facilities and medical institutions when it is prolonged over a long period of time in the big cities.

c) Overturning of Motor Vehicles

The exact number of motor vehicles that were overturned is not known when this typhoon struck Hachijojima, but the several cases were reported. It is anticipated that when motor vehicles are overturned, and if it happens in the big cities and in their suburbs where traffic is heavy, it will cause serious traffic problems. This is a problem which should be examined in the future.

8. Conclusion

The characteristics of the high wind brought about by Typhoon No. 7513 to Hachijojima, taking into account the wind and the configuration of the land, have been described. And the possible damage by typhoons hitting the big cities were examined through an analysis of wind damage caused by this typhoon. Among other things, the destruction of large windowpanes in large buildings, the collapse of electric poles, and the overturning of motor vehicles were discussed.

Finally, the fact that this typhoon did not cause any death tolls in spite of serious damage to houses and structures should be mentioned. The Miyakojima Typhoon II which recorded a maximum wind speed of 85.3 m/s caused no death tolls either. This is very fortunate, but this cannot be expected in all typhoons. In 1934, the Muroto Typhoon I with a peak gust of 60.0 m/s in Osaka destroyed a primary school building and caused the death of 400 pupils of that school. The fact that the typhoon hit Hachijojima on Sunday and that the peak gust was recorded in the day time, was part of the reason for the few number of casualties. It is also of interest to know what kind of refuge measures were taken by people to minimize the damage of the high wind which caused the total destruction of 275 buildings.

References

Ishizaki, H. et al (1968): The Structural Damage Caused by the Miyakojima Typhoon II Disaster Prevention Research Institute Annuals, No. 11A.

Mitsuta, Y. et al (1968): Severe Wind Storm Caused by the Miyakojima Typhoon II, Disaster Prevention Research Institute Annuals No. 11A.

Meteorological Agency (1967): Report on the Muroto Typhoon II (No. 6118, Nancy), Technical Report of the Japan Meteorological Agency No. 54, Mar. 1967.

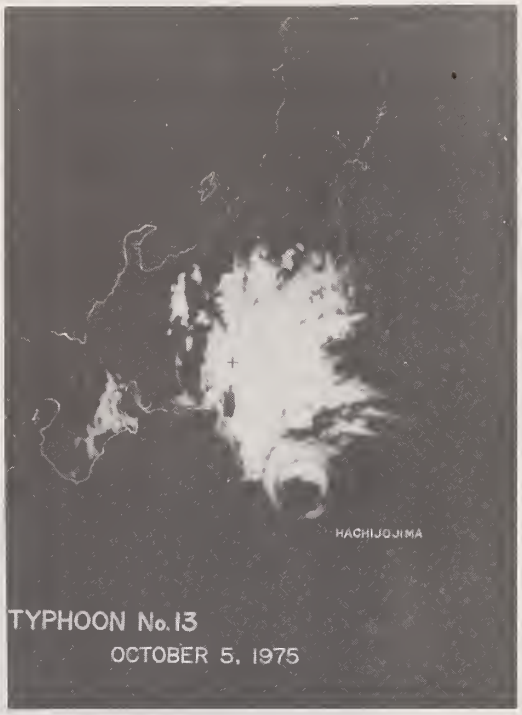

Photo. 1.

Typhoon No. 7513 taken by the Radar at top of Mt. Fuji; Hachijojima is located on the southern part of the typhoon eye wall.

Photo. 2
Examples of houses damage on Hachijojima.

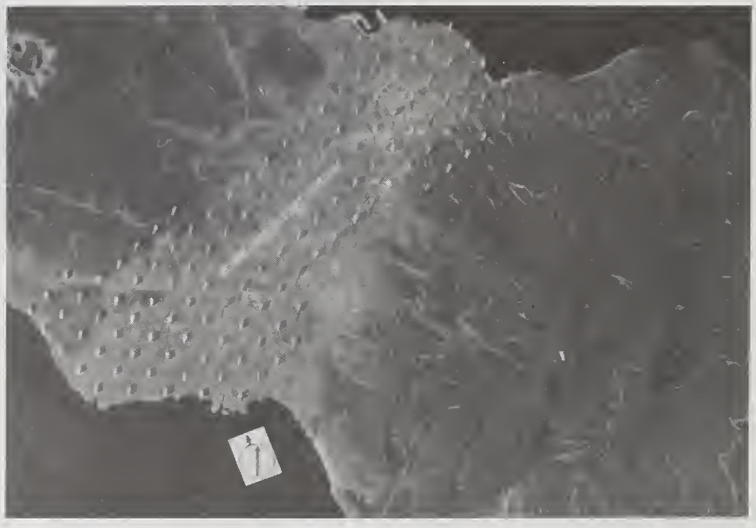

Photo. 3
An example of distribution of wind by wind tunnel experiment. The fixed wind is SSW, and the measuring equipment is small flags made of styloform.

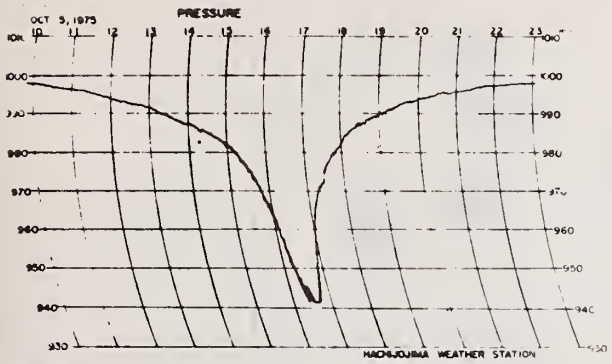

Fig. 1
Atmospheric pressure change of typhoon No. 7513 recorded at the Hachijojima Weather Station.

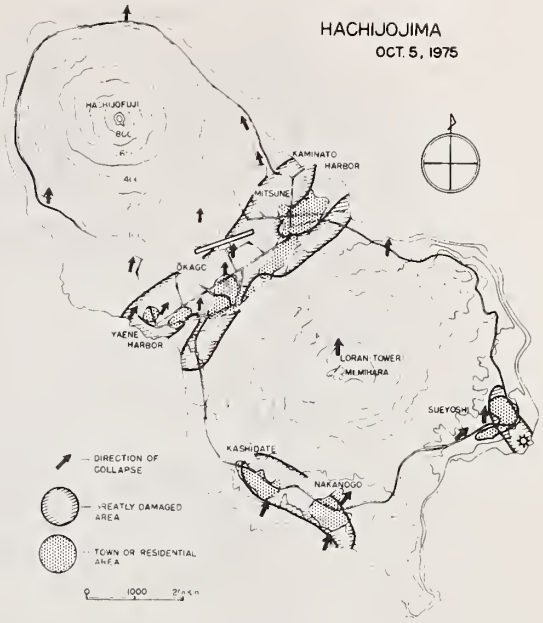

Fig. 2
Distribution of wind damage on Hachijojima.

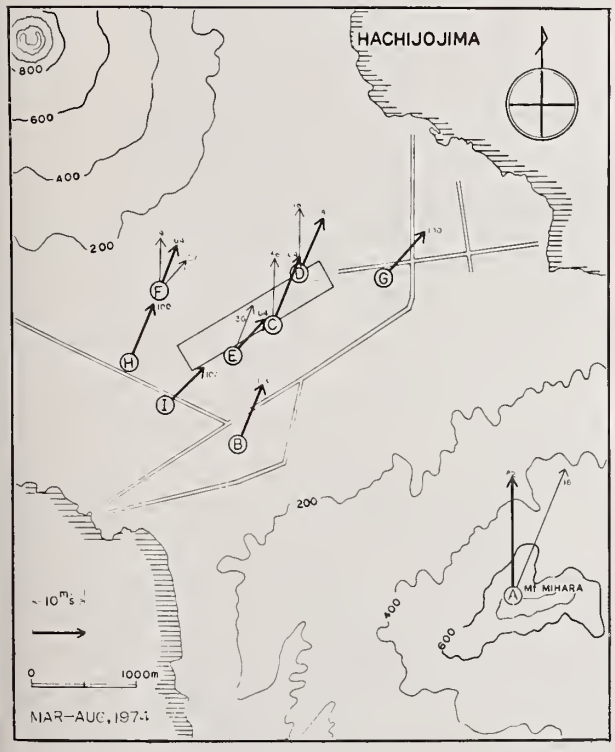

Fig. 3
Distribution of wind shown by vector formula various sites, when the Weather Station indicated SSW (Based on special observation data between 1973 and 1974).

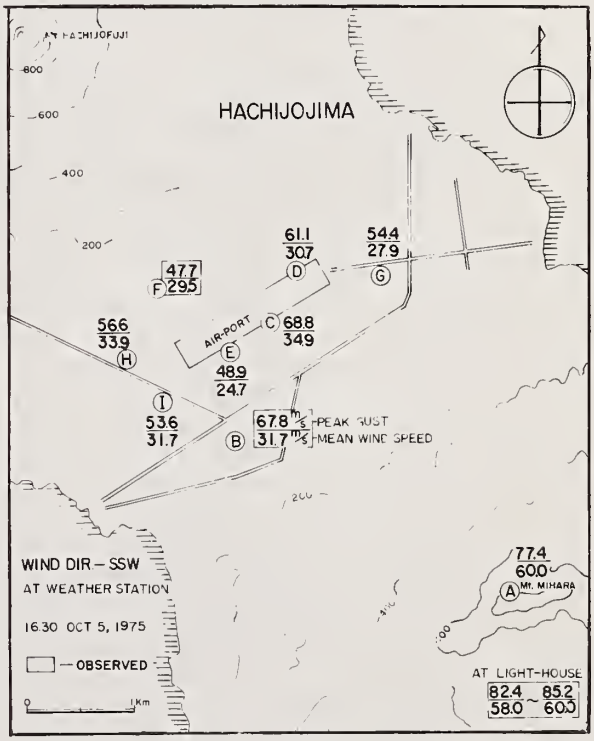

Fig. 4
Estimated mean wind speed (denominator) and peak gust (numerator) at each locations at 16.30, on the 5th.

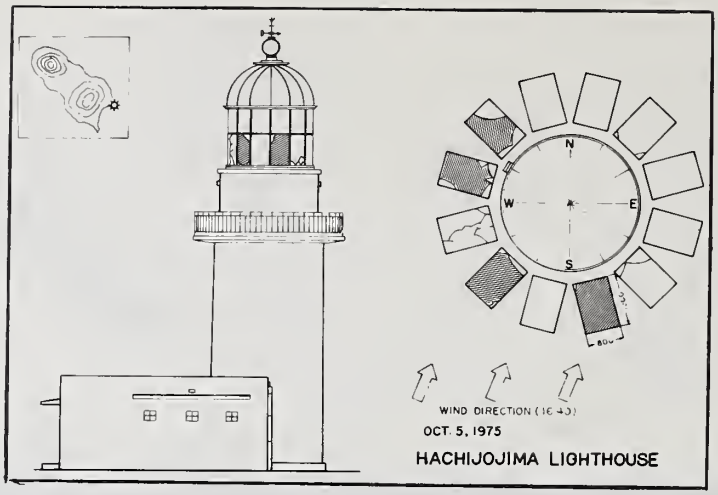

Fig. 5
Damage of lantern panes at the Hachijojima lighthouse. Arrow shows wind direction at 16.40.

Table 1.

PEAK GUST OBSERVED AT HACHIJOJIMA WEATHER STATION

WIND / DATE	WIND DIRECTION	WIND SPEED (m/s)	PERIOD
1938, 9.19	SSW	60.0	1937-1974
1938, 10,21	W	57.0	
1940, 9,18	NNE	54.3	
1943, 10,10	WSW	51.2	
1954, 11,28	NNW	51.0	
1975, 10, 3	SSW	67.8	1975

Table 2. MEAN WIND AND GUST FACTOR (OCT. 5, 1975)

HACHIJOJIMA WEATHER STATION					HACHIJOJIMA LIGHTHOUSE			
TIME	W. D.	U (m/s)	P. G. (m/s)	G. E.	W. D.	U (m/s)	P. G. (m/s)	G. F.
13.00	S	10.0	21.3	2.13	S	17.4	25.5	1.47
14.00	SSW	12.2	25.5	2.09	S	19.4	27.5	1.42
14.30	S	13.5	26.9	1.99	S	22.8	36.0	1.58
15.00	S	15.9	32.5	2.04	S	25.6	32.5	1.27
15.30	S	15.3	35.4	2.31	S	34.3	48.5	1.41
16.00	S	22.1	50.5	2.29	S	42.7	58.8	1.38
16.10	S	23.0	54.6	2.37	SSW	47.4	(67.3)	—
16.20	S	29.9	60.0	2.01	SSW	53.2	(75.5)	—
16.30	SSW	31.7	67.8	2.14	SSW	58.0—60.0	(82.4—85.2)	—
16.40	WSW	29.3	59.5	2.03	SW	—	77.0	—
16.50	W	28.0	55.5	1.98	SW	—	58.5	—
17.00	W	35.5	66.2	1.86	WSW	—	42.0	—
17.10	W	25.9	46.0	1.78	WSW	—	43.6	—
17.20	W	20.9	36.6	1.75	WSW	—	21.0	—
17.30	W	19.8	37.0	1.87	WSW	—		—
18.00	W	14.4	27.4	1.90	WSW	—	15.5	—
				MEAN 2.07				MEAN 1.42

( )---ESTIMATED VALUES OF WIND SPEED FROM MEAN WIND SPEED AND GUST FACTOR

Table 3. DAMAGE RATE OF HOUSES (OCT. 5, 1975)

District	No. of house-holds	Completely destroyed (Damaged more than 70%)		Half destroyed (Damaged 69-[illegible]%)		Partly destroyed (Damaged less than 20%)		Total	
		No. of houses	Rate (%)	No. of houses	Rate (%)	No. of houses	Rate (%)	No. of houses	Rate (%)
Mitsune	1587	116	7.3	217	13.6	[illegible]	30.2	813	51.2
Taigago	1247	97	7.7	216	16.8	417	33.4	724	[illegible]
Kashidate	270	20	7.4	30	11.1	67	24.3	117	43.3
Takanoso	427	13	3.0	36	8.4	[illegible]	39.6	218	51.1
Sueyoshi	254	29	11.4	24	9.4	[illegible]	58.3	201	[illegible]
	Total 3785	Total 275	Mean 7.3	Total 517	Mean 13.7	Total [illegible]	Mean 33.8	Total 2073	Mean 54.8

Table 4. WIND RATIO TO THE VALUE OBSERVED AT HACHIJOJIMA WEATHER STATION (B)

SITE	A Mt.M	B W.S.	C A.P.	D	E	F	G	H	I
WIND RATIO TO (B)	1.89	—	1.10	0.97	0.78	—	0.88	1.07	1.00
ESTIMATED WIND SPEED (m/s)	60.0	31.7	34.9	30.7	24.7	29.5	27.9	33.9	31.7

□ ---- OBSERVED VALUE AT 16:30, OCT. 5, 1975

Table 5. GUST FACTOR AND PEAK GUST (ESTIMATED)

SITE	A Mt.M	B W.S.	C A.P.	D	E	F	G	H	I
GUST FACTOR	1.29	2.14	1.97	1.99	1.98	1.62	1.95	1.67	1.69
ESTIMATED PEAK GUST (m/s)	77.4	67.8	68.8	61.1	48.9	47.7	54.4	56.6	53.6

□ ---- OBSERVED VALUE AT 16:30, OCT. 5, 1975

High Winds in the United States, 1975

by

Arnold R. Hull*
Environmental Data Service
National Oceanic & Atmospheric Admin., Washington, D.C. 20235

and

Thomas D. Potter
National Climatic Center, EDS
National Oceanic & Atmospheric Admin., Asheville, N.C. 28801

and

Nathaniel B. Guttman
National Climatic Center, EDS
National Oceanic & Atmospheric Admin., Asheville, N.C. 28801

During 1975, high winds in the United States were associated with tornado and thunderstorm activity, major extra-tropical storms and Hurricane Eloise.

Hurricane Eloise reached the coast of Florida with an observed minimum pressure of 95.5 kPa and sustained surface winds estimated at 202 km/h (56 m/s). Associated gale winds were reported from Cedar Key, Florida, to southeastern Louisiana and northward over most of Alabama, western Georgia, and extreme southeastern Tennessee. A unique set of hourly meteorological data and some oceanographic data was collected by two buoys during the approach and passage of the eye of Hurricane Eloise. These data, along with simultaneous ship, aircraft, and satellite data are being assembled and packaged for hurricane research studies.

During 1975, 918 tornadoes and numerous storms with high winds caused damage estimated in excess of 2 billion dollars.

A devastating January blizzard dumped up to 58 cm (.58 m) of snow in some areas of the North Central States and was accompanied by winds of up to 130 km/h (36 m/s). In contrast, a severe sandstorm struck southern California on June 17-18, bringing near zero visibility and windspeeds of 144 km/h (40 m/s). Damage to power lines, poles, and other facilities exceeded $100,000.

Key Words: Extra-tropical storms; Hurricanes; Thunderstorms; Tornadoes; Wind; Wind damage

---

* Deceased.

High Winds in the United States, 1975

1. INTRODUCTION

During 1975, high winds in the United States were associated with Hurricane Eloise, tornado and thunderstorm activity, and major extra-tropical storms. High winds occurred somewhere in the United States during each month of the year, and almost every state received extensive damage at least once. Property losses exceeded two billion dollars from the more than 1,500 separate storms that were reported.

2. 1975 TORNADO SEASON

Last year 918 tornadoes were reported[1] throughout the United States on 204 days. They occurred in all states except Alaska, Idaho, New Hampshire, Rhode Island, Utah, Vermont, and Washington. The season began on January 7 and ended on New Year's Eve. During the year, 60 people were killed, 1,504 were injured and property damage exceeded 500 million dollars. Over 1,120 mobile homes were destroyed by tornadoes.

A total of 53 tornadoes was reported in the United States as a whole during the month of January, eclipsing the old record of 39 in 1967. New state records were set as follows:

Month	State	New Record Number	Previous Record
January	Alabama	13	5 (1974)
February	Florida	10	8 (1970)
	Oklahoma	6	4 (1961)
	New York	1	0
March	Mississippi	13	7 (1950)
	North Carolina	8	7 (1956)
	Virginia	4	2 (1969)
April	Florida	13	12 (1973)
	Louisiana	17	7 (1967)

[1] National Oceanic and Atmospheric Administration, National Climatic Center, Storm Data, Vol. 17 (1975).

Month	State	New Record Number	Previous Record
May	Louisiana	12	10 (1950)
June	Montana	9	6 (1971)
	Virginia	4	2 (1969)
	West Virginia	2	1 (1973)
July	Maryland	6	2 (1971)
August	Delaware	2	1 (1967)
	Florida	13	8 (1974)
	Virginia	4	2 (1962)
September	Florida	9	7 (1967)
November	Iowa	9	3 (1960)
December	Iowa	1	0
	North Carolina	3	2 (1967)

On 10 January twenty-six tornadoes reported in Alabama, Louisiana, and Mississippi killed 10 people, injured 286 and caused over 30 million dollars worth of damage. The severe outbreak resulted from a squall line preceding a cold frontal passage.

In March, a tornado struck Warren, Arkansas. Seven people lost their lives. A major industrial area sustained extensive damage. A total of 151 buildings were destroyed, 100 others received major damage and 200 others sustained minor damage. Later in the month a tornado moved through Atlanta, Georgia, at 79 km/h (22 m/s). It killed three people, injured 152, and did 56 million dollars worth of damage. The storm struck a major industrial area, two large apartment complexes, many businesses, hundreds of fine homes and the Governor's Mansion. There were 550 families left homeless.

The worst tornado disaster in Omaha, Nebraska, since Easter Sunday 1913 occurred on 6 May 1975. Three tornadoes killed three, injured 133, and caused damage in excess of 400 million dollars. The storms moved through residential and business areas causing extensive damage to apartments, homes, businesses, schools, autos, trucks, and trees. In places the damaged area was a quarter-mile wide.

Figure 1. Row of houses twisted off foundations (courtesy R. Paskach, Omaha World-Herald).

Figure 2. Houses twisted off foundations (courtesy R. Paskach, Omaha World-Herald).

Figures 1-4 depict some of the damage in Omaha. The first two photographs show frame houses twisted off cement foundations. Winds in this area were estimated at approximately 324 km/h (90 m/s)[2]. The pattern of debris in Figure 3 is also indicative of strong vortex motion. The fourth photograph was taken in an area where residences were completely flattened. Figure 5 vividly portrays the human suffering caused by the tornadoes.

---

[2]T. Fujita, personal communication (1976).

Figure 3. Debris pattern indicative of strong vortex motion (courtesy R. Paskach, Omaha World-Herald).

Figure 4. Area of worst destruction
(courtesy J. Denney, Omaha World-Herald).

Figure 5. Human suffering from tornadoes
(courtesy S. Melingagio, Omaha World-Herald).

On 23 July, Canton, Illinois, was hit by a tornado that killed two and injured 69. This was the first storm to kill anyone in the State of Illinois during the month of July since records have been kept. About 20 million dollars worth of property was damaged in Canton. In a five block area in the central portion of the city, 127 businesses were damaged; some buildings were totally destroyed while others were so badly damaged that they had to be demolished. About 100 homes and 50 mobile homes were destroyed; 300 other homes and 100 other mobile homes were damaged.

3. EXTRA-TROPICAL STORMS

A devastating mid-January blizzard wreaked havoc over Illinois, Indiana, Iowa, Michigan, Minnesota, Missouri, Nebraska, North Dakota, South Dakota, and Wisconsin. The low pressure system moved across Oklahoma into eastern Kansas on the 9th and reached Missouri by daybreak on the 10th. It then curved sharply to the north-northeast, deepening rapidly and intensifying as it moved over eastern Iowa into southeastern Minnesota. The storm track is shown in Figure 6. During the night of the 10-11th, record low pressures were reported at Rochester (97.0 kPa), Minneapolis/St. Paul (96.9 kPa), and Duluth (96.7 kPa), Minnesota.

Wind gusts of up to 130 km/h (36 m/s) were observed in Minnesota, 122 km/h (34 m/s) in Iowa, 112 km/h (31 m/s) in Indiana and Wisconsin, and 97 km/h (27 m/s) in Illinois, Nebraska, and North Dakota. Strong winds and cold temperatures resulted in wind chills below -62°C (211°K) in Minnesota, North Dakota, and South Dakota. Snowfall measured up to 58 cm (.58 m) in Minnesota, 48 cm (.48 m) in Nebraska, 38 cm (.38 m) in Iowa, and 25 cm (.25 m) in North Dakota.

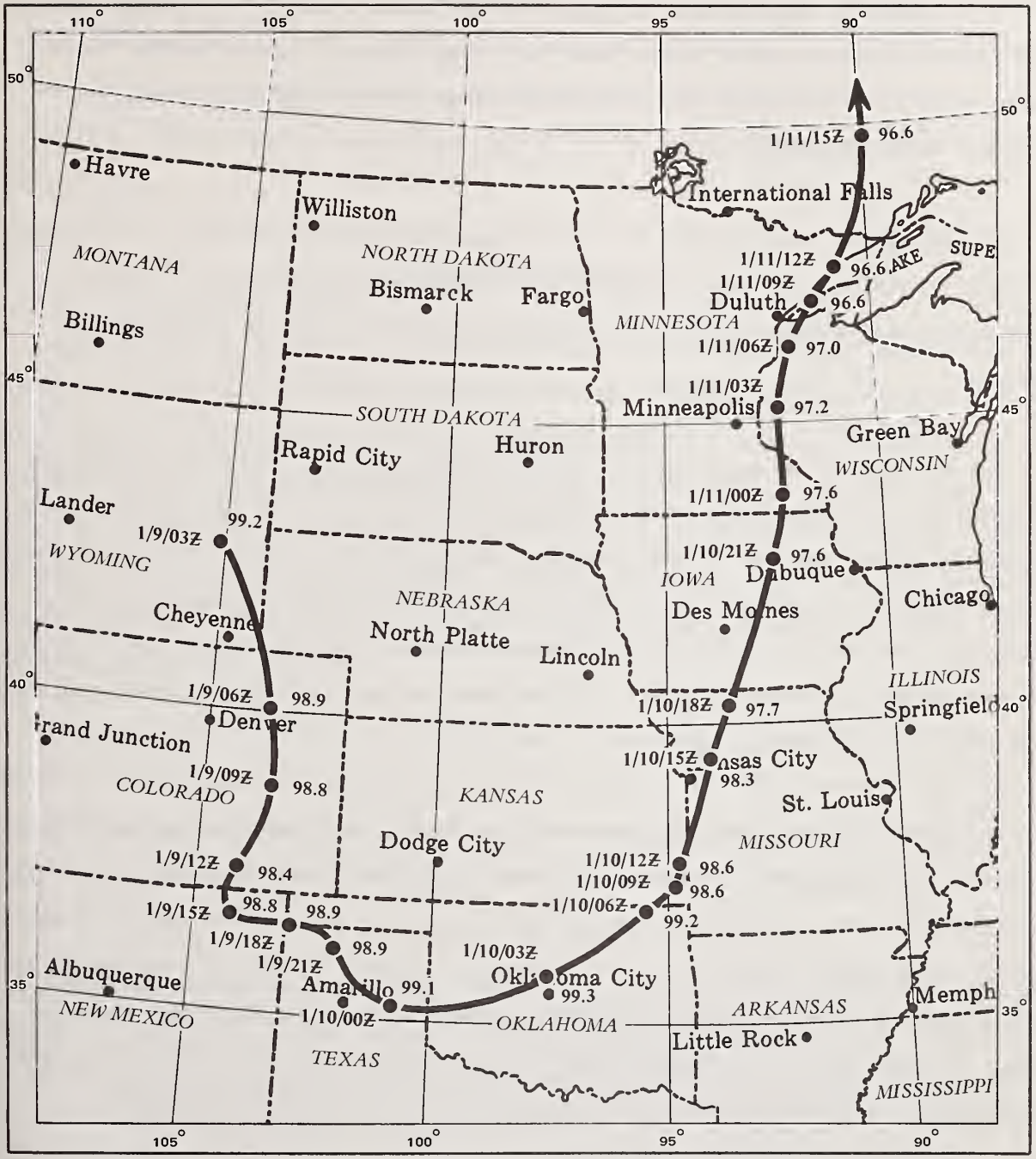

Figure 6. Storm track and central pressures (kPa) of the mid-January blizzard.

The blizzard caused 31 deaths and hundreds of injuries. Damage from the wind, snow and cold temperatures consisted of towers blown down, roofs blown off, broken windows, fallen trees, severe livestock losses and collapsed buildings. Power outages were common and transportation was stalled.

Another January extra-tropical storm swept across the State of Washington. Gusts near 112 km/h (31 m/s) toppled trees, flipped aircraft and caused widespread power outages. Considerable wind damage to irrigation equipment in the eastern part of the State was reported.

One of the worst March blizzards since 1951 struck Wisconsin, Minnesota, and Michigan on the 23-24th. Official observations recorded gusts in excess of 130 km/h (36 m/s), while unofficial reports exceeded 162 km/h (45 m/s). Wind-driven waves of 6.1 m pounded the shore of Lake Superior washing away large sections of the beach and causing extensive flooding. Wind, snow, ice, and water resulted in collapsed buildings, towers and signs, power outages, and cancellations of most activities. Six days later the area was struck by another blizzard with winds up to 112 km/h (31 m/s).

A severe storm struck Maryland, West Virginia, Pennsylvania, New York, and New England on 2-5 April. Western New York recorded the worst April snowstorm since 1894 as 61 cm (.61 m) of snow fell. Winds associated with the storm reached 241 km/h (67 m/s) atop Mt. Washington, New Hampshire, 162 km/h (45 m/s) in Maryland, 148 km/h (41 m/s) in Pennsylvania, 140 km/h (39 m/s) in Maine, and 126 km/h (35 m/s) in Massachusetts. Buildings were destroyed, power lines were downed, trees were broken, mobile homes were blown over, windows and signs were broken, and fishing equipment along the Atlantic coast was extensively damaged.

An intense low pressure system spread across the Midwest on 9-10 November. Winds in excess of 97 km/h (27 m/s) were reported at several stations in Illinois, Indiana, and Iowa. One hundred twenty-six km/h (35 m/s) winds were recorded in Michigan. On 29-30 November another low pressure system moved across the Midwest with similar wind speeds reported. During both storms, damage was widespread to power lines, trees, windows, buildings, and mobile homes.

4. OTHER SEVERE WINDSTORMS

Thunderstorms in the United States during 1975 often produced locally damaging winds in excess of 79 km/h (22 m/s). One of the more intense thunderstorm outbreaks occurred on 22 May in Minnesota and South Dakota. Several areas in these states reported winds above 162 km/h (45 m/s) that destroyed farm buildings, mobile homes, aircraft, trees, and power lines. An outbreak on 16 June in Nebraska and Oklahoma also caused winds of about 162 km/h (45 m/s). Damage to crops, farm equipment, and mobile homes was extensive. On 13 December, thunderstorms in Kansas resulted in winds estimated at 184 km/h (51 m/s) that damaged farm buildings, mobile homes, and trees.

Dust-laden winds gusting to 115 km/h (32 m/s) in the northern two-thirds of Arizona in May caused widespread property damage. Many mobile homes were damaged, sections of roofs were blown away, storm windows were blown out, signs were blown down and large trees fell on houses, cars, and power lines. Traffic accidents were numerous as dust reduced the visibility to zero.

California experienced a sandstorm in June. At the height of the storm a wind speed of 144 km/h (40 m/s) was recorded. Damage to utility company facilities was about $100,000. In addition thousands of automobiles and trucks had paint blasted off, pitted windshields and chrome, and damaged engines. In one area more than 100 automobiles were half-buried in sand.

5. HURRICANE ELOISE

The track of Hurricane Eloise across the Caribbean Sea and Gulf of Mexico is shown on Figure 7. On 23 September, she moved onshore in the Florida Panhandle with a minimum pressure of 95.5 kPa. Above normal tides and high winds caused considerable damage, even though the storm rapidly lost strength as it moved northward over the land.

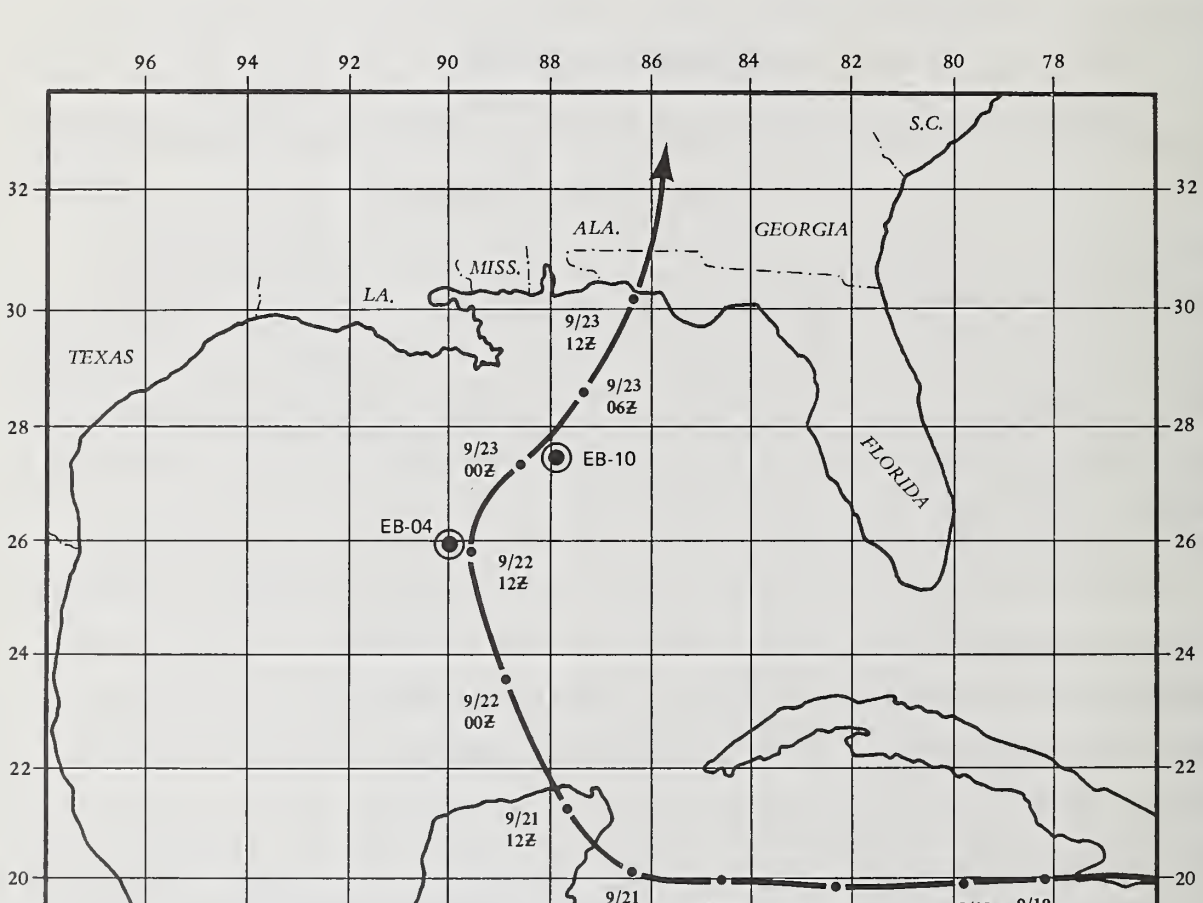

Figure 7. Storm track of Hurricane Eloise.

Northwest Florida was battered by sustained winds as high as 202 km/h (56 m/s) and gusts as high as 248 km/h (69 m/s). Tides along an 80 km strip of shoreline were 3.7 to 4.9 m above normal. Damage in this part of Florida was estimated at 150 million dollars. Wind-driven storm tides eroded 9.1 to 21.3 m of sand and undermined beach front structures. Eighty-five to 90 percent of the buildings between Fort Walton Beach and Panama City on the water side of the coastal highway were severely damaged or destroyed. Airplanes and boats were also destroyed. The hurricane affected one million acres of timber, and crop damage was severe.

Away from the center of the hurricane, wind gusts of up to 194 km/h (54 m/s) were reported in Alabama and 130 km/h (36 m/s) in Georgia. Gale winds associated with the storm were reported as far west as Louisiana and as far north as Tennessee. Crop damage in these states exceeded one million dollars - 50,000 pecan trees were uprooted, the corn crop was virtually a total loss, and the cotton and soybean crops were severely damaged. In addition, hundreds of buildings were damaged and some were destroyed, numerous mobile homes were either damaged or destroyed, power outages were widespread, and thousands of trees were felled.

A unique set of hourly meteorological data and some oceanographic data was collected by two buoys during the approach and passage of the eye of Hurricane Eloise. These data, along with simultaneous ship, aircraft, and satellite data are being assembled for hurricane research studies.

From 19-25 September buoy EB-04 at 26.0 N, 90.0 W collected air pressure, air and surface water temperature, dew point, solar radiation, wind speed and direction, surface salinity and surface current direction data. The second buoy, EB-10, at 27.5 N, 88.0 W collected from 20-26 September the above data plus wave height, wave period and precipitation; and subsurface temperature, pressure, salinity and current information. In addition, wave spectra are available from 20-24 September. Most of the data collected are 15 minute

averages. Time series of sea level pressure and wind speed at EB-10 are shown on Figure 8. The passage of the eye on 23 September is distinctly represented by the sharp drop and rapid recovery of both the pressure and wind speed.

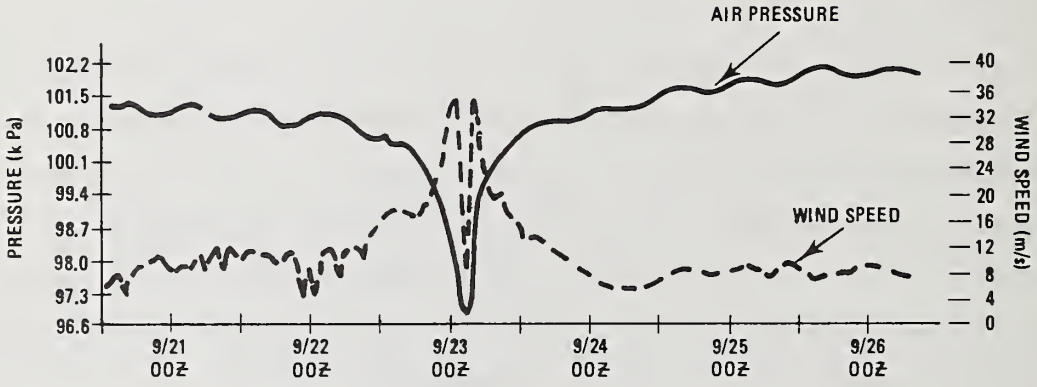

Figure 8. Time series of the sea level pressure and wind speed for buoy EB-10 during the passage of Hurricane Eloise.

The assembled data package from the National Climatic Center will contain digitized buoy data, land station data (surface and upper air), ship observations and satellite data. It will also contain microfiche of records of climatological observations, National Hurricane Center bulletins and advisories, barograms, hourly precipitation data and meteorological observations forms. Surface and upper air synoptic charts and forms, satellite photographs, reconnaissance data and radar logs will be microfilmed, and 16 mm films of satellite and radar data will be available. In short, a complete data package on Hurricane Eloise will be available at the National Climatic Center for researchers.

6. SUMMARY

Several severe windstorms caused loss of life and extensive damage in the United States during 1975. During each month some location in the United States was battered by strong winds from either relatively short-lived meso-scale storms (like tornadoes) or long-lived large scale storms (like hurricanes or severe extra-tropical storms). Some new records on frequency of storms and on damage were established during 1975. But the year was not highly unusual -- new records of some sort are established somewhere in the United States almost every year. Engineers designing systems to withstand wind damage must be cognizant of the likelihood of such extreme winds and of the establishment of new records. Meteorologists must continue work to better define the extreme wind environment.

7. ACKNOWLEDGEMENTS

The help of Mr. Henry Vigansky of the National Climatic Center is greatly appreciated. The cooperation of the management of the Omaha World-Herald, Omaha, Nebraska, for granting permission to use their photographs is also appreciated.

MEAN SPEED PROFILES OF HURRICANE WINDS

EMIL SIMIU
Structural Research Engineer
Center for Building Technology
National Bureau of Standards
Washington, D.C.

VIRENDRA C. PATEL
Associate Professor
Division of Energy Engineering
University of Iowa
Iowa City, Iowa

JOHN F. NASH
Vice President
Sybucon, Inc.
Atlanta, Georgia

ABSTRACT

A numerical solution of the hurricane boundary layer problem is presented in which the hurricane is modeled as a steady, axisymmetric, neutrally stratified flow. The turbulence effects in the flow are accounted for by the phenomenological relations proposed by Bradshaw et al, and Nash, which provide a considerably more realistic picture of the actual flow than the pseudolaminar model used in previous solutions of the boundary layer problem. The results of the calculations obtained on the basis of the model just described suggest that: (1) in the height range of interest to the structural designer, say up to a height of 400 m above ground, it is permissible to use the logarithmic law to represent the mean velocity profile of hurricane winds and (2) if the relation between wind speeds in different roughness regimes which is valid in extratropical storms is applied to hurricane winds, the speeds over built-up terrain, calculated as functions of speed over open terrain, may be underestimated by about 10% and 10-20% in suburban and in urban exposure, respectively. The corresponding mean loads are then underestimated by about 15% and 30%, respectively.

Key Words: Boundary layer; Hurricanes; Loads (forces); Natural analysis; Tall buildings; Wind Profiles.

1. Introduction

In view of the considerable influence upon tall building design of the assumptions regarding the variation of mean winds with height, the question has been raised as to whether or not mean wind profiles in mature hurricanes differ significantly from profiles typical of extratropical storms [6, 16, 21]. In the Southern Standard Building Code [19] it is assumed that hurricane wind speeds increase with height only up to an elevation of 100 ft (30.5 m) above ground and are constant above that elevation, i.e., that hurricane winds are characterized by flatter profiles than winds associated with inland storms.

On the other hand, in both the 1955 and the 1972 versions of the American National Standard A58.1 [1, 2] it is assumed that there are no differences between profiles in the two types of storms.

Several attempts to provide a description of the boundary layer in a mature hurricane have been reported in the literature. However, as noted in Ref. 16, the results obtained so far have been largely inconclusive. Hurricane wind speed data recorded in Florida suggest that mean profiles are considerably flatter in hurricanes than in extratropical storms. However, these data were discounted by Gentry [6, 21] as being of dubious reliability. It has also been argued [2] that no inferences valid for mature hurricanes can be drawn from data measured at Brookhaven, N.Y. in 1950, which are representative of a hurricane in the decaying stage. Finally, existing analytical solutions [4, 14, 18] are based upon the unrealistic assumption of pseudolaminarity and are therefore capable of providing, at best, a qualitative picture of the flow.

The occurrence of a hurricane at any one location is a rare event. It is therefore difficult to obtain relevant measurements on the variation of hurricane speeds with height and on the relation between hurricane wind speeds in different roughness regimes. This being the case, it appears reasonable to attempt an analytical solution of the hurricane boundary layer problem, based on a realistic representation of the turbulent flow. Such a solution is described herein. Numerical results corresponding to typical situations of interest to the designer and code writer are presented. Current building code provisions on hurricane winds are then assessed in the light of these results.

2. Analytical Model Method of Solution

Following Rosenthal [14], Carrier et al [4] and Smith [18], it is assumed that the hurricane boundary layer flow is steady, axisymmetric and neutrally stratified. Except in the immediate proximity of the eye, where the boundary layer assumptions break down [18], the Reynolds equations may be written as

$$U \frac{\partial U}{\partial R} + W \frac{\partial U}{\partial z} - \frac{V^2}{R} - fV + \frac{1}{\rho} \frac{dp}{dR} - \frac{1}{\rho} \frac{\partial \tau_u}{\partial z} = 0 \qquad (1)$$

$$U \frac{\partial V}{\partial R} + W \frac{\partial V}{\partial z} + \frac{UV}{R} + fU - \frac{1}{\rho} \frac{\partial \tau_v}{\partial z} = 0 \qquad (2)$$

The equation of continuity is

$$\frac{\partial}{\partial R} (RU) + \frac{\partial}{\partial z} (RW) = 0 \qquad (3)$$

Here, R is the radial distance measured from the storm center, z is the distance measured normal to the earth surface, U, V and W are the radial, circumferential and normal (vertical) mean velocities, respectively, ρ is air density, p is static pressure, f is the Coriolis parameter (in this work it was assumed $f = 5 \times 10^{-5}\ s^{-1}$) and τ_u and τ_v are the turbulent Reynolds stresses (the molecular stresses being negligibly small) in the radial and circumferential directions, respectively.

According to Rosenthal [14], measurements indicate that the expression

$$\frac{1}{\rho}\frac{dp}{dR} = \frac{\Delta p}{\rho R^2} R_{vm} \exp\left(-R_{vm}/R\right) \tag{4}$$

is quite representative of the pressure field in hurricanes. In Eq. 4, R_{vm} = value of the radius, R, at which the gradient wind, V_{gr}, is a maximum and Δp = difference between the high pressure in the far field ($R \simeq 1000$ km, say) and the low pressure at the storm center. The relation between pressure gradient and gradient velocity is given by the classical frictionless balance equation in cyclonic flow [7],

$$\frac{1}{\rho}\frac{dp}{dR} = \frac{V_{gr}^2}{R} + fV_{gr} \tag{5}$$

The boundary conditions, at the top and bottom edges of the boundary layer region were expressed as follows:

$$z = 0 \qquad U = 0 \qquad V = 0 \qquad W = 0 \tag{6}$$

$$z \to \infty \qquad U \to 0 \qquad V \to V_{gr} \tag{7}$$

In actual computations, condition (7) is satisfied with sufficient accuracy at some finite distance of the order of the boundary layer thickness δ.

Previous experience [4, 18] has shown that the solution of the equations of motion is not unduly sensitive to small variations in the boundary conditions at the far field radius. In this work, it was assumed that at R = 1000 km, the velocity and shear stress profiles are the same as in horizontally homogeneous flow over a rough plane surface, with a boundary layer thickness δ = 1.4 km.

To solve the equations of motion, phenomenological relations must be specified that describe the Reynolds stresses τ_u, τ_v. In this work, the relations proposed by Bradshaw et al. [3] and Nash [8] have been employed. These relations have been shown to result in successful predictions in a variety of boundary layer problems [11, 17] and have recently been also employed in micrometeorological work [13]; as shown by Nash [8], they are particularly suitable for use in the three-dimensional boundary layer problems. For the case of the hurricane boundary layer, and assuming, as in Ref. 8, that the directions of Reynolds stress vector and of the mean rate-of-strain vector coincide, the closure relations may be

written in the form

$$U \frac{\partial \tau}{\partial R} + V \frac{\partial \tau}{\partial z} + 2a_1 \left\{ \tau_v \frac{\partial U}{\partial z} + \tau_u \frac{\partial V}{\partial z} \right\} + 2a_1 \frac{\partial}{\partial z} (a_2 \tau) + \frac{\tau}{L} \sqrt{\frac{\tau}{\rho}} = 0 \tag{8}$$

and

$$\frac{\tau_u}{\frac{\partial U}{\partial z}} = \frac{\tau_v}{\frac{\partial V}{\partial z}} \tag{9}$$

In Eq. 8, which may be interpreted as an empirical model of the equation expressing the conservation of the turbulence kinetic energy, $\tau = (\tau_u^2 + \tau_v^2)^{1/2}$, a_1 is an absolute convective constant (= 0.15), and a_2 and L are universal functions of z/δ which model, respectively, the diffusion and dissipation of turbulence energy across the boundary layer. The empirical functions L and a_2 used are the same as those given in Ref. 9.

The system consisting of the Reynolds equations, the equation of continuity and the closure relations, with the given boundary conditions, was solved numerically using a time-relaxation procedure developed by Patel and Nash and described in some detail in Ref. 12. The numerical solution of the boundary layer equations was terminated at a height above ground of 0.05 times the local boundary layer thickness and then matched with the logarithmic law

$$\frac{Q}{u_*} = \frac{1}{\kappa} \ln \frac{z}{z_o} \tag{10}$$

assumed to be valid below that height. In Eq. 10, u_* = shear velocity = $(\tau_w/\rho)^{1/2}$, τ_w = resultant shear stress at the ground, ρ = air density, Q = resultant mean wind velocity, κ = von Karman constant, z_o = roughness length.

3. Numerical Results

Nine cases were investigated, covering four different roughness regimes. Values of the parameter z_o were used in the calculations that correspond, roughly, to flow over open water (z_o = 0.0023 m), flow over open terrain (z_o = 0.012 m and z_o = 0.03 m), flow over suburbs or towns (z_o = 0.35 m) and flow over large cities (z_o = 0.90 m). For simplicity, the terrain roughness was assumed to be uniform. The profiles were calculated at a distance, R, from the storm center equal to the radius of maximum gradient winds, R_{vm}, except that in one case the profile was also calculated at R = 2 R_{vm}, in addition to R = R_{vm}. Typically, it was assumed R_{vm} = 30 km and Δp = 100 mb. These assumptions are consistent with observed data (see for example, Ref. 20) in hurricanes of great intensity. To assess the influence upon the results of the magnitude of Δ_p and R_{vm}, additional calculations were performed with Δp = 60 mb, Δp = 140 mb and R_{vm} = 50 km. The values of the

parameters for the various cases investigated are given in Table 1. The results of the calculations, based on Eqs. 1-9, are listed in Table 2 [columns (1), (2), (3), (5), (7), (9)]. Table 2 also includes mean speeds calculated in accordance with the logarithmic law [columns (4), (6), (8), (10)].

$$V(z) = \frac{1}{\kappa} u_* \ln \frac{z}{z_o} \qquad (11)$$

4. Interpretation of Results

a) Logarithmic Profiles and Calculated Hurricane Wind Speeds.

It can be seen from Table 2 that, in the height range of interest to the structural designer, hurricane wind speeds, as determined on the basis of Eqs. 1-9, are smaller by less than 3% than speeds determined in accordance with Eq. 11.

(It is noted that the results reported in Ref. 12 show that the differences between the resultant mean speed Q(z) and the tangential component V(z) are negligibly small - of the order of 1% or less). Since the logarithmic law is an excellent representation of wind profiles in the lower few hundred meters of extratropical storms [10, 15], it follows, according to the results of Table 2, that mean profiles in hurricanes and in extratropical cyclones may be assumed to have approximately the same shape. It thus appears that, insofar as the power law is an approximation of the logarithmic law, the assumption regarding mean wind profiles used in the A58.1 Standard [1,2] is justified, and that, on the other hand, the assumption implicit in the Southern Building Code [19], according to which, at elevations higher than 30 m above ground, hurricane winds do not increase with height, may be unsafe from a structural design viewpoint.

b) Wind Speed Reduction due to Increased Roughness of Terrain.

In terrain that is built-up over a sufficiently large getch, the higher friction at the ground will retard the flow more effectively than is the case over open terrain. Thus, at any elevation within the boundary layer, mean wind speeds will be lower in built-up, than in open terrain.

Wind maps included in the A58.1 Standard 1972 [2] specify wind speeds at 30 ft (9.15 m) above ground in open terrain. To calculate the corresponding speeds over built-up terrain (suburban or urban) it is necessary that a model be assumed, describing the relation between wind speeds in different roughness regimes. Two such models are currently in use [2, 15]. The model presented in Ref. 15, referred to as the similarity model, is based on recent results of theoretical and experimental boundary layer research [5], and rests on the assumption that the flow in the free atmosphere is geostrophic. In accordance with this model, the friction velocities, u_{*1} and u_*, over terrains of roughness length z_{o1} and z_o, respectively, are related as follows [15]:

$$\frac{u_{*1}}{u_*} \simeq \left[\frac{20.25 + \ln^2 \frac{u_*}{fz_o}}{20.25 + \ln^2 \frac{u_{*1}}{fz_{o1}}}\right]^{1/2} \qquad (12)$$

where f = Corolis parameter. The model included in Ref. 2, referred to as the power law model, assumes the validity of the equation

$$V(z) = V(10)\ (\frac{z}{10})^{\alpha} \qquad (13)$$

where $\alpha = 1/7$ in open terrain, $\alpha = 1/4.5$ in suburban terrain and $\alpha = 1/3$ in urban terrain. This model assumes, in addition, that the gradient height (i.e., the thickness of the boundary layer) is $z_g = 275$ m, $z_g = 366$ m and $z_g = 458$ m in open, suburban and urban terrain, respectively. The magnitude of the wind speed at 10 m above ground in open terrain being specified, the corresponding speed over suburban or open terrain is easily obtained using Eq. 13, in which for all values of α, the gradient wind, $U(z_g)$, is the same [2].

Implicit in the power law model, which is in effect an empirical approximation of the similarity model, is the assumption that the flow in the free atmosphere is geostrophic. This assumption does not hold in the case of hurricane winds. Nevertheless, the power law model is applied in the A58.1 Standard [2] not only to extratropical storms, for which it may indeed be assumed that the flow is approximately geostrophic, but to hurricane winds as well.

The question thus arises as to whether it is permissible to apply the same relation between speeds in different roughness regimes - based on the assumption of geostrophic flow - to both extratropical storms and hurricanes. This question will now be examined in the light of the results of Table 2.

A direct comparison between these results, based on the model consisting of Eqs. 1-9, and those obtained if the power law model is employed would present difficulties insofar as the two models use different roughness parameters, vix., the roughness length, z_o, and the exponent, α, respectively. It will therefore be more convenient to compare the results of Table 2 with those obtained if the similarity model is used.

Let $z_o = 0.03$ m and $z_{o1} = 0.0023$ m, $z_{o1} = 0.012$ m, $z_{o1} = 0.35$ m and $z_{o1} = 0.90$ m. The ratios $(u_{*1}/u_*)_{extr}$, obtained using Eq. 12 are given in Table 3, in which the ratios, $(u_{*1}/u_*)_{hurr}$, based on Eqs. 1-9 and obtained from Tables 1 and 2 (cases 3, 6, 7, 8, 9) are listed for purposes of comparison (the subscripts extr, and hurr, indicate that the quantities involved are calculated for extratropical storms and for hurricanes, respectively). The quantities $[V(z)]_{hurr}$ and $[V(z)]_{extr}$ in Table 3 are mean speeds over terrain of roughness z_{o1}, calculated in accordance with Eqs. 1-9 and with Eq. 12 (in which $z_o = 0.03$ m), respectively. Assuming the model consisting of Eqs. 1-9 to be correct, it is seen that the similarity model (Eq. 12) results in underestimates of the mean speeds in suburban and urban terrain of the order of 5-15% and, therefore, underestimates of the mean load (which

is proportional to the square of the mean speeds) of the order of 10-30%.

The results of Tables 2 and 3 are based on the assumption that the terrain roughness is uniform throughout the area swept by the hurricane. In reality, the roughness corresponding to suburban or urban terrain only prevails over a small part of this area and thus the flow over rougher terrain is retarded somewhat less effectively than indicated by the results of Table 2. It may therefore be expected that the actual ratios $(u_*l/u_*)_{hurr}$ and $[V(z)]_{extr}$ for the suburban and urban terrain cases are larger than indicated in Table 3.

It thus appears that if Eq. 12 - which does not take into account the presence of inertia forces in the hurricanes - is used in structural engineering applications for calculating hurricane wind speeds over suburban terrain, the error involved is for z_{ol} = 0.20 - 0.35 m, of the order of 5-10%. If Eq. 12 is applied for calculating hurricane wind speeds over urban terrain (z_{ol} = 0.40 - 0.90 m), according to the results reported herein, the calculated speeds may be underestimated by about 10-20%.

5. Conclusions

A numerical solution of the hurricane boundary layer problem was presented in which the hurricane was modeled as a steady, axisymmetric, neutrally stratified flow with a pressure field represented by Rosenthal's expression [14] (Eq. 4). The turbulence effects in the flow are accounted for by the phenomenological relations proposed by Bradshaw et al [3] and Nash [12], which provide a considerably more realistic picture of the actual flow than the pseudolaminar model used in previous solutions of the boundary layer problem [4, 14, 18].

The results of the calculations obtained on the basis of the model just described suggest that:

1. In the height range of interest to the structural designer, say up to a height of 400 m above ground, it is permissible to use the logarithmic law to represent the mean velocity profile of hurricane winds. Accordingly,
   (a) the assumption used in the A58.1 Standard [2], according to which the variation of mean winds with height follows the same law in both extratropical storms and hurricanes is acceptable.
   (b) the assumption implicit in the Southern Standard Building Code [27], according to which, at elevations higher than 100 ft (30.5 m) above ground, hurricane wind speeds do not increase with height, may be unsafe from a structural design viewpoint.
2. If the relation between wind speeds in different roughness regimes which is valid in extratropical storms is applied to hurricane winds, the speeds over built-up terrain, calculated as functions of speed over open terrain, may be underestimated by about 5-10% and 10-20% in suburban and in urban exposure, respectively. The corresponding mean loads are then underestimated, roughly, by 15% and 30%, respectively.

Acknowledgements

The work presented herein is part of a study of hurricane effects on port facilities conducted by the Center for Building Technology, National Bureau of Standards and supported by the Maritime Administration, U.S. Department of Commerce. The calculations presented herein were planned and carried out by Sybucon, Inc.

Appendix I - References

1. "American Standard Building Code Requirements for Minimum Design Loads in Buildings and Other Structures," American Standards Association, New York, N.Y., 1955.

2. "American National Standard Building Code Requirements for Minimum Design Loads in Buildings and Other Structures A58-1," American National Standards Institute, New York N.Y., 1972.

3. Bradshaw, P., Ferris, D.H., Atwell, N.P., "Calculation of Boundary-Layer Development Using the Turbulent Energy Equation," Journal of Fluid Mechanics, Vol. 28, 1967, pp. 593-616.

4. Carrier, G.F., Hammond, A.L., George, O.D., "A Model of the Mature Hurricanes," Journal of Fluid Mechanics, Vol 47, pp. 145-170, 1971.

5. Csanady, G.T., "On the Resistance Law of a Turbulent Ekamn Layer," Journal of the Atmospheric Sciences, Vol. 24, Sept., 1967, pp. 467-471.

6. Gentry, R.C., discussion of "Nature of Wind" by R.H. Shelock, Journal of the Structural Division, ASCE, Vol. 85, No. ST3, Proc. Paper, 1988, Part 1, Mar., 1959, pp. 170-172.

7. Haltiner, G.J. and Martin, F.L., Dynamical and Physical Meteorology, McGraw-Hill Book Co., Inc., New York, N.Y., 1957.

8. Nash, J.F., "The Calculation of Three-Dimensional Turbulent Boundary Layers in Incompressible Flow," Journal of Fluid Mechanics, Vol. 37, 1969, p. 625-642.

9. Nash, J.F. and Patel, C.V., Three Dimensional Turbulent Boundary Layers, S.B.C. Technical Books, Atlants, 1972.

10. Pasquill, F., "Wind Structure in the Atmospheric Boundary Layer", Philosophical Transactions of the Royal Society of London, A. 269, 1971, pp. 439-456.

11. Patel, V.C. and Nash, J.F., "Some Solutions of the Unsteady Turbulent Boundary-Layer Equations," Proceedings, IUTAM Symposium, Quebec, 1972.

12. Patel, V.C. and Nash, J.F., "Numerical Study of the Hurricane Boundary Layer Mean-Wind Profiles," Report prepared for the National Bureau of Standards by Sybucon, Inc., Atlanta, Georgia, June, 1974.

13. Peterson, E.W., "Modification of Mean Flow and Turbulent Energy by a Change in Surface Roughness," Quarterly Journal of the Royal Meteorological Society, Vol. 95, 1969, pp. 560-575.

14. Rosenthal, S.L., "A Theoretical Analysis of the Field of Motion in the Hurricane Boundary Layer", Report No. 56, National Hurricane Research Project, U.S. Department of Commerce, Washington, D.C.

15. Simiu, Emil, "Logarithmic Profiles and Design Wind Speeds," Journal of the Engineering Mechanics Division, ASCE, Vol. 99, No. EM5, Proc. Paper 10100, October, 1973, pp. 1073-1083.

16. Simiu, E., "Variation of Mean Winds with Hurricanes," Journal of the Engineering Mechanics Division, ASCE, Technical Note, Vol. 100, No. EM4, Proc. Paper 10692, Aug., 1974, pp. 833-837.

17. Singleton, R.E. and Nash, J.F., "A Method for Calculating Unsteady Turbulent Boundary Layers in Two- and Three-Dimensional Flows," AIAA Journal, Vol. 12, No. 5, May 1974.

18. Smith, R.K., "The Surface Boundary Layer of a Hurricane," Tellus, Vol. 20, 1968, pp. 473-484.

19. Southern Standard Building Code, Birmingham, Alabama, 1965, p. 5-12 .

20. "Survey of Meteorological Factors Pertinent to Reduction of Loss of Life and Property in Hurricane Situations," Report No. 5, National Hurricane Research Project, U.S. Department of Commerce, Washington, D.C., 1957.

21. "Wind Forces on Structures," Final Report by Task Committee on Wind Forces, Transactions, ASCE, Vol 126, Paper No. 3269, Part II, 1961, pp. 1124-1198.

Appendix II - Notations

a_1	Convective constant in the turbulent shear stress equations
a_2	Diffusion constant
L	Dissipation length
f	Coriolis parameter
p	Static pressure
Q	Resultant mean wind velocity
R	Radial distance from the storm center
R_{max}	Radial location of maximum pressure gradient
R_{vm}	Radial location of maximum gradient wind
u_*, u_{*1}	Shear velocity in terrain of roughness length z_o, z_{o1}, respectively
U	Radial mean wind velocity
V	Circumferential mean wind velocity
V_{gr}	Gradient wind
W	Vertical mean wind velocity
z	Vertical distance above the ground
z_o	Terrain roughness length
Δp	Pressure depression
δ	Boundary-layer thickness
κ	Karman constant in the Law of the Wall
ρ	Air density
τ_u	Reynolds shear stress in the radial direction
τ_v	Reynolds shear stress in the circumferential direction
τ_w	Resultant shear stress at the ground

Table 1 - Values of Parameters for the Various Cases Investigated

Case Number	R_{vm} kilometers	Δp millibars	z_o meters	R^a kilometers
1	30	60	0.0023	30
2	30	140	0.0023	30
3	30	100	0.0023	30
4	30	100	0.0023	60
5	50	100	0.0023	50
6	30	100	0.012	30
7	30	100	0.03	30
8	30	100	0.35	30
9	30	100	0.90	30

[a]radius at which profile was calculated

Table 2 - Calculated Hurricane Wind Speeds in meters/second [12]

Case	δ	u_*	z (meters)							
	meters	meters/second	100		200		300		400	
	(1)	(2)	(3)	(4)	(5)	(6)	(7)	(8)	(9)	(10)
1	1,590	1.45	38.5	(38.8)	40.6	(41.3)	41.8	(42.8)	42.3	(43.9)
2	1,600	2.24	59.3	(59.8)	62.6	(63.6)	64.3	(65.9)	65.1	(67.5)
3	1,610	1.89	49.9	(50.3)	52.7	(53.7)	53.2	(55.5)	54.9	(56.9)
4	3,430	1.59	42.3	(42.3)	44.8	(45.1)	46.1	(46.7)	47.0	(47.9)
5	2,480	1.80	48.0	(48.0)	50.6	(51.2)	52.2	(53.0)	53.2	(54.3)
6	1,950	2.16	48.8	(48.8)	51.7	(52.6)	53.5	(54.8)	54.5	(56.3)
7	2,200	2.36	47.7	(47.7)	51.0	(51.8)	53.1	(54.2)	54.2	(55.9)
8	3,200	3.06	43.2	(43.2)	48.0	(48.5)	50.5	(51.6)	52.3	(53.8)
9	3,790	3.44	40.6	(40.6)	46.0	(46.5)	48.9	(50.0)	50.9	(52.5)

Note. Numbers in parentheses represent wind speeds calculated using the logarithmic law (Eq. 11).

Table 3 - Calculated Ratios u_{*1}/u_* and $[V(z)]_{hurr}/[V(z)]_{extr}$

z_{o1} (meters)	$(u_{*1}/u_*)_{hurr}$	$(u_{*1}/u_*)_{extr}$	$\frac{[V(z)]_{hurr}}{[V(z)]_{extr}}$	$\frac{[V(z)]^2_{hurr}}{[V(z)]^2_{extr}}$
0.0023	0.862	.800	.93	.86
0.012	0.951	.916	.96	.91
0.03	1.000	1.000	1.00	1.00
0.35	1.189	1.229	1.09	1.19
0.90	1.257	1.463	1.16	1.36

Planning and Design of Strong-Motion Instrument Networks

R. B. MATTHIESEN
U.S. Geological Survey, Menlo Park, California

ABSTRACT

The types of research studies that utilize strong-motion data may be classified as: source mechanism studies, ground motion studies, soil failure studies, studies of the response of typical structures (including soil-structure interaction effects), and studies of the response of equipment.

In planning networks and arrays to make these studies, criteria must be established based on the tectonic setting, the seismicity or recurrence of strong ground motions, the reliability of operations in different regions, and a cost/benefit analysis of the data that may be obtained. A review of the strong-motion records that have been obtained during the past 40 years indicates significant variations in the recurrence of strong ground motions in the seismically active regions of the western United States. When combined with instrument costs, maintenance costs, and the reliability of operations, these recurrence relations can be interpreted in terms of the cost per record for different levels of motion. The benefits to be derived from each type of study in each region need to be established.

Current plans call for additional arrays to be installed in California, the Mississippi embayment, the Yellowstone Park region, and Alaska to study the spectral characteristics of strong ground motions in these regions. Special studies of local site effects and structural response are being planned in the more seismically active regions of California. Similar criteria and planning should be applied in the establishment of arrays of strong-motion instruments on a worldwide basis.

Key Words: Cost effectiveness; ground motion; network design; strong-motion record.

INTRODUCTION

The primary input for the design of strong-motion instrument arrays comes from the research needs in strong-motion seismology and earthquake engineering. The impetus behind much of that research is the application of the research results in engineering design and reduction of earthquake hazards. This input defines general objectives to be accomplished by an appropriately designed network but does not constrain the development of the network geographically. A secondary input comes from the mission-oriented and regulatory agencies that desire to monitor the response of critical facilities to assess their response during potentially damaging earthquakes. The location of this instrumentation is constrained to the specific structure or system being monitored but may add significant data to that obtained from a network of research instruments. The mission-oriented agencies also influence the design of the network through their need for additional research results on a timely basis.

The types of studies that utilize strong-motion data may be classified as follows:

- Studies of the source mechanism.
- Studies of the spectral characteristics of strong ground motion and of the variations of these characteristics with the nature of the source, the travel path and regional geology, or the local site conditions.
- Studies of soil failures such as soil liquefaction or landslides.
- Studies of the response of representative types of structures and interconnected systems at potentially damaging levels of response and of the influence of the foundation conditions on this response.
- Studies of the response of equipment which may be free-standing or mounted on structures.

The first of these studies is a fundamental study in seismology. The remainder conveniently divide into ground motion studies and structural response studies and may involve the use of instrumentation for either the research or monitoring function.

CRITERIA FOR NETWORK DESIGN

The development of criteria for the planning and design of networks and arrays of instrumentation to measure ground motions involves the following steps: (1) the ground motions must be estimated; (2) the costs of operations must be evaluated; and (3) the benefit to be derived from the data must be assessed. A similar process is also required as the first step in the process of planning instrumentation arrays for structures (Rojahn, 1976).

The estimation of ground motions involves a determination of the tectonic setting, the seismicity of the region, and the recurrence of strong ground motions. This is similar to the process of obtaining ground motions for use in analyses of seismic risk or for use in establishing design levels for critical facilities (Algermissen and Perkins, 1972; Hays, et al, 1975). In this basic approach to estimating ground motions, the source characteristics are modeled in terms of the recurrence of earthquakes of different magnitudes; the transmission of the motion is modeled as an attenuation of peak acceleration; and the motion at the site is obtained as a recurrence relation for particular site conditions (see fig. 1). More refined techniques are the subject of current research in which the source characteristics are modeled in terms of the expected stress drop and source dimension; the transmission of the motion is modeled in terms of the wave propagation, attenuation, and dispersion; and the site effects are modeled in terms of their influence on the spectral characteristics of the motion.

Several authors have gathered a considerable amount of data indicating that for appropriately large source regions, the recurrence of earthquakes of different magnitudes can be represented as straight lines on semi-log plots (see Algermissen, 1969, for example). On the other hand, the existing data on the attenuation of strong ground motions indicate that there is a considerable amount of scatter in the relation of the peak acceleration, velocity, or displacement to the distance from the source. Figure 2 presents the attenuation of maximum acceleration with distance from the source for all of the data recorded during the San Fernando earthquake (see Maley and Cloud, 1971). An order of magnitude difference may be seen in the peak accelerations recorded at any one distance. Figure 3 presents the attenuation of peak accelerations with distance from the epicenter for all data recorded at Ferndale, Calif., during the past 40 years. A considerable amount of scatter is evident in this plot also. This large amount of scatter in

the data casts some doubt on the validity of the simplified model of transmission of motion.

The availability of data from several stations that have been installed for about 40 years provides a more direct approach to the evaluation of the recurrence of strong ground motions. For example, the results obtained from Ferndale are shown in figures 4 and 5. In figure 4, the cumulative numbers of events for which peak accelerations have exceeded selected levels are plotted versus the year in which the event occurred. The levels of peak acceleration used in figure 4 were selected to illustrate the approach used. Similar results can be obtained for each of the levels of peak acceleration recorded at this site. No attempt has been made to distinguish between foreshocks, main events, and aftershocks in compiling these data. Straight lines have been fitted to the data, and the slopes of these lines define the "events per year" for each of the selected values of peak acceleration.

All levels of peak acceleration from the complete set of records obtained at Ferndale were used to construct figure 5, in which the cumulative distribution of events per year is plotted versus the peak acceleration values. The end points are shown as circles in this figure, signifying an insufficiency in these data. (The value at a peak acceleration of 10 cm/sec^2 appears to be too low as a result of the fall off in the number of low level events that are recorded by an instrument that is triggered by the event being recorded, whereas the values for the highest peak accelerations are obtained from fewer than five events, and this is considered to be an insufficient amount of data). The amount of scatter in the data in figure 5 is relatively small compared with the amount of scatter indicated by the attenuation plots in figures 2 or 3.

Data of the type shown in figure 5 have been obtained for all of the strong-motion instrument sites that have been in place for about 40 years (table 1). Only in three cases (Ferndale, Hollister, and El Centro) are the data sufficient to provide statistically meaningful results for peak accelerations up to 100 cm/sec^2. Of equal importance, however, is the fact that at several sites in these "seismically active" areas, no estimate of recurrence could be made after 40 years of recording. For example, in the San Francisco Bay region, no reliable estimates of recurrence could be made for Golden Gate Park or San Jose, although a maximum value of greater than 100 cm/sec^2 has been recorded at each site. In the Los Angeles basin, no reliable estimates can be made for Westwood or Pasadena.

Similarly, although 12 records have been obtained at Helena, Mont., only three of these have been recorded since 1940 and none since 1960. The results in California are in sharp contrast to other estimates of recurrence that yield equal rates along most segments of the San Andreas fault. These results are also an indication of the serious difficulties in any attempt to provide a rational plan for obtaining the desired strong-motion records: potentially damaging earthquakes in any one area occur infrequently, and our basic understanding of the processes and recurrence of potentially damaging ground motions is therefore inadequate.

The cost of maintenance has been found to be about three times the cost of the instruments themselves (depreciated over a 20-year life). As a result, the procedures used in instrument maintenance need to be critically evaluated. In particular, the service interval may be lengthened if an evaluation indicates that this will not result in serious depreciation in either the quality or number of records recovered. The results of a study of the length of the service interval is shown in figure 6. In the early days of the program, a service interval of 2 months had been established. As the numbers of instruments being maintained dramatically increased in the late 1960's, this interval was perforce increased to 3 months. More recently, a general policy of servicing at a nominal 4- month interval has been adopted (a selected group of instruments are being serviced at 6-month intervals). Since the current cost figures are based on a nominal 3-month service interval, an increase to a 6-month interval will significantly decrease the maintenance costs, although they are not expected to decrease by half since it is planned that more time should be spent at each instrument when the service interval is lengthened. As a part of the evaluation of maintenance procedures, all of the older instruments are being replaced with modern instruments, and the modern types of instruments in service are being modified to bring them up to present specifications. This upgrading of the instruments should raise the lower of the two sets of lines shown in figure 6.

From the recurrence data summarized in table 1 and the average costs of instruments and maintenance ($400 per year), the costs per record for records with peak accelerations greater than specified amounts can be obtained (see table 2). At most sites, the cost doubles as the level of peak acceleration doubles. Estimates of these costs for other sites must be determined if planning criteria are to be firmly established. Since peak accelerations on the order of 200 cm/sec^2 are the minimum levels of potentially damaging motions, significant costs must be anticipated if we are to record potentially damaging

levels of ground motion at many of these sites.

The benefits that will be derived from the data that will be obtained must be estimated in order to assess the proper significance of these costs. Obviously, the first set of data that will permit some of the unanswered questions regarding the nature of the strong ground motions from earthquakes in the eastern part of the United States will be of considerable benefit, whereas additional records at 50 cm/sec^2 obtained at many of the sites in California are of little benefit. It is clear, in general, that those studies that can be accomplished in the more active areas may cost one tenth as much as they would in other areas of California. Thus, studies of local site effects should be planned for Ferndale, Hollister, and El Centro, if the local soil conditions permit. Studies of low-rise buildings should be conducted in these same regions, whereas studies of high-rise buildings can be conducted only in the San Francico or Los Angeles areas.

GENERAL OBSERVATIONS

Most of the strong-motion records obtained to date have been obtained in California, and the techniques for estimating ground motion spectra are largely based on these records. Preliminary evaluations for other regions of the United States suggest that the Mississippi embayment and Yellowstone Park regions may provide as much data, and as inexpensively, as some of the less active areas of California. On the other hand, high maintenance costs in Alaska offset the advantage of the generally high level of activity in that region.

General information on the influence of local site conditions on the spectral amplitudes of ground motion may be obtained from the regional networks by placing instruments in different geologic settings or at sites with different soil conditions. More detailed studies will require an expensive instrumentation program including down-hole instruments. These should be conducted in regions where the seismic activity is sufficiently high to insure an adequate return on the investment in instrumentation and its maintenance.

Similarly, instrumentation designed to study soil failures through liquefaction or landsliding can be incorporated into the regional arrays if areas subject to soil failure are identified. Remotely recording instruments should be placed on the area of potential landslide or liquefaction as well as on nearby stable ground. Extensive instrumentation for these studies should be installed only in highly active areas.

The information necessary to assess the costs of obtaining strong-motion data from all parts of the world should be assembled so that the greatest benefit may be derived for all concerned with earthquake hazards and the loss of life that has occurred in past earthquakes.

REFERENCES

Algermissen, S. T., "Seismic Risk Studies in the United States", Proceedings Fourth World Conf. on Earthquake Engr., Santiago, Chile, 1969.

Algermissen, S. T. and Perkins, D. M., "A Technique for Seismic Zoning", Proceedings Conference on Microzonation, Vol II, Seattle, 1972.

Hays, W. W., et al, Guidelines for Developing Design Earthquake Response Spectra, TR M-114, Construction Engineering Research Laboratory, June 1975.

Maley, R. P., and Cloud, W. K., "Strong-Motion Accelerograph Records", Strong-Motion Instrumental Data on the San Fernando Earthquake of Feb. 9, 1971, Seismological Field Survey and Earthquake Engr. Res. Lab., California Institute of Technology, Pasadena, 1971.

Rojahn, Christopher, "California Building Strong-Motion Instrumentation Program", Proc. Conference on Dynamic Reponse of Structures: Instrumentation, Testing Methods, and System Identification, UCLA, Los Angeles, March 1976.

Table 1 - Recurrence times for stations installed for 40 years

Total Number Years	Number of Records	Maximum Accel cm/sec^2	Station Location	Years/Event		
				a > 25	a > 50	a > 100
					a in cm/sec^2	
40	45	274	FERNDALE	1.5	3	6
40	11	230	EUREKA	8	(15)	-
40	3	124	GOLDEN GATE PARK	-		
39	6	52	ALEXANDER BUILDING	(20)	-	
39	11	48	SOUTHERN PACIFIC BLDG	(10)	-	
40	6	45	OAKLAND CITY HALL	(12)	-	
40	6	56	BERKELEY	(15)	-	
41	4	138	SAN JOSE	-		
30	32	191	HOLLISTER	2	4	8
40	9	172	SANTA BARBARA	10	-	
40	3	100	WESTWOOD	-		
40	7	220	HOLLYWOOD	(30)	-	
40	9	110	OCCIDENTAL BLDG	14	-	
41	11	210	VERNON	10	20	-
41	10	250	LONG BEACH	10	(25)	-
40	4	100	PASADENA	-		
40	10	46	COLTON	12	(25)	-
41	24	314	EL CENTRO	3	6	12
41	9	30	SAN DIEGO	(20)	-	
40	13	38	BISHOP	8	-	
36	7	42	HAWTHORNE	10	-	
38	12	115	HELENA	-		

Numbers in parentheses are based on an insufficient amount of data.

Table 2 - Summary of costs per record

Station Location	Maximum Accel cm/sec^2	Cost/Record in Dollars		
		a > 25	a > 50	a > 100
			a in cm/sec^2	
FERNDALE	274	600	1200	2400
EUREKA	230	3200	(6000)	-
GOLDEN GATE PARK	124	-		
ALEXANDER BUILDING	52	(8000)	-	
SOUTHERN PACIFIC BLDG	48	4000	-	
OAKLAND CITY HALL	45	(4800)	-	
BERKELEY	56	(6000)	-	
SAN JOSE	138	-		
HOLLISTER	191	800	1600	3200
SANTA BARBARA	172	4000	-	
WESTWOOD	100	-		
HOLLYWOOD	220	(12000)	-	
OCCIDENTAL BLDG	110	5600	-	
VERNON	210	4000	8000	-
LONG BEACH	250	4000	(10000)	-
PASADENA	100	-		
COLTON	46	5000	(10000)	-
EL CENTRO	314	1200	2400	4800
SAN DIEGO	30	(8000)	-	
BISHOP	38	3200	-	
HAWTHORNE	42	4000	-	
HELENA	115	-		

Numbers in parentheses are based on an insufficient amount of data.

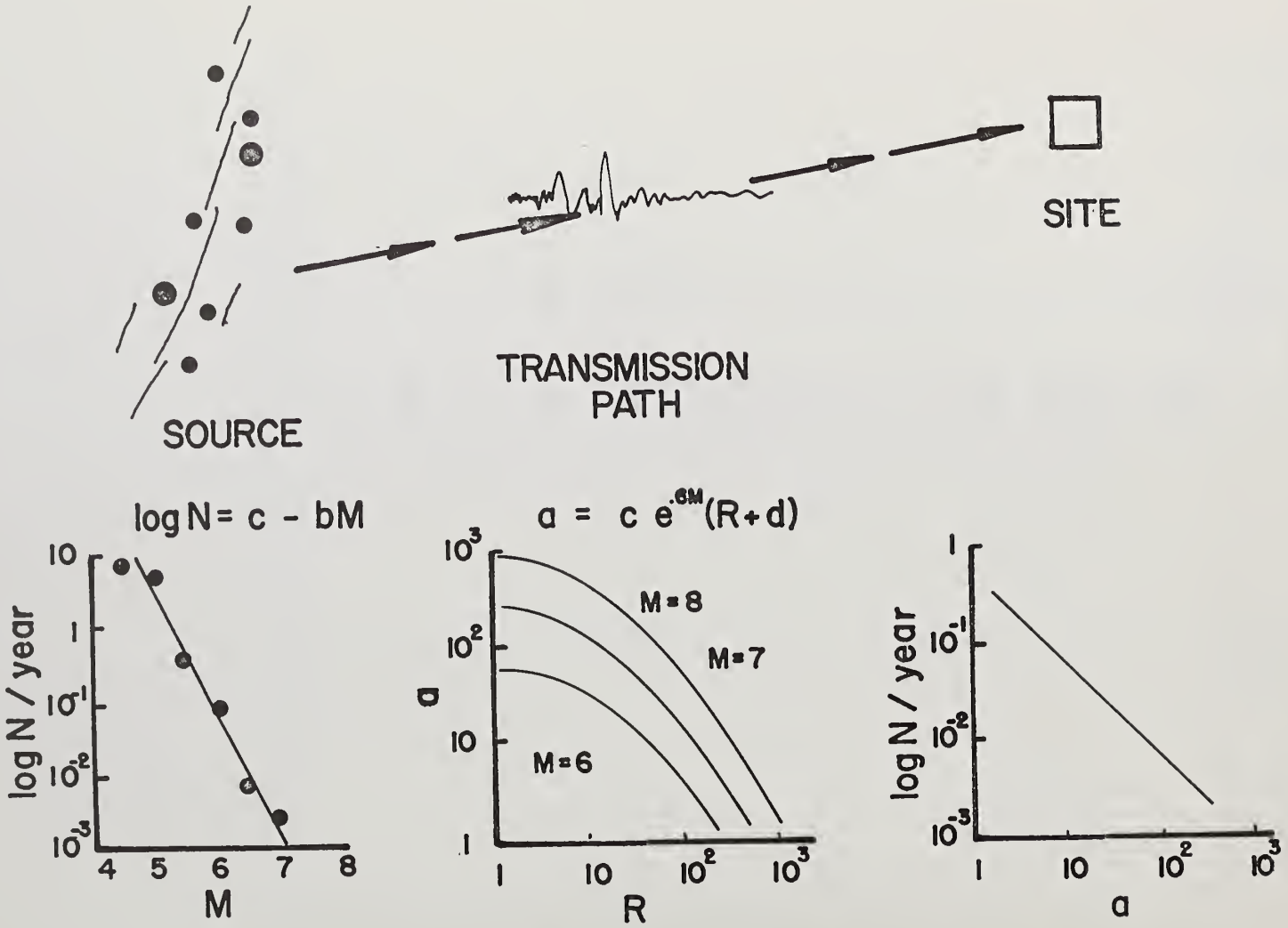

Figure 1. SCHEMATIC MODEL OF TRANSMISSION OF MOTION FROM SOURCE TO SITE

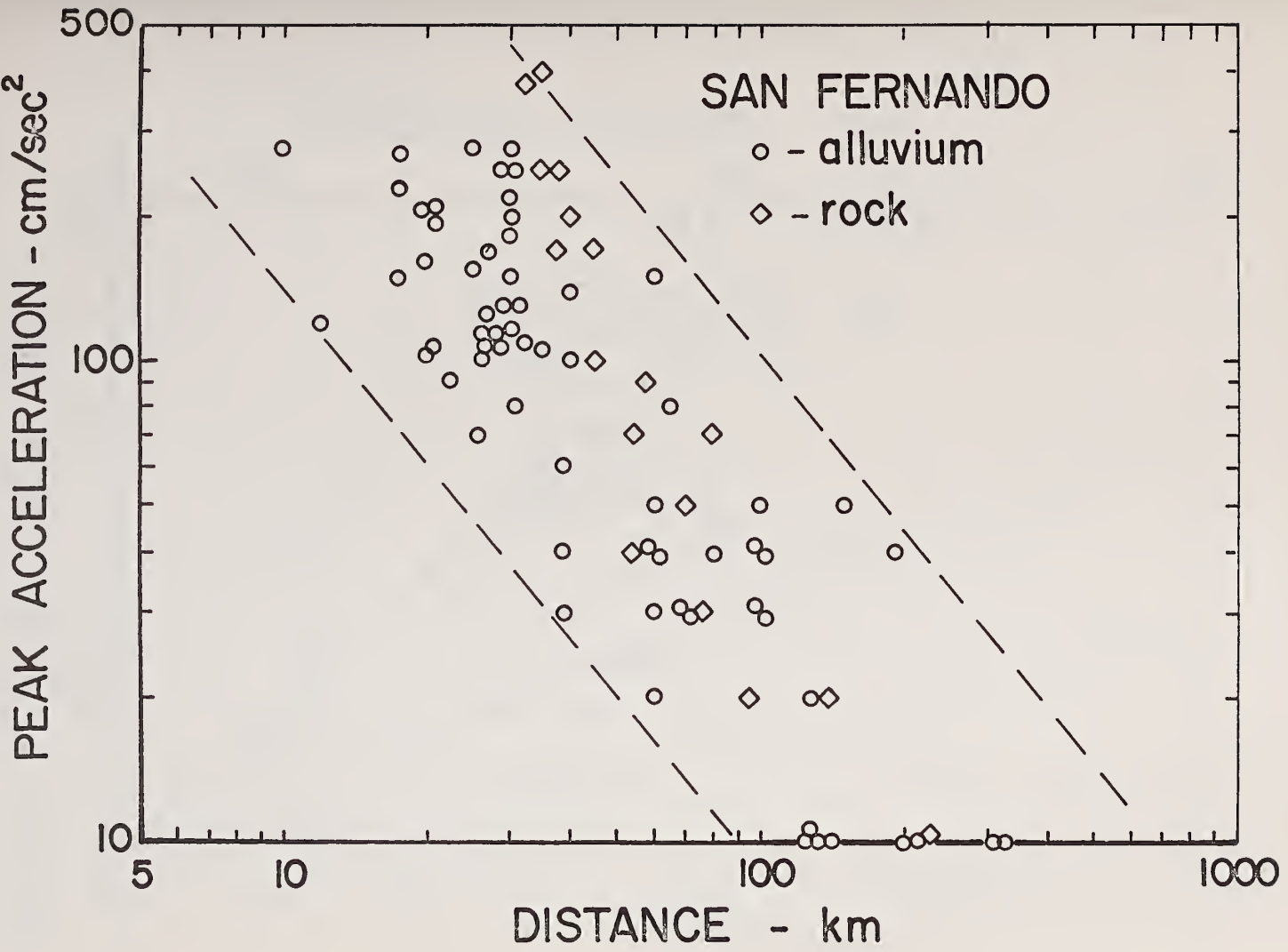

Figure 2. ATTENUATION OF PEAK ACCELERATION WITH DISTANCE - SAN FERNANDO EARTHQUAKE

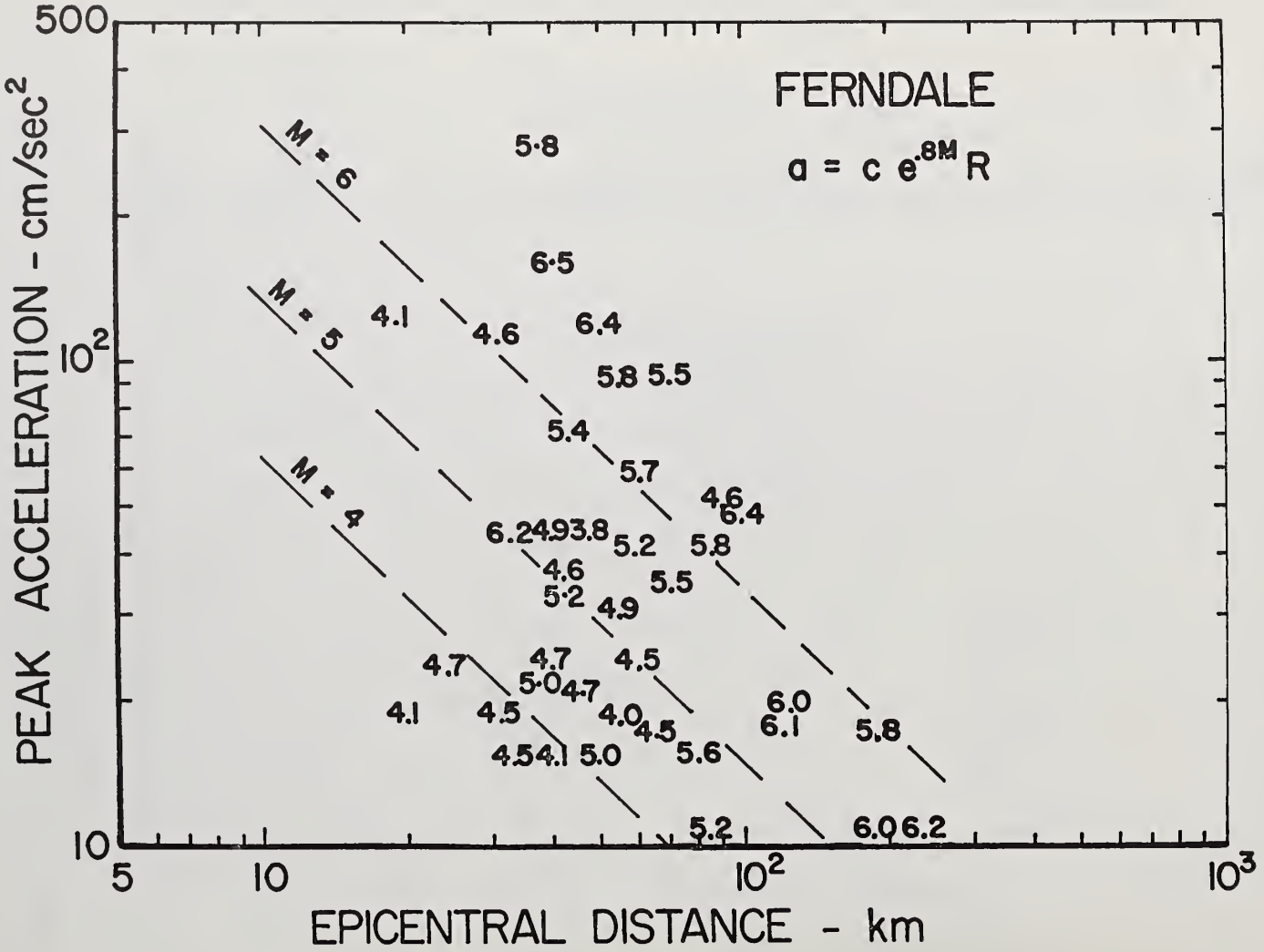

Figure 3. ATTENUATION OF PEAK ACCELERATION WITH DISTANCE - FERNDALE RECORDS

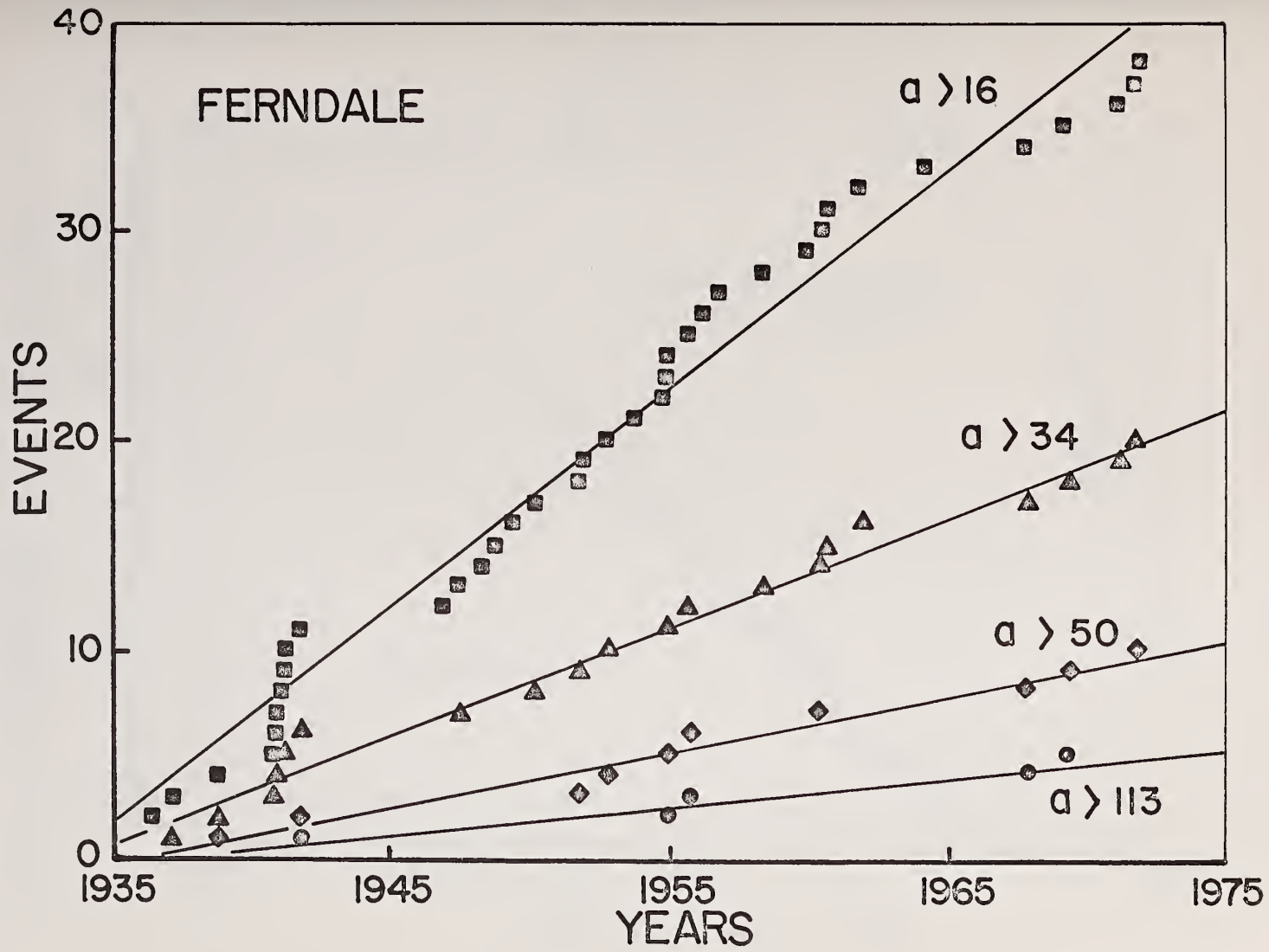

Figure 4. CUMULATIVE NUMBER OF EVENTS VERSUS TIME - FERNDALE RECORDS

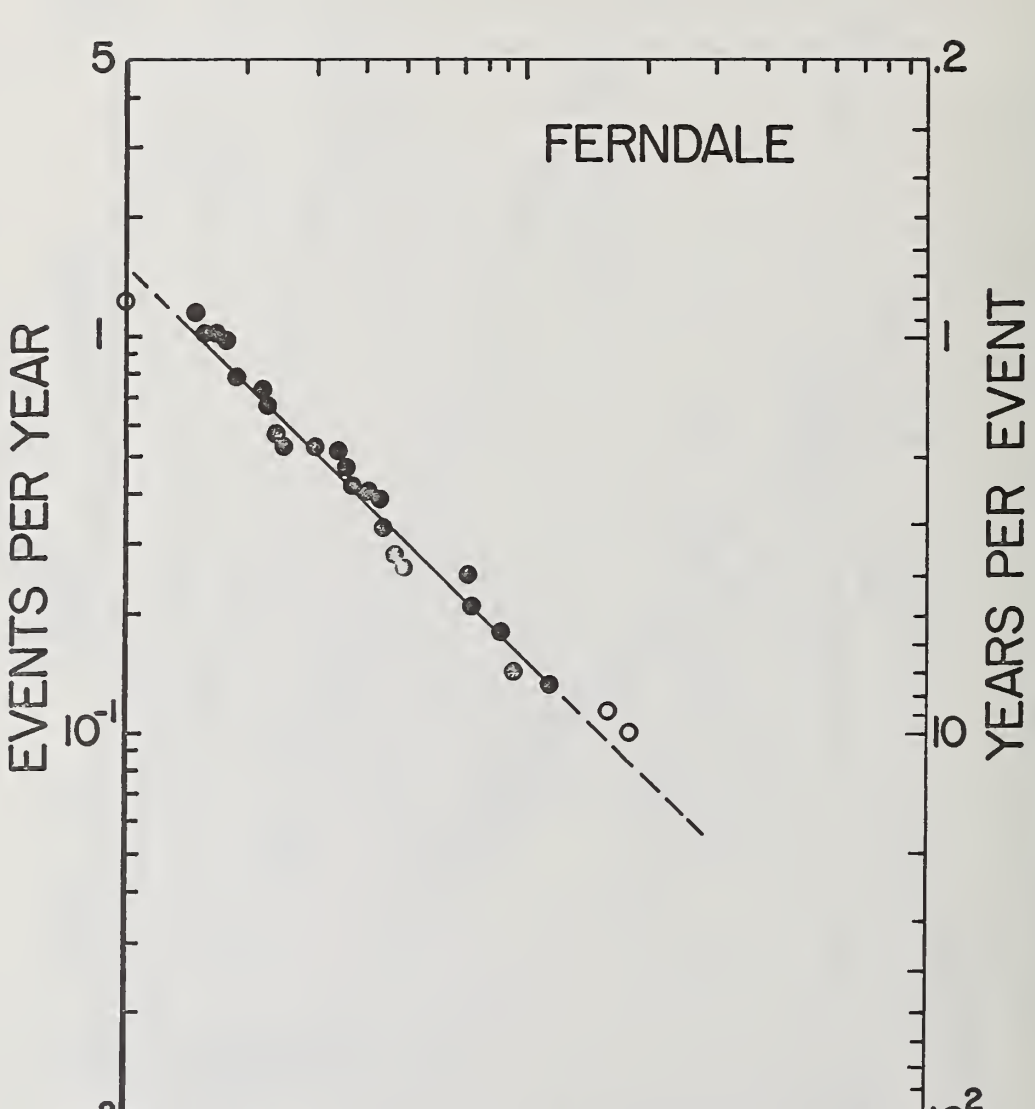

Figure 5. EVENTS PER YEAR VERSUS PEAK ACCELERATION - FERNDALE RECORDS

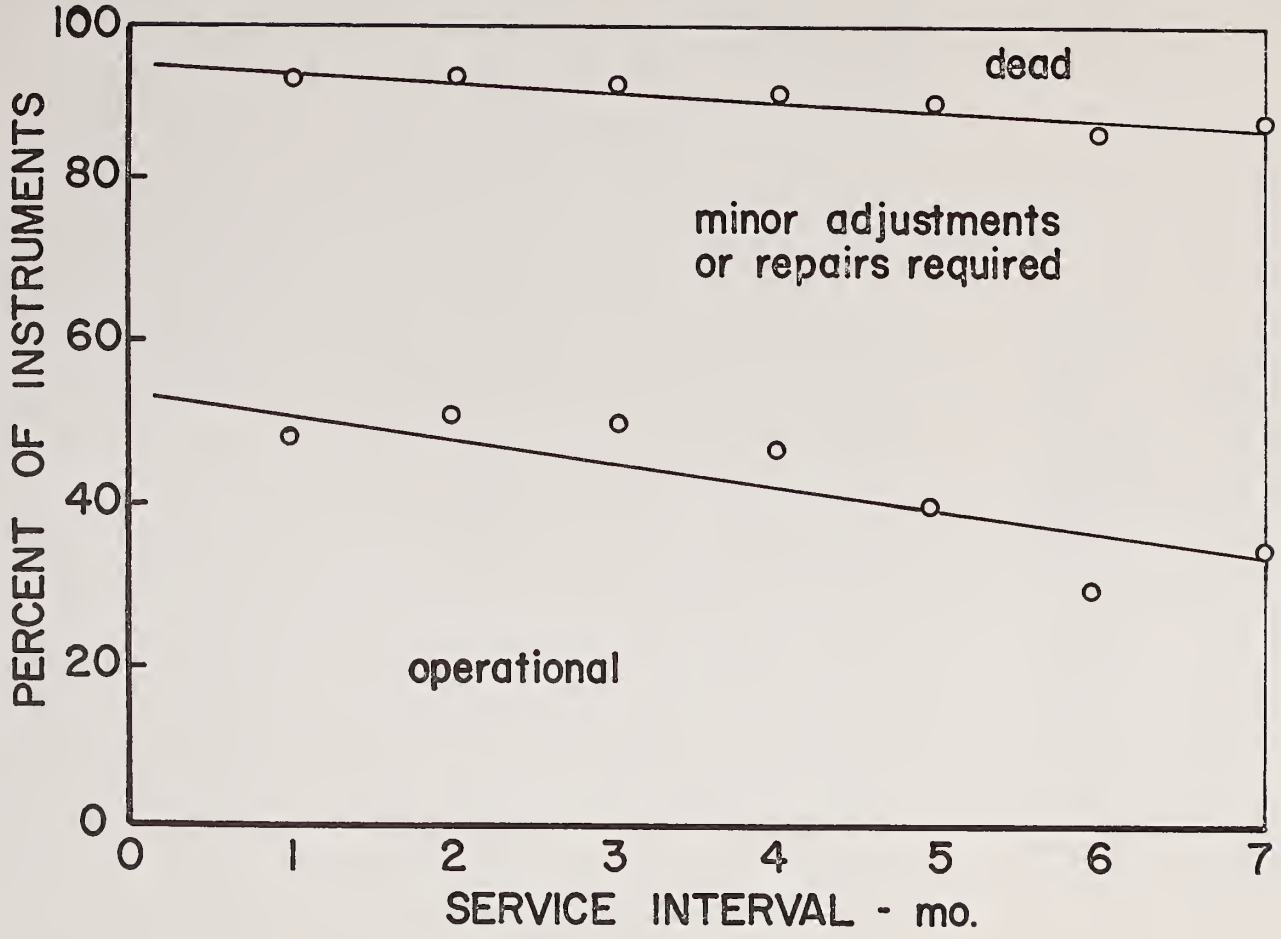

Figure 6. INSTRUMENT STATUS FOR DIFFERENT SERVICE INTERVALS

OBSERVATION OF EARTHQUAKE RESPONSE OF GROUND WITH HORIZONTAL AND VERTICAL SEISMOMETER ARRAYS

SATOSHI HAYASHI
Head, Structures Division
Port and Harbour Research Institute
Ministry of Transport, Japan

HAJIME TSUCHIDA
Chief, Earthquake Resistant Structures Laboratory
Structures Division
Port and Harbour Research Institute
Ministry of Transport, Japan

EIICHI KURATA
Earthquake Resistant Structures Laboratory
Structures Division
Port and Harbour Research Institute
Ministry of Transport, Japan

ABSTRACT

A horizontal seismometer array, having six observation points along a straight line of 2500 meters in length, have been established at the Tokyo International Airport. Each observation point is equipped with two horizontal seismometers. Downhole seismometer arrays have also been established at two points, one at the end of the observation line and the other at a point 500 meters inside from the other end of the line. The observation started in April 1974 and since then 28 earthquakes has been recorded as of June 1975. Correlations among the ground motions at the points on the ground surface and the two points in the ground where the downhole seismometers have been installed, have been studied. The relative displacements between the points have also been studied.

It was assumed that there had been a straight pipeline made of steel along the observation line and the pipe motions had been equal to the observed ground motions. Then, the stresses in the pipe were estimated, and it was found that the stresses due to axial deformations were remarkably larger than those due to the bending deformations.

Key Words: Arrays, Earthquakes, Ground motion, Records, Results, Seismometers.

1. Introduction

The Earthquake response analysis of ground over an area where a structure extends has been recognized to be important and investigated by researchers and practicing engineers. This is very important especially for extending structures such as pipelines and subaqueous tunnels. Stresses in such structures due to earthquake ground motions depend not only on acceleration but also on the relative displacement of the ground along the route. For that reason, the earthquake response analysis of the ground along extended structures is important.

The data to be collected during earthquake studies should include the simultaneous recording of earthquake ground motions at several points distributed along a line or in an area. The strong motion earthquake instruments currently being operated in the world, however, are installed to record ground motions at separate points. Only a few observations of earthquake ground motions, with seismometers arranged along lines, have been utilized to obtain basic field data (1, 2).

The authors have established a horizontal seismometer array which consists of six sets of seismometers located at an equal spacing of 500 meters along an observation line of 2500 meters in length. Each set has two horizontal seismometers. Two downhole seismometer arrays also have been established. The observation system was briefly reported at the 6th Joint Meeting, U.S.-Japan Panel on Wind and Seismic Effects, U.S.-Japan Cooperative Program in Natural Resources (3).

The observations were started in April 1974 and as of June 1975, 28 earthquakes have been recorded. In this paper, some observation results and analyses of three of the 28 earthquakes will be presented. Observations, however, are being continued as is the analysis.

2. Seismometer Arrays

The horizontal seismometer array has been established in the Tokyo International Airport, parallel to the C-runway, as shown in Fig. 1. The soil profile beneath the array is shown in Fig. 2; the profile was constructed by engineering geologists based on the two borings made for installation of the downhole seismometers and 69 borings which had been made for planning and construction of the airport facilities.

The seismometers, to observe ground surface motions, are installed at six observation points, designated as points A through F shown in Fig. 1. The distance between adjoining points is 500 meters and total length of the observation line is 2500 meters. Each point is equipped with transducers to observe the longitudinal and transverse components of ground accelerations. At the points A and E the vertical seismometer arrays are installed; the lower seismometers are at depths 67.2 meters and 49.6 meters below the ground surface respectively. The downhole seismometers have three transducers to observe longitudinal, transverse, and vertical components of the ground accelerations.

All the seismometers are of moving coil type where the output are recorded with four electro magnetic oscillographs. Frequency ranges of the seismometers (within 10%) are 0.1 to 35Hz for the seismometers on the ground surface and 0.5 to 50Hz for the downhole seismometers. The oscillograms were digitized for analyses with a computer on-line digitizer at equal time intervals of 0.01 seconds.

3. Observation Results

Parameters of the three earthquakes, which are designated as TIA-3, TIA-6, and TIA-9, included maximum accelerations at the observation points and other parameters are listed in Table 1. The locations of the epicenters are shown in Fig. 3, in which the direction of the horizontal seismometer array is indicated as D.H.A. The ground acceleration

records (longitudinal component) of the earthquake TIA-3 at the points A, C, and E are shown in Fig. 4, which is a computer plot of the digitized records.

4. Displacement

Displacements of the earthquake ground motions were calculated from the observed acceleration time histories. For the calculation, operation of a seismograph to the observed ground acceleration was simulated with an analog computer. The seismograph has a pendulum with a natural period of 6.0 seconds and amped at 55% of critical. The seismograph that was used is also being used in the network by the Japan Meteorological Agency. Filtering was applied to the input and the output of the simulated seismographs in order to eliminate components with periods longer than 10 seconds. The procedure used to calculate the displacement was compared with the procedure developed at the California Institute of Technology in the United States in their processing of strong motion accelerograms. The displacements calculated by both procedures agrees very well, when the difference between the frequency ranges of the integrations in both procedures are taken into account.

The calculated displacements for the earthquake TIA-3 are shown in Figs. 5 and 6. It can be seen from these figures that the displacement time histories, at all the observation points, are very similar to each other. The wave forms of the earthquake TIA-6 was similar to earthquake TIA-3 as shown in Figs. 5 and 6. However, earthquake TIA-9 did not show any similarity as the case of the other earthquakes. The maximum ground displacements at the points are listed in Table 1.

From the calculated ground displacements, the relative displacements of the two points adjoining each other were examined. The maximum relative displacements are listed in Table 1.

5. Wave Propagation

The cross correlation functions were calculated between the time histories of the calculated ground displacements at the points. The time-shifts for maximum correlation were then obtained, as given in Table 2. The time histories at point F were used for all calculations of the cross correlation function.

If it is assumed that the waves propagated from the epicenters straight along the ground surface, the velocities of the wave propagations are estimated as 5.3, 5.9, and 4.4 km/sec for the earthquakes TIA-3, TIA-6, and TIA-9, respectively. It should be noted, however, that regardless of the locations of the epicenters the cross correlation analysis implies that the waves will arrive at point F sooner than at point A.

Fig. 7 is a hodograph at point E from 10 to 20 seconds after the origin of the record of the earthquake TIA-3.

6. Stresses in Underground Pipeline

Based on the earthquake records, induced stresses in steel pipelines due to the ground motions were calculated. In performing these calculations the following assumptions were made: 1) steel pipes of different diameters were buried in the ground along the observation line. 2) displacements of the pipes at the observation points were equal to the ground displacements calculated from the recorded ground accelerations.

Maximum axial strains of the pipes were calculated from the maximum relative longitudinal displacements between two adjoining observation points. Where the axial strain means a strain due to the longitudinal component of the ground motion. The axial strain was assumed to be uniform between the two points.

In calculating the maximum bending stresses, using the deflection curves of the pipelines, were estimated as follows; three adjoining observation points were selected and a parabolic curve was fitted to the displacements at the three points. This curve was considered as the deflection curve of the pipelines, and the maximum bending strain in a segment of the pipelines under consideration was then calculated. This procedure was applied to four combinations of the observation points and for different 0.01 second time intervals, over significant part of the ground motion records. Then, with the maximum bending strain of the earthquake under consideration, the largest value was selected among the maximum bending strains calculated for different segments and times.

The calculated maximum axial strains and the maximum bending strains were converted into stresses and listed in Table 3.

Engineering requirements for oil pipelines have been established under Oil Pipelines Enterprise Law (5, 6), and a design formula to estimate stresses in steel pipelines due to earthquake ground motions is given. Comparison ratio of the maximum acceleration recorded by the downhole seismometers to the acceleration of gravity was taken as a design seismic coefficient. Stresses were then calculated by the formula in the assumed pipelines along the observation line with the results shown in Table 3. In these calculations the displacement of pipeline was considered to be equal to that of the ground. It will be noted, however, that other engineers may reach slightly different results with the same formula, since the details of application of the formula depends on judgement of each engineer.

7. References

1) Akio Sakurai, Tadashi Takahashi, Hajime Tsutsumi, Hiroshi Yajima, Toshiro Noguchi, and Toru Iwakata: Dynamic Stresses of Underground Pipelines during Earthquakes (A Study Based on the Observed Records in the Matsushiro Earthquakes), Report No. 67058, Technical Laboratory, Central Research Institute of Electric Power Industry, 1967.

2) Choshiro Tamura, Katsuyuki Kato, and Hiroshi Maeda: On Characteristics of Earthquake Ground Motion along a Line on Soft Ground, Proceedings of the 29th Annual Meeting for Research Presentations, The Japan Society of Civil Engineers, Part I, October 1974.

3) Satoshi Hayashi and Hajime Tsuchida: Observation and Analysis of Ground Response in Earthquakes, Proceedings of the 6th Joint Meeting, U.S.-Japan Panel on Wind and Seismic Effects, U.S.-Japan Cooperative Program in Natural Resources, May 1974, Washington, D.C.

4) M.D. Trifunac and V.W. Lee: A Note on the Accuracy of Computing Ground Displacements from Strong-Motion Accelerograms, Bulletin of the Seismological Society of America, Vol. 64, No. 4, August 1974, pp. 1209-1219.

5) Ministrial Ordinance on Engineering Requirements for Facilities for Oil Pipelines Enterprise, Ordinance No. 2 of Ministry of International Trade and Industry, Ministry of Transport, Ministry of Construction, and Ministry of Automomy, 1972.

6) Ministrial Notification on Details of Engineering Requirements for Facilities for Oil Pipelines Enterprise, Notification No. 1 of Ministry of International Trade and Industry, Ministry of Transport, Ministry of Construction, and Ministry of Autonomy, 1973.

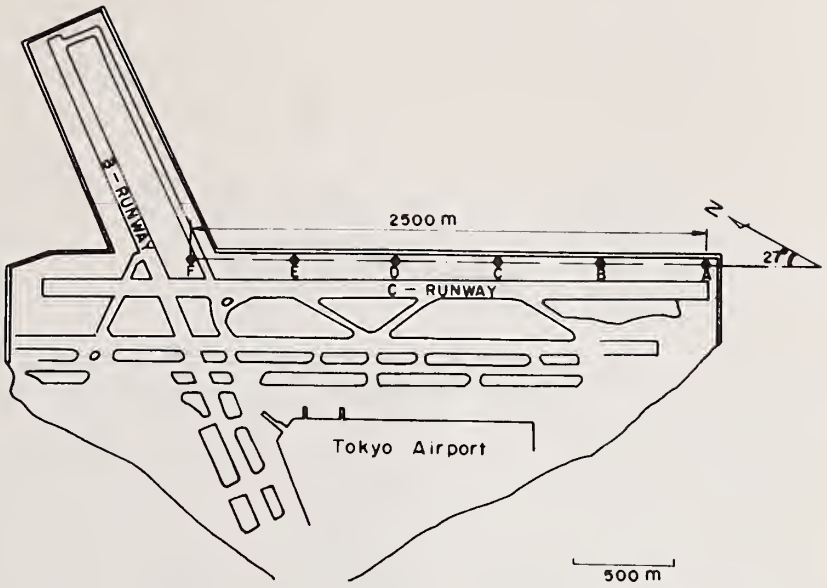

Fig. 1 Plan of seismometer array site

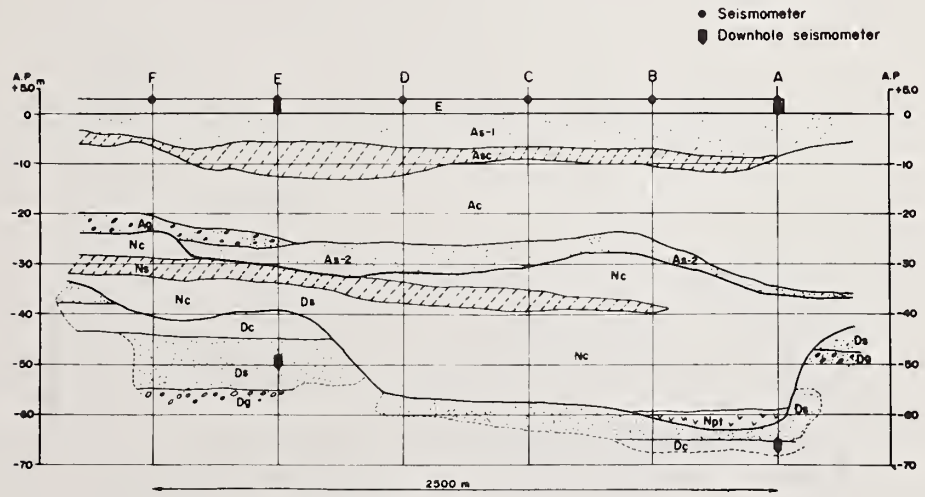

Key (Fill) E:Fill, (Alluvial deposit) A_{s-1}:Sand, A_{sc}:Silty sand
A_c:Silty clay, A_{s-2}:Sand, A_g:Sandy gravel, (Diluvial deposit)
N_c:Silty clay, N_s:Silty sand, N_{pt}:Peat, D_s:Sand,
D_g:Sandy gravel, D_c:Silt

Fig. 2 Soil profile at seismometer array site

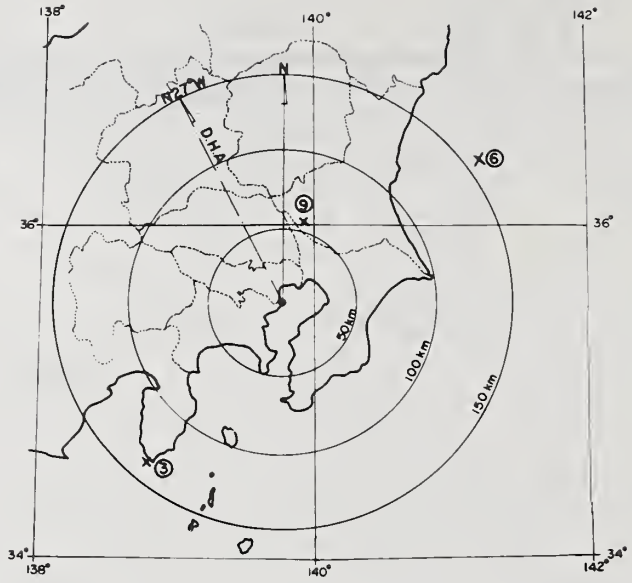

Fig. 3 Locations of epicenters of earthquakes TIA-3, 6, and 9

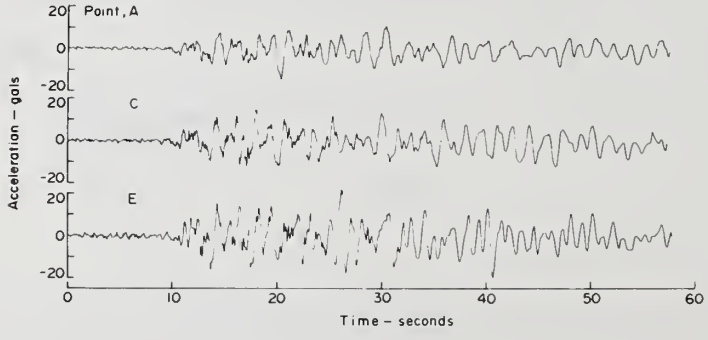

Fig. 4 Acceleration records at points A, C, and E
Earthquake TIA-3, Longitudinal component

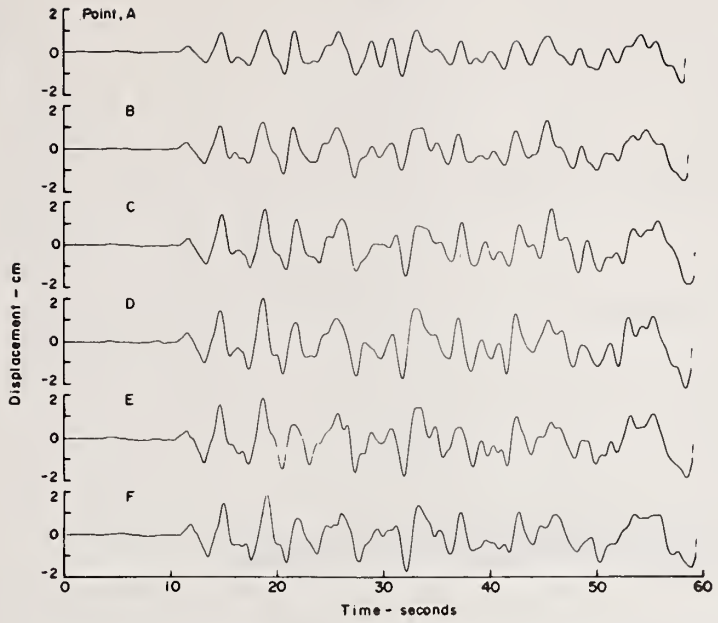

Fig. Ground displacements, Earthquake TIA-3, Longitudinal component

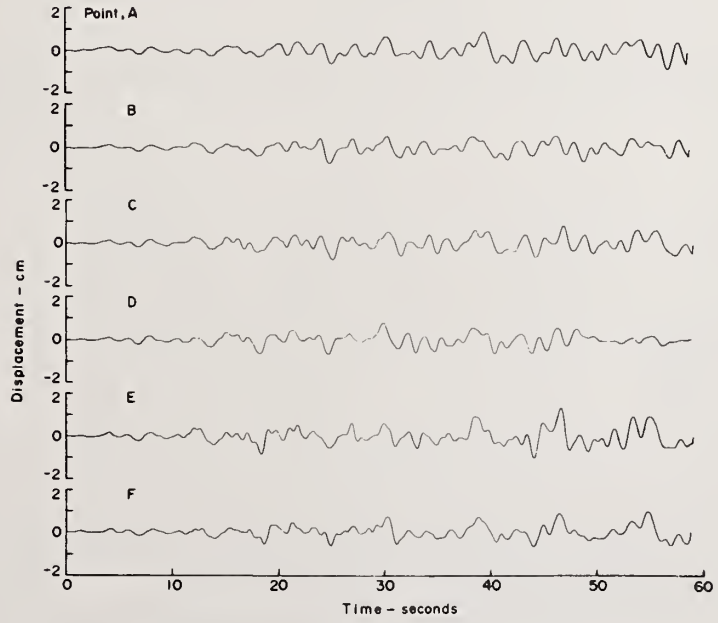

Fig. 6 Ground displacements, Earthquake TIA-3, Transverse component

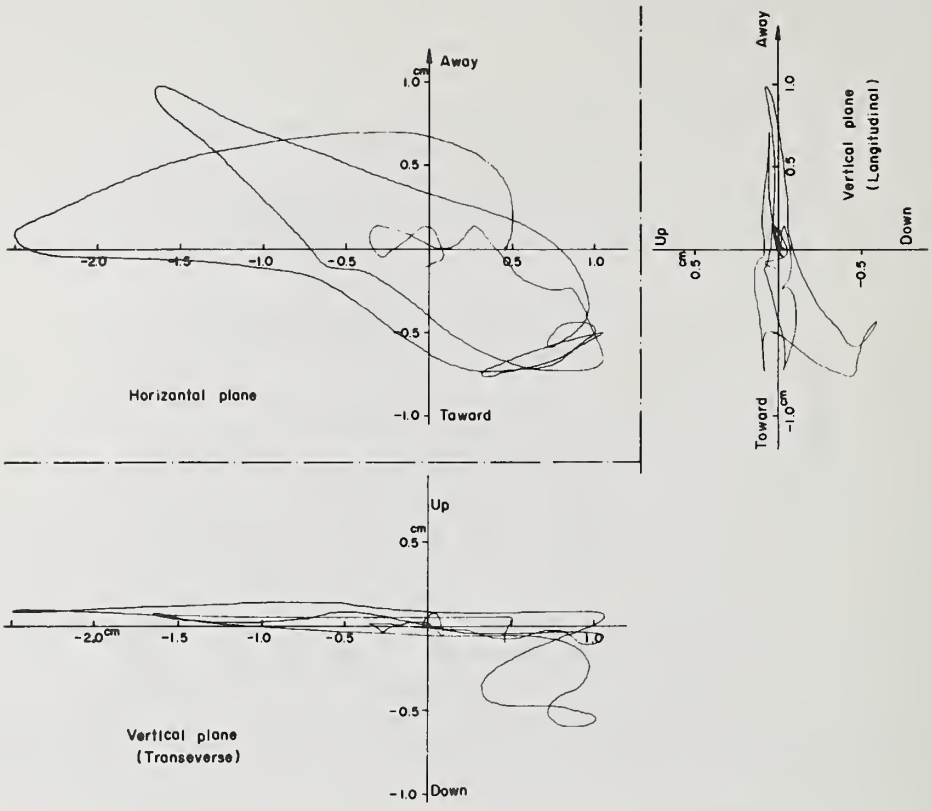

Fig. 7 Hodograph at point E, Earthquake TIA-3, from 10 to 20 seconds after origin of record

Earthquake	TIA-3		TIA-6		TIA-9	
Obser. or design*	Obs.	Des.	Obs.	Des.	Obs.	Des.
Axial stress	3040	9120	2840	6080	2060	21280
Bending stress						
Diameter: 20 cm	1	30	0	21	1	71
: 60 cm	3	91	1	61	4	213
:100 cm	6	152	2	101	7	310
Total stress**	3040	16080	2840	10790	2060	37560

Unit:kN/m^2 (International unit system, 1kg/cm^2 =98.0665kN/m^2)
* Obser.:Stress derived from observed ground motions.
Design:Stress derived from design formula.
** In calculation of total stress only axial stress is taken into acco

Table 3 Comparison of observed and design stresses in underground pipeline due to earthquake ground motions

Record designation	TIA-3		TIA-6		TIA-9	
Date	May 9, 1974		July 8, [illegible]4		Aug [illegible] 4, 1974	
Time	08:33		14:15		03:[illegible]	
Hypocenter	Near S Coast		Off Ibaraki		SW Ibaraki	
Location	of Izu Pen.		Prefecture		Prefecture	
Latitude	33.6°N		36.4°N		36.0°N	
Longitude	138.8°E		141.2°E		139.[illegible]°E	
Depth	10 km		40 km		50 km	
Magnitude	6.9		6.3		5.8	
Epicentral distance	140 km		161 km		54 km	
Component	Long.	Tran.	Long.	Tran.	Long.	Tran.
Maximum acceleration in gals						
Point A	15.0	9.1	6.4	6.1	20.6	24.6
B	14.0	9.8	11.4	8.3	47.3	35.8
C	16.2	12.8	9.6	7.5	36.6	31.0
D	21.7	11.2	11.7	9.1	29.3	22.5
E	23.2	19.2	10.7	11.[illegible]	51.8	32.4
F	18.5	13.0	11.7	11.[illegible]	40.9	34.7
Maximum displacement in cm						
Point A	1.34	0.91	0.52	0.63	0.40	0.38
B	1.48	0.76	0.59	0.83	0.42	0.87
C	1.83	0.85	0.54	0.[illegible]	0.63	0.52
D	2.14	0.81	0.81	0.79	0.46	0.39
E	1.96	1.26	0.49	0.83	0.4[illegible]	0.58
F	1.92	0.94	0.51	0.66	0.5[illegible]	0.55
Maximum relative displacement in cm						
Points A & B	0.50	0.59	0.16	0.[illegible]	0.[illegible]	0.31
B & C	0.37	0.64	0.19	0.[illegible]	0.22	0.87
C & D	0.71	0.61	0.13	0.25	0.51	0.34
D & E	0.74	0.53	0.32	0.21	0.34	0.27
E & F	0.64	0.64	0.[illegible]	0.24	0.23	0.26

Table 1 Earthquakes, maximum accelerations, maximum displacements, and maximum relative displacements

Earthquake	Component	Points				
		F-A	F-B	F-C	F-D	F-E
TIA-3	Longitudinal	0.18	0.15	0.15	0.[illegible]9	0.0[illegible]
	Transverse	0.20	0.17	0.16	0.01	0
TIA-6	Longitudinal	0.15	0.11	0.[illegible]8	0.02	0
	Transverse	0.18	0.12	0.11	0	0
TIA-9	Longitudinal	0.44	0.3[illegible]	0.17	0.12	0
	Transverse	0.43	0.25	[illegible].23	0.[illegible]0	0.0[illegible]

Table 2 Time-shift for maximum correlation in second

Building Strong-Motion Earthquake Instrumentation

CHRISTOPHER ROJAHN
U.S. Geological Survey, Menlo Park, California

ABSTRACT

Based on the recommendations of a special ad-hoc committee, twenty-one geographic areas will be instrumented under the building instrumentation phase of the California Strong-Motion Instrumentation Program, a statewide program established by law in 1971 and funded through an assessment of estimated construction costs collected statewide from building permits. The areas were selected on the basis of population density, locations of buildings already instrumented, and the probability for potentially damaging earthquakes. Buildings to be instrumented will be of typical construction, simple in framing and design, and of various heights with the instrumentation of low-rise buildings emphasized. Remote recording instrumentation, consisting of single or multiaxial accelerometers connected via data cable to a central recorder, will be installed in each building. The accelerometers will be placed on the lowest level, at the roof level, and, in many cases, at one or more intermediate levels. The instrumentation will be situated so as to separately record both translational and torsional response.

On the basis of current projected revenues, and instrument procurement, installation and maintenance expenses, it is estimated that as many as 400 buildings may be instrumented under the State program.

Key Words: Buildings, Instruments, Strong Motion

INTRODUCTION

In 1971 the State of California established a Strong-Motion Instrumentation Program to assure the development of a scientifically sound distribution of strong-motion instruments throughout the State. The California Division of Mines and Geology (CDMG) operates the program with the advice of an Advisory Board. Funding is provided by a .007 percent (7¢ per $1000) assessment of estimated construction costs collected statewide from building permits.

During the first two years the program was in effect (1972-73), the instrumentation of ground or "freefield" sites was emphasized and all available funding was used to purchase and install strong- motion accelerographs for that purpose. In 1974, with the "freefield" instrumentation phase of the program well established, a large segment of the available funding was channeled for use in instrumenting buildings, the second priority of the program. At the request of the CDMG and its Advisory Board, a set of detailed guidelines for selecting and instrumenting buildings was developed by a special ad-hoc committee. Those guidelines, their background and subsequent implementation, are the subject of this paper. Similar guidelines, not discussed herein, have also been developed for a third phase of the program in which dams throughout the State are being instrumented.

The basic objectives for the building instrumentation phase of the State program were adopted by the Advisory Board's Site Selection Committee in mid-1973 as follows: to place a high priority on instrumenting buildings in Zone III of the Preliminary Map of the Maximum Expectable Earthquake Intensity in California, figure 1 (Alfors, Burnett, and Gay, 1973), and a lower priority on instrumenting buildings in Zone II; to place the highest priority on instrumenting buildings located within five miles of the major faults along which there is significant activity; to seek the assistance of the Structural Engineers Association of California in selecting buildings to be instrumented under the program; to select representative types and heights of buildings; to instrument many buildings moderately rather than a few buildings extensively; and to use remote recording accelerograph systems with accelerometers located so as best to record both translational and torsional response of each building. With these objectives and at the request of the Site Selection Committee, the specially appointed ad-hoc committee (the Subcommittee on Instrumentation for Structures) developed a series of guidelines defining where, which types, and how buildings should be instrumented under the program. Those guidelines, discussed in detail below, are now being implemented.

GEOGRAPHIC DISTRIBUTION OF INSTRUMENTED BUILDINGS

In adopting its objectives for the building instrumentation program, the Site Selection Committee stipulated that areas within Zone III (zone of maximum expected intensity) of the Preliminary Map of Maximum Expectable Earthquake Intensity in California, and especially areas within five miles of the major active fault zones, should be given highest priority for the instrumentation of buildings. In light of these stipulations and considering population densities, locations of buildings in which strong-motion instrumentation had already been installed, and a best-educated-guess on the probability for potentially damaging earthquakes in various areas throughout the State, the Subcommittee on Instrumentation for Structures established a list of 21 areas recommended for instrumentation and suggested how many buildings should be instrumented in each area (expressed as a percentage of the total number of buildings to be instrumented). With the exception of the highly populated San Diego area, all selected areas were either in or immediately adjacent to Zone III. The area along the Hayward fault between Milpitas and Geyserville was selected for the largest number of buildings because of the high concentration of buildings adjacent to the fault, high probability for potentially damaging earthquake activity, and lack of existing instrumented buildings. The area along the San Andreas fault between Los Gatos and Fort Bragg was chosen for similar reasons. In Los Angeles, where a large number of mid- and high- rise buildings have already been instrumented under the terms of the city ordinance, the concentration of buildings and probability for potentially damaging earthquake activity were also considered to be high and the need to instrument low-rise buildings was considered to be great. A slightly lower number of buildings were recommended along the Calaveras fault system as it extends from San Jose to Napa, along the San Jacinto fault from Cajon Pass to Hemet and from Hemet to El Centro, and along the San Andreas fault from Cajon Pass to Calipatria. These areas were considered to have a high probability for potentially damaging earthquake activity, moderately dense populations, and few instrumented buildings. In the remaining selected areas, a relatively small number of buildings were recommended because of lower population densities and postulated lower potential for seismic activity.

Because of the manner in which seismic waves propagate and attenuate in the California region (high frequencies tend to attenuate more quickly with distance than lower frequencies, which tend to be more pronounced away from the source of energy release) and

the fact that the natural periods of vibration of buildings are approximately proportional to the number of stories (the higher the building, the longer the fundamental period), recommendations were made on the distribution of the height of instrumented buildings relative to the distance from potentially active faults. Those recommendations, shown in table 1, suggest that instrumented low-rise buildings (one to six stories) should be within 10 miles (16 km) of the fault of interest, that most of the instrumented mid-rise buildings (seven to fifteen stories) should be within a 25-mile (40-km) range, and that most of the instrumented high-rise buildings (greater than fifteen stories) should be in the 5- to 25-mile (8- to 40-km) range.

SELECTION OF TYPES AND HEIGHTS OF BUILDINGS

In its interpretation of the legislation creating the State program, the Advisory Board indicated that one of the primary objectives should be to provide data on which to base improvements in engineering design practice. In light of this objective and the general stipulation that representative buildings throughout the State should be instrumented, it was recommended that: all major building types, construction techniques, and materials should be equitably represented; each instrumented building should be relatively simple in framing and design so that the response can be readily interpreted; and the instrumentation of low-rise buildings should be emphasized.

In regard to building type, an attempt was made to ascertain an equitable distribution of the types of buildings shown in table 2. No recommendations were made with regard to date of design or construction although it was believed that the instrumentation of buildings designed since the Long Beach earthquake of 1933 should be emphasized.

With respect to the percentage distribution of instrumented building heights, it was suggested that 28% of the instrumented buildings should be in the one to two-story range, 32% in the three to six-story range, 26% in the seven to fifteen-story range, and 14% greater than fifteen stories (table 1). This distribution reflects the attitude that low-rise buildings (one to six stories) should make up 60% of the total number of buildings instrumented under the State program. The emphasis on low-rise buildings stems from the fact that they are vastly more numerous throughout the State than their high-rise counterparts, and that they have historically been more hazardous when subjected to strong ground shaking (all known deaths in the 1971 San Fernando earthquake, for example,

occurred in low-rise buildings). Furthermore, relatively few low-rise buildings had been instrumented prior to the development of the State program.

SELECTION AND PLACEMENT OF INSTRUMENTS IN BUILDINGS

In general, it was recommended that all buildings instrumented under the State program should be instrumented using remote recording instrumentation, consisting of single or multiaxial accelerometers connected via data cable to a central recorder(s), and that the accelerometers should be installed at locations prescribed by the guidelines for instrumenting buildings developed by the author and R. B. Matthiesen (Rojahn and Matthiesen, 1975).

Remote recording systems were recommended rather than triaxial optical-mechanical self-contained accelerographs (triaxial accelerographs are presently required by the city of Los Angeles and other municipalities that adopted similar ordinances) because remote recording systems give greater flexibility for accelerometer placement, space requirements are minimized, and the recorder can be centrally located for easy maintenance and record retrieval. Furthermore, triaxial systems like those presently required by the city of Los Angeles do not provide enough data to isolate translational and torsional response, a capability that forced-vibration tests (Goebler, 1969; Hart, DiJulio and Lew, 1974; Jennings, Matthiesen and Hoerner, 1972) as well as analyses of records from the 1971 San Fernando earthquake (Blume and Associates, 1973; Gates, 1973) indicate is vital even in highly symmetrical buildings.

As a minimum, accelerometers should be placed on the lowest level and at the main roof level. On the lowest level, it is recommended (as a minimum) that three orthogonal accelerometers (two horizontal and one vertical) be attached firmly to the foundation or floor near the center of plan with the horizontal accelerometers oriented parallel to the transverse and longitudinal axes of the building. If the foundation conditions are such that differential horizontal motion may occur (Yamahara, 1970), one or more additional horizontal accelerometers are recommended. In a building that is large and relatively square in plan, two additional accelerometers should be positioned along and parallel to two adjacent outside walls, whereas in a building that is very long in comparison with its width, one additional accelerometer positioned and parallel to one of the outside end

walls may be sufficient (figure 2a). If the building has a rigid mat foundation and rocking motion is expected, two additional vertical accelerometers are recommended. These should be positioned so that rocking motion can be recorded along any azimuth, i.e., one vertical accelerometer should be positioned in each of three corners of the building (figure 2b). In a building that is quite large in plan with significantly varying foundation conditions, it is recommended that additional triaxial packages be installed on the different foundation materials.

Instrumentation at the main roof level, as well as at all instrumented intermediate floors, should consist of an array of remote horizontal accelerometers arranged so as separately to record both translational and torsional motion. If the roof or instrumented floor is very stiff and is expected to be rigid in the horizontal plane, only three horizontal accelerometers are required. A biaxial pair should be located at the predicted or known center of rigidity so as to record pure translational motion along the transverse and longitudinal axes of the building. The third accelerometer should be positioned along and parallel to the most distant outside end wall so as to record torsional motion (figure 3a). If the roof is not expected to be rigid in the horizontal plane, one or more additional horizontal accelerometers is recommended. The location of each of these will be dependent upon the expected response of the roof (floor). For example, in the case of a rectangular-plan exterior shear-wall building with the roof (floor) diaphragm flexible in the transverse direction and not in the longitudinal direction, one additional accelerometer is recommended. It should be positioned so as to facilitate the interpretation of relative motion in the transverse direction between the end walls and the center of the roof (floor) diaphragm (figure 3b). Because the most significant motions in building response to strong ground shaking are normally in the horizontal direction, vertical accelerometers are not felt to be as crucial above ground level as horizontal accelerometers. If vertical response is of interest, however, vertical accelerometers sufficient in number to determine all significant relative motions should be installed. In masonry-wall buildings, for example, where ultimate strength is a function of bearing stress (Mayes and Clough, 1975), the vertical accelerometers should be aligned vertically on the wall(s) of interest at various heights throughout the building, including the lowest level. Likewise, if the vertical response of a floor slab or beam is of interest (in any type of building), multiple vertical accelerometers should be installed at the slab edges, or

beam ends, and the mid-span.

The number of intermediate levels at which instrumentation should be installed is a functon of the structural framing system, number of stories, architectural configuration and known dynamic characteristics of the building. Unless mode shapes have been predetermined by forced-vibration or in-depth ambient vibration tests and intermediate level instrumentation is not considered to be necessary, instrumentation should be placed at as many intermediate floors as is economically feasible because the accuracy with which a building's response to earthquake motion can be determined is largely proportional to the number of levels instrumented. As a minimum, it is recommended that at least two intermediate levels be instrumented in buildings having more than six stories above ground and at least one be instrumented in buildings having three to six stories. The level(s) should not coincide, if at all possible, with a nodal point of any of the modes of predominant response (usually some or all of the first four modes). Close examination of the mode shapes in figure 4 indicates the most optimal "anti-node" areas for buildings uniform in plan with height are located at about 25%, 40% and 70% of the above ground building height. If no other information is available, it is recommended that one or two of these levels be instrumented. If, however, mode shapes based on a computerized model of the building are available, such mode shapes should be used to determine the optimal locations. Stiffness discontinuities must also be considered in the process and should be instrumented whenever their effect on mode shapes is unknown. Instrumentation at such locations could either serve as or complement the intermediate level instrumentation recommended as minimal. In some buildings, such as one having a slender tower on a wide base, the discontinuity is obvious, whereas in others, stiffness discontinuities may be revealed only through a thorough investigation of the structural framing system.

Other recommendations designed to enhance and facilitate the analysis of records obtained from instrumented buildings are as follows: "free-field" accelerographs should be located near each instrumented building in order to obtain data on site-structure resonance effects and soil-structure interaction; the CDMG should collect and archive plans, specifications, calculations, and pertinent construction and inspection records for each instrumented building as well as site soil and geology descriptions.

IMPLEMENTATION OF THE PROGRAM

The above guidelines were submitted to the Advisory Board in mid-1974 and approved shortly thereafter with the stipulation that they be regularly updated (perhaps annually) as more geologic, seismological, engineering analysis and other pertinent information becomes available. After approval, the CDMG solicited and received from the Structural Engineers Association of California (SEAOC) a list of 54 buildings to be instrumented under the first phase of the program. The size and location distribution of this first set of buildings (figure 5) are not in exact adherence to the criteria established by the above guidelines, though the basic intent of the guidelines certainly has been met. Significant deviations from the recommended distributions will be rectified in subsequent phases of the program.

On the basis of current projected revenues, and instrument procurement, installation and maintenance expenses, it is estimated that as many as 400 buildings may be instrumented under the State program (California Division of Mines & Geology, unpublished report to the California Legislature). The installation phase of the program is expected to be completed in the year 2035, the time at which program revenues are expected to be sufficient only for covering instrument maintenance (a major cost), personnel (minimal staff), and data analysis expenses.

ACKNOWLEDGMENTS

The author gratefully acknowledges Dr. R. B. Matthiesen of the U.S. Geological Survey and the Subcommittee on Instrumentation for Structures--L. Leroy Crandall, Jack F. Meehan, John O. Robb, Roland L. Sharpe, William M. Wells, and Edwin G. Zacher--for providing the support and advice that made these guidelines possible. Thanks also go to the SEAOC Strong-Motion Instrumentation Committees, chaired by Kenneth K. Honda and John O. Robb, who have assumed responsibility for selecting buildings to be instrumented under the program.

REFERENCES

Alfors, J. T., Burnett, J. L. and Gay, T. E., Jr., 1973, Urban geology master plan for California: California Division of Mines and Geology Bulletin 198, p. 20.

Blume, John A. and Associates, 1973, Sheraton-Universal Hotel, Bank of California, Holiday Inn (Orion Avenue), Holiday Inn (Morengo Street), Bunker Hill Tower: San Fernando, California Earthquake of February 9, 1971, ERL/NOAA/U.S. Dept. of Commerce, v. 1, p. 307-444.

Bowkamp, J. G. and Blohm, J. K., 1966, Dynamic response of a two-story frame structure: Seismol. Soc. America Bull., v. 56, p. 1289-1303.

Gates, W. E., 1973, KB Valley Center, Muir Medical Center, Kajima International Building, Certified Life Building: San Fernando, California Earthquake of February 9, 1971, ERL/NOAA/U.S. Dept. of Commerce, v. 1, p. 449-574.

Goebler, H. W., 1969, Three-dimensional modeling and dynamic analysis of the San Diego Gas and Electric Company Building: California Univ., Los Angeles, M. S. thesis, 72 p.

Hart, G. C., DiJulio, R. M., Jr. and Lew, M., 1974, Torsional response and design of high-rise buildings: Cincinnati, Ohio, ASCE Structural Engineering Convention Meeting Preprint, 30 p.

Jennings, P. C., 1969, Spectrum techniques for tall buildings: World Conference on Earthquake Engineering, (4th), Santiago, Chile, Proc., p. 61-74.

Jennings, P. C., Matthiesen, R. B. and Hoerner, J. B., 1972, Forced-vibration of a tall steel-frame building: Earthquake Engineering and Structural Dynamics, v. 1, p. 107-132.

Mayes, R. L. and Clough, R. W., 1975, Cyclic shear tests on fixed-ended masonry piers: New Orleans, Louisana, ASCE National Structural Engineering Convention Meeting Preprint, 30 p.

Moran, D. F. and Bockemohle, L. W., 1973, History and philosophy of California earthquake codes and elements of lateral force design: San Fernando, California Earthquake of February 9, 1971, ERL/NOAA/U.S. Dept. of Commerce, v. 1, p. 24.

Rojahn, C. and Matthiesen, R. B., 1975, Guidelines for strong-motion instrumentation of buildings: presented at the ASCE National Structural Engineering Convention, New Orleans, Louisiana.

Yamahara, Hiroshi, 1970, Ground motions during earthquakes and the input loss of earthquake power to an excitation of buildings: Soils and Foundations (The Japanese Society of Soil Mechanics and Foundation Engineering), v. X, n. 2, 14 p.

Table 1 - Proposed Distribution of Instrumented Buildings as a Function of Distance from Fault of Interest, in percent

Distance from fault in miles (km) \ Number of stories	1-2	3-6	7-15	>15
0-5 (0-8)	16	16	4	0+
5-10 (9-16)	12	16	12	4
10-25 (16-40)	0+	0+	8	8
>25 (>40)	0+	0+	2	2

Table 2 - Recommended Types of Buildings to be Instrumented

I. One and two-story buildings.
   - A. Open frame type - gymnasiums, auditoriums.
   - B. Continuous frame - school classrooms, offices.
   - C. Box structures - commercial masonry or concrete wall structures with flexible diaphragms.

II. Three to six-story buildings.
   - A. Frame.
   - B. Shearwall.
   - C. Combination.
   - D. Precast structural elements.

III. Buildings over six stories.
   - A. Frame.
   - B. Shearwall.
   - C. Combination.

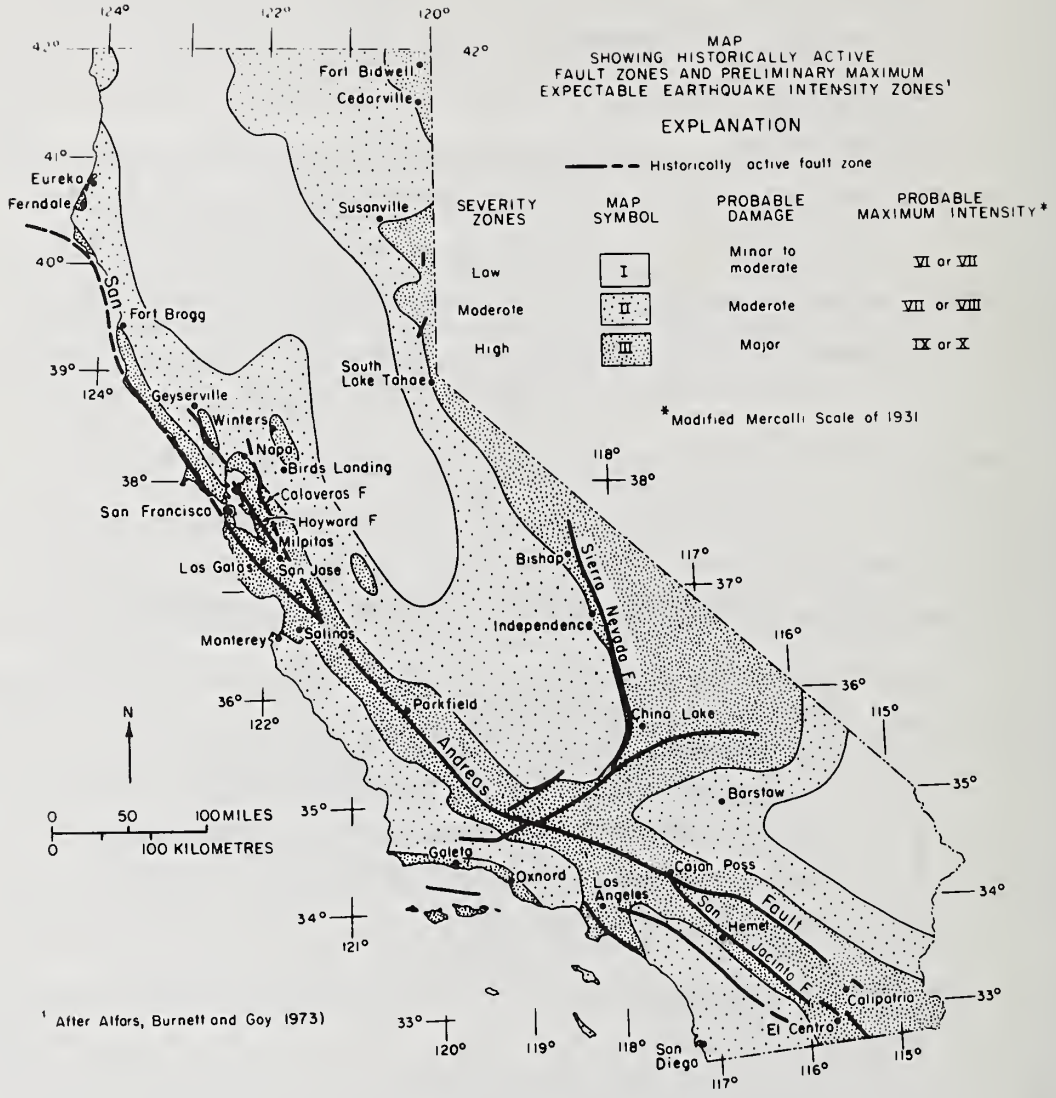

Figure 1.- Map showing historically active fault zones and preliminary maximum expectable earthquake intensity zones (Alfors, Burnett, and Gay, 1973).

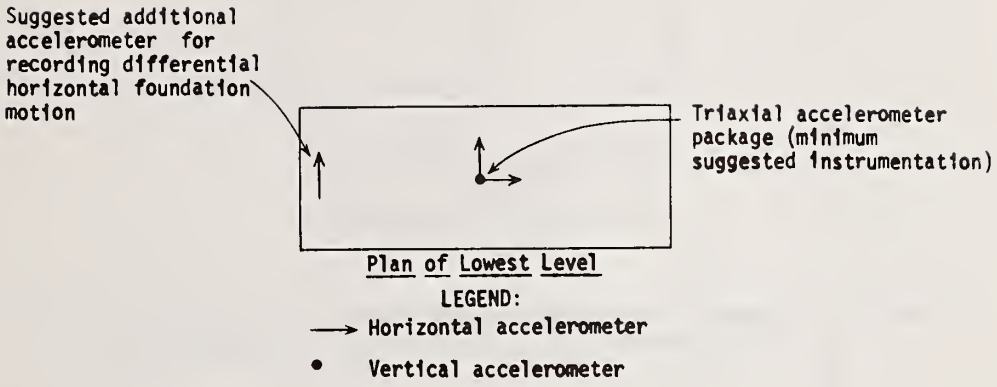

Figure 2a.- Suggested strong-motion instrumentation scheme for recording differential horizontal foundation motion in a building whose length is very large in comparison with its width.

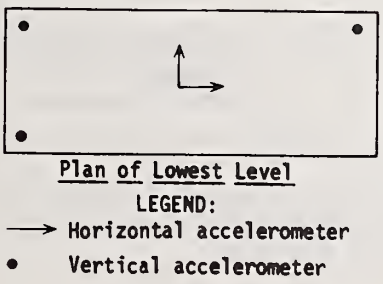

Figure 2b.- Suggested strong-motion instrumentation scheme for recording rocking motion at lowest level.

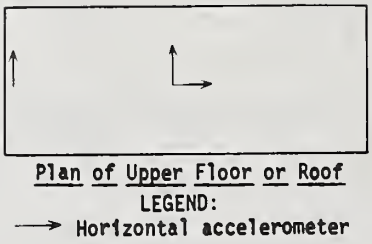

Figure 3a.- Suggested strong-motion instrumentation scheme for roof (or floor) expected to be rigid in the horizontal plane.

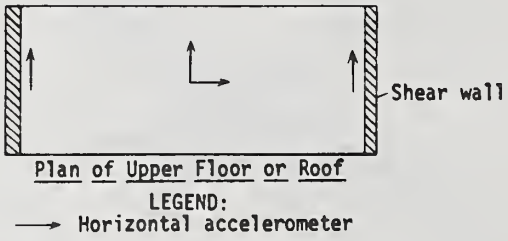

Figure 3b.- Suggested strong-motion instrumentation scheme for roof (or floor) where relative diaphragm motion is expected in the transverse direction.

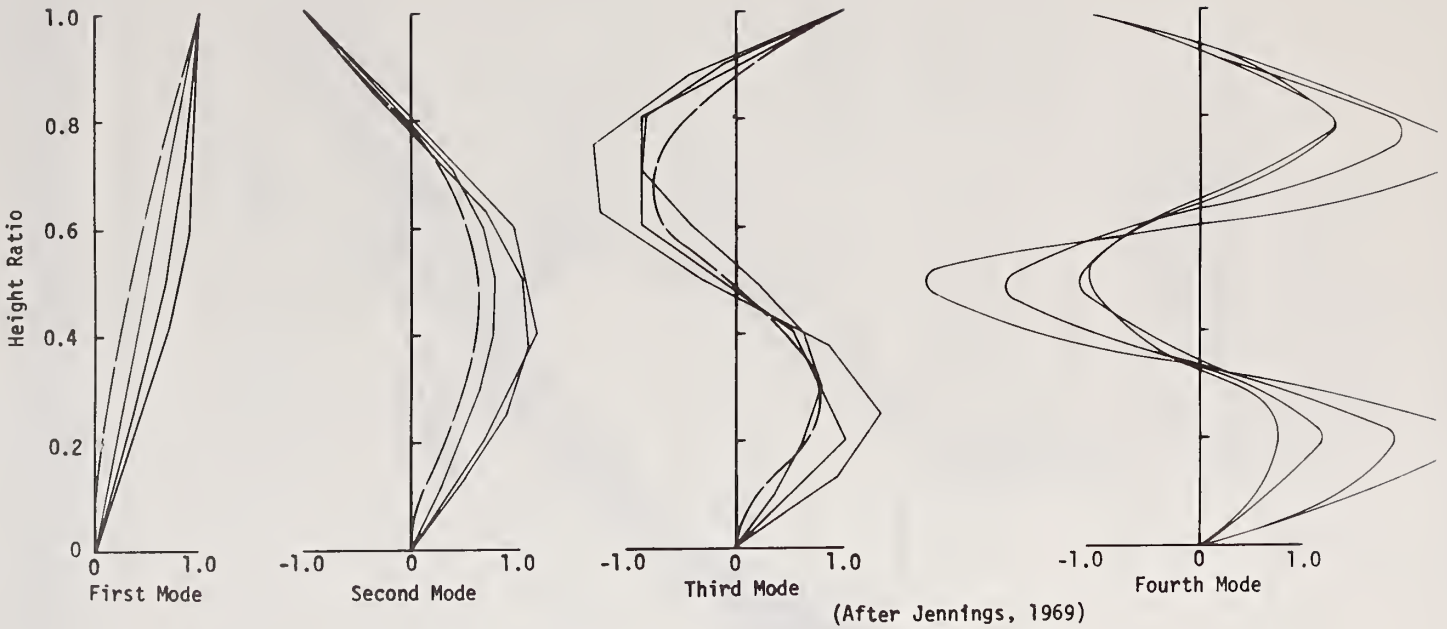

Figure 4.- Experimental and analytical mode shapes for buildings.

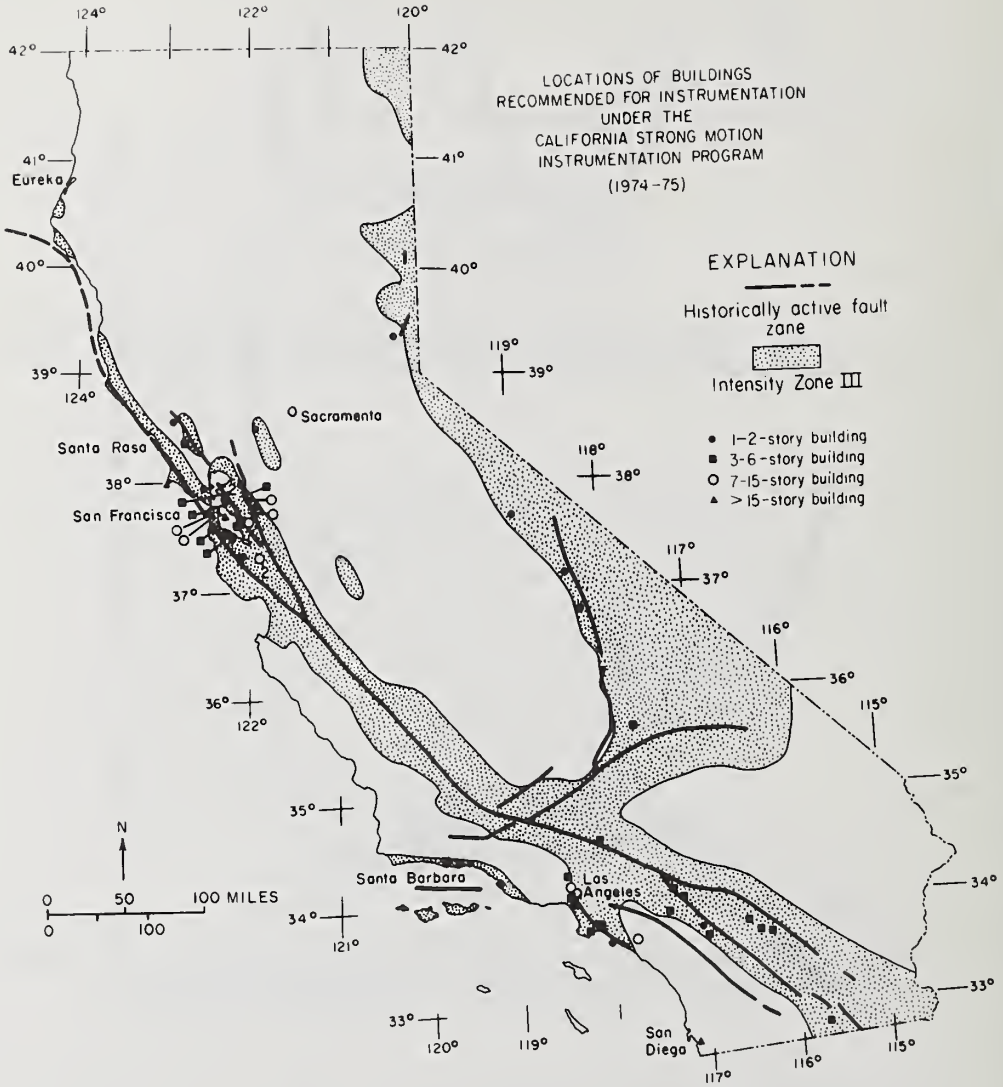

Figure 5.- Locations of buildings recommended for instrumentation under the California Strong-Motion Instrumentation Program (1974-1975).

CHARACTERISTICS OF UNDERGROUND SEISMIC MOTIONS AT FOUR SITES AROUND TOKYO BAY

TOSHIO IWASAKI
Chief, Ground Vibration Section
Public Works Research Institute
Ministry of Construction
4-12-52 Anagawa, Chiba, Japan

SUSUMU WAKABAYASHI
Research Engineer
Public Works Research Institute
Ministry of Construction
4-12-52 Anagawa, Chiba, Japan

FUMIO TATSUOKA
Research Engineer
Public Works Research Institute
Ministry of Construction
4-12-52 Anagawa, Chiba, Japan

ABSTRACT

This paper discusses the dynamic behavior of subsurface soil and rock layers on the basis of acceleration records triggered during actual small to moderate earthquakes. Borehole accelerometers are installed at four sites around the Bay of Tokyo. These were installed in 1970-74, in connection with the Tokyo Bay Loop Highway Project proposed by the Ministry of Construction.

Important acceleration records were obtained during sixteen moderate earthquakes (Magnitude - 4.8 - 7.2) which occurred near the area in September, 1970 through February 1975. From distributions of maximum accelerations at the four stations, it seems that the surface magnification factors (ratios of the surface acceleration to the base acceleration) are large (2.5 to 3.5) at the soft clayey soil site, small (about 1.5) at the rocky site, and medium (1.5 to 3) at sandy soil sites.

Response spectrum curves from typical acceleration records are shown. Comparison of the spectral curves from records obtained at three (or four) levels of one station during an earthquake suggests that frequency characteristics at the several depths are comparatively similar. Also it seems that frequency characteristics of earthquake ground motions are influenced by seismic conditions (such as magnitudes, epicentral distances, etc) as well as soil conditions at the sites.

Key Words: Acceleration records; dynamic behavior; earthquakes; response spectra, soils.

1. Introduction

At the present there are more than 200 strong motion accelerographs (mostly SMAC type) installed at the ground surface of various sites throughout Japan, which provide us with ground motion records during strong earthquakes. The number of stations, however, where borehole seismometers are installed in the underground is comparatively less. To analyze the dynamic behavior of the soil layers during earthquakes, the measurements of the earth-

quake motions at the deeper levels below the ground surface seem very important. This paper intends to present the results of seismic observation with use of borehole accelerometers installed at four stations around Tokyo Bay.

2. Outline of Observation Stations

The Public Works Research Institute and the Kanto Regional Construction Bureau have been measuring underground seismic motions at four stations around the Bay of Tokyo (1). As shown in Fig. 1 the stations are located in Futtsu Cape, Chiba Prefecture; Ukishima Park; Kawasaki City; Kannonzaki, Yokosuka City; and Ohgishima, Yokohama City. These were installed in 1970 through 1974, in connection with the Tokyo Bay Loop Highway Project proposed by the Ministry of Construction.

Depths of the borehole accelerometers and soil profiles at the four stations are shown in Figs. 2 and 3 respectively. At the site of Futtsu Cape, where a comparatively uniform sand layer exists, 3-component borehole accelerometers are set up at three levels, the surface, -70 m, and -110 m. At Ukishima Park, consisting of reclaimed soils, silts, clays, and sands, four pickups are installed at the surface, -27 m, -67 m, and -127 m. At Kannonzaki, indicating a rocky layer (siltstone) with a shallow topsoil, three accelerometers are set up at the surface, -80 m. and -120 m. Furthermore, at Ohgishima, a newly reclaimed island consisting of deep reclaimed sands and stiff clays, four acceleration transducers are installed at the surface, -15 m, -38m, and -150 m. Each accelerometer has three components - one vertical and two horizontal. Time dependent acceleration waves are triggered on oscillograph papers.

3. Acceleration Records

Table 1 indicates a list of the earthquake records obtained during sixteen small and moderate earthquakes (Magnitude = 4.8 to 7.2) which broke out near the area between 1970 and 1975. In the table the maximum accelerations in the three directions are listed, together with the dates and magnitudes of the earthquakes. In the column of remarks of the table H denotes the hypocentral depths and D means the ranges of the distance from the epicenter to the stations. An example of the records triggered is shown in Fig. 4, which is a set of acceleration records obtained at Ukishima Park during the earthquake (M = 4.8) of September 30, 1970. Most earthquake records including those in Table 1 are digitized, and their spectral characteristics are obtained (2).

4. Distribution of Maximum Accelerations Relative to Depth

The variation of maximum accelerations with respect to depths and the three components, is illustrated in Fig. 5 for six typical earthquakes. The normalized distribution of maximum accelerations are obtained by averaging all data in Table 1. In the upper part of the figure the maximum acceleration at the surface is taken as a unit, and in the lower part the deepest is taken as a unit. From the figures the following conclusions can be derived, relative to the distribution of underground accelerations during small and moderate earthquakes.

(a) The vertical distribution of underground accelerations with respect to depths varies with stations, directions, earthquake properties, etc.

(b) Depths where the accelerations become one half of the surface accelerations at Futtsu Cape, Ukishima Park, Kannonzaki, and Ohgishima are about 70^{m}, 50^{m}, more than 120^{m}, and 150^{m}, respectively.

(c) Accelerations at the deeper layers are close among the values at the four stations. Accelerations at the surface, however, differ greatly among the four stations. Furthermore, accelerations at the deeper layer of each station do not change with respect to depths.

(d) Ratios of the surface acceleration to the deepest acceleration are large (2.5 to 3.5) at the soft clayey soil site (Ukishima Park), small (about 1.5) at the rocky site (kannonzaki), and medium (1.5 to 3) at the sandy soil sites (Futtsu Cape and Ohgishima).

(e) Vertical accelerations are generally smaller (1/3 to 1/2) than the horizontal acceleration.

5. Characteristics of the Response Spectra for Underground Motions

In order to show the frequency characteristics of underground motions, response spectral curves for horizontal components of typical records are illustrated in Fig. 7 (3). The abscissa denotes the natural period of a single degree of freedom system. The ordinate indicates the maximum absolute response acceleration of the system with a damping ratio of 2%, when subjected to time dependent accelerations recorded at respective levels of each station. These spectral curves indicate the following:

(a) It is apparent that frequency characteristics of acceleration records obtained at one station during an earthquake are very similar among the three or four layers of the station.

(b) By comparing (A) with (B) of Fig. 7, it is seen that frequency characteristics at one station considerably differ between records obtained during the two different earthquakes. Fig. 7 (A) shows the spectra at Ukishima Park for a small and near earthquake ($M = 4.8$, $\Delta = 10$ km), and Fig. 7 (B) shows the spectra at the same station for a moderate and distant earthquake ($M = 7.2$, $\Delta = 320$ km). The characteristics of these two spectra are very different.

(c) By comparing the spectra at two stations (whose soil conditions are considerably different, for example, Fig. 7 (B) and (D) during an earthquake, it is seen that the general characteristics are very close, and that the responses in the range of longer periods are predominant at the soft soil site (Ukishima Park).

6. Conclusions

From the analyses of underground seismic acceleration records, obtained during small and moderate earthquakes with magnitudes of 4.8 to 7.2, the following conclusions can be drawn.

(a) The distribution of the maximum accelerations, with respect to depths, changes considerably with the change of soil conditions near the ground surface. Ratios of the

surface acceleration to that at the deeper layer (110 to 150m) are about 1.5 at a rocky ground, 1.5 to 3 at sandy grounds, and 2.5 to 3.5 at a very clayey ground.

(b) Although the acceleration values are smaller at deeper layers, frequency characteristics of underground seismic motions are close to those of the surface motions.

(c) It appears that the characteristics of earthquake ground motions are influenced by seismic conditions such as magnitudes of earthquakes, epicentral distances, etc., as well as soil conditions at the site.

Acknowledgements

The observation of the underground seismic motions described in this paper was realized under the strong promotion of Dr. Tadayoshi Okubo and Mr. Eiichi Kuribayashi at the Public Works Research Institute. The authors appreciate their achievements to attain this project. Acquisition of acceleration records was made by the staff members at the Kanto Regional Construction Bureau, and digitization and computer analysis were conducted with an assistance of Mr. Shunichi Horiuchi, former engineer at the Public Works Research Institute. The authors wish to thank them for their strenuous efforts.

References

1) Toshio Iwasaki, Susumu Wakabayashi, Fumio Tatsuoka, "Seismic Behavior of Subsurface Ground Layers", Proceedings, 4th Japan Earthquake Engineering Symposium, November, 1975, Tokyo, Japan.

2) Toshio Iwasaki, Susumu Wakabayashi, Shunichi Horiuchi, "Strong-Motion Earthquake Records at Undergrounds (Vol 1, Vol. 2)", Technical Memorandum of the Public Works Research Institute No. 1103, March, 1976.

3) Eiichi Kuribayashi, Toshio Iwasaki, Yutaka Iida, Katunari Tuji, "Effects of Seismic and Subsoil Conditions on Earthquake Response Spectra", 5th World Conference on Earthquake Engineering, Rome, Italy, June, 1973.

Table 1 Maximum Accelerations during 16 Moderate Earthquakes Since Sept., 1970 (in gals)

EQ No.	Date Magnitude Epicenter	Component	Futtsu Cape			Ukishima Park				Kannonzaki			Ohgishima				Remarks
			0 m	-70m	-110m	0 m	-27m	-67m	-127m	0 m	-80m	-120m	0 m	-15m	-38m	-150m	
1	9.30,1970 M=4.8 Eastern Kanagawa-ken	NS	28.2	16.0	7.8	11.8	10.7	5.5	4.3								H=40 km △≒10~30km Mouth of Tama River
		EW	29.4	9.8	11.2	17.8	11.2	6.0	3.4								
		UD	8.4	4.2	6.4	7.8	3.8	1.8	2.0								
2	7.23,1971 M=5.3 Eastern Yamanashi-ken	NS	5.6	2.5	2.7	16.8	13.3	5.6	6.4	12.4	5.3	4.9					H=40 km △≒60~80 km
		EW	8.6	2.6	4.3	12.3	11.8	5.0	3.5	6.7	5.5	8.5					
		UD	2.2	1.2	1.3	5.7	3.3	3.0	2.6	5.4	4.1	3.4					
3	2.29,1972 M=7.2 E OFF Hachijo	NS	46.1	32.3	18.6					10.3	13.1	12.2					H=70 km △≒300 km
		EW	51.6	23.6	21.6					8.6	14.9	14.6					
		UD	17.2	10.9	13.3					6.0	11.3	10.4					
4	10.18,1972 M=5.1 Northern Chiba-ken	NS	6.4	3.5	2.1	6.5	5.8	3.7	3.1	6.1	4.6	3.1					H=80 km △≒50~70 km
		EW	8.0	3.3	2.5	12.0	9.6	2.1	3.6	17.2	3.0	3.5					
		UD	2.8	1.3	1.2	4.2	2.8	1.6	1.1	4.0	2.1	1.8					
5	11 6,1972 M=5.1 SW Ibaraki-ken	NS	2.8	1.6	0.8	3.3	3.2	2.0	1.8								H=40 km △≒60~90 km
		EW	3.2	1.4	1.4	8.1	6.3	2.5	1.6								
		UD	1.8	0.9	0.9	2.2	1.4	0.9	0.9								
6	12. 4,1972 M=7.2 E Off Hachijo	NS				20.0	14.6	7.4	6.4	6.5	10.1	10.4					H=50 km △≒300~320km
		EW				15.6	11.3	7.1	4.7	7.3	10.6	10.7					
		UD				4.1	3.6	3.0	3.0	—	—	—					
7	12. 8,1972 M=4.8 Northern Tokyo Bay	NS	12.3	7.2	3.2	10.1	9.3	5.3	4.4	8.3	5.0	4.2					H=90 km △≒20~40 km
		EW	7.0	3.6	8.5	13.4	10.4	4.2	3.3	16.8	5.9	5.3					
		UD	4.0	1.8	2.1	3.7	2.4	1.6	1.5	6.1	2.5	2.5					
8	3.27,1973 M=4.9 Tokyo Bay	NS	47.5	30.7	7.4					18.6	25.9	16.8					H=60 km △≒20~40 km
		EW	42.1	12.3	13.7					31.5	26.7	—					
		UD	7.1	6.5	5.8					8.5	9.3	5.4					
9	12.22,1973 M=5.0 Southern Chiba-ken	NS	10.5	8.5	2.6					13.0	6.4	6.0					H=70 km △≒50~55 km
		EW	7.6	4.3	7.8					18.4	7.3	7.4					
		UD	3.4	1.8	2.3					6.3	3.0	3.9					
10	5. 9,1974 M=6.9 S Coast of Izu Pen.	NS	38.0	22.3	28.7					30.0	14.7	11.5					H=10 km △≒110~120km Off Izu Pen. Eq.
		EW	40.6	26.4	13.7					37.7	17.7	22.4					
		UD	13.9	6.8	7.1					12.5	6.9	5.5					
11	7. 8,1974 M=6.3 Off Ibaraki-ken	NS	4.1	2.4	0.9	4.2	2.0	2.9	1.0	3.5	1.9	1.5					H=40 km △≒160~190 km
		EW	3.3	1.9	2.0	3.3	0.7	1.3	1.7	3.6	1.9	2.0					
		UD	2.3	1.7	1.3	1.5	1.0	1.0	1.0	2.0	1.9	1.2					
12	8. 4,1974 M=5.8 SW Ibaraki-ken	NS				13.6	10.6	6.5	5.1	12.5	6.5	4.9	12.1	7.1	8.5	6.2	H=50 km △≒60~90 km
		EW				12.9	7.7	5.5	4.4	15.0	7.1	6.5	8.2	6.0	10.8	4.8	
		UD				5.8	3.1	2.0	1.9	4.5	4.5	3.2	10.7	4.7	—	3.4	
13	9.27,1974 M=6.5 SE Off Boso pen	NS	11.8	7.0	5.0	7.0	5.9	3.7	3.1				4.7	5.0	5.0	2.9	H=40 km △≒240 km
		EW	10.2	7.1	5.9	5.5	5.0	3.3	1.9				5.9	3.9	5.5	3.2	
		UD	6.9	4.0	3.0	3.1	2.0	1.3	1.3				4.5	2.5	2.3	1.6	
14	11 16,1974 M=6.1 Near Choshi Chiba-ken	NS				4.8	4.0	3.0	2.8				5.4	3.4	2.9	1.8	H=40 km △≒140 km
		EW				4.8	2.6	2.2	1.7				3.6	4.2	3.3	1.9	
		UD				1.7	1.2	1.6	1.2				3.1	2.8	2.9	1.4	
15	11 30,1974 M=7.5~7.75 Near Torishima	NS	11.6	8.5	4.0	6.2	7.0	2.5	2.8				6.2	3.2	5.6	4.2	H=350 km △≒550 km
		EW	8.5	5.8	4.5	5.3	5.0	2.9	2.2				6.2	3.4	6.8	3.6	
		UD	4.7	3.1	2.8	2.3	1.7	1.3	1.1				3.7	2.2	2.4	1.5	
16	2. 8,1975 M=5.4 Northern Chiba-ken	NS				14.2	9.3	4.8	4.2								H=50 km △≒50 km
		EW				18.9	16.6	7.5	5.5								
		UD				5.6	3.1	2.6	2.0								

Fig. 1 Stations of Borehole Accelerometer Installation

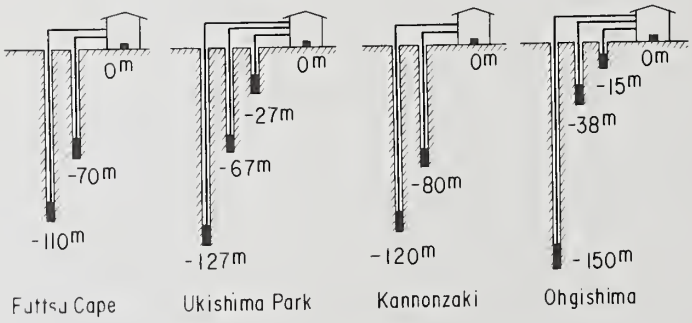

Fig. 2 Depths of Acceleration Pickups

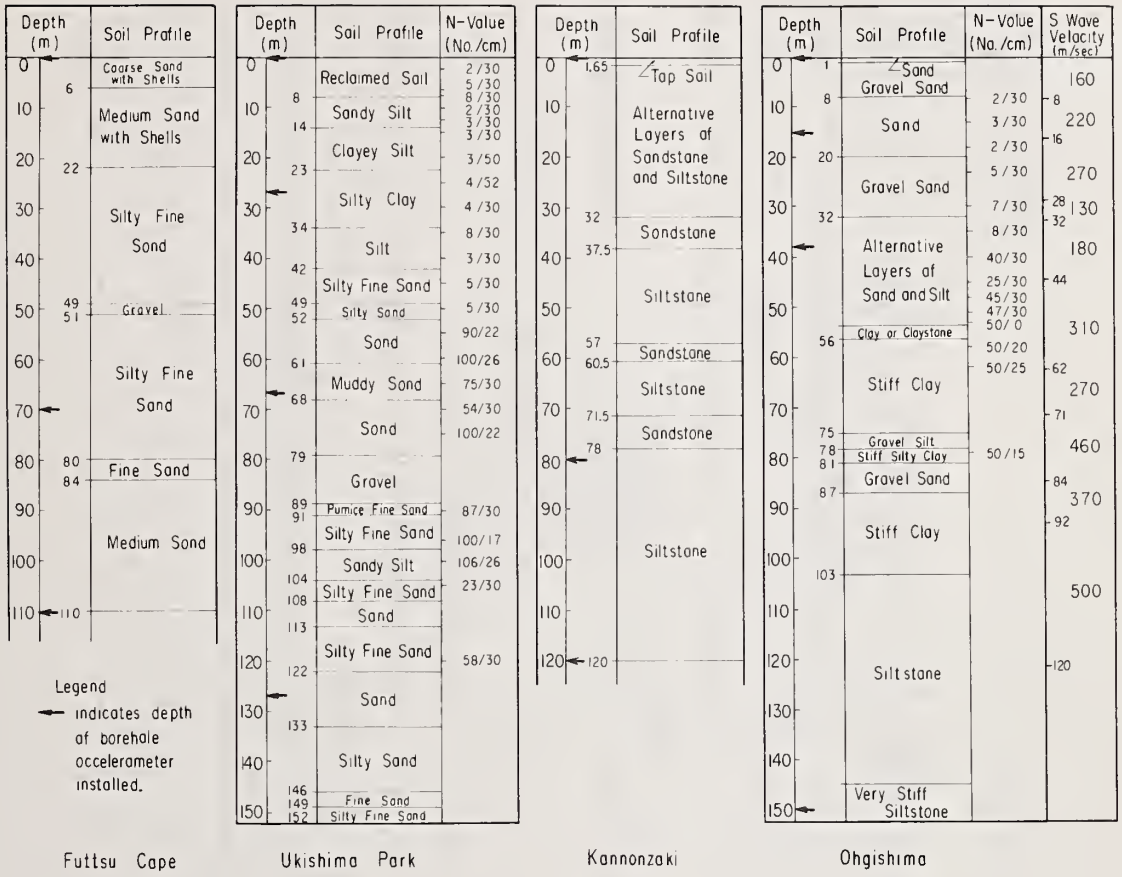

Fig. 3 Soil Profiles at Four Observation Stations

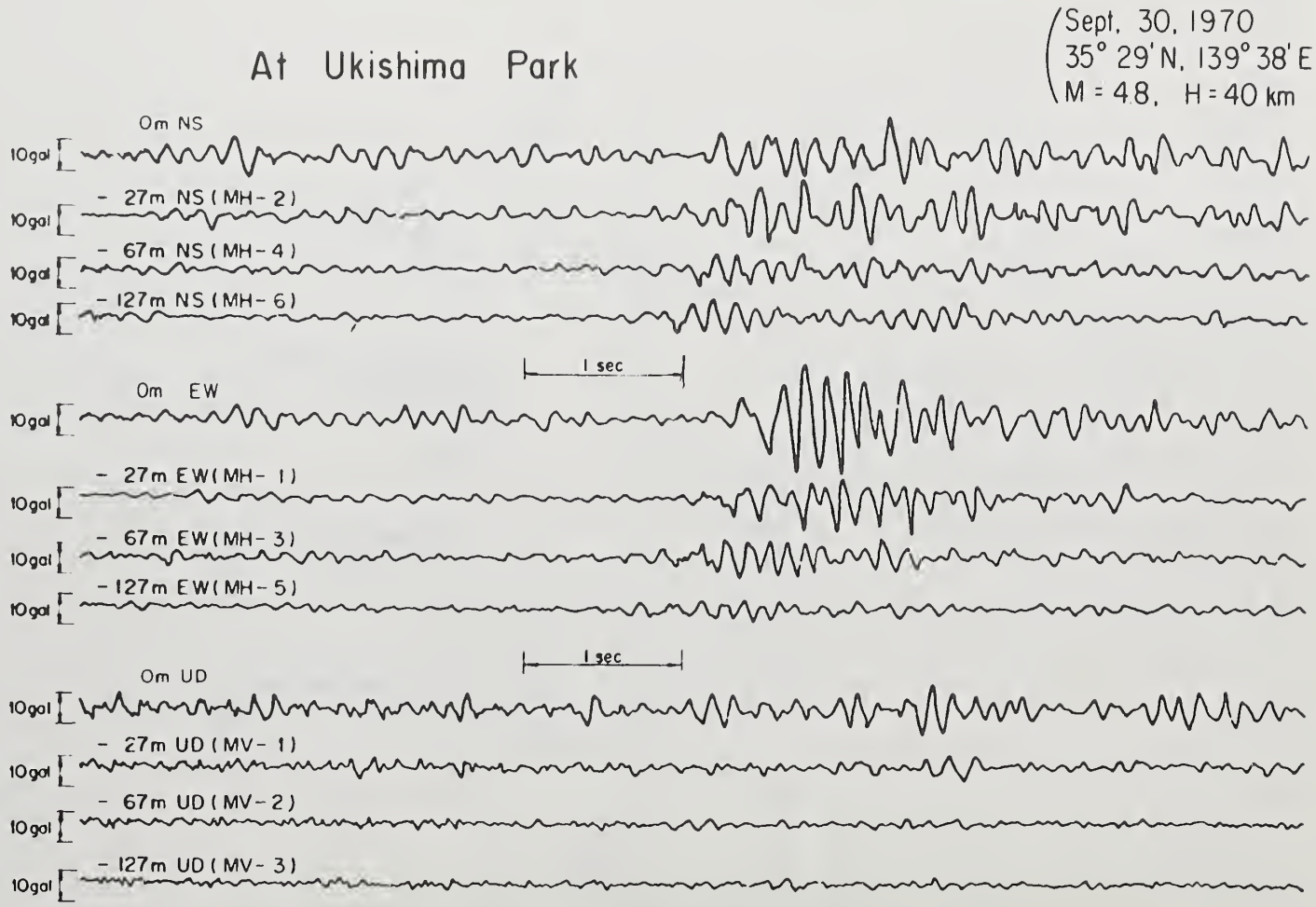

Fig. 4 Example of Records from Borehole Accelerometers

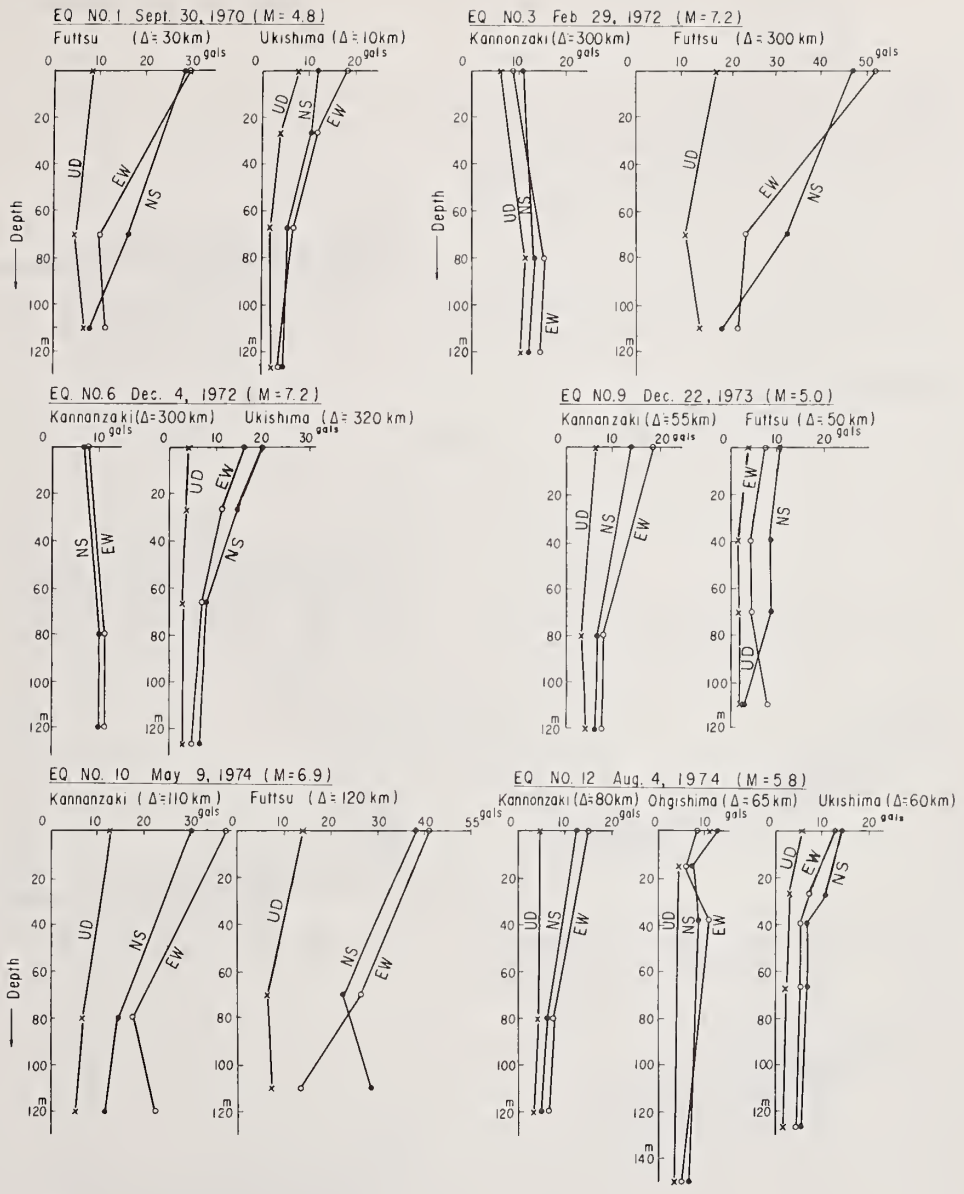

Fig. 5 Vertical Distribution of Maximum Accelerations during Six Earthquakes

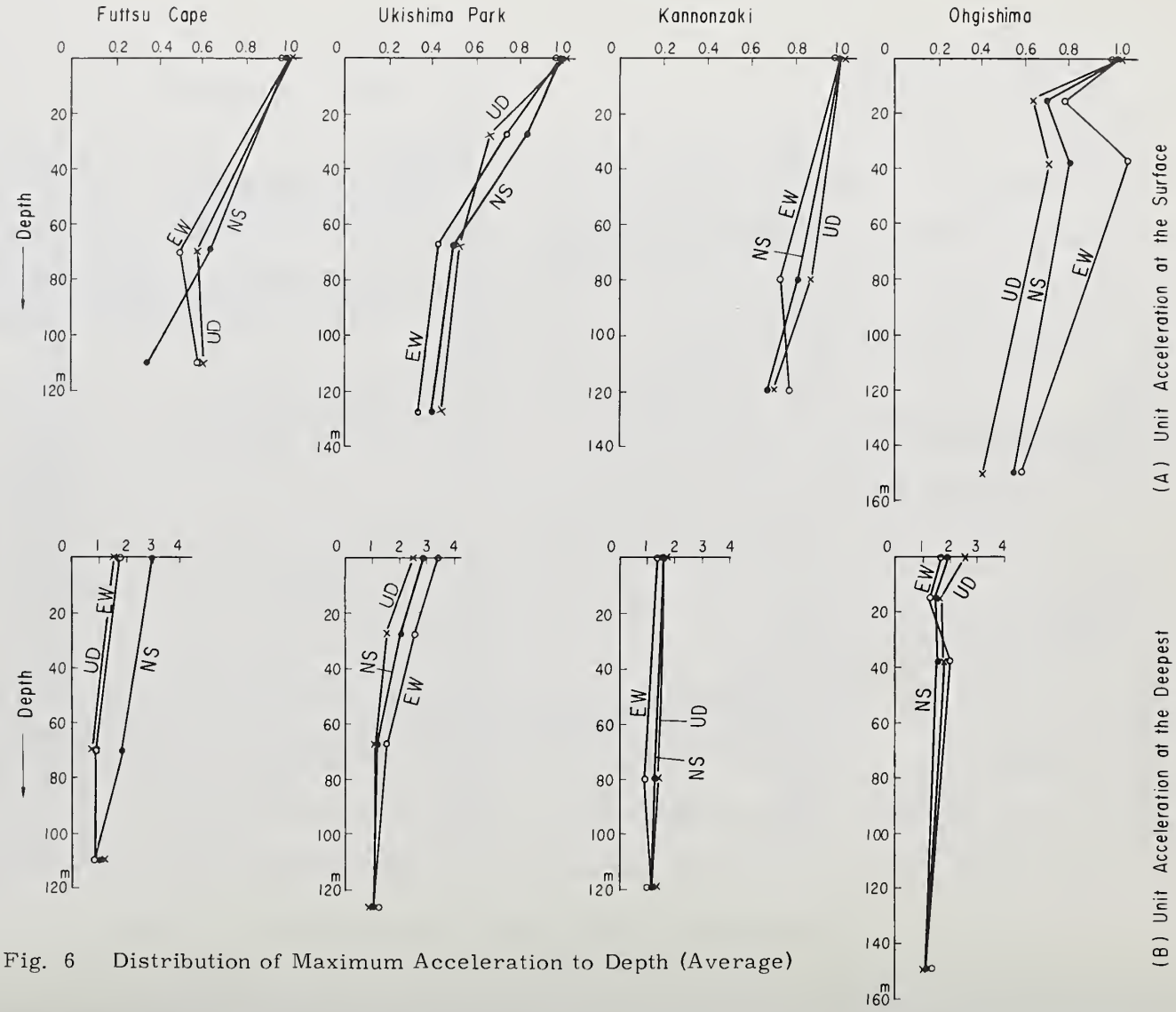

Fig. 6 Distribution of Maximum Acceleration to Depth (Average)

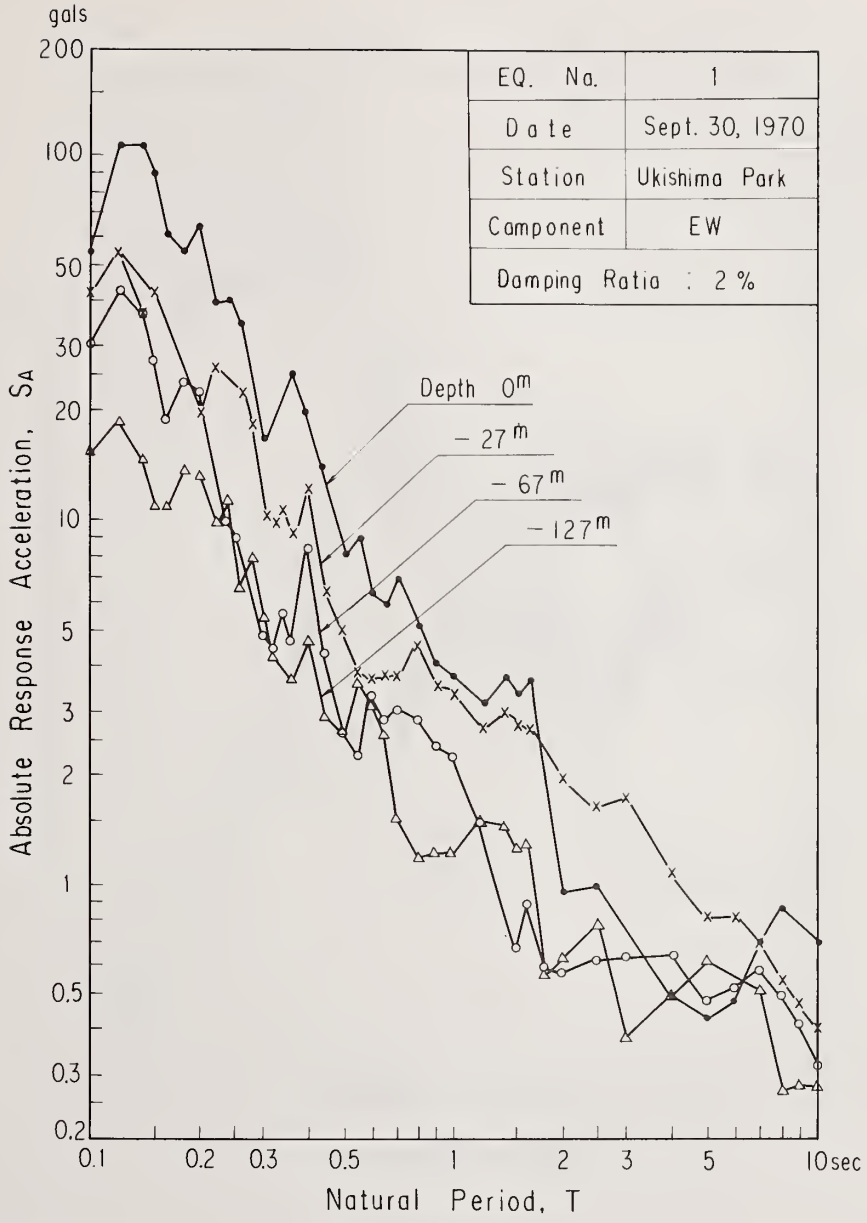

(A) Ukishima Park, EQ. NO. 1

Fig. 7 Response Spectral Curves

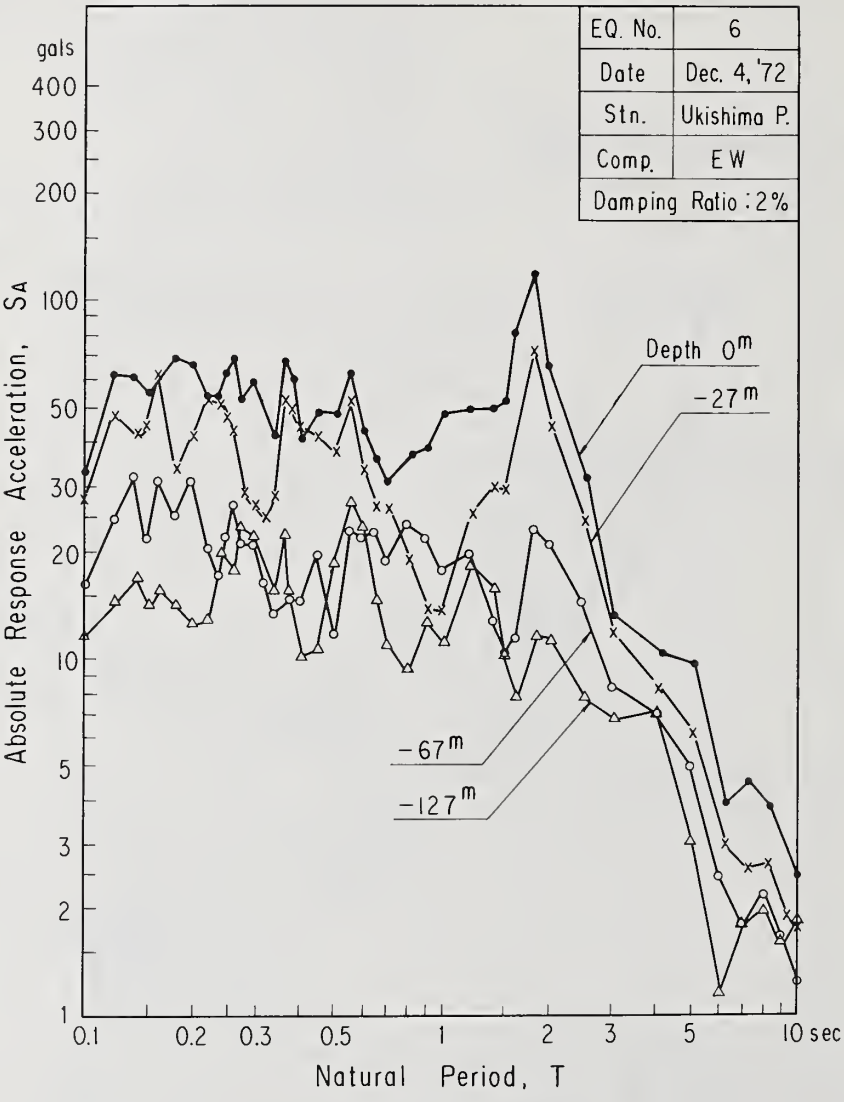

(B) Ukishima Park, EQ. NO. 6

Fig. 7 Response Spectral Curves

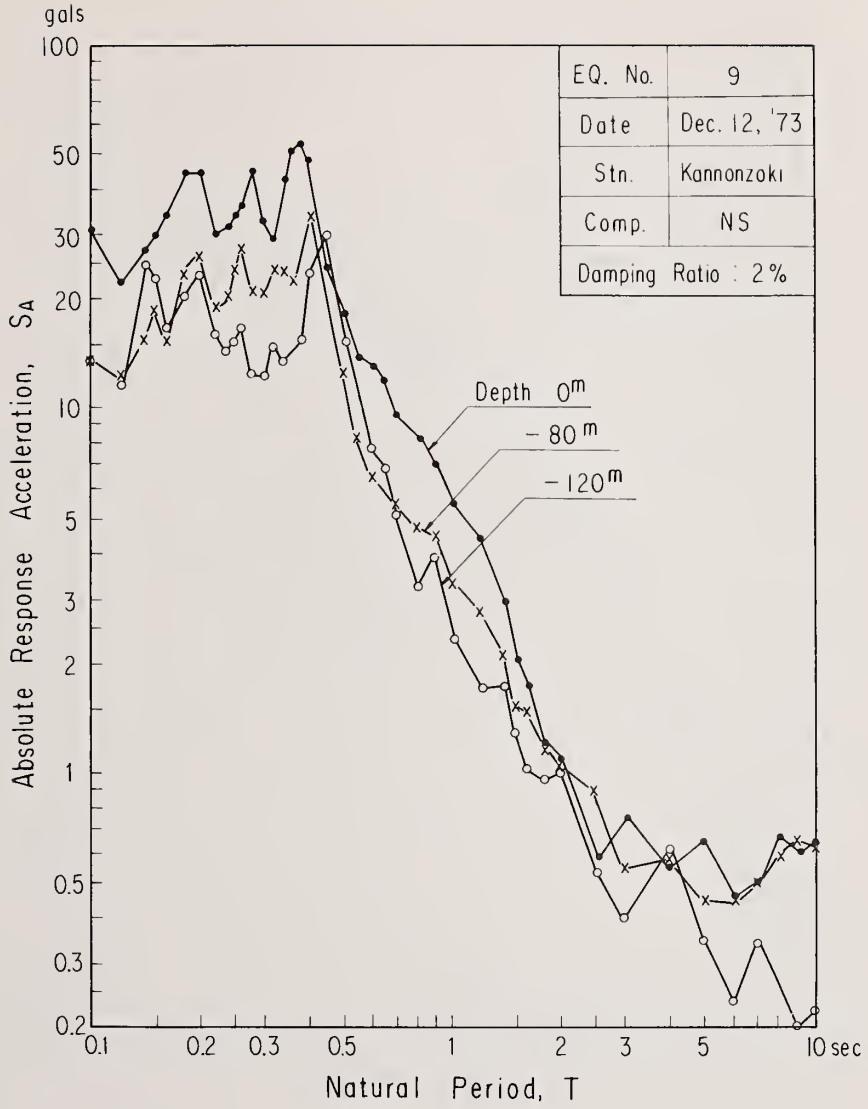

(C) Kannonzaki, EQ. NO. 9

Fig. 7 Response Spectral Curves

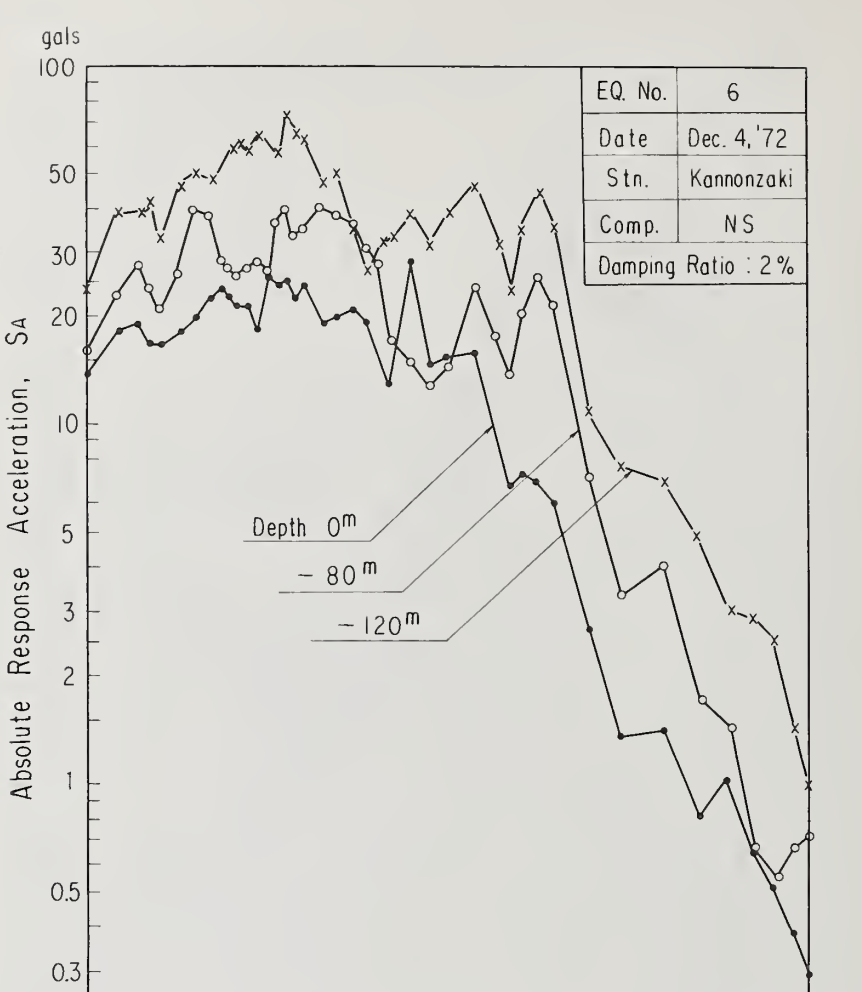

(D) Kannonzaki, EQ. NO. 6

Fig. 7 Response Spectral Curves

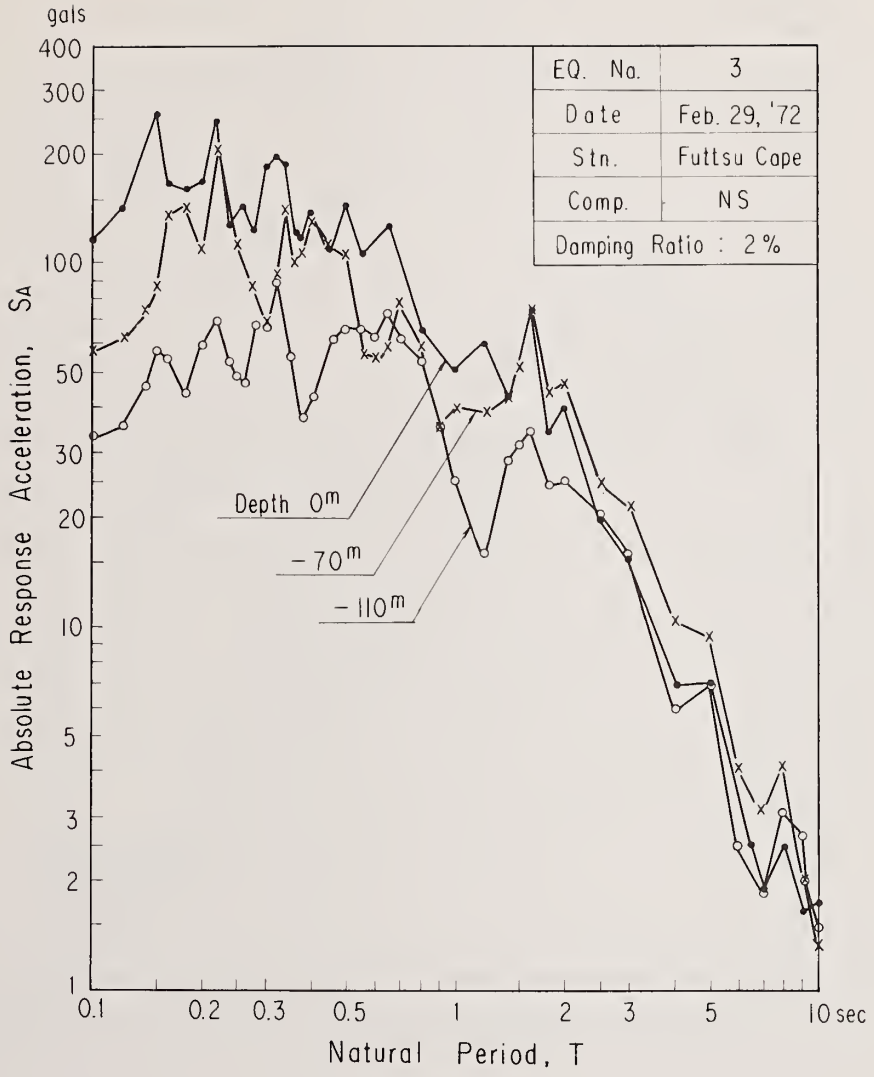

(E) Futtsu Cape, EQ. NO. 3

Fig. 7 Response Spectral Curves

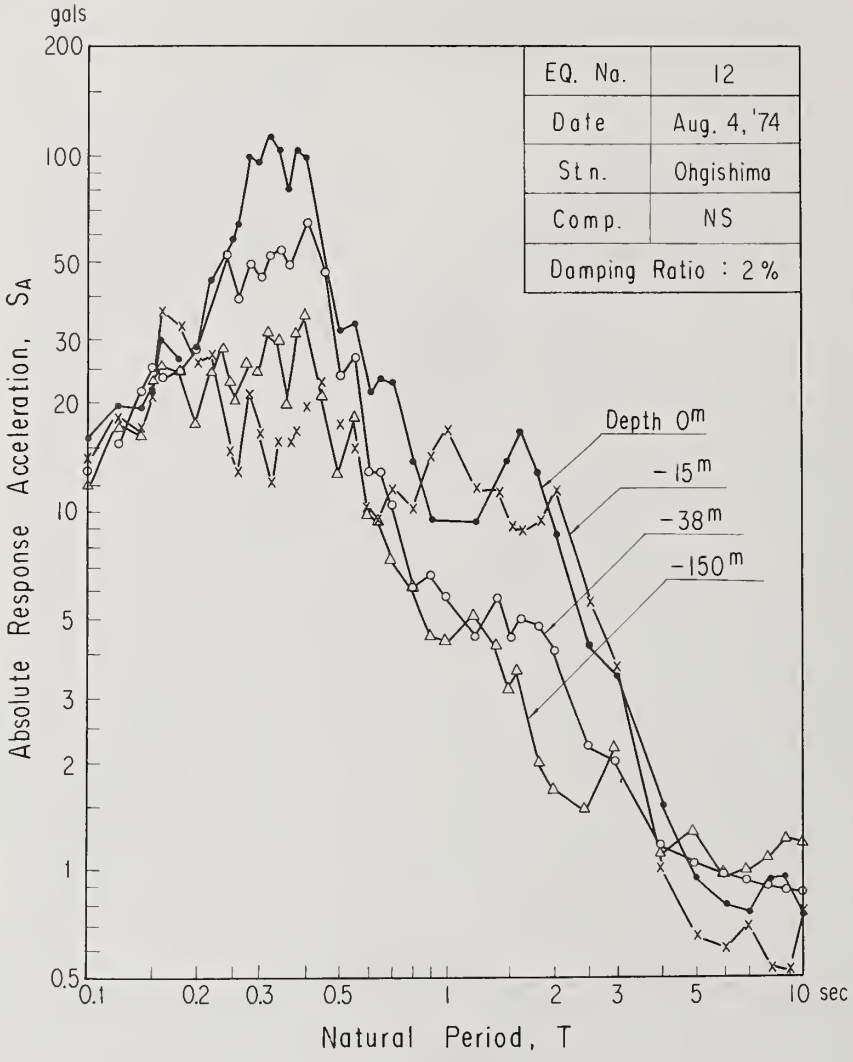

(F) Ohgishima, EQ. NO. 12

Fig. 7 Response Spectral Curves

RELATIONSHIP BETWEEN EARTHQUAKE DAMAGE OF EXISTING WOODEN HOUSES AND SEISMIC INTENSITIES

EIICHI KURIBAYASHI
Chief, Earthquake Engineering Section
Public Works Research Institute
Takayuki Tazaku
Research Member

TAKAYUKI HADATE
Research Member

ABSTRACT

This report discusses a quantitative relationship between a ratio of earthquake damage of existing wooden houses and seismic intensities.

The ratio of earthquake damage of the houses is useful not only for understanding house and building design criteria but for presuming the damage ratio of other structures such as bridges, roads, public utilities, etc.

Using statistics of disaster documents on short distant earthquakes; Fukui Earthquake (M = 7.3, 1948), Isuhanto-Oki Earthquake (M = 6.8, 1974) and Ebino Earthquake (M = 6.1, 1968) the relationship between the ratio of razed houses and epicentral distances or magnitudes of earthquakes was analyzed. The equivalent ratio of razed houses in earthquakes (D1) and the original ratio of razed houses (D2) are defined as;

$$D_1 = \frac{\text{Number of Razed Houses} + 0.5 \times \text{Number of Half Razed Houses}}{\text{Total Number of Existing Houses}} \times 100 \ (\%)$$

$$D_2 = \frac{\text{Number of Razed Houses}}{\text{Total Number of Existing Houses}} \times 100 \ (\%)$$

Conclusively D_1 in the area of diluvium or tertiary (given as D_{1I}) and in the area of alluvium (given as D_{1II}) can be tentatively expressed as follows:

$$D_{1I} = K_I \times 10^{k_I}$$

$$D_{1II} = K_{II} \times 10^{k_{II}}$$

where K_I and K_{II} are respective constant values, K_I and K_{II} are functions of epicentral distances and earthquake magnitudes.

Moreover D_1 and D_2 correlate with each other and D_{2II} (in the area of alluvium) is greater than D_{21} (in the area of diluvium or tertiary).

Key Words: Classification, Damage, Seismic, Intensity, Wooden Houses.

1. Introduction (1, 2)

This report discusses relationships among damage of houses, loss of human life, epicentral distances and earthquake magnitudes, using documents obtained in earthquake disasters relative to the Fukui Earthquake (M = 7.3, 1948), Isuhanto-Oki Earthquake (M = 6.8, 1974) and Ebino Earthquake (M = 6.1, 1968).

2. Classifications of Damage Due to Earthquake (2)

Damage due to earthquakes can roughly be classified from the disaster documents, as shown in Fig. 1.

3. Analyses on Distributions of Earthquake Damage Ratios

In order to analyze earthquake damage of existing wooden houses, earthquake damage ratios are defined as follows,

$$D_1 = \frac{\text{number of razed houses + 0.5 x number of half razed houses}}{\text{total number of existing houses}} \tag{1}$$

$$D_2 = \frac{\text{number of razed houses}}{\text{total number of existing houses}} \tag{2}$$

$$D_3 = \frac{\text{number of houses burnt}}{\text{total number of existing houses}} \tag{3}$$

$$D_4 = \frac{\text{number of houses lost by floods}}{\text{total number of existing houses}} \tag{4}$$

$$D_5 = \frac{\text{number of houses inundated}}{\text{total number of existing houses}} \tag{5}$$

where

D_1 ; equivalent ratios of razed houses due to earthquakes,
D_2 ; original ratios of razed houses due to earthquakes,
D_3 ; ratios of houses burnt due to earthquakes,
D_4 ; ratios of houses lost by floods due to earthquakes,
D_5 ; ratios of houses inundated due to earthquakes.

Similarly, earthquake damage ratio for human lives are defined as follows.

$$D_6 = \frac{\text{number of death by razed houses + number of injured by razed houses}}{\text{population respected}} \tag{6}$$

$$D_7 = \frac{\text{number of death by razed houses}}{\text{population respected}} \tag{7}$$

$$D_8 = \frac{\text{number of heads burnt to death + number of injured by fires}}{\text{population respected}} \tag{8}$$

$$D_9 = \frac{\text{number of heads burnt to death}}{\text{population respected}} \quad (9)$$

$$D_{10} = \frac{\text{number of heads drowned}}{\text{population respected}} \quad (10)$$

where

D_6 ; ratios of death and injured due to earthquake,
D_7 ; ratios of death by razed houses,
D_8 ; ratios of heads burnt and injured by fires,
D_9 ; ratios of heads burnt to death,
D_{10} ; ratios of heads drowned.

b) Earthquakes Employed

In this analyses, three earthquakes, so called short distant earthquakes are employed as follows,

(1) 1948, June, 28 Fukui Earthquake (5, 6); magnitude M = 7.3, focal depth H = 20 km.

(2) 1968, February, 21 Ebino Earthquake (7); magnitude M = 6.1, focal depth H = 0 km.

(3) 1974, May, 9 Isuhanto-oki Earthquake (8); magnitude M = 6.8, focal depth H = 20 km.

c) Distribution of the Ratios of Razed Houses

The relationships among the ratios of the razed houses, the epicentral distances and magnitudes of the subgrounds are classified in two types;

type 1; deluvium and Tertiary

type 2; alluvium (9)

According to preliminary analyses, relationships between the equivalent ratios and epicentral distances can approximately be expressed by exponential functions as shown in Fig. 2 (5, 10). Since the above, the damage ratio is assumed as follows,

$$D_1 = \alpha \cdot 10^{\beta \cdot \Delta} \quad (\log D_1 = \beta \cdot \Delta + \log \alpha) \quad , (11)$$

where α and β are coefficients statistically obtained from topographical distributions of actual damage ratio and Δ is the epicentral distance.

α and β with respect to the earthquakes and the types of subground properties, are estimated as shown in Fig. 3. Substituting the values of α and β into Eq. (11), D_1 with respect to the type of subground properties can be expressed as follows,

$$D_{II}(\Delta \cdot M) = \frac{1}{164} \times 10^{0.625M+0.0025\Delta M-0.272\Delta} \quad , (12)$$

$$D_{III}(\Delta \cdot M) = \frac{1}{73} \times 10^{0.576M+0.0263M-0.248\Delta} \quad , (13)$$

where D_{1I}; is the equivalent ratio in respect of type 1 of subground properties and D_{1II}; is the equivalent ratio in respect of type 2.

Equations (12) and (13) are applicable to following cases,

$$6.0 \leq M \leq 7.0 \text{ and } 5.0 \text{ KM} \leq \Delta \leq 40.0 \text{ KM}$$

where Fig. 4 shows various relationships.

d) Correlations Between the Equivalent Ratios of Razed Houses and Original Ratios of the Razed Houses

In Fukui Earthquake, correlation between the original ratios and the types of subgrounds, are shown in Fig. 5. Further details on the subground type 1 are shown in Fig. 6, where the numbers with circles represent the following;

1 ; mean values of the ratio,
2 and 3 ; limits for confidence levels with five percent,
4 and 5 ; limits for confidence levels with two percent and
6 and 7 ; limits for confidence levels with one percent.

As shown in Fig. 6 four out of fourteen data are scattered beyond the domain of the one percent interval because of the rough classification of the types of subgrounds and nonuniformity of capable loads of the houses.

Regression coefficients of the ratios (gradients) increase with increases of earthquake magnitude, as shown in Fig. 7.

4. Losses of Human Lives (5, 12)

H. Kawasumi relationships between damage of houses and losses of human lives are used and are given as follows, (11)

number of razed houses ; $N = 0.2 \times 10^{2(M-5)}$, (14)

number of houses burnt ; $B = 10^{-5} N^2$, (15)

number of death ; $n = 10^{-2} N^{1.25} \quad 10^{1.125} B^{0.625}$, (16)

where M means earthquake magnitudes.

Eq. (16) is available only to estimate total numbers of death and not the ratio of death. With respect to the type 2 subground properties in the Fukui Earthquake, relationships between the equivalent damage ratio and the ratio of death can be expressed as follows,

the ratio of death and injured ; $2 \times 10^{-3} D_{III}^2$, (17)

the ratio of death ; $3 \times 10^{-4} D_{III}^2$, (18)

where D_{III} means the equivalent ratio of razed houses.

The above indicated that death and injury increases progressively with increase of the damage ratio.

5. Conclusions

a) According to the statistical analyses using documents concerning earthquake disasters, the damage ratios of wooden houses can be expressed as functions with respect to the types of subground properties, epicentral distances and magnitudes of earthquakes. The trend between the ratio and the components is as follows;

subground properties;

Relatively small damage ratios for subground type 1 (stiff and sound) and relatively large damage ratios for subground type 2 (soft).

epicentral distances;

Larger damage ratios for shorter distances, and magnitudes of earthquakes (Richter scale);

Larger damage ratios for larger magnitudes

b) Although the value of the functions of the ratios near epicenters statistically exceeds 100 percent in some cases it seems that the capacity of the structural material is smaller than the actual vibratory loads induced in the earthquakes concerned.

c) Under a constant value of equivalent damage ratio, the trend of the original damage ratio is as follows,

subground properties;

Relatively small damage ratios for subground type 1 and relatively large damage ratios for subground type 2 in Fukui Earthquake, and magnitudes of earthquakes;

Larger damage ratios for larger magnitudes when comparing Fukui and Ebino Earthquakes.

References

1. E. Kuribayashi et al; Quantitative Relations Between Magnitudes of Earthquake and Damage (in Japanese), proc., Kanto District, Japan Society of Civil Engineers, Tokyo, January 1976.

2. K. Kuribayashi et al; Distributions of Damage Due to Recent Short Distant Earthquakes (in Japanese), Technical Memorandum of Public Works Research Institute No. 1106, P.W.R.I. Ministry of Construction, March 1976.

3. N. Koiwai and K. Miyawaki, Determination of Earthquake Hazards in Densely Populated Areas and Preventive Measures to be Considered in Urban Planning, Proc. of 5th Joint Meeting U.S. and Japan Panel on Wind and Seismic Effects, UJNR, Tokyo, May 14-16, 1973.

4. Earthquakes Experienced and Their Disasters in Nagoya City (in Japan), Disaster Prevention Council, Nagoya City, June 1974.

5. Fukui Earthquake Disaster History (in Japanese), Fukui prefecture, June 28, 1949.

6. Report on Hokuriku Earthquake Disaster (in Japanese), Report of Public Works Research Institute, P.W.R.I., Ministry of Construction, March 1949.

7. Memorandum of Ebino Earthquake (in Japanese), Miyazaki prefecture, September 30, 1969.

8. Preliminary Report of 1974 Isuhanto-Oki Earthquake (in Japanese), Building Research Institute, Ministry of Construction, May 23, 1974.

9. Classified maps of subground (in Japanese), Development Bureau, Economy and Planning Agency, Prime Minister's Office, 1974.

10. Report of Statistic Survey on Housing (in Japanese), Japan Statistics Agency, 1948, 1968.

11. H. Kawazumi, Intensity and Magnitude of Shallow Earthquakes, Bureau Central Seismology, International Series A, Tran., Sci., 19, (1954).

12. Report of Census 1970 (in Japanese), Japan Statistics Agency.

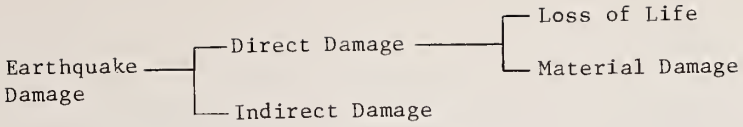

Fig. 1. Classifications of earthquake damage

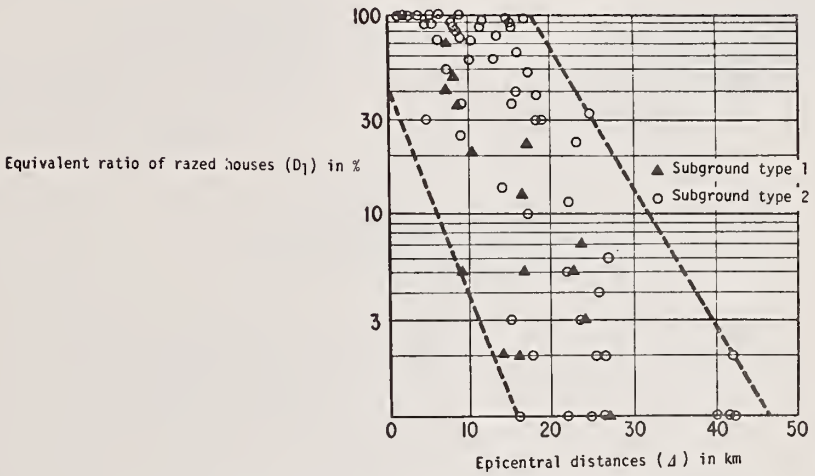

Fig. 2. Relationships between D_1 and Δ in Fukui Earthquake

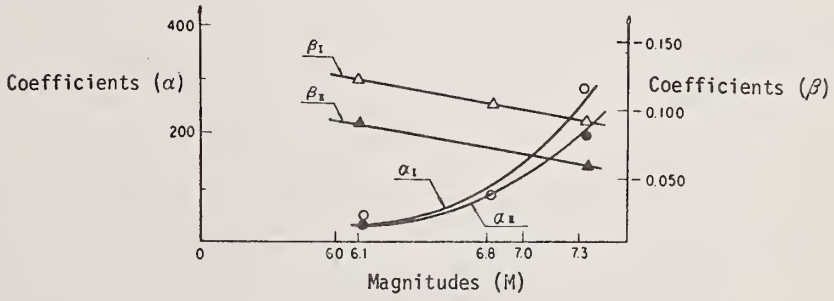

Subground	α	β	α	β
Type 1	○	△	$\alpha_I = 10^{0.625M}/164$	$\beta_I = 0.025M - 0.272$
Type 2	◐	▲	$\alpha_{II} = 10^{0.576M}/73$	$\beta_{II} = 0.026M - 0.248$

Fig. 3. Relationships between M and coefficients α or β

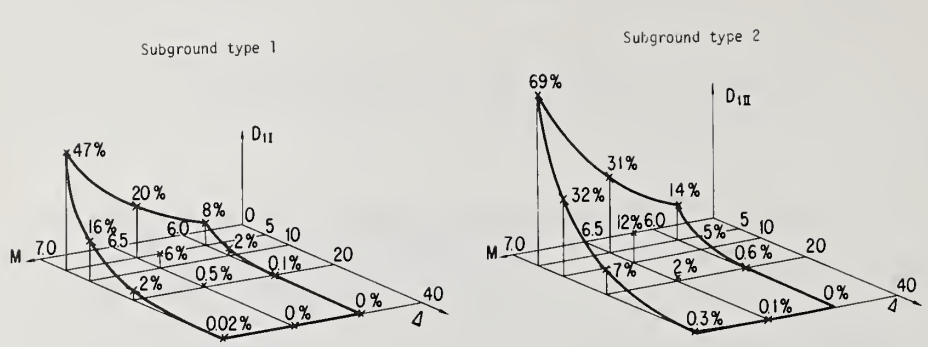

note) D_{II} ; Equivalent ratio in respect of type 1 in %
D_{III}; Equivalent ratio in respect of type 2 in %
Δ ; Epicentral distance in km
M ; Earthquake magnitudes

Fig. 4. Equivalent damage ratios by Eq.(12) and (13)

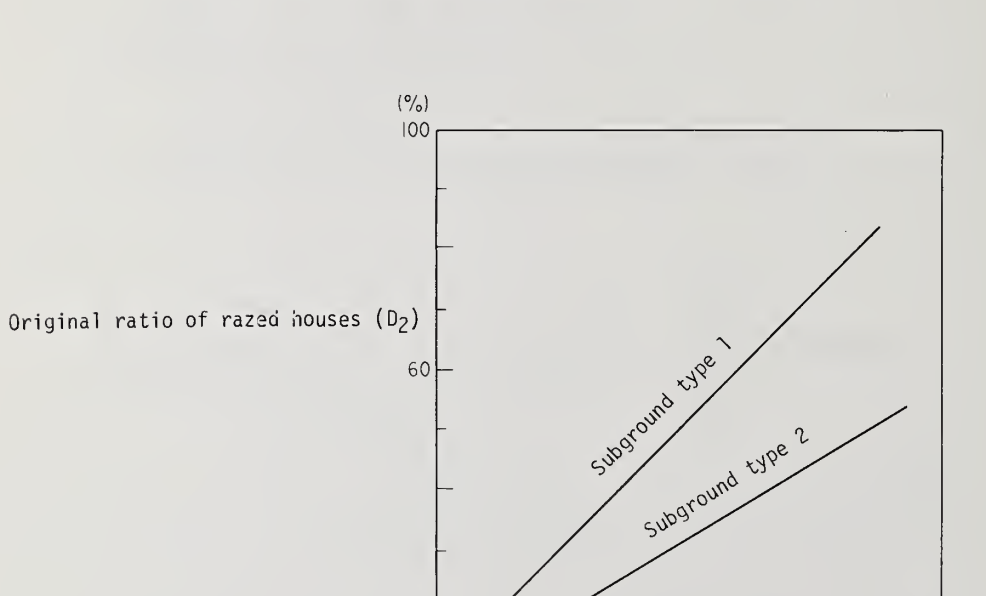

Fig. 5. Correlations between D_1 and D_2 in respect of subground types

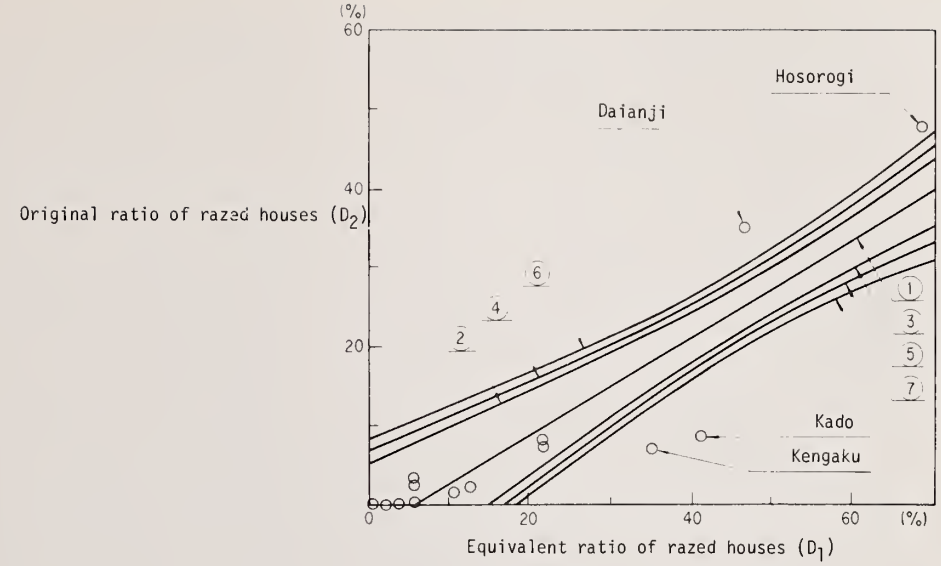

Fig. 6. Correlations between D_1 and D_2 in respect of subground type 1 in Fukui Earthquake

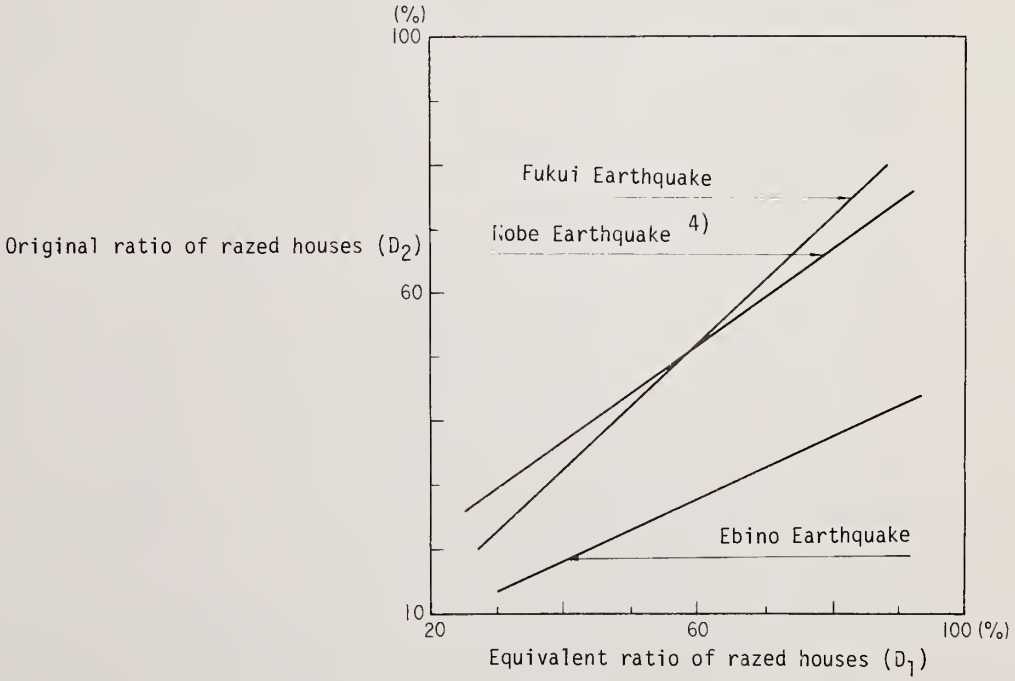

Fig. 7. Correlations between D_1 and D_2 in respect of subground type 1 in Fukui Earthquake

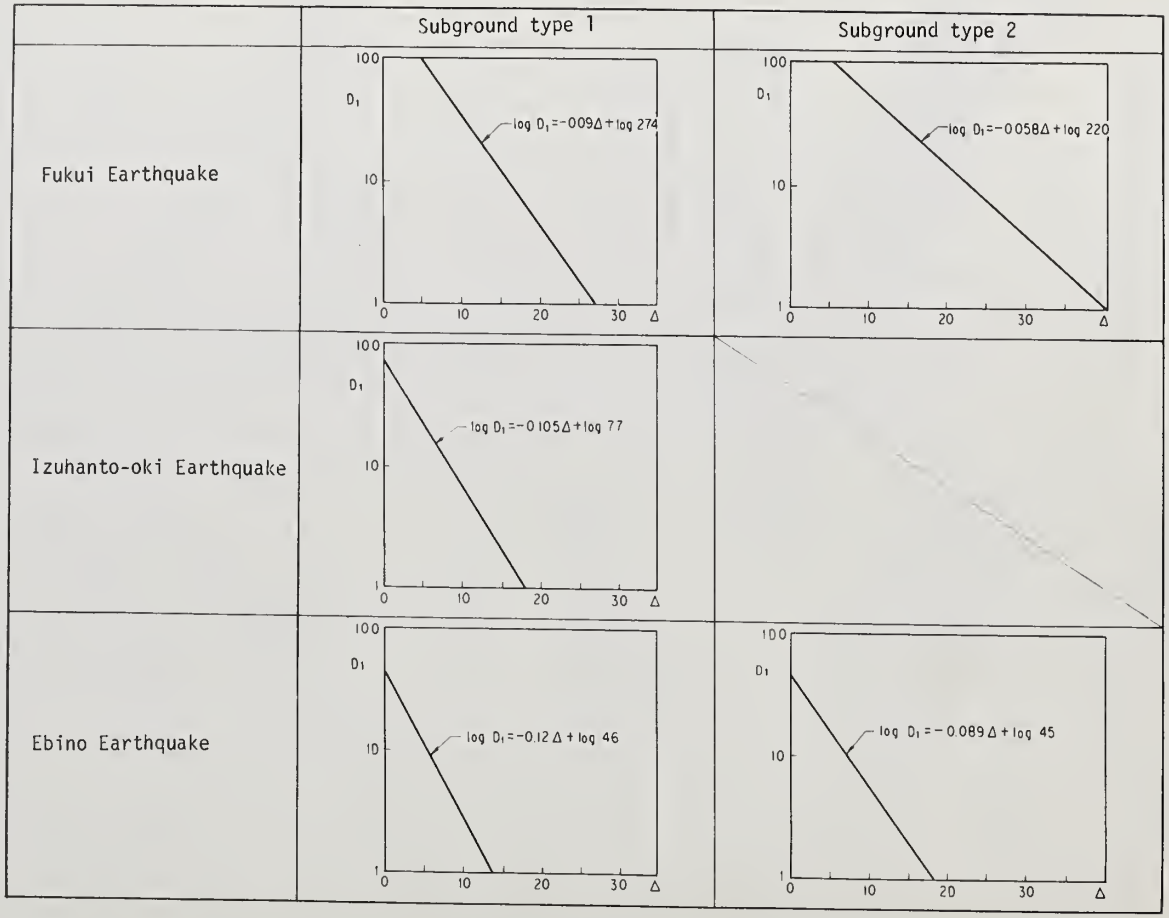

Fig. a. Relationships between the equivalent ratio of razed houses (D_1) in % and epicentral distance (Δ) in km

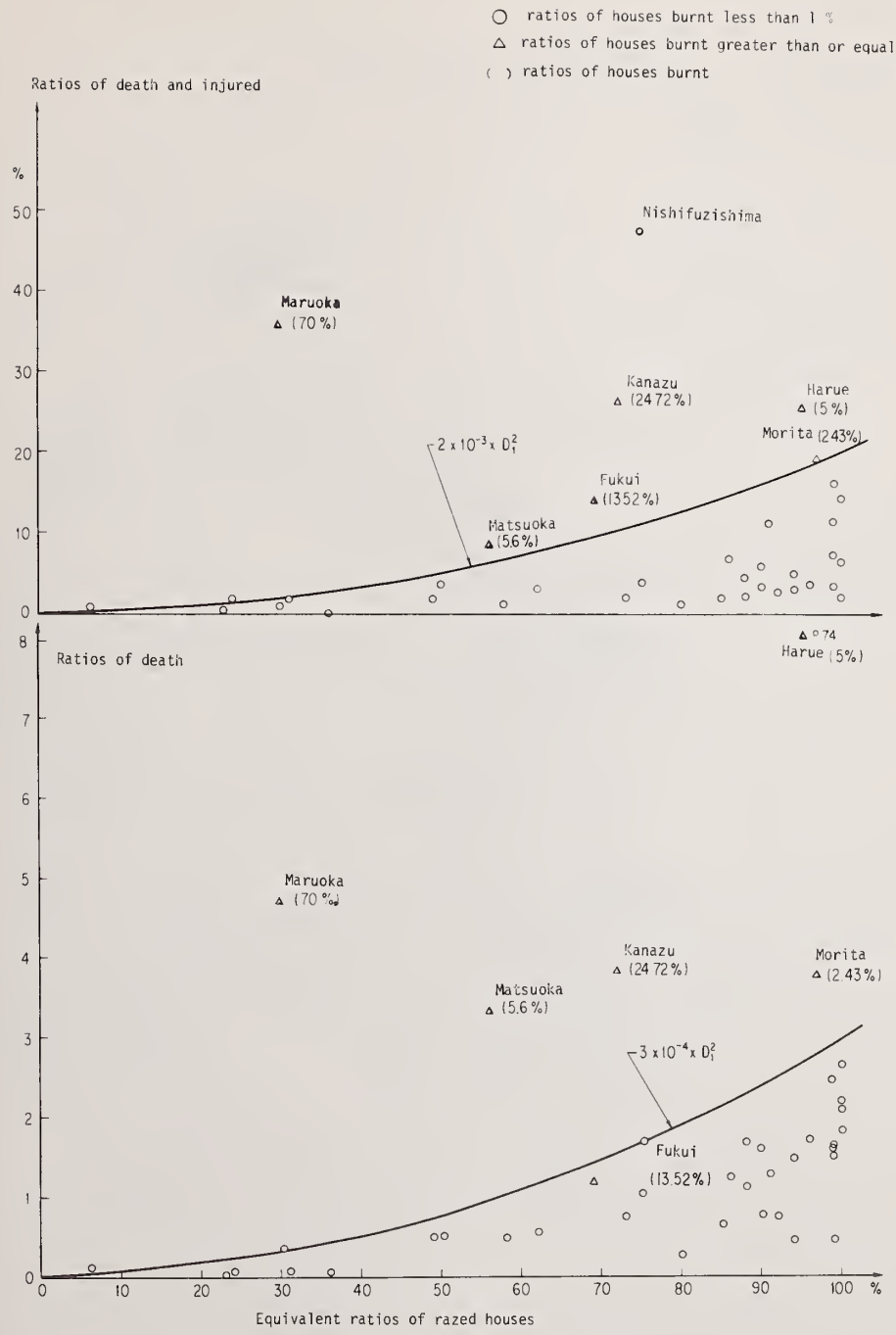

Fig. b. Relationships between D_1 and losses of lives

Fig. c Distribution of earthquake damage of Wooden houses in Fukui Earthquake

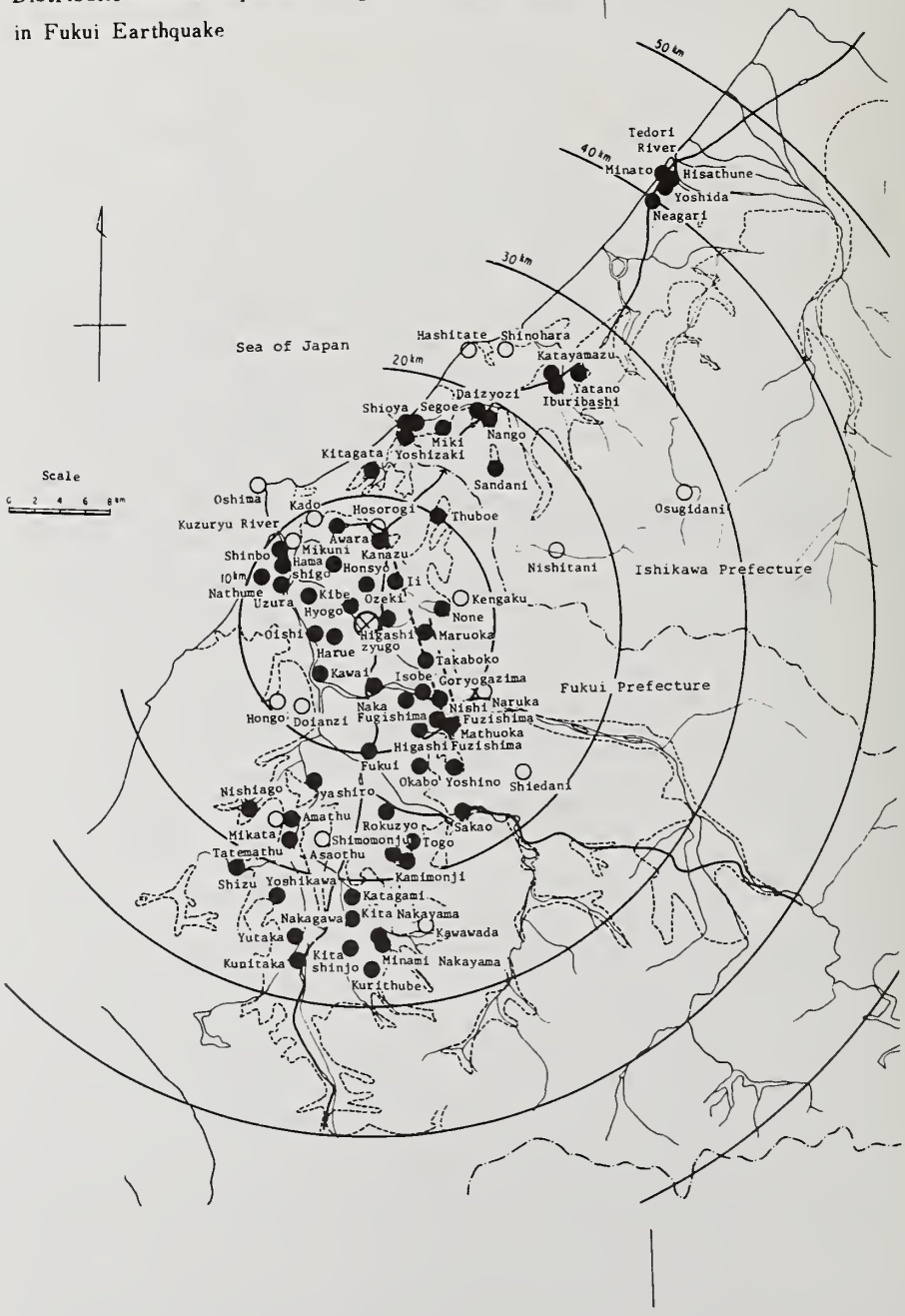

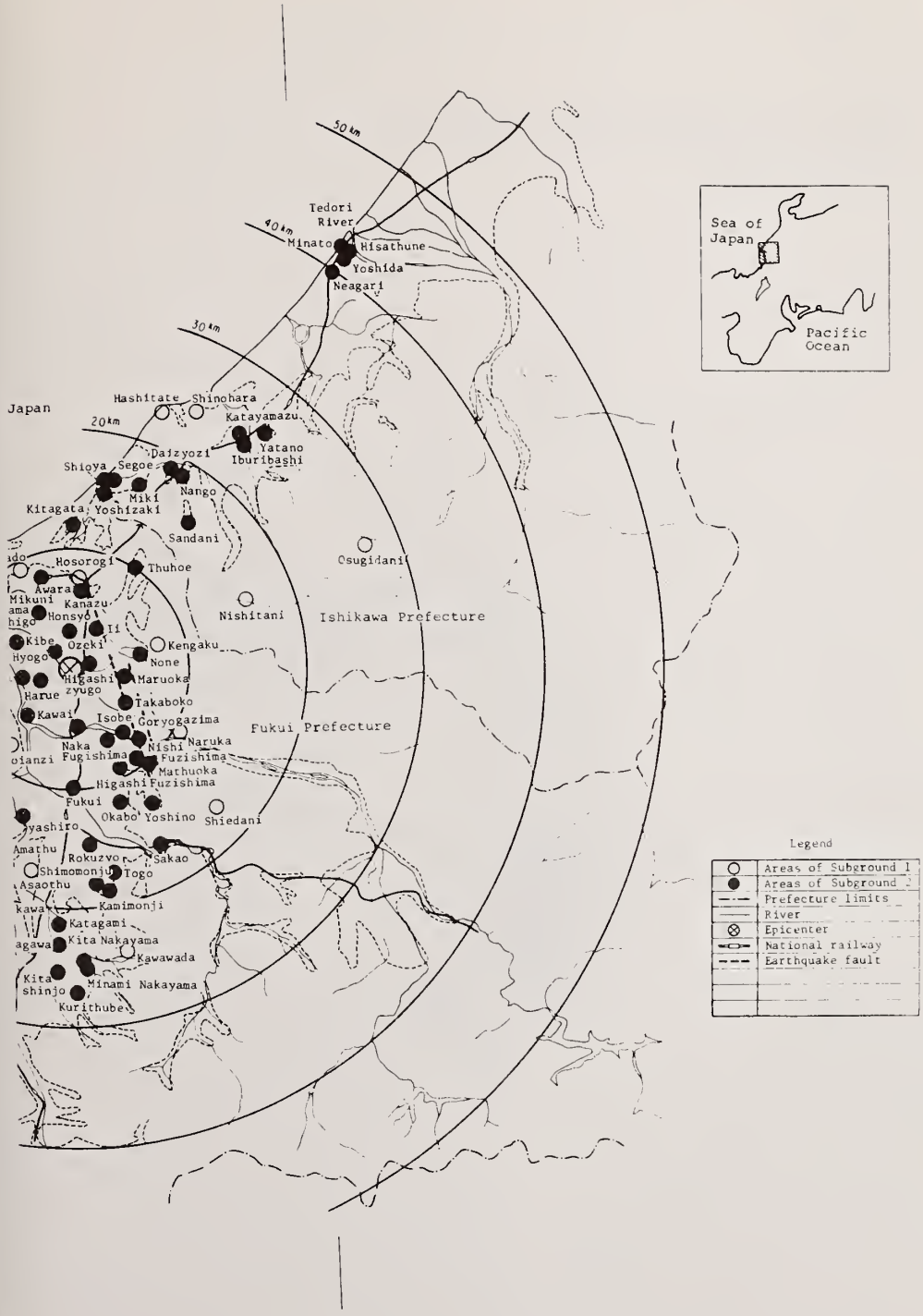
50 km
40 km
30 km
20km
Tedori River
Minato
Hisathune
Yoshida
Neagari
Hashitate
Shinohara
Katayamazu
Yatano
Iburibashi
Daizyozi
Shioya
Segoe
Miki
Nango
Kitagata
Yoshizaki
Sandani
Osugidani
Hosorogi
Thuhoe
Awara
Kanazu
Honsyo
Ii
Kibe
Ozeki
Kengaku
None
Higashi zyugo
Maruoka
Takaboko
Kawai
Isobe
Goryogazima
Naruka
Naka Fugishima
Nishi Fuzishima
Mathuoka
Higashi Fuzishima
Fukui
Okabo
Yoshino
Shiedani
Rokuzyo
Sakao
Shimomonju
Togo
Kamimonji
Katagami
Kita Nakayama
Kawawada
Minami Nakayama
Kurithube
Nishitani
Ishikawa Prefecture
Fukui Prefecture
Japan
Sea of Japan
Pacific Ocean
Legend
Areas of Subground 1
Areas of Subground 2
Prefecture limits
River
Epicenter
National railway
Earthquake fault

Fig. d Distribution of earthquake damage of Wooden houses in Ebino Earthquake

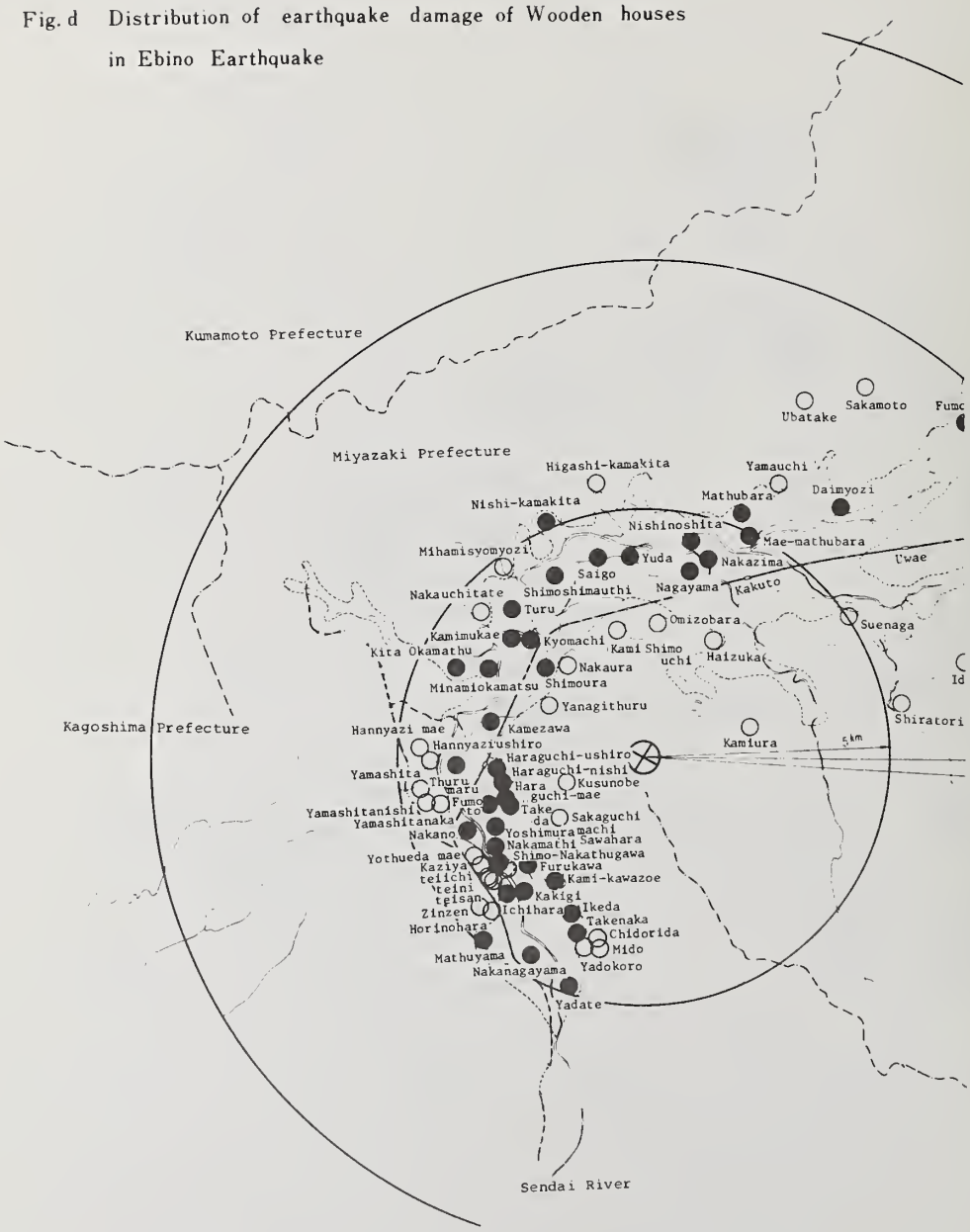

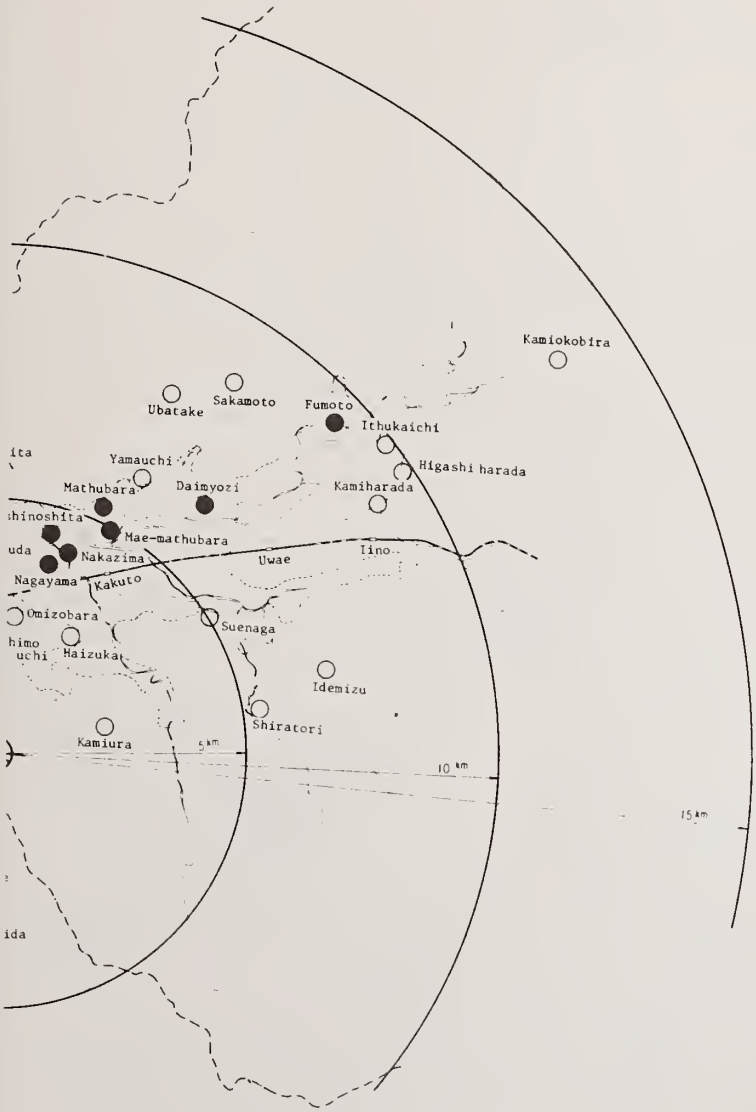

Legend

○	Areas of Subground 1
●	Areas of Subground 2
	Prefecture limits
	River
⊗	Epicenter
	National railway
	Earthquake fault

Fig. e Distribution of earthquake damage of Wooden houses in Izuhanto-Oki Earthquake

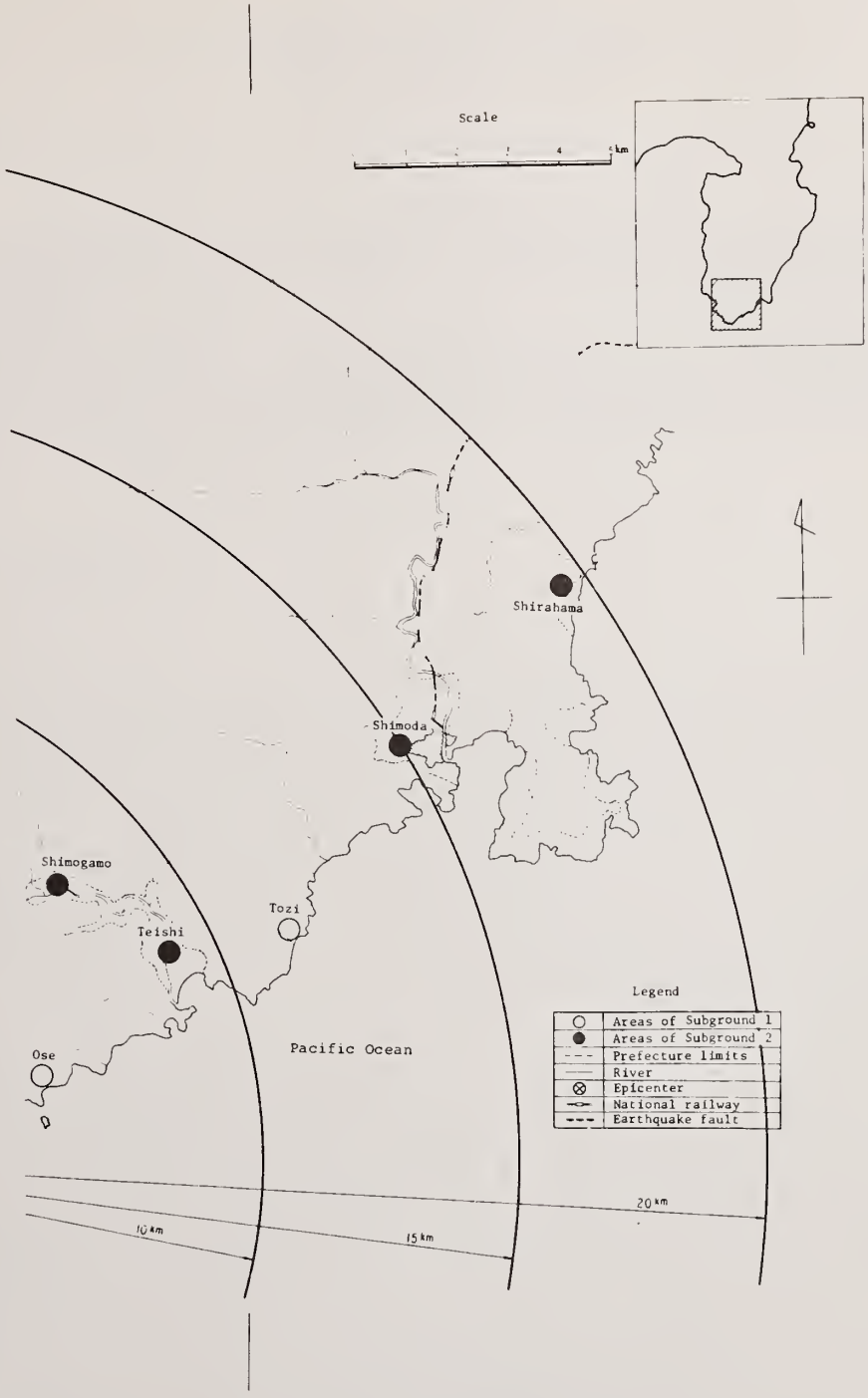
Scale
km
Shirahama
Shimoda
Shimogamo
Teishi
Tozi
Ose
Pacific Ocean
Legend
Areas of Subground 1
Areas of Subground 2
Prefecture limits
River
Epicenter
National railway
Earthquake fault
20 km
15 km
10 km

A METHOD FOR CALCULATING NONLINEAR SEISMIC RESPONSE IN TWO DIMENSIONS

WILLIAM B. JOYNER
Office of Earthquake Studies
Branch of Earthquake Hazards
U.S.G.S
Menlo Park, California

ABSTRACT

A method is presented for calculating the seismic response of two-dimensional configurations of soil testing on bedrock. The method, which is based on a rheological model suggested by Iwan, takes account of the nonlinear, hysteretic behavior of soil and offers considerable flexibility for incorporating laboratory data on soil behavior. An approximate treatment of the boundary conditions is employed which permits energy to be radiated into the underlying medium. Examples are shown to illustrate the method.

Key Words: Bedrock, Modeling; Rheological, Two-dimensions, Seismic Response.

1. Introduction

Numerical calculations of the effect of local site conditions on strong earthquake ground shaking play a major role in the design of important structures for earthquake resistance. Most such calculations at present employ one or both of two major simplifications. The first simplification is the use of one-dimensional models. In such models conditions at the site are represented by a system of horizontal soil layers resting on a semi-infinite elastic medium. The source of earthquake energy is represented by a vertically-incident shear wave in the underlying medium. Serious reservations have been expressed about such models (Hudson, 1972; Newmark and others, 1972), and their range of applicability is a subject of considerable dispute.

The second major simplification has to do with the nonlinearity of the stress-strain relationships of soils. The one-dimensional problem was solved for the case of linear visco-elastic layers by Kanai (1952) some years ago. When we are dealing with input motion sufficiently intense to cause severe damage to structures, however, we cannot assume linear behavior over the entire range of strain. To do so would imply stresses many times greater than the strength of typical materials as measured in the laboratory. To circumvent this difficulty, the method in common use is what is called the "equivalent linear method" (Idriss and Seed, 1968; Schnabel, Seed, and Lysmer, 1972). It is based on the assumption that the response of the system can be approximated by the response of a linear model whose properties are chosen in accord with the average strain that occurs in the model during excitation. The average strain level is found by iterative calculation. The equivalent linear method has been applied to two-dimensional as well as one-dimensional models (Idriss and Seed, 1974).

Recently, a number of workers have developed truly nonlinear methods of solving the one-dimensional ground response problem (Streeter, Wylie, and Richart, 1974; Constantopolous, 1973; Faccioli, Santoyo V., and Leon T., 1973; Papastamatiou, written communication; Chen and Joyner, 1974; Joyner and Chen, 1975). Streeter, Wylie and Richart (1974) have extended their method to two dimensions by replacing the continuum with a latticework of one-dimensional elements.

The method of Chem and Joyner (1974) is based on a rheological model proposed by Iwan (1967). In his paper Iwan extended the one-dimensional model to three dimensions. Application of the extended Iwan model leads to a rigorous and efficient method for computing the seismic response of two-dimensional soil configurations. The present paper describes that method.

Two-dimensional computations have potential application for determining free-field site response in cases where one-dimensional models are inadequate. In addition, such computations have a special application of particular importance in evaluating the response of earth dams.

2. Basic Computational Scheme

The computations are done step by step in time over a grid of discrete points. The displacements of grid points are considered small, and the movement of material relative to a fixed frame of reference is neglected. The soil mass is divided into prismatic elements of infinite length, either square or right-triangular in cross section. The soil is underlain by a semi-infinite elastic medium representing bedrock. The velocities of both P and S waves in the underlying medium are assumed large compared to the velocities in the soil. The sources of seismic disturbance lie in the semi-infinite medium. Figure 1 is a schematic illustration of a possible configuration.

For square elements the mass is divided equally among the adjoining nodes. In some of the examples presented later, the mass of triangular elements is divided equally between the two nodes on the horizontal leg of the triangle. In others the mass is divided equally among all three adjoining nodes. The latter procedure is preferable, but the difference should not be significant.

The behavior of the system is described in terms of the three components of particle velocity V_i at the nodes and the nine components of total stress S_{ij} and strain E_{ij} for the elements. The state of initial stress prior to seismic disturbance may be included in the formulation of the problem. Mean stress σ_M and deviatoric stress σ_{ij} are defined by the equations

$$\sigma_M = S_{kk}/3$$

$$\sigma_{ij} = S_{ij} - \sigma_M \delta_{ij}$$

where the repeated index denotes summation and δ_{ij} is the Kronecker delta. Mean strain e_M and deviatoric strain e_{ij} are defined by the corresponding equations

$$e_M = E_{kk}/3$$
$$e_{ij} = E_{ij} - e_M \delta_{ij}. \tag{1}$$

For both deviatoric stress and deviatoric strain only five components are independent.

A simplified outline of the sequence of computations is as follows:

1. At each node the components of particle velocity V_i are known at time t, and, for each element, the mean stress σ_M and deviatoric stress σ_{ij} are known at time $(t - \Delta t/2)$.

2. The values of V_i at time t are used to compute the change in mean strain Δe_M and deviatoric strain Δe_{ij} for a time interval Δt centered about t.

3. The values of Δe_M and Δe_{ij} are used in conjunction with the constitutive relations described in the next section to obtain the change in mean stress $\Delta\sigma_M$ and the change in deviatoric stress $\Delta\sigma_{ij}$, which are used to update the stress components to time $(t + \Delta t/2)$.

4. From the stress components at time $(t + \Delta t/2)$, the corresponding force on each node is determined and this is added to the gravitational force to give the total force on the node.

5. Values of the total force on a node at time $(t + \Delta t/2)$ are used to update the particle velocity V_i to time $(t + \Delta t)$.

The increment in strain over a time Δt is given by

$$\Delta E_{ij} = 1/2 \left(\frac{\partial V_i}{\partial x_j} + \frac{\partial V_j}{\partial x_i}\right) \Delta t \tag{2}$$

Once the increment in total strain is known, the increment in mean strain and deviatoric strain can readily be found using equations (1).

Particle velocities are assumed to be independent of the x_2 coordinate, so that

$$\frac{\partial V_i}{\partial x_2} = 0$$

The quantity $\partial V_i / \partial x_j$, for values of j other than 2, is approximated in terms of the particle velocities at the nodes. Consider the two elements diagrammed in Figure 2 with the nodes numbered as shown. For the triangle assume that the velocity within an element is a linear function of position. This leads to the expression

$$\frac{\partial V_i}{\partial x_1} \approx (V_i(3) - V_i(1))/\Delta x$$
$$\frac{\partial V_i}{\partial x_3} \approx (V_i(3) - V_i(2))/\Delta x \tag{3}$$

where Δx is the nodal spacing and the numbers in parenthesis refer to the nodes. Corresponding expressions can be derived for triangles of other orientations. The square

elements are considered as two triangles within each of which velocity is a linear function of position. It does not matter which diagonal is used to divide the square into triangles, the result is the same. Averaging the values from the two triangles gives for the square elements

$$\frac{\partial V_i}{\partial x_1} \approx (V_i(4) + V_i(3) - V_i(1) - V_i(2))/2\Delta x$$

$$\frac{\partial V_i}{\partial x_3} \approx (V_i(1) + V_i(4) - V_i(2) - V_i(3))/2\Delta x \qquad (4)$$

Equations (1) through (4) are used to obtain the strain increments Δe_M and Δe_{ij} for the elements from the velocities V_i at nodes. The strain increments are used with constitutive relations described in the next section to obtain stress increments $\Delta\sigma_M$ and $\Delta\sigma_{ij}$, which are accumulated to give the stresses σ_M and σ_{ij} in the elements.

In order to advance from one time step to the next, it is necessary to compute the forces on the nodes. The force on each boundary segment of an element resulting from stress in that element is computed using Cauchy's formula (Fung, 1965, p. 63). Half the force on the boundary segment is applied to the node at one end of the segment and half to the node at the other end. The total force on an internal node is simply the sum of the contributions from all the boundary segments connected to that node plus the gravitational force on the node. The nodes along the outer boundary of the basin are subject to an additional force resulting from stresses in the external medium. The part of the additional force that is constant in time is computed from the initial state of the system by applying the requirement of equilibrium. The dynamic boundary resulting from seismic disturbance is handled by methods described in a subsequent section of the report.

From the total force F_i acting on an internal node, the velocity of that node in the next time step is given by

$$V_i(t + \Delta t) = V_i(t) + F_i\Delta t/m \qquad (5)$$

where m is the mass lumped at the node. Computation of V_i for nodes along the boundary with the underlying medium is described in the section on boundary conditions.

3. Constitutive Relations

The stress-strain model used in the computations was given by Iwan (1967). The one-dimensional version of that model for simple shear is shown in Figure 3. It is composed of simple linear springs and Coulomb friction units arranged as shown. The friction units remain locked until the stress on them exceeds the yield stress Y_i. Then, they yield, and the stress across them during yielding is equal to the yield stress. Generally, the yield stress Y_1 of the first unit is set to zero. The spring constants G_i are chosen so as to reproduce stress-strain behavior measured in the laboratory.

The type of hysteresis loops that such a model produces is shown in Figure 4, which illustrates the behavior of a single soil element subject to cyclic shear loading of increasing amplitude. The loops of Figure 4 are plotted in terms of reduced stress and reduced strain - scaled in such a way that the maximum stress on the sample is one unit and the low-strain modulus has a value of one. The spring constants of the model were chosen to give the behavior as a function of strain indicated by the experimental work of Hardin and Drnevich (1972a, 1972b). The model of Figure 4 contains 50 springs and 50 friction units.

In order to extend the model to three dimensions, Iwan (1967) introduced an extension of the standard incremental theory of plasticity (Fung, 1965). Instead of a single yield surface in stress space, Iwan postulated a family of yield surfaces. The development of the constitutive relations given below follows Iwan with minor modifications.

The relationship between mean stress and mean strain is presumed elastic so that

$$de_M = d\sigma_M/3K \tag{6}$$

where K is the bulk modulus. The deviatoric stress σ_{ij} is considered as a vector in nine-dimensional space, and a family of yield surfaces is postulated, represented by the yield functions

$$F_n(\sigma_{ij} - \alpha_{nij}) = k_n^2$$

where k_n is a constant characteristic of the nth surface and α_{nij} represents the "origin" of the surface. The total deviatoric strain e_{ij} is presumed to consist of the sum of an elastic strain e_{Eij} plus plastic strain components e_{Pnij} each associated with the nth yield surface. Kinematic hardening of the Prager type is assumed so that

$$d\alpha_{nij} = C_n\, de_{Pnij} \tag{7}$$

where C_n is a constant associated with the nth surface.

The plastic strain increments must be normal to the corresponding yield surfaces. This gives

$$de_{Pnij} = L_n\, h_n \frac{\partial F_n}{\partial \sigma_{ij}} \tag{8}$$

where

$L_n = 0$ if $F_n < k_n^2$ or $\frac{\partial F_n}{\partial \sigma_{ij}}\, d\sigma_{ij} < 0$;

$L_n = 1$ if $F_n = k_n^2$ and $\frac{\partial F_n}{\partial \sigma_{ij}}\, d\sigma_{ij} \geq 0$.

The requirement that loading from a plastic state must lead to another plastic state can be used to determine h_n (Fung, 1965, p. 147-151).

$$h_n = \frac{1}{C_n} \frac{(\partial F_n/\partial \sigma_{rs})\ d\sigma_{rs}}{(\partial F_n/\partial \sigma_{kl})(\partial F_n/\partial \sigma_{kl})} \tag{9}$$

The elastic deviatoric strain is given by

$$e_{Eij} = \sigma_{ij}/2G_o$$

where G_o is the low-strain shear modulus.

Summing elastic and plastic strain increment components and substituting from equations (8) and (9) gives the total deviatoric strain increment

$$de_{ij} = Q_{ijrs}\ d\sigma_{rs} + d\sigma_{ij}/2G_o \tag{10}$$

$$\text{where } Q_{ijrs} = \sum_n \frac{L_n\ (\partial F_n/\partial \sigma_{ij})(\partial F_n/\partial \sigma_{rs})}{C_n\ (\partial F_n/\partial \sigma_{kl})(\partial F_n/\partial \sigma_{kl})}$$

Equation (10) is to be solved for $d\sigma_{rs}$ in terms of de_{ij}, but first it should be noted that only five of the components of $d\sigma_{rs}$ are independent. Five independent components are selected, and using the relationships

$$\sigma_{rs} = \sigma_{sr}$$

and

$$\sigma_{11} + \sigma_{22} + \sigma_{33} = 0$$

equation (10) is rewritten in terms of the independent components.

$$de_{ij} = P_{ij11}\ d\sigma_{11} + P_{ij12}\ d\sigma_{12} + P_{ij13}\ d\sigma_{13} + P_{ij23}\ d\sigma_{23} + P_{ij33}\ d\sigma_{33} \tag{11}$$

where (i,j) takes on the values (1,1), (1,2), (1,3), (2,3), and (3,3). The coefficients are given by

$$P_{ij11} = \sum_n \frac{L_n (\partial F_n/\partial \sigma_{ij})(\partial F_n/\partial \sigma_{11} - \partial F_n/\partial \sigma_{22})}{C_n (\partial F_n/\partial \sigma_{kl})(\partial F_n/\partial \sigma_{kl})}$$

$$P_{ij12} = \sum_n \frac{L_n (\partial F_n/\partial \sigma_{ij})(\partial F_n/\partial \sigma_{12} + \partial F_n/\partial \sigma_{21})}{C_n (\partial F_n/\partial \sigma_{kl})(\partial F_n/\partial \sigma_{kl})}$$

$$P_{ij13} = \sum_n \frac{L_n (\partial F_n/\partial \sigma_{ij})(\partial F_n/\partial \sigma_{13} + \partial F_n/\partial \sigma_{31})}{C_n (\partial F_n/\partial \sigma_{kl})(\partial F_n/\partial \sigma_{kl})}$$

$$P_{ij23} = \sum_n \frac{L_n (\partial F_n/\partial \sigma_{ij})(\partial F_n/\partial \sigma_{23} + \partial F_n/\partial \sigma_{32})}{C_n (\partial F_n/\partial \sigma_{kl})(\partial F_n/\partial \sigma_{kl})}$$

$$P_{ij33} = \sum_n \frac{L_n (\partial F_n/\partial \sigma_{ij})(\partial F_n/\partial \sigma_{33} - \partial F_n/\partial \sigma_{22})}{C_n (\partial F_n/\partial \sigma_{kl})(\partial F_n/\partial \sigma_{kl})}$$

By solving equation (6) and (11), the stress increments are obtained from the strain increments. Gaussian elimination is used in solving equation (11). Since the equation must be solved for each element at each time step some care was taken to insure that the programming of the solution was efficient.

The coefficients in equation (11) depend on $\partial F_n/\partial \sigma_{ij}$, C_n, and L_n. The yield condition of von Mises is used so that

$$F_n = 1/2\ (\sigma_{ij} - \alpha_{nij})(\sigma_{ij} - \alpha_{nij}) \qquad (12)$$

and

$$\frac{\partial F_n}{\partial \sigma_{ij}} = \sigma_{ij} - \alpha_{nij}.$$

With that choice the parameter k_n in the equation that described the yield surface represents the initial yield stress in simple shear. The values of k_n and C_n are chosen in order to fit laboratory data on the stress-strain behavior of the material. In order to determine the value of L_n we need to know the value of F_n and the sign of the quantity $(\partial F_n/\partial \sigma_{ij})\ d\sigma_{ij}$. The first is no problem, but the second requires a knowledge of $d\sigma_{ij}$, which is the unknown in equation (11). This difficulty is avoided by a procedure that is the equivalent of choosing L_n in accordance with the sign of $(\partial F_n/\partial \sigma_{ij})\ d\sigma_{ij}$ during the previous time step. The adequacy of this approximation has been checked by comparing with the results of one-dimensional calculations for which the approximation was not made.

If during a given time step yielding takes place on the nth surface, the quantities α_{nij} are changed. In order to ensure that the stress point always remains exactly on a yielding surface, equation (7) is not used to calculate the change in σ_{nij}. Coincidence of the stress point and the yielding surface is maintained by using the following equation

$$\alpha'_{nij} = \sigma'_{ij} - \frac{K_n(\sigma'_{ij} - \alpha_{nij})}{[1/2\ (\sigma'_{kl} - \alpha_{nkl})(\sigma'_{kl} - \alpha_{nkl})]^{1/2}} \tag{13}$$

where the unprimed quantities represent values at time $(t-\Delta t/2)$ and the primed quantities values at time $(t+\Delta t/2)$.

The actual sequency of computations is given below, where the primed quantities are computed in the current time step and the unprimed quantities are inherited from the previous time step.

1. New values of the stress components σ'_{ij} are obtained from

$$\sigma'_{ij} = \sigma_{ij} + \Delta\sigma_{ij}$$

2. The quantity T_n is evaluated as

$$T_n = [1/2\ (\sigma'_{kl} - \alpha_{nkl})(\sigma'_{kl} - \alpha_{nkl})]^{1/2}$$

3. The quantities $\partial F_n/\partial\sigma_{ij}$ are evaluated. The equation used can be derived by noting that form (12)

$$\frac{\partial F_n}{\partial \sigma_{ij}} = \sigma'_{ij} - \alpha'_{nij}.$$

Combining with equation (13) gives

$$\frac{\partial F_n}{\partial \sigma_{ij}} = \frac{k_n}{T_n}(\sigma'_{ij} - \alpha_{nij}). \tag{14}$$

4. The coefficients of equation (11) are evaluated using (14). Equation (11) is then solved to give the new stress increments $\Delta\sigma_{ij}$. Factors of (k_n/T_n) from (14) appearing in the numerator and denominator of the expressions for the coefficients of (11) cancel out, simplifying the calculations.

5. Equation (13) is used to evaluate α'_{nij}.

Determination of the constants C_n is accomplished by considering the behavior of the system in simple shear. Iwan (1967) showed that the behavior of the three-dimensional model in simple shear is equivalent to the behavior of the one-dimensional model, which is illustrated in Figures 3 and 4 of this paper. It is assumed that the loading curve from an initial state of zero deviatoric stress and strain is known. In principle it could be determined from laboratory measurement. With the proper choice of coordinate axes the non-vanishing components of stress and strain in simple shear are

$$\sigma_{13} = \sigma_{31}$$

$$e_{13} = e_{31}$$

The parameter k_n represents the yield stress in simple shear for the nth yielding surface. A set of values of k_n is chosen to cover the range of stress the system is expected to encounter, and the values are distributed so that the initial loading curve can be faithfully represented. From the initial loading curve a set of values e_n (n=1, N) is obtained for the shear strain corresponding to the stress values k_n. A stress value σ_{N+1} is chosen larger than k_N and larger than any stress that is expected to occur. A corresponding strain value e_{N+1} is obtained from the loading curve. For the case of simple shear equation (10) becomes

$$de_{13} = \frac{d\sigma_{13}}{2G_o} + Q_{1313}\, d\sigma_{13} + Q_{1331}\, d\sigma_{31}.$$

Evaluating Q_{1313} and Q_{1331} with the aid of equations (9) and (12), gives

$$de_{13} = \left(\frac{1}{2G_o} + \sum_{n=1}^{j} \frac{1}{C_n}\right) d\sigma_{13} \qquad (15)$$

where j is the index of the surface with the largest yield stress of all the surfaces that are in the yielding state.

Equation (15) leads to a simple recursion relationship for determining C_j

$$\frac{1}{C_j} = \frac{e_{j+1} - e_j}{k_{j+1} - k_j} - \frac{1}{2G_o} - \sum_{n=1}^{j-1} \frac{1}{C_n}.$$

The evaluation of C_N is the same except that σ_{N+1} is used in place of the undefined k_{N+1}.

In order to simplify the computations, stress and strain are normalized in a way similar to that used by Hardin and Drnevich (1972b). Stress is normalized by multiplying by $1/\sigma_{max}$, where σ_{max} is the maximum stress the material can withstand in simple shear, and strain is normalized by multiplying by $2G_o/\sigma_{max}$. The normalized stress-strain curve has a limit of 1.0 for high strain and an initial slope at the origin of 1.0. The computa-

tions are simplified by using the same normalized initial loading curve, and therefore the same set of normalized C_n and k_n, for all of the soil elements in the model. The differences in soil behavior from one element to another result from differences in the values of σ_{max} and G_o assigned to the different elements.

For the examples presented later in this report, the following set of values was adopted for k_n and σ_{N+1}:

$$k_n = 0.1\ n \qquad 1 \leq n \leq 9$$

$$k_{10} = 0.99$$

$$\sigma_{N+1} = 0.9999$$

A hyperbolic initial loading curve (Hardin and Drnevich, 1972b) was used and normalized strain was expressed in terms of normalized stress by the equation

$$e_n = \frac{k_n}{1-k_n}$$

The method described here in no way depends on the hyperbolic relationship; a purely empirical stress-strain curve derived from laboratory measurements could be used just as well.

The method of normalization and the use of a hyperbolic stress-strain curve is similar to the approach of Hardin and Drnevich (1972b), but some differences should be noted. The stress-strain curve considered by Hardin and Drnevich is the curve formed by the loci of the endpoints of hysteresis loops formed in cyclic loading experiments at differing peak strain levels. The stress for the Hardin and Drnevich curve is the shear stress on a horizontal plane applied to a sample with an initial geostatic stress state characterized by non-vanishing deviatoric stress. The stress-strain curve referred to in this report, on the other hand, is an initial loading curve in simple shear from an initial state of zero deviatoric stress. Given the constitutive relationships adopted in this report, an initial loading curve is identical to the loci of endpoints of hysteresis loops. The difference in initial state of stress, however, may be significant.

Total stress rather than effective stress is used in this report to describe soil behavior under seismic loading conditions. That is essentially equivalent to using the undrained strength principle (Whitman, 1961, p. 587-589), the presumption being that undrained conditions prevail during seismic deformation. The parameter σ_{max} is therefore related to the undrained strength, which is commonly used property in soils engineering. Seismic deformation implies relatively rapid loading conditions, however, and values of undrained strength measured by quasi-static methods should not be used for σ_{max} without considering the effect of loading rate.

The assumption of an elastic relationship for volumetric stress and strain coupled with the use of the von Mises yielding condition is about the simplest set of choices that

could be made. It does not incorporate in any direct way the effects of dilatancy, the tendency of soils to change in volume when undergoing shear. The effect of dilatency upon shear strength (through its effect on pore pressure) can be incorporated indirectly, however, by choosing C_n values to satisfy laboratory data on the stress-strain relationship. With the flexibility that comes from the choice of C_n and k_n values, this rather simple model may give an adequate representation of the behavior of a wide range of material. Extension to more elaborate models poses no obvious difficulties except for possible increase in computation costs.

4. Dynamic Boundary Conditions

Problems involving the response of soils to seismic motion in the underlying bedrock are commonly solved by assigning the particle velocity (or acceleration or displacement) along the boundary between rock and soil. This is an approximation, because in the real case the reaction of the soil will modify the motion of the boundary. The accuracy of the approximation depends on the contrast in properties across the boundary. Assigning particle velocity at the soil-rock boundary is the equivalent of assuming infinite rigidity and incompressibility for the rock. Such as assumption has the disadvantage of allowing no energy to be radiated out of the soil system. If the rate of energy dissipation within the soil is small, multiple reflections may give rise to resonances that are significantly stronger than would occur in a system that allowed energy to be radiated from the boundary. This may be true even for systems with substantial contrasts in rigidity and incompressibility at the boundary. The method presented in this paper, which assumes zero energy loss in compressional deformation, is particularly sensitive to this problem. For low amplitude motion the energy loss in shear would be small and the problem would occur for shear waves also.

To minimize this problem, the writer has adopted a method for approximating the boundary conditions that is based on the method used in one dimension by Papastamatiou (written communication). The approach is similar to that of Lysmer and Kuhlemeyer (1969). At every point on the boundary a vector function V_F is defined which is the particle velocity that would be produced by the given seismic sources if the boundary were a free surface. The actual motion V of the point is then approximated by substituting for the sources an equivalent combination of plane P and S waves normally incident on the boundary.

The velocity V of a boundary node is obtained by solving an equation involving all of the forces acting on the node. In general, a node along the boundary is associated with two boundary segments (Figure 5). The forces on half of each segment are considered to be applied to the given node. Consider one segment at a time. Define a new coordinate system x_i', rotated so that x_3' is normal to the boundary (Figure 5). The specified input function when transformed to the prime coordinate system is given by

$$V_{Fi}' = \beta_{ij} V_{Fj}$$

where β_{ij} is the matrix of the transformation. Since the x_2 axis is the axis of rotation

$$\beta_{22} = 1.0$$

$$\beta_{12} = \beta_{21} = \beta_{23} = \beta_{32} = 0$$

The motion V_i of the boundary node is considered the sum of incident and reflected P, SV, and SH waves with ray paths normal to the boundary node is considered the sum of incident and reflected P, SV, and SH waves with ray paths normal to the boundary segment in question.

$$\begin{aligned} V'_3 &= V'_{PI} + V'_{PR} \\ V'_1 &= V'_{SVI} + V'_{SVR} \\ V'_2 &= V'_{SHI} + V'_{SHR} \end{aligned} \tag{16}$$

V_{Fi}; is defined such that

$$\begin{aligned} V_{F3}' &= 2V_{PI}' \\ V_{F1}' &= 2V_{SVI}' \\ V_{F2}' &= 2V_{SHI}' \end{aligned} \tag{17}$$

To compute for forces on the node due to the input motion, note that V_{PI}' and V_{PR}' are considered plane waves in the underlying medium. The corresponding particle displacements can be expressed as follows:

$$U_{PI}' = U_{PI}' (x_3' - v_p t)$$

$$U_{PR}' = U_{PR}' (x_3' + v_p t)$$

where v_p is the compressional wave velocity in the underlying medium.

$$\frac{\partial U_{PI}'}{\partial x_3'} = \frac{-V'_{PI}}{v_p}$$

$$\frac{\partial U_{PR}'}{\partial x_3'} = \frac{V'_{PR}}{v_p} .$$

The strain components in the underlying medium due to the hypothesized incident and reflected P waves are

$$E'_{PI33} = \frac{-V'_{PI}}{v_p}$$

$$E'_{PR33} = \frac{V'_{PR}}{v_p} .$$

The corresponding stress components are

$$S'_{PI33} = \frac{-(K+4G_o/3)\ V'_{PI}}{v_p}$$

$$S'_{PR33} = \frac{(K+4G_o/3)\ V'_{PR}}{v_p}$$

The equations above can be rewritten

$$S'_{PI33} = -\rho v_p\ V_{PI}'$$

$$S'_{PR33} = \rho v_p\ V_{PR}'$$

Substituting from equations (16) and (17) and adding gives

$$S_{P33}' = \rho v_p\ (V_3' - V_{F3}').$$

A corresponding argument gives

$$S'_{SV31} = S'_{SV13} = \rho v_s\ (V_1' - V_{F1}')$$

$$S'_{SH32} = S'_{SH23} = \rho v_s\ (V_2' - V_{F2}')$$

where v_s is the shear wave velocity in the underlying medium. The other stress components are zero.

The force F_{ai}' applied to the given node from boundary segment a is then

$$F_{a3}' = -\rho v_p\ (V_3' - V_{F3}')\Delta s_a/2$$

$$F_{a1}' = -\rho v_s\ (V_1' - V_{F1}')\Delta s_a/2$$

$$F_{a2}' = -\rho v_s\ (V_2' - V_{F2}')\Delta s_a/2$$

where Δs_a is the length of boundary segment a.

Transforming to the original coordinate system and adding the forces from boundary segments a and b gives

$$F_{ai} + F_{bi} = -A_{ij}\ (V_j - V_{Fj}) \qquad (18)$$

where the non-zero components of A_{ij} are given by

$$A_{11} = (\beta_{11}^{-1} v_s \beta_{11} + \beta_{13}^{-1} v_p \beta_{31})_a \rho \Delta s_a / 2$$
$$+ (\beta_{11}^{-1} v_s \beta_{11} + \beta_{13}^{-1} v_p \beta_{31})_b \rho \Delta s_b / 2$$

$$A_{13} = (\beta_{11}^{-1} v_s \beta_{13} + \beta_{13}^{-1} v_p \beta_{33})_a \rho \Delta s_a / 2$$
$$+ (\beta_{11}^{-1} v_s \beta_{13} + \beta_{13}^{-1} v_p \beta_{33})_b \rho \Delta s_b / 2$$

$$A_{31} = (\beta_{31}^{-1} v_s \beta_{11} + \beta_{33}^{-1} v_p \beta_{31})_a \rho \Delta s_a / 2$$
$$+ (\beta_{31}^{-1} v_s \beta_{11} + \beta_{33}^{-1} v_p \beta_{31})_b \rho \Delta s_b / 2$$

$$A_{33} = (\beta_{31}^{-1} v_s \beta_{13} + \beta_{33}^{-1} v_p \beta_{33})_a \rho \Delta s_a / 2$$
$$+ (\beta_{31}^{-1} v_s \beta_{13} + \beta_{33}^{-1} v_p \beta_{33})_b \rho \Delta s_b / 2$$

$$A_{22} = \rho v_s (\Delta s_a + \Delta s_b) / 2.$$

All the other forces acting on the given node point are accounted for in the basic computational scheme. Denoting the sum of those other forces by F_i, Newton's second law requires that

$$F_i + F_{ai} + F_{bi} = ma_i \qquad (19)$$

where m is the mass and a the acceleration of the node.

$$a_i = (V_i - V_{Li})/\Delta t \qquad (20)$$

where V_{Li} is the value of V_i from the previous time step. Substituting from equations (18) and (20) into equation (19) gives

$$F_i = A_{ij} (V_j - V_{Fj}) + (V_i - V_{Li}) m/\Delta t.$$

Slight rearrangement gives

$$F_i = (A_{ij} + \delta_{ij}\, m/\Delta t)(V_j - V_{Fj}) + (V_{Fi} - V_{Li})m/\Delta t \qquad (21)$$

The solution of equation (21) for V_i in terms of the other quantities is

$$V_i = V_{Fi} + N_{ij}\,(F_j + (V_{Lj} - V_{Fj})m/\Delta t)$$

where N_{ij} is the inverse of the matrix $(A_{ij} + \delta_{ij}\, m/\Delta t)$.

Components of the matrix N_{ij} are computed for each boundary node at the beginning of the computer program and are stored for use at each time step.

Possible methods of synthesizing realistic input motion are not taken up in this paper. There has been much progress recently in computing expected ground motion using dislocation theory (Boore and Zoback, 1974; Trifunac, 1974), and it is hoped that such methods could be used for generating the required input motion. For the examples presented later in this report, simple plane waves are used as input. Calculations using simple input motion may give valuable insight into the character of earthquake ground response even though the motion itself is not totally realistic.

5. Resolution, Stability, and Convergence

In choosing the mesh size Δx, the rule suggested by Boore (1972b) was adopted which requires 10 mesh points per wavelength for the highest frequency wave for which faithful representation is desired. Once Δx is chosen, the choice of Δt is limited by the requirement of stability. No attempt was made to do a stability analysis of the nonlinear system. The stability requirement derived by Alterman and Loewenthal (1972) for the corresponding linear elastic system is

$$v_p\, \Delta t \leq \Delta x \left[1 + \left(\frac{v_s}{v_p}\right)^2\right]^{-1/2} \qquad (22)$$

In the nonlinear system, v_s is a function of strain level, but for the strain-softening behavior characteristic of soils v_s never exceeds the low-strain limit. Values of Δt chosen in accordance with (22), using the low-strain limiting value for v_s, have not led to any stability problems in nonlinear calculations done by the method described in this report.

Convergence was investigated by repeating an experimental run with Δx and Δt reduced to one-half. The agreement was satisfactory.

6. Examples

Examples are shown for the purpose of illustrating and testing the method. They are not intended as a basis for any general conclusions regarding the response of soil to earthquake motion.

The first example is a linear elastic problem for which Boore, Larner , and Aki (1971) have published a solution calculated by a finite difference method. The problem is a symmetrical basin filled with soft material, excited by a shear wave vertically incident from below with particle motion parallel to the basin axis. A diagram showing half of the symmetrical basin is given in Figure 6. The shear velocity is 0.7 km/sec in the basin and 3.5 km/sec in the underlying medium. The rigidity ratio between the basin material and the underlying medium is 0.0286. The incident wave has the form of a Ricker wavelet.

As explained in a previous section, the input motion for the method described in this report is specified in terms of the motion that would be produced on the soil-rock interface if that interface were a free surface. In this example the motion is approximated at each point on the interface by doubling the amplitude of the incident wave. The approximation neglects the diffractions generated in the underlying medium by the non-planar portions of the interface. The calculations were made using a nodal spacing of 100 meters and a time step of 0.01 second.

The solid lines in Figure 7 show particle displacement calculated by the method of this report. The dashed lines give the results of Boore, Larner, and Aki (1971) for comparison. The agreement is satisfactory, in view of the approximate specification of the input motion and the approximate boundary conditions used in computing the solid lines.

The second example demonstrates the method for a case in which the input motion is strong enough to give a highly nonlinear response. As in the first example, input particle motion is parallel to the long axis of the two-dimensional configuration. The grid is shown in Figure 8. It represents a simple, hypothetical basin 90 meters deep and 540 meters wide at the surface. The nodal spacing is 9 meters and the time step 0.005 second. The basin is filled with cohesive alluvial material with a plasticity index of 20 percent, a density of 2.05 gm/cm^3, and a P velocity of 1.69 km/sec. The material is overconsolidated near the surface, having a maximum past vertical effective stress of 2.94 bars. Complete water saturation prevails throughout. In the underlying medium the density is 2.6 gm/cm^3, the P velocity 3.7 km/sec and the S velocity 2.0 km/sec.

The key material parameters are the maximum shear stress σ_{max} and the low strain shear modulus G_o. Both parameters are strongly dependent upon the effective stress prior to seismic excitation, which in turn depends upon depth. An attempt was made to assign values to these parameters as functions of depth in a reasonably realistic manner. The approach taken relies heavily on the work of Hardin and Drnvich (1972b). The approach is described in some detail to show how the parameters might be estimated for a real problem.

In the normally consolidated part of the section σ_{max} was assumed proportional to effective stress,

$$\sigma_{max} = C_s P_{ve}$$

where P_{ve} is the vertical effective stress prior to seismic excitation. P_{ve} can readily be calculated given the density and the depth. The coefficient C_s was evaluated by assuming that no pore-pressure change occurs during shear and using the Mohr's circle construction in Figure 9. This gives

$$\sigma_{max} = \frac{1 + K_o}{2} \sin \bar{\phi} P_{ve}$$

where $\bar{\phi}$ is the angle of drained shear resistance and K_o is the coefficient of earth pressure at rest. Estimation on the basis of the plasticity index of the material gives a value of 31° for $\bar{\phi}$ (Terzaghi and Peck, 1967, p. 112) and 0.55 for K_o (Brooker and Ireland, 1965). Carrying out the computations gives a value of 0.4 for C_s.

The assumption of no pore pressure change will tend to lead to an over-estimate of the strength and thereby of the capacity of the material to transmit shear. Normally consolidated clays tend to contract with shear, increasing the pore pressure and reducing the strength.

For the overconsolidated part of the section it was assumed that σ_{max} obeyed the following relationship

$$\sigma_{max} = C_s P_{ve} (OCR)^T$$

where OCR is the overconsolidation ratio in terms of vertical effective stresses. Analysis of undrained strength data from Ladd and Edgers (1972) gave a value of 0.75 for T.

Hardin and Black (1969; Hardin and Drnvich, 1972b) have shown that for a wide variety of undisturbed cohesive soils, and sands as well, the low-strain shear modulus G_o is given by an equation which can be rewritten in the form

$$G_o = C_G P_{me}^{1/2} (OCR_m)^H$$

where P_{me} is the mean effective stress, OCR_m is the overconsolidation ratio in terms of mean effective stresses, C_G is a constant depending on void ration, and H depends on plasticity index. For a PI of 20 percent H has a value of 0.18.

It is more convenient in the present case to deal in terms of vertical stresses. Using K_o values from Brooker and Ireland (1965) to convert from mean stress to vertical stress, it was found that the values of equation (23) could be reproduced within a few percent over the range of 1.0-32 in OCR by the following equation

$$G_o = C_G P_{ve}^{1/2} (OCR)^Q$$

where Q takes on a value of 0.28 for a PI of 20 percent. A value of 0.9×10^6 $(dynes/cm^2)^{\frac{1}{2}}$ was chosen for C_G based on shear velocity on shear velocity measurement in a 180 meter drill hole in alluvium in the San Francisco Bay Area (Warrick, 1974). With these choices

the low-strain shear velocity in the basin ranges from about 200 to 300 meters/sec. The vertical transit time through the basin for shear waves at low strain is 0.3 second. This implies a fundamental resonant frequency of 0.8 Hz for the equivalent plane layer at low strain. The resolution for low strain excitation is approximately 2.5 H_z. At high strain levels this will be reduced somewhat.

Initial values for the total vertical and horizontal stress are specified for each element. Vertical total stress is readily calculated given the depth and the density. Vertical total stress is converted into vertical effective stress by subtracting the fluid pressure. Horizontal effective stress is then calculated from vertical effective stress using K_o data from Brooker and Ireland (1965) for the assumed PI of 20 percent. Finally, horizontal total stress is obtained by adding the fluid pressure.

The input consists of a plane SH wave incident from the left at an angle of 30° from the vertical. The time history of the particle velocity, after doubling to allow for the effect of the bedrock surface, is that of the integrated N21E component of the Taft accelerogram multiplied by a factor of 4, giving a peak velocity of 67 cm/sec. (The Taft accelerogram was recorded during the 1952 Kern County, California, earthquake.) No attempt was made to correct the input motion to account for departure of the bedrock surface from a plane. This approximation should be adequate because the dimensions of the sloping portions of the basin are small compared to a wavelength in the underlying medium (Boore, 1972a).

Results are shown in Figure 10, which gives the horizontal component of particle velocity in the direction of the long axis of the basin at the points on the surface designated in Figure 8. The peak particle velocity at the midpoint of the basin is larger than that of the input motion by about 25 percent. Computations with a one-dimensional method (Joyner and Chen, 1975) give a particle velocity time history almost identical to that for the two-dimensional calculation at the midpoint of the basin. The peak values differ by less than one percent.

Even though the input motion has a component only in the direction of the basin axis, the components of particle velocity in the plane perpendicular to the axis do not vanish, as they would in the elastic case. Because of the initial stress and the nonlinear material behavior, antiplane strain motions (motions parallel to the long axis of the structure) are not uncoupled from plane strain motions (motions in the plane perpendicular to the long axis). The plane strain components (x_1 and x_3) are very small, however, the peak being no more than three percent of the peak antiplane strain component for nodes 1 through 5 on Figure 8. This suggests the feasibility of developing simplified models in which only antiplane strain motion is permitted. Such models would reduce computation time by a large factor, in part because the number of computations per time step would be significantly reduced, but also because larger time steps could be used. This is true because, if compressional deformation is excluded from the model, the stability requirement on Δt (Boore, 1972b) is much less restrictive. Plane strain models are subject to the same stability requirement as the general model, but they, too, offer savings in

computation time by reducing the number of computations per time step.

For a model restricted to antiplane strain it is necessary to ignore initial stress and carry out the computations in terms of stress departures from an unspecified initial state rather than in terms of absolute stress. Computations made with both antiplane strain and plane strain input motions indicate that this is feasible. The results of runs made with initial deviatoric stress set to zero show little difference from those with initial stress assigned by the methods described previously. Ignoring initial stress and dealing in terms of stress departures from an initial state is convenient in the plane strain case, though not necessary as with antiplane strain.

For the example of Figures 8 and 10, the computations required 740 seconds on the CDC 7600 at the Lawrence Berkeley Laboratory. This is the equivalent of 360 microseconds per element per time step and indicates that the method is fast enough to be useful. (Running time is essentially proportional to the product of the number of elements and the number of time steps.) The larger time step permissible with an antiplane strain model would reduce the computation time on this example by a factor of six. A further reduction by about a factor of two would result from the reduction in the number of computations per time step in an antiplane strain model. Even with the reductions, however, the cost of the computations will place a practical limit of the size of the problem that can be solved for a given frequency resolution.

The final example involves plane strain input motion and illustrates the application of the method to calculating the response of earth dams. As in the previous example, the input motion is strong enough to produce a highly nonlinear response. The configuration, as shown in Figure 11, represents a simplified model of an earth dam. The nodal spacing is 9 meters and the time step 0.005 second. The elements marked with dots represent the clay core of the dam and the other elements represent granular material. For simplicity all elements are assigned a density of 2.05 gm/cm^3, a P velocity of 1.69 km/sec and a low strain shear velocity of 300 meters/sec. This gives a low-strain frequency resolution of 3.3 Hz. The maximum shear σ_{max} is 0.9×10^6 $dynes/cm^2$ for the clay core and 1.2×10^6 $dynes/cm^2$ for the granular material. In the underlying medium the density is 2.6 gm/cm^3, the velocity 3.7 km/sec and the S velocity 2.0 km/sec. The initial stress is ignored and the computations are carried out in terms of stress departures from the unspecified initial state. Only plane strain motions are permitted.

The input motion consists of a vertically incident plane shear wave with particle motion confined to the plane of the section shown in Figure 11. The time history of particle velocity for the input motion is the same as in the previous example, with the amplitude doubled, as in the previous example, to allow for the effect of the bedrock surface.

The results are shown in Figure 12, which gives the horizontal particle velocity for the points on the surface indicated in Figure 11. The peak velocity at the crest is approximately 30 percent greater than the peak for the input. The computations required 200 seconds on the CDC 7600, which represents 210 microseconds per element per time step.

7. Conclusions and Applications

The Iwin rheological model leads to an efficient method for two-dimensional soil response calculations that takes account of the nonlinear, hysteretic behavior of soil and allows flexibility for incorporating laboratory data on soil behavior. The method can be used to compute free-field response at sites where the soil configuration cannot be adequately represented by simple plane layers. For a given frequency resolution, however, the size of such models is limited by computer time requirements. The method has particular promise for use in calculating the response of earth dams. It could also be adapted to the calculation of soil-structure interaction in two or three dimensions.

8. Acknowledgments

The writer is indebted to Harold W. Olsen for his advice on questions relating to soils dynamics and to David M. Boore and D.J. Andrews for helpful suggestions concerning two-dimensional finite mesh calculations. D.J. Andrews and Albert T.F. Chen read the manuscript and suggested a number of improvements.

References

1. Alterman, Z., and D. Loewenthal (1972). Computer generated seismograms, in Methods in Computational Physics, Vol. 12, Seismology, Body Waves and Sources, Bruce A. Bolt (ed.), Academic Press, New York, 35-164.

2. Boore, D.M. (1972a). A note on the effect of simple topography on seismic SH waves, Bull. Seism. Soc. Am., 62, 275-284.

3. Boore, D.M. (1972b). Finite difference methods for seismic wave propagation in heterogeneous materials, in Methods in Computational Physics, Vol. 11, Seismology, Surface Waves and Earth Oscillations, Bruce A. Bolt (ed.), Academic Press, New York, 1-37.

4. Boore, D.M., K.L. Larner, and K. Aki (1971). Comparison of two independent methods for the solution of wave-scattering problems: Response of a sedimentary basin to vertically incident SH waves, J. Geophys. Res., 76, 558-569.

5. Boore, D.M., and M.D. Zoback (1974). Two-dimensional kinematic fault modeling of the Pacoima Dam strong-motion recordings of the February 9, 1971, San Fernando earthquake, Bull. Seism. Soc. Am., 64, 555-570.

6. Brooker, E.W., and H.O. Ireland (1965). Earth pressures at rest related to stress history, Canadian Geotechnical Journ., 2, 1-15.

7. Chen, A.T.F., and W.B. Joyner (1974). Multi-linear analysis for ground motion studies of layered systems, Report No. USGS-GS-74-020, NTIS No. PB232-704/AS, Clearinghouse, Springfield, VA 22151.

8. Constantopoulos, I.V. (1973). Amplification studies for a nonlinear hysteretic soil model, Research Report R73-46, Department of Civil Engineering, Massachusetts Institute of Technology, 204 p.

9. Faccioli, Ezio, Enrique Santoyo V., and J.T. Leon T. (1973). Microzonation criteria and seismic response for the city of Managua, Proceedings of the Earthquake Engineering Research Institute Conference on the Managua, Nicaragua, Earthquake of December 23, 1972, Vol. I, 271-301.

10. Fung, Y.C. (1965). Foundations of Solid Mechanics, Prentice-Hall, Englewood Cliffs, New Jersey.

11. Hardin, B.O., and W.L. Black (1969). Vibration modulus of normally consolidated clay (discussion), Proc. Am. Soc. Civil Engin., Journ. Soil Mech. and Found. Div., 95, 1531-1537.

12. Hardin, B.O., and V.P. Drnevich (1972a). Shear modulus and damping in soils: Measurement and parameter effects, Proc. Am. Soc. Civil Eng., Journ. Soil Mech. and Found. Div., 98, 603-624.

13. Hardin, B.O., and V.P. Drnevich (1972b). Shear modulus and damping in soils: Design equations and curves, Proc. Am. Soc. Civil Eng., Journ. Soil Mech. and Found. Div., 98, 667-692.

14. Hudson, D.E. (1972). Strong motion seismology, Proceedings of the International Conference on Microzonation, Seattle, Washington, Vol. I, p. 29-60.

15. Idriss, I.M., and H.B. Seed (1968). Seismic response of horizontal soil layers, Proc. Am. Soc. Civil Eng., Journ. Soil Mech. and Found. Div., 94, 1003-1031.

16. Idriss, I.M., and H.B. Seed (1974). Seismic response by variable damping finite elements, Proc. Am. Soc. Civil Eng., Journ. Geotechnical Eng. Div., 100, 1-13.

17. Iwan, W.D. (1967). On a class of models for the yielding behavior of continuous and composite systems, Jour. of Applied Mechanics, 34, 612-617.

18. Joyner, W.B., and A.T.F. Chen (1975). Calculation of nonlinear ground response in earthquakes, Bull. Seism. Soc. Am. (in press).

19. Kanai, K. (1952). Relation between the nature of surface layer and the amplitudes of earthquake motions, Bull. Earthq. Res. Inst., Tokyo Univ., 30, 31-37.

20. Ladd, C.C., and Lewis Edgers (1972). Consolidated-undrained direct-simple shear tests on saturated clays, Research Report R72-82, Department of Civil Engineering, Massachusetts Institute of Technology, Cambridge, Mass.

21. Lysmer, John, and R.L. Kuhlemeyer (1969). Finite dynamic model for infinite media, Proc. Am. Soc. Civil Eng., Journ. of the Eng. Mechanics Div., 95, 859-877.

22. Newmark, N.M., A.R. Robinson, A.H.-S. Ang, L.A. Lopez, and W.J. Hall (1972). Methods for determining site characteristics, Proceedings of the International Conference on Microzonation, Seattle, Washington, Vol. I, p. 113-129.

23. Schnabel, P., H. Bolton Seed, and J. Lysmer (1972). Modification of seismograph records for effects of local soil conditions, Bull. Seism. Soc. Am., 62, 1649-1664.

24. Streeter, V.L., E.B. Wylie, and F.E. Richart (1974). Soil motion computations by characteristics method, Proc. Am. Soc. Civil Eng., Journ. Geotechnical Eng. Div., 100, 247-263.

25. Terzaghi, Karl, and R.B. Peck (1967). Soil Mechanics in Engineering Practice (2d ed.), Wiley, New York.

26. Trifunac, M.D. (1974). A three-dimensional dislocation model for the San Fernando, California, earthquake of February 9, 1971, Bull. Seism. Soc. Am., 64, 149-172.

27. Warrick, R.E. (1974). Seismic investigation of a San Francisco Bay mud site Bull. Seism. Soc. Am., 64, 375-385.

28. Whitman, R.V. (1961). Some considerations and data regarding the shear strength of clays, in Research Conference on Shear Strength of Cohesive Soils, American Society of Civil Engineers, New York, 581-614.

Figure Captions

Figure 1 - Schematic diagram of computational grid.

Figure 2 - Diagram showing the different types of elements and the numbering of the nodes.

Figure 3 - Rheological model in one dimension (Iwan, 1967).

Figure 4 - Hysteresis loops produced by the model of Figure 3 under cyclic loading with increasing amplitude.

Figure 5 - A portion of the boundary.

Figure 7 - Horizontal particle displacement for the soft basin problem. Solid lines represent results of the method described in this report and dashed lines are from Boore, Larner, and Aki (1971)

Figure 8 - Grid for hypothetical basin described in text.

Figure 9 - Mohr's circle construction for determining σ_{max}. The inner circle represents the intital geostatic stress state and the outer circle represents the limiting state.

Figure 10 - Horizontal component of particle velocity in the direction of the long axis of the basin at the points on the surface designated in Figure 8.

Figure 11 - Grid for simplified model of earth dam described in text. The elements marked with dots represent the clay core.

Figure 12 - Horizontal particle velocity at the points on the surface designated in Figure 11.

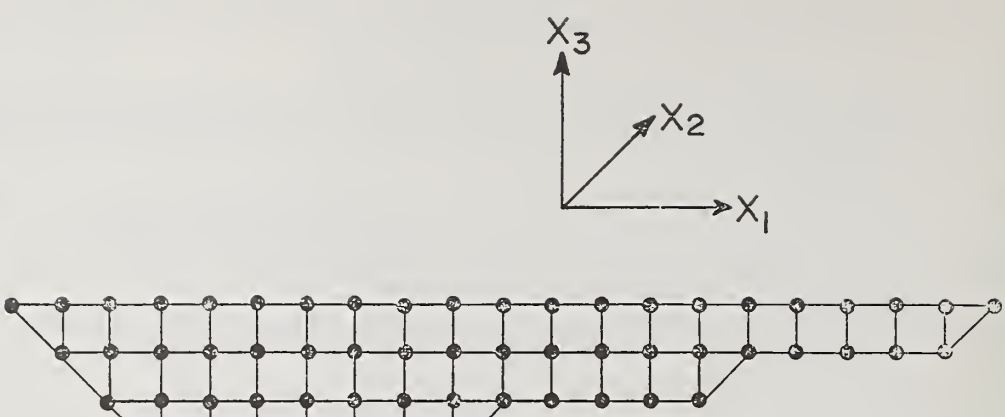

Figure 1

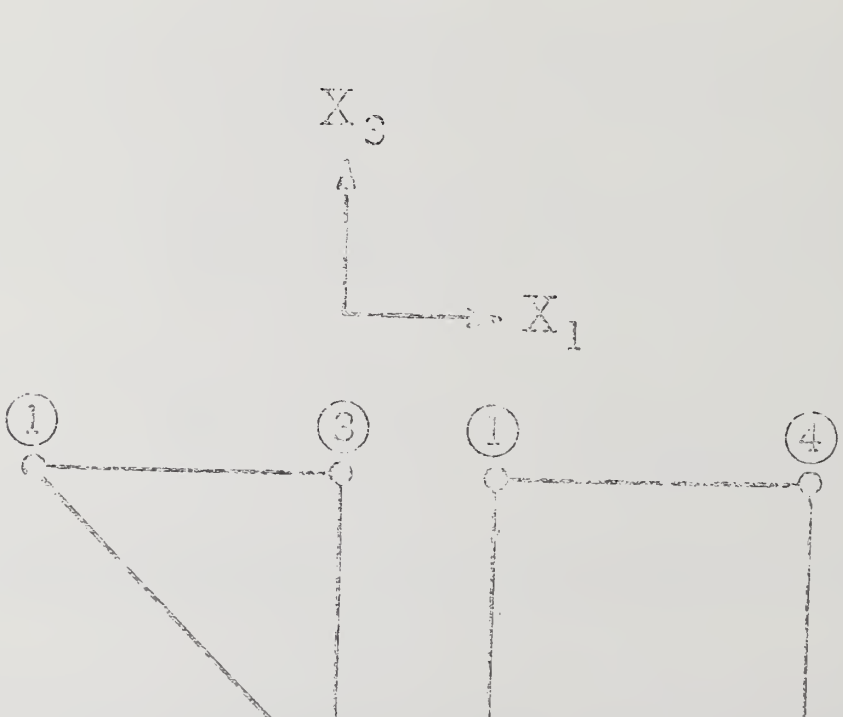

Figure 2

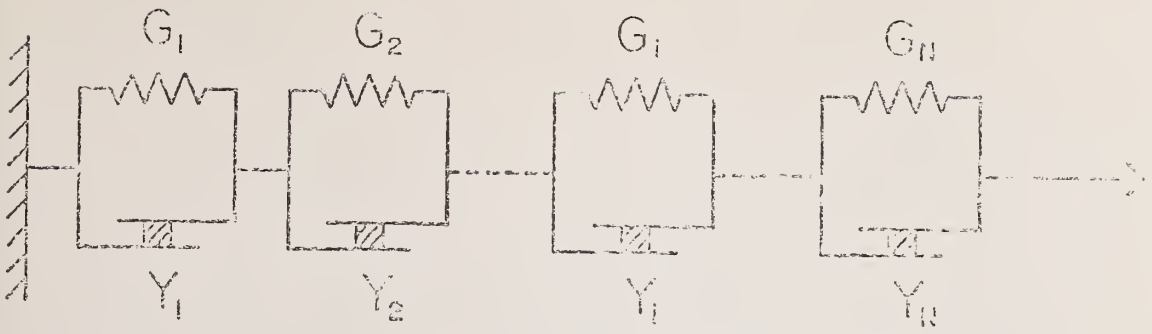

Figure 3

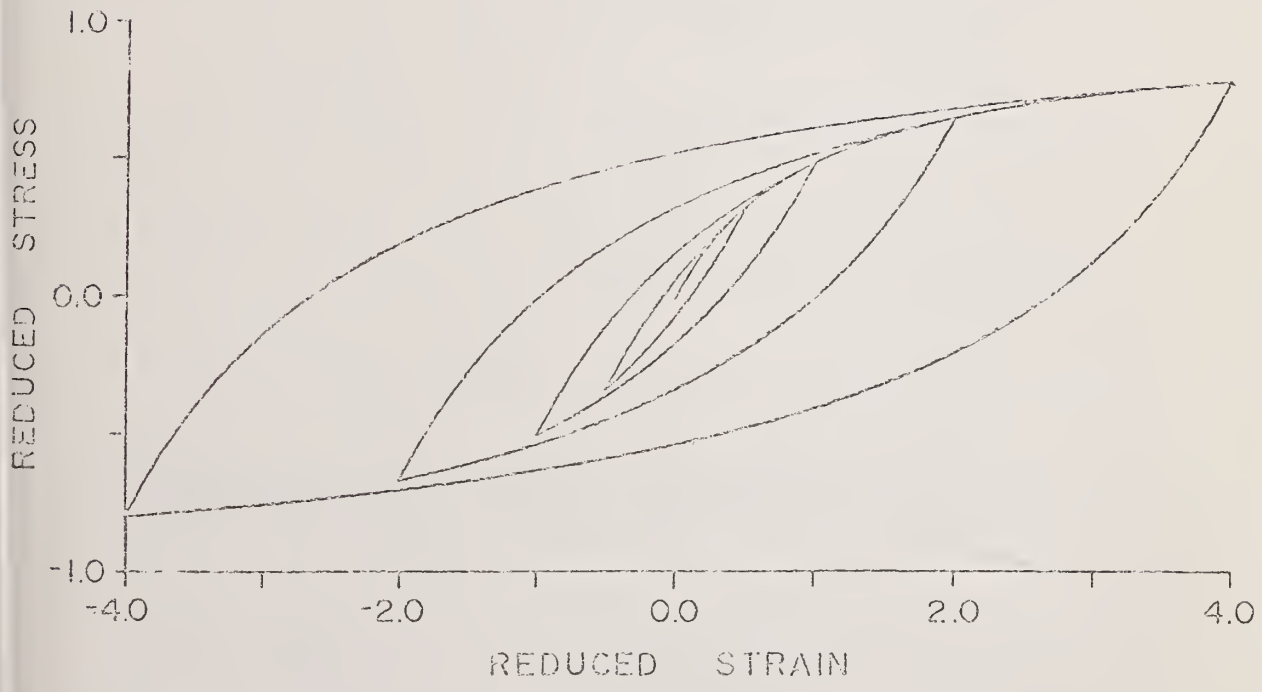

Figure 4

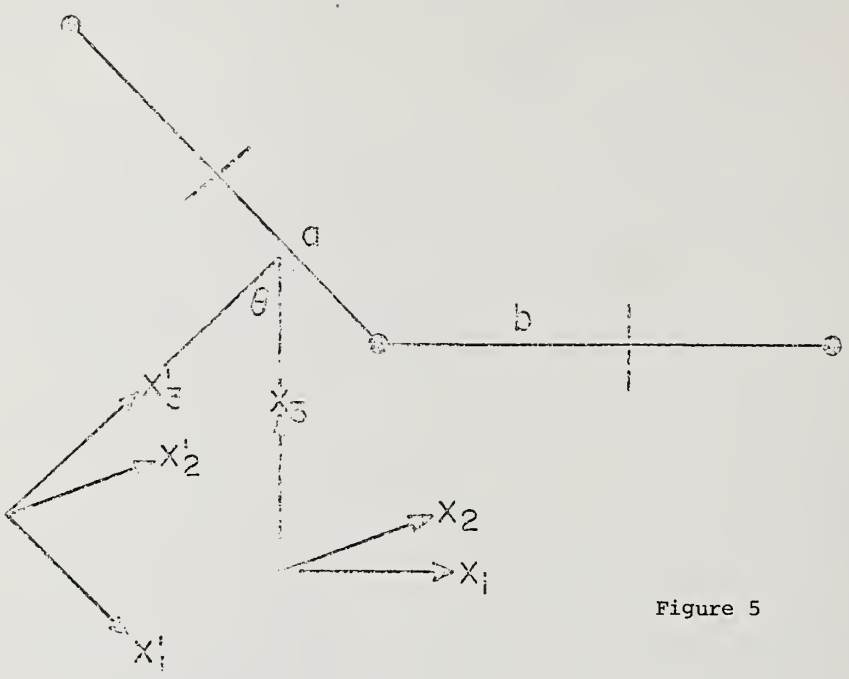

Figure 5

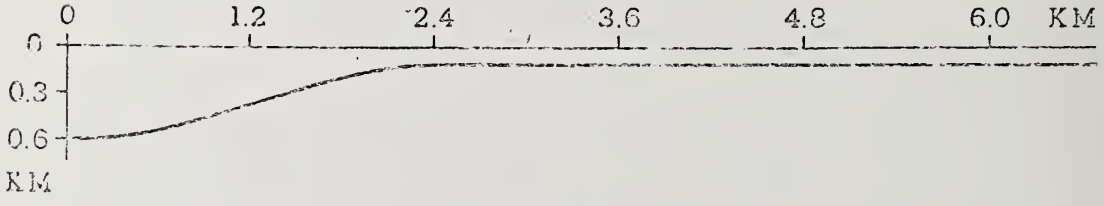

Figure 6

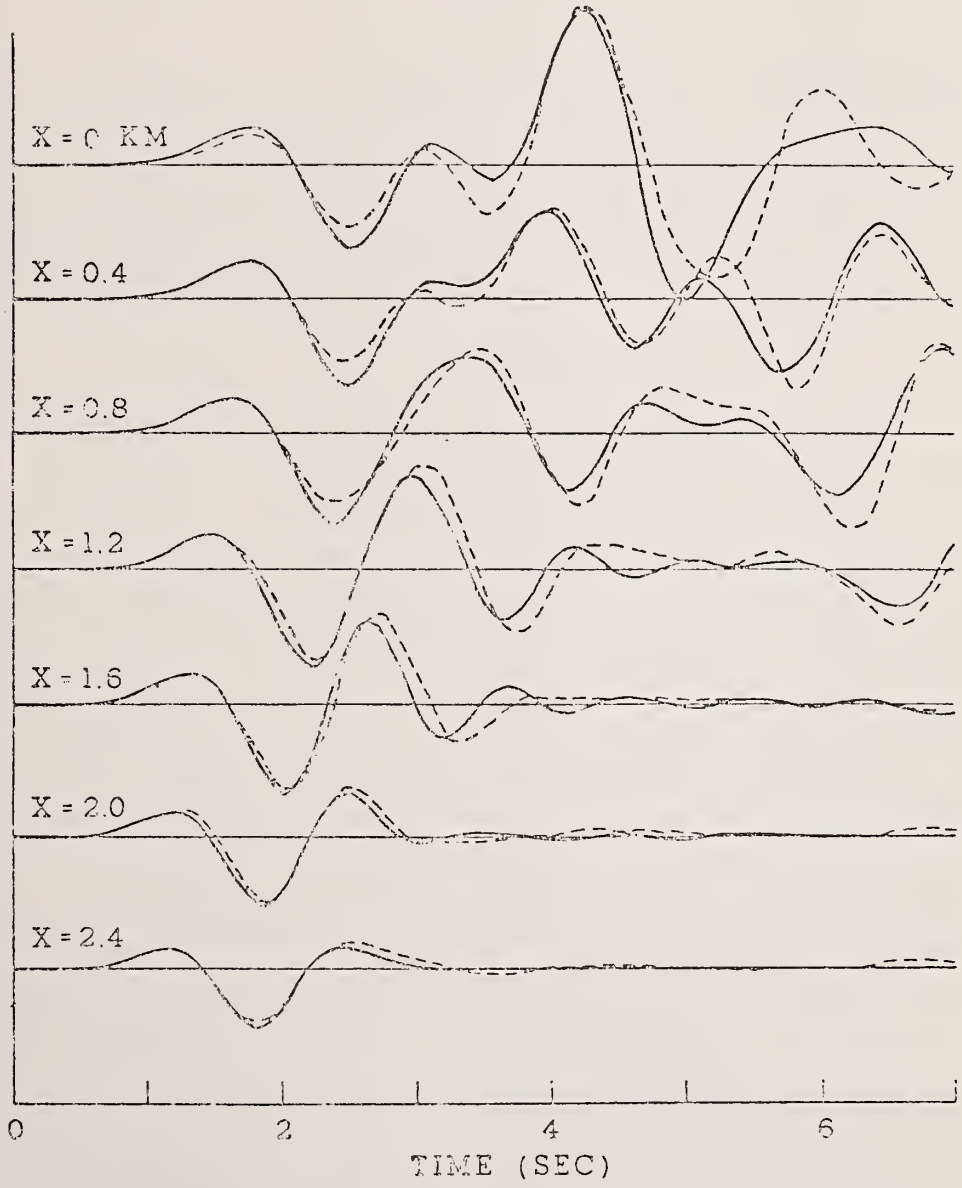

Figure 7

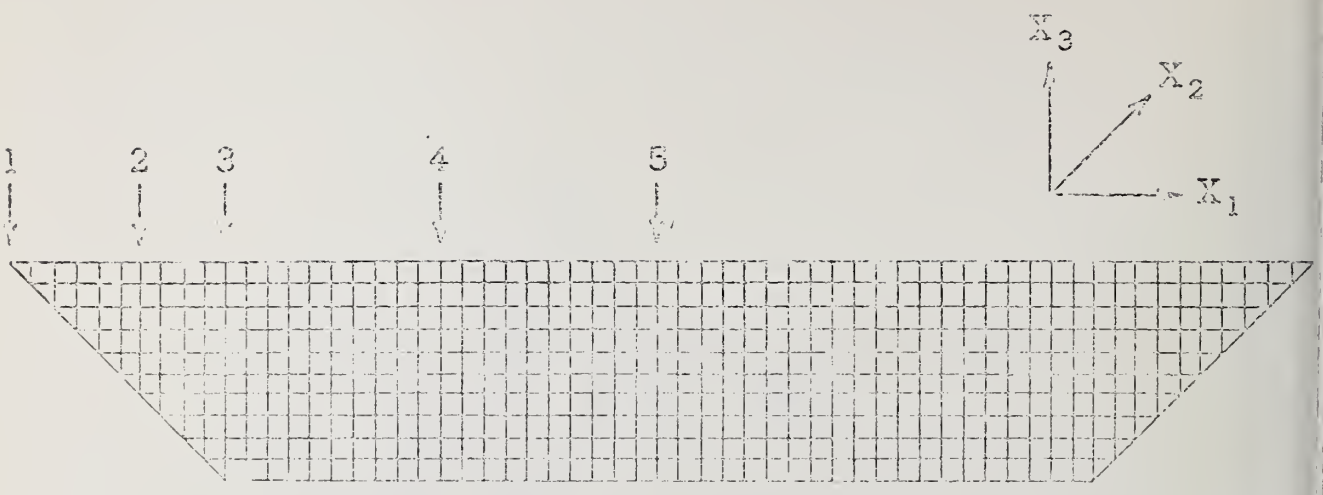

Figure 8

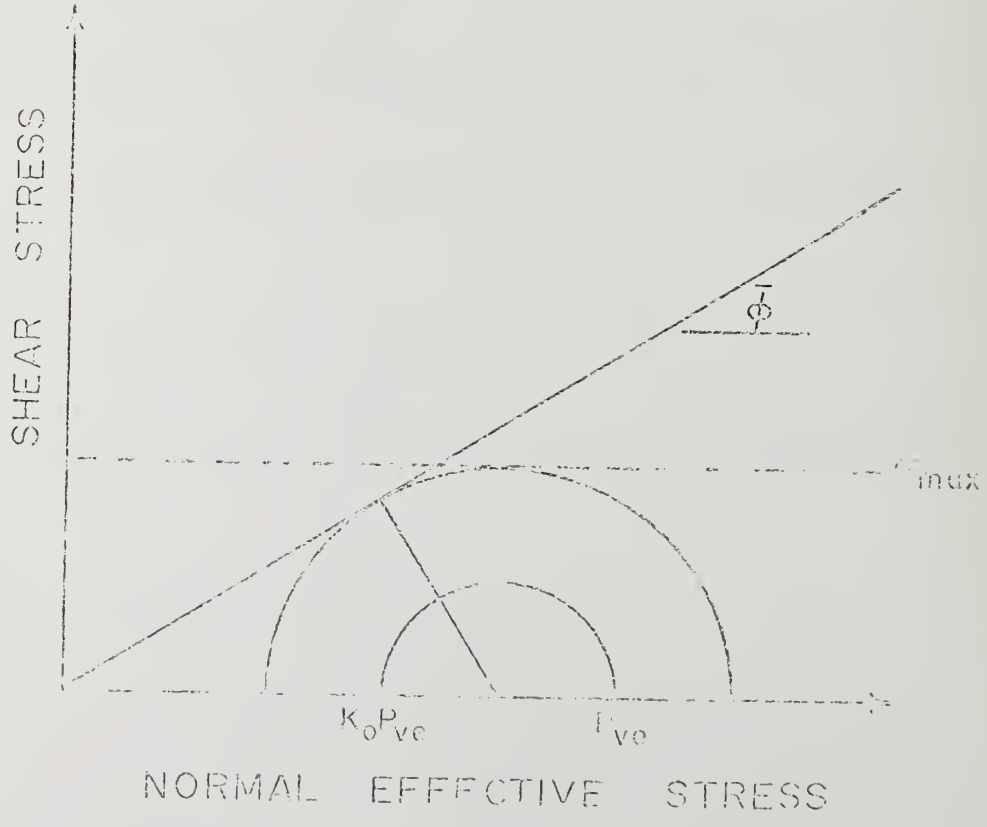

Figure 9

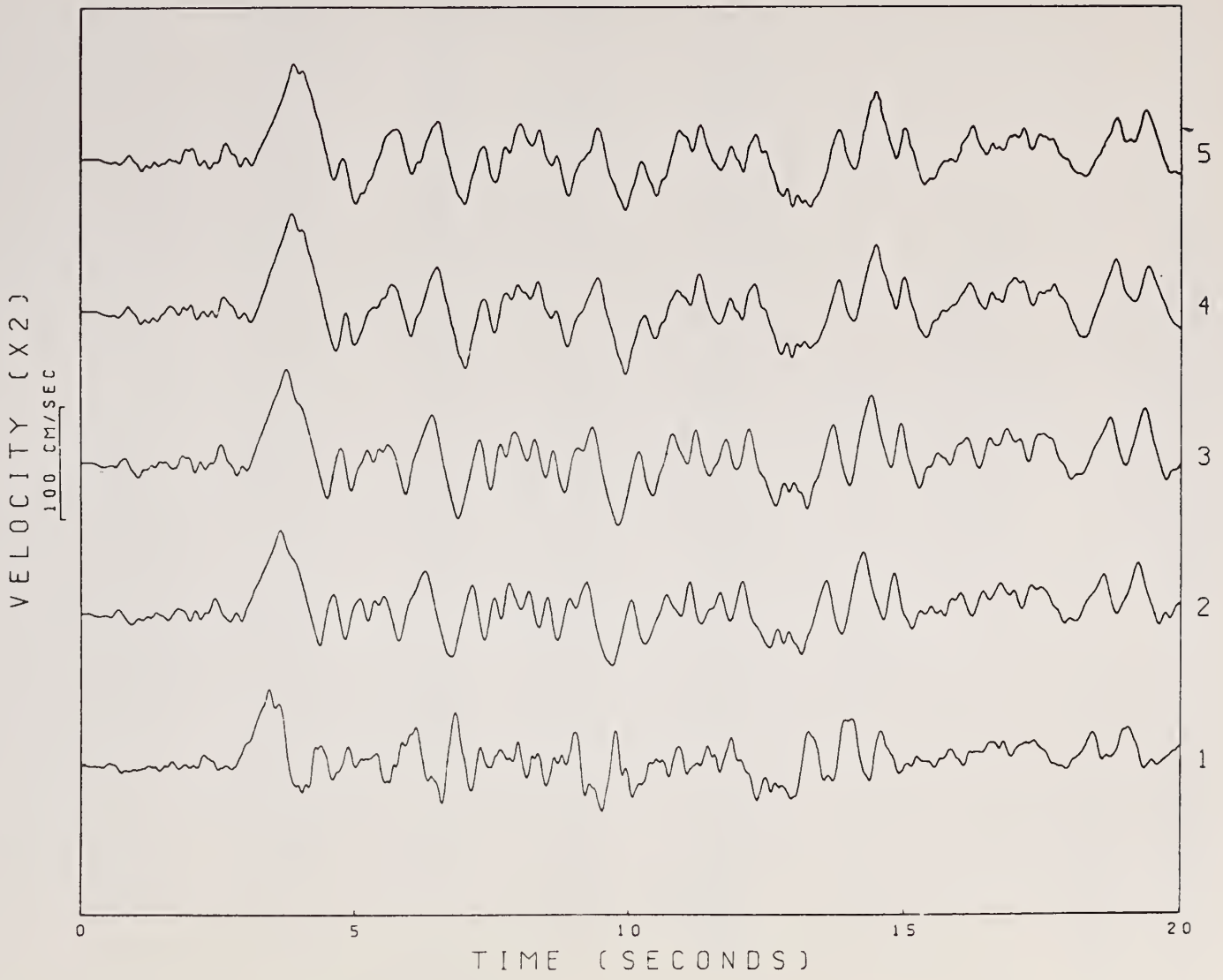

Figure 10

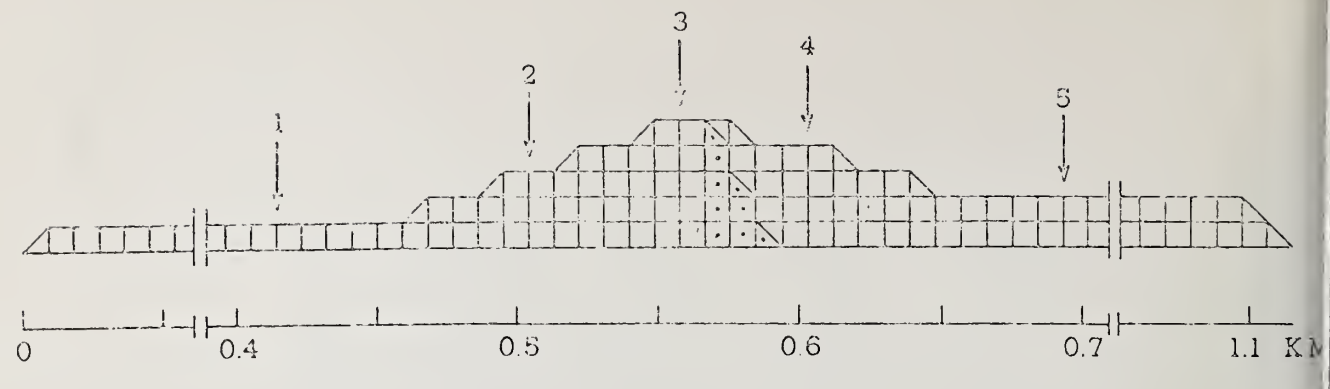

Figure 11

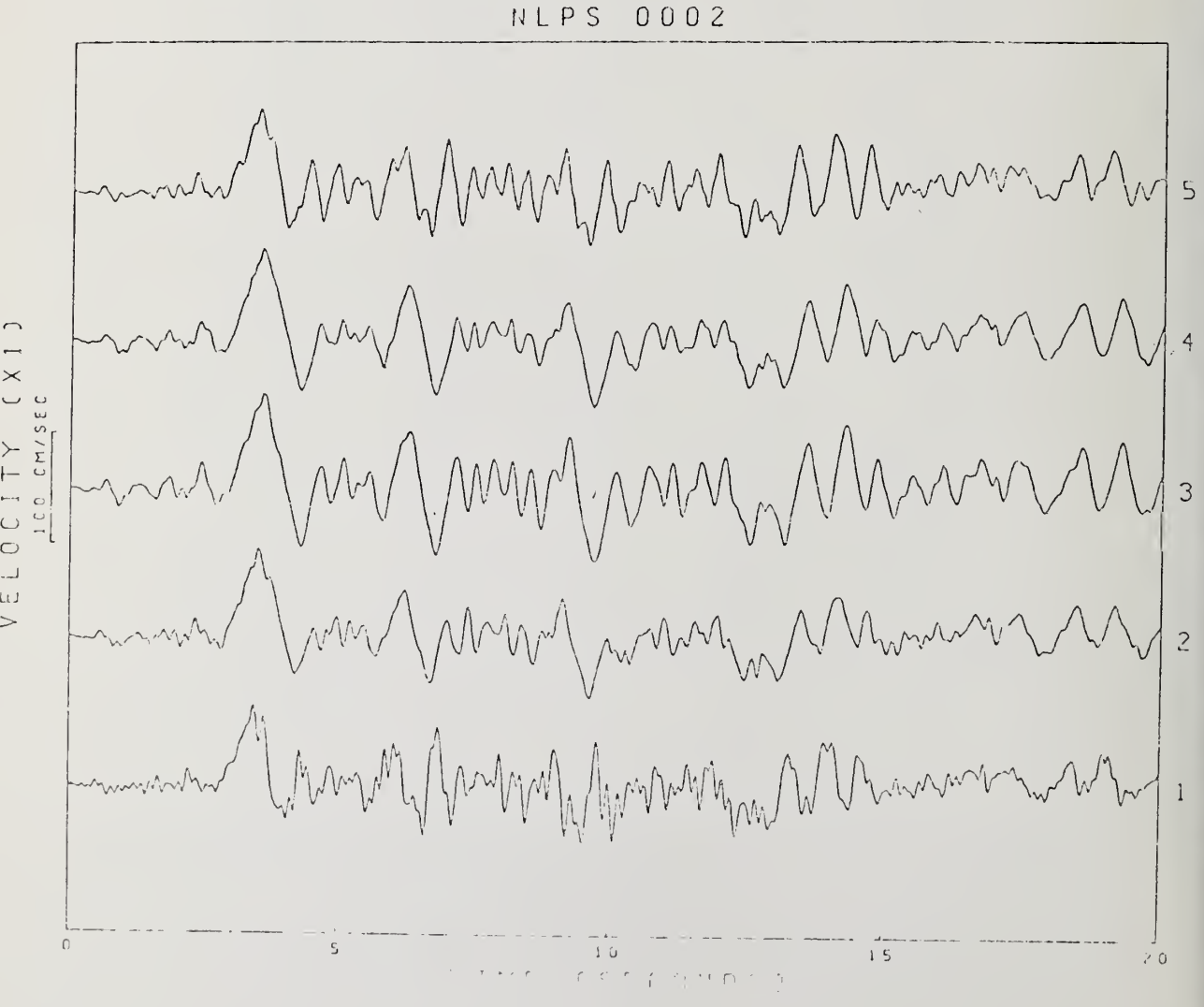

Figure 12

A NEW SCALE REPRESENTING THE "QUAKE-SENSITIVITY" AT A CERTAIN REGION

TSUTOMU TERASHIMA
Chief, Seismology Section
International Institute of Seismology
and Earthquake Engineering
Building Research Institute
Ministry of Construction
Japan

TETSUO SANTO
Head
International Institute of Seismology
and Earthquake Engineering
Building Research Institute
Ministry of Construction
Japan

ABSTRACT

The nature of ground motions due to earthquakes, depends on the property of the superficial materials of the ground, which vary in different areas. In this paper, the different characteristics of the ground motions is normalized by a new scale designated as "Quake-Sensitivity." This scale is defined as a ratio of N(I)/S, where N(I) is the annual mean frequency of seismic intensity of more than III (in J.M.A. scale) and S is seismicity index which has been defined previously by the authors.

A seismic zoning map was then made for Japan Islands relative to the "Quake-Sensitivity". The area having a large value of N(I)/S means that the area is sensitive to earthquake motions or the neighboring area has moderate earthquakes.

Key Words: Earthquake; Index; Quake-Sensitivity; Seismic Index; Seismicity.

1. Introduction

In the previous seventh joint meeting in Tokyo of this Panel (May 20-23, 1975), we introduced "Seismicity Index S" as a quantitative seismicity scale being defined as follows:

$$S = (N(M)/T)_{\Delta \leq 100\text{km}} \qquad T = 100 \text{ years},$$

in which N(M) is the frequency of shallow earthquake with the magnitude M greater than 6.

If a geological structure in a certain region is uniform, the earthquake with the magnitude greater than 6 shakes the ground with seismic intensity of more than approximately III inside a circular area with diameter of 100 km. The distribution of the seismicity index S above defined, therefore, might also represent a regionalization with regard to the annual frequency distribution of a seismic intensity of more than III due to the occurrence of earthquake of $M \geq 6.0$ during 100 years.

In practice, however, the intensity distribution due to a certain earthquake is almost always distorted from a circular configuration because of the different superficial conditions from region to region (Fig. 1). Moreover, if we also take into account the intermediate or deep earthquakes, the distortion of the isoseismal distribution from the circular shape due to the passing and/or the absorption of short period seismic waves caused by the penetration of a rigid slab (Fig. 2) (Utsu et al., 1968). In other words, the distribution of the seismicity index S is not directly related to the distribution of the intensity larger than III.

The present paper is a first step in determining the distribution of the regions which were subjected to an intensity of more than a certain level, say the intensity III on the Japanese scale. Such intensities are caused by special superficial conditions and/or the geographical situations against the distributions of deeper shocks and abnormal situations in the upper mantle being underthrusted by a slab. For this purpose, a new scale representing the "Quake-Sensitivity" of the ground, is proposed.

2. Definition of the "Quake-Sensitivity"

As was mentioned in the previous section, our final purpose is to select special regions where the ground is subjected to abnormally high intensities. The following quantity will be used to describe this intensity;

$$Q.I. = N(I)/S,$$

where the quake intensity is given by the ratio of the frequency of seismic intensity more than a certain level N(I) to the seismicity index S. Taking this ratio, we can exaggerate the regions where the grounds were frequently quaked either due to the occurrence of near ($\Delta < 100$ km) earthquakes of $M < 6.0$ or due to particularly worse situations related to the superficial and/or upper mantle conditions.

3. Analytical Example

Distribution of "Quake-Sensitivity" thus defined is surveyed for Japan. As for N(I), frequency of seismic intensity greater than III (J.M.A. scale) in period 1921-1973 at every stations (Terashima, 1976) are used. As for Seismicity Index S, the result by T. Terashima (1973) is also used directly.

Fig. 3 shows the contour lines of the annual mean frequency of seismic intensity greater than III. Fig. 4 shows the distribution of N(I)/S as derived by superimposing Fig. 3 on Fig. 5 and shows the distribution of seismicity index S in and near Japan. Fig. 4 is further rearranged as given in Fig. 6. From the distribution of high numbers in Fig. 4 and Fig. 6, we can suggest the regions where the ground can be easily quaked. From these maps, the following is recognized:

1, There are sensitive regions for seismic motions even if the seismicity is low. For instance, seismicity indexes S of northern and middle regions in Hokkaido, Niigata prefecture and western part of Kyushu are smaller than Pacific side of Tohoku and Kwanto

regions. But, N(I)/S of those regions are larger than those of Pacific side of Tohoku and Kwanto regions. This means that the regions quite often suffer from the seismic motions compared with Pacific side of Tohoku and Kwanto regions due to smaller events or due to the geological situations.

2. There are non-sensitive regions even if seismicity is active. For instance, seismicity indexes S on Pacific side of Tohoku and Kwanto regions show the largest values in and near Japan. But N(I)/S are not large compared with the other regions. This means that these regions have been quaked mainly due to the events with magnitudes larger than 6.

4. Conclusions

A new scale of "Quake-Sensitivity" which is a ratio of the annual mean frequency of seismic intensity to seismicity index, has been proposed. Regionalization of this Q.I. were made for the Japan Islands (Fig. 4 and Fig. 6) for an example. These maps show the regions in which the ground is frequently quaked due to the following situations:

1. Seismic activity of the earthquakes with the magnitude less than 6 is high in the neighborhood ($\Delta < 100$ km) of the position.

2. The region with bad superficial geological conditions or the region whose locations are such that the high intensities due to the deeper shocks easily appear by the penetrating slab.

Among these conditions, regionalizations due to the second cause is more important by eliminating the effect due to the first cause. We shall aim to make this kind of regionalization as a next step for various intensity levels.

References

1. Utsu, T. and H. Okada, 1968, Anomalies in Seismic Wave Velocity and Attenuation Associated with a Deep Earthquake Zone (II). Jour. Faculty of Science, Hokkaido Univ., Ser. VII, (Geophysics), Vol. 3, No. 2, 65-84.

2. Terashima, T., 1973, Quantification of Seismicity, Bull. Inter. Inst. Seism. Earthq. Engg., 11, 33-41.

3. Terashima, T., 1976, Frequency Distribution of Seismic Intensity in Every Station Belongs to Japan Meteorological Agency, Kenchiku Kenkyu Shiryo, (in press).

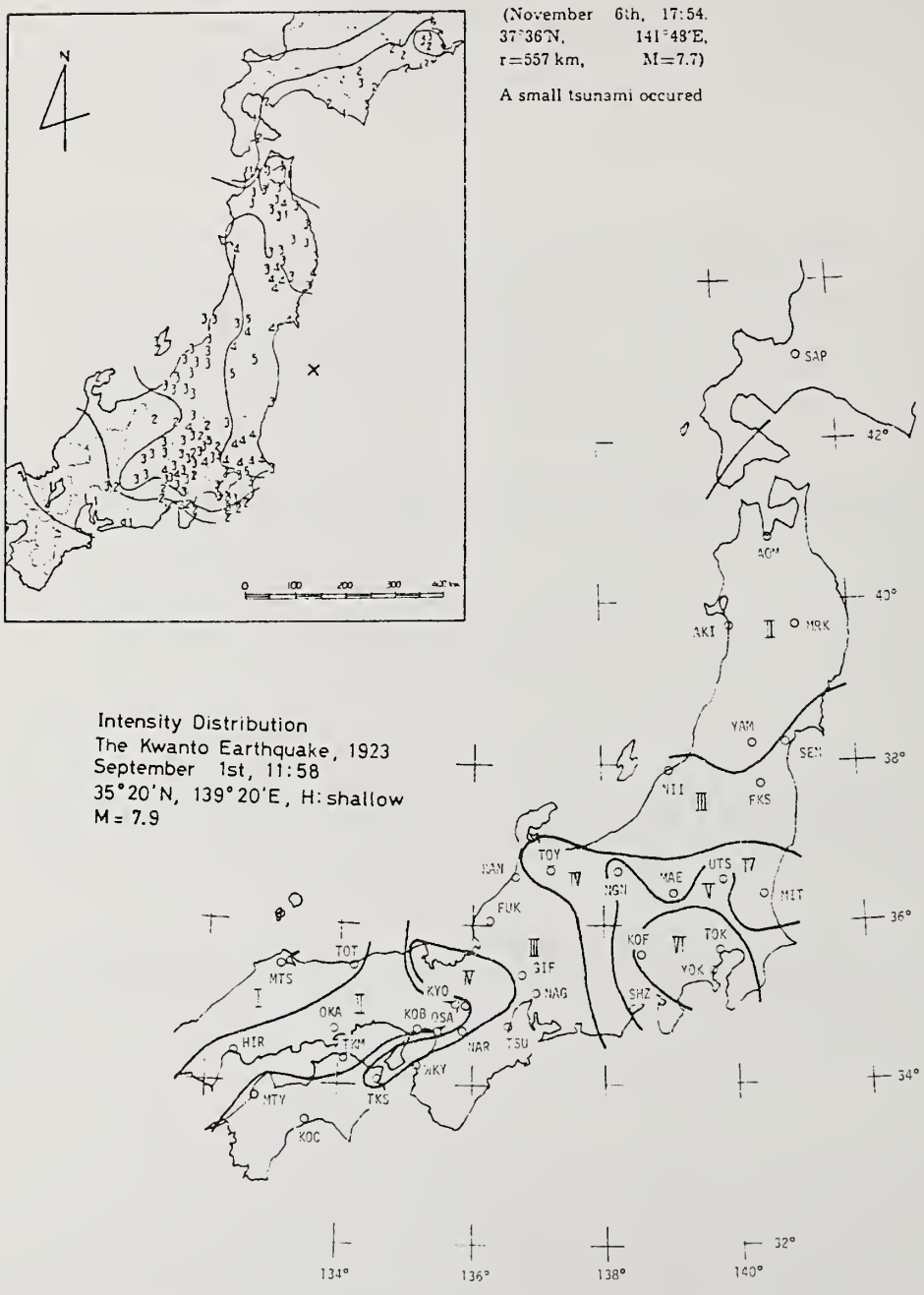

Fig.1. Examples of complicated distribution of seismic intensity.

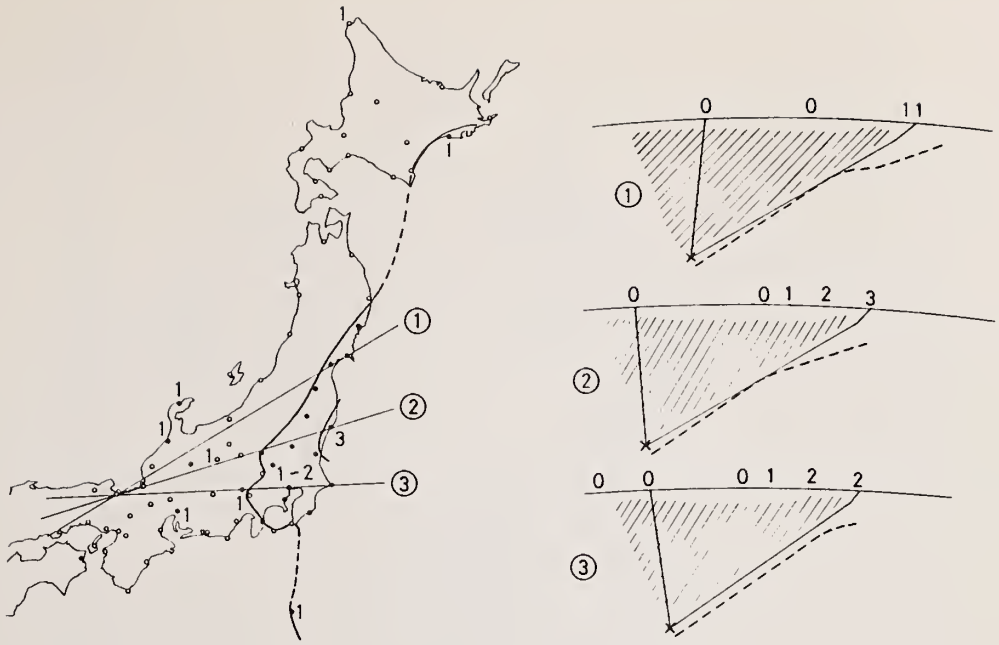

Fig.2. Constitutions of crust and upper mantle of the earth and regions of abnormal seismic intensity.

Fig.3. Mean annual frequency of seismic intensity more than III (J.M.A. scale) at every station and the isoplethic curves.

Fig.4. Distribution of $\bar{N}(I)/S$ obtained from Fig.3 and 5.

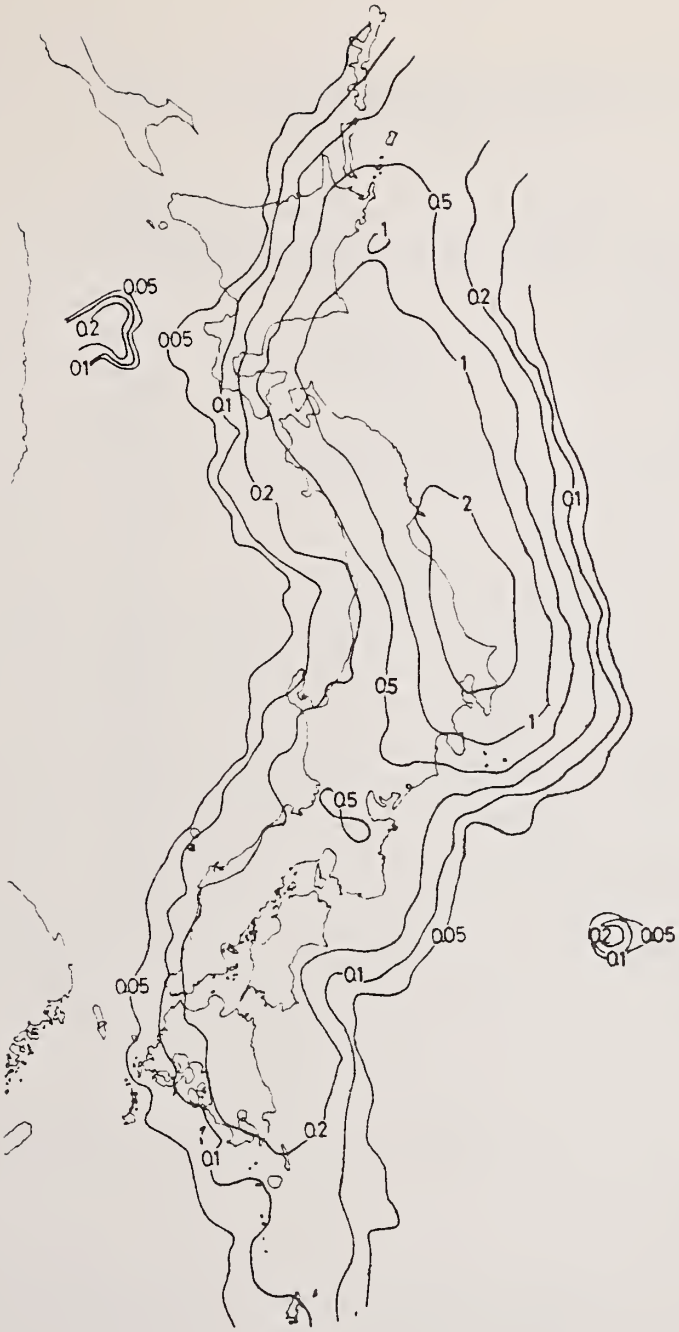

Fig.5. Distribution of seismicity index S in and near Japan.

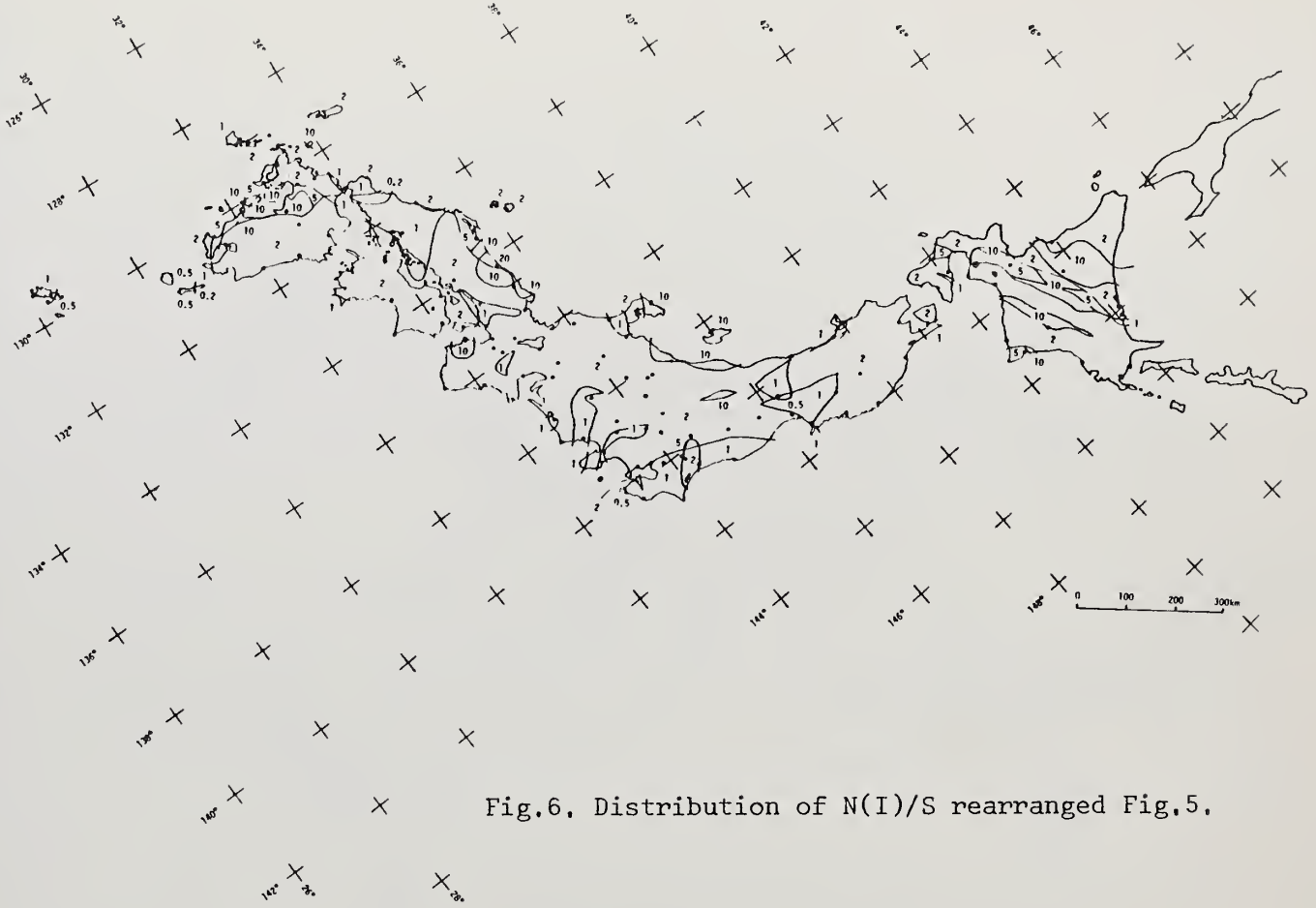

Fig.6. Distribution of N(I)/S rearranged Fig.5.

DAMAGE TO THE CIVIL ENGINEERING STRUCTURES IN HACHIJOJIMA ISLAND BY TYPHOON 7513

T. OKUBO
Head, Planning and Research Administration Division
Public Works Research Institute
Ministry of Construction, Japan

N. NARITA
Chief, Structure Section
P.W.R.I

K. YOKOYAMA
Research Engineer
Structure Section, P.W.R.I.

ABSTRACT

Typhoon 7513 passed across Hachijojima Island on 16:40, October 5, 1975 and caused damage to property, houses and public service. The Public Works Research Institute performed a field investigation in Hachijojima Island. In this paper the record of strong wind and the state of damage are introduced. Typhoon 7513 is classified as a small but strong typhoon, and the maximum wind speed, averaged over ten minute intervals was 35.5 m/s, and the maximum instantaneous wind speed was 67.8 m/s.

The number of the wounded was 85, but fortunately no one was killed. A great deal of damage was done to houses, trees, poles and fences. The damage, with regard to public service was the destruction of a school and hospital building, and the interruption of electric power, telephone, and roads. The damage to large scale structures consisted of the destruction of a guyed tower 30 meters high, a panzer-mast, a bridge and four arc lamp standards.

Key Words: Damage; Structures; Typhoon; Wind; Wind Effects.

1. Introduction

Typhoon 7513 passed the southeast of Okinotorishima Island on October 2, 1975, then continued to the north, and grew to a small but strong typhoon. The typhoon then advanced to the sea south of Honshu (Mainland of Japan) and passed through the Hachijojima Island on 16:40, October 5. This typhoon 7513, caused damage to property, houses, and public service such as electric power, telephone and roads.

The Public Works Research Institute performed a field investigation throughout Hachijojima Island, from October 9 through October 11.

In this paper, the record of the strong winds and the damage situation on Hachijojima Island are introduced.

2. Strong Wind Characteristics

a) Abstract of the Typhoon 7513

According to the announcement of the Meteorological Agency, typhoon 7513 passed near Hachijojima Island on 16:40, October 5 as shown in Fig. -1. At that time the central pressure of the typhoon was 945 mb, the maximum wind speed was 45 m/s. The scale of storm area, in which wind speed was more than 25 m/s, was about 230 km long to the southeast and 140 km long to the northwest as shown in Fig. -2. Typhoon 7513 can be classified as "a small but strong storm" according to the standard classification of typhoons shown in Tables-1 and-2.

The observed wind at the Hachijojima Weather Station is shown in Table -3. This data indicates that the characteristics of the typhoon, are as follows:

1. The maximum wind speed, at its center, was high in comparison to its scale. (No damage occurred to the Aogashima Island, 60 km from the Island.)

2. Typhoon 7513 had a strong intensity and a clear eye, until it came near Hachijojima Island.

3. The stormy zone area was small and the travelling speed was as high as 60 km/h, a strong wind of 15 m/s was observed for a short period of time. (3 hours from 15:00 to 18:00, October 5 in Hachijojima Island).

4. The total precipitation on Hachijojima Island was only 25.5 mm, and most part of the damage was caused by the strong wind.

The strong wind caused by typhoon 7513 and previous strong wind observations are given in Table -4 and Fig. -3. From these data it can be stated that;

(a) There are more possibilities to have hard winds on the Hachijojima Island than on the Honshu Island.

(b) The maximum wind speed caused by typhoon 7513 is the seventh worst during the past 47 years, such a storm has not occurred during the past 15 years.

(c) The frequency of such a strong wind due to a typhoon, is about 7 years.

(d) The time when the maximum instantaneous wind speed was observed did not coincide with the time when the maximum wind speeds averaged over a ten-minute intervals was observed. The gust factor was 1.9 relative to values of 1.2-1.5 as usually observed.

b) The Characteristics of Topography and Wind on Hachijojima Island

Hachijojima Island is located 300 km south of Tokyo and has a circumference of about 60 km. As shown in Fig. -4, Mt. Hachijo-Fuji (854.3 m high) is located in the northwest and Mt. Mihara (704 m high) is located in the southeast, and has facilities such as an airport and town offices, between two mountains. The wind direction was south during the typhoon, and was west when it was leaving; it appears that the wind was influenced by the two mountains.

Wind observation was performed, not only at the Hachijojima Weather Station, but the Hachijojima Lighthouse in Sueyoshi and at the Hachijojima Airport in Ohkago. The wind record traces at these stations, are shown in Fig. -5. The Hachijojima Weather Station is on a hill 79.7 m above the sea level and 1 km distance from the seashore in Ohkago, and has instruments which are on a building as shown in Photo -1. The observed

wind speed is thus influenced by the topography.

Hachijojima Lighthouse is located on a bluff located at the southeast tip of the island as shown in Photo -2. The intensity of the wind turbulence is very low, in comparison with the wind record trace of the weather station shown in Fig. -5 (1), (2). When the typhoon passed through, the wind direction changed from south to west and the wind speed became weak due to the effect of the topography.

Hachijojima Airport is located at the foot of Mt. Hachijo-Fuji. Anemometers have been installed on the top of the building and at the east tip and west tip of the runway at this airport. The wind speed observed at the airport was nearly the same at that recorded at the weather station.

The wind data at each station, as given in Fig. -6, 7 and Table -5, reveal the following comparison:

1. The wind speed observed in the lighthouse is higher than that in the weather station, where the magnification factor is from 1.25 to 2.0.

2. The wind speed observed in the airport is nearly the same as that in the weather station.

The wind characteristics at Hachijojima Island, due to typhoon 7513, are summarized as follows:

1. The wind direction was south while the typhoon was approaching, with strong wind of low intensity and turbulence blowing in the Yaene and Sueyoshi district near the seashore.

2. The wind direction changed from south to west accompanied with passage of the typhoon. The wind speed became weak in the Sueyoshi district, because the wind from the west is blocked by the mountains. The wind was negligible in the Ohkago and Mitsume district located between Mt. Hachijo-Fuji and Mt. Mihara.

3. At the district located in the rear of Mt. Hachijo-Fuji and Mt. Mihara, the wind became so weak that these areas had minimal damage.

3. Examination of Damage

a) Abstract of Damage

The statistics of damage is shown in Tables-6 and-7. The number of the wounded was 85, but fortunately no one was killed. On the other hand a great deal of damage occurred to the houses, where the number of fully and halfly collapsed houses were 304 (8.0%) and 539 (14.2%), respectively. The damage occurred when wooden houses leaned and fell, the roofs was peeled off or blown away and the window glass was broken into pieces as shown in Photos -5 and-6. Galvanized steel roofing is widely used in Hachijojima, and the damage of the roofs, for the most part, occurred to these galvanized steel roofs. As an example of the damage to window glass, the Hachijojima Kokusai Kanko Hotel had extensive damage as shown in Photo -7. The window glass with 8 mm thick at the south side of building and was broken into pieces when hit by blowing pebbles etc. It was also noted that in some instances the aluminum window frames yielded, in spite of this the glass did not break as shown in Photo -8. The damage relative to public service was the destruction

of a school and hospital building, and the interruption of electric power, telephone and roads. The number of damaged major structures, except buildings, has few, and consisted of destruction of a guyed tower, a panzermast, a bridge and four arc lamp standards, this is because there are only a few large structures in Hachijojima.

b) Damage to Roads

Roads were lightly damaged and no large scale landslide occurred as the total precipitation was only 25.5 mm. The roads were cut off at 150 places by such obstacles as fallen trees and pieces of broken houses, but they cleared in a few days. Many trees, at the slope in Yokomagaura, fell due to the typhoon. The inclination of the slope at Yokomagaura is steep and therefore, preventative work had been conducted in order to avoid future landslides.

c) Damage to Structures

(1) Bridges and Breakwater

A girder bridge, with 15 m span at the Yaene Harbor, was damaged by waves as shown in Photo -10. This bridge consisted of 17 PC beams which fixed on the abutment with bolts and a concrete slab. Due to typhoon 7513 the slab was lost and some anchor bolts sheared so that some of girders fell into the sea.

The breakwater at the Aegae Harbor was partially destroyed at the concrete joint. The state of damage is as shown in Photo. -11

(2) Guyed tower of the Loran Long Range Navigation Station

Hachijojima Laran Station, of the Maritime Safety Agency is located on the top of Mt. Mihara, and has a guyed tower 80 m high and a panzer-mast 20 m high. During the storm both the tower and mast collapsed.

The guyed tower was constructed in 1966. It consisted of 16 blocks of triangular truss with a side length of 60 cm, and block length of 5 m. The tower is stiffened by 4 layers and 3 direction guys as illustrated in Fig. -8. The state of damage is shown in Photo -12. The tower failed at the base in the north direction (leeward). The 4th block from the base of the truss yielded and the others remained without deformation. The guy was cut near the tower as illustrated in Fig. -8.

The state of destruction of this tower was presumed as follows:

1. Excessive wind loads acted on the tower, and the guy on the windward and at the lowest layer fractured.

2. This resulted in an induced severe bending moment to act on the truss and thus caused failure of the 4th block of the truss.

3. Consequently, the whole tower fell in leeward direction.

This tower was designed using the standard for structural designs of steel towers (Architectural Institute of Japan). Namely, the design wind load is calculated by the following equation and the design wind speed is 60 m/s.

$P = qCA$ where P: wind pressure (kg)

q: design velocity pressure (kh/m^2)

C: coefficient of drag

$q = 120\sqrt[4]{h}$ A: projected area (m^2)

h: height above the ground (m)

$C = KFMC_0$ K: coefficient of wind force for latticed structure

F: aspect ratio

M: modification factor of wind pressure

C_0: modification factor for circular member

Because the highest tension acts on the highest guy according to these calculations, it is difficult to assume that the lowest guy had first featured. But these calculations assume that the vertical wind profile is peculiar.

The wind at this site influences its height and the effect of the topography, namely the tower existed on the top of Mt. Mihara and its height is 704 m. As an example, the convergence of the wind at the top of a mountain is shown in Fig. -9, as a result of wind tunnel experiments.

(3) Arc Lamp Standard

Arc lamp standards at the Mihara Junior High School and Hachijo High School broke near the base. The panzer-mast consisted of 8 pipes, at length 2 m, thickness of 2 mm, diameter at the base of 55 cm and a material of high-tensile-steel. The dimension of the lamp is as shown in Table -8. The layout of school is as shown in Table -8, and the state of the damage is shown in Photos -14 through 16.

The lamp standard fell down toward the north which coincides with the wind direction, therefore, the standards fell down due to an excessive wind load. A gap, shown in Photo -14, was left at the base between the ground and the standard did not fall down. The direction of this gap is perpendicular to the wind direction, thus the standards vibrated due to Karman vortex where the amplitude at the top of the standard reached more than 10 cm. The fact that only 2 standards among 6 standards were damaged, shows that wind affects were very local, thus, the existence of buildings or others blocks or the wind, had an effect on the intensity of the wind.

(4) Poles and Fences

Many concrete telegraph poles broke and fell in the Ohkago and Mitsune district (Photos -17, 18). Most of damaged poles broke near the base, but some of them broke in the middle. The standard for concrete poles is provided by JIS (Japanese Industrial Standard) and the configuration and design loads are as shown in Table 9. The length and design loads on poles used in Hachijojima are 12 m and 350 kg, respectively, and the design wind speed is 50 m/s (for reference, 40 m/s in Tokyo).

Many concrete block fences and net fences fell. Concrete block fences, shown in Photo -18, broke at the boundary between the foundation and blocks. Net fences, shown in Photo -19 were damaged, although its frequency ratio was small.

4. Conclusion

Results from this examination are summarized as follows:

1. According to the observed data, the wind speed over a ten-minute interval was 35.5 m/s and the maximum instantaneous wind speed was 67.8 m/s, therefore the gust factor

was over 1.9 and is larger than the usual value.

2. After performing some calculations on the return period of annual maximum wind speeds, the return period of a strong wind due to the typhoon 7513 is 7 years, which is very small. Hence, it is necessary to consider wind effects in future design of structures in Hachijojima.

3. A great deal of damage was done to public service. This interruption to public service produces a powerful effect on the civilian populations, thus the design wind speed has to be determined with due regard to the importance of the public.

4. The design wind speed for the design of structures is considered to be the wind speed over a ten-minute interval. However the destruction of structures is related to the maximum instantaneous wind speed. Therefore it is necessary to examine such effects by engineers.

Acknowledgments

Many persons have assisted the writers in the collection and evaluation of the information presented herein. We thank each of these people for their help.

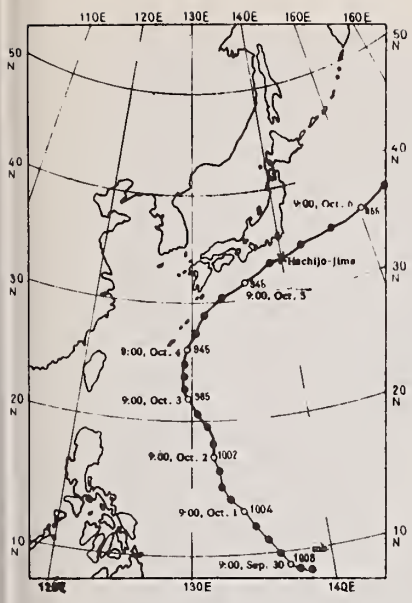

Fig.-1 The trace of typhoon 7513.

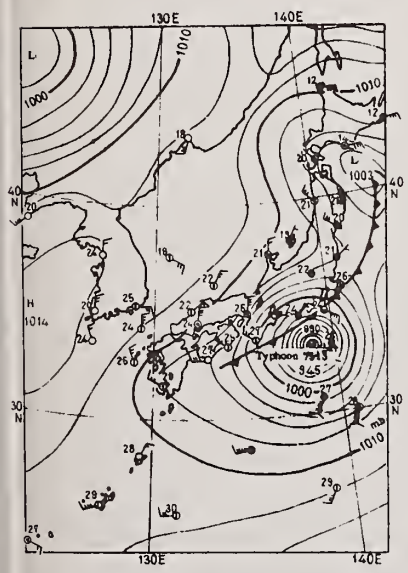

.-2 weather chart (at 15:00, October 5, 1975)

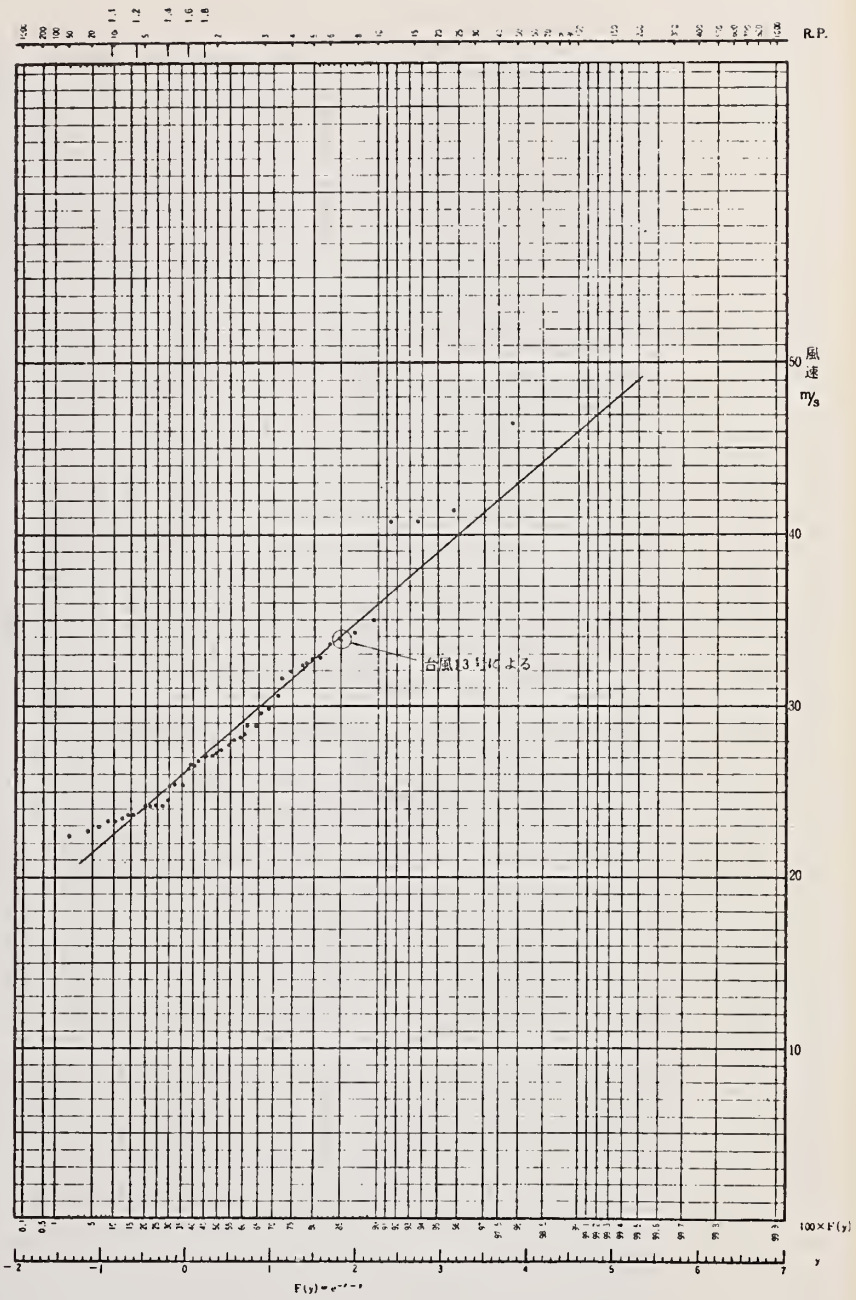

Fig.-3 Annual maximum wind speed vs. return period

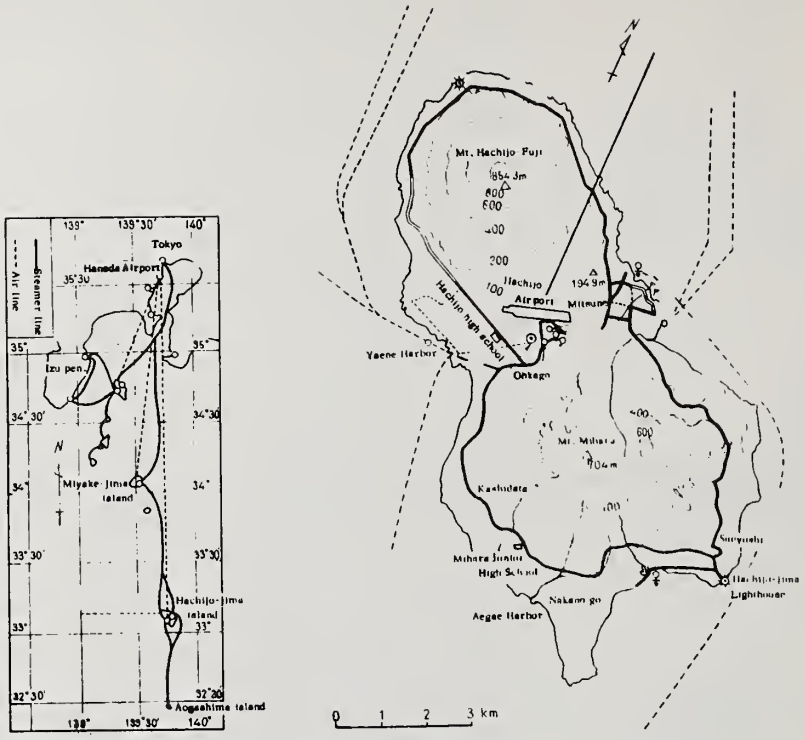

Fig.-4 General view of Hachijo-jima island

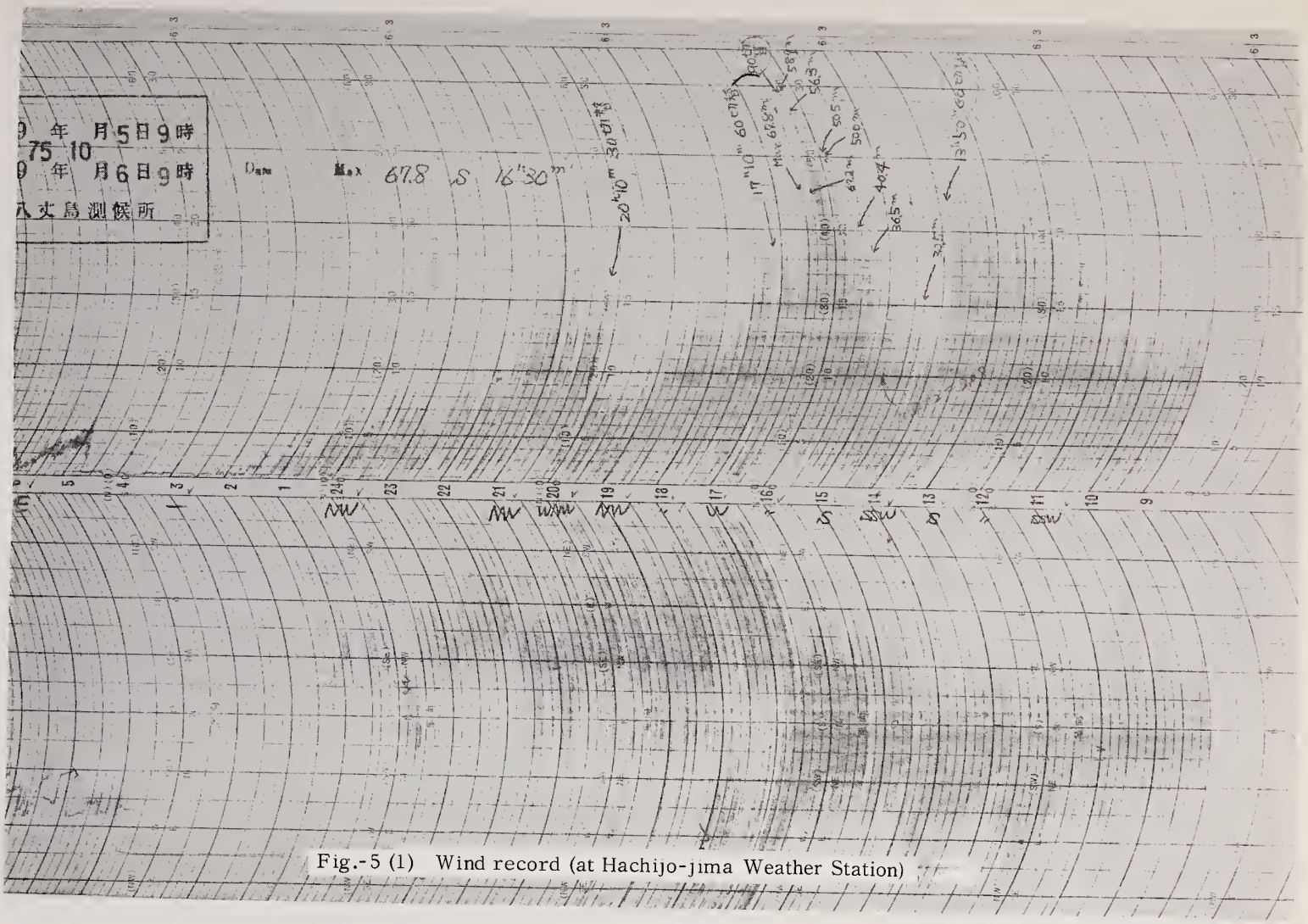

Fig.-5 (1) Wind record (at Hachijo-jima Weather Station)

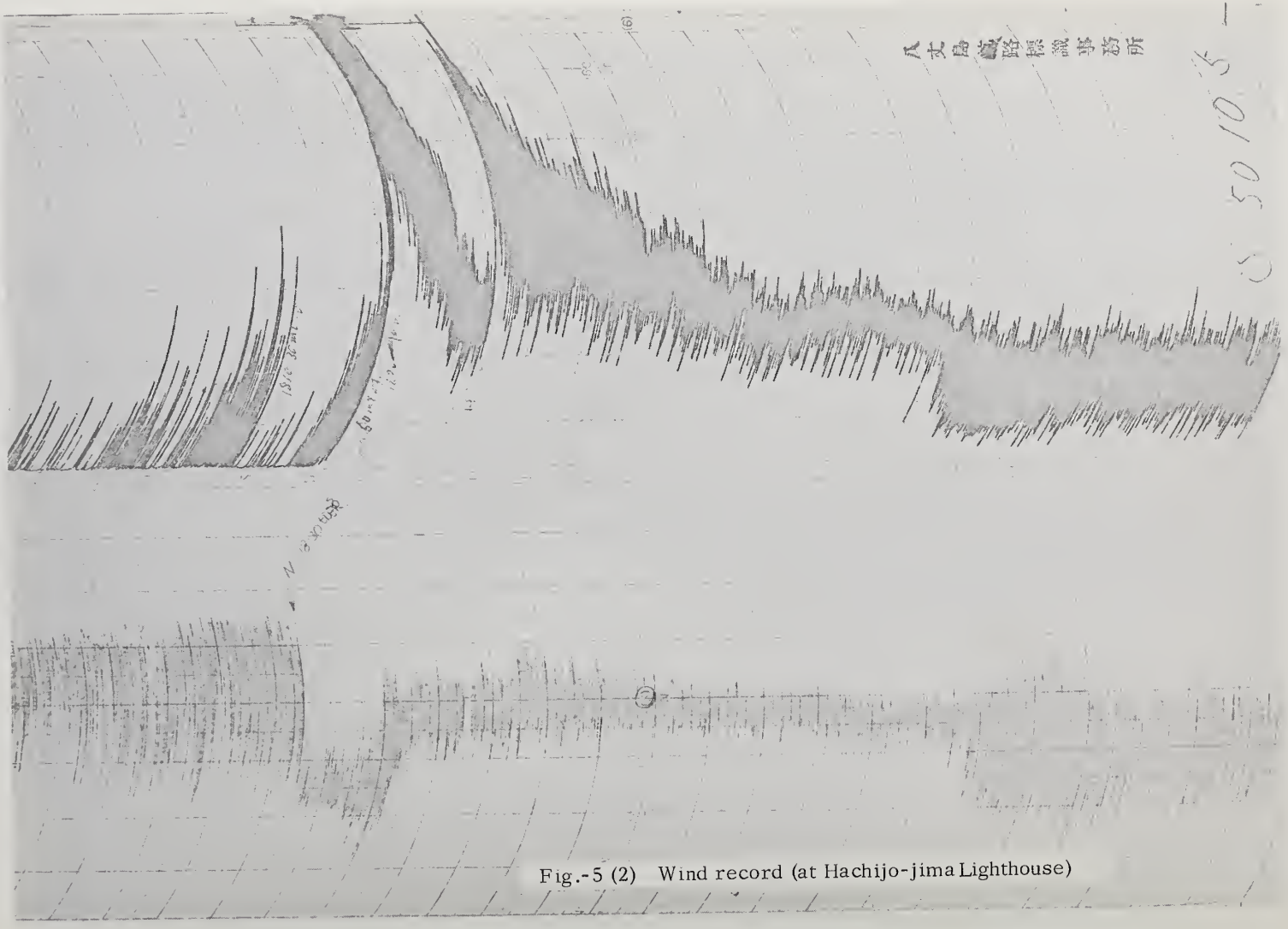

Fig.-5 (2) Wind record (at Hachijo-jima Lighthouse)

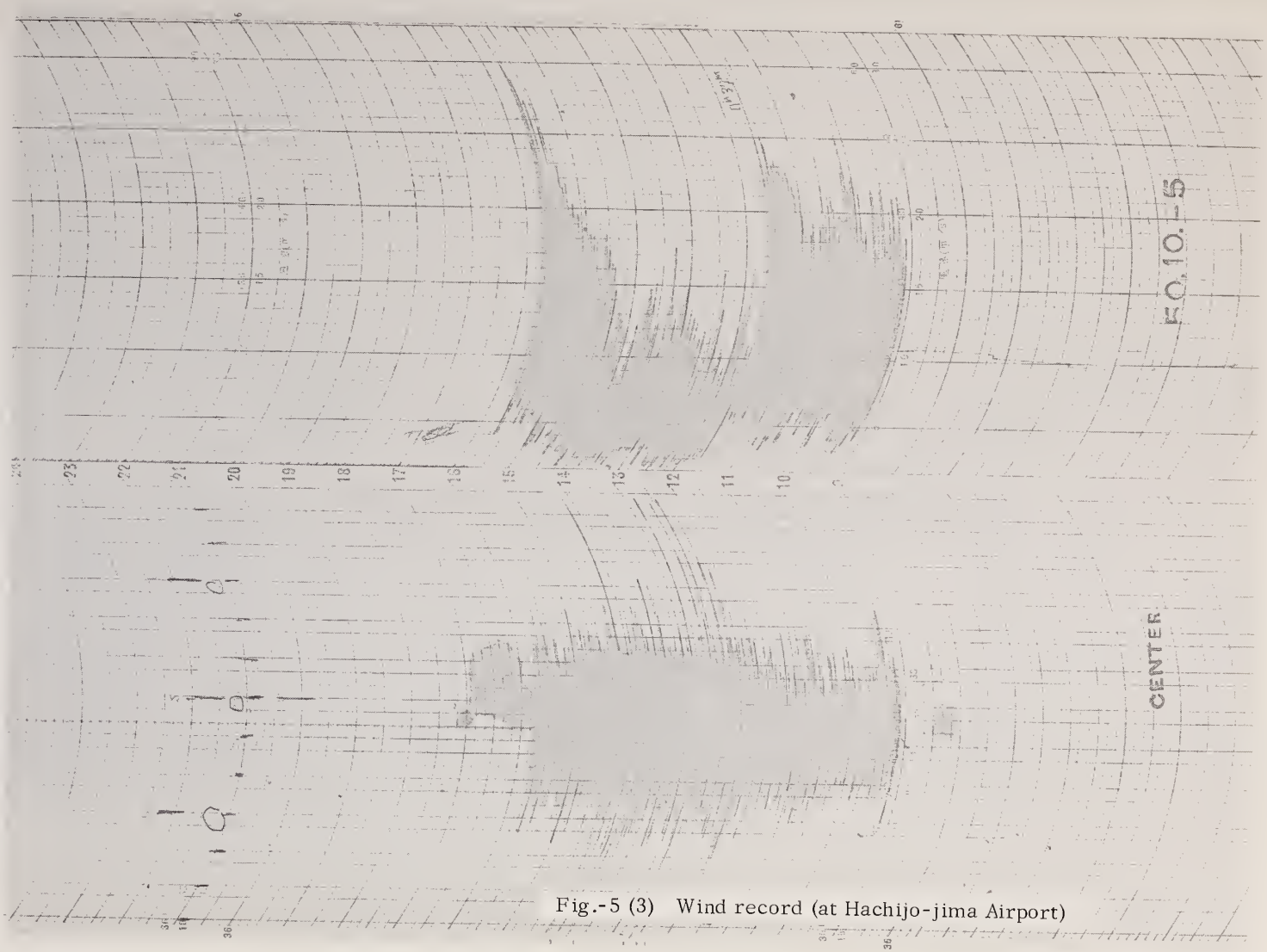

Fig.-5 (3) Wind record (at Hachijo-jima Airport)

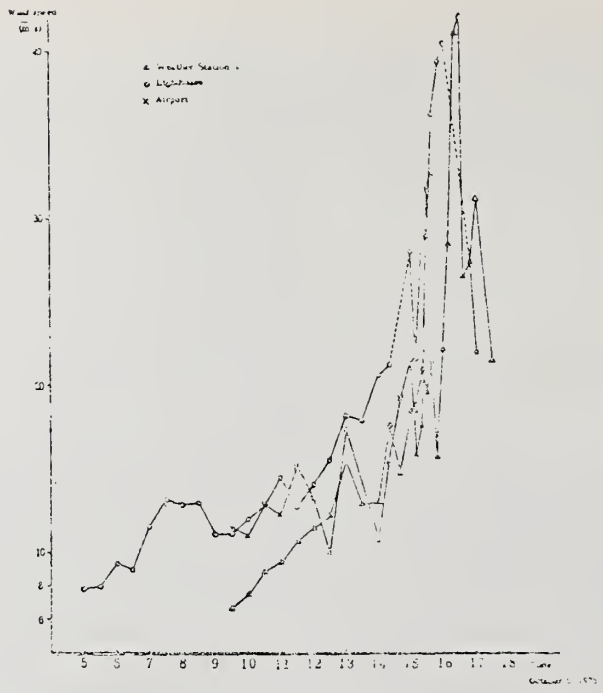

Fig.-6 Observation data of wind speed (typhoon 7513)

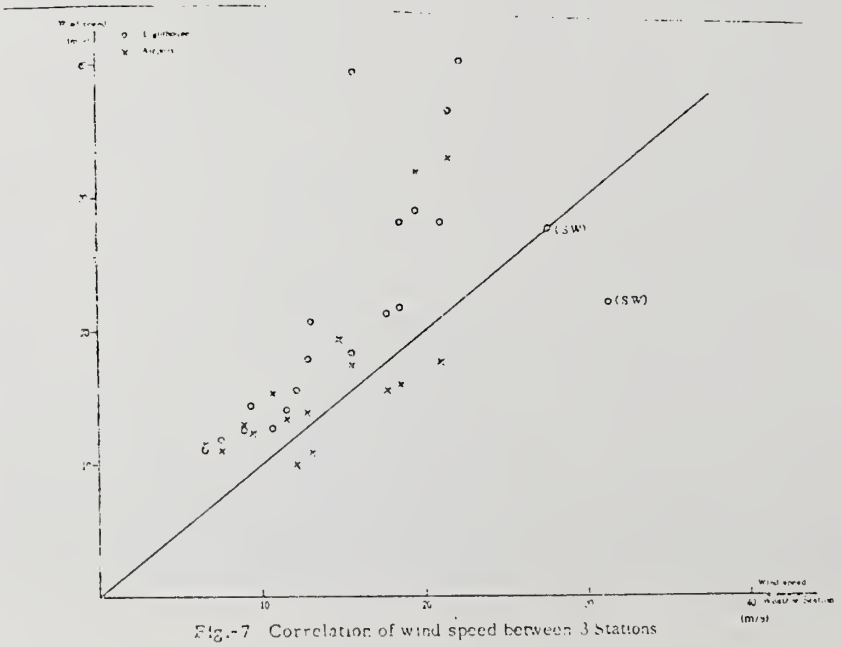

Fig.-7 Correlation of wind speed between 3 Stations

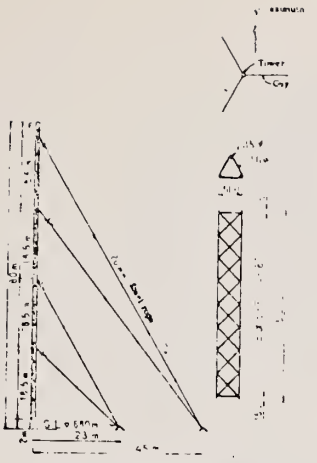

Fig.-8 The general view of the guyed tower

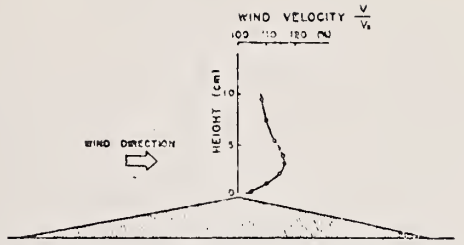

Fig.-9 Wind profile over the summit of mountain (After the result of wind tunnel experiment)

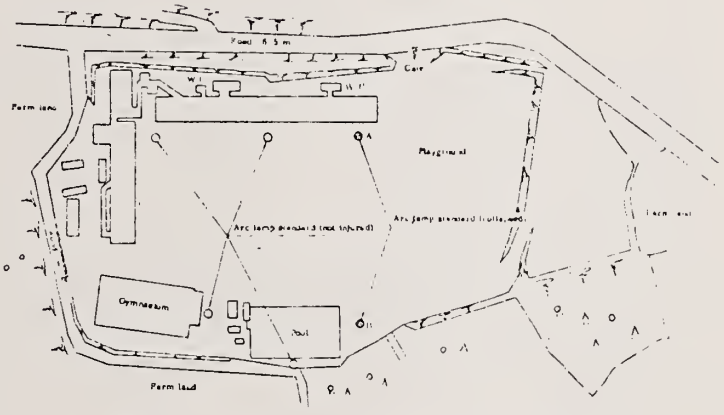

Fig.-10 (1) The plane view of Mihara Junior High School

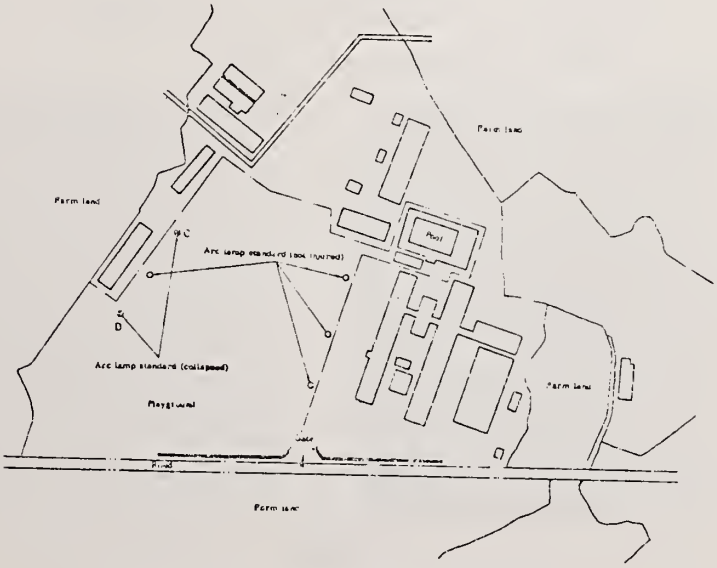

Fig.-10 (2) The plane view of Hachijo High School

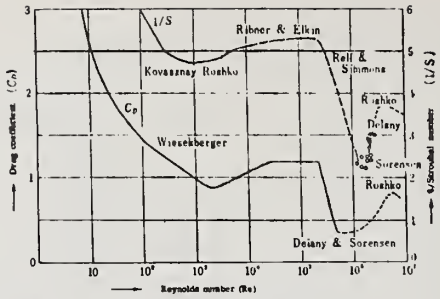

Fig.-11 Effect of Reynolds number on drag coefficient and Strouhal number.

Table-1 Classification of scale of typhoon

Grade	The radius of isobar "1000 mb"	The radius of area in which wind speed is more than 25 m/s (for reference)	The radius of maximum circular isobar (for reference)
Extremely large	More than 600 km	400 km or over	More than 800 km
Large	300 - 600	about 300 km	400 - 800
Medium	200 - 300	about 200 km	300 - 400
Small	100 - 200	about 100 km	200 - 300
Extremely small	Less than 100 km	–	Less than 100 km

Table-2 Classification of strength of typhoon

Grade	Central atmospheric pressure	Maximum wind speed (for reference)
Weak	More than 990 mb	Less than 25 m/s
mean	950 - 989	25 - 34
Strong	930 - 949	35 - 44
Extremely strong	900 - 929	45 - 54
Violent	Less than 900 mb	More than 55 m/s

Table-3 Observed data at Weather Stations

Hachijo-jima

Date	Time	Pressure at sea level	Temperature ℃	Humidity %	Wind direction	Wind speed m/s	Precipitation mm	Weather
4	21	1010.2	26.5	87	SW	5.8	–	◎
	24	1009.7	25.3		SW	5.2	–	◎
5	3	1008.7	26.2	87	SW	6.6	–	◎
	6	1008.5	25.5		SSW	5.1	–	◎
	9	1007.8	26.1	87	S	6.7	0.0	◎
	11	1005.2	26.3	87	SSW	7.5	–	◎
	12	1002.7	26.5	86	SSW	8.7	–	◎
	13	1000.3	26.4	84	S	10.0	0.0	◎
	14	998.0	28.3	87	SSW	12.2	0.0	●
	15	990.4	26.5	88	S	15.9	10.5	●
	16	972.7	24.7	94	S	22.1	6.6	●
	17	966.3	25.4	93	W	36.6	4.6	●
	18	991.0	26.3	96	W	14.4	1.5	●
	19	998.4	23.4	86	NW	12.2	1.0	◎
	20	1002.3	23.8	82	WNW	12.0	–	◎
	21	1005.0	24.3	78	NW	7.0	–	◎
	24	1007.8	22.6		NW	3.8	2.0	●
6	3	1009.4	21.6	89	–	0.0	0.6	◎
	6	1011.4	21.4		NE	1.9	–	◑
	9	1013.5	25.0	65	ENE	5.4	0.0	◑

Miyake-jima

Date	Time	Pressure at sea level mb	Temperature ℃	Humidity %	Wind direction	Wind speed m/s	Precipitation mm	Weather
4	21	1008.4	25.6	88	SW	4.4	–	◎
	24							
5	3	1007.2	25.4	84	SW	4.7	–	◑
	6		25.4		SW	3.6	–	
	9	1006.8	26.3	81	S	4.6	0.5	◎
	11							
	12	1003.0	25.9	87	SE	5.3	0.0	◎
	13	1000.5	25.4	89	SE	4.1	2.0	●
	14	997.7	26.1	90	SE	6.8	6.5	●
	15	993.9	25.0	92	SSE	9.4	6.0	●
	16	989.8	25.1	92	E	15.8	16.0	●
	17	989.1	25.1	88	NNE	17.5	1.5	●
	18	993.6	21.9	91	NNE	16.2	12.5	●
	19	996.9	23.0	89	N	11.2	3.5	●
	20	1000.6	23.6	85	N	8.8	0.0	●
	21	1003.7	23.3	79	N	5.9	0.0	●
	24							
6	3	1006.5	22.7	66	E	4.8	–	●
	6							
	9	1014.1	24.5	60	NE	4.4	–	◑

● : Rain
◑ : Cloud
○ : Fine

Table-5 Observed data of wind (typhoon 7513.)

Observation point / Time	Weather Stations		Lighthouse		Airport	
	Wind speed	Wind direction	Wind speed	Wind direction	Wind speed	Wind direction
5 : 00			7.85	S W		
30			7.90	S W		
6 : 00			9.35	S S W		
30			8.95	S S W		
7 : 00			11.55	S S W		
30			13.15	S S W		
8 : 00			12.80	S S W		
30			12.90	S S W		
9 : 00			11.05	S S W		
30	6.55	S	11.10	S S W	11.25	S S W
10 : 00	7.50	S	11.90	S S W	11.00	S S W
30	8.90	S	12.70	S S W	12.85	S S W
11 : 00	9.35	S S W	14.45	S S W	12.25	S S W
30	10.75	S S W	12.75	S S W	15.20	S S W
12 : 00	11.50	S S W	14.00	S S W	13.25	S S W
30	12.15	S S W	15.50	S	10.00	S S W
13 : 00	15.50	S	18.15	S	17.40	S S W
30	12.85	S S W	17.90	S	13.75	S S W
14 : 00	13.00	S S W	20.55	S	10.75	S S W
20	17.75	S S W	21.20	S	15.50	S S W
40	14.75	S	(Over)	S S W	19.25	S S W
15 : 00	18.50	S S W	28.00	S	21.50	S S W
10	18.50	S S W	21.75	S	15.85	S S W
20	21.00	S	28.00	S	17.50	S S W
30	19.50	S	28.50	S	31.75	S S W
40	21.50	S	39.25	S S W	32.75	S S W
50	15.75	S	39.40	S S W		
16 : 00	22.25	S	40.50	S		
10	28.50	S	(Over)	S		
20	41.10	S	〃	S		
30	42.15	S S W	〃	S S W		
40	26.50		〃	S S W		
50	27.50		27.50	S W		
17 : 00	31.25		22.00	S W		
30	19.50			S W W		

Table-4 Annual maximum wind speed (Hachijo-jima)

Year	Date	Wind speed	Wind direction	Wind speed*	Year	Date	Wind speed	Wind direction	Wind speed*
1929	9. 30	32.1	WSW	34.2	1953	12. 25	24.8	W	23.2
30	4. 2	27.9	NE	29.7	54	9. 18	34.0	SW	33.7
31	9. 10	38.2	ENE	40.8	55	2. 20	32.8	W	32.3
32	11. 14	39.4	WSW	41.5	56	12. 5	29.2	W	28.1
33	3. 26	22.9	NE	24.1	57	3. 8	28.4	W	27.1
34	12. 29	26.0	NNW	27.4	58	9. 18	33.0	SSW	32.6
35	3. 25	24.1	WNW	25.6	59	10. 21	25.9	NNE	24.1
36	10. 3	38.7	SW	40.8	60	1. 17	29.8	W	28.7
37	12. 2	25.2	W	26.5	61	10. 10	32.9	SW	31.5
38	10. 21	44.2	W	46.5	62	11. 16	28.5	ENE	27.3
39	10. 27	25.6	NE	27.0	63	3. 13	29.3	NE	28.0
40	2. 20	27.7	SW	26.5	64	3. 27	23.8	W	22.8
41	3. 27	29.5	W	28.3	65	5. 27	24.7	SW	23.6
42	9. 19	25.2	SW	24.1	66	1. 4	25.2	W	24.1
43	10. 10	36.5	WSW	35.0	67	9. 14	28.0	ENE	26.7
44	2. 24	26.5	SW	25.2	68	1. 15	26.5	W	25.3
45	12. 17	27.3	SW	25.6	69	3. 12	24.5	WSW	23.4
46	12. 9	29.0	W	27.9	70	1. 5	24.7	W	23.6
47	4. 21	33.3	W	31.9	71	1. 5	25.2	W	24.1
48	9. 15	30.8	SW	29.5	72	4. 1	23.8	W	22.7
49	8. 31	33.2	SW	32.8	73	12. 22	24.3	W	23.2
50	1. 10	31.1	W	30.4	74	3. 22	23.5	W	22.4
51	12. 27	29.8	W	28.7	75	19. 5	35.5	W	33.9
52	6. 24	25.5	SW	24.0					

*Wind speed at the height of 10 meters above the ground

Table-8 Dimension of [illegible] lamp standard

Term		
Total height		17.26 m
Height above the ground		14.76 m
Length under the ground		2.50 m
Diameter of the top		206 mm
Diameter of the bottom		613 mm
Weight		488 kg
Allowable tension on the top	Wind pressure (v = 60 m/s)	480 kg
	Wind pressure (v = 40 m/s)	540 kg
	Calm	600 kg

Table-6 The state of damage

District \ Term	Population	Household	Human damage: Death	Human damage: Major injury	Human damage: Minor injury	Damage of houses: Fully collapsed	Damage of houses: Halfly collapsed	Damage of houses: Partially collapsed	
Mikuni	2,614	1,587			42	124	229	512	Public service (school, etc.) 12
Ohkago	2,073	1,247		1	32	117	216	424	
Kashidate	336	270			3	20	30	70	Others (garage, etc.) 361
Nakanogo	706	427			2	13	37	173	
Sugiyoshi	638	254		2	3	30	27	152	
Total	6,767	3,785	0	3	82	304	539	1,331	

Table-9 Standard of concrete pole (JIS-A5309)

D_1 cm			12		14			17			19						22
Strength load kgf (kN)			120 (1.18)	200 (1.96)	150 (1.47)	200 (1.96)	250 (2.45)	300 (2.92)	200 (1.96)	270 (2.65)	340 (2.94)	300 (2.94)	350 (3.43)	430 (4.22)	500 (4.90)	600 (5.88)	700 (6.87)	(kN) (9.81)
L_1 m	H_1 m	H_2 m																
6	4.75	1.0	○															
6.5	5.15	1.1	○															
7	5.55	1.2			○									○		○		
7.5	5.95	1.3				○								○		○		
8	6.35	1.4		○		○			○					○		○		
9	7.25	1.5		○		○	○			○	○		○	○		○		
10	8.05	1.7		○			○			○		○	○	○	○	○		
11	8.85	1.9		○				○				○	○	○	○	○		
12	9.75	2.0										○	○		○			
13	10.55	2.2										○	○		○		○	
14	11.35	2.4										○	○		○		○	○
15	12.25	2.5										○	○		○		○	○
16	13.25	2.5											○		○		○	○
17	14.25	2.5													○			

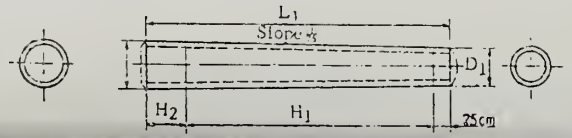

Table-7 Damage of public service

Term	Number	Sum
School	11	230,308,000 yen
Hospital	4	23,850,000
Road	2	1,920,000
Ship	4	10,000,000
Telephone	3,600	
Harbor	2	48,000,000
Landslide	1	3,000,000
Collapsed trees	50,000	50,000,000
Road (closed to traffic)	42	
Sweeping obstacles on road	111	11,060,000

Photo-1. Hachijojima Weather Station

Photo-2. Hachijojima Lighthouse

Photo-3. Hachijojima Airport (control office)

Photo-4. Hachijojima Airport (west side of runway)

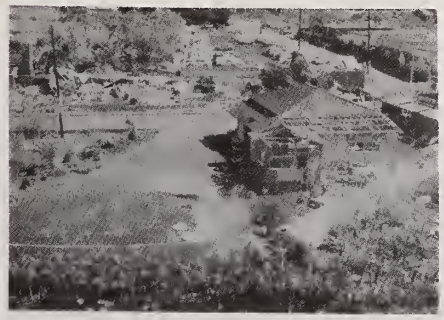

Photo-5. Damage to wooden house (Ohkago)

Photo-6. Damage to wooden house (Ohsato)

Photo-7. Damage to Hachijojima Kokusai Kanko Hotel

Photo-8. Damage to window frame (Hachijo High School)

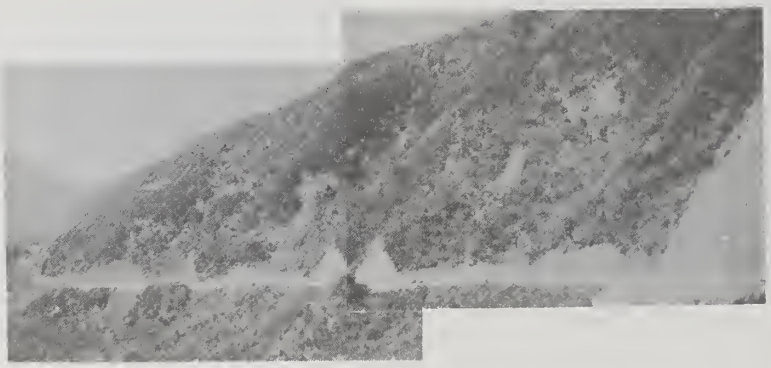

Photo-9. Fallen trees in slope (Yokomagaura)

Photo-10. Damage to bridge

Photo-11. Damage to breakwater

Photo-12. Damage to guyed tower (on top of Mt. Mihara)

Photo-13. Damage to arc lamp standard (Mihara Junior High School)

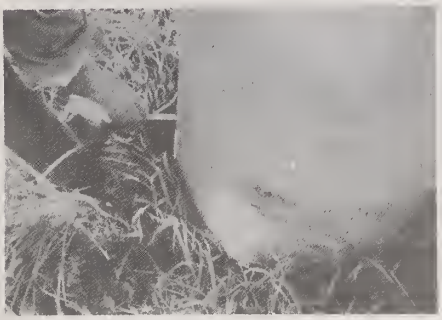

Photo-14. Close-up of the base of arc lamp standard

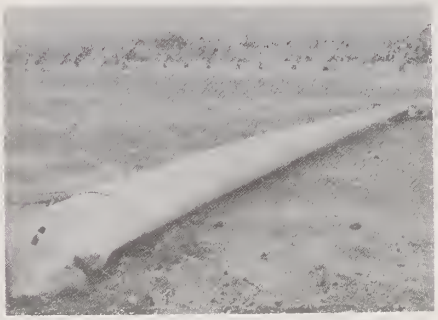

Photo-15. Damage to arc lamp standard (Hachijo High School)

Photo-16. Damage to telegraph pole

Photo-17. Damage to telegraph pole

Photo-18. Damage of concrete block fence

Photo-19. Damage of net fence

CYCLONE TRACY

RICHARD D. MARSHALL
Center for Building Technology
Institute for Applied Technology
National Bureau of Standards
Washington, D.C.

ABSTRACT

During the early morning hours of December 25, 1974, the city of Darwin was devastated by the most damaging cyclone ever to strike the Australian Continent. Winds of up to 75 m/s caused extensive damage to housing in particular, requiring the evacuation of approximately half of the 45,000 residents to other major cities in Australia. This report is a result of the author spending several days on temporary assignment with the Department of Housing and Construction-Australian Government to inspect the damage, and to participate in discussions regarding the establishment of new design criteria and construction practices for cyclone areas. The fact that most of the damage was caused by wind forces rather than a combination of wind and storm surge greatly simplified the assessment of damage and structural performance. The experience at Darwin points out the danger in depending too heavily upon past experience and intuition in the design of housing. It also makes clear the need for additional research into the behavior of certain building materials under repeated loads and missile impact, and the racking strength of walls subjected to uplift loads.

Key words: Buildings; Cyclones; Disasters; Structural Engineering; Tides; Wind.

1.0 INTRODUCTION

Cyclone Tracy, which struck Darwin, N.T. in the early morning of December 25, 1974, was the most damaging cyclone ever to strike the Australian Continent. In the four to five hours required for the storm to pass over Darwin, approximately 50 lives were lost and damage in excess of $300,000,000 (US) was done to buildings and other structures. This report is an attempt to describe the more common types of buildings in Darwin and their performance under extreme wind conditions. Some residential areas suffered almost complete destruction while other areas of the city experienced only moderate damage. The wide variety of construction and the fact that most damage was due entirely to wind effects rather than a combination of wind and storm surge make possible some important and meaningful deductions and point up several areas that should be given closer attention in designing structures for wind-prone areas.

2.0 STORM SUMMARY

2.1 DEVELOPMENT AND LANDFALL

Cyclone Tracy originated as a tropical depression in the Arafura Sea near 8S-134E early on December 20, 1974. The storm system moved off in a southwesterly direction and was classified as a tropical cyclone during the evening hours of the 21st. On the morning of the 22nd, Tracy was located at 9S-131E, or approximately 200 km north of Darwin. It continued to move toward the southwest for the next two days, entering the Timor Sea and passing some 50 km west of Bathurst Island on the morning of December 24. Shortly thereafter Tracy made an abrupt change in direction and headed southeast, directly toward Darwin. At midnight Tracy was located just off Point Charles or 30 km WNW of Darwin, moving to the ESE at approximately 8 km/hr (see Fig. 1). Landfall (passage of the leading eye wall) is believed to have occurred somewhere between East Point and Nightcliff shortly after 0300 hours on the 25th, the eye passing directly over the Royal Australian Air Force (RAAF) Base and Darwin International Airport (see Fig. 2). Extreme winds persisted over the greater Darwin area until approximately 0600 hours. Tracy continued on a southeasterly course, dissipating over Arnhem Land during the remainder of the 25th.

2.2 WIND SPEEDS

The only detailed wind speed record obtained during the passage of Tracy was that of the Bureau of Meteorology at the airport. The Dines anemometer was mounted on a 10-meter mast and the recorded gusts correspond to an averaging period of from 2 to 3 seconds. Gusts of 12 m/s were recorded over the period 1300 to 1930 hours on the 24th with a steady increase up to 24 m/s at midnight. Gusts of 40 m/s were being recorded at 0200 hours on the 25th and the peak recorded gust of approximately 57 m/s occurred just after 0300 hours. At this point, the anemometer was struck by flying debris and no further wind speed measurements were obtained.

Estimates of maximum wind speeds (3-second gust at 10 meters) in Cyclone Tracy range from 60 to 75 m/s. Based upon peak departures from the mean just prior to failure of the airport anemometer and the observed passage of the eye wall shortly thereafter, a maximum speed of 70 m/s seems reasonable. Several observers are of the opinion that wind speeds on the rear edge of the eye exceeded those on the leading edge. There is no way to confirm this, but many structures apparently suffered the heaviest damage just after passage of the eye. The average speed of passage is believed to have been 6 to 8

km/hr. Winds in excess of 50 m/s extended outward 10 to 12 km from the center.

2.3 BAROMETRIC PRESSURE

The barograph record obtained by the Bureau of Meteorology dropped below 990 mb at 0030 hours, reached a minimum of 940-950 mb at 0400 hours and recrossed 990 mb at approximately 0730 hours. This record was obtained at the city office which is located just to the south of the estimated eye path. The diameter of the eye is believed to have been about 10 km, based on radar pictures obtained at 0400 hours while Tracy was passing over Darwin. The diameter of the calm area would have been slightly less than this since the radar image represents the location of the rain bands.

2.4 STORM SURGE

The maximum surge level (departure from predicted tide) recorded at Darwin Harbor was 1.6 meters at 0215 hours on December 25 [1][1]. The maximum predicted tide of 5.3 meters occurred at 0116 hours [2]. Since the astronomical tidal range at Darwin is approximately 8 meters, the storm surge caused very little structural damage. The eye of Cyclone Tracy passed to the north of Darwin Harbor, thus creating higher surge levels at the northern beaches due to the clockwise circulation. It is estimated that a maximum water level of 9 meters (8 meters above town datum) occurred at Casuarina Beach [1]. This level includes wave effects and is approximately 4 meters above predicted high tide. Had Cyclone Tracy coincided with the highest astronomical tide, some of the lower sections of Darwin would have been flooded to a depth of approximately 3 meters.

2.5 COMPARISON WITH OTHER INTENSE TROPICAL STORMS

Whatever the maximum wind speeds, Cyclone Tracy must be ranked as an extremely intense tropical storm and compares with two notable U.S. hurricanes; Hurricane Camille which struck the Mississippi Gulf Coast in 1969 and Hurricane Celia which caused heavy damage to Corpus Christi, Texas in 1970 [3, 4, 5]. Significant characteristics of these storms are listed below:

	Tracy	Camille (1969)	Celia (1970)
Central pressure (mb)	940-950	905-915	940-950
Maximum wind speed (m/s)	60-75	75-85	70-75
Diameter of eye (km)	8-10	8-10	20-30
Radius of winds > 50 m/s (km)	10-12	30-50	25-30
Forward speed (km/hr)	6-8	20-25	20-25
Maximum storm surge (meters)	1.6	7.4*	2.8*

(*) Includes astronomical tide.

Other notable cyclones affecting Darwin occurred on January 7, 1897 and on March 10, 1937 [6]. The 1897 event is believed to have been the most intense cyclone to strike Darwin prior to Tracy with extensive damage to the city and trees either flattened or stripped of branches. Twenty-eight deaths were recorded and a minimum barometric pressure of 950 mb was observed at Point Charles Lighthouse. As with Tracy, the direction of travel was SE. The 1937 cyclone approached from the NW and caused very rough seas with waves breaking over the cliffs at Fannie Bay and Emery Point. Wind

[1] Figures in brackets indicate literature references

gusts of 44 m/s and a minimum pressure of 975 mb were recorded. Most trees were stripped of branches.

3.0 TYPES OF BUILDINGS AND DISTRIBUTION OF DAMAGE

3.1 GENERAL

All areas of Greater Darwin suffered substantial wind damage, the severity depending upon the type of construction and degree of wind exposure. The purpose of this section is not to describe the damage in detail, which will be covered in subsequent sections, but rather to describe the predominant types of buildings by subdivision and the general distribution of damage.

3.2 TYPES OF BUILDINGS BY SUBDIVISION

The following tabulations are necessarily subjective and are intended to convey a general description of types of buildings located in the various subdivisions of Darwin. See Figure 2 for subdivision locations.

Darwin City: Commercial buildings up to three stories, government administration buildings, city office buildings and several historic buildings constructed prior to 1900. Three recently constructed reinforced concrete buildings of 10 and 11 stories, one 8-story load-bearing brick masonry building, several apartment buildings of two and three stories. Some industrial buildings and petroleum storage tanks in the railway area along Francis Bay. Several transit sheds and a power plant next to Darwin Harbor. Very few single-family dwellings.

Larrakeyah: Military area on Emery and Elliot Points, Darwin Hospital, one-and two-story commercial buildings, apartment buildings and single-family dwellings.

Stuart Park: Railway workshops, some light industrial buildings, several apartment buildings and single-family dwellings.

Fannie Bay and Parap: Single-story commercial buildings, primarily single-family dwellings and some apartment buildings of two and three stories along Fannie Bay. Darwin High School.

Winnellie: Large steel-framed warehouses and multiple-bay industrial buildings.

Narrows: Single-family dwellings and apartment buildings.

Ludmilla: Single-story commercial buildings and single-family dwellings.

Coconut Grove and Nightcliff: Single-family dwellings, apartment buildings up to 4 stories and some single-story commercial buildings.

Northern Suburbs: Includes all subdivisions north of airport and east of Nightcliff. Primarily single-family dwellings, schools, shopping centers and a few apartment buildings.

Darwin International Airport: Terminal building, aircraft hangars, RAAF operations buildings and military housing adjacent to Narrows and Ludmilla subdivisions.

3.3 DISTRIBUTION OF DAMAGES

Shortly after the passage of Cyclone Tracy, a survey of damage to houses in Darwin was carried out by the Northern Territory Housing Commission [7]. Approximately 85 percent of the houses in Darwin (estimated at 8,000 units) were surveyed, the subdivisions of Tiwi and Anula (see Figure 2) being excluded because many of these houses were still under construction and the destruction in these subdivisions was very close to 100 percent. RAAF housing was also excluded from this survey. The results are as follows:

Subdivision	Destroyed (Percent of houses in each subdivision)	Intact
Darwin City	38	9
Larrakeyah	29	4
Stuart Park	24	10
Fannie Bay and Parap	33	11
Narrows	5	29
Ludmilla	32	6
Nightcliff	54	4
Millner	33	3
Rapid Creek	37	6
Jingili	51	7
Moil	75	2
Alawa	57	3
Wagaman	72	2
Nakara	97	0
Wanguri	86	0

It is fairly obvious from the above tabulation that the major damage occurred in the northern suburbs and that Narrows and, to some extent, Stuart Park suffered less damage to housing than did most other areas of Darwin. The Narrows area runs along the upper reaches of Ludmilla Creek and is at a lower elevation than adjacent subdivisions. Stuart Park is located on fairly irregular terrain and while many buildings were directly exposed to the wind, several sections were protected by hills and ridges. The northern suburbs, on the other hand, had very little protection, particularly after the surrounding trees had been stripped of their branches. The entire area rises gently from Casuarina Beach north of Nightcliff and thus experienced scant reduction in wind speeds due to terrain roughness. It is quite likely that Winnellie, Stuart Park, Larrakeyah and Darwin City did benefit from terrain effects, particularly in the early stages of the storm passage.

Because of the different styles of construction and changes in design criteria and construction materials that accompanied the growth of Darwin, it is not possible to deduce local maximum wind speeds on the basis of housing damage alone. A comprehensive study of simple structures such as road signs and flagpoles which showed no evidence of missile impact provided valuable information on extreme speeds and wind direction [8]. Based on this study the following description of wind conditions during the passage of Tracy was deduced:.

Location	Maximum Speeds	Range of Direction
Darwin City & Larrakeyah	50-60	NE to SSE
Fannie Bay & Parap	55-65	NE to S
Winnellie & Narrows	55-65	NE to SSW
Airport	60-70	NE to SW
Nightcliff	60-70	NNW to SW
Northern Suburbs	65-75	NW to WSW

4.1 HOUSES

4.1.1 Background

The vast majority of houses in Darwin were constructed for the Department of Housing and Construction or for the Northern Territory Housing Commission. There are some privately constructed houses and several prefabricated housing systems which were introduced within the past two or three years. The design of housing was largely based upon intuition and experience with very little attention given to the rational estimation of wind loads and load capacity. An exception to this was the newer prefabricated housing systems whose designs were subjected to a careful review prior to acceptance by local authorities. Design wind speeds for Darwin varied somewhat through the years and included adjustments for type of exposure, expected life of structure and height above ground. Design speeds of 45 to 50 m/s were used from 1951 to 1972 at which time the new code provisions for wind loads (AS CA34.2) were adopted [9]. This code, subsequently re-issued as AS 1170 Part 2-1973 specifies a basic design speed of 56.4 m/s for Darwin and allows reductions for terrain roughness. Following the adoption of AS CA34.2, a category 3 (mean velocity profile described by a power law with an exponent of approximately 0.25) terrain was assumed with a corresponding basic design speed of 39.4 m/s. Hindsight suggests that category 2 terrain (exponent of 0.15) or a design speed of 56.4 m/s would have been more appropriate.

Of approximately 7,000 houses surveyed, more than 50 percent were damaged beyond repair and only some 400 units could be considered to be intact with minor damage to roofing, wall cladding and windows. Of those considered to be repairable, the vast majority suffered substantial damage to roofing. The following sections describe some of the more common housing systems and their performance during Cyclone Tracy.

4.1.2 High-Set Houses

By far the most popular style of house in Darwin is the so-called "high-set" house constructed for the Department of Housing and Construction. Although there are several variations the basic unit consists of an elevated platform and light timber frame with a gable roof (see Figure 3). The plan dimensions are approximately 7 x 16 meters with the platform some 2.5 meters above ground. Prior to 1968 galvanized steel pipe columns with cross-bracing were used to support the platforms (see Figure 4). These were superceded by concrete columns on simple spread footings and the cross-bracing was replaced by concrete block shear walls installed between 4 adjacent columns, the resulting enclosure serving as a laundry room or storage space.

The frames of the older high-set houses were constructed of 2 x 4 in. (nominal) wood studs with let-in diagonal bracing and the 6 mm (1/4-inch) asbestos cement wall cladding was not counted on to provide principal resistance to racking. In more recent construction the let-in bracing was eliminated, the stud sizes were reduced to 2 x 3-in. (nominal) and both the corrugated galvanized iron (CGI) roof cladding and asbestos cement wall cladding were assumed to provide sufficient resistance to racking in the roof and wall planes. Following Cyclone Althea which struck Townsville in 1971, certain changes were introduced to improve the wind resistance of new housing in tropical areas. These changes included the addition of steel rods or "cyclone bolts" extending from the roof trusses

down through the walls to the underside of the floor joists. Nails were replaced by self-drilling wood screws with neoprene washers for the attachment of CGI cladding and reinforced concrete bond beams were added to the concrete block shear walls. Another important feature of the high-set houses, and most other houses in Darwin for that matter, is the widespread use of prefabricated wall panels containing jalousie windows and ventilation louvers. The frames and mullions in these units are extruded aluminum sections.

The high-set houses performed reasonably well in the older subdivisions such as Fannie Bay and Larrakeyah where there was some protection provided by other buildings and trees and where the wood frames contained diagonal bracing. Many of these older houses were roofed with corrugated asbestos cement sheets. In the northern suburbs, however, the new high-set houses suffered extensive damage. The failure of upwind buildings created a source of missiles which undoubtedly played a major role in the widespread damage observed in the northern suburbs. This tended to be a self-sustaining effect as other structures failed downwind. The sequence of failure is believed to have been loss of roof cladding and purlins, followed by collapse of roof trusses and large unsupported walls, particularly in the living rooms. The racking strength of the walls was reduced by missiles fracturing the asbestos cement cladding and these sheets completely failed once racking deformations occurred. In many cases the entire wood frame was removed from the elevated platform (see Figure 5). The piers and platforms generally remained intact, but there were cases where the entire structure collapsed or where the piers were racked following failure of the concrete masonry shear walls due to overturning (see Figure 6). No failures of the older steel pipe columns were observed (see Figure 4). A typical connection between the concrete pier and floor beam is shown in Figure 7. Note that the floor joists are toenailed to the nailing strips which are attached to the steel beams by "Ramset" studs. Some high-set houses used metal cladding on the endwalls as seen in Figure 6 and this generally performed very well, being much more resistant to missile impact than the asbestos cement cladding. The cyclone bolts which were installed in all houses built after mid-1972 (see Figure 8) do not appear to have made any significant difference in performance since the main problem was a lack of racking strength once the asbestos cement cladding had failed. Many instances of endwall failure were observed (see Figure 9), suggesting inadequate corner connections and roof-wall connections at the gable ends. The performance of roof cladding is dealt with in a separate section of this report.

4.1.3 Conventional Single-Story Houses

Houses constructed for the Northern Territory Housing Commission were, for the most part, single-story slab-on-grade structures. There were several variations of this system but the cavity wall with bond beams was by far the most common. A typical cavity wall is shown in Figure 10. In several cases bond beams were provided only along the sidewalls and were inadequately tied through the walls to the footings (see Figure 11). This system generally performed very poorly with many cases observed in which the entire roof structure was removed intact and the ties between inner and outer leafs or wythes (each continuous vertical section of wall one masonry unit in thickness) of the cavity walls appeared to be inadequate. Both brick and concrete block were used for the exterior wythe. A few of the newer houses were of timber frame construction with brick veneer on the endwalls. Overall performance of this type of construction was generally poor. Some units in Wanguri and Anula, under construction at the time of Cyclone Tracy, utilized precast-tiltup concrete panels and performed exceptionally well.

4.1.4 Prefabricated Houses

Of the several prefabricated housing systems used in Darwin, only two were investigated in some detail and are described herein. The first is a high-set house with the same general floor plan and overall dimensions as the timber high-sets constructed for the Department of Housing and Construction (see Figure 12). All components are of precast concrete with welded and grouted beam-column connections. Columns are 200 x 200 mm in cross-section and the beams are 300 mm deep and 75 mm wide. The floor and roof panels are approximately 50 mm thick except for the edges which are 100 mm thick. A screed course is placed over the floor panels and the roof panels are bolted into sockets provided in the top edge of the beams. Wall panels lock into slots provided in the beams and columns. Conventional aluminum window frames, jalousie windows and metal louvers are also used in these houses. A conventional truss-purlin-CGI roof is placed over the ceiling panels, the timber plate being bolted down with the precast ceiling panels. This system would have performed very well had it not been for the fact that anchor bolts were installed only along the perimeter of the roof, even though the interior ceiling beams contained bolt sockets (see Figure 13). The result was that many of the panels were lifted from the interior beams, causing the perimeter anchors to fail.

Some of the ceiling panels shifted enough to drop off of their supporting beams, causing damage to wall and floor panels. In some cases the ceiling panels were flipped over and fractured adjacent panels (see Figure 14). This occurred after loss of the CGI roof cladding and roof trusses. One house had obviously received a heavy missile impact, causing failure of a second story corner column. The beam-column connection detail revealed by this failure is shown in Figure 15.

The second prefabricated system inspected is a single-story dwelling with a gable roof as shown in Figure 16. The walls are sandwich panels of 6 mm asbestos cement with a polyurethane core. The panels are framed with steel "H" sections (two channels back to back) and the roof system consists of welded, light-gage steel members. Roofing varied from structure to structure, the type shown here being "Decramastic," a steel sheeting stamped into the shape of tiles and coated with an asphaltic compound. Sandwich panels are also used for the ceiling, the channel framing also serving as the bottom chords of the trusses. This detail allowed the ceiling to act very effectively as a diaphragm. Although there were some window failures and substantial loss of roofing, this system performed exceptionally well. The walls and roof trusses exhibited no permanent deformations and the resistance of the sandwich panels to missiles was far superior to the ordinary asbestos cement cladding used on the high-set houses.

4.1.5 Privately Constructed Houses

Several privately constructed houses performed well with damage being limited to loss of CGI roof cladding or tiles and some broken windows. The house shown in Figure 17 is located in Nakara and has a welded steel frame with brick veneer. Note that the roof tiles have been replaced since the storm. Commercially produced timber connectors were used in many of these houses to attach purlins and trusses.

4.2 SCHOOL BUILDINGS

4.2.1 General

Several school buildings were constructed in Darwin over the past two years, particularly primary schools in the northern suburbs. Time did not permit a detailed study of all school buildings, but it is generally agreed that most of these buildings performed very well. Darwin High School served as the main center for recovery operations and provided temporary shelter for victims of Tracy while evacuation plans were being formulated. Design wind speeds for the newer schools in Darwin are not known to the author, but were probably between 50 and 55 m/s. It is important to note that most of these structures would have served well as community shelters during the passage of Tracy. The buildings described in this section were quite closely inspected and are believed to be representative of recent school construction in Darwin.

4.2.2 Millner Primary School

This complex consists of an auditorium and two-story classroom buildings connected by covered walkways. Construction is steel frame with concrete and brick masonry walls and roofing is steel pan-type sheet with hidden locking clips. The entire auditorium roof and most of the cladding over the covered walkways failed as did some portions of the roofing on the classroom buildings (see Figure 18). It is believed that the loss of roofing followed the failure of window panels on the windward side of the buildings. Two large infill masonry walls were blown in, falling onto the stairway leading to second-floor classrooms.

Of particular interest at this school were the temporary classrooms shown in Figure 19. Construction is cold-formed steel frame and steel cladding. They suffered a number of missile impacts and some loss of windows, but remained intact. The anchorage system depended solely on the dead weight of the concrete piers and footings and performed very well. One case of partial anchorage failure due to overturning of the piers was observed. Again, these units would have provided adequate refuge.

4.2.3 Darwin Community College

Darwin Community College is located just west of Nakara and was one of the more interesting complexes inspected because of some rather unusual structural failures. The main classroom building is a two-story reinforced concrete structure with masonry spandrel walls. The roof system consists of pan-type steel sheet carried by bar joists which are bolted to the column tops. A view of one-half of the north or windward wall is shown in Figure 20 and it is obvious that cracking has occurred in all of the columns just above the level of the second floor. The other half of the windward face of the building is shown in Figure 21. The roof structure has been folded over the exposed interior wall, and the second-story spandrel wall and several columns have failed. It was originally believed that the column failures were due to a poor splice detail, i.e., insufficient bar lap and column ties. However, a closer inspection revealed a quite different mode of failure. Following loss of the windows and/or spandrel walls the bottom chords of the bar joists failed in compression due to the high uplift pressures on the roof cladding and absence of any lateral bracing of the bottom chords. This, in turn, displaced the column tops and caused them to fail in combined bending and tension. This sequence of events was quite clear, both in the failed section and in the portion which was still standing.

A number of failures of masonry walls were observed in the buildings housing the metal and woodworking shops of Darwin Community College. These buildings have structural steel frames and concrete block walls as seen in Figure 22. The walls were unreinforced and are believed to have failed by direct wind loading since there was no source of debris upwind of these structures. There was no apparent damage to the steel frames.

Damage to student housing, located downwind of the main classroom building, is covered in a subsequent section.

4.3 APARTMENT BUILDINGS

No damage statistics on apartment buildings were available at the time the author visited Darwin. However, it was quite obvious that apartment buildings performed considerably better than did houses. It was observed that a substantial number of the people remaining in Darwin after Tracy were being lodged in apartments and that the highest density of apartments is in the subdivisions of Stuart Park, Larrakeyah and Darwin City. These subdivisions are believed to have had slightly lower wind speeds than did other parts of the city, but the relatively good performance of this class of structure can be largely attributed to better structural detailing. These buildings are typically two or three stories with reinforced concrete floor slabs and loadbearing walls of brick or concrete masonry. Roof decks are either steel purlins and CGI cladding or reinforced concrete. Figure 23 shows typical units in Darwin City.

Structural failures generally involved loss of roof decks and, in a few cases, collapse of masonry walls on the top floors following loss or buckling of purlins. Most roof failures are believed to have been initiated by breakage of windows or failure of doors on windward faces. No cases of primary structural damage were observed in apartment buildings with reinforced concrete roof decks. The building shown in Figure 24 is located in Millner, very close to the center of estimated storm track. Damage was limited to some broken windows, loss of an infill wall in the stairwell and partial failure of an equipment enclosure on the roof.

4.4 PUBLIC BUILDINGS

4.4.1 Government Office Blocks

These buildings are concentrated in the SE portion of Darwin City and are typically two and three story structures with steel or reinforced concrete frames. Design wind speeds are believed to have been in the range 49 to 58 m/s and maximum speeds in this area during the passage of Tracy are estimated at 50 to 60 m/s. Damage was generally limited to broken windows and partial loss of roofing. The amount of debris available for missile damage was markedly less than in other parts of Darwin. A very interesting observation was the effectiveness of sunscreens in protecting windows from missiles. Note the impact points in Figure 25. It is also possible that the sunscreens served to reduce the wind loading on cladding panels and windows.

4.4.2 Darwin Hospital

Darwin Hospital is located in Larrakeyah adjacent to the military area on Emery Point and was designed for a wind speed of 58 m/s. It is a 3-story reinforced concrete structure with sunscreens (see Figure 26) and has a relatively clear wind exposure. This building performed very well and continued to function during the storm, switching over to emergency power when the main distribution system failed. Maximum wind speeds in this area were probably in the range 55-60 m/s. As with the city area, relatively small amounts of debris were available to cause missile damage.

4.4.3 Historic Buildings

Several buildings constructed prior to 1900 have been preserved as historic buildings and are of interest because of their previous exposure to intense cyclones. These buildings are all quite similar in physical size and type of construction, having timber roof trusses and load-bearing walls of native stone approximately 400 mm thick. Most of these buildings suffered extensive damage in the cyclones of 1897 and 1937. Typical damage is shown in Figure 27.

4.5 TALL BUILDINGS

Several new hotels and office buildings have been constructed in Darwin since 1970. These include the 10-story MLC Building and the 11-story Travelodge (Figures 28 & 29) in the Darwin City area. Both are of reinforced concrete flat plate construction with concrete shear walls. Most wind damage was superficial, being limited mainly to loss of pan-type roof cladding and broken windows. There proved to be no substance to the rumor that a large missile caused the partial failure of the brick and concrete block endwalls of the Travelodge (see Figure 29). An identical failure occurred at the same level on the opposite end, undoubtedly due to extremely low surface pressures downstream of the separation points. The change in wind direction in this area would have been sufficient to create identical pressure distributions at each end of the building. The design speeds are not known, but inspection teams reported no evidence of cracking or plastic action in either structural system. Occupants did report noticeable oscillations during the storm passage. Water damage was extensive in these and other tall buildings following loss of roof cladding and glass breakage.

4.6 INDUSTRIAL BUILDINGS

Most of the industrial buildings are located in Winnellie and Stuart Park. Maximum speeds in Winnellie are believed to have been 55-60 m/s and slightly lower in Stuart Park. Structural details and materials used in most of these buildings are very similar to U.S. practice; i.e., cold-formed rafter sections, purlins and girts with 26 ga. CGI cladding. Wind bracing was usually limited to diagonal rods in one or two wall panels, the cladding being counted on for most of the in-plane stiffness. Most buildings had a concrete masonry infill wall and small office area at one end, the other end consisting of girts and CGI wall cladding. In many cases the purlins were tied directly into the concrete masonry wall, the end rafter being eliminated.

The overall performance of industrial buildings was good, but damage to these light-frame structures in some areas of Winnellie was heavy. It was quite apparent that these buildings had little variation in ultimate load capacity; if one building of a particular type failed, most others of that same type also failed. It is quite likely that failure of rollup doors, windows, and flashing led to gross cladding failure because of sudden increases in internal pressure. Many cases of purlins being buckled upward were observed and this often led to failure of the masonry endwalls to which they were anchored. In other cases the roof cladding was removed by direct pullout of the fasteners, but was more often due to fatigue failure in the material adjacent to the fasteners. This often resulted in total collapse, particularly where the cladding provided the only source of racking strength in the roof planes. A typical failure is shown in Figure 30. Several buildings suffered complete loss of roof and wall cladding without the frame collapsing. In these cases, however, a conventional system of diagonal bracing had been installed in the roof and wall planes.

The buildings shown in Figure 31 are located in Stuart Park and, excepting some loss of wall cladding, they performed very well. These buildings have 22 ga. CGI cladding with 16 mm washers under the fastener heads. This detail, in conjunction with the ridge ventilators undoubtedly had much to do with the overall good performance. Ridge ventilators effectively lower the internal pressure and reduce the uplift load on the roof. This observation has been made in previous surveys of wind damage.

5.0 PERFORMANCE OF MATERIALS AND STRUCTURAL SYSTEMS

5.1 GENERAL

The behavior of certain materials and subsystems under repeated loading and attack by windborne debris was an important factor in the overall performance of buildings in Darwin and deserves special attention in this report. It raises serious questions as to the validity and application of design criteria based solely upon static load tests of buildng elements and structural subsystems. Although many of the failures observed can be explained by extreme loading, poor workmanship or poor design, there was overwhelming evidence of consistently poor performance of certain materials and structural subsystems during the passage of Cyclone Tracy. These are discussed in the following sections.

5.2 CORRUGATED GALVANIZED IRON CLADDING (CGI)

As with other tropical regions of Australia and, in fact, throughout the world, CGI cladding is widely used in Darwin. There are many variations in the sheet profiles and types of fasteners, by far the most common being a sinusoidal cross section with self-drilling, self-tapping fasteners equipped with a neoprene sealing washer. Immediately following Cyclone Tracy, laboratory tests and field inspections of single-family dwellings and industrial buildings were carried out by the Housing Research Branch, Department of Housing and Construction to establish the reasons for the widespread failure of CGI in Darwin [10]. These investigations are continuing, but preliminary findings indicate that low-cycle fatigue was the predominant failure mode. Repeated load tests carried out at approximately 30 percent of the ultimate static load capacity produced failures after 2000 to 3000 cycles. A typical failure is shown in Figure 32. Data obtained in recent full-scale investigations of wind

loading [11] suggest that this combination of load and number of cycles would have been exceeded in slightly less than one hour for the wind speeds occurring in the northern suburbs. This suggests that the fastening system in current use (typically 15 mm diameter screw heads with screws installed at every second or third crest) will have to be radically altered. Possible improvements include:

a) Installation of fasteners in valleys rather than on ridges
b) Larger washer or screwhead diameter
c) Battens placed over the CGI and bolted into the purlins

5.3 ASBESTOS CEMENT CLADDING

The asbestos cement cladding used on most of the high-set houses and some of the single-story dwellings proved to be very susceptible to missile impact. This was a major factor in the poor performance of those structures which depended entirely on cladding for racking strength. Static load tests did not reveal this deficiency and it is likely that performance would have been substantially better had a tougher material such as plywood been used. It is interesting to note the drastic improvement in impact resistance where the same material is used in sandwich panel construction (see Figure 33). Conventional nailing of asbestos cement sheets subjected to repeated racking loads deserves additional study.

5.4 MASONRY CAVITY WALLS

Many failures of masonry cavity walls were observed. Lack of bond beams and lateral loading due to purlin buckling were often the cause of these failures. However, a number of cases were observed where the crossties were either inadequate or improperly installed and the inner and outer wythes did not act together in resisting lateral loading. Since Australian practice with respect to masonry cavity wall construction is quite similar to that here in the U.S., this high incidence of failure is cause for concern. Most load tests on masonry walls have been carried out with vertical compression loads applied to simulate deadload. This load condition overestimates resistance to racking and lateral loads when uplift forces are sufficient to offset the deadload. In many cases observed in Darwin, it is likely that the uplift forces transmitted through the purlins were sufficiently high to place the entire wall in tension.

6.0 UTILITIES

6.1 POWER GENERATION AND DISTRIBUTION

6.1.1 Stokes Hill Power Station

The Stokes Hill Power Station supplies the entire greater Darwin area with electrical power and is located at the extreme southern tip of the city. It does not function as part of a grid system and was thus essential to recovery operations. Damage was primarily due to water entering switch gear following loss of roof cladding. A trawler was washed ashore directly over the cooling water outlet structure, but this did not require any immediate repair work. The one reinforced concrete and three steel stacks at the station suffered no apparent damage and the station was placed in partial operation within two days after the storm.

6.1.2 Electrical Distribution

With the exception of the main transmission line running across Darwin to the northeast (conventional steel space-truss towers), most distribution lines were heavily damaged and required complete replacement. Most power poles were either steel lattice structures or prestressed concrete and failures were generally due to accumulation of CGI cladding on the conductors and poles. Many lamp standards also failed due to debris loading (see Figure 34). Primary distribution lines were put back in service within one to two weeks after the storm.

6.2 COMMUNICATIONS

Darwin is connected through a microwave link to the national communications network and most lines in the city are buried. The microwave tower and related equipment in Darwin City experienced only light damage and telephone communications were thus partially restored within hours after the passage of Tracy.

6.3 WATER AND SEWERAGE SYSTEMS

Damage to water and sewerage systems was minimal, primarily due to the fact that there was very little erosion due to storm surge and wave action. Most of the disruption was caused by lack of electrical power at pumping stations. Of the half-dozen or so large elevated water tanks in Darwin, none suffered any noticeable structural damage. The extremely heavy damage in the northern suburbs required that most of the water mains in that area be shut down until individual service taps could be closed.

7.0 CONCLUSIONS

Cyclone Tracy was an extremely intense storm which passed directly over the city of Darwin. The unusually slow forward speed (6-8 km/hr) and long duration of extreme winds is believed to have been a key factor in the extensive damage to buildings, housing in particular, and revealed weaknesses in structural systems that would quite likely have resisted an equally intense storm of shorter duration. While certain construction practices and building materials used in Darwin are not commonly found in the U.S., much of what happened should be given proper attention in future revisions of wind load design criteria and indicates a need for additional research in the following areas:

a) Behavior of CGI cladding and fastening systems under repeated loads
b) Resistance of brittle materials such as asbestos cement and fiber board to missile impact
c) Racking strength of wall panels subjected to uplift loads
d) Behavior of housing systems subjected to unusually high internal pressures resulting from failure of doors and windows
e) Performance of brick and concrete masonry cavity walls for various conditions of edge support and load combinations, including uplift.

8.0 ACKNOWLEDGEMENTS

The author wishes to express his special thanks to Dr. George R. Walker, Senior Lecturer, Department of Engineering, James Cook University of North Queensland, for making most of the technical data contained in this report available and for providing invaluable assistance and guidance during the brief period available for the inspection of damage. This report is the result of the author spending several days on temporary assignment with the Department of Housing and Construction, and the assistance of members of the engineering staff, both in Darwin and Melbourne, is gratefully acknowledged.

9.0 REFERENCES

1. Wilkinson, F.L., "Interim Report - Cyclone Tracy Storm Surge at Darwin, 25 December, 1974," Report No. 57, Department of Housing and Construction, Maritime Works Section, Melbourne, Vic., January 1975.

2. "The Port of Darwin Tide Tables - 1974," Compiled at Naval Headquarters, Darwin, NT.

3. Thom, H.C.S. and Marshall, R.D., "Wind and Surge Damage Due to Hurricane Camille." Journal of the Waterways, Harbors and Coastal Engineering Division, ASCE, Vol. 97, No. WW2, May 1971.

4. DeAngelis, R.M. and Nelson, E.R., "Hurricane Camille, August 5-22." Climatological Data, National Summary, ESSA, Vol. 20, No. 8, Washington, D.C. 1969.

5. Condon, C.R. "North Atlantic Tropical Cyclones - 1970" Climatological Data, National Summary, NOAA, Vol. 21, No. 13, Washington, D.C., 1970.

6. "Is Darwin Prepared for a Cyclone?" Report by the Cyclone Subcommittee of the Institution of Engineers, Australia - Darwin Group, April 1974.

7. Walker, G.R., "Report on Cyclone Tracy - Effect on Buildings." Vol. 1, Department of Housing and Construction, Melbourne, Vic., March 1975.

8. Halpern Glick Pty. Ltd., "Indications of Wind Velocities During Cyclone Tracy From the Behavior of Simple Structures." Report on Cyclone Tracy-Effect on Buildings, Vol. 2, Appendix 1, Department of Housing and Construction, Melbourne, Vic., March 1975.

9. SAA Loading Code, Part II - Wind Forces (AS CA34, Part II - 1971). Standards Association of Australia, Sydney, NSW, 1971.

10. Beck, V.R., "Appraisal of Roof Cladding Under Dynamic Wind Loading - Cyclone Tracy, Darwin, 1974." Technical Report No. 1 (Preliminary), Housing Research Branch, Department of Housing and Construction, Melbourne, Vic., February 1975.

11. Marshall, R.D., "A Study of Wind Pressures on a Single-Family Dwelling in Model and Full-Scale." NBS Technical Note 852, National Bureau of Standards, Washington, D.C., 40 pages (October 1974).

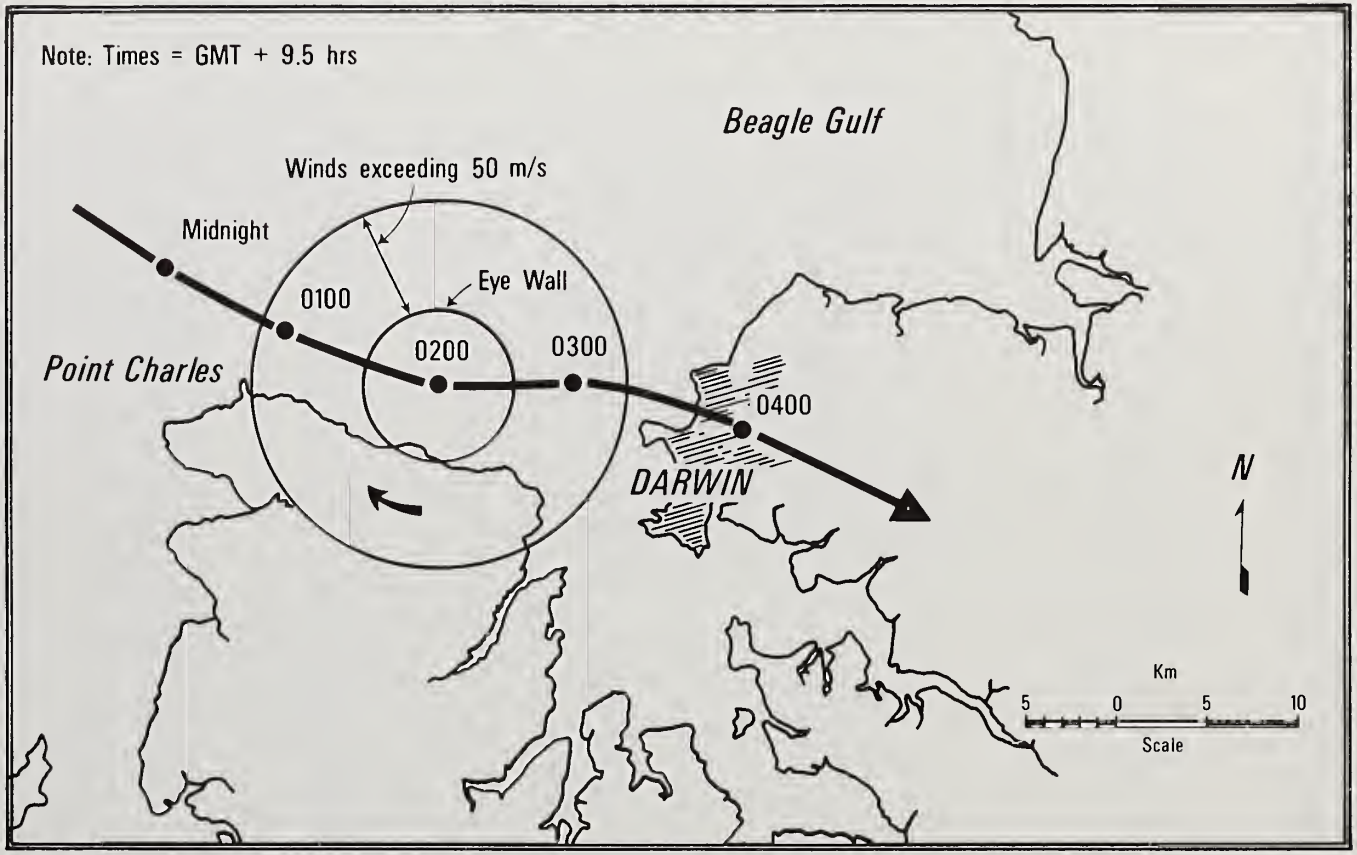

Fig. 1. Approximate track and position of Cyclone Tracy at 0200 hrs., December 25

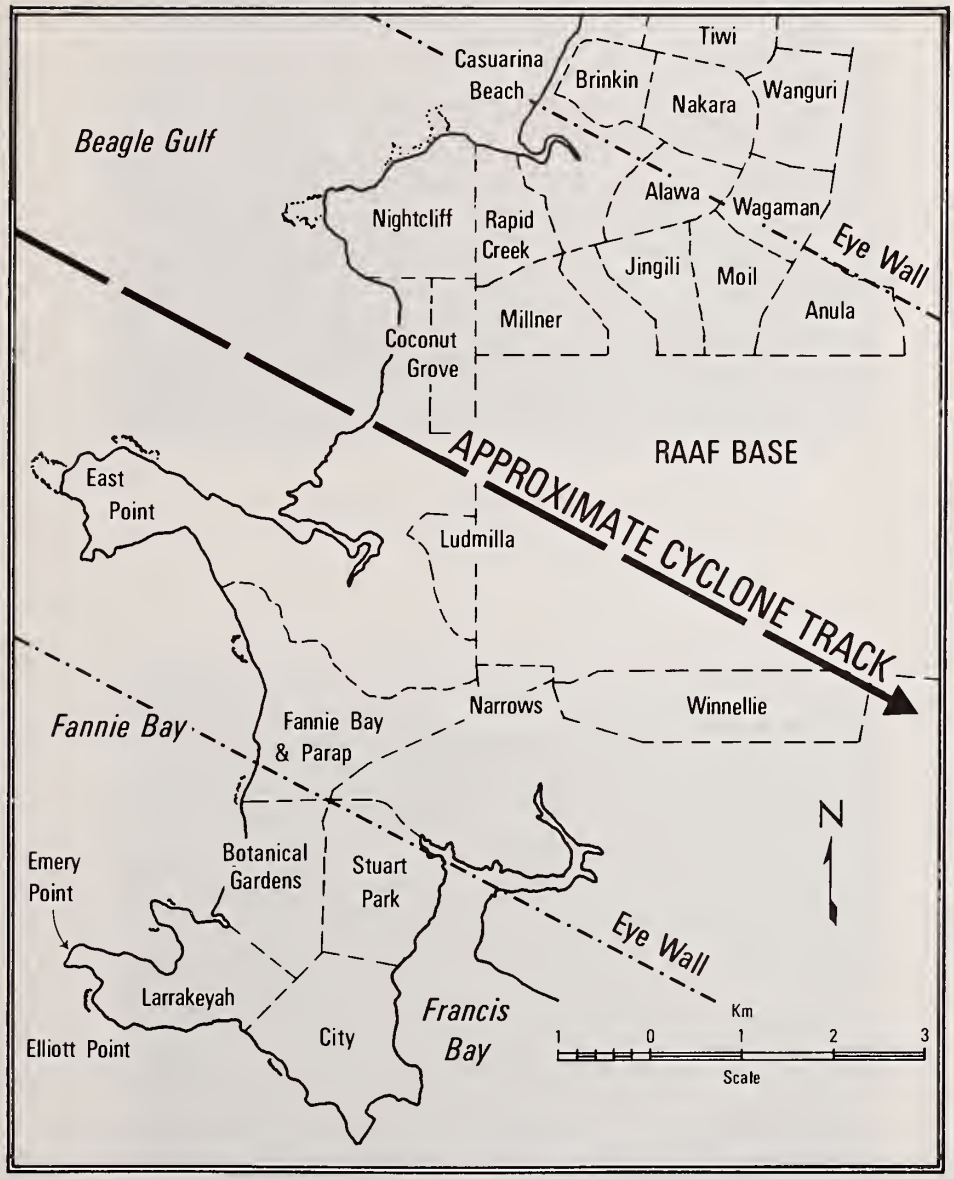

Fig. 2. Approximate cyclone track across Darwin

Fig. 3. Typical high-set house

Fig. 4. Pipe columns used in older construction

Fig. 5. Severe racking and loss of timber deck

Fig. 6. Failure of concrete block shear walls and racking of concrete piers

Fig. 7. Typical floor systems and pier anchorage

Fig. 8. Cyclone bolt and rafter connection

Fig. 9. Failure of endwall

Fig. 10. Failure of brick and concrete block cavity wall

Fig. 11. Concrete bond beam and timber plate (single-story construction)

Fig. 12. High-set house with precast concrete frame and interlocking precast concrete panels.

Fig. 13. Ceiling panel anchorage - bolt and adjacent panel missing

Fig. 14. Overturned ceiling panels - CGI cladding and roof framing completely removed.

Fig. 15. Beam to column connection - precast concrete high-set

Fig. 16. Prefabricated house with asbestos cement-polyurethane sandwich panels and steel wall and roof frames

Fig. 17. Privately constructed residence with welded steel frame and brick veneer

Fig. 18 Auditorium - Millner Primary School

Fig. 19. Temporary classrooms - Millner Primary School

Fig. 20. Academic Block - Darwin Community College

Fig. 21. Failure of second story (view immediately to right of Fig. 20)

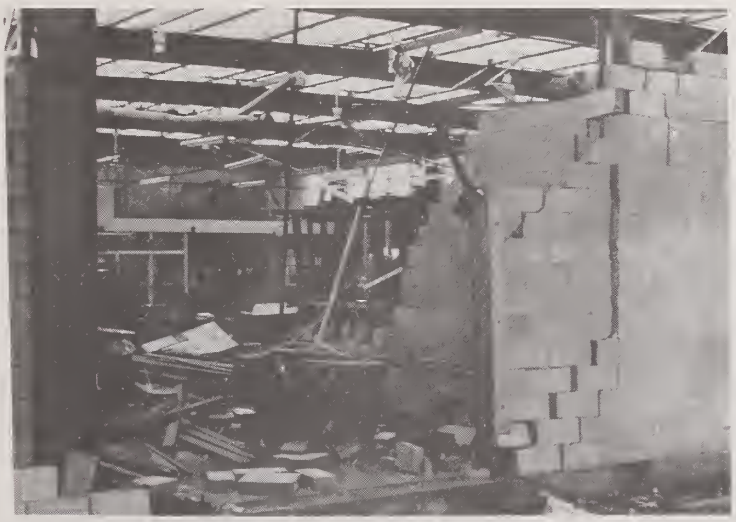

Fig. 22. Woodworking shop - Darwin Community College

Fig. 23. Apartment buildings in city area

Fig. 24. Apartment building in Millner

Fig. 25. Sunscreen showing points of missle impact

Fig. 26. Darwin Hospital - Larrakeyah

Fig. 27. Historic building in Darwin City - hip roof completely removed

Fig. 28. MLC Building - Darwin City

Fig. 29. Travelodge - Darwin City (similar damage at opposite end)

Fig. 30. Industrial building - Winnellie

Fig. 31. Railway shops - Stuart Park

Fig. 32. Typical fatigue failure of CGI cladding

Fig. 33. Missile damage to asbestos cement-polyurethane sandwich panel

Fig. 34. Failure of lamp standard due to debris loading

ON THE DAMAGE TO BUILDINGS IN HACHIJOJIMA CAUSED BY TYPHOON NO. 7513

TATSURO MUROTA
Chief, Structure Section
Structure Division
Building Research Institute
Ministry of Construction, Japan

ABSTRACT

On October 5, 1975 Typhoon No. 7513 hit Hachijojima Island, Tokyo and the maximum peak gust of 67.8 m/s was observed. The damage to this island was severe and widespread, damage to buildings, services, crops, trees, electric power lines and telephone lines occurred. The wind records and the rate of damage to buildings was one of the largest in Japan.

The Building Research Institute investigated the damage to the buildings in Hachijo-jima Island from 9 to 16, October. This paper describes results of the investigation.

Description of the typhoon and meteorological environment in the Island during the passage of the typhoon are referred in detail by Soma (1) and therefore are not referred to herein.

Key Words: Damage; Typhoon; Wind; Wind Effects.

1. Definition of Terms

In order to express the extent of damage the following terms and notations will be used in this paper:

"completely destroyed" = damaged to the extent that the floor area damaged exceedes 70% of the total floor area, or the expense of repairs is more than 50% of the current price of the building.

"badly damaged" = damaged to the extent that the floor area damaged are 20 to 70% of the total floor area or the expense of repairs is more than 50% of the current price of the building.

"rate of completely destroyed houses = R_c = rate of the number of completely destroyed houses to the total number of households in a certain district.

"rate of badly damaged houses" = R_b = rate of the number of badly damaged houses to the total number of households in a certain district.

"rate of damaged houses; = R_t = sum of the two rates defined above.

2. Description of Damage to Buildings

a) Statistics and Regional Distributions of Damage to Houses

Quoting from the damage statistics published by Hachijo-Cho Town Hall under date of October 9, damage to houses in every administrative district in Hachijojima Island is

as shown in Table 1. Concerning the rate of completely destroyed houses, the average was 7.9% and by administrative district the highest rate was 11.4% in Sueyoshi. Concerning the rate of damaged houses it was 18.6% by administrative district 21.8% in Okaho which was the largest. It is worthy to note that in Nakanogo district both of these rates were considerably lower than others.

In each administrative district in Hachijojima there are small sections where scores of people are living. The rate of damage houses R_t for each section was investigated and the result is illustrated in Fig. 1, where the rate of damaged houses was classified into 5 steps 10% each.

The maximum rate was 58.1% (25/43, Section No. 6, Obata, Mitsune District) and the minimum rate was 1.5% (1/64, Sec. No. 14, Sakuradaira, Mitsune Dist.). In addition to the large difference between these extremes, it was very surprising that these two sections are located side by side. Similar behavior of damage rates were observed in several other places. One of the reasons for this inconsistency was the effect of the topography.

b) Relation Between the Rate of Damage and the Maximum Peak Gust

According to Takahashi (1) the amount of damage to structures is proportional to the wind speed. Ishizaki et al. (2) applied this theory to damage of houses caused by three severe typhoons: the 2nd and 3rd Miyakoj-ma Typhoon (1966 and 1963) and Isewan Typhoon (1959), and plotted the relation between the rates of completely destroyed houses R_c and maximum peak gusts as shown in Fig. 2. A mark Δ in this figure was plotted by the present author for comparison. It will be noted from this figure that the value of R_c 7.9% in a severe wind of maximum peak gust 67.8 m/s was not exceptional when comparing those damages caused by the past three typhoons.

3. Features of the Damage to Buildings

a) Wooden Buildings

Wooden buildings are most popular in Hachijojima Island. Most of the houses have a gable roof or a hip roof with a slope of 2/10 to 2.5/10. Their roofings, almost without exception, consist of a thin metal plate roof nailed to bed rafters where "bed rafters" are structural members of square cross-sections and are set on common rafters in a direction perpendicular to the common rafters.

Damage to the wooden buildings occurred to the roofs and openings on the external walls. Roof damage in which only the metal roof was removed was rare, in most cases, removal of the bed rafter, common rafters, purlins, roof posts or ridges occurred together with the removal of metal roof. Such damage was caused by the imperfection of connections between roof structural members.

b) Reinforced Concrete Buildings

Damage to reinforced concrete buildings occurred only at openings on the external walls. Such damage occurred at a hotel in Hachijojima. This hotel was six stories and suffered severe damage to its windows. From the 2nd to 6th floor, 30% of the windows on windward surface were broken. At the 1st floor of the hotel there was a lobby surrounded by glass walls and these glass walls had been broken on both of windward and leeward

sides. This damage was caused by wind generated missiles and also the small flexural rigidity of the window sashes.

In the design of buildings having many windows on exterior walls, it is necessary to take the breakdown of window glasses into account, because the breakdown of windows lead to an increase of interior pressure and for some part of the building the overload may be caused by this pressure increase.

c) Steel Frame Buildings

Steel frame buildings suffered damage to the finish of the external surfaces. Most of the damage was precipitated by the structural engineer for not checking the safety of those finishings into detail. It is necessary that structural engineers recognize that the wind pressure acts on finishings on external surfaces of buildings.

The other point which is considered to be important, is that several buildings of flat roofs using steel roof decks suffered serious damage: bodily removal of the roofs. These roofs had considerably long eaves and roof surfaces were more flexible than other types of roofs. In wind resistant design of these roofs it is necessary to take the dynamic effect of pressure fluctuations into account.

4. Concluding Remarks

On October 5, 1975 Typhoon No 7513 hit Hachijojima Island. Maximum peak gust of 67.8 m/s was observed at Hachijojima Weather Station. 7.9% of houses in the island were completely destroyed by the severe wind caused by this typhoon. This damage was one of the severest in Japan.

Lessons obtained from this disaster are as follows:

1. Light weight roofs suffer damage very easily. When flexural rigidity of the roof surface is small, like some flat roofs with steel roof decks, it is necessary in structural design to take the dynamic effect of wind pressure fluctuations into account. Investigations will be necessary concerning this problem.

2. Damage to openings and finishings on external walls was observed on many buildings. Such damage may be a trigger to more serious damage and therefore it is necessary to recognize the importance of the design of details.

References

1. K. Takahashi, et al.,Reports of the Damage Caused by Isewan Typhoon, Jour. of Architecture and Building Science, Vol. 75, 1960, pp. 111-115.

2. H. Ishizaki, et al.,On the Damage to Houses Caused by the Third Miyakojima Typhoon, Annals, Disaster Prevention Institute, Kyoto Univ., No. 13A, 1970, pp. 449-461.

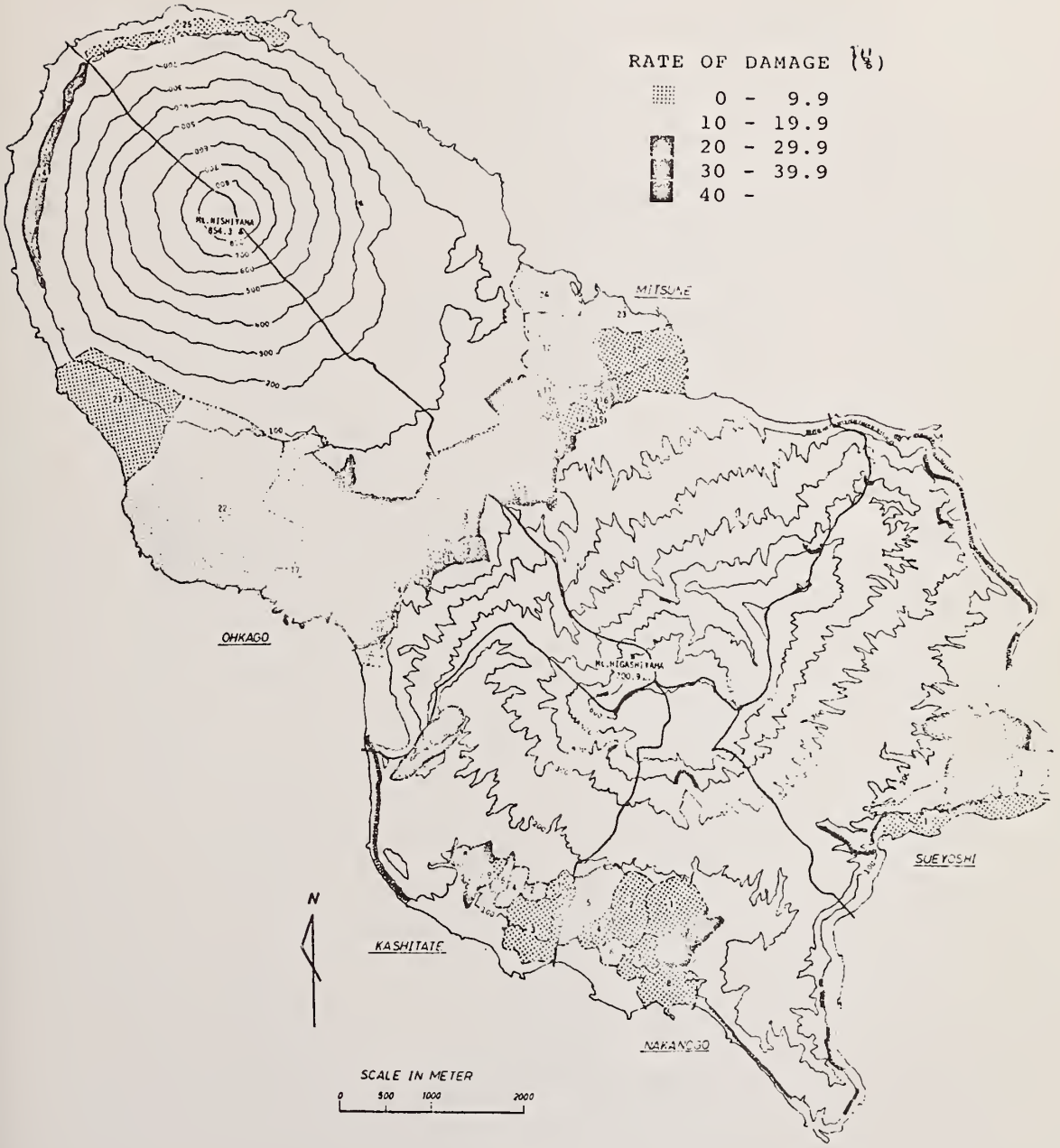

Fig. 1 Distribution of the rate of damaged houses, Rt

Fig. 2 Relation between the rate of completely destroyed houses, R_c and the maximum peak gust.

- ⊙ Isewan Typhoon
- × The 2nd Miyakojima Typhoon
- ○ The 3rd Miyakojima Typhoon
- △ Typhoon No. 7513

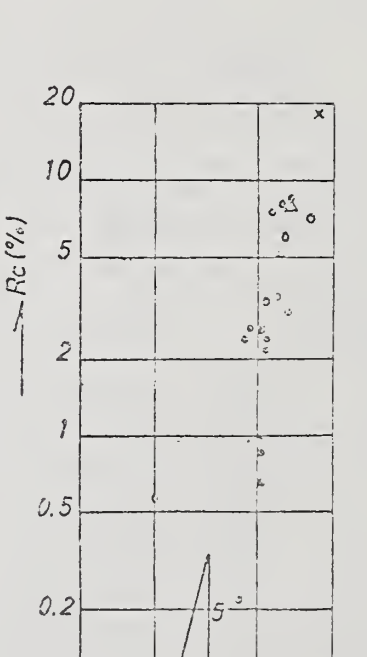

Table 1 Statistics of house damaged

Administrative District	Number of Households	No. of completely Destroyed Houses	No. of badly Destroyed Houses	Rc (%)	Rt (%)
Mitsune	1587	113	184	7.1	18.7
Okago	1247	121	151	9.7	21.8
Kashitate	270	21	22	7.8	15.9
Nakanogo	427	13	30	3.0	10.1
Sueyoshi	254	29	21	11.4	19.7
Total	3785	297	408	7.9	18.6

SEISMIC RESPONSE OF REINFORCED CONCRETE HIGHWAY BRIDGES

J. PENZIEN
Professor of Structural Engineering
University of California, Berkeley

W.G. GODDEN
Professor of Civil Engineering
University of California, Berkeley

M.C. CHEN
Assistant Research Engineer
University of California, Berkeley

D. WILLIAMS
Assistant Research Engineer
University of California, Berkeley

K. KAWASHIMA
Assistant Specialist
University of California, Berkeley

ABSTRACT

Presented is a brief progress report of an investigation entitled "An Investigation of the Effectiveness of Existing Bridge Design Methodology in Providing Adequate Structural Resistance to Seismic Disturbances" which was initiated in 1971 within the Earthquake Engineering Research Center, University of California, Berkeley, under the sponsorship of the U.S. Department of Transportation, Federal Highway Administration.

Key Words: Bridges; Design; Experiments; Nonlinear Response; Reinforced Concrete.

1. Introduction

In the past, numerous highway bridges have suffered extensive damages due to strong motion earthquakes (1,2). The older bridges, consisting of single or multiple simple truss or girder spans supported on massive piers and abutments, were particularly vulnerable to the action of strong ground motions. Seismic damages were most commonly caused by foundation failures resulting from excessive ground deformation and/or loss of stability and bearing capacity of the foundation soils. As a direct result, the substructures often tilted, settled, slid, or even overturned; thus severe cracking or complete failure was often experienced. These large support displacements also caused relative shifting of and damage to the superstructures, induced failures within the bearing supports, and even caused spans to fall off their supports. It is significant to note that very little damage occurred to these older structures as a direct result of structural vibration effects.

Certain types of modern highway bridges may, on the other hand, be quite susceptible to damage from strong ground vibration effects. This fact became very evident during the

San Fernando earthquake of February 9, 1971, when numerous reinforced concrete highway bridges which were designed by the traditional elastic approach, i.e., by the equivalent static seismic coefficient method similar to that previously adopted for buildings, suffered severe damages (3,4,5). Because of this experience, it was immediately apparent that the seismic requirements used were inadequate and that the design methodology should be critically examined. Action was quickly taken following the earthquake to correct certain design deficiencies (6); however, the basic static approach to design still remains in effect.

Recognizing the urgent need for both theoretical and experimental research related directly to seismic effects on bridge structures, an investigation entitled "An Investigation of the Effectiveness of Existing Bridge Design Methodology in Providing Adequate Structural Resistance to Seismic Disturbances" was initiated in 1971 within the Earthquake Engineering Research Center, University of California, Berkeley, under the sponsorship of the U.S. Department of Transportation, Federal Highway Administration. This investigation consists of the following six phases:

1. A thorough review of the world's literature on seismic effects on highway bridge structures including damages to bridges during the San Fernando earthquake of February 9, 1971.

2. An analytical investigation of the dynamic response of long, multiple-span, highway overcrossings of the type which suffered heavy damages during the 1971 San Fernando earthquake.

3. An analytical investigation of the dynamic response of short, single and multiple span highway overcrossings of the type which suffered heavy damages during the 1971 San Fernando Earthquake.

4. Detailed model experiments on a shaking table to provide dynamic response data similar to prototype behavior which can be used to verify the validity of theoretical response predictions.

5. Correlation of dynamic response data obtained from shaking table experiments with theoretical response and modification of analytical procedures as found necessary.

6. Preparation of recommendations for changes in seismic design specifications and methodology as necessary to provide adequate protection of reinforced concrete highway bridges against future earthquakes.

Final reports covering Phases 1, 2, and 3 have been published (1,7,8) and similar reports covering Phases 4 and 5 are now in preparation. Phase 6 of the overall investigation will be completed during summer and fall of 1976.

The brief progress report presented in this paper concentrates on Phases 4 and 5 with some mention of the results obtained in Phases 2 and 3.

2. Analytical Studies

a) Long Multiple-Span Bridges (7,9,10)

The primary objective of the investigation in Phase 2 was to develop suitable pro-

cedures for linear and nonlinear three-dimensional earthquake response analysis of long, multiple-span, modern highway bridges of the type which suffered heavy damages during the 1971 San Fernando earthquake and to identify and investigate the important parameters which significantly affect the response of this type of bridge system. To achieve these objectives linear and nonlinear mathematical models suitable for modelling the dynamic characteristics of this type of bridge were defined and analytical procedures and computer programs were developed for determining the seismic response of the complete bridge system to arbitrary, but prescribed, earthquake excitations.

Linear and nonlinear seismic analyses were performed on three typical major overcrossings using earthquake ground motions of several intensities. These bridges were (1) the South Connector Overcrossing of the Golden State freeway and Antelope Valley freeway interchange (5/14 South Connector Overcrossing), (2) the proposed curved Figueroa Street Undercrossing Connector in the Los Angeles area, and (3) a straightened version of the Figueroa Street Undercrossing Connector. Various parameter studies were carried out for these bridges and the results were correlated with the apparent behavior of this type of structure during the San Fernando earthquake. In particular, the causes of collapse of the 5/14 South Connector Overcrossing were identified and examined.

Based on the results of this investigation, the following conclusions were deduced:

1. The basic mathematical models, analytical procedures, and computer programs developed provide a rational and effective means for determining the seismic response of curved and straight, multiple-span, long, highway overcrossings.

2. The collapse of the 5/14 South Connector Overcrossing during the San Fernando earthquake was due to the inability of the longitudinal restrainer ties to constrain the joint separation at expansion joints; thus allowing two central spans to fall off one end support, resulting in the collapse of the spans along with their common supporting column.

3. The proposed curved Figureoa Street Undercrossing Connector can safely withstand severe ground shaking of an intensity similar to those experienced during the San Fernando earthquake; however, some flexural damage is likely to occur at the bases of the columns supporting the central spans.

4. The strength and distribution of bridge columns in each deck segment between expansion joints are the primary factors which most significantly affect the seismic response characteristics of the bridge structure. Thus expansion joints in the deck should be located in a manner such that each substructural segment possesses a reasonably adequate amount of lateral stiffness.

5. Under severe shaking conditions similar to those experienced during the San Fernando earthquake, the maximum horizontal acceleration response at the deck level substantially exceeded those values specified by the "Bridge Planning and Design manual," California State Division of Highways (5) which was in effect prior to the San Fernando earthquake of February 9, 1971.

6. Because of their effectiveness in reducing the amplitude of the seismic displacement response of curved bridges, longitudinal restrainer ties should be provided at expansion joints. They should have sufficiently high strength and ductility to constrain the

joint separation within the limit of the supporting ledge dimension. Vertical restrainers should also be provided at expansion joints in order to prevent the lifting of spans from their supports.

7. For curved bridges, a bigger expansion joint gap appears to be desirable to prevent biased seismic response and to avoid a shake-down situation under severe shaking conditions.

8. The required expansion joint ledge dimension and joint gap can be estimated from the maximum horizontal displacement obtained from a seismic analysis.

9. Under moderate to severe shaking, the overall seismic response of a bridge structure is considerably affected by vertical ground accelerations. The effect is particularly noticeable for curved bridges in which coupling exists between vertical and horizontal modes of vibration. Thus the vertical component of ground acceleration should always be included in a seismic analysis.

10. For a normally proportional bridge structure under moderate to severe shaking, flexural yielding is more likely to occur at the base of the columns. Yielding in columns should be avoided under moderate shaking but can be permitted to limited levels under severe shaking conditions. It is therefore important that column reinforcement be sized and detailed in such a manner that the columns can develop full yield strengths and maintain their yield capacities throughout their specified ranges of ductility. Flexural yielding should be prevented from developing at the top of columns in order to avoid damage penetrating the deck.

11. The effect of expansion joint Coulomb friction on high seismic response of the bridges considered is small.

12. Linear seismic responses analysis provides a reasonable estimate of the maximum displacement response of a bridge system; however, substantial error may result in predicting the internal forces in the structure. Thus it is essential that nonlinear seismic analyses be carried out for major bridge structures under severe shaking conditions.

b) Short Single or Multiple-Span Bridges (8)

The primary objective of the investigation in Phase 3 was to develop suitable procedures for linear and nonlinear two- and three-dimensional earthquake response analysis of short single or multiple-span highway bridges of the type where soil-structure interaction effects are important.

For the two-dimensional studies, the bridge system was modelled mathematically using six different sub-elements (1) finite modelling was used for the backfill soils, (2) bridge deck, piers, and abutments were modelled using prismatic beam elements, (3) a frictional element was used to model the discontinuous behavior at the interface of backfill soils and abutments, (4) discontinuous type expansion joint elements were included, (5) linear spring elements were used to provide flexibility at the vertical soil boundaries, and (6) the soil foundation flexibilities under columns were determined using elastic half-space theory. In the non-linear mathematical model, the effects of separation and impact at the interface between abutments and backfills, the yielding at concrete

columns and backfill solid and slippage at the expansion joints were taken into consideration.

Parameter studies were first carried out considering a rigid wall backfill soil system A short, stiff, three-span bridge was then investigated with full soil-structure interaction effects included. It was found from these studies that soil-structure interaction effects must be considered when analyzing the dynamic response of short, stiff, single or multiple span bridges and it was shown that the mathematical modelling and computer programs developed provide an effective means of conducting such analyses.

For the three-dimensional studies, the bridge system was modelled by four different sub-elements (1) the linear elastic three-dimensional beam element was used to model the bridge girder, pier columns, and pile cap, when necessary, (2) the linear elastic three-dimensional solid finite element was used to model backfill soils and abutment walls, (3) a nonlinear three-dimensional friction element was used to simulate separation and impact between backfills and abutment walls, and (4) linear elastic spring elements having six degrees of freedom, 3 translational and 3 rotational, were used to model column foundations.

The same bridge used in the above two-dimensional analysis was treated again in a three-dimensional skewed form to study the influence of torsion about a vertical axis. Parameter studies included effects of skewness, impact and separation between abutment walls and backfill soils, and type of model (linear vs. nonlinear) used for the backfill soils. Results of the analyses showed that significant torsional response can occur due to skewness of the deck coupled with out of phase abutment forces resulting from various causes.

3. Experimental Studies (11,12,13)

a) Model Design

A 1/30 true-scale microconcrete model of a simplified symmetrical version of a typical high curved bridge structure was constructed and subjected to appropriately scaled simulated seismic motions of varying intensity using the 20 ft x 20 ft shaking table at the U.C. Earthquake Simulator Laborabory. The model consisted of three deck segments, separated by expansion joints and supported at the abutments and on 3 ft high columns. The radius of curvature was 9 ft., the deviation angle was 125° and the total span approximately 22 ft.

In order to gain as much experimental data as possible from the basic model, it was designed as an assemblage of replaceable components. This procedure has the obvious advantages of making the structure easily repairable when damaged, of facilitating certain property changes between test series, and of enabling linear and nonlinear characteristics to be determined by prior component testing.

In relation to the prototype, the quantities scaled included all bending and torsional stiffnesses, self-weight effects and inelastic effects both in the expansion joint restrainers and in the columns. The model was designed so that damage would be confined to these two locations while the remainder of the deck system remained elastic.

Inelastic cyclic bending tests of the column elements have confirmed that the nonlinearity of well designed prototype reinforced concrete columns was adequately simulated.

The model was weight-distorted; thus deficiency weight in the form of lead blocks equivalent to 30 times the self-weight of the model (based on the prototype box girder section) was added to the model. The resulting time ratio was 1/5.5. The lower mode shapes and frequencies of the scaled prototype structure were consequently reproduced in the model.

b) Model Response

Three types of simulated earthquake excitation were applied to the model, (1) horizontal excitation alone in the asymmetric longitudinal direction, (2) horizontal excitation alone in the symmetric transverse direction, and (3) horizontal excitation in the symmetric transverse direction with simultaneous vertical excitation. The response of the model, primarily the global relative displacements, was measured by means of LVDTs and recorded in digitized form by the data acquisition system. The response of the model was also recorded by a high speed movie camera.

In all cases of high intensity excitation, severe damage occurred to the bridge deck at the zone of the expansion joints. The inclusion of ductile steel ties across the joints to prevent excessive separation of the girders and subsequent collapse of the structure did not prevent damage to the expansion joint region. The damage generally considered consisted of failure of the shear key and severe shear cracking across the hinge seat. Furthermore, the joint restrainers were subjected to large ductility demands. In the case of longitudinal excitation, spalling of the adjacent joint faces also occurred. It was caused by the large shear and impacting forces at the joints during the dynamic response of the structure and served to emphasize the undesirability of such discontinuities in this type of structure. For these particular test structures the column damage was insignificant.

The objective of these tests was to indicate trends of behavior, and also to provide test data on which to check the validity of computer analyses developed in Phase 2 of the project. The experimental studies clearly demonstrated the complexity of the 3-dimensional nonlinear response of curved bridges to earthquakes, some of the problems associated with the mathematical modelling of the phenomena, and the need for a more careful spatial arrangement and detailing of expansion joints in bridges when conditions necessitate their use.

4. Correlation of Experimental and Analytical Response

a) Formulation of Analytical Model

The experimental bridge model was idealized by a discrete parameter system consisting of 55 nodal points, 24 three-dimensional curved beam elements representing the superstructure, 24 straight beam elements representing the columns, 2 expansion joint elements, and 2 boundary elements representing the abutments. The stiffness properties of the superstructure, columns, and abutments were determined either from the results of static

load-deformation tests or by calculation using section and material properties. Since the expansion joints have many constraints as provided by shear stiffness of support pads, friction at support interfaces, transverse shear key, etc., their overall constraint to the girder is difficult to define accurately. Therefore, it was decided to determine this constraint so that the dynamic properties of the analytical model would match those of the experiment model. As a first requirement the natural frequencies of the analytical model should match the frequencies of the experimental model derived from low-amplitude free vibration and forced harmonic tests. The constraint of the expansion joints was modelled by a set of elastic springs which resist relative translational and rotational motions between adjacent girders. The stiffnesses of these springs were adjusted so that the calculated natural frequencies of the analytical model matched the measured natural frequencies of the experimental model. These frequencies were approximately 5.0, 6.6, and 9.5 H_z for the longitudinal, transverse, and vertical normal modes, respectively. This procedure established the basic linear analytical model which matched the low-amplitude vibration characteristics of the experimental model.

b) Experimental Tests Chosen for Correlation Purposes

Six basic tests were carried out in the experimental investigation, i.e., Phase 4 of the overall research program. Three of these designated as H1, H3, and HV2 were selected for correlation purposes. The primary features of these tests are shown in Table 1. Tests H1 was carried out using only horizontal excitation in the transverse direction of low intensity (peak acceleration - 0.11g). During this test the expansion joint tie bars remained elastic, no collisions occurred in the expansion joints, and no failures occurred to the shear keys. Test H3 used high intensity (peak acceleration = 0.50 g) excitation in the horizontal transverse direction. In this test, yielding of tie bars occurred, multiple collisions took place in the expansion joints, and failure of a shear key resulted. Tests HV2 was carried out using both horizontal transverse and vertical excitations having peak accelerations equal to 0.47 g and 0.27 g, respectively. In this test yielding of tie bars occurred and multiple collisions took place in the expansion joints. No failure of shear key occurred in this test.

c) Correlation of Experimental Results with Linear Analytical Model

The linear analytical model described above was used in the correlation of experimental results obtained in Test H1. A damping ratio of 6% of critical was used for the analytical model which agreed with the measured damping ratio of the experimental model. Upon comparing time histories of displacement of the analytical model with experimental results, it was found that the overall stiffness of the analytical model was greater than that of the experimental model. Further adjustments of stiffnesses in the expansion joints were then made to minimize the observed phase lag discrepancies in response. The analytical time histories of displacement now agreed quite well with the experimental results except that the calculated responses showed symmetric motions relative to the outward and inward directions while the measured responses were somewhat unsymmetrical due to the fact that the tie bars resist outward motion but not inward motion.

The linear analytical model was also used in the correlation Studies of tests H3 and HV2. However, due to the presence of multiple collisions and yielding of tie bars, very poor correlation of analytical and experimental responses were obtained. Obviously, linear analytical modelling is unacceptable for cases of high intensity excitation which produces significant nonlinearities to develop in the structural system.

d) Correlations of Experimental Data With Nonlinear Analytical Model

Based on the experience derived from the linear correlation studies, it was apparent that linear modelling of expansion joint behavior was inadequate for cases of high intensity excitation. The linear expansion joint element was then replaced by a nonlinear element which hopefully would properly model the yielding of tension tie bars and the collision phenomenon. Coulomb friction was also introduced into the analytical model to present the sliding forces at the support interfaces. Correlation of the nonlinear analytical responses now showed good agreement with the experimental nonlinear responses measured in tests H3 and HV2, except for the later part measured in test H3. In this case, failure occurred to a shear key midway in the test which allowed a drift of the displacement response which was not predictable by the analytical model.

5. Concluding Statement

Based on the excellent correlations finally achieved in Phase 5 of the overall investigation between analytical and experimental results, it is concluded that accurate data was obtained in Phase 4 and that the analytical procedures develop in Phase 2, which were modified and improved in Phase 5, predict realistically the nonlinear response of bridge systems under high intensity seismic excitation.

Acknowledgement

The investigation summarized in this paper was sponsored by the U.S. Department of Transportation, Federal Highway Administration, under contract No. DOT-FH-7798.

Disclaimer

The contents of this paper reflect the views of the authors but do not necessarily reflect the official views of the U.S. Department of Transportation.

References

1. Iwasaki, T., Penzien, J., Clough, R., "Literature Survey - Seismic Effects on Highway Bridges," EERC Report No. 71-11, Earthquake Engineering Research Center, University of California, Berkeley, November, 1972.

2. Iwasaki, T., Penzien, J., Clough, R., "An Investigation of the Effectiveness of Existing Bridge Design Methodology in Providing Adequate Structural Resistance to Seismic Disturbance, Phase I: Literature Survey," FHWA-RD-73-13, Federal Highway Administration, November, 1972.

3. Penzien, J., "Seismic Effects on Bridges, San Fernando Earthquake, 9, February 1971," III Congreso Nacional de Ingenieria Sismica, Acapulco, Gro. Mexico, November, 1971.

4. Jennings, P.C., "Engineering Features of the San Fernando Earthquake, February 9, 1971," EERL 71-20, Earthquake Engineering Research Laboratory, California Institute of Technology, June, 1971.

5. "Bridge Planning and Design Manual," California State Division of Highways," Vol. 1 - Design Specifications, March, 1968.

6. Elliot, A.L., "The San Fernando Earthquake: A Lesson in Highway and Bridge Design," Civil Engineering, ASCE, Special Issue, September, 1972.

7. Tseng, W.S. and Penzien, J., "Analytical Investigations of the Seismic Response of Long, Multiple-Span Highway Bridges," Report No. EERC 73-12, Earthquake Engineering Research Center, University of California, Berkeley, June, 1973.

8. Chen, M.C., and Penzien, J., "Analytical Investigations of Seismic Response of Short, Single or Multiple-Span Highway Bridges," Report No. EERC 75-4, January, 1975.

9. Tseng, W.S., and Penzien, Jr., "Seismic Analysis of Long Multiple-Span Highway Bridges," International Journal of Earthquake Engineering and Structural Dynamics, Vol. 4, 1975.

10. Tseng, W.S. and Penzien, J., "Seismic Response of Long Multiple-Span Highway Bridges," International Journal of Earthquake Engineering and Structural Dynamics, Vol. 4, 1975.

11. Williams, D., and Godden, W.G., "Seismic Behavior of High Curved Over-crossings," Proceedings U.S. National Conference on Earthquake Engineering, Ann Arbor, Michigan, EERI, June, 1975.

12. Williams, D., and Godden, W.G., "Multidirectional Seismic Response of a Curved Highway Bridge Model," Bulletin of the New Zealand National Society for Earthquake Engineering, Vol. 8, No. 3, September, 1975.

13. Williams, D. and Godden, W.G., "Seismic Response of Bridge Model," Transportation Research Board Record, National Research Council. (Accepted for publication.)

TABLE - 1 FEATURES OF SEISMIC EXCITATION TESTS

EXCITATION TEST NO.	PEAK TABLE ACCELERATION [G]		OBSERVED FEATURES IN EXCITATION		
	HORIZONTAL	VERTICAL	YIELDING OF TIE BARS	COLLISIONS OF GIRDERS	FAILURE OF SHEAR KEY
H1	0.11	---	NO	NO	NO
H3	0.50	---	YES	YES	YES
HV2	0.47	0.27	YES	YES	NO

AN EVALUATION METHOD FOR THE EARTHQUAKE RESISTANT CAPACITY OF REINFORCED CONCRETE AND STEEL REINFORCED CONCRETE COLUMNS

MASAKAZU OZAKI
Head, Structure Division
Building Research Institute, Japan

YUJI ISHIYAMA
Chief Research Engineer, Structure Division
Building Research Institute, Japan

ABSTRACT

An evaluation method for the earthquake resistant capacity of reinforced concrete and steel reinforced concrete columns by utilizing the force deflection relationship of column specimens subjected to axial force and repeated and reversed lateral loading of considerable intensity is proposed.

An approximate response analysis for a non-linear structural system was developed based on random vibration theory and was applied to models represented by a single-degree-of-freedom system subjected to a constant white noise acceleration. The mean expected maximum response values of the models with two different natural periods 0.1 and 0.5 sec. were calculated. Each model has a degrading stiffness system and various hysteretic envelope slopes after four different yield point levels. The viscous damping ratio is considered to be 5% of the critical damping for the entire processes of the models, and the hysteretic damping ratio after yielding is assumed to increase according to the increase of ductility factor. The ductility factors of the models calculated by the non-linear response analysis are shown in tables and figures.

The maximum strength of the linear model having the equivalent earthquake resistant capacity of a column specimen can be assumed if the yield point, hysteretic envelope slope tangent, coefficient of hysteretic damping ratio and ductiltiy factor of the specimen are measured by testing.

A facility was designed for testing large models of reinforced concrete and steel reinforced concrete columns under action simulating gravity load and ground motion in order to standardize the testing techniques and to forestall possible errors that may be induced by the use of different types of testing facilities.

An example of evaluation for the earthquake resistant capacity of a reinforced concrete column is presented by utilizing the force deflection relationship of the specimen obtained by the testing facility.

It is confirmed that yield point level, hysteric envelope slope, hysteretic damping ratio and ductility factor are the most important components of earthquake resistant capacity.

Keywords: Columns; Earthquake; Concrete; Hysteretic Envelope; Reinforced; Strength.

1. Introduction

A number of modern reinforced concrete buildings have had severe damage during recent strong earthquakes. Some reinforced concrete buildings have suffered damage in the columns, due to the shearing instituted by the earthquakes, resulting in collapse of entire buildings.

Large scale model tests of reinforced concrete and steel reinforced concrete column specimens, have been conducted in order to investigate the earthquake resistant capacity of such columns. Force deflection relationships were obtained from these test results and were reported in various technical papers.

There is, however, no reasonable evaluation method for testing of column specimens with ductility after yielding.

This paper deals with a method for determining the earthquake resistant capacity of reinforced concrete and steel reinforced concrete columns with ductility after yielding. The method utilizes the force deflection relationship of column specimens subjected to axial force and repeated and reversed lateral loading of considerable intensity.

It is considered that the same method is applicable to the evaluation for the earthquake resistant capacity of girders, joints of girders and columns shearing walls and any building structures constructed of reinforced concrete and steel reinforced concrete.

2. Assumptions

a) Stationary acceleration spectrum of duration 30 sec. without any predominant frequency (white noise) was utilized to represent strong motion earthquake excitation.

One of the most significant contributions to the field of earthquake engineering was the introduction of the idea of the earthquake response spectrum which was first introduced by M.A. Biot, E.C. Robinson, G. Housner and others. Using the eight components of the four strongest ground motions recorded to date, Housner normalized each accelerogram to a common intensity level and by averaging the velocity spectra resulting therefrom obtained what is now commonly known as Housner's standard velocity spectra. Even though the number of samples may be small in this case, Housner's standard velocity spectra give the mean value of maximum (or peak) response due to earthquakes of an intensity level which is generally considered a good measure of the expected damage to structures having fundamental period in the range $0.1 \leq Tn \leq 2.5$ sec.

Using an analog computer, Bycroft studied the possibility of using a white noise acceleration process to represent earthquake ground motion of a given intensity level. Bycroft's results would seem to indicate that white noise is a reasonable simulation of earthquake excitation.

A more accurate method of predicting the maximum or peak response when concerned with long period and low damping ratio and when assuming a white noise acceleration process of finite duration is the method presented by Rosenblueth and Bustamante. The results were compared with Housner's standard velocity spectra and quite good agreement between them over the entire ranges of damping and period was reported in Reference (5). Therefore,

a stationary acceleration represented by a white noise was utilized for this evaluation.

b) Non-linear structural models with a degrading stiffness system represented by a single-degree-of-freedom system were used as shown in Fig. 1. A non-linear dynamic response analysis for the models subjected to a stationary white noise acceleration was carried out by utilizing the force deflection curves obtained by large model tests of column specimens. An idealized force deflection curve with a degrading stiffness system is shown in Fig. 2.

In general, reinforced concrete and steel reinforced concrete column specimens show a tendency that the maximum strengths at each step of deflection after yielding reduced due to repeated and reversed loading. An envelope line which plots the reduced maximum strength corresponding to each step of deflection can be approximated by a straight line, as shown in Fig. 2. The slope of the straight line is defined as the hysteretic envelope slope, and the ratio of the hysteretic envelope slope tangent to the initial stiffness slope tangent is named the slope tangent ratio of ductility.

The damping factor induced by viscous damping (viscous damping ratio ζv) is considered to be 0.05 of the critical damping for the entire processes of the models. The damping factor induced by hysteretic damping (hysteretic damping ratio ζH) can be calculated by measuring the areas of hysteretic loops corresponding to each step of deflection of specimens. For example, the hysteretic damping ratio at the deflection ${}_2\delta y$ is simply obtained, if the hysteretic loops are symmetrical with respect to the original point, as follows;

$$\zeta_{H(\delta={}_2\delta_y)} = \frac{1}{\pi} \frac{\text{Area } 2.3.5}{\text{Area } 2.\textcircled{2}5 + \text{Area } 2.\textcircled{2}3} \qquad (1)$$

where δy is the deflection at the yielding point of specimens.

In the case of reinforced concrete and steel reinforced concrete specimen tests, the hysteretic damping ratio ζH can be assumed to increase proportionally to the increase of $\sqrt{(\delta-\delta y)/\delta y}$ after yielding. Therefore, the hysteretic damping ratio at the deflection δ is approximated by

$$\zeta_H = {}_c\zeta_H \sqrt{\frac{\delta - \delta y}{\delta y}} \qquad (\delta \geq \delta y) \qquad (2)$$

where $c\zeta H$ is defined as the coefficient of hysteretic damping ratio.

By using the method of least squares, the coefficient of hysteretic damping ratio can be obtained from the hysteretic damping ratios ζHn at the deflections $\delta n (n=1,2,....n)$ as

$${}_c\zeta_H = \sqrt{\delta y} \frac{\sum_1^n \zeta_{Hn}}{\sum_1^n \sqrt{(\delta n - \delta y)}} \qquad (3)$$

In calculation, the hysteretic damping with a loop was transformed to the equivalent viscous damping for a linear system. Therefore, the equivalent viscous damping ratio ζ was obtained by adding the viscous damping ratio ζV to the hysteretic damping ratio ζH.

3. Numerical Calculation

The mean expected maximum response values of the structural models having a degrading stiffness system shown in Fig. 2 were calculated by a non-linear response analysis when they were subjected to a stationary white noise acceleration.

The models with natural period Tm 6.1 sec. (m = 1.0 ton sec ^{2}/cm, K = 4 942.0 ton/cm) were divided into four types according to the four different yield point levels, where the yield point levels of Model 1, 2, 3, and 4 are 1/2, 1/3, 1/4 and 1/5 of the mean expected maximum response values in a linear system respectively. Where the mean expected maximum response value in a linear system is defined as the mean of the maximum response values, the structural model has a linear system without the yield point. In other words, the mean maximum response value in the degrading stiffness system can be replaced by the strength of the linear model with the equivalent earthquake resistant capacity.

In each model, the slope tangent ratio of ductility varies as 0.8, 0.6, 0.4, 0.2, 0.1, 0.0, ...-0.1 after yielding. The ductility factors of the models were calculated by a non-linear response analysis when the coefficient ζH of hysteretic damping ratio varies from 0.03 to 0.12.

For example, if the maximum response value of a column having a linear system is three times the yield point level of the column having a non-linear system, the ductility indicated in Fig. 3b will be required to prevent the complete collapse from the structure, when the structure is subjected to a strong earthquake. In other words, if the yield point, hysteretic envelope slope tangent, coefficient of hysteretic damping ratio and ductility factor of a column are measured by testing, the maximum strength of the linear model having the equivalent earthquake resistant capacity of the column can be presumed.

Table 3 and 4 show the increment ratio of the equivalent maximum strength of linear models to the yield point levels of column specimens due to the increase of the earthquake resistant capacity by ductility for the cases of Type 1 and Type 2. Therefore, a new allowable strength level of columns can be defined by taking the collapse of structures into consideration.

The models with natural period Tr = 0.5 sec. were also calculated in the same manner. There is however, little difference between the models with the different natural periods for the calculated response values.

In this calculation, an approximate non-linear response analysis was developed based on random vibration theory and was applied to models with a single-degree-of-freedom system subjected to a constant white noise acceleration. The non-linear response analysis based on random vibration theory is introduced in Reference (4) and examined by the method of simulation in Appendix I.

4. Testing Facility

A facility was designed for testing large models of reinforced concrete and steel reinforced concrete columns under action simulating gravity load and ground motion in order to standardize the testing techniques and to forestall possible errors that may be induced by the use of different types of testing facilities. The elevation of this facility is shown in Fig. 5. Main features of this facility are as follows;

a) Models of columns with sectional area of 25 cm x 25 cm for reinforced concrete and 30 cm x 30 cm for steel reinforced concrete and length varying from 50 cm up to 150 cm can be tested.

b) Models of columns can be subjected to axial force and repeated and reversed lateral loading of considerable intensity.

c) Models can be subjected to very large lateral deformations by the repeated and reversed lateral loading.

d) In case the top of a specimen of the models is considerably displaced in lateral direction, the specimen is subjected to bending moment and shearing force induced by the eccentric gravity in addition to the bending moment and sheering force by the repeated lateral load acting at the top of the specimen. In other words, P - δ effects are considered.

e) The facility is safe even in the case of sudden and brittle failure of the specimens.

f) Stresses and deformations induced in the specimens under test can be easily measured and progressive pattern of damages and mechanism of failure up to collapse can be visually observed.

g) The setting or removal of the specimens can be accomplished easily.

5. Examples

The earthquake resistant capacity of a reinforced concrete column specimen is evaluated by utilizing the force deflection relationship obtained by the testing facility shown in Fig. 5. The dimensions and bar arrangement of the specimen are indicated in Table 5 and Fig. 6. The force deflection curve of the specimen is shown in Fig. 7.

Section	B x D = 25 cm x 25 cm
Length	L = 50 cm
Axial force ratio	N/BD = 26.25 kg/cm^2
shear span ratio	M/QD = 1.5
Strength of concrete	Fc = 245 kg/cm^2
Main reinforcing bars	6 - D 13 (SD30)
Hoops	9 ϕ - @ 45.5 (SR24)
Tensile bar ratio	Pt = 0.61%
Web reinforcement ratio	Pw = 1.12%

This specimen showed a shear-type collapse at the lateral deflection of 4.0 cm. The yield strength of 18.5 ton and the corresponding yield displacement of 0.2 cm were observed. The hysteretic envelope slope defined in Section 2 was determined by a straight line as shown in Fig. 7.

Measuring the hesteretic damping ratios at the displacements δ = 0.5, 1.0, 1.5 and 2.0 cm, the coefficient of the hysteretic damping ratio can be calculated by the method of least squares given in Eq. (3).

The four important components of earthquake resistant capacity were obtained as follows:

1.	Yield point level	19.25 ton
2.	Slope tangent ratio of ductility	-0.054
3.	Coefficient of hysteretic damping ratio	0.073
4.	Ductility factor at collapse	20.0

The specimen with the above values of ductility satisfies the ductility requirement shown in Fig. 3b. The maximum strength of a linear model having the equivalent earthquake resistant capacity of this specimen is presumed to be about 57.75 ton by multiplying the yield strength times the increment ratio of maximum strength by ductility shown in Table 3.

Let us consider a particular problem of an irregular frame model shown in Fig. 8a. This model has two columns with different length. In order to evaluate the earthquake resistant capacity of this model, each column cannot be discussed separately, because the whole structure will be destroyed if one of the columns collapses. Therefore, the superposed force deflection curve must be taken into consideration, as shown in Fig. 8b.

It should be noted that the smaller deflection capacity of the shorter column gives the deflection capacity of the whole structure in the case of this irregular frame model.

6. Conclusions

It is confirmed that yield point level, hysteretic envelope slope, hysteretic damping ratio and ductility factor are the most important components of earthquake resistant capacity, when reinforced concrete and steel reinforced concrete columns are subjected to a white noise ground motion.

In order to maintain desirable hysteretic envelope slope after yielding, it will be recommended to avoid the shear-type failure of columns. It is also important to use sufficient ductile materials such as steel and reinforcing bars in columns to increase hysteretic damping ratio and ductility factor of columns. When a column without sufficient ductility is used, the allowable strength level should be estimated lower than the conventional one in the case of strong earthquakes.

It will be reasonable to use this evaluation method for the earthquake resistant capacity of reinforced concrete and steel reinforced concrete columns, if it is difficult to determine a specific strong earthquake input for designing a building structure.

Acknowledgments

The authors are deeply indebted to Dr. Minouru Wakabayashi, Professor of Kyoto University for his valuable suggestion for designing the testing facility.

References

1. Tajimi, H., Introduction to Structural Dynamics, Corona-sha, Tokyo, Japan, 1964.

2. Ozaki, M. and Others , Earthquake Response Prediction and Failure of Reinforced Concrete Buildings due to Repeated Shearing Forces, Part I. Theoretical Analysis of Earthquake Response Prediction, Research Paper of the Building Research Institute, No. 40, 1969, Japan.

3. Ozaki, M. and Yamazaki, Y., Dynamic Response Prediction of Buildings subjected to Earthquakes, Part II. Numerical Analysis, Research Paper of the Building Research Institute, No. 42, 1970, Japan.

4. Ozaki, M. and Ishiyama, Y., Earthquake Response Prediction of Reinforced Concrete Buildings, The 5th World Conference on Earthquake Engineering, 1973.

5. Penzien, J., Application of Random Vibration Theory in Earthquake Engineering, Bulletin of the International Institute of Seismology and Earthquake Engineering, Vol. 2, 1965.

6. Bycroft, C.N., White Noise Representation of Earthquakes, Proceedings of the American Society of Civil Engineers, Vol. 86, No EM4, April, 1960.

7. Housner, G.W., Behavior of Structures during Earthquakes, Proceedings of the American Society of Civil Engineers, Vol. 85, No. EM4, October, 1959.

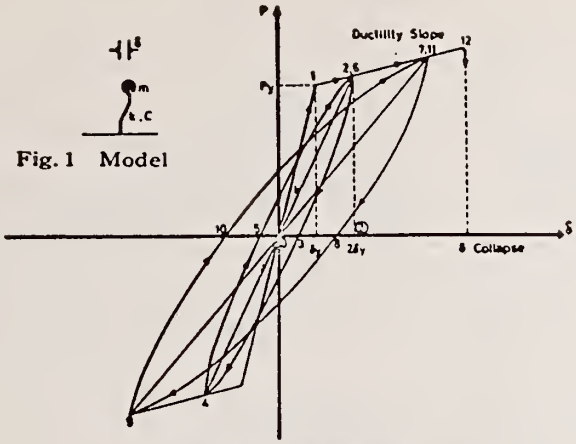

Fig. 1 Model

Fig. 2 Hysteretic Curve

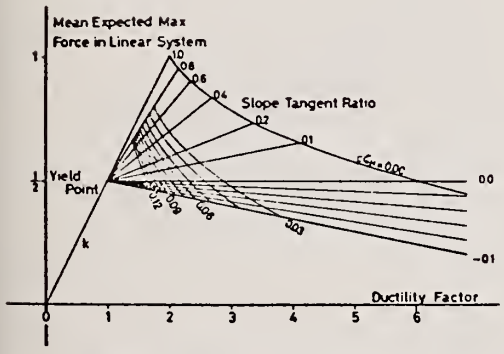

Fig. 3a Ductility Requirement (Model 1)

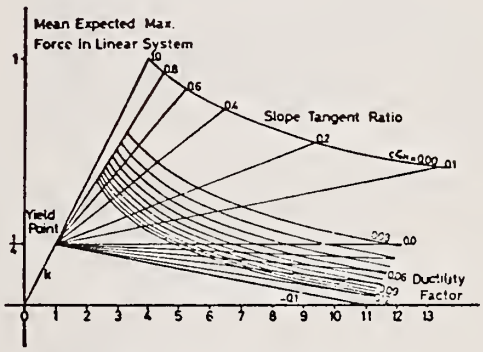

Fig. 3c Ductility Requirements (Model 3)

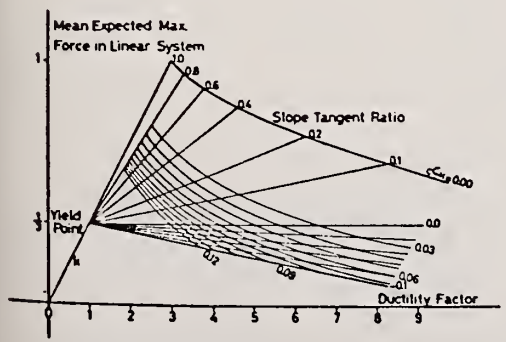

Fig. 3b Ductility Requirement (Model 2)

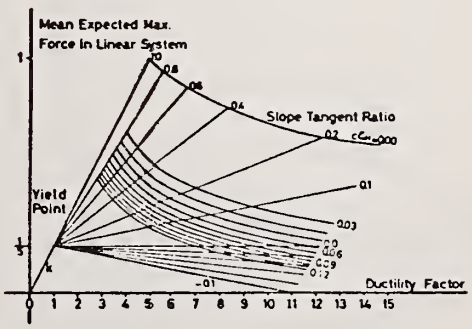

Fig. 3d Ductility Requirements (Model 4)

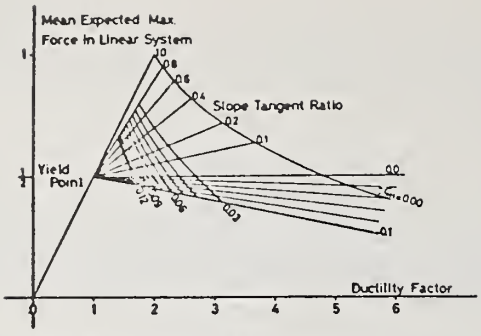

Fig. 4a Ductility Requirements
(Model 1 of Type 2) Tn=0.5sec

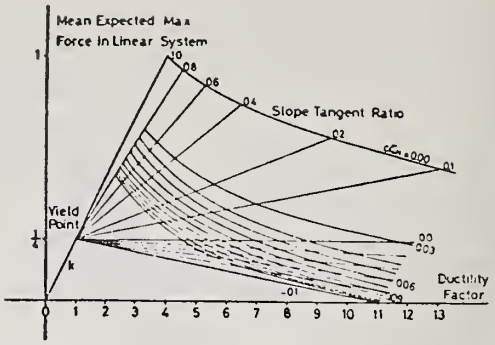

Fig. 4c Ductility Requirements
(Model 3 of Type 2) Tn=0.5sec

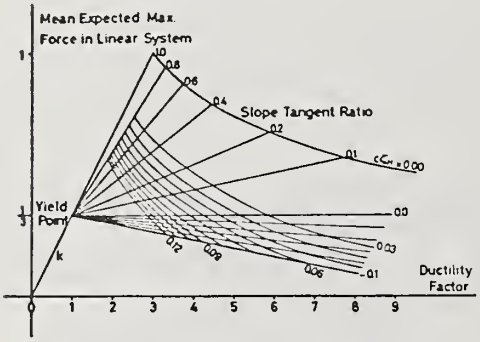

Fig. 4b Ductility Requirements
(Model 2 of Type 2) Tn=0.5sec

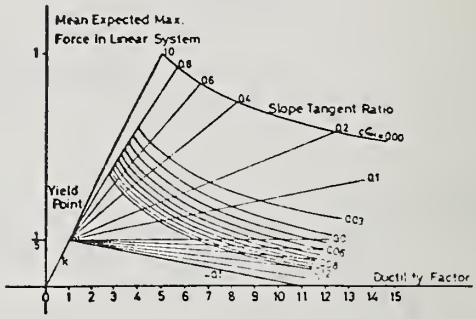

Fig. 4d Ductility Requirements
(Model 4 of Type 2) Tn=0.5sec

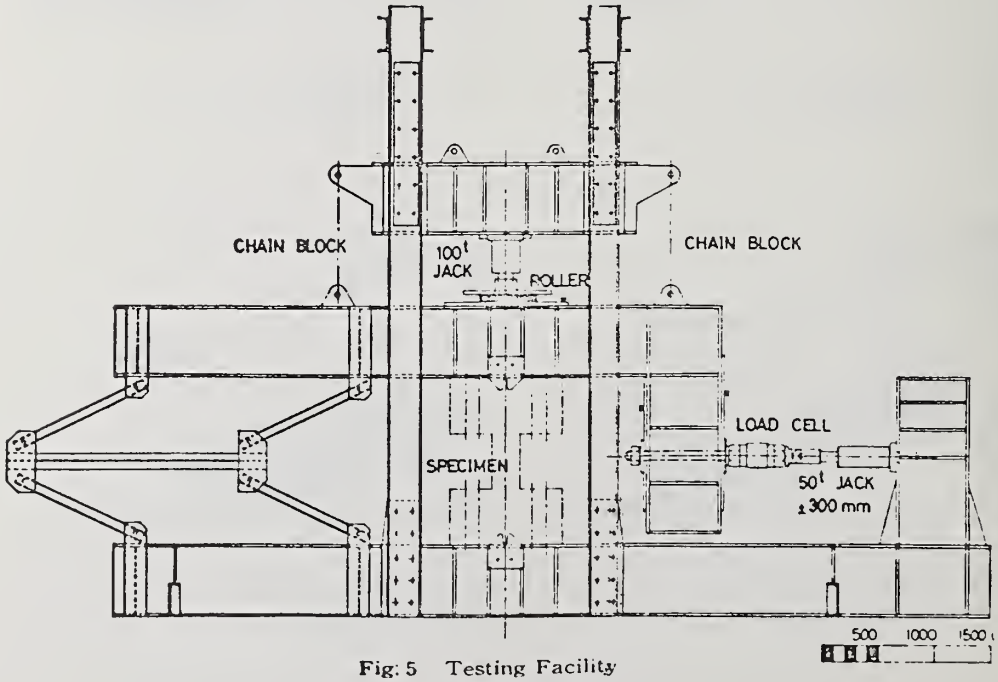

Fig. 5 Testing Facility

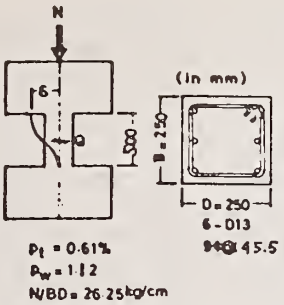

Fig. 6 Specimen

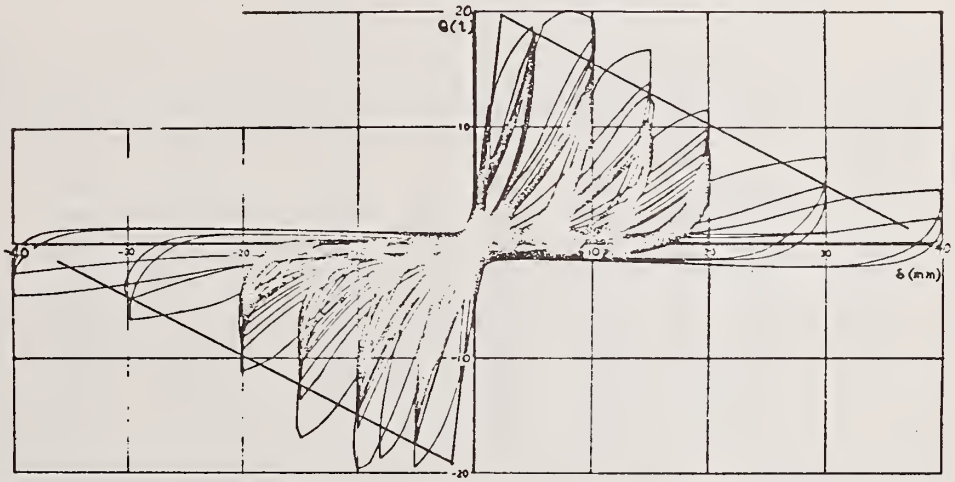

Fig. 7 Force-Deflection Relationship of Specimen

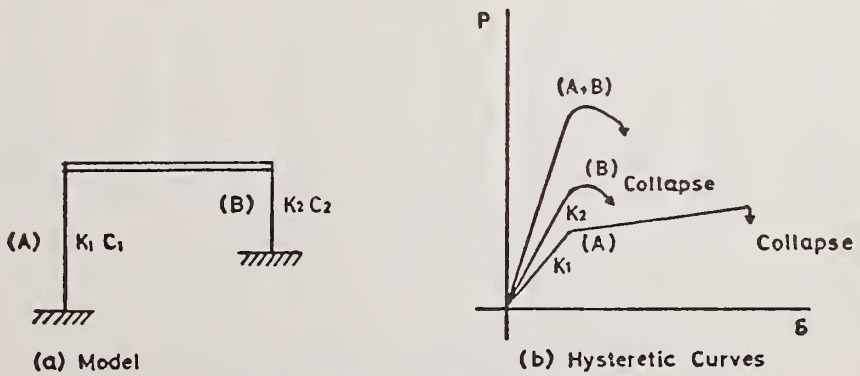

Fig. 8 Irregular Frame

Slope Tangent Ratio	Coefficient of Hysteretic Damping Ratio c_{eh}									
	0.00	0.03	0.04	0.05	0.06	0.07	0.08	0.09	0.10	0.11	0.12
1.0	2.00										
0.8	2.14	1.76	1.68	1.62	1.58	1.54	1.50	1.47	1.44	1.42	1.40
0.6	2.35	1.86	1.77	1.70	1.64	1.59	1.55	1.51	1.48	1.45	1.43
0.4	2.69	2.01	1.90	1.81	1.73	1.67	1.62	1.58	1.54	1.50	1.4
0.2	3.34	2.26	2.10	1.97	1.87	1.79	1.72	1.67	1.62	1.57	1.54
0.1	4.04	2.47	2.26	2.10	1.98	1.88	1.80	1.73	1.67	1.62	1.58
0.00	6.02	2.84	2.53	2.30	2.14	2.00	1.90	1.82	1.74	1.68	1.63
- 0.02	7.12	2.95	2.60	2.36	2.18	2.04	1.93	1.84	1.76	1.70	1.65
- 0.04	9.92	3.08	2.69	2.42	2.22	2.08	1.95	1.86	1.78	1.71	1.66
- 0.06		3.26	2.80	2.50	2.27	2.12	1.98	1.89	1.80	1.73	1.67
- 0.08		3.49	2.93	2.58	2.34	2.16	2.02	1.91	1.83	1.75	1.69
- 0.10		3.82	3.09	2.68	2.41	2.21	2.00	1.94	1.85	1.77	1.71

Table 1a Ductility Requirement for Model 1 of Type 1
(T_n = 0.1 sec., P_y = 1/2 P_{max}.)

Slope Tangent Ratio	Coefficient of Hysteretic Damping Ratio c_{eh}									
	0.00	0.03	0.04	0.05	0.06	0.07	0.08	0.09	0.10	0.11	0.12
1.0	3.00										
0.8	3.31	2.53	2.39	2.28	2.19	2.12	2.05	1.99	1.94	1.90	1.86
0.6	3.78	2.77	2.60	2.47	2.36	2.27	2.19	2.13	2.07	2.01	1.96
0.4	4.55	3.15	2.93	2.76	2.62	2.50	2.40	2.32	2.24	2.17	2.11
0.2	6.27	3.87	3.54	3.28	3.07	2.90	2.76	2.64	2.53	2.44	2.36
0.1	8.50	4.61	4.14	3.78	3.50	3.27	3.08	2.92	2.78	2.66	2.56
0.0	21.10	6.55	5.55	4.88	4.46	3.99	3.68	3.43	3.23	3.05	2.83
- 0.02		7.54	6.20	5.32	4.71	4.24	3.89	3.59	3.36	3.17	3.0
- 0.04		9.74	7.31	6.02	5.17	4.60	4.15	3.81	3.53	3.31	3.1
- 0.06			10.97	7.44	5.99	5.11	4.54	4.09	3.76	3.48	3.27
- 0.08					8.28	6.15	5.14	4.54	4.07	3.74	3.45
- 0.10							6.92	5.36	4.60	4.08	3.74

Table 1b Ductility Requirement for Model 2 of Type 1
(T_n = 0.1 sec., P_y = 1/3 P_{max}.)

Slope Tangent Ratio	Coefficient of Hysteretic Damping Ratio c_{eh}									
	0.00	0.03	0.04	0.05	0.06	0.07	0.08	0.09	0.10	0.11	0.12
1.0	4.00										
0.8	4.48	3.27	3.07	2.92	2.79	2.68	2.59	2.51	2.44	2.38	2.32
0.6	5.21	3.65	3.41	3.22	3.07	2.94	2.83	2.73	2.65	2.57	2.50
0.4	6.45	4.27	3.95	3.70	3.50	3.33	3.19	3.07	2.96	2.86	2.78
0.2	9.31	5.50	5.00	4.62	4.32	4.07	3.86	3.68	3.52	3.38	3.26
0.1	13.30	6.90	6.17	5.61	5.18	4.82	4.53	4.28	4.07	3.88	3.72
0.00	50.70	11.82	9.83	8.45	7.50	6.75	6.15	5.68	5.29	4.96	4.66
- 0.02		16.74	12.65	10.31	8.82	7.72	6.94	6.31	5.79	5.39	5.05
- 0.04				20.36	12.38	9.82	8.41	7.36	6.65	6.05	5.58
- 0.06								10.89	8.58	7.36	6.56
- 0.08											11.82
- 0.10											

Table 1c Ductility Requirement for Model 3 of Type 1
(T_n = 0.1 sec., P_y = 1/4 P_{max}.)

Slope Tangent Ratio	Coefficient of Hysteretic Damping Ratio c_{eh}										
	0.00	0.03	0.04	0.05	0.06	0.07	0.08	0.09	0.10	0.11	0.12
1.0	5.00										
0.8	5.65	3.99	3.74	3.54	3.37	3.23	3.12	3.02	2.93	2.85	2.77
0.6	6.64	4.51	4.20	3.95	3.75	3.59	3.44	3.32	3.21	3.12	3.03
0.4	8.35	5.35	4.94	4.62	4.36	4.14	3.96	3.80	3.66	3.54	3.43
0.2	12.38	7.11	6.45	5.96	5.56	5.23	4.96	4.72	4.52	4.43	4.18
0.1	18.19	9.21	8.23	7.49	6.90	6.43	6.04	5.71	5.42	5.17	4.94
0.0	97.80	18.56	15.23	12.98	11.41	10.22	9.27	8.49	7.87	7.35	6.90
-0.02			27.64	19.47	15.54	13.20	11.50	10.27	9.32	8.54	7.88
-0.04								18.33	13.54	11.52	10.03
-0.06											
-0.08											
-0.10											

Table 1d Ductility Requirement for Model 4 of Type 1
(Tn = 0.1sec., Py = 1/5 Pmax.)

Slope Tangent Ratio	Coefficient of Hysteretic Damping Ratio c_{eh}										
	0.00	0.03	0.04	0.05	0.06	0.07	0.08	0.09	0.10	0.11	0.12
1.0	2.00										
0.8	2.13	1.77	1.70	1.64	1.60	1.56	1.52	1.49	1.47	1.45	1.43
0.6	2.31	1.86	1.78	1.71	1.66	1.62	1.58	1.54	1.51	1.48	1.46
0.4	2.60	2.00	1.89	1.81	1.74	1.69	1.64	1.60	1.56	1.53	1.51
0.2	3.11	2.21	2.07	1.95	1.87	1.79	1.73	1.68	1.64	1.60	1.57
0.1	3.63	2.37	2.20	2.06	1.95	1.87	1.80	1.74	1.69	1.64	1.60
0.0	4.72	2.64	2.39	2.22	2.08	1.97	1.88	1.81	1.75	1.70	1.65
-0.02	5.15	2.71	2.44	2.26	2.11	1.99	1.90	1.83	1.76	1.71	1.66
-0.04	5.76	2.80	2.50	2.30	2.15	2.02	1.92	1.85	1.78	1.72	1.68
-0.06	6.73	2.89	2.57	2.35	2.18	2.05	1.95	1.87	1.80	1.74	1.69
-0.08	10.23	3.01	2.65	2.39	2.23	2.09	1.97	1.89	1.82	1.75	1.70
-0.10		3.14	2.75	2.46	2.27	2.12	2.00	1.91	1.84	1.77	1.71

Table 2a Ductility Requirement for Model 1 of Type 2
(Tn = 0.5sec., Py = 1/2 Pmax.)

Slope Tangent Ratio	Coefficient of Hysteretic Damping Ratio c_{eh}										
	0.00	0.03	0.04	0.05	0.06	0.07	0.08	0.09	0.10	0.11	0.12
1.0	3.00										
0.8	3.30	2.54	2.41	2.31	2.22	2.14	2.08	2.03	1.98	1.94	1.89
0.6	3.72	2.77	2.61	2.48	2.38	2.29	2.21	2.15	2.09	2.04	2.00
0.4	4.43	3.12	2.91	2.75	2.62	2.51	2.41	2.33	2.26	2.19	2.14
0.2	5.92	3.76	3.45	3.21	3.02	2.87	2.73	2.62	2.52	2.44	2.36
0.1	7.69	4.38	3.96	3.64	3.38	3.17	3.01	2.86	2.74	2.63	2.54
0.0	14.53	5.77	4.99	4.45	4.05	3.74	3.48	3.26	3.09	2.95	2.82
-0.02	23.51	6.34	5.40	4.73	4.27	3.92	3.63	3.38	3.19	3.04	2.90
-0.04		7.19	5.96	5.13	4.54	4.13	3.81	3.54	3.31	3.14	2.99
-0.06		9.15	6.85	5.72	4.95	4.42	4.03	3.72	3.46	3.26	3.09
-0.08			9.44	6.72	5.59	4.83	4.33	3.96	3.66	3.40	3.22
-0.10					6.85	5.58	4.76	4.28	3.92	3.61	3.37

Table 2b Ductility Requirement for Model 2 of Type 2
(Tn = 0.5sec., Py = 1/3 Pmax.)

Slope Tangent Ratio	Coefficient of Hysteretic Damping Ratio c_{eh}										
	0.00	0.03	0.04	0.05	0.06	0.07	0.08	0.09	0.10	0.11	0.12
1.0	4.00										
0.8	4.46	3.29	3.09	2.95	2.82	2.72	2.63	2.55	2.48	2.43	2.37
0.6	5.14	3.65	3.42	3.23	3.09	2.96	2.85	2.76	2.68	2.61	2.5
0.4	6.29	4.23	3.92	3.68	3.49	3.33	3.19	3.08	2.97	2.88	2.8
0.2	8.84	5.35	4.88	4.53	4.24	4.00	3.81	3.64	3.49	3.36	3.25
0.1	12.13	6.55	5.89	5.38	4.98	4.66	4.38	4.16	3.97	3.80	3.65
0.0	32.08	10.10	8.58	7.50	6.71	6.13	5.66	5.26	4.93	4.64	4.41
-0.02		12.34	10.06	8.58	7.51	6.73	6.15	5.68	5.29	4.96	4.67
-0.04			13.51	10.65	8.94	7.75	6.88	6.28	5.79	5.38	5.03
-0.06					13.34	10.10	8.42	7.29	6.56	6.01	5.56
-0.08								11.03	8.44	7.12	6.43
-0.10											

Table 2c Ductility Requirement for Model 3 of Type 2
(Tn = 0.5sec., Py = 1/4 Pmax.)

Slope Tangent Ratio	Coefficient of Hysteretic Damping Ratio c_{eh}										
	0.00	0.03	0.04	0.05	0.06	0.07	0.08	0.09	0.10	0.11	0.12
1.0	5.00										
0.8	5.63	4.01	3.76	3.57	3.41	3.27	3.16	3.06	2.97	2.90	2.83
0.6	6.56	4.51	4.20	3.96	3.77	3.61	3.47	3.35	3.25	3.16	3.08
0.4	8.16	5.31	4.91	4.50	4.34	4.14	3.96	3.81	3.68	3.56	3.46
0.2	11.80	6.92	6.30	5.83	5.46	5.15	4.89	4.67	4.47	4.30	4.16
0.1	16.78	8.77	7.86	7.18	6.64	6.20	5.84	5.53	5.27	5.04	4.84
0.0	57.91	15.51	12.99	11.25	10.01	9.08	8.33	7.71	7.19	6.75	6.37
-0.02		23.05	17.43	14.27	12.17	10.67	9.62	8.79	8.11	7.54	7.0
-0.04					22.00	15.47	12.67	10.86	9.75	8.89	8.1
-0.06										13.59	10.86
-0.08											
-0.10											

Table 2d Ductility Requirement for Model 4 of Type 2
(Tn = 0.5sec., Py = 1/5 Pmax.)

Slope Tangent Ratio	Ductility Factor	Coefficient of Hysteretic Damping Ratio c_{ch}									
		0.03	0.04	0.05	0.06	0.07	0.08	0.09	0.10	0.11	0.12
	2	2	2	2	2	2	2	3	3	3	3
	3	3	3	4	4	4	4	4	5	5	5
	4	5	5	5	5	5	5	5			
0.8	5										
	6										
	7										
	8										
	9										
	2	2	2	2	2	2	2	2	2	2	3
	3	3	3	3	4	4	4	4	4	4	4
	4	4	4	5	5	5	5	5	5	5	5
0.6	5	5	5								
	6										
	7										
	8										
	9										
	2	1	2	2	2	2	2	2	2	2	2
	3	2	3	3	3	3	3	3	4	4	4
	4	3	4	4	4	4	5	5	5	5	5
0.4	5	4	5	5	5	5					
	6	5									
	7										
	8										
	9										
	2	1	1	2	2	2	2	2	2	2	2
	3	2	2	2	2	3	3	3	3	3	3
	4	3	3	3	3	3	4	4	4	4	4
0.2	5	3	4	4	4	4	5	5	5	5	5
	6	4	4	5	5	5					
	7	4	5								
	8	5									
	9										
	2	1	1	1	2	2	2	2	2	2	2
	3	2	2	2	2	2	2	3	3	3	3
	4	2	2	3	3	3	3	3	3	4	4
0.1	5	3	3	3	3	4	4	4	4	4	5
	6	3	3	4	4	4	4	5	5	5	
	7	4	4	4	5	5	5				
	8	4	4	5							
	9	4	5								
	2	1	1	1	1	2	2	2	2	2	2
	3	2	2	2	2	2	2	2	2	2	3
	4	2	2	2	2	3	3	3	3	3	3
0.0	5	2	2	3	3	3	3	3	3	4	4
	6	2	3	3	3	3	3	4	4	4	4
	7	3	3	3	3	4	4	4	4	4	5
	8	3	3	3	4	4	4	4	5	5	
	9	3	3	4	4	4	4	5			

Slope Tangent Ratio	Ductility Factor	Coefficient of Hysteretic Damping Ratio c_{eh}									
		0.03	0.04	0.05	0.06	0.07	0.08	0.09	0.10	0.11	0.12
	2	1	1	1	1	1	2	2	2	2	2
	3	2	2	2	2	2	2	2	2	2	3
	4	2	2	2	2	2	3	3	3	3	3
-0.02	5	2	2	2	3	3	3	3	3	3	3
	6	2	2	3	3	3	3	3	4	4	4
	7	2	3	3	3	3	4	4	4	4	4
	8	3	3	3	3	4	4	4	4	4	5
	9	3	3	3	4	4	4	4	4	5	
	2	1	1	1	1	1	2	2	2	2	2
	3	1	2	2	2	2	2	2	2	2	2
	4	2	2	2	2	2	2	3	3	3	3
-0.04	5	2	2	2	2	3	3	3	3	3	3
	6	2	2	2	3	3	3	3	3	3	4
	7	2	2	3	3	3	3	3	4	4	4
	8	2	3	3	3	3	3	4	4	4	4
	9	2	3	3	3	3	4	4	4	4	4
	2	1	1	1	1	1	2	2	2	2	2
	3	1	2	2	2	2	2	2	2	2	2
	4	2	2	2	2	2	2	2	3	3	3
-0.06	5	2	2	2	2	2	3	3	3	3	3
	6	2	2	2	3	3	3	3	3	3	3
	7	2	2	2	3	3	3	3	3	3	4
	8	2	2	3	3	3	3	3	3	4	4
	9	2	2	3	3	3	3	3	4	4	4
	2	1	1	1	1	1	1	2	2	2	2
	3	1	2	2	2	2	2	2	2	2	2
	4	2	2	2	2	2	2	2	2	3	3
-0.08	5	2	2	2	2	2	2	2	3	3	3
	6	2	2	2	2	2	3	3	3	3	3
	7	2	2	2	2	3	3	3	3	3	3
	8	2	2	2	2	3	3	3	3	3	3
	9	2	2	2	3	3	3	3	3	3	3
	2	1	1	1	1	1	1	2	2	2	2
	3	1	1	2	2	2	2	2	2	2	2
	4	2	2	2	2	2	2	2	2	2	3
-0.10	5	2	2	2	2	2	2	2	3	3	3
	6	2	2	2	2	2	2	2	3	3	3
	7	2	2	2	2	2	3	3	3	3	3
	8	2	2	2	2	2	3	3	3	3	3
	9	2	2	2	2	2	3	3	3	3	3

Table 3 Increment Ratio of Maximum Strength by Ductility

Type 1 (T_n = 0.1 sec.)
Blank indicater 5 of more than 5.

Slope Tangent Ratio	Ductility Factor	Coefficient of Hysteretic Damping cch									
		0.03	0.04	0.05	0.06	0.07	0.08	0.09	0.10	0.11	0.12
	2	2	2	2	2	2	2	2	3	3	3
	3	3	3	4	4	4	4	4	5	5	5
	4	4	5	5	5	5	5	5			
0.8	5	5									
	6										
	7										
	8										
	9										
	2	2	2	2	2	2	2	2	2	2	3
	3	3	3	3	3	4	4	4	4	4	4
	4	4	4	5	5	5	5	5	5	5	5
0.6	5	5	5								
	6										
	7										
	8										
	9										
	2	2	2	2	2	2	2	2	2	2	2
	3	2	3	3	3	3	3	3	4	4	4
	4	3	4	4	4	4	5	5	5	5	5
0.4	5	4	5	5	5	5					
	6	5									
	7										
	8										
	9										
	2	1	1	2	2	2	2	2	2	2	2
	3	2	2	2	2	3	3	3	3	3	3
	4	3	3	3	3	3	4	4	4	4	4
0.2	5	3	4	4	4	4	5	5	5	5	5
	6	4	4	5	5	5					
	7	5	5								
	8										
	9										
	2	1	1	1	2	2	2	2	2	2	2
	3	2	2	2	2	2	2	3	3	3	3
	4	2	3	3	3	3	3	3	4	4	4
0.1	5	3	3	3	4	4	4	4	4	4	5
	6	3	4	4	4	4	5	5	5	5	
	7	4	4	4	5	5					
	8	4	5	5							
	9	5									
	2	1	1	1	1	2	2	2	2	2	2
	3	2	2	2	2	2	2	2	2	3	3
	4	2	2	2	2	3	3	3	3	3	3
0.0	5	2	3	3	3	3	3	3	4	4	4
	6	3	3	3	3	3	4	4	4	4	4
	7	3	3	3	4	4	4	4	4	5	5
	8	3	3	4	4	4	4	5	5		
	9	3	4	4	4	4	5				

Slope Tangent Ratio	Ductility Factor	Coefficient of Hysteretic Damping c_{eh}									
		0.03	0.04	0.05	0.06	0.07	0.08	0.09	0.10	0.11	0.12
	2	1	1	1	1	2	2	2	2	2	2
	3	2	2	2	2	2	2	2	2	2	3
	4	2	2	2	2	3	3	3	3	3	3
-0.02	5	2	2	3	3	3	3	3	3	4	4
	6	2	3	3	3	3	3	4	4	4	4
	7	3	3	3	3	4	4	4	4	4	4
	8	3	3	3	4	4	4	4	4	5	5
	9	3	3	4	4	4	4	5	5		
	2	1	1	1	1	1	2	2	2	2	2
	3	2	2	2	2	2	2	2	2	2	3
	4	2	2	2	2	2	3	3	3	3	3
-0.04	5	2	2	2	3	3	3	3	3	3	3
	6	2	3	3	3	3	3	3	4	4	4
	7	2	3	3	3	3	4	4	4	4	4
	8	3	3	3	3	4	4	4	4	4	4
	9	3	3	3	4	4	4	4	4	5	5
	2	1	1	1	1	1	2	2	2	2	2
	3	2	2	2	2	2	2	2	2	2	2
	4	2	2	2	2	2	2	3	3	3	3
-0.06	5	2	2	2	3	3	3	3	3	3	3
	6	2	2	3	3	3	3	3	3	3	4
	7	2	3	3	3	3	3	3	4	4	4
	8	2	3	3	3	3	3	4	4	4	4
	9	2	3	3	3	3	4	4	4	4	4
	2	1	1	1	1	1	2	2	2	2	2
	3	1	2	2	2	2	2	2	2	2	2
	4	2	2	2	2	2	2	3	3	3	3
-0.08	5	2	2	2	2	3	3	3	3	3	3
	6	2	2	2	3	3	3	3	3	3	3
	7	2	2	3	3	3	3	3	3	3	4
	8	2	2	3	3	3	3	3	3	4	4
	9	2	2	3	3	3	3	3	4	4	4
	2	1	1	1	1	1	2	2	2	2	2
	3	1	2	2	2	2	2	2	2	2	2
	4	2	2	2	2	2	2	2	3	3	3
-0.10	5	2	2	2	2	2	3	3	3	3	3
	6	2	2	2	2	3	3	3	3	3	3
	7	2	2	2	3	3	3	3	3	3	3
	8	2	2	2	3	3	3	3	3	3	3
	9	2	2	2	3	3	3	3	3	3	3

Table 4 Increment Ratio of Maximum Strength by Ductility

Type 2 (T_n = 0.5sec.)
Blank indicates 5 or more than 5.

APPENDIX I: Non-linear Response by Random Vibration Theory and Simulated Deterministic Analysis

Non-linear response values for one degree-of-freedom system introduced in Reference (4) were examined by the method of simulation. Both response values are compared in Table I.

The values of the response ratio γ is almost unity for the building subjected to the strong motion earthquake excitation having a normal probability density function with zero mean value.

Earthquake		Building		Maximum Displacement Response by 10 Artificial Waves (cm)												Ran (cm)	γ	β
T_o, ω_g, ζ_g	S_o (cm^4/sec^2)	m,k,h,P_y	ky/k	1	2	3	4	5	6	7	8	9	10	Ave	σ			
T_o=20.0 (sec)	10.78	m=0.1 (ton·sec^2/cm)	1.0	2.11	2.72	2.15	2.58	2.50	2.87	2.15	3.02	2.40	2.69	2.52	0.30	2.42	1.04	1.90
			0.8	2.27	2.29	2.39	3.26	2.53	2.91	2.44	3.25	2.42	3.02	2.68	0.37	2.54	1.06	2.00
			0.6	2.37	2.93	3.36	3.56	2.56	2.89	2.48	3.36	2.89	2.96	2.94	0.38	2.64	1.11	2.08
			0.4	2.66	3.11	3.59	3.87	3.47	2.58	2.52	3.44	3.29	3.43	3.20	0.44	2.72	1.18	2.15
			0.2	2.44	3.23	2.94	3.97	3.63	2.38	2.66	3.48	2.79	2.97	3.05	0.49	2.80	1.09	2.21
			0.0	2.64	3.01	2.52	3.87	2.77	3.15	3.82	3.28	2.40	4.43	3.19	0.63	2.91	1.10	2.30
		k=15.79 (ton/cm)	1.0	4.21	5.44	4.29	5.16	5.01	5.74	4.30	6.05	4.81	5.37	5.04	0.59	4.85	1.04	3.83
			0.8	4.81	5.01	5.41	6.70	5.23	5.83	4.85	6.75	5.17	5.68	5.54	0.67	5.22	1.06	4.12
ω_g=13.36	43.11		0.6	4.81	6.41	7.05	6.28	7.20	4.90	5.14	6.60	6.02	7.01	6.14	0.86	5.48	1.12	4.33
			0.4	6.02	6.30	4.53	7.57	7.34	5.89	6.05	6.08	5.07	6.19	6.10	0.86	5.72	1.07	4.52
(rad/sec)		h=h_y	0.2	6.24	5.45	4.73	5.67	7.88	4.30	7.14	6.51	6.26	8.54	6.27	1.17	6.21	1.01	4.90
		=0.05	0.0	8.98	6.49	7.81	7.45	7.82	6.87	6.19	8.28	9.54	6.23	7.57	1.10	8.17	0.93	6.45
			1.0	6.32	8.16	6.44	7.75	7.51	8.62	6.45	9.07	7.21	8.06	7.56	0.91	7.27	1.04	5.74
			0.8	6.95	8.68	8.57	9.90	8.42	8.70	7.10	10.19	8.21	8.43	8.51	0.97	7.90	1.08	6.24
			0.6	7.31	9.42	9.59	9.81	10.50	7.20	8.89	9.06	9.32	10.06	9.12	1.03	8.31	1.10	6.56
ζ_g=0.242	96.99	P_y=20	0.4	9.24	9.21	6.30	8.48	8.74	9.60	11.49	8.98	9.87	9.16	9.03	1.19	8.75	1.03	6.92
		(ton)	0.2	9.50	8.91	11.42	14.82	12.75	9.49	11.98	8.56	10.55	11.94	10.99	1.94	9.93	1.11	7.64
			0.0	22.15	19.94	16.99	10.39	17.67	17.53	13.84	25.22	16.13	19.69	17.96	3.95	18.94	0.99	14.24

σ = Standard Deviation

β = Ductility Factor

TABLE I: Comparison of Response Values

THE EARTHQUAKE ENGINEERING PROGRAM OF THE NATIONAL SCIENCE FOUNDATION

JOHN. B. SCALZI
National Science Foundation
Washington, D.C.

ABSTRACT

The general research program, supported by the National Science Foundation, is given in general terms. The required interaction between the social, economic and technology is described.

Key Words: Earthquake; Program; Research; Seismic.

1. Introduction

Earthquakes pose a regularly determined threat to man and his total surroundings. The relatively recent earthquakes which devasted Anchorage, Alaska in 1964 and crippled San Fernando, California in 1971 bear stark, vivid evidence to the vulnerability of our most modern cities and communities. Earthquake destruction need not be widespread chaos and disruption of life if we can learn to design our buildings, bridges, life lines, and total systems to resist the forces caused by the abrupt crustal movements of the earth's surface. Although complete life safety and zero property damage is a goal worthy of achievement, as realists, we can only hope to approach that objective. Technology and research capabilities are available today throughout the country to sucessfully support a major program of disaster mitigation to a respectable level to the advantage of the general public and the nation.

The popular conception of the earthquake hazard in the United States often limits it to the Pacific Coast, especially California, and to such well known disasters as the San Francisco earthquake in 1906, Long Beach in 1933, the Alaskan Coast in 1964, and San Fernando in 1971. Major earthquakes are by no means unknown to the rest of the country where seismic events have occurred in the St. Lawrence River region on several occasions, in the vicinity of Boston in 1755; the central Mississippi Valley (New Madrid, Missouri) in 1811 and 1812; Charleston, South Carolina in 1886 and Hebgen Lake, Montana in 1959.

The dense population of the United States, particularly in those areas of substantial earthquake vulnerability, is a relatively recent development. While there have been many reported earthquakes prior to 1860; the quality of the reported characteristics and resultant damage associated with these events is variable and unreliable. During this period, 36 damaging earthquakes have occurred resulting in cumulative property losses of two billion dollars and over sixteen-hundred lives lost.

In estimating earthquakes losses, it should be noted that property damage is only one aspect of the loss which accrues. Other important losses include; loss of life, injuries, economic loss due to injuries, loss of income due to business disruption, cost of emergency operations, and many others. There is little available data on the extent of these

costs although they most certainly exceed the direct costs involved.

Losses from earthquakes are not limited to the direct effects of ground faulting and shaking. Tsunamis are sea waves generated by submarine crustal disturbances, often associated with earthquakes and volcanic eruptions. They are scarsely perceptible at sea, but as they enter the coastal margin their crests may build to great heights depending on the energy stored in the waves and on the coastal configuration. Tsunamis are limited in destructive effects to areas immediately adjacent to the coastline where they destroy by the impact of water and the subsequent inundation. Affected areas are not necessarily proximate to the earthquake site. For example, in 1960, Hilo, Hawaii suffered from the Chilean earthquake and Northern California was hit by the effect of the Alaska event. Thirteen twentieth century tsunamis affected the United States with a loss of 400 lives and property damages of more than one-hundred sixty million dollars.

Although the most earthquake prone areas of the United States are along the Circum-Pacific belt, many other sections of the country are also affected. Parts of the coastal portion of California are among the most densely populated and rapidly urbanizing sections of the country and therefore become more vulnerable. Much of the rest of the United States has had notable seismic events also. Maps have been developed by seismologists and engineers to delineate in a approximate way zones of earthquakes "vulnerability". From a study of the maps and population distribution, it was found that thirty-five percent of the population of the United States resides in areas subject to major or moderate risks. Table I presents a population analysis by risk zone. Thirty-nine states have regions that are in either zone 2 or 3 or both.

We need only to look at the record of losses of two relatively recent earthquakes to realize the impending devastation which is now lying dormant, and would be quickly awakened, if another strong motion earthquake were to occur somewhere in the United States. The San Fernando Earthquake of 1971 and the Alaska Earthquake of 1964 have the following statistics:

San Fernando	65 Lives Lost	$511 Million, Property Damage
Alaska	131 Lives Lost	$500 Million, Property Damage

Although the magnitudes for lives lost and property damages appear to be low, we must recall that the Alaska event was in a sparsely populated area and the San Fernando region is a residential suburb of Los Angeles. If the San Fernando shock had struck closer to the business district of Los Angeles, the gruesome statistics may have been more frightening.

Although there was an intervening period of seven years between the San Fernando and Alaska Earthquakes, evidence of damage and study of design and construction practices appear to indicate that very little new information was brought to bear on the methods of design and construction. In the general codes for buildings and bridges only a few small changes were noted, except in those areas where earthquakes are generally considered to be a more frequent occurrence. Other areas of the country generally remained complacent.

Estimates of an annual investment in construction in the United States are in excess of fifteen-billion dollars in regions of high seismic activity and the year two-thousand

an investment of three-hundred-seventy-five billion dollars of new construction will be exposed to the possibility severe earthquakes. It is prudent to hope that in the interim buildings will be designed for maximum safety, economy and functional operation.

Estimates of future damage to be expected in the year two-thousand, if a high intensity earthquake were to reoccur, are indicated below:

San Francisco	Property loss $20 Billion, Lives Lost 10,000
New Madrid	Property loss $ 6 Billion, Lives Lost 3,000

If the New Madrid event were to shift northward by one hundred miles, the damage estimate would be tripled because a more populated region including Chicago would be effected.

Other factors would also affect the estimates, such as increased growth rates, greater population density, construction standards used in the next twenty-five years, the extra physical wealth, the ages of buildings, the materials and quality of construction. All of these factors may not be controlled by good engineering practices, but those factors that can be controlled should be undertaken soon to mitigate all possible losses.

To assist the professionals in their efforts, research is underway by many organizations, private and public, which will lead to a better understanding of earthquakes forces and their effect on man made structure. Foremost among the organizations which sponsor research in earthquake engineering are the various agencies of the Federal Government of which the National Science Foundation (NSF) is a prominent participant. NSF supports basic and applied research projects principally at universities. The program includes two major areas of interest, Geophysics and Earthquake Engineering.

The NSF Geophysics program supports basic research in the areas of seismology, gravity, geodesy, geomagnetism, paleomagnetism, earth currents, heat flow and materials properties. The dynamic process of the earth's crust leading to earthquakes are studied by investigations in plate tectonics, crustal mechanisms, faulting mechanisms, local material response and propagation characteristics and location of the events. From this research, realistic assessments of the risk of an earthquake at a particular site and in a given time span can be pursued.

The NSF Earthquake Engineering program supports a broad, basic and applied research activity in all aspects of engineering, geotechnical geology, social and behavioral sciences which are aimed at developing methods and procedures for the mitigation of earthquake disasters. As such, the NSF program is the lead Federal agency in earthquake engineering research.

The general objectives of the NSF Earthquake Engineering program are to support research projects leading to:

1. Development of economically feasible design and construction methods for building earthquake resistant structures of all types.

2. Development of procedures for integrating information on seismic risk with ongoing land use planning processes.

3. Development of an improved understanding of social and economic consequences of individual and community decisions on earthquake related issues.

4. Presentation of program results in forms useable by the affected interest communities to control the vulnerability to earthquakes.

The general objectives are supported by several specific technical program elements which are described below. These elements have been developed to treat the specific technical problems of analysis, design, and synthesis of engineering and scientific knowledge to control the consequences of earthquakes which are measured in terms of life loss, property and functional loss.

2. Ground Motion and Data Services

Destructive ground motions resulting from earthquake actions are of several different types, including heavy ground shaking, slow or rapid fault slip, subsidence and land slides. Fundamental to an understanding of any of these damaging phenomena, however, is an accurate knowledge of the actual earthquake ground motion. Fundamental to the validation of structural design and analysis procedures is the actual structural response generated by the ground motion.

The measurement of destructive ground motions in the epicentral region of large earthquakes and the associated response of structures is achieved by placing a network of instruments at a variety of sites where earthquakes are likely to occur. These instruments include both passive and active recording devices. The strong motion accelerograph record the history of acceleration in three component directions. It begins recording after an acceleration threshold has been exceeded. These instruments are the most generally used types and find application in most activities of data gathering. Other active recording systems include pore pressure gauges to measure the liquid pressure in saturated soils, with pressure gauges to measure the inertial effects of soil usually on a foundation wall, strain gauges and displacement meters. Among the passive instruments are the seismoscope, a conic pendulum that records motion on a smoked glass, scratch strain gauges and extensometers.

The measurements obtained are directed at achieving three principal objectives:

1. To support the research program by measuring pertinent quantities to validate, calibrate and/or formulate theories of earthquake response.

2. To support the designer's need for earthquake motion information at varying geological and seismological sites.

3. To obtain a comprehensive data base to perform microoregionalization of earthquake risk areas based on events in the area.

3. Soils Response and Analysis

One of the greatest potential sources of property loss is damage to structures that rest on soils or on foundations which, although adequate to support the structures under ordinary circumstances, might fail during an earthquake. A great potential for loss of life resides

in the possibility of a dam failure. The following areas represent forms of soil failure under consideration by the program: settlement of cohesionless soils, bearing capacity failures, embankment failure; soil liquefaction, and water front bulkhead failures.

The dynamic behavior of structure during an earthquake depends on the shaking transmitted to it by the surrounding soil. These motions are imparted to the structure through the interaction between its foundation and the supporting soil and/or bedrock and include amplification effects.

The objectives of this element are to:

1. Develop methods to evaluate and control soil failure potentials.
2. Develop analysis and design methods to evaluate and control soil amplification.
3. Develop design and analysis methods to characterize the loadings transmitted to structures through soil foundation interaction.

4. Structural Response and Analysis

The realization of a structure rests on two complementary activities, analysis and design. Analysis forms the basis for design. The ability to analyze a hypothetical structure and determine the stresses and displacements that would be produced by a specified loading is an essential part of the design process. The more accurately this can be done the resulting design will be more efficient and economical with a more reliable design factor of safety. The analysis of a structure can be exceedingly difficult because ordinary structures are exceedingly complex dynamic system; and because the ground motions which the structure will be subjected to during its lifetime are probabilistic, and the construction process leads to a structure which is not precisely known. The analysis of structural response requires knowledge of the full system, including foundations, adjacent soils and in some cases the properties of adjacent structures.

The objectives for this program element are to:

1. Determine appropriate models for element (e.g., beam, column, plate, etc.) response to strong motion excitation from analytical and experimental studies.
2. Develop digital computer methods of analysis that predict earthquake response of structural systems comparable in complexity to real structures.
3. Validate and calibrate these models by comparison with earthquake measured motions and damage of structural systems and elements.

The basic problem of earthquake design is to synthesize the structural configurations; the size, shape, and materials of the structural elements; and the methods of fabrication, so that the structure will safely and economically withstand the action of earthquake ground motions. The object of design is to control the effects of an earthquake on a structure and keep damage within acceptable limits. A further series of objectives for this element are:

4. Determine the dynamic properties of structures, elements and materials under conditions of large strains, beyond the yield point and up to failure.

5. Develop reliable, practical and simplified methods of earthquake design for widely used and special important structures: for example low rise residential, low rise commercial, school houses, high rise buildings, dams, bridges and industrial structures.

6. Thoroughly study structures that failed during an earthquake, as well as those that did not fail, to refine design principles.

7. Develop design and analysis methods for non-structural elements and mechanical components of structures.

5. Systems Response

Previous elements of the research program have dealt almost exclusively with localized structures, that is, a single building, dam, etc. The operation of the community during the emergency and recovery periods is dependent on the functioning of utility and public service facilities that function as a system with elements located at many sites in the affected area. The failure of an element can cause the total system to malfunction or be inoperative. Thus the design of system elements must consider the seismic characteristic requirements of the extended system. Both physically connected and non-connected systems are to be investigated. An example of a connected system is fire water distribution (storage, pumping stations, water mains, etc., while a non-connected system is represented by emergency health care facilities (hospitals, clinics, laboratories, etc.).

The objectives of the element are to:

1. Develop principles of planning and designing facilities for minimum disruption of operations due to earthquake ground displacements.

2. Develop design procedures for special structures and equipment of each type of utility and public service facility, among these are:

a) Fire fighting and emergency transportation

b) Emergency power and communications

c) Hospitals and emergency agencies

d) General Communications

e) Water services and sewage disposal

f) Electrical power and natural gas or fuel supplied

g) General transportation facilities.

6. Coastal and Inland Waterways

An earthquake at sea may generate a tsunami, (tidal wave as it is commonly known), that presents a real danger to coastal and island regions of the United States. The risk posed by tsunamis may best be controlled by land use regulation in vulnerable areas. Verification of the occurrence of a tsunami permits the evacuation of potential affected areas.

If a dam fails, an inundation wave may be generated when the reservoir empties, and can cause serious downstream damage. Structuring downstream land use, with this potential hazard in mind can reduce life and property loss. When a reservoir behind a dam is filled a series of earthquakes often occurs in the vicinity of the impoundment. The increment risk these quakes cause above the natural risk is at present uncertain.

The objectives of the element are to:

1. Develop methods to verify that an ocean-based earthquake has generated a tsunami.

2. Develop methods to anticipate tsunami run-up in coastal regions.

3. Develop methods to anticipate downstream inundation levels.

4. Determine the incremental seismic risk associated with filling a reservoir and the degree that this risk should be part of the design criteria for the dam.

7. Technology Transfer

Within the Earthquake Program, utilization activities have been centralized and formulated as a specific program thrust. The objectives in this element are to:

1. Maintain a technical reference collection of published reports, papers and unpublished data available to researchers and professionals, to provide for information dissemination.

2. Maintain a software center to archive, document, validate and distribute computer programs developed for earthquake engineering applications.

3. Consolidate the best knowledge regarding design and analytical methods from current and completed research and professional experience in building codes, design criteria and standards for use by professionals and regulatory bodies.

4. Conduct regular conferences and workshops to act as foci for dialogues between the research and professional communities.

5. Conduct post-earthquake inspections to obtain engineering data and to identify unfulfilled research needs.

8. Implementation Studies

Advances in civil engineering methods are implemented through two types of actions: individual professional applications; and adoption of regulatory or enforcement agencies. The latter process is primarily political, while for former is educational. The structuring of the flow of technological developments from research to implementation is a particularly arduous one, involving a vast complex of institutions, special interest groups and secondary agendas. The way in which this process works is not too well understood by most people. An understanding of the process is a first step in structuring a methodology to fore-shorten the period from research to practice. The objectives of this program element are to:

1. Develop an understanding of the implementation process.

2. Develop a methodology to program the education of professionals to the best earthquake engineering practice.

3. Develop a strategy of program results to be processed through the community into regulatory and enforcement agency regulations in a timely fashion.

4. Advocate the accomplishment by public and private groups of the developed plan.

9. Social and Behavioral

The mitigation of earthquake effects may depend on a variety of actions not directly associated with the assurance of safe structures. The possibilities of earthquake control and prediction present different technical methods that may lead to mitigation. Community actions during and following the event may significantly affect the consequences of the quake. Condemnation and redevelopment attitudes, insurance programs and economic assistance may markedly affect the vulnerability of a community to future events. With a view to filling important gaps in our understanding of earthquakes as they impact man and his social environment, research in the social and behavioral sciences, and in economics, will be undertaken to:

1. Develop policy alternatives for the community to provide emergency, rescue, recovery and redevelopment services.

2. Develop policy alternatives for the dissemination of earthquake warnings.

3. Assess the consequences of technical developments and policy alternatives on the achievement of disaster mitigation.

New areas of research to be undertaken and initiated in the coming fiscal year will extend the NSF Program to fill several important voids in knowledge which have been identified as essential elements to the research program.

Particular emphasis will be placed on the following general topics:

1. Development of vulnerability methods for assessing the risk posed by structures not designed and constructed to be earthquake resistant.

2. Extension of experiments begun in 1976 on the three-dimensional non-linear behavior of structural components to include typical building elements. Current design methods are based on two-dimensional failure models.

3. Research initiations on the design and analysis of earthquake performance of lifeline facilities, utility, transportation, and communication systems which are critical to the performance of the community.

4. Expansion of FY 1976 activities to develop an understanding of the impediments of the incorporation of research results into seismic hazard regulations for construction.

5. Research initiations to discover how private vulnerability decisions are made and may be affected, since business decisions are a major factor in developing the physical environment and, thus, affect the seismic vulnerability of entire communities.

In addition to the earthquake forces other environmental loads are closely related to the design of structures by their dynamic nature. These load effects are: extreme winds, accidents, explosions, projectiles, wave actions, surges, and floods. These dynamic hazards account for an annual financial loss in excess of $1 Billion. The nature of these hazards is reasonably well known and the analytical and design methods developed for seismic resistance can be adopted to these additional forces at a relatively small cost.

The research related to these dynamic hazards will; adopt, where appropriate, seismic and analysis methods to other individual dynamic hazards to buildings and develop proceedures and methods that integrate the effects of multiple loads sources and types and that are suitable for professional use and regulatory adoption.

Several other Government Agencies are engaged in research problems involving earthquake engineering which effect the successful operation of their day to day mission assignment. Close cooperation between agencies and departments assure that duplicative effort by academic researchers is eliminated as much as possible.

A review of the program technical elements described above indicates the breadth and scope of the NSF Earthquake Engineering Program. It is a broad program designed to provide the necessary research to develop improved building design provisions, design criteria, evaluation of risks, and preparation for an event should it occur anywhere in the United States. The main thrust of the program is to mitigate the losses from earthquakes which may occur anywhere throughout the country. With the assistance of the academic researchers, engineers, architects, building officials, code writing bodies, contractors and other future earthquake events may be only simple momentary disruptions rather than devastating chaos.

LARGE-SCALE TESTING PROGRAMS RELATED TO WIND AND SEISMIC EFFECTS CURRENTLY UNDERWAY IN JAPAN

SEIICHI INABA
Earthquake Engineering Laboratory
National Research Center for Disaster Prevention
Science and Technology Agency
Japan

ABSTRACT

This list has been prepared in order to discuss cooperative research problems in the area of large-scale testing of structures at the 8th Joint Meeting of U.S.-Japan Panel on Wind and Seismic Effects. The Japan Panel selected for following four members to work on the task committee on the large-scale testing program.

Seiichi Inaba, National Research Center for Disaster Prevention
Makoto Watabe, Building Research Institute
Kenkichi Sawada, Public Works Research Institute
Nobuyuki Narita, Public Works Research Institute

In accordance with the exchange of letters between Dr. C. Culver of the National Bureau of Standards of the U.S. Panel and Mr. S. Inaba of the Japan Panel, this list has been drafted to inform the U.S.-Japan Panel of work being conducted in this area. The list includes the large-scale testing programs currently underway in Japan, the organization, the name of individuals in charge, and a brief description of the objectives, status and time schedule.

Key Words: Earthquake; Research Programs; Seismic; Testing; Wind.

1. Program: Dynamic Tests of Structures by Use of A Two-Dimensional Shake Table
Organization: National Research Center for Disaster Prevention
Names in Charge: Seiichi Inaba, Nobuyuki Ogawa; Earthquake Engineering Laboratory.
Description of the Objectives: It is planned to study the effects of the vertical earthquake shaking of structures using the two-dimensional shake table, which is going to be built in the National Research Center for Disaster Prevention. The table will be 6 m x 6 m and have a maximum test weight of 60 tons which can apply simultaneous vertical and horizontal vibrations with a maximum displacements of $\pm$100 mm in the horizontal and $\pm$50 mm in the vertical. Maximum velocities of 60 cm/sec in the horizontal and 40 cm/sec in the vertical, and a maximum accelerations of 1.2 G in the horizontal and 0.8 G in the vertical direction can be achieved as well as a frequency range between D.C. and 30 Hz.

Dynamic test programs have been planned for large-scale models of embankments and other soil structures, building structures, plant structures, foundation structures and so forth.

Status: Soil exploration of the foundation site was performed in 1974. A feasibility study of the two-dimensional shake table has been conducted. A small-scale model simulator of the table, 1 m x 1 m, was constructed in March, 1976.

Time Schedule: Designs of the shake table, foundation and laboratory building are being conducted in 1976, and the construction of foundations will start in 1977. Dynamic tests will start in 1980, after completion of the construction.

2. Program: Dynamic Tests of Composite Breakwater

Organization: Port and Harbour Research Institute, Ministry of Transport

Names of Individuals in Charge: Setsuo Noda, Tatsuo Uwabe, Hajime Tsuchida, and Satoshi Hayashi

Description of the Objectives: Recently, several high composite breakwaters are under planning in Japan. The composite breakwater consists of a rock-fill or sand-fill mound and concrete caissons resting on the mound. The largest breakwater of this type in Japan has been constructed in Ofunato Bay, to protect the coastal area along the bay from hazard by tsunami; the breakwater is 40 meters in height. The breakwater against tsunami must have sufficient seismic stability, since it is certain that the breakwater will be shaken due to earthquake ground motions preceding tsunami arrival.

The Port and Harbour Research Institute (PHRI) is planning to examine the seismic stability of the composite breakwater by model tests. At present tests are expected to be performed on a shaking table in PHRI, which is an electric-dynamic random shaking table having frequency range from 0.2 to 100Hz. The size of a container on the table is 5 meters in length in the direction of table motions, and is 1.5 meters in width and 1.5 meters in depth. A wave absorbing channel can be connected with a flexible joint to the container to eliminate disturbance by waves generated and reflected by an end wall.

Through the tests stability of rock-fill mound, dynamic water pressure to the mound and the caissons, and relative displacement between the mound and the caissons will be studied.

PHRI has been observing earthquake ground motions at the site of the tsunami breakwater in Ofunato Bay and its earthquake response. The records obtained during the observation will be analysed as a part of the study.

Status: PHRI has some experiences on dynamic tests of such a composite breakwater; in the tests, however, a small model was used and the model was tested in air.

The earthquake ground motion records at the site of the breakwater and records of its earthquake responses were once briefly analysed and reported in the following report:

> Hajime Tsuchida, Tatsuo Uwabe, Eiichi Kurata, and Satoshi Hayashi: Observation and Analysis of Earthquake Response of Fill Type Breakwater, Proceedings of the Japan Earthquake Engineering Symposium 1973 in commemoration of the 50th anniversary of the Kwanto earthquake, August and September 1973, pp. 375-364.

Time schedule: The tests are expected in late 1976 or in 1977 Japanese fiscal year (from April to March).

3. Program: Experimental Investigation into the Seismic Behavior of Full-size Reinforced Concrete Structures Utilizing the Large Scale Testing Facilities.

Organization: Building Research Institute, Ministry of Construction

Names of Individuals in Charge: M. Watabe, M. Hirosawa, S. Nakata.

Description of the Objectives: Up to date many experimental studies were made on the columns, beams and shear walls. However there are many fields still unexplored; such as the stress distribution among each member of structures at the variable plastic stages, yielding mechanisms of a structure and ductility of each member during yielding and development of mechanisms in the structure. For example the aseismic tests (static and dynamic) of a full size structure with slabs, shear walls and foundations need to be conducted. These test results would make clear the difference between the behavior of a structure and a unit member, especially the anchorage of main bars or ground effects on walls. Hitherto laboratory studies on the structural damage due to earthquake were based only on member tests, and the behavior of an entire structure had to be based on engineering judgement. Such judgements may lead the serious errors. Therefore, full size structural testing should be made in order to avoid such errors.

As a first stage of the testing project, we propose to test a 3-story building with shear walls. The kind of shear walls will include normal types, precast walls and slit walls. By performing this test the behavior of shear walls, effects of foundations, soil conditions and mechanisms during structural yielding can be explored. Various types of buildings, such as follows, will also be included in the project, i.e., structures without shear walls with short columns or long columns, long span structures and many types of ground conditions.

The Large Scale Loading Facility of the Building Research Institute, can be used for static and dynamic tests of full size structures by use of hydraulic sero actuators, which are now under construction and can be used by 1979. All the testing systems, loading, vibration and measurement are directly controlled by a computer system in this facility. The total cost of this project is expected to be 12 billion yen (40 million dollars).

Status: M. Watabe et al.,"A Proposal to the Joint Research Program on the Aseismic Properties of R.C. Structure by the Full Size Specimens." 7th Joint Meeting U.S.-Japan Panel on Wind Seismic Effects, UJNR, Tokyo, May 20-23, 1975.

Exchange of Research Personnel: 1976----E. Pfrang (N.B.S.), A. Sozen (Univ. of Illinois), R. Hanson (Univ. of Michigan), H. Umemura (Univ. of Tokyo), H. Aoyama (Univ. of Tokyo), M. Watabe (B.R.I.). 1977----J. Penzien (E.E.R.C.), R. Clough (E.E.R.C.), P. Jennings (T.I.C.), T. Okada (Univ. of Tokyo), M. Murakami (chiba Univ.), Y. Yamazaki (B.R.I.) 1978----M. Duke (U.C.L.A.), E. Popov (E.E.R.C.), M. Hirosawa (B.R.I.), A. Shibata (Tohoku Univ.), Y. Matsushima (B.R.I.). 1979----R. Bresler (E.E.R.C.), J. Penzien (E.E.R.C.), R. Clough (E.E.R.C.), Y. Ohsawa (E.R.I., Univ. of Tokyo), S. Nakata (B.R.I.)

4. Program: Dynamic Test of Structures for Nuclear Power Plants
Organization: Center for Nuclear Safety Engineering Research
Names in Charge: Resources and Energy Agency, Ministry of International Trade and Industry
Description: Construction of a shake table for testing of nuclear power plant structures is planned in order to prove the safety of nuclear power plants during and after future destructive earthquakes. Part of the funds have been obtained from the government since 1975.

The structures that will be dynamically tested will include containers, pressure vessels, elements of reactors and piping of main-coolant system for both PWR and BWR nuclear power plants.

The shake table under planning will have dimensions of 15 x 15 m, maximum test weight of 1000 tons, maximum horizontal stroke of $\pm$ 200 mm and a vertical stroke of $\pm$100 mm. The table can be driven with simultaneous vibrations in the horizontal and vertical directions up to accelerations of 2 g in the horizontal and 1 g in the vertical with a velocity of 70 cm/sec in the horizontal and 35 cm/sec in the vertical direction.

The total cost of construction, including the shake table, foundation and the laboratory building is expected to be 24.8 billion yen (83 million dollars) and the construction cost of a test structure will be about 2 billion yen (7 million dollars).

The model scale of the test structures will be 1/4 for a container of 800 NWe PWR and 1/2 for that of a 1100 MWe BWR power plant.
Status: Construction of the table and the research work will be carried out by the Center for Nuclear Safety Engineering Research, which has been established under the control of the Resources and Energy Agency in February, 1976. The center is a joint government-private foundation supported by the government and the electric power companies, constructors and manufacturers.
Time Schedule: It will take 5 years to build the shake table and the laboratory and other testing facilities. The shake tests will begin in 1981.

5. Program: Dynamic Experiments on Earthquake Resistance of Civil Engineering Structures
Organization: Public Works Research Institute, Ministry of Construction
Name in Charge: Ground Vibration Section and Earthquake Engineering Section, Public Works Research Institute, Ministry of Construction.
Description: Construction of a shake table is planned to prove the earthquake resistance of engineering structures such as suspension bridges, prefabricated submerged tunnels, underground pipelines, embankments, etc.

There are two kinds of shake-table facilities that have been planned. One will have the dimension of 6 meter x 8 meter, maximum test weight of 130 tons, maximum stroke of $\pm$75 mm, maximum velocity of 60 cm/sec, maximum acceleration of 0.7 g in the horizontal direction. The other will have 4 shake tables, and each table will have the dimension of 2 meter x 3 meter, maximum test weight of 30 tons, and other specifications that are almost the same as the above large scale shake table. These two kinds of shake tables will use 4 common actuators.

The total cost of construction including the shake tables, foundations and laboratory building is expected to be 12. billion yen (4 million dollars).

Status: Dynamic tests of submerged tunnels and underground pipes, using the large scale shaking table which belongs to the Earthquake Engineering Laboratory, National Research Center for Disaster Prevention, Science and Technology Agency, had been conducted several years ago. An experiment on the dynamic behavior of sandy grounds during earthquakes are now being conducted, using the shake table which have the dimensions of 1.5 meter x 2 meter, maximum test weight of 5 tons in the horizontal direction.

Time Schedule: The construction of the shake tables and the laboratory and other testing facilities at Tukuba Science City will start in 1977, and it will take 2 years to complete a part of those facilities. Dynamic tests are expected to begin in 1979.

6. Program: Dynamic Test of the Suspension Bridge Foundation Model

Organization: Honshu-Shikoku Bridge Authority

Name in Charge: Keiichi Komada, Chief of the Third Design Division

Summary: In order to prove the safety of the bridge foundations at the time of an earthquake, dynamic model tests by use of a large scale shake table is planned in 1976. It is aimed to clarify the interaction between the foundation and ground. Thus the response of the foundation and ground will be measured for various depths of the foundation model.

An outline of the test and analysis is as follows:

1. Model:
   Foundation Model: 60 x 80 x 100 cm (Weight: 1 t)
   Ground Model: 400 x 900 x 150 cm
2. Exciting Waves:
   Sinusoidal Wave, Random Wave and Earthquake Wave
3. Measurements:
   Acceleration Response of the Foundation and Ground
4. Analysis:
   Experimental Analysis of Resonance Curves, Vibration Modes and Others
   Theoretical Analysis of Response by the Finite Element Method

Status: Honshu-Shikoku Bridge Authority has been executing the dynamic test in order to develop an earthquake proof design for various types of foundations, since 1971. These details are shown in Table 1.

7. Program: Dynamic Test of Embankment

Organization: Public Works Research Institute

Names in Charge: Kenkichi Sawada, Yasuyuki Koga: Soil Dynamics Section

Description of the Objectives: The object of our research is to explain the dynamic behavior of an embankment, using the large-scale shake table established at the National Research Center for Disaster Prevention.

The height of the test embankment is 1.5 m and the depth of the ground base is 1.5 m. The total length of the model is 12 m perpendicularly to the embankment axis and the width is 2 m. In addition to this basic model, embankments protected with the steel sheet piles and horizontal sand berms are to be tested. The model embankment is constructed in a water tight steel box on the shake table and the model is perfectly or partially submerged in water, depending on the test program.

The test of the embankment of a saturated ground soil is a fundamental and important case. Data on the increase of pore water pressure and acceleration of the model can be obtained. Analysis using the slice method to evaluate the stability of the embankment can be applied to explain the slope failure due to the dynamic vibration in which the effects in the increase of pore water pressure on embankments and ground soil is considered. Analysis will also be performed in the liquefaction problem under anisotropic stress conditions.

Status: Results of this test program have been published in a Technical Report of Public Works Research Institute and presented at the Annual Conference of the Japan Society of Soil Mechanics and Foundation Engineering. A paper on the settlement of saturated sands due to vibration was presented at the UJNR U.S.-Japan Joint Panel on Wind and Seismic Effects in 1975.

Time Schedule: We have been engaged in the research program for 5 years beginning in 1970. Our future program is to examine the behavior of vertical vibrations of embankments, soil-foundation interaction, and soil structures constructed with other materials such as steel piles, concrete slabs, and retaining walls.

8. Program: Aerodynamic Test for Long-Span Bridges and High-Rise Towers

Organization: Public Works Research Institute, Ministry of Construction

Names of Individuals in Charge: N. Narita, Chief, Structure Section and K. Yokoyama Res. Eng., Structures Section.

Description: Two large wind tunnels are now being constructed. The main feature of these wind tunnels is as follows:

1. Wind tunnel for flutter testing of bridge and tower structures:

   Dimension of test section: 2.5 x 4.0 m (10 m long)

   Maximum wind speed: 25.0 m (without coarse grid)

2. Wind tunnel for aerodynamic testing of bridge and tower structures under turbulent flow.

   Dimension of test section: 6.0 x 3.0 (30 m long)

   Maximum wind speed: 15.0 m/s

3. Location of the facilities

   Tsukuba Science City in Ibaraki Prefecture about 60 kilometers northeast of Tokyo.

4. Completion

   The construction work will be completed in May 1977.

The following wind tunnel tests are scheduled to be carried out:

1. Measurement of aerostatic and aerodynamic forces acting on bridge or tower structures.

2. Measurement of critical fluttle speed of the structures.

3. Measurement of aerodynamic response of the structures under gusty and turbulent wind.

Acknowledgments

The following three experts have cooperated with our task committee on the preparation of the list.

Hajime Tsuchida, Port and Harbour Research Institute

Yoshio Komada, Honshu-Shikoku Bridge Authority

Yukiyoshi Ibe, Resources and Energy Agency

The author, serving as co-chairman of the task committee, is responsible for the entire work in the preparation of this list, contact with the U.S. Panel, and proposals to the Japan Panel.

Table 1 Details of Experiments

Year	Type of Foundation	Ground Material	Measurement
1971	Rigid Foundation and Multi-Column Foundation	Rubber	Acceleration and Displacement
1972	Rigid Foundation and Multi-Column Foundation	Grouting Material	Acceleration and Displacement
1973	Rigid Foundation and Rigid Foundation with Piles	Grouting Material	Acceleration and Displacement
1974	Rigid Foundation	Sand	Acceleration, Displacement, Soil Pressure and Pore Pressure

EARTHQUAKE DAMAGES TO EARTH STRUCTURES

KENKICHI SAWADA
Director
Soil Dynamics Section
Public Works Research Institute
Ministry of Construction
Japan

ABSTRACT

This paper will present the problems associated with the damage to earth structures during earthquakes, and how some of the problems have been solved. In addition this paper will present the principle of the design of earth structures, that to date have not been discussed.

Initially, data has been collected on the amount of damage to earth structures during earthquakes, how they have failed and relationships to such failures. These data are then used in formulating the mechanics of the failure.

Finally, the details of the repair work required, as listed by field engineers engaged in this repair work was examined.

Key Words: Construction; Dams; Earthquake; Earth Structures; Roads; Survey.

1. Foreward

We can investigate the damage caused to earth structures by recent earthquakes by actually visiting the site. However, details of past failures and damage can only be obtained from literature, but little quantitative data is available.

In this report, details of earthquake damages to soil structures, both past and present, will be given. The earth structures will include sliding of slope, settlement of embankment and displacement of retaining walls.

2. Damage

The expression "There are many cracks in the ground and the land slide dam up river and overflow has caused a flood" which relates to a geophysical phenomenon given in literature 1000 years ago. This indicates that the mechanism of the disaster in the Edo-period resembles todays earthquakes. During this period people constructed riverlevees extensively, and many people lived near the river. Therefore the scale of disaster for these geophysical structures was quite extensive.

Fire was propagated due to earthquakes during this period. This was due in part by the thickly populated areas with houses and the type of fuel used. "Expanded disaster was the result of human activity" has generally evolved as a truism, where today we find the fire and flood associated by earthquakes.

The utilization of information, collected during failure of buildings and bridges has permitted establishment of specifications during the past 30 years. However, these specifications are limited to only steel and concrete structures.

During this period, several large scale geophysical disasters have occurred, such as the Kanto earthquake ('23 M=7.9) in Nebukawa along the coast of Sagami Bay where a land slide (H = 90 m L = 2000 m) occurred, resulting in the soil pushing a standing train into sea. Also the Kitaizu earthquake ('30 M=7.0) induced failure of an old dike reservoir, the Nankai earthquake ('46 M=8.0) in Yanokawa along south part of Kii peninsula, created a large scale slope failure (H = 80.8 m I = 1/25). In all instances crack and settlement of road embankments were noted, however, the resulting reports describing these earthquakes, contain no quantitative data.

After the Fukui earthquake ('48 M = 7.3), valuable engineering analysis began, resulting in procedures in the collection of earthquake data. The epicenter of the Fukui earthquake was in the Fukui alluvial plain, therefore damage was limited in this plain, which is one reason why the investigation was simple to perform. Now we know the type of serious damage which can occur to the earth structures during earthquakes, which include; failure of roads, railway embankments, river levees, slidings of sand hills and overturning of retaining walls. The maximum volume of soil, to be removed during these failures was several thousand m^3.

At the Niigata earthquake (-64 M = 7.5) many types of investigations in the earthquake engineering field were conducted. The main theme of the investigation in soil mechanics, was liquefaction of the soft sandy ground. The analysis of the settlement and sliding of the road and railway embankment and river levee were due to the liquefaction of the ground. The railway embankment (H = 7 m L = 150 m) was damaged and its material shifted 115 m, shows the severety of the damage.

Though similar damage to earth structures have occurred, it was the experience gained by many engineers who were engaged in soil mechanics, that increased the state of the art. Although they were able to obtain a solution, research work was initiated after the '68 Tokachioki earthquake.

The '68 Tokachioki earthquake ('68 M = 7.9) was an important investigation relative to damage of an earthquake damage, in which Liquefaction of an embankment occurred.

The precipitation of 100 - 200 mm, two days before the shock occurred was a condition to soil liquefaction of the relatively uniform graded volcanic soil. The new embankment of the National railway suffered serious damages to this embankment which consisted of this volcanic soil. The maximum height of the embankment was 15 m. The national route No. 4 which was seriously damaged, was located at Metoki. The entire portion of the embankment (H = 5 m L = 110 M) was constructed on a swamp, failured and spread more than 40 m. Another case was damage to a hill side slope (H = 20 m) where the saturated soil spread 100 m and the ground of the middle school (H = 12.3 m I = 1/1.5). Another case involved an earth dam (H = 8 m L = 200 m) used for irrigation, spread 160 m.

Even at the relatively small earthquakes, large scale earth structures were damaged. During the Oitakenchubu earthquake ('75 M = 6.4), a large slope of an embankment

(H = 22 m L = 90 m) slid and stopped traffic flow along a toll road. In addition to that special case, there are many other cases of land slides which have been increasing in numbers.

Land slides and ground fissure designed as an index Intensity VI of the JMA. So in the area VI there have to be land slides and cracks. But recently there has been an opinion that land slides and cracks should have an index of V.

As already mentioned, there are many facts relative to damage, but little useful data. In reporting disaster surveys, there are many ways in describing the frequency, length and soil volume during failure. It is easy to attribute this reason to the complexibility of the soil composition and field conditions, but we must examine the real cause more closely. Because of the inaccuracies in soil dynamics describing the behavior of earth structures during the earthquake, we can not obtain accurate results. At present it appears that a universal theory to predict the behavior of such structures is not possible.

3. Analysis

Next I will present the results of various analysis of the failure of earth structures, and their differences. The first is a study by Professor Kawakami, of Tohoku University, refered to the Miyagikenhokubu earthquake ('62 M = 6.5). In this case an embankment of a road, railway and river levee concentrated in relatively narrow area (40 x 40 Km^2), were damaged. The investigator attempted to gather stochastic data, which might explain the influence of the soil property and aging of the soil to the scale of failure. As a result he states that a seismic area VI existed in which almost all embankments were damaged seriously, and in seismic area V there wasn't any damage. Further he presents a table which gives relationships between the ratio of failure and the geophysical condition of the base, the soil property of the alluvial deposit and the depth of the alluvial deposit.

I think that such arrangements need more data, such as the scale of the sampling range on the stochastic results and moreover the method in arranging the data gathered at different earthquakes must be established. These are important points of the stochastic arrangement especially for the earthquake problems.

The next example is the slope stability analysis of a river levee damaged during the Niigata earthquake. A slice method is used to analyze the dynamic problem. The river levee (H = 6 m I = 1/2) as located at the left bank of the Sinano river. In selecting the values of c and ϕ, which is the most important procedure in this analysis,a correlation table between N and c, ϕ is used. Supposing that the horizontal and vertical acceleration is 0.14, 0.1 and 0.15, 0.10 respectively, then the safety factor of the sliding was computed as less than 1.0. This static slice method for the dynamic problem, requires numerous solutions, but the vibration test, using the embankment model made of 40 m^3 sand on the large shake table can clearify the validity of this method. Also the Institute of National railway has conducted large scale embankment tests, related to the '68 Tokachioki earthquake damage. In order to reproduce the in-situ failure pattern and analyze the numerical relation and assure the aseimic design of embankment, many tests were conducted.

Data from the Izuhantooki earthquake ('74 M = 6.9), which involved an embankment failure is valuable as its base is hard. In the manual of road construction there is a table giving the standard slope inclination and critical height for each soil property. Where the soil property is classified into five categories these classifications are (1) well graded sand, gravel soil, (2) poorly graded sand, (3) rock or gravel, (4) sandy soil hard clay, (5) soft clay. Computing the C, and Ø using the slice method for each soil gives; C = 1.0 t/m^2 and Ø = 21° 9° 27° 15° 3° respectively. Also for the other soils gives; C = 4 t/m^2 and 37°, C = 3 $t.m^2$ and Ø = 22° and C = 2 t/m^2 and Ø = 7° respectively for III, IV and V soil. The above values can be considered design values, having a safety surplus. Most embankments which failed due to the Izuhantooki earthquake, were made of soil I and the embankment in Nagaturo is the largest, having a 15 m height. Using the above determined C, the Ø stability of the Nagaturo embankment was analyzed. The results give a static state safety factor of 1.66, which became 1.06 under vibration of a 200 gal acceleration, when the maximum horizontal shock acceleration is presumed to be 400 gal.

The research work on liquefaction is advanced in the earthquake area. If we limit the problem to the criteria of liquefaction, we can use various data and get successful results. In the case of perfect liquefaction the soil has no shearing resistance, and thus, the phenomenon is easy to explain. But there is an increasing rate of pore pressure, than there is data.

Recent papers have provided various data concerning soil dynamics. However, little has been done to apply these results to analyze the failure mechanism of earth structures. The gap between knowledge in the laboratory and field practice is surprisingly wide.

As shown previously, the analysis of earth structures damaged by earthquakes has advanced slowly, and there is minimal effort these studies have on the reconstruction and design of new earth structures. The planning and reconstruction of damaged structures, will therefore, not be presented.

4. Reconstruction

In the paper concerning the Kanto earthquake, "the earthquake caused the roads to be closed, but they were opened the next day" is described. How the field engineers were able to provide such service, will now be described.

Due to the '68 Tokachioki earthquake, the National route No. 4, was seriously damaged at Metoki, which is on the border between Aomori and Morioka prefecture. The road embankment (H = 5 m) was constructed on a swamp and between the road and hill there was a pond and another hill opposite to the pond beyond 40 m plain. At the time of the shock movement the body of the embankment crossed the plain and ran toward the opposite hill, and then the pavement fell. The embankment was constructed on a wood frame, usually used in river works as the bearing capacity of the swamp was insufficient. Therefore, the reconstruction work was primarily a problem of drainage. The reconstruction of the road first required the pond to be drained, then the centerline of the road was shifted off the pond area and a large drain pipe was buried under the toe of the slope. Therefore, the stability of the embankment could be improved. However, we can not judge the maximum

Seismic Intensity that the embankment can withstand. It took 2 days for the temporary repair design, 10 days for a complete design, and 60 days for the final construction.

The next paragraph will describe some episode as detailed by a bus driver. He was driving the bus on to the embankment when the earthquake occurred, at which point he went back to the safety area. At that time, the embankment had just failed. At the same time in Hokkaido, one motor car had overturned as the wheel fell into cracks on the road surface. Description of the later cases are given in an investigation report.

Due to the Niigata earthquake, the National route No. 7, was damaged and the Ebigase surface of the road settled and shifted about 4 meters as a result of liquefaction of the base. Traffic was reopened in the same day. Temporarily, reconstruction consisted of filling in of the cracks and settled area to maintain drainage and application of an asphalt coat to prevent dust. The design of the reconstructed pavement used the bearing capacity of the temporary fill as the design value. In such a design, the pavement base property which was liquefied at the shock, was not improved.

Therefore if an earthquake should occur in this area again, the same damage will occur.

Another example of the strengthening of a structure involves the river levee of the Mogami River due to the Niigata earthquake. The usual method of repair is to fill the levee with additional soil to the previous height. However, in this case, the base soft clay material was replaced with good material. This method of reconstruction was tested by experiments in the laboratory, in order to determine how effective this method was against future earthquake shocks.

The greatest change in road occurred during the Izuhantooki earthquake. The original road passed through the bottom of a cliff near the seashore, but during the earthquake this road was completely burried under the collapsed soil. The road was not reconstructed, but a tunnel built instead. The opinion that tunnels can serve not only as roads but also as a shelter against wind and rain is an effective decision. This is because this road and the people living here were always threatened by land slides caused by rainfall and earthquakes. There was no requirement that the repair work must be finished early, therefore enough time was available to discuss the plan of reconstruction.

Another example is the reconstruction of a high embankment which failed in the Ohitachubu earthquake. There were several points to be considered in the planning of this reconstruction. These are that the additional cutting of a hill must be avoided, removement of the collapsed soil from the swamp must be avoided, thin over lays on the slope of the embankment must be avoided and the results of a test boring must be utilized. The detailed plans are as follows; 1) shift the centerline, construct the embankment with a slope having 1/1.5 inclination and build a buttress retaining wall (H=9 m) at the bottom, 2) keep the centerline, and construct the embankment having a well crib wall and construct the bridge. The second proposal was adopted. We can notice here that the plan of execution was the main interest and there was no special attention to earthquakes and thus nothing was attained.

From examination of the above examples, we can understand the principle of how earthquake damage to earth structures are treated. Design methods of earth structures, considering dynamic effects, are not concrete.For field emergencies, the requirement to repair quickly is an important factor in design. And thus the probability of damage to this structure again by some earthquake is overlooked. In the case where failure of the earth structure causes injury to many people and many days repair, it must be designed to withstand greater earthquake shocks.

5. Final Remarks

Examining many principles, it can be concluded that the design of earth structures is not established. Many earth structures have been constructed and have been damaged by earthquakes. Analysis is not sufficient and the requirements for reconstruction have not been consistent.

DYNAMIC TEST OF A CIRCUIT BREAKER FOR TRANSFORMER SUBSTATION

SEIICHI INABA
SHEGIO KINOSHITA
Earthquake Engineering Laboratory
National Research Center for Disaster Prevention
Science and Technology Agency

ABSTRACT

During earthquakes, dependability of electric power supply systems, is required. However, earthquake damage to the electric power industry has resulted from the structural failure of porcelain insulators, which are commonly used for electric transmission equipment.

Dynamic tests of a circuit breaker of capacity 72/84 kilovolts used for a transformer substation was conduced using the large-scale shaking table of the National Research Center for Disaster Prevention in 1975. The test was performed under the sponsorship of Meidensha, a Japanese Manufacturer of electric power equipment. The purpose of the test was to determine the dynamic characteristics of the prototype structure shielded with the porcelain insulator. Sinusoidal waves of resonant frequency and earthquake simulated waves were applied to the test structure. It was found that the failure of the porcelain insulator governs the seismic resistibility of the circuit breaker and the maximum allowable acceleration at the top of the structure is 8.0 g.

Key Words: Circuit Breaker; Data; Experiment; Shake Table; Testing; Transformer.

1. The Objectives

The purpose of the dynamic test was to investigate the earthquake effects of a circuit breaker. The three wave resonance method was applied to the test specimen. The three waves resonance method is a dynamic test procedure which induced three successive waves at the same frequency as that of the resonant vibration of the test structure, then the earthquake resistance is evaluated as defined by the first excursion failure.

2. N-waves Resonance Dynamic Test

Since there are no general input waves during a vibration test, the selection of appropriate input waves is required for each test. Determinate function waves, such as sinusoidal waves or earthquake simulated waves, are used for the test. Resonant vibration of the sinusoidal waves are also used as an earthquake loading. N-waves resonance method gives N cycles of sinusoidal waves at resonant frequency of the structure and provides an observation of the treatment transient state of vibration. The main purpose of the dynamic test is to evaluate the structural failure defined as the first excursion failure, where any deflection, strain, or stress of the structure reaches the fracture

limit due to the dynamic force. While fatigue failure occurs during a stationary state of a structure, the first excursion failure is for the transient state, in which N-waves resonance method is appropriate as the dynamic test procedure for evaluating the first excursion failure.

a) N-waves Resonance Vibration of a Spring-Mass System with Damping

We shall consider here a viscously damped spring-mass system excited by harmonic waves at resonant frequency. The equation of the motion can be written as;

$$\frac{d^2y}{dt^2} + 2h_n w_n \frac{dy}{dt} + w_n^2 y = -\frac{d^2u}{dt^2} \qquad \text{--- 1}$$

$$u(t) = \sin w_n t \quad ; \quad 0 < t < NT_n = 2\pi N / w_n \qquad \text{--- 2}$$

where w_n is the natural frequency in radians per second, h_n is the damping factor, y(t) is the relative displacement and u(t) is the foundation displacement. The solution is expressed as

$$\frac{d^2y}{dt^2} = \frac{w_n^2}{2h_n} \cos w_n t - \frac{w_n^2 D_n}{2} \sin\left(w_n (1-h_n^2)^{\frac{1}{2}} t + \theta_n \right) \exp(-h_n w_n t) \qquad \text{---3}$$

where D_n, and θ_n are written as

$$D_n = 1/(h_n(1-h_n^2)^{\frac{1}{2}}) \ , \quad \theta = -\tan^{-1}((1-h_n^2)^{\frac{1}{2}}/h_n) \qquad \text{---4}$$

The maximum response, in terms of acceleration amplification during N-waves of resonance vibration, is;

$$A_N(h_n) = \frac{1}{w_n^2} \left| \frac{d^2y}{dt^2} + \frac{d^2u}{dt^2} \right|_{max} \qquad \text{---5}$$

For the stationary state of resonant vibration,

$$A(h_n) = \left(\frac{1+4h_n^2}{4h_n^2} \right)^{\frac{1}{2}} \qquad \text{---6}$$

Computed values of $A_N(h_n)$ are shown in Fig. 1.

b) Analysis of the Porcelain Insulator

A circuit breaker is constructed with a frame and a porcelain insulator, which is divided into two parts the breaker insulator and the supporting insulator. An analytical model of a continuous system is shown in Fig. 2 where the equation of vibration excited by the harmonic motion is written as,

$$\frac{\partial^2 y}{\partial t^2} + k^2 b^2 \frac{\partial^4 y}{\partial x^4} = -\frac{\partial^2 u}{\partial t^2} \ , \quad u(t) = \sin w_n t \qquad \text{---7}$$

where u(t) is the motion at x = 0, y(x,t) is the relative motion of the system, k is the inertia radius of the section, and $b^2 = E/\rho$. E is Young's modulus and ρ is the density. The frequency equation is given as,

$$1 + \cos m \cosh m = 0 \qquad \text{---8}$$

and the natural circular frequency is written in terms of solution m_j as,

$$w_j = kb(m_j^2/l^2) \ , \ j=1,2,3,\cdots \qquad \text{--- 9}$$

the normal function at $m = m_j$ is

$$v_j(x)=\cos\frac{m_j}{l} x - \cosh\frac{m_j}{l} x - \frac{\cos m_j+\cosh m_j}{\sin m_j+\sinh m_j}\left(\sin\frac{m_j}{l}x - \sinh\frac{m_j}{l} x\right) \text{---10}$$

and the solution of equation 7 is

$$y(x,t) = \sum_{j=1} v_j(x)\, q_j(t) \qquad \text{--11}$$

where $q_j(t)$ is the generalized coordinates. The equation of nth mode is equivalent to the motion of a one-degree-of-freedom spring-mass system with viscous damping which is written as,

$$\ddot{q}_n + 2h_n w_n \dot{q}_n + w_n^2 q_n = - \beta_n \ddot{u} \qquad \text{---12}$$

where β_n is the participation factor and it is written as,

$$\beta_n = \int_0^1 v_n(x)\, dx / \int_0^1 v_n^2(x)\, dx \qquad \text{---13}$$

Therefore, the amplification factor due to the N waves resonance excitation is given as,

$$v_n(x)\beta_n A_N(h_n) \qquad (0 \leq x \leq 1) \qquad \text{---14}$$

Table 1 shows the participation factor ρ_j (j=1,2,3,...), and the normal function v_j(j=1, 2,3,...) is given in Fig. 3. Considering these results, the bending moment of the system for the 1st mode of vibration is written as,

$$M(x,t)= EI\frac{\partial^2 y(x,t)}{\partial x^2} = EI\frac{d^2 v_1}{dx^2} q_1 = \frac{EIm_1^2}{l^2} v_1(1-x)\, q_1 \qquad \text{--- 15}$$

where v_1 is maximum at x=1, and M(x,t) is the maximum at x=0, then

$$M_{max} = M(0,t) = \frac{E I m_1^2}{l^2} v_1(1)\, q_1 \qquad \text{--- 16}$$

Therefore M_{max} is proportional to the relative displacement at the top of the porcelain insulator, and stress and strain will be given as,

$$\sigma(x,t) = M(x,t)/ Z(x) , \quad \epsilon(x,t) = \sigma(x,t)/ E \qquad \text{--- 17}$$

3. Dynamic Test of the Circuit Breaker

Vibration tests on the shaking table were conducted in order to observe the dynamic response of the structure, and also possible leakage of the air-pressure and defects in the equipment. The equipment was tested before and after the table excitation. No functional deficiency was found even after loading up to the acceleration of 0.3 g, was applied.

a) Test Structure

The test structure was a circuit breaker of 72/64 kilovolts and 1200 ampere which was constructed with a frame and a porcelain insulator as shown in Fig. 4. The porcelain insulator is composed of an upper breaker insulator and a lower supporting insulator. The insulator of each phase has dimensions of 2.2 m in height and 900 kg of weight and composed of porcelain. The lowest end of the supporting insulator has a larger diameter in order to increase its strength and is cemented and bolted to the frame structure. Therefore, the maximum stress of the insulator is measured at the second fold from the lowest end, where the critical strain related to the first excursion failure can be observed.

The result of the static test shows that the critical strain for failure is 780×10^{-6} ($= \varepsilon_o$), and the static allowable stress is 5.85 kg/mm^2 since the Young's modulus of porcelain is 7500 kg/mm^2. Insulators of each phase are called A, B, and C phase insulator respectively. For the test on the shake table, the supporting frame was bolted to a steel panel and the panel was fixed to the shake table with bolts.

b) Instrumentation and Measurement

Two horizontal excitation directions were chosen for the test as given in Fig. 4, and are named short axis test and long axis test. Accelerations and strains of the porcelain insulator were measured using accelerographs and strain gages as shown in Fig. 4, in which points of G_1 - G_8 are the accelerographs and points of S_1 - S_{17} are the strain gages.

c) Vibration

Harmonic excitation of sinusoidal waves in the frequency range between 0 Hz and 10 Hz , which cover the frequency range of earthquake waves, were induced to find the frequency characteristics of the system including the support frame and to decide the test frequency during three waves of vibration. Before the harmonic oscilation , the table was driven by an instantaneous step displacement of 0.5 mm in order to induce the free

vibration of each phase insulators and to decide the approximate natural frequency and damping factor. Then the sinusoidal wave, at the acceleration level of 0.03 g, was applied to the structure until the stationary response was observed at each frequency. This wave function was changed between 1 Hz and 10 Hz by the pitch of 0.2 Hz near the resonance. These harmonic excitations were applied in two directions as mentioned previously.

The Meidensha, the manufacturer of the circuit breaker, was primarily interested in the three waves resonance vibration test. Resonant frequency was defined as the frequency where the maximum amplification was measured in terms of the acceleration at the top of the porcelain insulator compared to the table acceleration.

Three successive sinusoidal waves at resonance frequency f_n, and also at the frequencies of $f_n \pm 0.2$ Hz, were applied to the specimen at the acceleration level of 0.3 g. Two directions of excitation were used and the equipment states for breaker-on stage and for breaker-off stage were tested.

Normal white noise input waves at the level of 0.05 g for 30 seconds and the simulated earthquake waves of El Centro 1940 N-S direction were also induced for the dynamic test.

4. Test Result and Discussion

The supporting frame and the porcelain insulators of the circuit breaker are physically coupled but they are considered to be structurally independent. However, when considering the earthquake effects on the system the porcelain insulators are more important than the frame.

a) Natural Frequency and Damping Factor

The damping factor and natural frequency of the insulator can be obtained from the analysis described in Section 2. From the dynamic test results the natural frequency of first mode is approximately 9 Hz in the long axis direction and 6.8 Hz in the short axis direction, and a damping factor of approximately 0.02. The natural frequencies of higher modes are given as

$$F_j = (m_j/m_1)^2 F_1 \qquad \text{---18}$$

The natural frequency of the second mode F_2 is 56 Hz, therefore, the vibration of first mode is important as the frequency range agrees with that of earthquake.

b) Acceleration of the Porcelain Insulator

The maximum acceleration of the insulator, due to the N waves resonance vibration of first mode, is

$$G_N(x,h_1,U) = v_1(x)\cdot\beta_1\cdot A_N(h_1)\cdot U \qquad \text{---19}$$

where U is the amplitude of the input acceleration, $A_N(h_1)$ is obtained from Fig. 1, and $v_1(x)$ is calculated from equation 10. Fig. 5 shows the maximum acceleration at N=3,

h_1=0.02, x=1, and the test results of G_2 and G_8. Even though the input frequency of the table is not the same as that of the frame, and the initial condition of excitation is not exactly the same as that of the analysis, results shown on Fig. 5 can be used as the criteria for the maximum acceleration at the top of the insulator.

c) First Excursion Failure

We consider the first excursion failure in terms of strain, where the strains were measured during dynamic tests. Maximum strains are observed at the second porcelain fold from the bottom and proportional to the relative motion at the top of the insulator.

The linear relationship between the maximum strains and the measured acceleration at the top was found from the dynamic tests, as shown in Fig. 6 and Fig. 7. The equation for this relationship is written as;

$$S \text{ (maximum strain)} = 100x\ 10^{-6} x\ G \text{ (maximum acceleration)} \qquad \text{---20}$$

Equation 20 is confirmed for the maximum strain of 570 x 10^{-6} from the test and the maximum fracture strain determined from the static test is 780 x 10^{-6}. Assuming that the equation 20 is valid for the strain of 780 x 10^{-6}, the first excursion failure will be induced at the acceleration of 8.0 g at the top of the insulator.

d) Earthquake Resistance of the Porcelain Insulator

We consider that the earthquake resistance of the porcelain insulator governs the entire system of the circuit breaker. The equation of first excursion failure determined from the N waves resonance vibration of the first mode is written as

$$G_N(1,h_1,U)=v_1(1)\beta_1 \cdot A_N(h_1) \cdot U = G_0 \qquad \text{---21}$$

where G_o is assumed to be 8.0 g from the test results. Since then the safety factor at the three waves resonance vibration for the input acceleration of U will be written as,

$$P_3(U) = G_o / (v_1(1) \cdot \beta_1 \cdot A_3(h_1) \cdot U) \qquad \text{---22}$$

Fig. 8 and Fig. 9 show the relationships between the safety factor $P_3(U)$ and the input acceleration of U. Fig. 10 shows the relationship between the safety factor $P_N(U)$ and the number of waves of resonant frequency of the first mode at the input acceleration U = 0.3 g, assuming h_1 = 0.02.

e) Seismic Effects on the Circuit Breaker

The main purpose of the dynamic test was to evaluate the effects of the earthquake vibration on the circuit breaker, including the porcelain insulator and supporting frame. The safety factor of the breaker obtained from the test is given as the following, where

the maximum strain of the support insulator at second fold is $\varepsilon_3(U)$,

$$Q_3(U) = \varepsilon / \varepsilon_3(U) \qquad \text{---23}$$

The test data of $Q_3(U)$ assuming $U = G_1$ are plotted on the Fig. 8 and Fig. 9. It was determined that the safety factor ($P_3(U)$ can be used as a more conservative criteria than that obtained from test data $Q_3(U)$ of the circuit breaker, we can then evaluate the seismic resistance of the circuit breaker on the bases of this criteria given from three waves resonance vibration test.

f) Earthquake Wave Test

Earthquake simulating waves of El Centro 1940 N-S direction were applied to the test structure. The maximum strains are approximately 40% of the three waves resonance vibration test in long axis direction, and 70% for the short axis direction. The three waves resonance test seemed to give conservative criteria for practical design compared to the earthquake simulating wave test.

5. Conclusions

Conclusions of the dynamic test of the circuit breaker are summarized as follows;

1. The allowable acceleration at the top of the porcelain insulater, related to the first excursion failure, is 8.0 g.

2. The maximum allowable input acceleration to the circuit breaker is greater than 0.6 g, where the safety factor equals unity.

3. The number of successive sinusoidal waves at resonance is more than 9, based on an assumption that the safety factor equals unity and the input acceleration is 0.3 g.

4. Acceleration of the strain response, due to a simulated earthquake, is less than the 70% of the maximum acceleration or strain observed for the three waves resonance vibration test at an input acceleration of 0.3 g.

Acknowledgments

Considerable assistance was received from other members of the Earthquake Engineering Laboratory, National Research Center for Disaster Prevention. In particular, Mr. Nobuyuki Ogawa and Mr. Chikahiro Minowa for arranging the input waves, and Mr. Haruo Iida and Mr. Takeshi Kubota in operating the large-scale shake table during the dynamic test. Additional assistance was received from Dr. Takeo Kinoshita, Head of the Large-scale Testing Division, National Research Center for Disaster Prevention. This project was a research program sponsored by Meidensha.

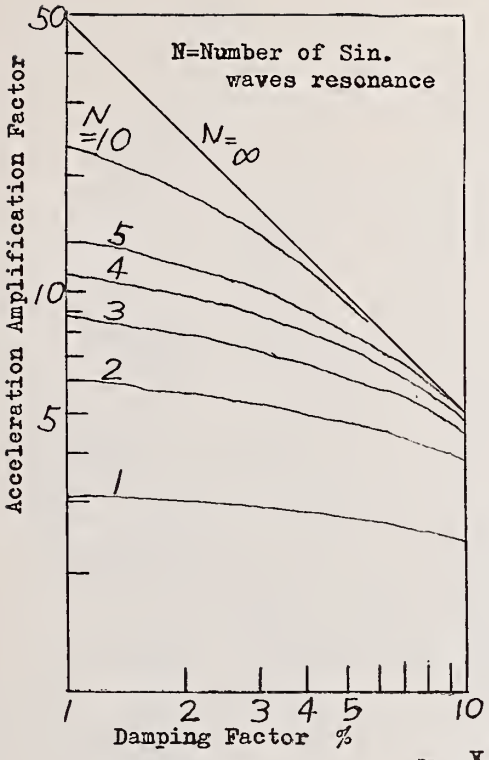

Fig. 1

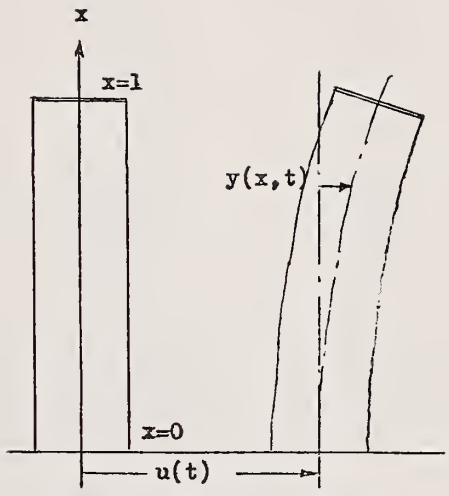

Fig 2 Model of Insulator

Table 1
Participation Factor β_j

j	m_j	β_j
1	1.8751	-0.87
2	4.6941	-0.43
3	7.8548	-0.25
4	10.9955	-0.18
5	14.1372	-0.14

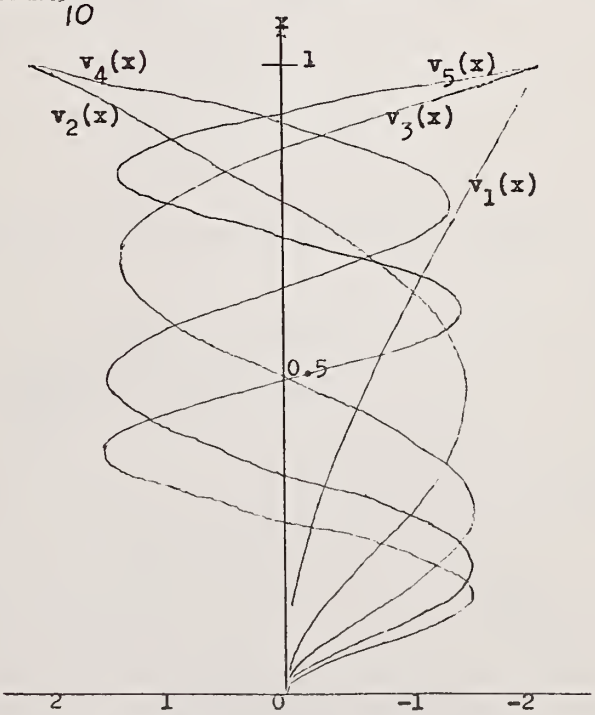

Fig. 3 Normal Function $V_j(X)$

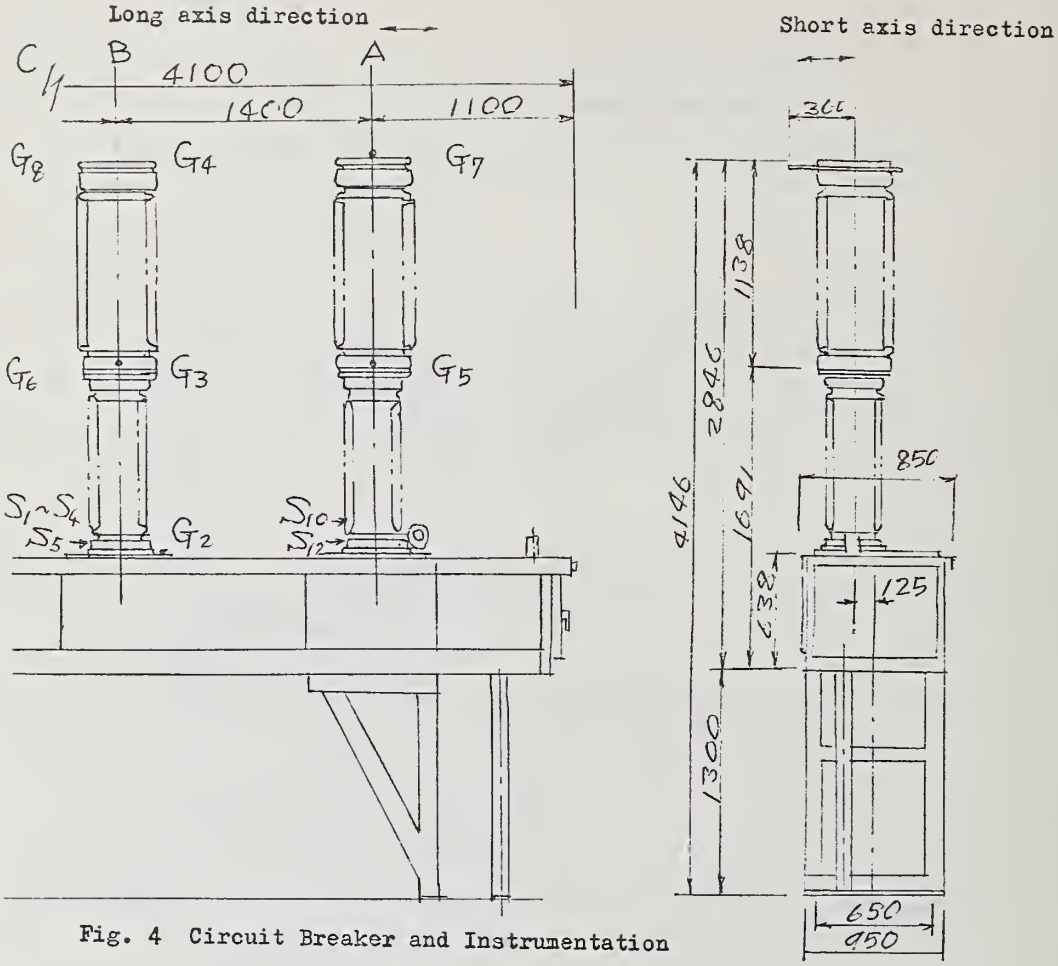

Fig. 4 Circuit Breaker and Instrumentation

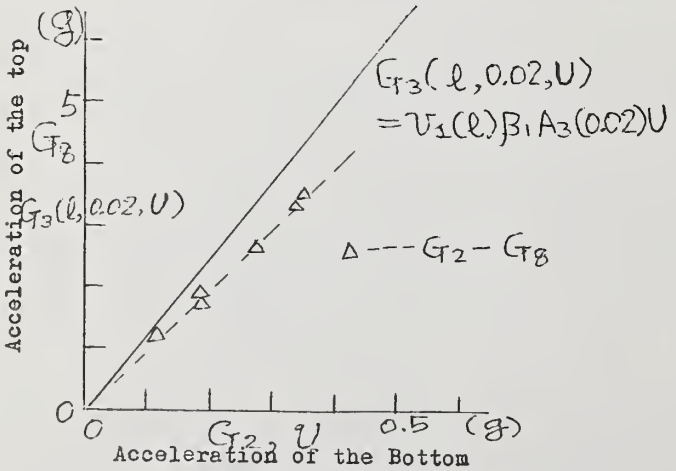

Acceleration of the Bottom

Fig. 5

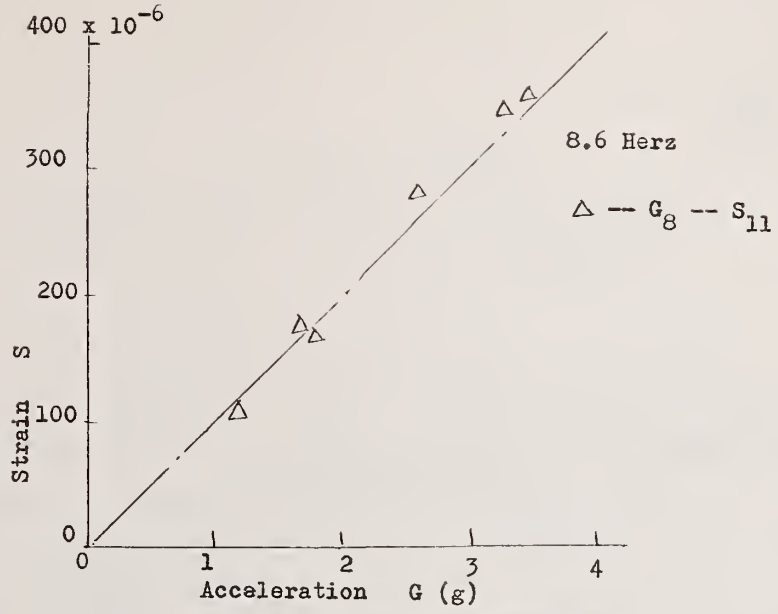

Fig. 6 Long Axis Direction

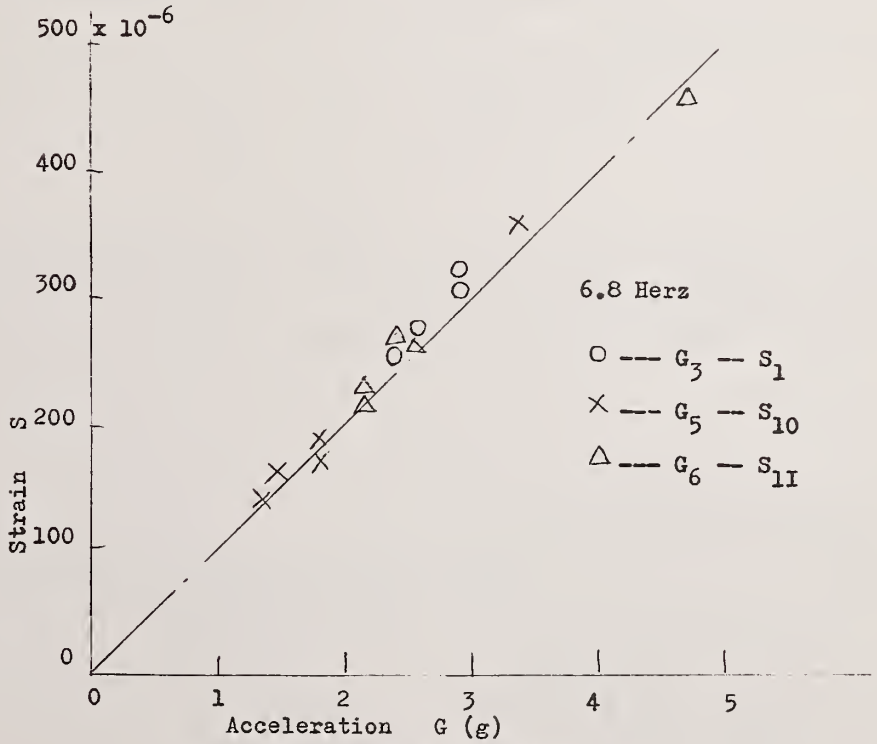

Fig. 7 Short Axis Direction

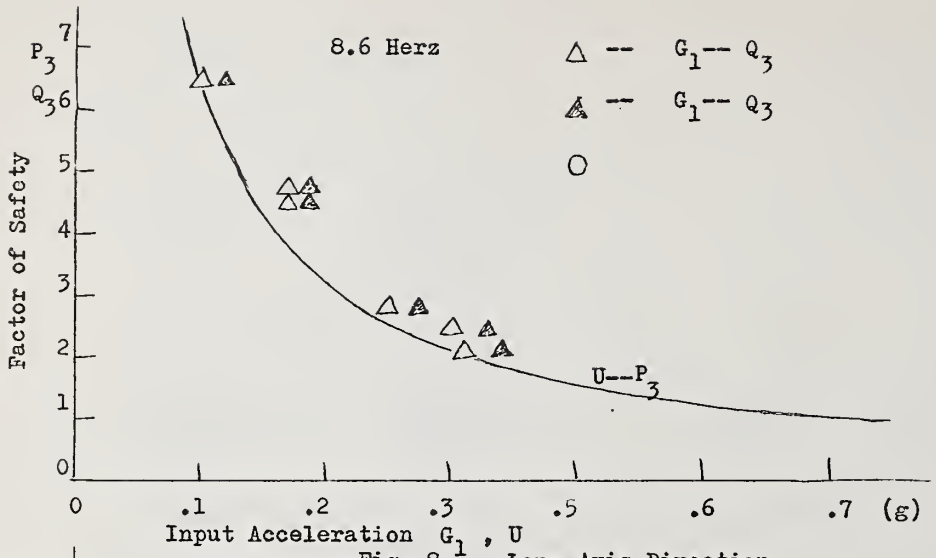

Fig. 8 Long Axis Direction

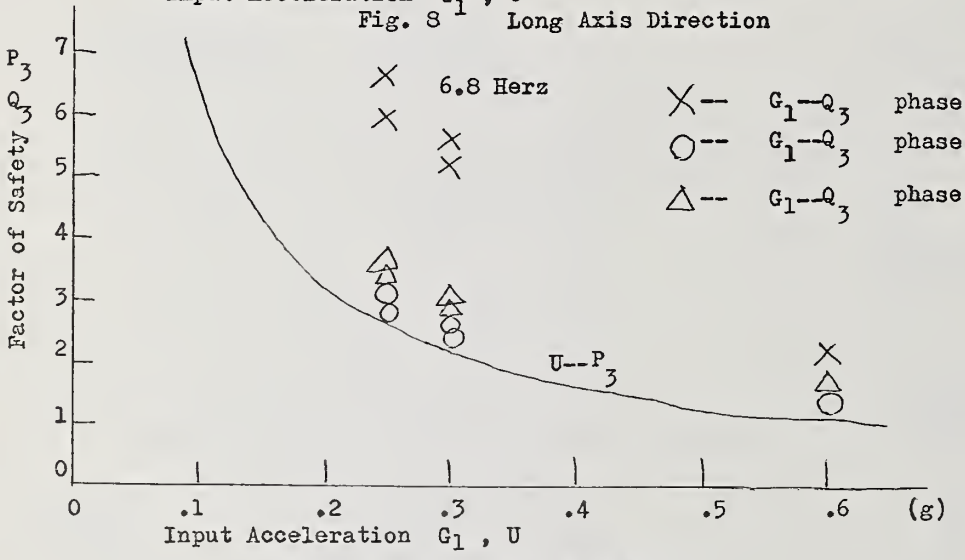

Fig. 9 Short Axis Direction

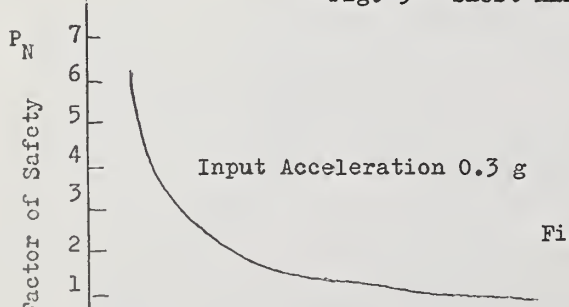

Fig. 10 Factor of Safety and Number of Waves of Resonance

COMPREHENSIVE SEISMIC DESIGN PROVISIONS FOR BUILDINGS
A STATUS REPORT

BY

CHARLES G. CULVER

National Bureau of Standards, Washington, D.C.

A review of the first draft of recently developed U.S. seismic design provisions for building is presented. The draft includes regulatory provisions suitable for inclusion as part of a building code and technical criteria for earthquake resistant design. The provisions are intended for implementation by standards organizations, model code groups, Federal agencies and other regulatory groups. Technical criteria for structural design, architectural and mechanical-electrical design, and existing buildings are discussed.

KEY WORDS: Buildings; building codes; design; earthquakes; structural engineering.

INTRODUCTION

In 1974 the National Science Foundation and the National Bureau of Standards, as part of the Cooperative Federal Program on Building Practices for Disaster Mitigation, undertook a project with the Applied Technology Council of the Structural Engineers Association of California to develop comprehensive nationally applicable seismic design provisions for buildings. It is intended that these design provisions be national in scope and reflect the current state-of-the-art in earthquake engineering in a form adaptable for implementation by standards organizations, model codes, Federal agencies and other regulatory groups. Approximately 90 professionals from throughout the United States representing the design professions, the university research community, and regulatory groups including the model codes and state and local building officials are participating in developing these provisions.

The development and organization of this activity were discussed at the Sixth Joint UJNR Panel meeting in May 1974 (1). In January of 1976 a first draft of the provisions (2) was circulated to professional organizations, trade associations, standards groups, Federal agencies and professionals throughout the United States soliciting their comments. The purpose of this paper is to briefly review this first draft. Since many of the provisions are still under study and specific requirements may change as the work proceeds, the review will only deal with overall concepts.

SCOPE AND ORGANIZATION

The provisions are comprehensive in nature and deal with earthquake resistant design of the structural system, architectural and non-structural elements and mechanical-electrical systems in buildings. Both new and existing buildings are included. The design provisions are presented in two parts: (1) Regulatory Provisions, and (2) Technical Criteria. The Regulatory Provisions are presented in the form of a short, legal document written in mandatory non-technical language suitable for inclusion as part of a building code. The technical criteria or recommendations for the design and construction of earthquake resistant buildings represent acceptable standards of practice and are intended for inclusion in design standards and materials specifications.

STRUCTURAL DESIGN

Three alternate procedures are presented for determining the seismic loads which the structural system must be designed to resist. Moments, shears and axial forces produced by these loads are to be determined using an elastic analysis. Selection of the procedure for determining the seismic loads is based on the type of facility or building use and the expected ground acceleration. For the majority of buildings in the United States located in areas where the ground acceleration in a 50 year period would not be expected to exceed 0.05g, the first or least rigorous procedure would be used. Except for buildings with large differences in stiffness or lateral

resistance between adjacent stories or unusual structural features, seismic forces for the remaining buildings would be determined using a procedure referred to as the equivalent lateral force procedure. For the remaining buildings, a modal analysis is required.

The equivalent lateral force procedure is similar to that currently used for design in the United States (3). The total lateral seismic design force or base shear is related to: (1) geographic location of the building, (2) soil conditions, (3) the type of structural system, (4) the period of the building, and (5) type of facility or building use. The design ground motion is described by a smoothed response spectra normalized to an "effective peak acceleration" or EPA. Values of EPA corresponding to a 75% to 95% probability of non-exceedence in a 50 year period are presented in the form of a contour map for the contiguous United States, Alaska and Hawaii. Using the contour map, an acceleration for use in design may be determined for a given geographic location.

The design acceleration is modified by a soil factor. Discrete values for the soil factor are defined in terms of the soil characteristics. Detailed site investigations are not required to establish these characteristics.

The design acceleration is further modified by a building response factor. This factor is defined in terms of the characteristics of the vertical and lateral load resisting systems and the horizontal system used to distribute the seismic forces to the lateral load resisting system. The factor is analogous to the current K factor (3) and is

intended to account for the type of performance to be expected from various systems.

The variation of design force as a function of building stiffness is accounted for through use of the building period. Approximate formulas, different from those currently specified in design codes, are given for determining this period. The formulas are expressed in terms of the dimensions of the building and the material used for the lateral load resisting system.

The use of the building also affects the design acceleration. Higher values are used for essential facilities or buildings which are required to be functional in the immediate post-earthquake period.

Numerous additional requirements related to design of the structural system are included in the provisions. Soil structure interaction, the distribution of seismic forces through the height of the building, torsion, overturning, vertical motions, interstory drifts and second order effects due to large displacements are included.

ARCHITECTURAL AND MECHANICAL-ELECTRICAL DESIGN

The provisions dealing with the design of architectural or nonstructural elements and mechanical and electrical equipment and components represent the greatest departure from current practice in terms of their scope. Under the new provisions, many building com-

ponents and systems not currently considered in the seismic design will need to be designed for specified seismic forces. These requirements reflect the increased concern for the need to design these items in view of observations following recent earthquakes.

Formulas for the design forces are given in much the same form as current requirements for parts or portions of buildings. The force levels for architectural components and their connections are specified in terms of performance levels which are in turn related to the type of facility and the potential hazard associated with failure of the component. Deformation limits for these components and considerations related to anticipated interstory drifts are given.

EXISTING BUILDINGS

The provisions for existing buildings consider evaluation of the potential seismic hazards associated with these buildings and emergency safety evaluations for post-earthquake use. For existing buildings, procedures are given for establishing priorities to select the buildings for evaluation. A two step evaluation procedure employing an initial examination of the design and construction documentation and an inspection of the building followed by an analytical evaluation is employed. In the analysis, the current lateral load resisting capability and the strength of non-structural components are compared with those required for new construction to provide a basis for determining the need for hazard abatement. The analysis is also used to

determine the time period within which any hazard abatement must be accomplished.

CONCLUSIONS

The first draft of the provisions includes a number of departures from current practice. Attempts have been made to reflect the current state-of-the-art. In some cases, such as architectural and non-structural elements and mechanical-electrical equipment design, they represent a significant increase in scope over current design requirements.

It is anticipated that the review of this first draft will identify areas for improvement. The review should insure that the final recommended design provisions to be issued in about a year are practically viable and represent a significant step toward improved earthquake resistant design.

REFERENCES

1. Culver, Charles G., "Comprehensive Seismic Design Provisions for Buildings," Wind and Seismic Effects, NBS Special Publication 444, (Proceedings of the Sixth Joint UJNR Panel Conference), April 1976.

2. Working Draft of Recommended Comprehensive Seismic Design Provisions for Buildings, Applied Technology Council, San Francisco, California, January 31, 1976.

3. Uniform Building Code Standards, 1973 Edition, International Conference of Building Officials, 5360 South Workman Mill Road, Whittier, California.

RETROFITTING OF VULNERABILITY IN EARTHQUAKE DISASTER MITIGATION PROBLEMS

KAORU ICHIHARA
Director, Public Works Research Institute

EIICHI KURIBAYASHI
Ministry of Construction, Japan
Earthquake Engineering Section

TADAYUKI TAZAKI
Ministry of Construction, Japan
Earthquake Engineering Section

ABSTRACT

This paper discusses a criterion for retrofitting of existing structures vulnerable to disastrous earthquakes.

It would be ideal if all structural damage could be avoided during earthquakes, however, to completely strengthen structures is not practical because of the limitation of resourses and land-space. On the basis of execution,it is necessary to classify the structures by functional importance and structural vulnerability. The first category of classification deals with the structure load. In the category dealing with the location, the densely inhabited and effectively utilized structure, should have preferential earthquake resistance, and this consideration is the basic philosophy of urban design including the countermeasure to earthquakes. The second category is classified according to the purpose of the structure. Life lines, such as traffic, transportation, water and energy transmission, and communication are indispensable during evacuation and rescue, so that these structures would be required to retain safety. This is especially true for roads, which are used not only for a path of evacuation but also for rescue space, fire fighting etc. immediately after earthquakes. However, it seems impossible that all existing roads can be modified to such a high standard of earthquake resistance because of the extreme cost involved. It is therefore more practical and rational to select the important routes which should be modified to meet specific earthquakes.

In this situation the following principles have been chosen in the retrofitting and the vulnerability for such a decision-making process.

If given certain model routes, retrofitting costs can be obtained for several methods, for example,perfect, medium and rough, for which the retrofitting cost should not be more than the cost of reconstruction. Next, suitable load-retrofitting relations and suitable load-safety relations are examined..... Using these quantitative results a final decision can be made.

Key Words: Costs; Existing Structures; Optimization; Retrofitting; Seismic.

1. Introduction

Due to progressive earthquake resistant design criteria, it is possible to design and construct various structures resistant to earthquake effects. However, with some exceptions, no one knows multilateral earthquake resistivities. Also immediately after earthquakes, continuity between rescue, transportation, communication, energy supply and circulation of water should be retained.

Concerning the above, this paper discusses the basic principle planning methodology for appropriate selection of structures for retrofitting corresponding to those of some vulnerability and for considerable assessment of the difference between reasonable capacity required and actual capacity of the structure in an earthquake.

Generally greater retrofitting is required for more earthquake resistivity, but perfect earthquake resistivity requires an infinite amount of investment to retrofit. It is not practical to make such an investment, because of the limitation of resources and land space. Therefore, an optimum amount of investment should be evaluated relative to the physical and socio-economic conditions. This of course requires consideration of the loss of human life and the decrease of the functions of the various structures.

2. Methodology of Selection

The criteria in selecting the structures to be retrofitted, consist of selection of various physical and socio-economic conditions. The items to be examined in selection of the structures are shown in Table 1. An example of the relationship between a structure, durability, and its physical conditions are given in Fig. 1.

Initially a method for retrofitting is determined. This is based on the retrofitting costs by several methods, which are not more than the cost of reconstruction. The capable load-retrofitting cost and the capable load-safety are examined. Using these quantitative results a final decision can then be made.

The next chapter described one method to evaluate the optimum amount of investment, considering only the physical conditions.

3. An Optimization of Initial and Running Costs of Structures Taking into Account the Probability of Failures Caused by Earthquakes

a) Assumptions

To optimize initial and running costs of structures, taking into account the probability of failure caused by earthquakes, the following is assumed relative to the physical conditions with respect to the probability of failure and expenditures;

1. Future earthquake intensities and recurrences can be estimated from trends of past earthquakes.

2. Probability of failure due to earthquakes can be obtained from existing information.

3. Earthquake resistances of individual structures can be obtained from codes and regulations.

4. Total costs consist of the cost of construction, retrofitting and loss of failure.

b) Principle in Determining the Safety of Structures in Earthquakes

Let R and S be the resistivity and the intensity of load. The probability P that structures will become limit states is given by Eq. (1);

$$p \equiv Pr\left[R<S\right] = \int_0^\infty F_R(x)\ f_s(x)dx \qquad (1)$$

where Pr [R<S]: probability of R<S

$F_R(x)$: cumulative distribution function of R

$f_x(x)$: random variable of S

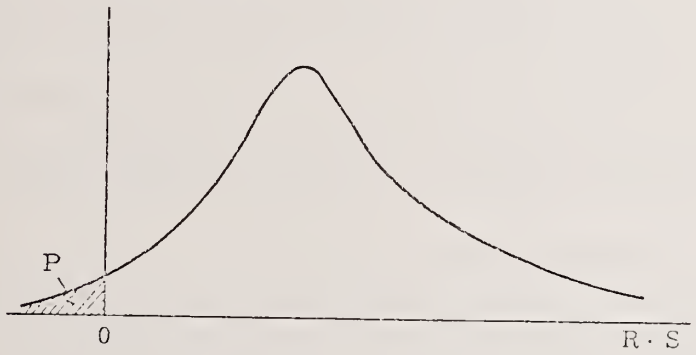

In the case of earthquake, let $f_{s(x)}$ be a random variable of maximum earthquake intensity in a year and $F_{R(x)}$ be a cumulative distribution function of the mean quake-resistivity in a year. The cumulative probability of failure of a structure during its life is therefore;

$$U_D = 1 - \prod_{t=1}^{T_D} (1 - p) \qquad (2)$$

U_D: cumulative probability of survival

T_D: durable life

If p is a constant during the life, eq. (2) can be written as;

$$U_D = 1 - (1 - p)^T \qquad (2)'$$

The assumption (b) given in a) means that;

$$U_D = U^* \qquad (3)$$

where U* represents social needs for safety during an earthquake.

Therefore the structures must be designed so satisfy eq. (3). However, existing structures, with low quake-resistivity and impossible structures to retrofit and thus satisfy eq. (3). In these cases (T_D - T), where T equals the served lives, can be substituted instead of (T_D) into eq. (2), which considers the fact that the existing structure will fail. This thought can be written as;

$$U = 1 - \prod_{t=1}^{T_D - T} (1 - p) \tag{4}$$

$$U = U^* \tag{5}$$

In Fig. 3 if the resistivity R of a structure A at time T corresponds to the constant level of cumulative probability, then structure A is safe. Structure B has also adequate safety because of a decrease of cumulative probability. Structure C needs to be retrofitted because the resistivity decreases more than A and the cumulative probability exceeds U*. To adopt this criteria, the initial resistivity R_0 is not required for retrofitting, but R_2 which brings cumulative probability U* during its residual life (T_D - T) is sufficient.

Now, let the total cost of a structure during its durable life be defined as follows;

$$C = C_C + C_R + C_F \tag{6}$$

where C : total cost of a structure
C_C: cost of construction
C_R: cost of retrofitting
C_F: loss of failure

Supposing that C_C depends only on the cumulative probability, C_C becomes

$$C_C = C_{CO}(1 - c \log U_0) \tag{7}$$

C_{CO}, C: constant
U_O: cumulative probability assuming that a structure is not retrofitted during its useful life (a structure without retrofitting $U_O = U_D$)

Suppose that the cost to retrofit a structure from quake-resistivity R to (R + Δ) is proportional to the difference between the cost of construction of R and (R + ΔR), then C_R becomes

$$C_R = \alpha \sum^{N} \left\{C_C(R + \Delta R) - C_C(R)\right\} \tag{8}$$

α: constant

N: number of times of retrofitting

$C_C(R + \Delta R)$, $C_C(R)$: cost of construction of $(R + \Delta R)$ and R

The cost of failure (C_F) will be divided into an independent part of the cumulative probability, such as the indirect losses of failure, and a dependent part on cumulative probability such as the cost of repair and reconstruction. Therefore, C_F becomes

$$C_F = \left\{C_{F0} + m\, C_{C0}(1 - c \log U_0)\right\} U_D \tag{9}$$

C_{FO}, m: constant

Under the conditions of equations (7) through (9), the total cost C should not be minimized.

c) Examples

Initially the social needs for safety during earthquake need to be given. Table 2 shows the number of destroyed bridges, after the Kanto earthquake (1923). In (1964) the Niigata earthquake it was reported that there were three bridges destroyed and 13 others damaged bridges, which had lengths longer than 20 m [9]. Accordingly the total number of bridges destroyed or functionally damaged during the Niigata earthquake can be estimated as

$$(3 + 13) \times \frac{4014 \text{ (Total Number of Bridges in Niigata Pref. in 1964)}}{609 \text{ (Number of bridges longer than 20 m)}}$$

$$= 107$$

The total number of the bridges destroyed or functionally damaged the after Kanto earthquake is estimated as;

$$22 \times \frac{107}{3} = 785$$

The increase in the number of bridges on the principal roads (national highways, prefectural roads and principal municipal roads) in Japan after 1948 is shown in Table 3. The increase after the Kanto earthquake is therefore estimated as given in Fig. 4. The average number of bridges after 1923 was 90040. Using the value 0.24, that is the ratio of the number of bridges on principal roads to that of total roads, the total number of bridges from 1923 becomes

$$90\ 040 \div 0.24 = 375\ 000$$

The cumulative probability converted to a useful life of 50 years, becomes

$$\frac{785}{375\ 000} \times \frac{50}{51} = 2.1 \times 10^{-3}$$

In this example U* is assumed to be 2.1×10^{-3}. As shown by eq. (1), the probability p is dependent on both the quake-resistivity R and the intensity of the load S, however, it is difficult to evaluate R; therefore it is assumed that R has no deviation but has a certain value and p is dependent only on S. Generally, the relationship between the earthquake intensity I_{JMA} and the probability p, which means the probability that an earthquake exceeding I_{JMA} occurs in a year, is well known and is as follows

$$\log p = \theta - \gamma I_{JMA} \qquad (10)$$

θ γ : constant

I_{JMA}: earthquake intensity of Japan Meteorological Agency

Applying the data given in the report of Katayama (12), $\theta = 3.24$ and $\gamma = 0.87$ for Tokyo is determined. (Fig. 5) The relationship between I_{JMA} and response I_B observed for road bridges is reported as (13)

$$I_B = \begin{cases} 2 \log \left\{ 0.528 \times \left(\frac{0.253}{1000} \times 10^{0.5 I_{JMA}} \right)^{\frac{1}{2}} \times \frac{1000}{0.253} \right\} \\ 2 \log \left\{ 0.264 \times \left(\frac{0.800}{1000} \times 10^{0.5 I_{JMA}} \right)^{\frac{1}{2}} \times \frac{1000}{0.800} \right\} \end{cases} \qquad (11)$$

Where the first equation corresponds to the earthquake of higher mangitude and the second equation of smaller magnitude. Using the average of both, eq. (11) becomes;

$$I_B = 0.5 I_{JMA} + 2.49 \qquad (11)'$$

Inserting p, which corresponds to the cumulative probability U_D of 2.1×10^{-3} given in eq. (2) into eq. (10) and inserting I_{JMA} to eq. (11), I_B equals 6.87. Thus if a structure has an initial quake-resistivity of $R_O = 6.87$, and the quake-resistivity is not changed during its life, the cumulative probability of 2.1×10^{-3} is ensured. In general practice, however, bridge quake resistivities are decreasing because of the decrease of the stength of materials, corrosion and fatigue. (Fig. 1) In this example the quake-resistivity at the end of a useful life is assumed as 75% of the initial value. The quake-resistivity

R(t), at time t, is assumed as;

$$R(t) = 1.012 \log (50 - t) + 5.15 \qquad (12)$$

based on $R_{t=0} = 6.87$ (Fig. 6)

The coefficients in eq. (7) through (9) can now be estimated. The constant c, in eq. (7), is independent of the cumulative probability and the value (c = 0.041) introduced into the reinforced concrete problems (8) is used herein. For example most typical bridges as of 1973, have a length of 30 m, width of 8 m, area of 240 m^2. The estimated cost of such a bridge, based on the assumption that the bridge has a cumulative property of 2.1×10^{-3}, will be;

$$C_{C0} = \frac{60000 \text{ (average cost of superstructure per unit area for 30 m span)} \times 240 \div 0.6 \text{ (ratio of cost of superstructure to that of the total bridge)}}{1 - 0.041 \log 2.1 \times 10^{-3}} = 2.16 \times 10^{7} \text{ (yen)}$$

Inserting $C_C(R + \Delta R)$ and $C_C(R)$ calculated by eq. (8) into eq. (7),

$$C_R = \alpha C_{C0} c \sum^{N} (\log U_R - \log U_{R+\Delta R})^{\gamma} \qquad (13)$$

where U_R and $U_{R+\Delta R}$ are the cumulative probabilities having quake-resistivity of R and R + ΔR during their residual lives. This value is the ratio of the cost of retrofitting to that of construction and the former exceeds the latter because of the scale merit and temporary conditions, therefore $\alpha = 2$ will be assumed.

It is assumed that C_{FO} in eq. (9) consists only of indirect losses, and is determined according to the ratio of indirect losses to direct losses as reported for the Niigata earthquake;

$$C_{F0} = \frac{122.1 \text{ billion yen (indirect losses)}}{130.0 \text{ billion yen (direct losses)}} \times C_{C0} = 2.12 \times 10^{7} \text{ (yen)}$$

The value m is assumed as 1.0

Substituting R for I_B in eq. (11) and inserting into eq. (10) gives;

$$p = 10^{7.57 - 1.74R} \qquad (14)$$

where R is given by eq. (12). Thus cumulative probability of the structure, for which the initial quake-resistivity if $R + \Delta R_1$, during its durable life can be written as

$$U_D = 1 - \prod_{t=1}^{T_D} (1 - 10^{7.57 - 1.74 (R + \Delta R_1)}) \quad (15)$$

Suppose that the initial quake-resistivity is $R + \Delta R_1$ and retrofitting is ΔR_2 at T years after construction. The probability of failure becomes;

$$U_D = 1 - \prod_{t=1}^{T_D - T} (1 - 10^{7.57 - 1.74 (R + \Delta R_1 + \Delta R_2)}) \prod_{T_D - T + 1}^{T_D} (1 - 10^{7.57 - 1.74 (R + \Delta R_1)}) \quad (16)$$

Table 4 shows the results for ΔR_1, ΔR_2, C_C, C_R, C_F and C. Taking into account the interest rate γ;

$$C = C_C + \frac{1}{(1 + \gamma)^T} (C_R + C_F)$$

Fig. 7, 8, 9 shows the total costs C corresponding to interest rates of 0.00, 0.05 and 0.10 respectively. If ΔR_1 is less than 0.20 and 0.40, corresponding to the retrofitting of 30 years and 40 years after construction, it is impossible to ensure the cumulative probability of 2.1×10^{-3}, then the results for that area are missing.

d) Considerations

1. The results noted above give the minimum cost under the condition of $U_D = U^*$. When γ is 0.00, the minimum cost is realized in case of high initial quake-resistivity and is not influenced by the time of retrofitting, because the cost of retrofitting is more expensive than that of construction (α=2.0). When γ is 0.05 or 0.10, it is profitable to retrofit and 30 through 40 years (γ=0.05) or 20 through 30 years (γ=0.10) after construction.

2. Using the method described in section 3c, the most economical quake-resistivity for an initial design can be obtained under a certain condition for the value of the cumulative probability during the durable lives. Concerning existing structures the level of retrofitting can be obtained for a certain value of cumulative probability. However, these methods should be applied to the structures of quake-resistivity that ensures U* at the beginning of construction. Therefore it is different from the methodology shown in Fig. 3, in that it is sufficient to ensure U* only during the residual lives. The former methodology should be applied to relatively new structures and the latter to the old structures.

4. Conclusions

a) To retrofit structures, physical and socio-economic conditions should be considered. However, it is hard to evaluate the socio-economic conditions quantitatively.

b) Relationships between the cost and the safety can be estimated from the following; method -- cost; cost -- capable load; and capable load -- safety relations.

c) With respect of the application, considering only the physical conditions, optimization for retrofitting can theoretically be obtained.

d) The methodology can be applied to reasonable retrofitting of vulnerable structures and also extensive urban renewals which are exposed to high levels of earthquake risk potentials and the socio-economic conditions are important.

References

1. Japan Urban Center: Investigations on the Planning of Urban Disaster Prevention.

2. City Bureau, Ministry of Construction: Draft of Manuals of Planning to Promote Countermeasures for Mitigation of Earthquake Disasters, Aug. 1975.

3. J. Cooper: Highway Bridges Seismic Research, Proc. of 7th Joint Meeting of Panel on Wind and Seismic Effect UJNR, Tokyo, May 1975.

4. Committee of Disaster Prevention, Tokyo Pref.: Investigations on Provision of Refuge Places for Fires by Earthquakes, Sept. 1973

5. Yokohama City: Risk Energy, 1972.

6. Committee of Disaster Prevention, Nagoya City: Investigations on the Evacuation Planning from Fires by Earthquakes in Nagoya, June, 1974.

7. Executive Office of the President Office of Emergency Preparedness: Report of the Congress, Disaster Preparedness, Jan. 1972.

8. Pugsley, A.G.: The Safety of Structures, Edward Arnold Publishers Ltd., 1966.

9. Report of the Public Works Research Institute, Ministry of Construction, Vol. 125, June 1965.

10. Annual Report of Statistics of Road, 1964.

11. Annual Report of Statistics of Road, 1973.

12. T. Katayama: Fundamentals of Probabilistic Evaluation of Seismic Activity and Seismic Risk, May 1975.

13. E. Kuribayashi, T. Iwasaki: Observed Earthquake Responses of Bridges, Proc. of 4th WCEE, Jan 1969.

14. Japan Road Association: Annual Report of Road Bridges, 1973.

15. Niigata Pref.: Records on Niigata Earthquake, June 1965.

TABLE 1 ITEMS TO EXAMINE FOR EARTHQUAKE DISASTER MITIGATION

CLASSIFICATIONS	FUNCTIONAL IMPORTANCE			DURABILITY	REPAIR AND RECONSTRUCTION
	CONTRIBUTION	NUISANCE	DUMMY		
VICINITY	○	○	○		
STRUCTURE	○	○	○	○	○
SCALE	○	○	○	○	○

TABLE 2 DESTROYED BRIDGES AFTER KANTO EARTHQUAKE

EARTHQUAKE	DATE	NUMBER OF DESTROYED BRIDGES
KANTO	1923. 9. 1	8
NANKAI	1946.12.21	1
FUKUI	1948. 6.28	10
NIIGATA	1964. 6.16	3
TOTAL		22

TABLE 3 TRANSITION OF NUMBER OF BRIDGES

YEAR	LONG SPAN BRIDGES	SHORT SPAN BRIDGES	TOTAL
1948	1, 730	105, 323	107, 053
1950	1, 901	113, 621	115, 522
1951	1. 934	116, 806	118, 740
1952	1, 994	119, 045	121, 039
1953	2, 054	112, 190	124, 253
1954	2, 094	123, 237	125, 331
1955	2, 137	123, 027	125, 164
1956	2, 234	124, 473	126, 707
1957	2, 257	124, 523	126, 780
1958	2, 282	124, 396	126, 678
1959	2, 350	123, 953	126, 303
1960	2, 397	123, 288	125, 685
1961	2, 436	123, 373	125, 809
1962	2, 549	123, 847	126, 396
1963	2, 599	123, 971	126, 570
1964	2, 701	123, 400	126, 101
1965	2, 797	124, 090	126, 887
1966	2, 883	124, 008	126, 891
1967	2, 992	125, 587	128, 579
1968	3, 116	124, 726	127, 842
1969	3, 344	126, 406	129, 750
1970	3, 520	126, 677	130, 197
1971	3, 725	127, 524	131, 249
1972	3, 925	128, 966	132, 891
1973	4, 107	130, 056	134, 163

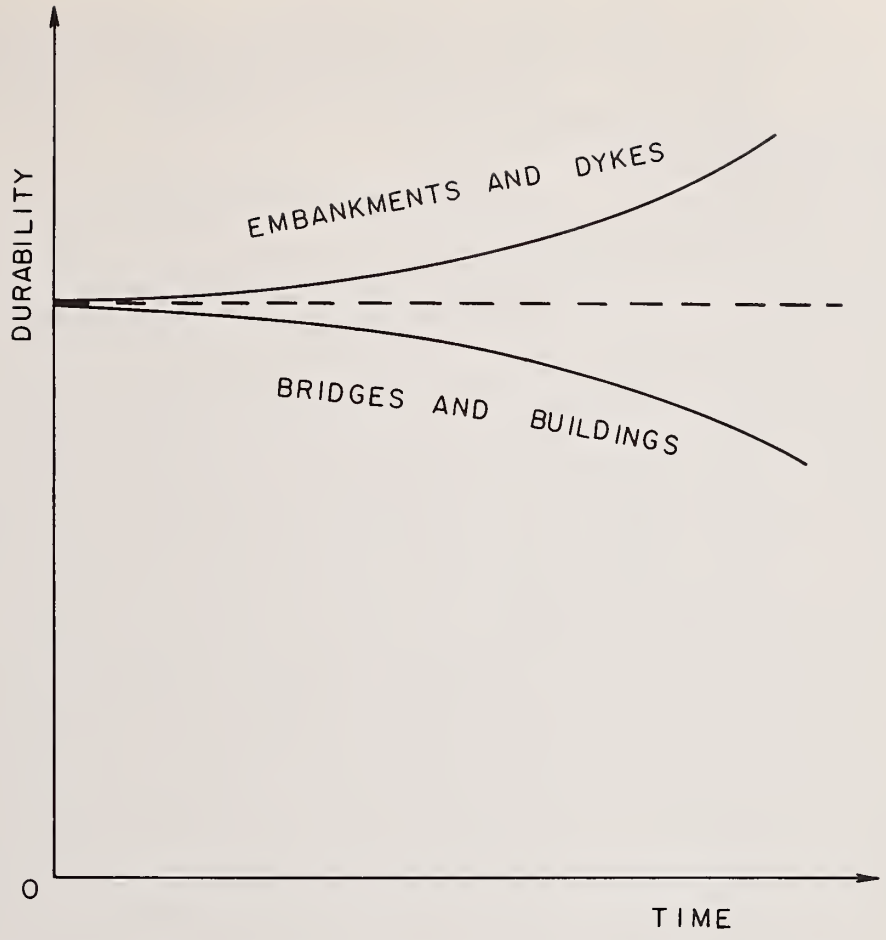

Fig.—1 CHARACTERISTICS OF DURABILITY OF EXISTING STRUCTURES

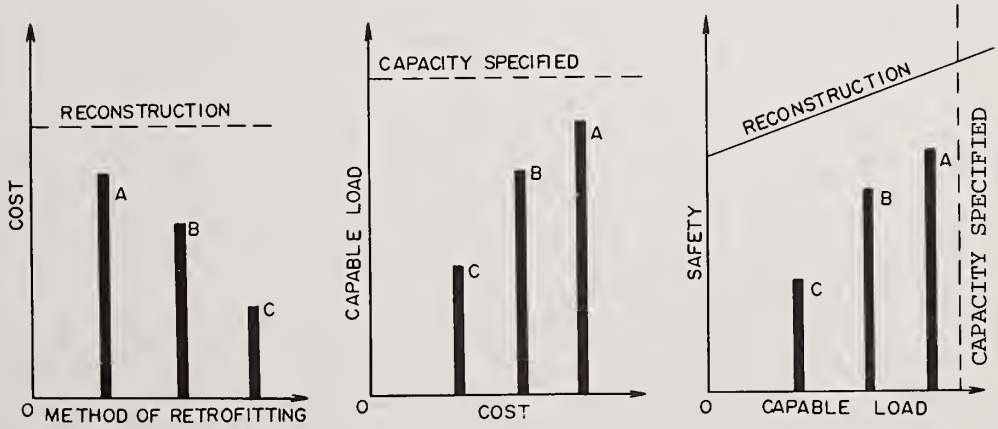

Fig.—2 INVESTMENTS AND RETROFITTING

TABLE 4 TOTAL COSTS OF STRUCTURES (COST : $\times 10^7$ YEN)

					$\gamma = 0.00$				$\gamma = 0.05$			$\gamma = 0.10$		
$\triangle R_1$	$\triangle R_2$	U_O	U_R	$U_R+\triangle R$	C_C	C_R	C_F	C	$C_R/(1+\gamma)^T$	$C_F/(1+\gamma)^T$	C	$C_R/(1+\gamma)^T$	$C_F/(1+\gamma)^T$	C
WITHOUT RETROFITTING														
0.90	–	0.00210	–	–	2.40	0.00	0.01	2.41	0.00	0.01	2.41	0.00	0.01	2.41
RETROFITTING AFTER 10 YEARS														
0.00	0.97	0.0749	0.0744	0.0016	2.26	0.29	0.01	2.56	0.18	0.00	2.44	0.11	0.00	2.37
0.10	0.84	0.0502	0.0409	0.0018	2.28	0.24	0.01	2.53	0.15	0.00	2.43	0.09	0.00	2.37
0.20	0.72	0.0338	0.0336	0.0019	2.29	0.22	0.01	2.52	0.14	0.00	2.43	0.09	0.00	2.38
0.30	0.61	0.0227	0.0226	0.0020	2.31	0.19	0.01	2.51	0.11	0.00	2.42	0.07	0.00	2.38
0.40	0.51	0.0153	0.0152	0.0020	2.32	0.16	0.01	2.49	0.10	0.00	2.42	0.06	0.00	2.38
0.50	0.41	0.0103	0.0102	0.0020	2.34	0.13	0.01	2.48	0.08	0.00	2.42	0.05	0.00	2.39
0.60	0.31	0.00688	0.00683	0.0020	2.35	0.09	0.01	2.45	0.06	0.00	2.41	0.04	0.00	2.39
0.70	0.21	0.00461	0.00458	0.0020	2.37	0.06	0.01	2.44	0.04	0.00	2.41	0.02	0.00	2.39
0.80	0.11	0.00310	0.00308	0.0020	2.38	0.03	0.01	2.42	0.02	0.00	2.40	0.01	0.00	2.39
0.90	0.01	0.00207	0.00205	0.0020	2.40	0.00	0.01	2.41	0.00	0.00	2.40	0.00	0.00	2.40
RETROFITTING AFTER 20 YEARS														
0.00	1.14	0.0749	0.0737	0.0008	2.26	0.35	0.01	2.62	0.13	0.00	2.39	0.05	0.00	2.31
0.10	0.91	0.0502	0.0494	0.0013	2.28	0.28	0.01	2.57	0.11	0.00	2.39	0.04	0.00	2.32
0.20	0.78	0.0338	0.0332	0.0015	2.29	0.24	0.01	2.54	0.09	0.00	2.38	0.04	0.00	2.33
0.30	0.63	0.0227	0.0224	0.0018	2.31	0.19	0.01	2.51	0.07	0.00	2.38	0.03	0.00	2.34
0.40	0.53	0.0153	0.0150	0.0018	2.32	0.16	0.01	2.49	0.06	0.00	2.38	0.02	0.00	2.34
0.50	0.43	0.0103	0.0101	0.0018	2.34	0.13	0.01	2.48	0.05	0.00	2.39	0.02	0.00	2.36
0.60	0.33	0.00688	0.00676	0.0018	2.35	0.10	0.01	2.46	0.04	0.00	2.39	0.02	0.00	2.37
0.70	0.23	0.00461	0.00454	0.0018	2.37	0.07	0.01	2.45	0.03	0.00	2.40	0.01	0.00	2.38
0.80	0.13	0.00310	0.00305	0.0018	2.38	0.04	0.01	2.43	0.02	0.00	2.40	0.01	0.00	2.39
0.90	0.03	0.00207	0.00203	0.0018	2.40	0.01	0.01	2.42	0.00	0.00	2.40	0.00	0.00	2.40
RETROFITTING AFTER 30 YEARS														
0.20	0.90	0.0338	0.0326	0.0009	2.29	0.28	0.01	2.58	0.06	0.00	2.35	0.02	0.00	2.31
0.30	0.69	0.0227	0.0220	0.0014	2.31	0.21	0.01	2.53	0.05	0.00	2.36	0.01	0.00	2.32
0.40	0.56	0.0153	0.0148	0.0016	2.32	0.17	0.01	2.50	0.04	0.00	2.36	0.01	0.00	2.33
0.50	0.44	0.0103	0.0099	0.0017	2.34	0.14	0.01	2.49	0.03	0.00	2.37	0.01	0.00	2.35
0.60	0.31	0.00688	0.00664	0.0019	2.35	0.10	0.01	2.46	0.02	0.00	2.37	0.01	0.00	2.36
0.70	0.21	0.00461	0.00445	0.0019	2.37	0.07	0.01	2.45	0.02	0.00	2.39	0.00	0.00	2.37
0.80	0.11	0.00310	0.00299	0.0019	2.38	0.03	0.01	2.42	0.01	0.00	2.39	0.00	0.00	2.38
0.90	0.01	0.00207	0.00199	0.0019	2.40	0.00	0.01	2.41	0.00	0.00	2.40	0.00	0.00	2.40
RETROFITTING AFTER 40 YEARS														
0.40	0.72	0.0153	0.0140	0.0008	2.32	0.22	0.01	2.55	0.03	0.00	2.35	0.00	0.00	2.32
0.50	0.52	0.0103	0.0094	0.0012	2.34	0.16	0.01	2.51	0.02	0.00	2.36	0.00	0.00	2.34
0.60	0.36	0.00688	0.00632	0.0015	2.35	0.11	0.01	2.47	0.02	0.00	2.37	0.00	0.00	2.35
0.70	0.23	0.00461	0.00424	0.0017	2.37	0.07	0.01	2.45	0.01	0.00	2.38	0.00	0.00	2.37
0.80	0.12	0.00310	0.00284	0.0018	2.38	0.04	0.01	2.43	0.00	0.00	2.38	0.00	0.00	2.38
0.90	–	0.00207	–	–	2.40	0.00	0.01	2.41	0.00	0.00	2.40	0.00	0.00	2.40

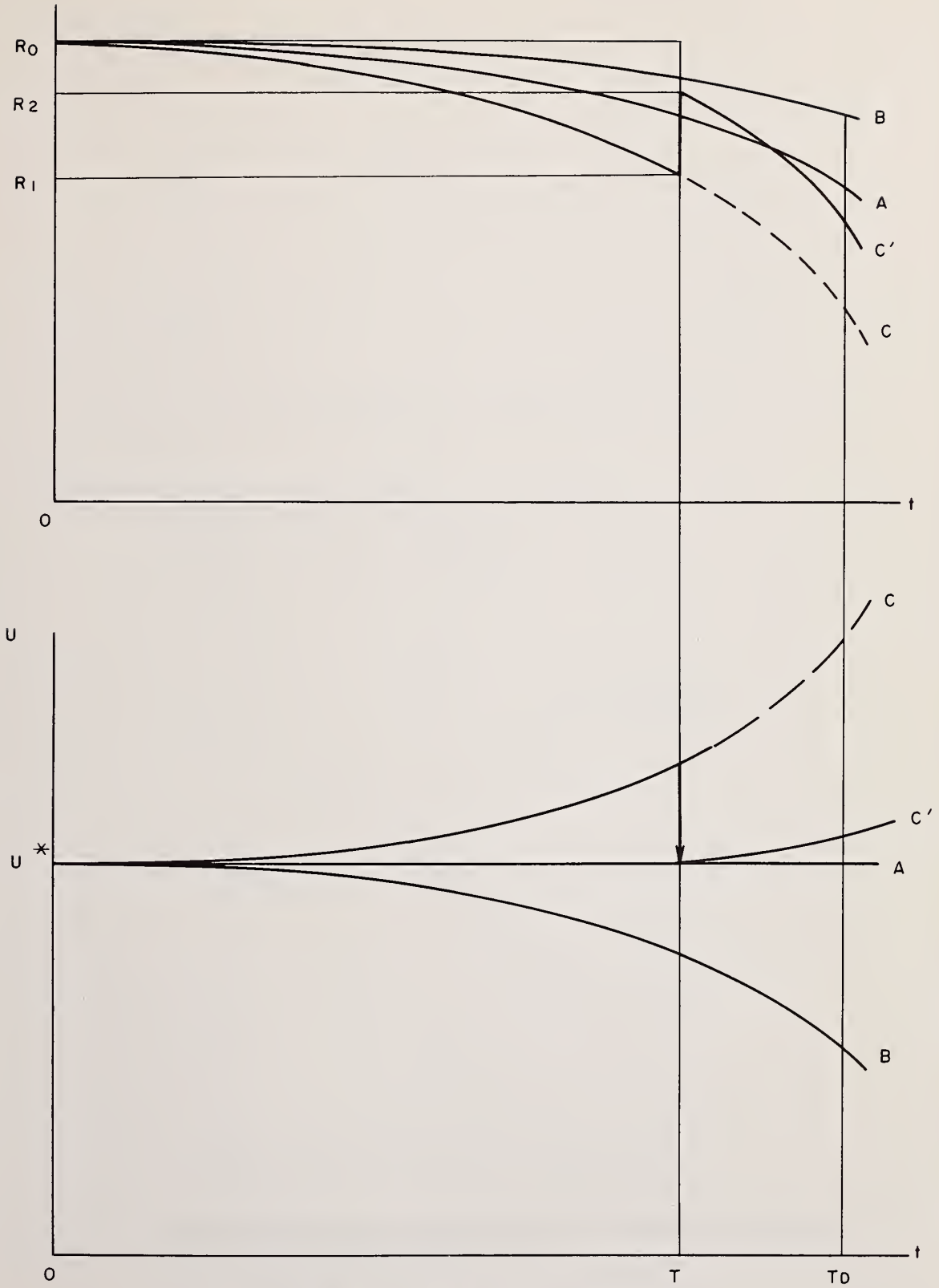

Fig. — 3 RETROFITTING OF EXISTING STRUCTURES

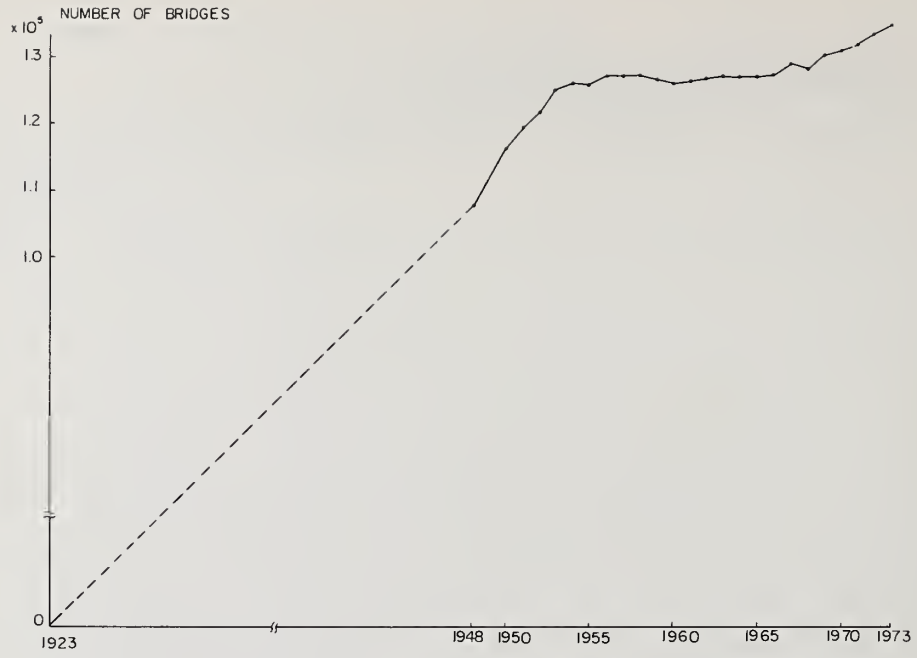

Fig.—4 TRANSITION OF NUMBER OF BRIDGES

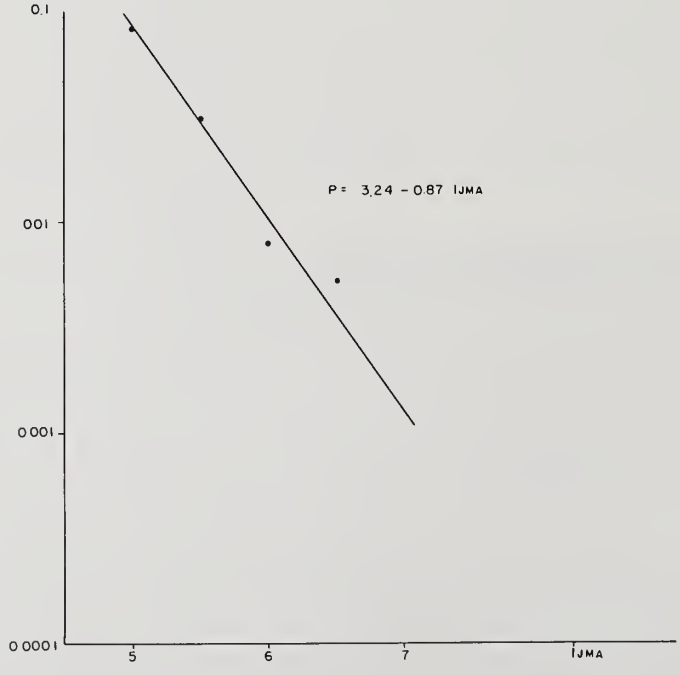

Fig.—5 PROBABILITY OF OCCURRENCE OF EARTHQUAKE TOKYO

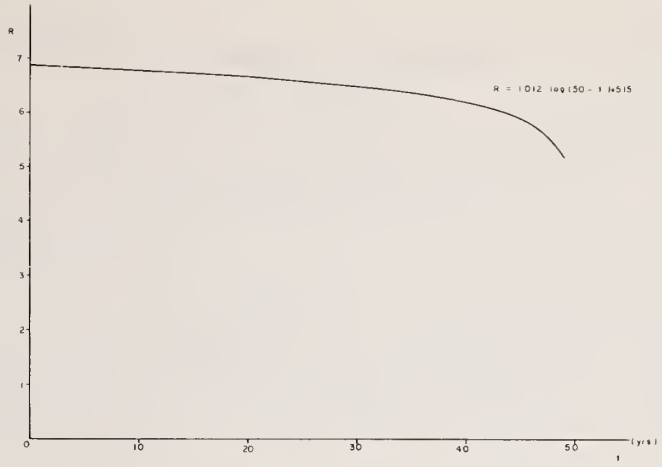

Fig.－6 ASSUMED TRANSITION OF EARTHQUAKE RESISTIVITY

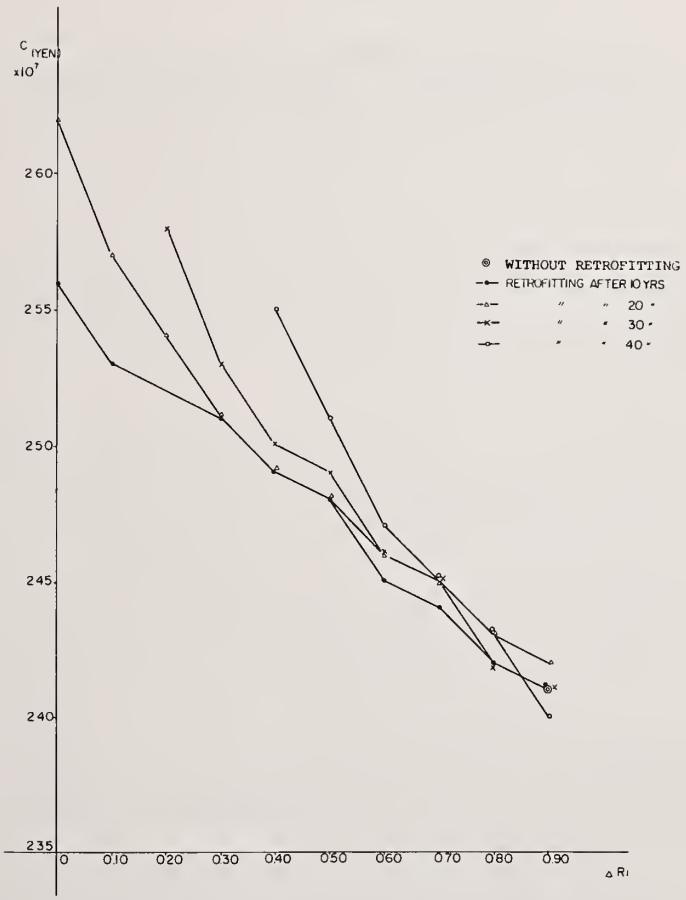

Fig.－7 RELATIONSHIP BETWEEN TOTAL COST AND INITIAL EARTHQUAKE RESISTIVITY, RETROFITTING TIME ($\gamma = 0.00$)

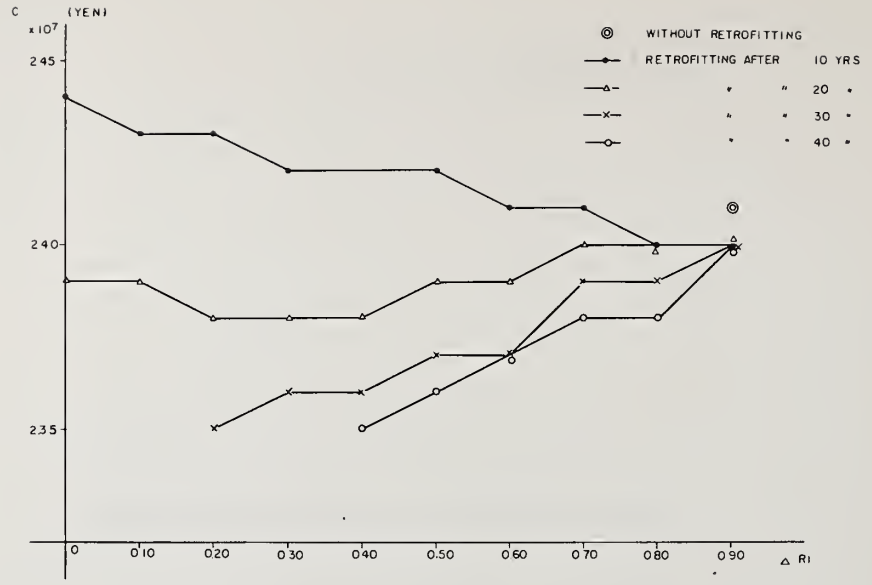

Fig.－8 RELATIONSHIP BETWEEN TOTAL COST AND INITIAL EARTHQUAKE RESISTIVITY, RETROFITTING TIME ($\gamma = 0.05$)

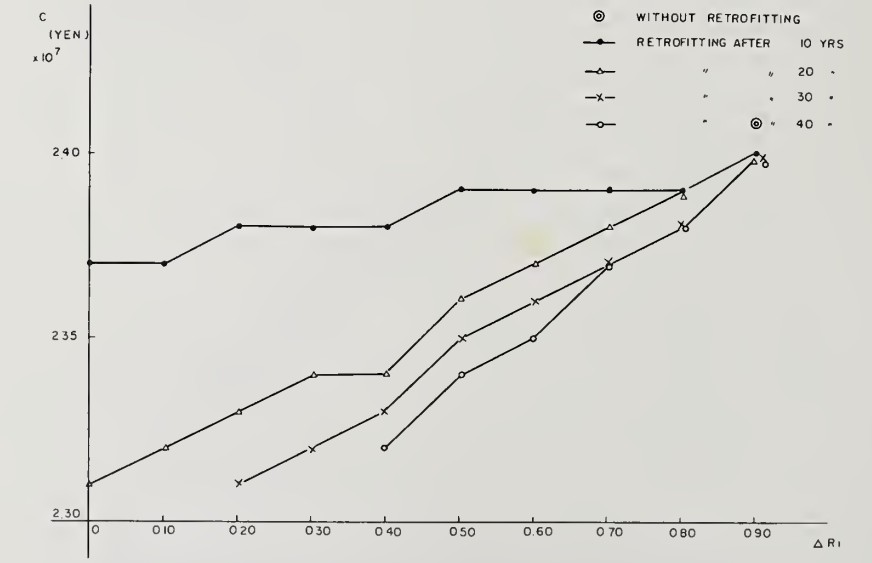

Fig.－9 RELATIONSHIP BETWEEN TOTAL COST AND INITIAL EARTHQUAKE RESISTIVITY, RETROFITTING TIME $\gamma = 0.10$)

DYNAMIC RESPONSE CHARACTERISTICS OF A MODEL ARCH DAM

CHARLES D. NORMAN, ROGER D. CROWSON, JIMMY P. BALSARA
Weapons Effects Laboratory
U.S. Army Engineer Waterways Experiment Station
P.O. Box 631, Vicksburg, Miss. 39180

ABSTRACT

The dynamic response characteristics of a model arch dam are given in detail. These characteristics were determined by subjecting the model to a vibratory loading. Resulting deformations and velocities are given.

Key Words: Arch Dam; Deflections; Dynamic Tests; Model; Structural Analysis; Velocities; Vibrations.

1. Introduction

a) In order to develop better design procedures for concrete dams subjected to earthquake forces, an understanding of the significant parameters that influence the dynamic properties of such structures is necessary. Assumptions regarding geometry, boundary conditions, and interaction with the foundation and reservoir can significantly affect earthquake response calculations. Vibration tests provide a means of determining dynamic properties of dams and evaluating the various parameters that influence these properties. The investigation of the North Fork Dam was undertaken to verify the use of physical models and linear three-dimensional (3-D) finite element analyses to determine the dynamic properties of an arch dam.

b) The North Fork Dam, located near Auburn, California, on the North Fork of the American River, was built in 1939 to trap sediments from upstream mining operations. It is a constant-angle arch with a maximum height of 155 ft*, a crest length of 620 ft., and a crown thickness that varies from 22 ft at the base to 6.8 ft at the crest. The overflow spillway is a section 200 ft long near the center of the dam and is depressed 3 ft below the normal crest elevation. The reservoir is very narrow, having a maximum width of about 700 ft and a length of about 5 miles.

c) Completion of the Auburn Dam 5 miles downstream will inundate the North Fork Dam completely. Prior to completion, full-scale tests similar to the model tests discussed in this report will be conducted to correlate model and full-scale test results.

2. Model Construction

a) Details of the first North Fork Dam model, which was destroyed by explosive tests, are discussed in Reference 1. In the second North Fork Dam model, the foundation, reaction mass, and reservoir of the first model, and a new dam and kicker slab were used. The kicker slab is a mass of concrete used to transmit the input vibratory load to the foundation. After complete removal of the original dam and slab, two-way steel reinforce-

ment was welded into position for the new slab. The reinforcement consisted of no. 6 steel bars placed between the foundation and loading plate. Commercially available concrete having a compressive strength of 4000 psi was used for the new slab. A plan view of the dam and slab showing reinforcement details is shown in Figure 1.

b) The foundation was slightly altered by cutting a 2-in. by 2-in. groove at the dam-foundation interface, thus forming a secure keyway after the dam was cast. The light-weight concrete forms used in the first model were again utilized. A specially prepared concrete grout with an average 28-day compressive strength of 5000 psi and an average density of 142.2 pcf was used. The concrete was allowed to cure for 28 days, after which the forms were removed and a curing compound applied. The new model is shown in Figure 2.

3. Test Procedures

a) Test Equipment: The electromagnetic (EM) and electrohydraulic (EH) vibrators used in the first test series (Reference 1) were again employed in this test. Instrumentation used for motion measurement consisted of velocity transducers connected by compatible electronics to two analog magnetic tape recorders. During the EM and EH vibrator tests, nine velocity transducers located along the dam crest and three on the crown contilever section were used to measure both radial and vertical motion. Hydrodynamic pressure measurements during both EM and EH tests were made with a pressure transducer mounted on a rod and hand-held at a constant distance of 1 in. from the dam face. Complete descriptions and specifications of the equipment are provided in Reference 1.

b) EM Tests: EM vibrator tests were conducted with the reservoir full (1 in. below top of spillway crest), 24 in. down, and empty. The two vibrators were placed on the crest at each end of the spillway and run in phase and 180 deg out of phase. A constant force level of 15.5 pounds per vibrator, applied in a radial direction, was maintained for all EM tests. The frequency was swept from 30 to 500 Hz at a rate of 1.0 Hz/sec. Other sweep rates ranging from 0.25 to 10 Hz/sec resulted in the same response curves. The vibrators were held at resonant frequencies for several minutes to allow amplitude buildup. However, no increase in amplitude was noted for any particular sweep test. Damping tests were conducted by running the EM vibrators at various resonant peaks and abruptly shutting off the power amplifier The logarithmic signal decay was measured to determine the damping ratio. Hydrodynamic pressure measurements were made at resonant frequencies by holding a pressure transducer 1 in. from the upstream dam face at various locations. A list of all EM tests conducted is presented in Table 1, and plan, profile, and section views of the model and equipment are shown in Figure 3.

c) EH Tests: Base excitation of the dam was provided by the EH vibrator. Vibratory loads were transferred to the dam foundation through a heavily reinforced concrete slab (Figure 1). Frequency sweeps and hydrodynamic pressure measurements were made at dynamic force input levels of 10,000-40,000 pounds. The frequency was swept from 10 to about 175 Hz at a rate of 0.5 Hz/sec. Hydrodynamic pressure measurements were made at a load of 20,000 pounds while the vibrator was held at various resonant frequencies.

4. Test Results

a) The experimental portion of this study was primarily concerned with determining natural frequencies, mode shapes, structural damping, and hydrodynamic pressures. Natural frequencies were obtained by analyzing velocity versus frequency plots, as shown in Plates 1-3 for the EM tests. Plate 4 shows velocity versus frequency plots for the EH test in which hydrodynamic pressures were measured. Mode shapes determined from EM tests are presented graphically in Plates 5-7. Damping ratios are given in Table 2, and hydrodynamic pressures are plotted in Plates 8-16. A comparison of natural frequencies obtained for the first model test (Reference 1) with those reported herein can be made using the data presented in Table 6. In comparing these data, consideration should be given to the fact that the first model had been damaged by explosive tests then repaired for the vibration tests. For the study reported herein, the EH tests were aimed at better designing hydrodynamic pressures and damping ratios. No significant peaks in the velocity data were noticed during the EH frequency sweeps and therefore natural frequencies could not be determined.

b) EM Tests: Data from the EM frequency sweep tests were recorded on magnetic tape and later played back through an X-Y plotter. The records for these tests are shown in Plates 1-3. During the tests, output from various velocity transducers was recorded on an X-Y plotter, and acceleration input to the vibrator mass was monitored on an oscilloscope. Oscillograph records were also made at resonant peaks to observe wave shapes and to provide a crosscheck of the analog-to-digital data used to determine the mode shapes.

c) EH Tests: The EH vibration test data were recorded in the same manner as were the EM data. The constant load feedback measured by a pressure transducer in the EH vibrator was monitored on an oscilloscope during all tests. After the tests were completed, all data channels were played back on the X-Y plotter.

d) Mode Shapes: The velocity versus frequency plots were carefully analyzed to determine resonant peaks. The 12 velocity data channels were converted at the resonant frequencies to digital records, which were then integrated to obtain displacements. Displacements for the symmetrical and asymmetrical mode shapes for both the radial crest and cantilever deflections are shown in Plates 5-7. With the reservoir full, the natural frequencies for the second through the fifth modes were 103, 147, 175, and 243 Hz, respectively. The first mode excited in the first model (Reference 1) could not be determined in this test series. With the reservoir empty, the frequencies were 133, 151, 213, and 297 Hz. Values for the second, fourth, and fifth natural frequencies increased 22-29 percent for the empty condition, whereas the third natural frequency increased only 3 percent.

e) Damping: For the DM tests, damping ratios were determined with the reservoir full and empty. Output from velocity transducers 3 and 6 (location of the vibrators) was recorded on an oscillograph record as the vibrators were abruptly shut off after being held at a resonant peak. The relative amplitude versus cycle of oscillation was measured, and the damping ratio D was determined from the formula;

$$D = \frac{1}{2\pi n} \ln \left(\frac{x_1}{x_n} \right)$$

where n = number of cycles of oscillation

x_1 = amplitude of 1st cycle

x_n = amplitude of nth cycle

A tabulation of all damping data is presented in Table 2. The damping ratios are quite uniform, as values ranged from 0.02 to 0.05 for all tests conducted. From the data collected, the reservoir level, frequency, and phasing of vibrators had no discernable effect on the damping ratios.

f) Hydrodynamic Pressure

1. For the EM tests, hydrodynamic pressure measurements were made at each velocity transducer location at 1-ft depth intervals. Readings were taken at each point while the vibrators were held at the second, third, and fourth natural frequencies (105, 147, and 196 Hz, respectively). The EM data are shown in Plates 8-10 as pressure versus depth. The maximum pressure recorded was 0.275 psi occurring at 175 Hz, 12 in. below velocity transducer 4.

2. Hydrodynamic pressure measurements for the EH tests were made in the same manner and at the same locations as were those for the EM tests. Readings were taken with the vibrator held at 80, 98, and 122 Hz. These frequencies were selected to provide pressure data at frequencies below the dam's fundamental mode and then considerably above the fundamental mode. The force level was 20,000 pounds. The data plots of pressure versus depth are shown in Plates 12-14. The maximum pressure recorded was 0.40 psi at 122 Hz, occurring at a depth of 1ft. below velocity transducer 5.

5. Finite Element Analysis

a) General

1. A 3-D finite element analysis was conducted to determine the vibration characteristics of the model dam. Specifically, mode shapes and corresponding natural frequencies were determined for two finite element models, one in which the foundation was included and one with the base fixed. For each grid, computations were made with the reservoir full and empty.

2. An eight-node 3-D solid element was used in the calculations. The element has three translational degrees of freedom (DOF) per node and contains incompatible deformation modes that greatly improve its bending behavior. A detailed description of this element is presented by Wilson in Reference 2. The small grid consists of the dam alone and contains 110 elements, 278 nodes, and 570 DOF. The large grid comprises the dam and the massive concrete foundation of the model. This grid has 916 elements, 1464 nodes, and 2916 DOF. The nodes at the base of the small grid are fixed against translation in all directions. In order that the effects of deformations in the dam foundation could be

studied, the large grid was used with outside foundation element nodes fixed against translation. The two grids are shown in Figures 4 and 5.

b) Reservoir Effects

1. The problems of hydrodynamic effects on submerged or partially submerged structures has received considerable attention in the recent past. One method of accounting for this phenomenon is to construct a large finite element grid modeling the structure and the water. This method presents problems for many systems since the number of unknowns can be great, and the lack of symmetry in the mass and the stiffness matrices increases the amount necessary computational effort.

2. Another approach to the fluid-structure interaction problem is the substructure concept (Reference 3). In this approach, the structure is discretized by finite elements, and the reservoir is treated as a continuum boundary value problem. Results of the continuum reservoir solution are used as input to the equations of motion, which are expected in modal coordinates. This method depends heavily on the geometry of the reservoir being simple, since solutions to the continuum boundary value problem are difficult for complex boundary geometries. Still another method for handling the hydrodynamic problem is to calculate an effective mass of water and add this mass to the structure. This concept was proposed by Westergaard (Reference 4) and is based on the idea that the hydrodynamic force is of an inertia type and can therefore be represented as an effective mass. A limitation of this technique is observed at frequencies above the fundamental frequency of the reservoir. This problem is discussed in detail by Chopra (Reference 5). A comparison of hydrodynamic pressure computed using Westergaard's theory and a theory for arch dam by Perumlaswami and Kar (Reference 6) with experimental data is shown in Plate 16. Westergaard's theory is based on a rigid vertical plane dam, while Perumalswami and Kar's theory is based on a rigid, constant-curvature arch dam. Both methods accurately predicted the hydrodynamic pressures at the deepest section of the dam-reservoir interface at a frequency at which the dam was moving essentially as a rigid body.

3. Due to the complex structure and reservoir geometries of the North Fork Dam, a finite element analysis of the complete system appeared uneconomical. Also, the complex reservoir geometry renders the continuum boundary value problem intractable. Based on these considerations and the comparison of Westergaard's theory with test data, the effective mass concept was used in the finite element analysis. The water mass was distributed at each vertical cross section of the dam based on the approximate equations presented in Reference 4, using the height as determined at the midsection of the dam crest. In using this approximate technique, it is assumed that the motion at a mass point is purely radial. Based on the model test data, this assumption was felt justified, especially in the more flexible regions of the dam where water mass effects would be greatest. Since the frequencies of interest for the dam were in the region of 100-200 Hz, limitation of the effective mass concept to frequencies below that of the reservoir was not thought to be a significant problem. As a crude approximation to the fundamental frequency of the reservoir, the frequency equation for a semi-infinite reservoir was used. For a 5.5-ft-deep reservoir, corresponding to the maximum height of the model dam, this frequency is

approximately 1240 Hz, much greater than the 100- to 200Hz band of interest for the model dam response.

c) Calculations of Mode Shapes and Natural Frequencies

1. Mode shape and natural frequencies of the model dam were determined through use of the Ritz analysis (Reference 2) and a subspace iteration in the finite element analysis. The Ritz analysis is based on selecting a set of force patterns with corresponding deflected shapes similar to the structure's vibration mode shapes. Obviously, this method requires some prior understanding of the structure's dynamic response. The subspace iteration technique, which is more efficient when the band width of the system is large, was developed by Bathe and is discussed in detail in Reference 7. Essentially, this technique relies on repeated application of the Ritz method, each step depending on the base vectors developed in the previous step until convergence to the desired eigenvectors is obtained. A simultaneous iteration on the mass and stiffness matrices is performed, beginning with a set of trial vectors.

2. In order to determine the sensitivity of the Ritz technique used in this study two runs were made. In the first run, only the crest elements were subjected to the static load patterns; in the second run, however, these crest elements plus elements below the crest sections were loaded. Efficiency in selecting elements to be loaded is discussed by Wright and Miles in Reference 8. In general, more elements in areas of greater flexibility should be loaded. The results of the two runs are given in Table 3. The average decrease in frequencies for the first four modes is approximately 19 percent. In Table 4, frequencies determined using the more accurate Ritz analysis are compared with those calculated using the subspace iteration scheme with 11 working vectors. As expected, the subspace iteration technique gave the lowest values of the calculated frequencies. The calculated results were still appreciably higher than those determined experimentally. The fixed-base assumption was then investigated by including the massive concrete foundation. The accuracy of this calculation based on a comparison with experimental data showed considerable improvement over the previous results. The results of the calculations made using the subspace iteration scheme for the dam fixed at the base and with the foundation included are compared with experimental data in Table 5. The comparisons are shown for both full and empty reservoirs. The effects of water mass in reducing the computed natural frequency are consistent with the reduction in frequency measured for the second and fourth modes. However, no significant reduction in frequency was measured for the third mode. The normalized mode shape calculated for the dam with the fixed base and foundation are compared with experimental results in Plates 17 and 18 for the symmetrical and asymmetrical modes, respectively. Results of both calculations agree equally well with the measured mode shapes.

6. Conclusions

a) Vibration tests conducted on the model dam showed that interaction with the reservoir decreases the natural of the dam. The frequencies decreased by 20-30 percent for all but the third mode. The decrease in the third mode was about 3 percent. Apparently,

the change in frequency due to reservoir interaction was not uniform for all modes.

b) Hydrodynamic pressures calculated using Westergaard's theory and that proposed by Perumalswami and Kar indicate that the effects of curvature are not great, at least for the lower natural frequencies. The point of major interest concerning hydrodynamic pressures was the magnification of pressures in the most flexible regions of the dam. This increase in pressure coupled with the lower moment capacity of this section should be given special attention in design considerations.

c) Since the load patterns used in the Ritz analysis reflect the manner in which the inertia distribution of the structure is being approximated (Reference 9), computational accuracy increases substantially when the number of loaded elements is increased. Methods discussed by Wright and Miles (Reference 8) should be considered in selecting the number and locations of nodes to be loaded. Since the first step of the subspace iteration method is essentially a Ritz analysis, results from the subspace scheme should yield a lower bound on computed frequencies. There were no striking dissimilarities in the mode shapes predicted through use of the two schemes. From these considerations, it can be seen that the Ritz analysis used in the early versions of the Structural Analysis Program can be attractive from an economical standpoint. However, when a higher degree of accuracy is required in the analysis of geometrically complex structures, the subspace iteration scheme seems very appropriate.

d) When complete fixity of the base is assumed in the finite element analysis, natural frequencies predicted are higher than those predicted when the fixity associated with the interaction of the dam and the foundation is used. With the reservoir full, the predicted frequencies for the case in which the foundation was completely fixed were 20-30 percent greater than those for the case in which the foundation was included in the analysis as such. The differences in the predicted frequencies were much less for the two cases when the reservoir was empty, which, however, represents a rather academic case.

e) Comparison of natural frequencies determined in the first model study (Reference 1) with those reported herein indicates that structural damage incurred during explosive tests resulted in the response characteristics of the first model dam being altered. For the EM tests, these differences are presented in Table 6. Also, a significant peak in the velocity versus frequency plots was observed in EH tests conducted on the first model. However, no such peak was noticed in the second model tests. It is felt that the crack in the first model changed the three-dimensional character of the dam and allowed a type of cantilever action to result. The altered structure could then respond more efficiently to the force levels attainable from the EH vibrator and, therefore, some low resonant peaks were observed. Having no crack, the second model was stiffer and required more energy from the EH vibrator to develop significant resonant peaks. Due to the amount of damping, both structural and radiation into the soil, the EH vibrator could not supply the level of energy required to produce distinguishable resonant peaks in the second model.

References

1. Balsara, J.P., Walker, R.E., and Fowler, J., "Vibration Characteristics of the North Fork Dam Model," Technical Report N-74-2, Mar 1974, U.S. Army Engineer Waterways Experiment Station, CE, Vicksburg, Miss.

2. Wilson, E.L., "SAP, A General Structural Analysis Program," Report No. SESM 70-20, Division of Structural Engineering and Structural Mechanics, University of California, Berkeley, 1970.

3. Chakrabarti, P., and Chopra, A.K., "Earthquake Response of Gravity Dams Including Reservoir Interaction Effects," Report No. EERC 72-6, Earthquake Engineering Research Center, University of California, Berkeley, 1972.

4. Westergaard, H.M., "Water Pressures on Dams During Earthquakes," Proceedings, American Society of Civil Engineers, 57, pp 1303-1318, 1931.

5. Chopra, A.K., "Hydrodynamic Pressures on Dams During Earthquakes," Journal, Engineering Mechanics Division, American Society of Civil Engineers, 93, No, EM6, pp 205-223, 1967.

6. Perumalswami, P.R. and Kar, L., "Earthquake Hydrodynamic Forces on Arch Dams," Journal, Engineering Mechanics Division, American Society of Civil Engineers, 99, No. EM5, pp. 965-977, 1973.

7. Bathe, K.J., "Solution Methods for Large Generalized Eigenvalue Problems in Structural Engineering," Report No. SESM 71-20, Division of Structural Engineering and Structural Mechanics, University of California, Berkeley, 1971.

8. Wright, G.C. and Miles, G.A., "An Economical Method for Determining the Smallest Eigenvalues for Large Linear Systems," International Journal for Numerical Methods in Engineering, 3, pp 25-33, 1971.

9. Dong, S.B., Wolf, J.A., Jr., and Peterson, F.E., "On a Direct-Iterative Eigensolution Technique," International Journal for Numerical Methods in Engineering, 4, pp 155-161, 1972.

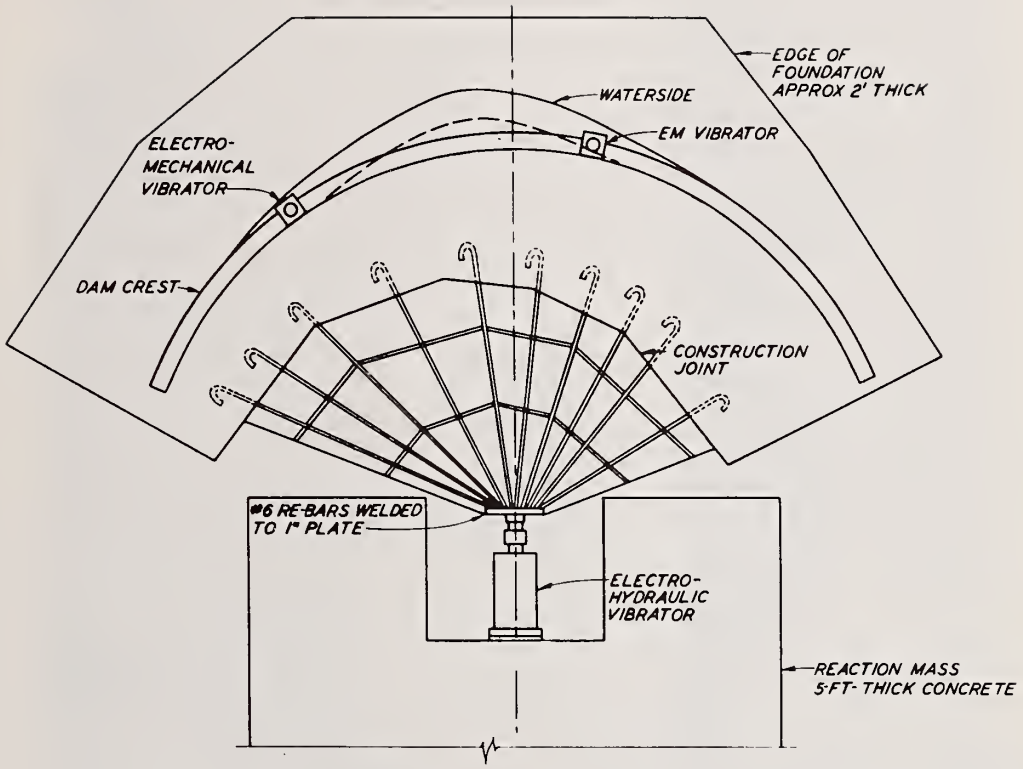

Figure 1. Two-way reinforcement of kicker slab

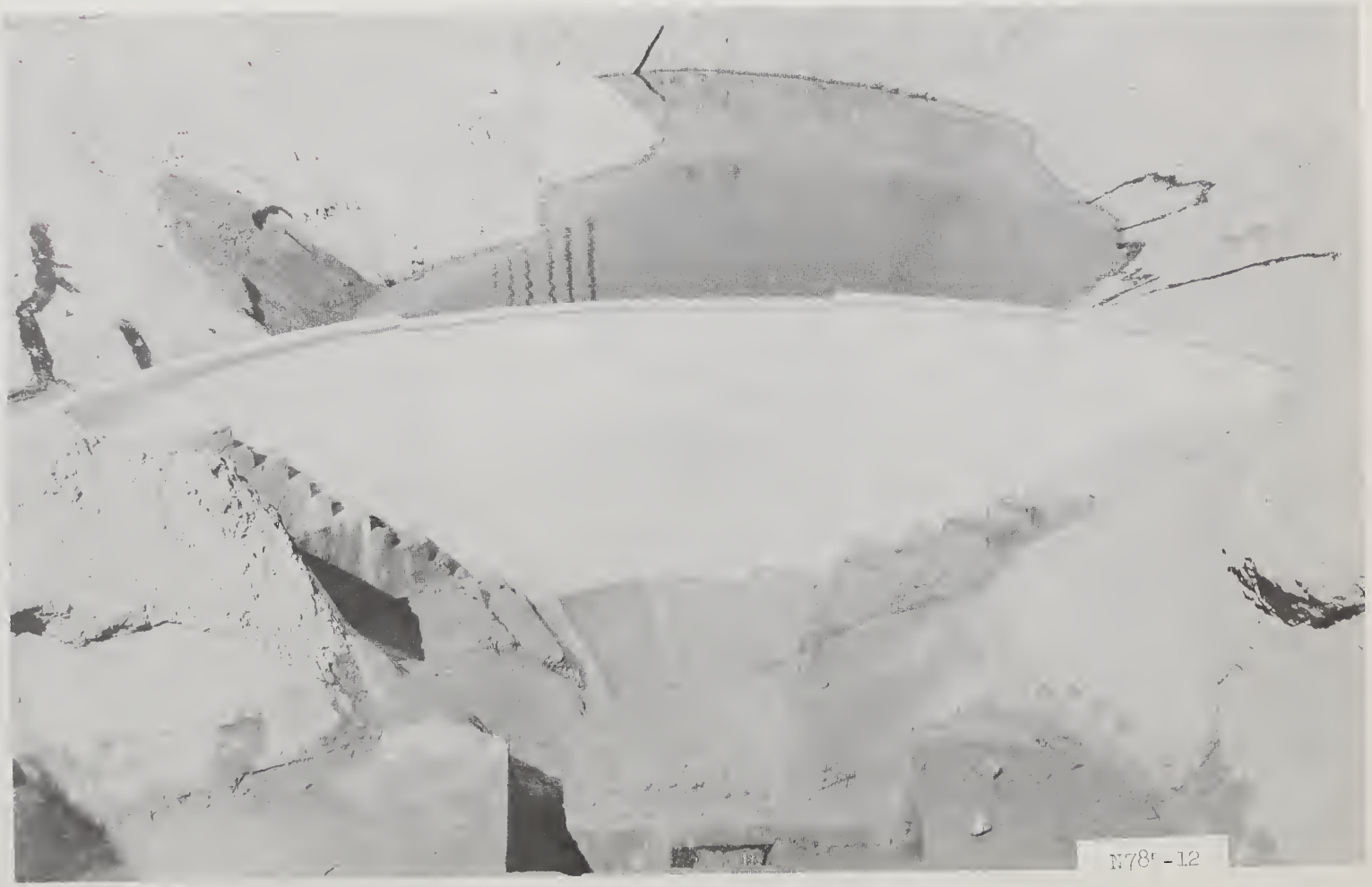

Figure 2. North Fork Dam model

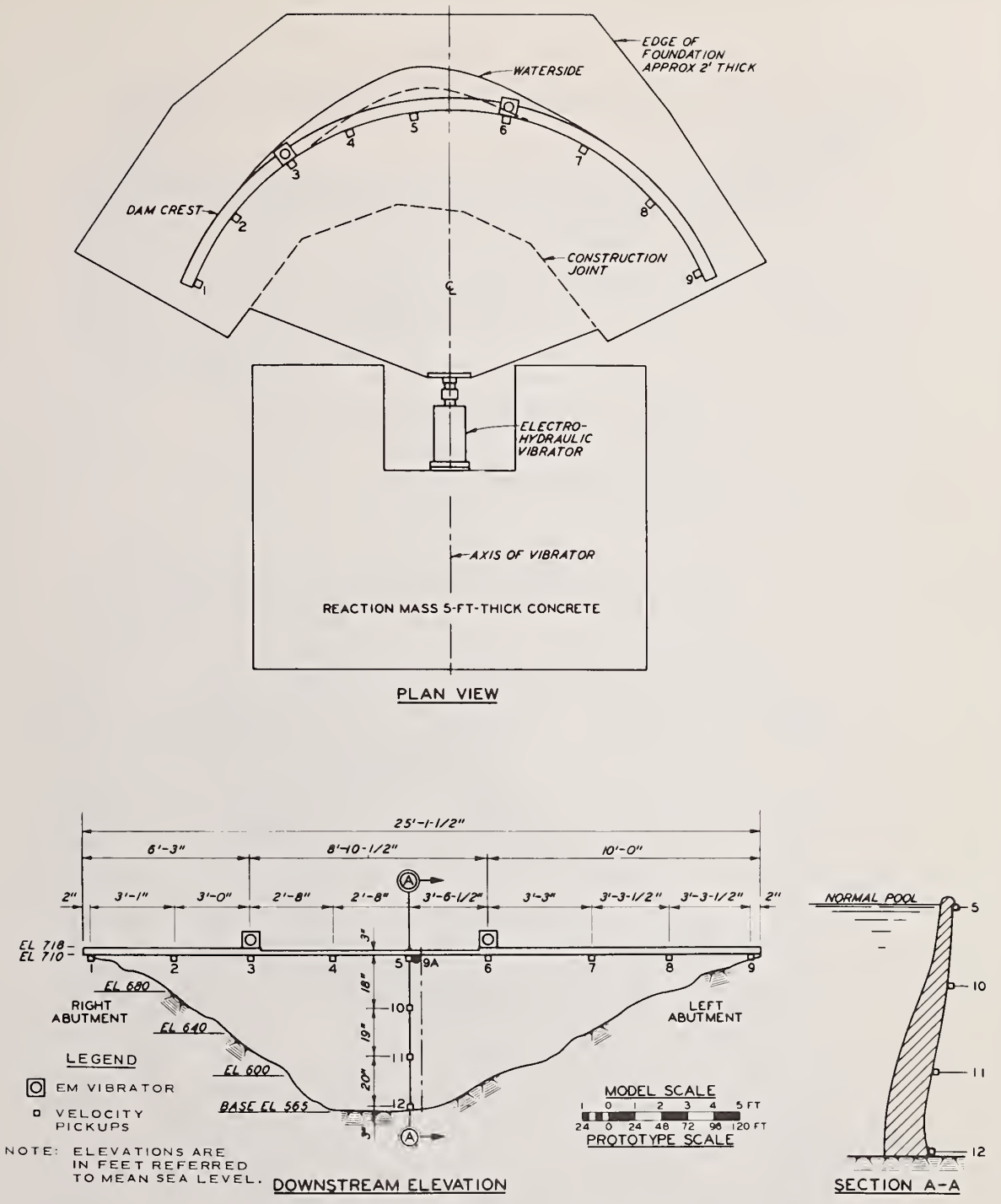

Figure 3. Plan, elevation, and section of North Fork Dam model

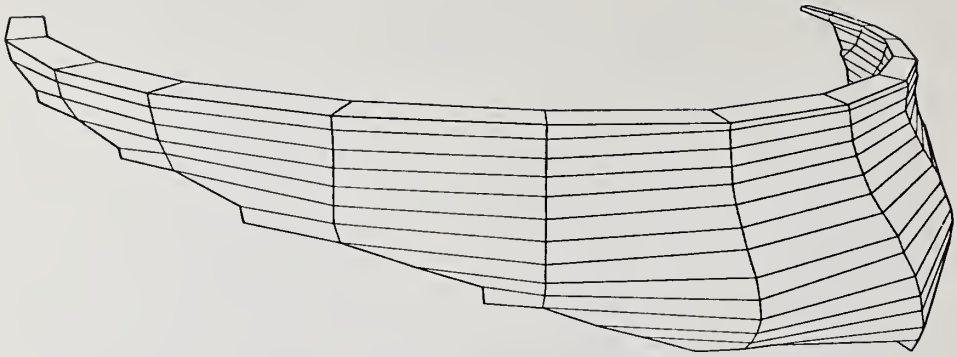

Figure 4. Small finite element grid

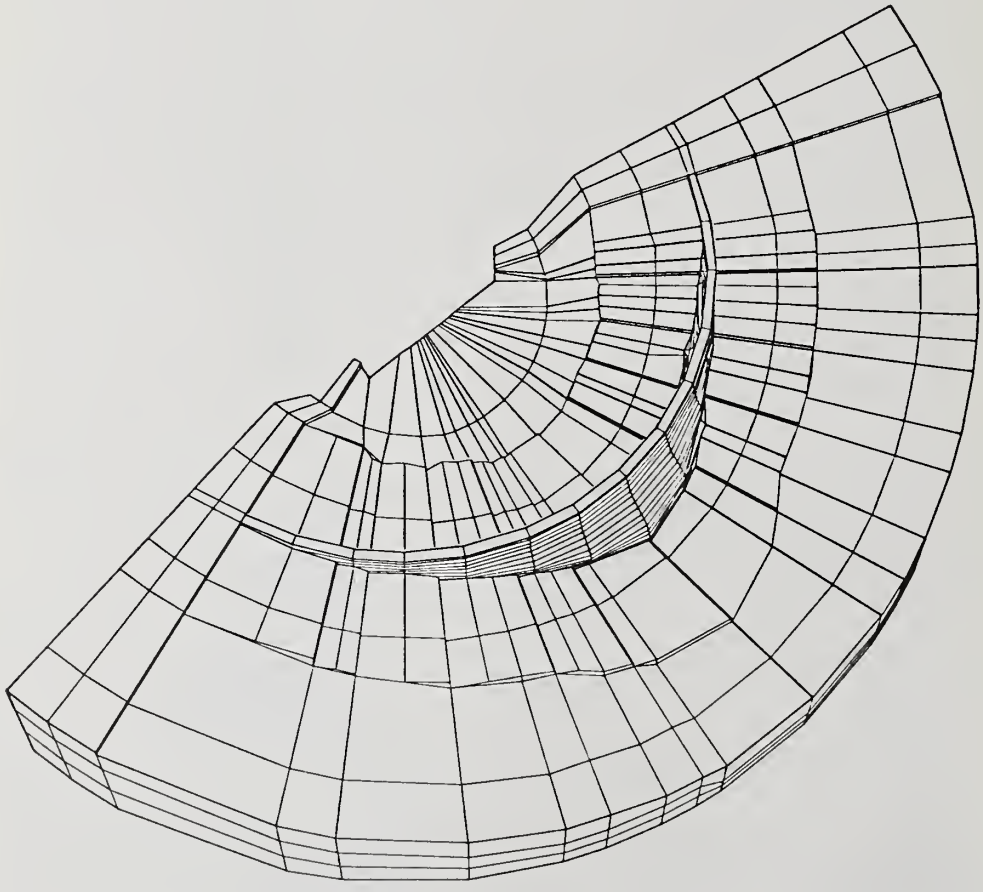

Figure 5. Large finite element grid including foundation

Table 1

EM Vibration Tests Conducted for North Fork Dam Model

Vibration System	Reservoir Level	Remarks
Two EM's	Empty	Frequency sweeps at 1 Hz/sec from 30 to 500 Hz, vibrators in phase and out of phase
Two EM's	Empty	Damping tests, vibrators shut off at various resonant peaks
Two EM's	Full	Frequency sweeps
Two EM's	Full	Damping tests
Two EM's	24 in. down	Frequency sweeps
Two EM's	Full	Pressure measurements at various resonant frequencies

Table 2

Damping Ratios with EM Vibrator and 15.5-Pound Force

Date (1973)	Vibrators In Phase (IP) or Out of Phase (OP)	Pickup Location	Frequency Hz	Damping Ratio
		Reservoir Empty		
21 Feb	IP	3	150	0.03
21 Feb	IP	3	297	0.02
21 Feb	IP	3	323	0.02
21 Feb	IP	6	150	0.04
21 Feb	IP	6	297	0.03
21 Feb	IP	6	323	0.02
21 Feb	OP	3	134	0.03
21 Feb	OP	3	150	0.04
21 Feb	OP	3	153	0.02
21 Feb	OP	6	134	0.05
		Reservoir Full		
22 Feb	IP	3	90	0.03
22 Feb	IP	3	106	0.04
22 Feb	IP	3	147	0.04
22 Feb	IP	6	90	0.04
22 Feb	IP	6	106	0.04
22 Feb	IP	6	147	0.03
22 Feb	OP	3	103	0.05
22 Feb	OP	3	104	0.04
22 Feb	OP	3	141	0.03
22 Feb	OP	3	175	0.02
22 Feb	OP	3	177	0.02
22 Feb	OP	6	103	0.05
22 Feb	OP	6	104	0.03
22 Feb	OP	6	141	0.02
22 Feb	OP	6	175	0.02
22 Feb	OP	6	177	0.03

Table 3

Sensitivity of Ritz Analysis to Load Pattern
with Reservoir Full and Fixed Base

Mode	Natural Frequency, Hz	
	Load Condition 1	Load Condition 2
1	183	159
2	232	177
3	271	219
4	335	274

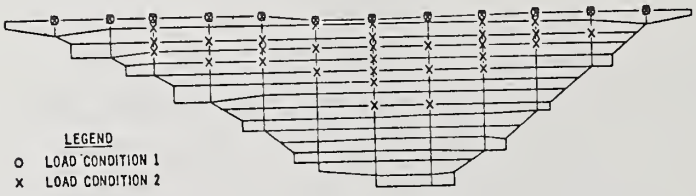

Table 4

Comparison of Natural Frequencies
Determined Using the Ritz Analysis
and the Subspace Iteration Technique
With Reservoir Full and Fixed Base

Mode	Natural Frequencies, Hz	
	Ritz Analysis	Subspace Iteration
1	159	151
2	177	162
3	219	197
4	274	229

Table 5

Comparison of Finite Element Frequency Calculations of Model Dam with Fixed Base and Foundation with Experimental Data

Mode	Reservoir Condition	Natural Frequency, Hz		
		Finite Element Model		
		Fixed Base	Foundation	Experimental
1	Full	151	124	--
1	Empty	171	160	--
2	Full	162	122	103
2	Empty	185	162	133
3	Full	197	151	147
3	Empty	226	196	151
4	Full	229	182	175
4	Empty	264	231	213

Table 6

Natural Frequencies for 1st and 2nd North Fork Dam Models (Reservoir Full)

Mode	Natural Frequencies, HZ	
	1st Model	2nd Model
1	94	--
2	102	103
3	118	147
4	150	175

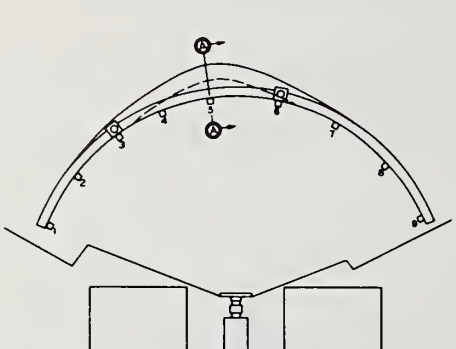

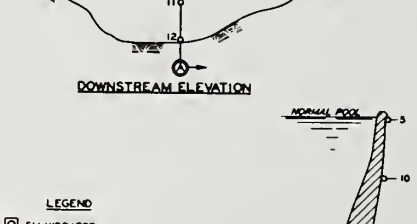

LEGEND
EM VIBRATOR
VELOCITY PICKUPS

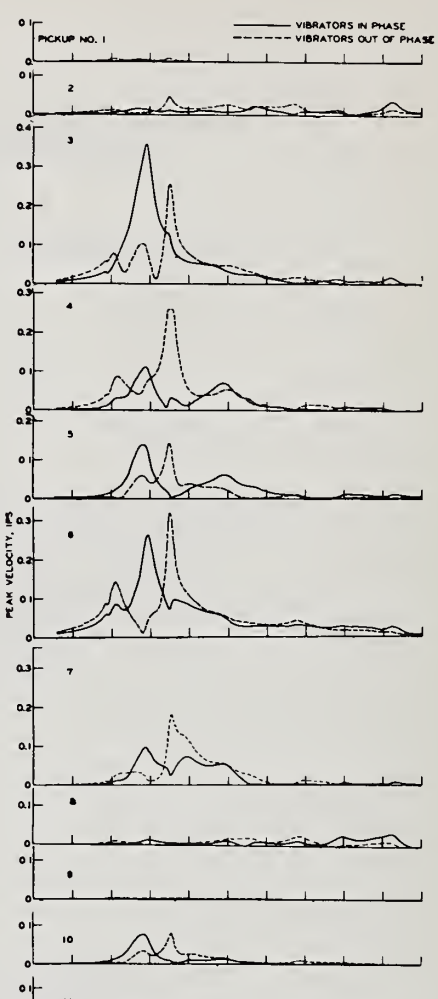

NORTH FORK DAM MODEL

VELOCITY VERSUS FREQUENCY

EM TESTS
RESERVOIR FULL

PLATE 1

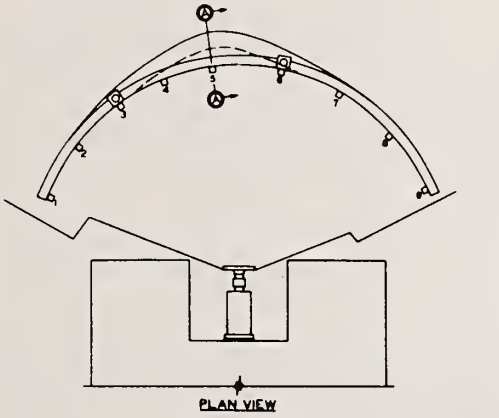

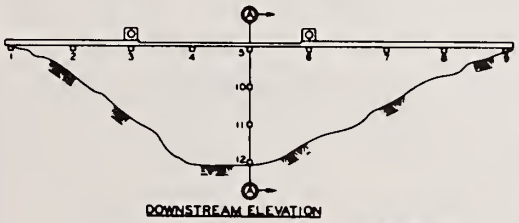

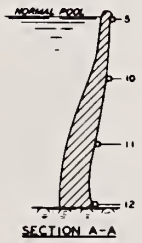

LEGEND

EM VIBRATOR

VELOCITY PICKUPS

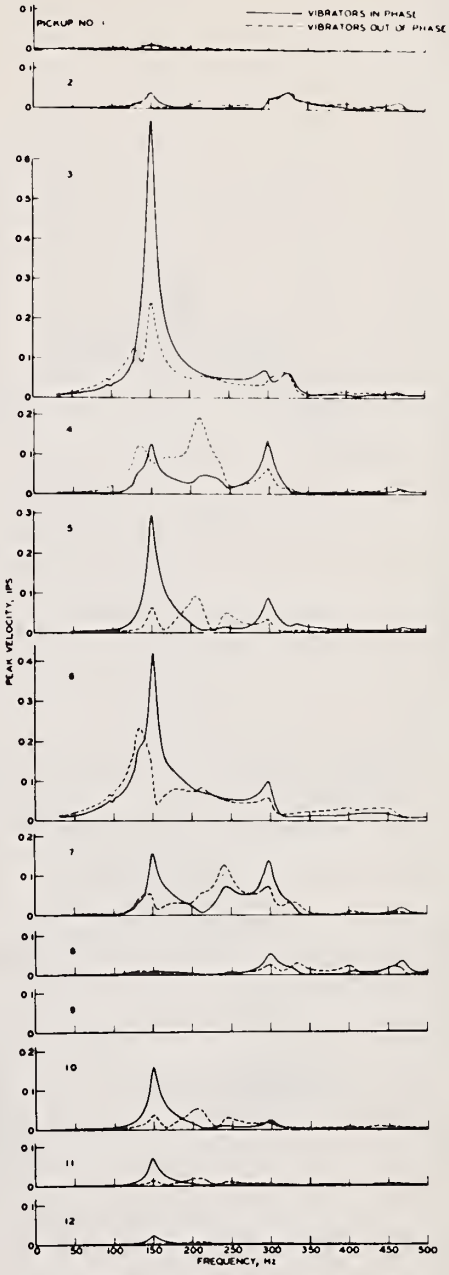

NORTH FORK DAM MODEL

VELOCITY VERSUS FREQUENCY

EM TESTS

RESERVOIR EMPTY

PLATE 2

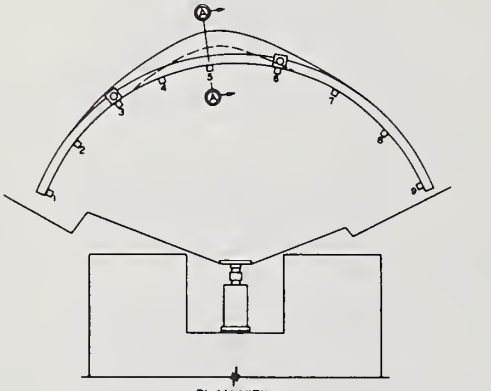

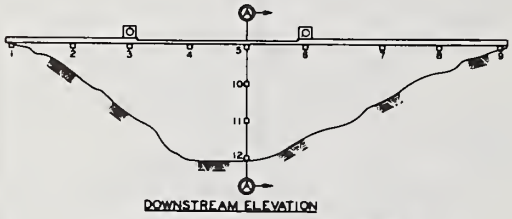

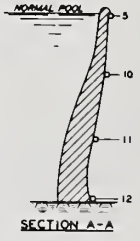

LEGEND

EM VIBRATOR

VELOCITY PICKUPS

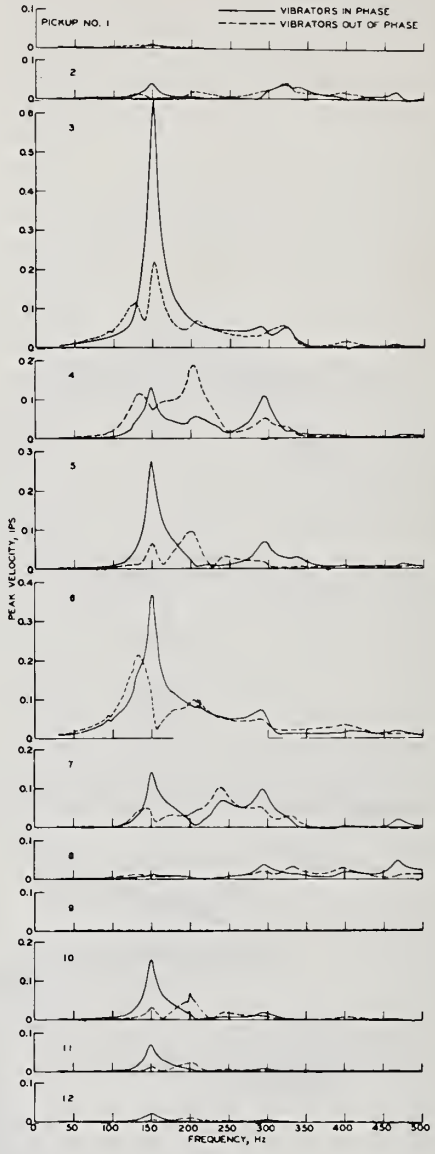

NORTH FORK DAM MODEL

VELOCITY VERSUS FREQUENCY

EM TESTS

RESERVOIR DOWN 24 IN.

PLATE 3

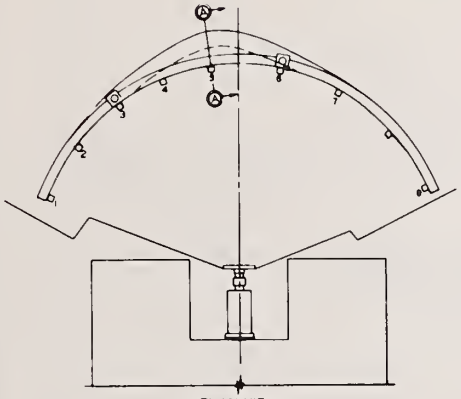

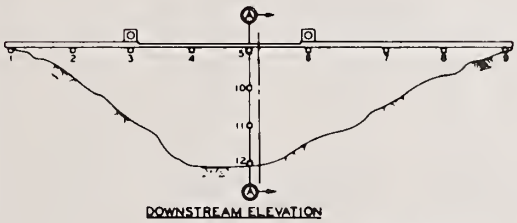

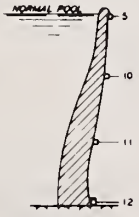

LEGEND

EM VIBRATOR

VELOCITY PICKUPS

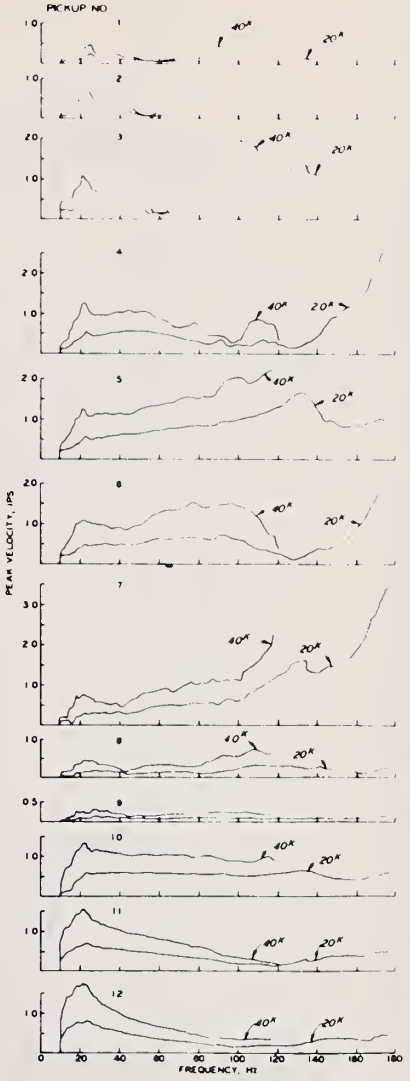

NORTH FORK DAM MODEL

VELOCITY VERSUS FREQUENCY

EH TESTS
RESERVOIR FULL

PLATE 4

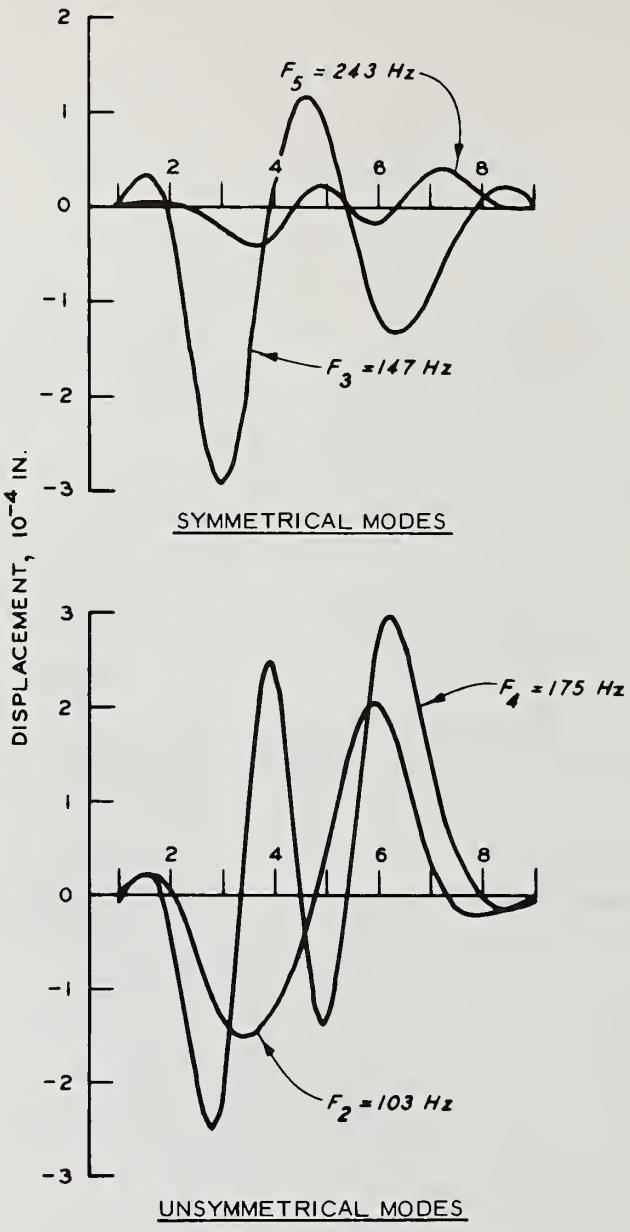

RADIAL CREST
DEFLECTIONS FOR MODES 2 – 5
EM VIBRATOR TESTS
RESERVOIR FULL

PLATE 5

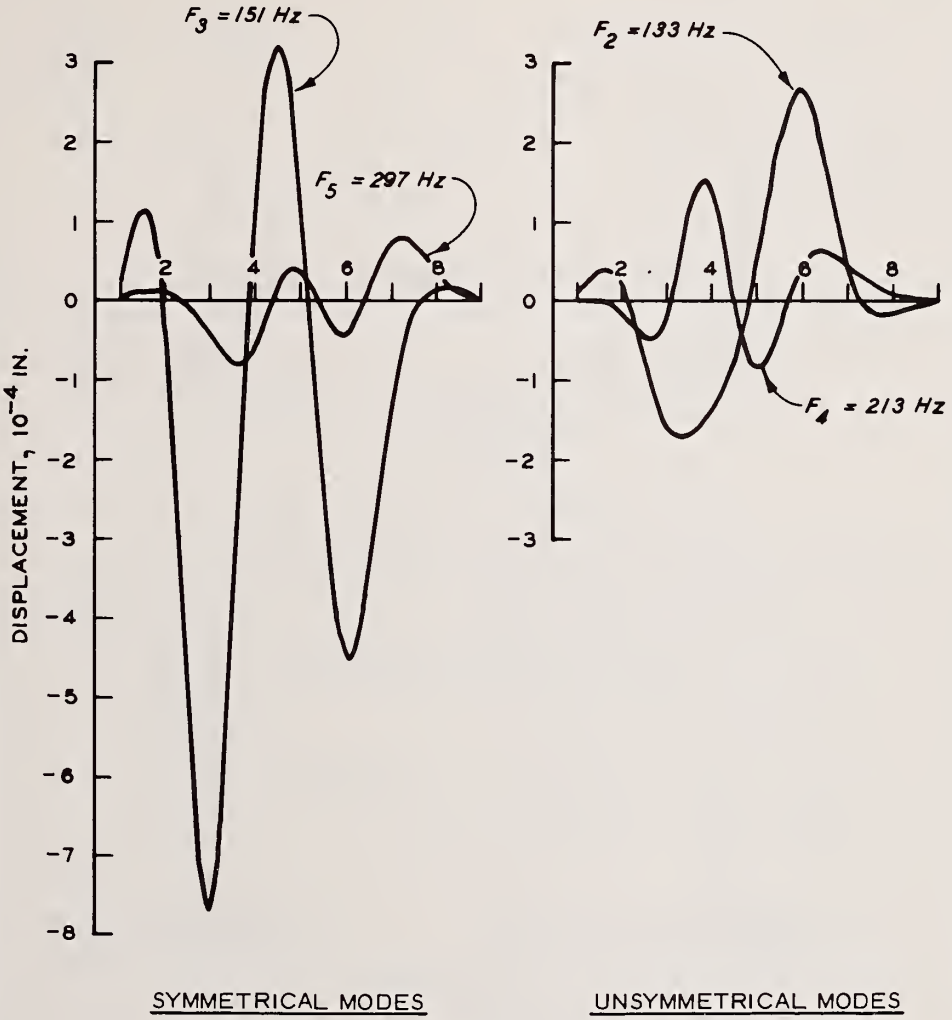

RADIAL CREST
DEFLECTIONS FOR MODES 2 – 5
EM VIBRATOR TESTS
RESERVOIR EMPTY

PLATE 6

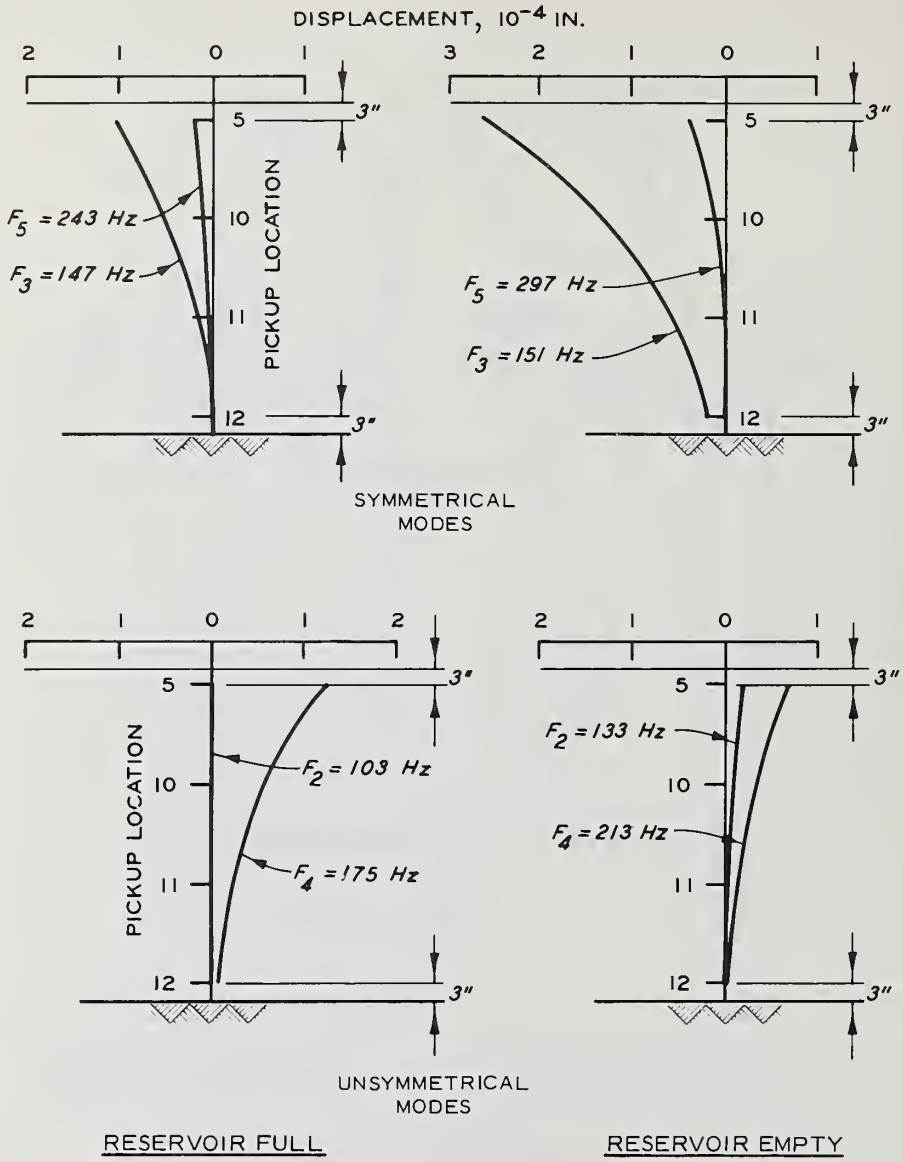

RADIAL CANTILEVER DEFLECTIONS NEAR CENTER LINE FOR MODES 2-5

EM VIBRATOR TESTS

PLATE 7

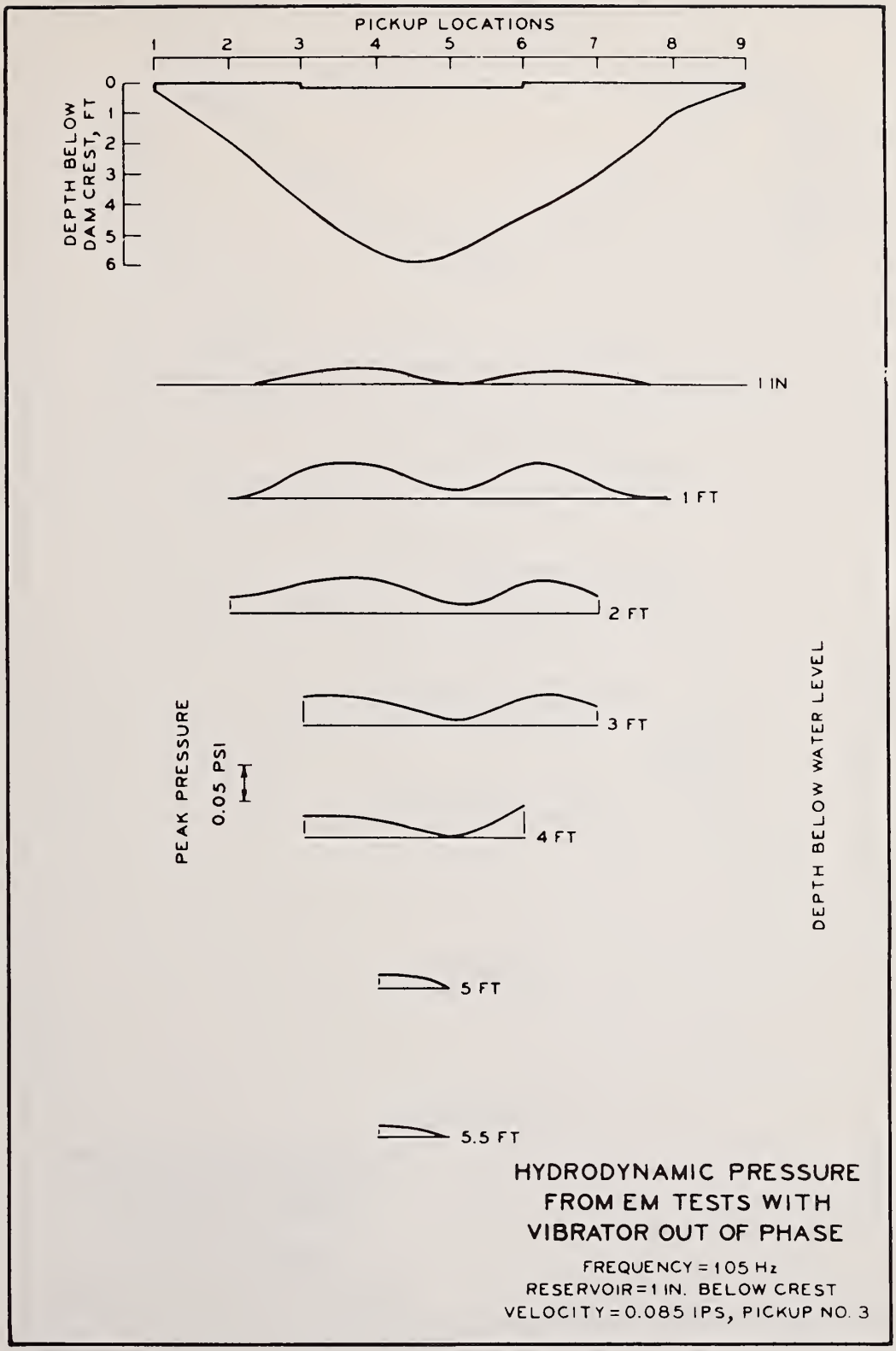
PICKUP LOCATIONS
1
2
3
4
5
6
7
8
9
DEPTH BELOW DAM CREST, FT
0
1
2
3
4
5
6
1 IN
1 FT
2 FT
3 FT
4 FT
5 FT
5.5 FT
PEAK PRESSURE
0.05 PSI
DEPTH BELOW WATER LEVEL
HYDRODYNAMIC PRESSURE FROM EM TESTS WITH VIBRATOR OUT OF PHASE
FREQUENCY = 1.05 Hz
RESERVOIR = 1 IN. BELOW CREST
VELOCITY = 0.085 IPS, PICKUP NO. 3

PLATE 8

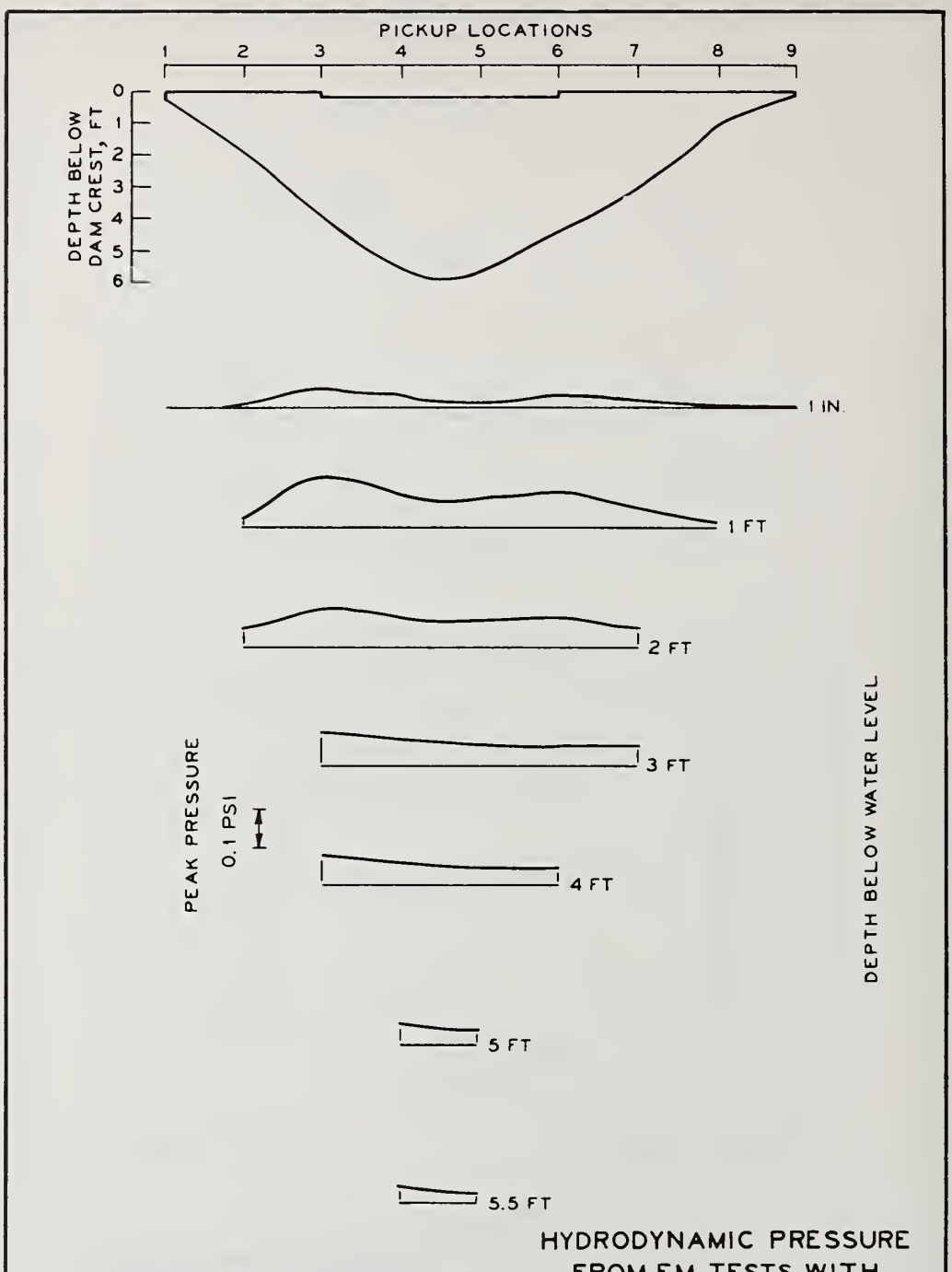

HYDRODYNAMIC PRESSURE FROM EM TESTS WITH VIBRATOR IN PHASE

FREQUENCY = 147 Hz
RESERVOIR = 1 IN. BELOW CREST
VELOCITY = 0.36 IPS, PICKUP NO. 3

PLATE 9

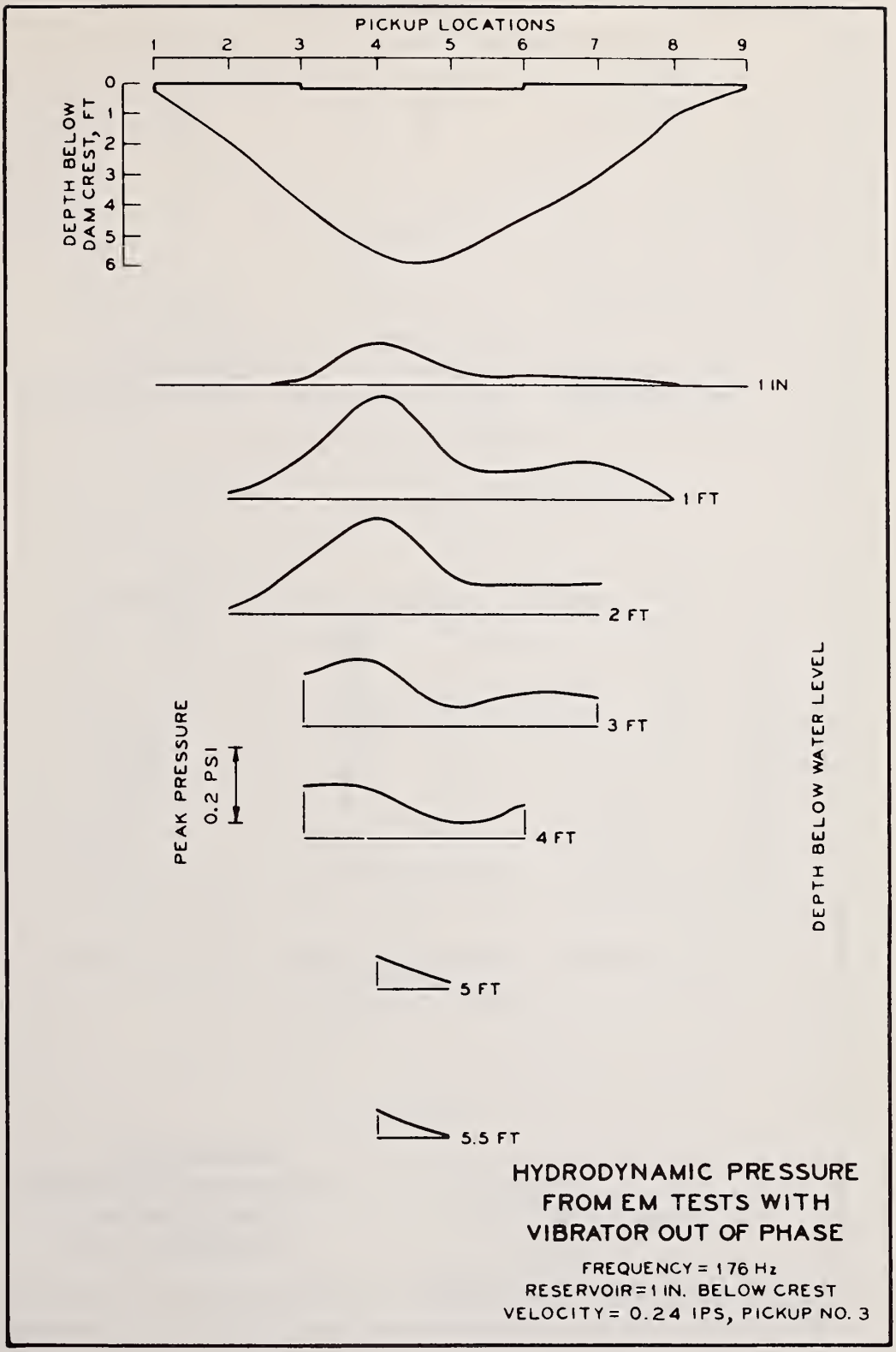

HYDRODYNAMIC PRESSURE FROM EM TESTS WITH VIBRATOR OUT OF PHASE

FREQUENCY = 1.76 Hz
RESERVOIR = 1 IN. BELOW CREST
VELOCITY = 0.24 IPS, PICKUP NO. 3

PLATE 10

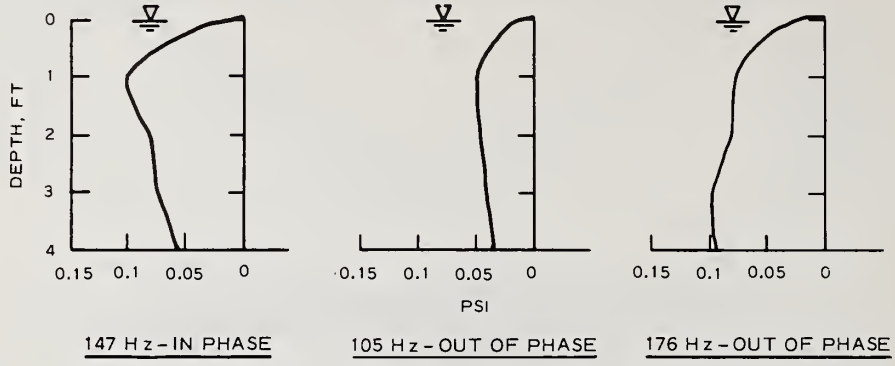

147 Hz - IN PHASE | 105 Hz - OUT OF PHASE | 176 Hz - OUT OF PHASE

VELOCITY TRANSDUCER NO. 6

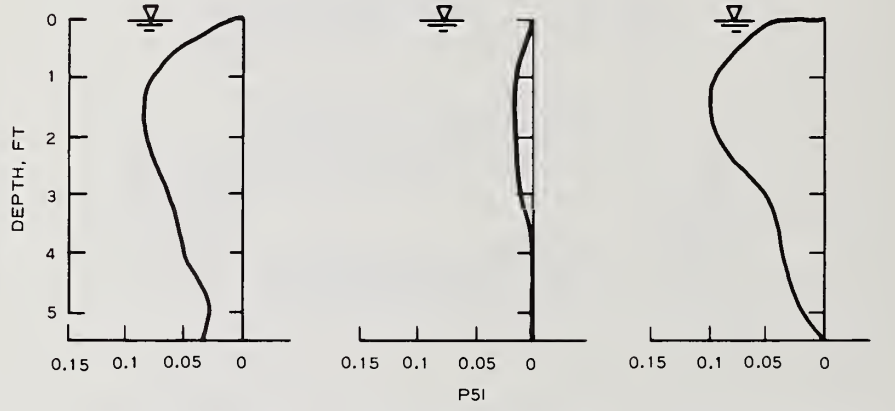

147 Hz - IN PHASE | 105 Hz - OUT OF PHASE | 176 Hz - OUT OF PHASE

VELOCITY TRANSDUCER NO. 5

VARIATION OF HYDRODYNAMIC PRESSURE WITH DEPTH

EM VIBRATOR TESTS

PLATE 11

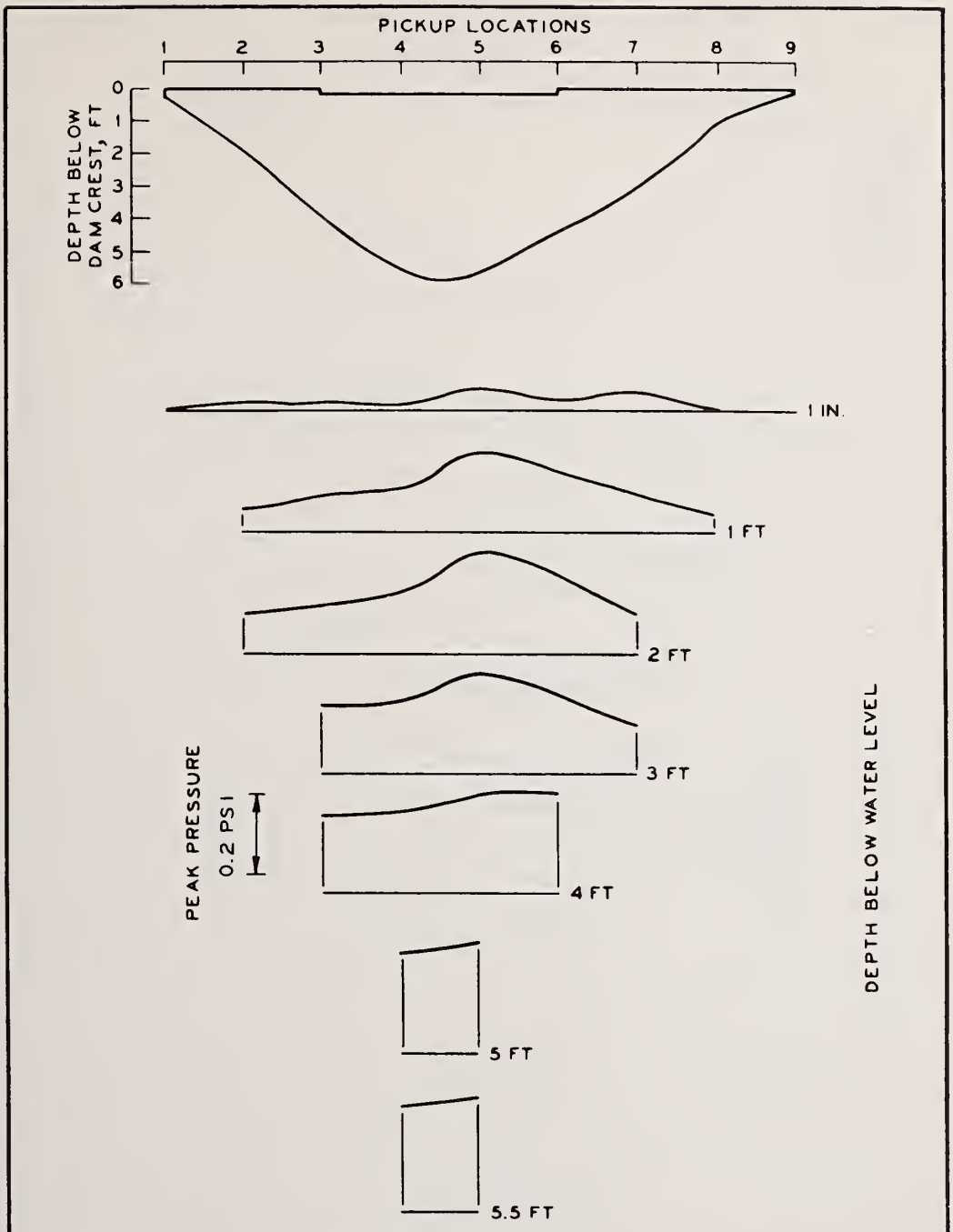

HYDRODYNAMIC PRESSURE FOR EH TESTS

FREQUENCY = 80 Hz
RESERVOIR = 1-3/8 IN. BELOW CREST
VELOCITY = 0.42 IPS, PICKUP NO. 5

PLATE 12

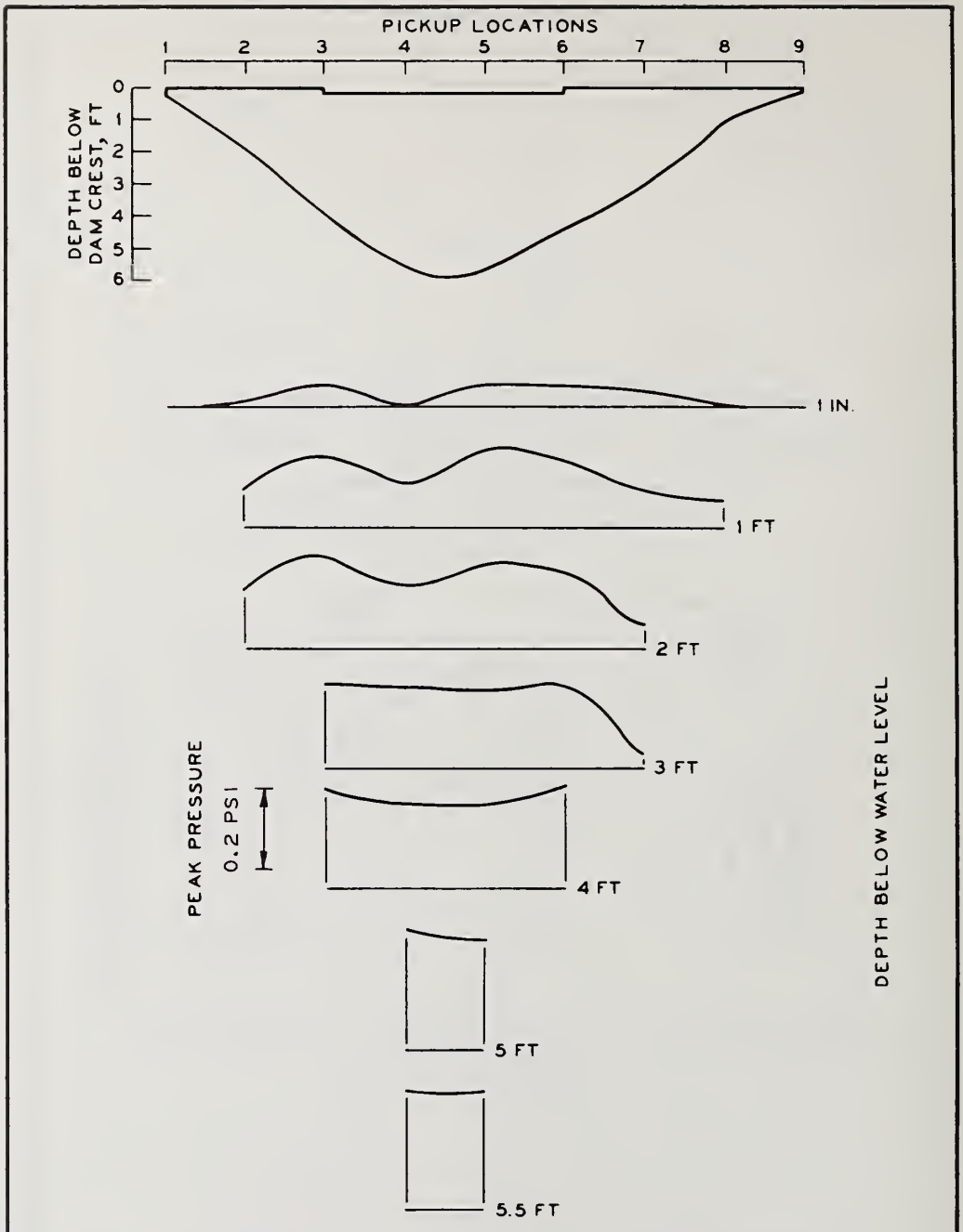

HYDRODYNAMIC PRESSURE FOR EH TESTS

FREQUENCY = 98 Hz
RESERVOIR = 1-3/8 IN. BELOW CREST
VELOCITY = 0.45 IPS, PICKUP NO. 5

PLATE 13

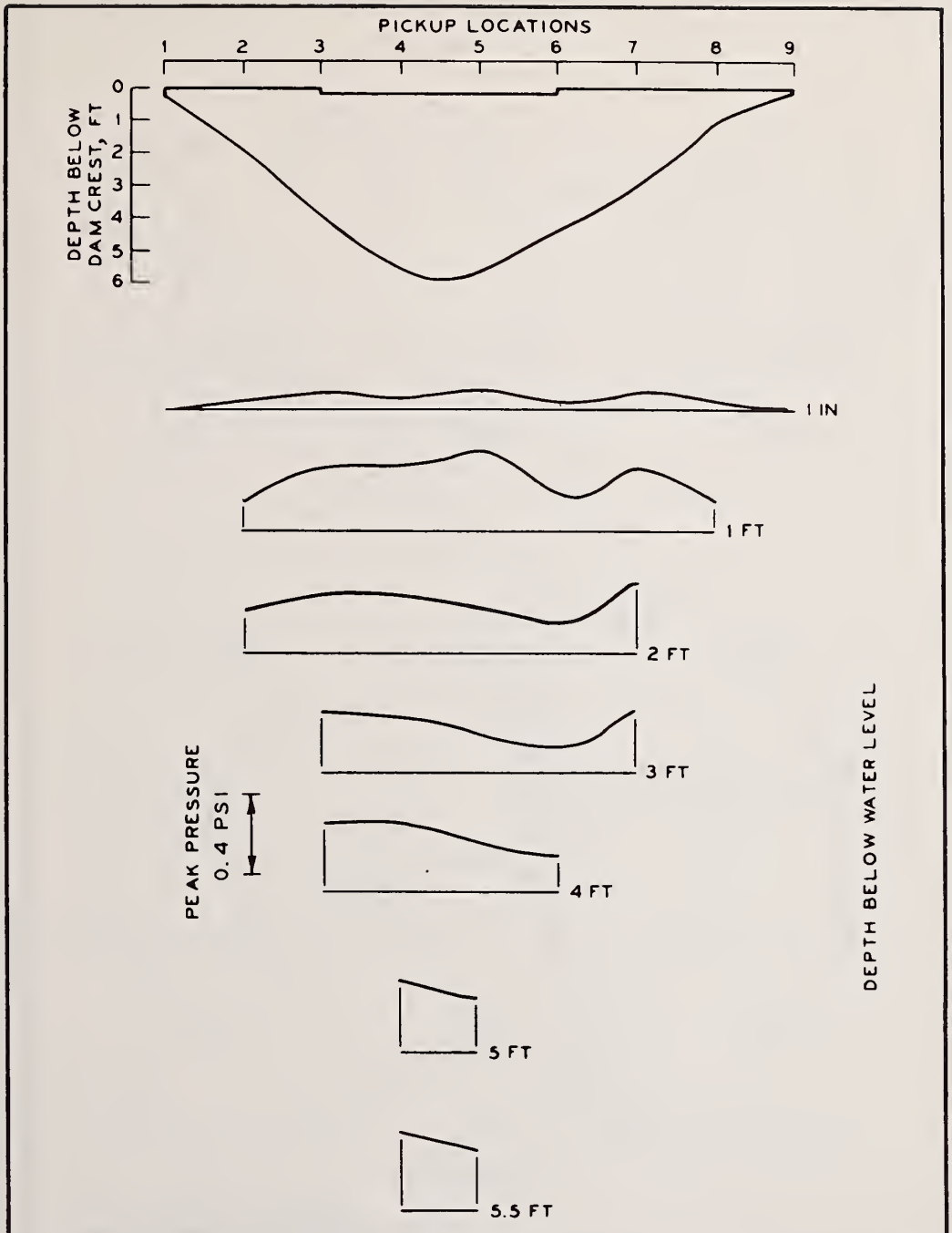

HYDRODYNAMIC PRESSURE FOR EH TESTS

FREQUENCY = 1.22 Hz
RESERVOIR = 1-3/8 IN. BELOW CREST
VELOCITY = 0.80 IPS, PICKUP NO. 5

PLATE 14

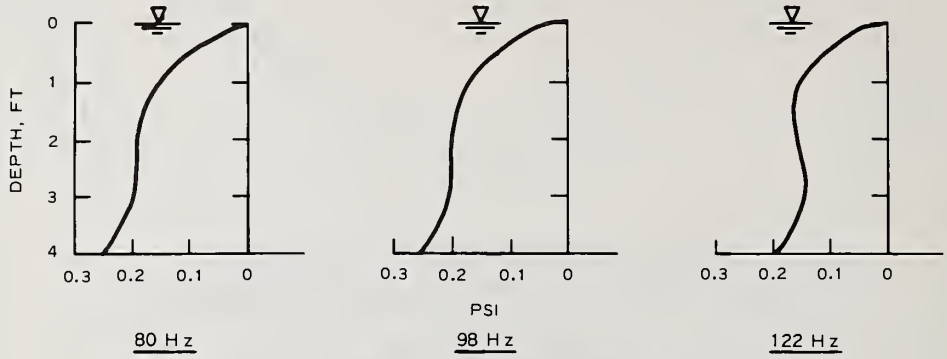

VELOCITY TRANSDUCER NO. 6

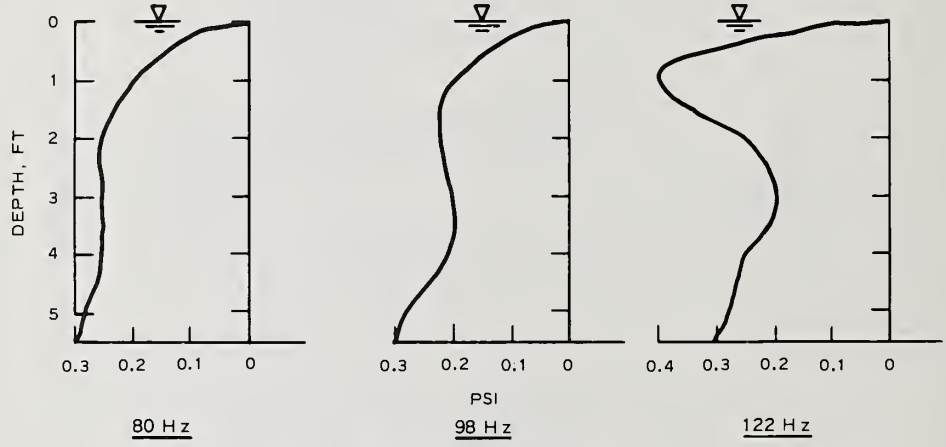

VELOCITY TRANSDUCER NO. 5

VARIATION OF HYDRODYNAMIC PRESSURE WITH DEPTH
EH VIBRATOR TESTS
AT 20^{K} FORCE

PLATE 15

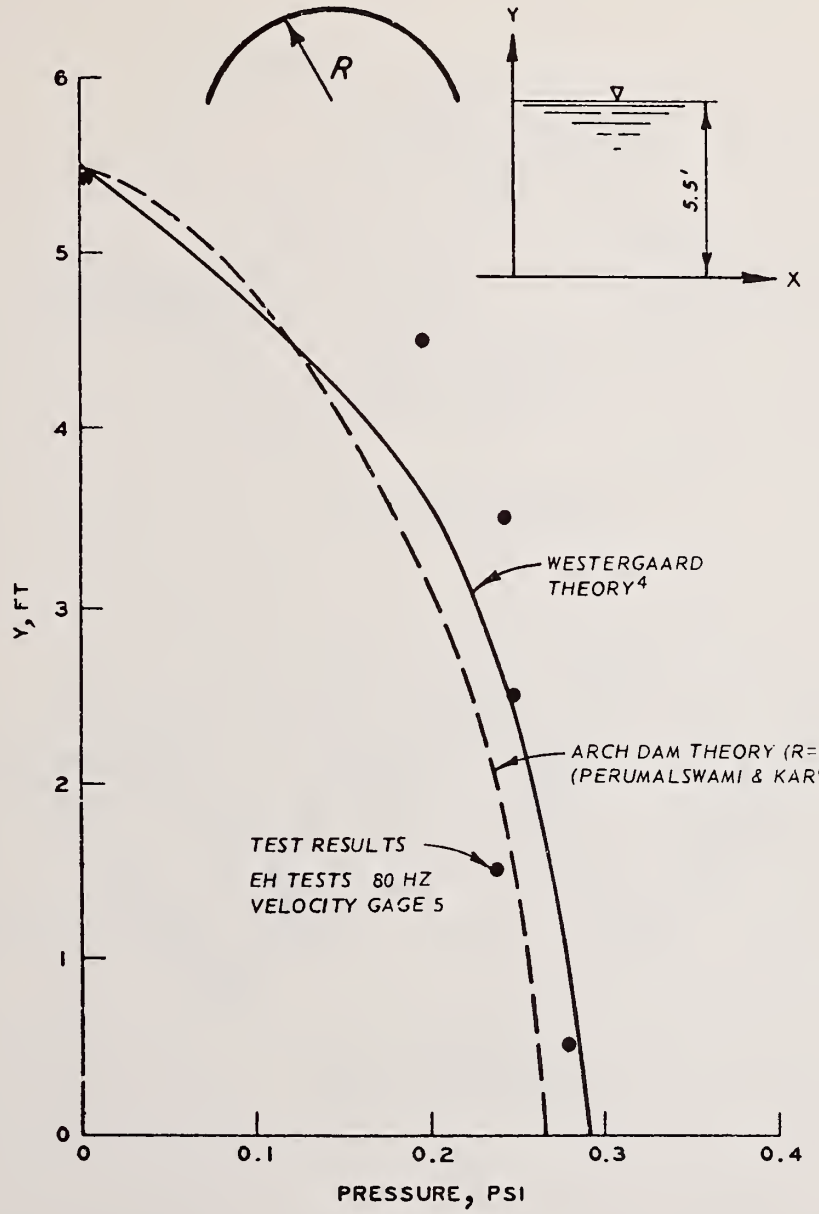

COMPARISON
OF THEORETICAL
AND EXPERIMENTAL
HYDRODYNAMIC PRESSURES

PLATE 16

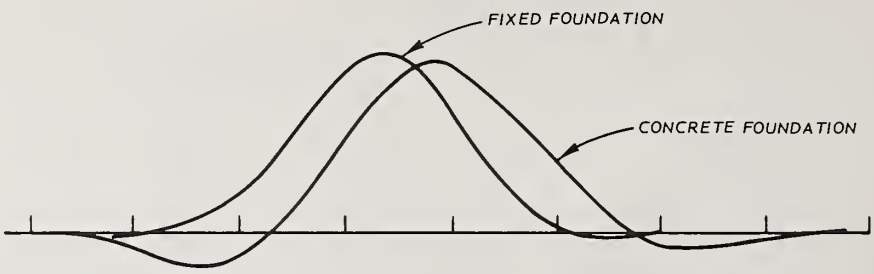

1ST SYMMETRICAL MODE

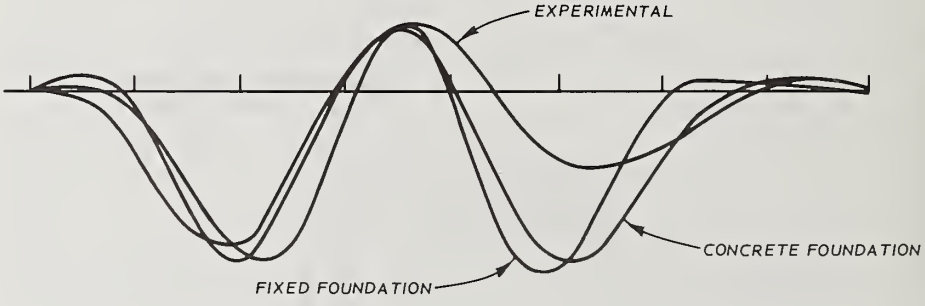

2ND SYMMETRICAL MODE

COMPARISON OF EXPERIMENTAL AND ANALYTICAL NORMALIZED MODE SHAPES

RESERVOIR FULL

SYMMETRICAL MODES

PLATE 17

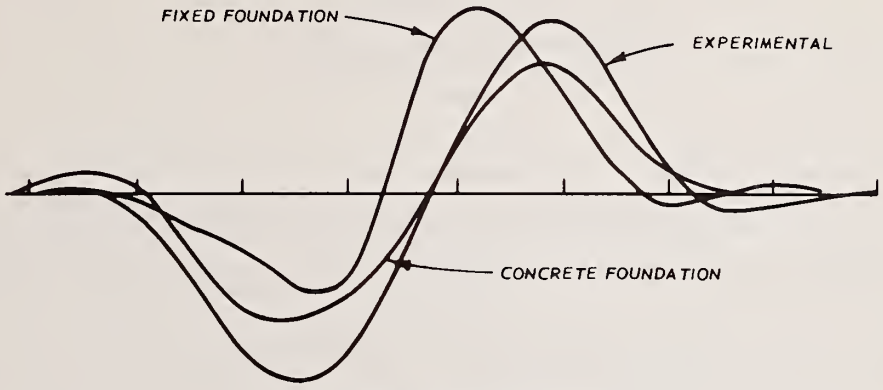

1ST ASYMMETRICAL MODE

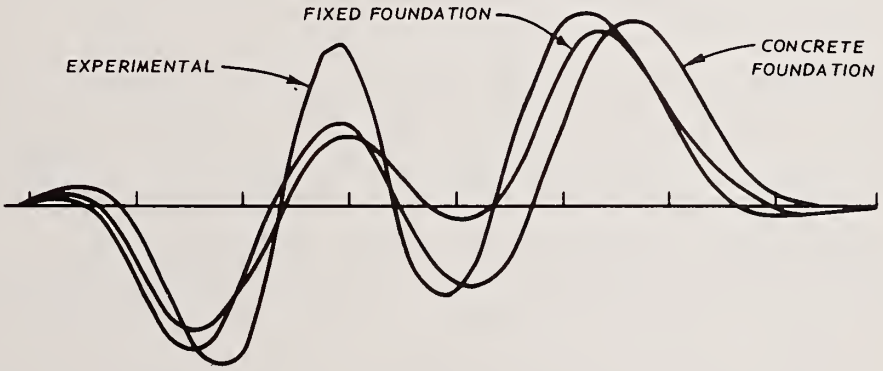

2ND ASYMMETRICAL MODE

COMPARISON OF EXPERIMENTAL AND ANALYTICAL NORMALIZED MODE SHAPES

RESERVOIR FULL

ASYMMETRICAL MODES

PLATE 18

THE MEASUREMENT OF THE DYNAMIC k-VALUE IN SITE AND ITS APPLICATION TO DESIGN

TETSUO KUNIHIRO
KANAME YAHAGI
MICHIO OKAHARA
Structure and Bridge Division
Public Works Research Institute
Ministry of Construction
Japan

ABSTRACT

The determination of the dynamic soil k property is determined by a series of bore hole tests. Results from these tests are discussed and the significance of these data are presented.

Key Words: Bore Hole; k Property; Soil; Stiffness; Property; Testing.

1. Introduction

The earthquake-proof design of structures including the foundation, is performed by the so-called seismic-coefficient method in which the dynamic phenomena is substituted by a staticphenomena. With recent advances in the method of structural analysis and computer systems, calculation of the complicated dynamic phenomena has become possible. However, in examining the effects of earthquakes relative to actual structures, it is important to know the nature of the structural materials. This is especially true concerning the dynamic characteristics of the ground, instead of mere knowledge of the nature of the dynamic load as an input and the adequate analytical method.

Calculation of horizontal resistance of piles is usually made by using the values of the modulus of lateral reaction of the ground, k-values, assuming that piles are beams on an elastic foundation. The k-values are obtained by utilizing the data from bore holes at the site. The evaluation of the k at the time of the earthquake is obtained from static tests and then multiplied by a certain conversion coefficient. Scientific research on the dynamic properties of soil has been conducted, to some extent, but few have applied the research to practical problem of design of foundations.

In this report, description of the development of a device for measurement of the dynamic k-values by utilizing boring holes, will be given. This will therefore meet the urgent need for determining k-values at the site.

2. Basic Problems Concerning k-Value

Definition of the modulus of dynamic lateral reaction force (k-values) of the ground, is quite difficult because of the following reasons: Complexity of the forms of stratums that compose the ground; even if the domain of strain is small the stress-strain relation is non-linear under the loaded conditions: change in the dynamic properties of the

ground becomes further complicated due to the extent the strain is sustained in each stratum.

If the ground is perfectly elastic, no change occurs in the k-values, even though the working stress may differ in its magnitude and velocity. However, the ground is not perfectly elastic. Therefore, in order to obtain a reasonable k-value, the effects of strain, load velocity, number of vibration, etc. should be taken into consideration in the evaluation of the real k-value.

In order to deal with the above problems, it may be necessary to obtain k-values by examination of many stratums and select k-values that are useful in the actual design from among the accumulated data during the actual measurements.

3. Basic Problems in Measurement of Static k-Values

The following methods can be used to measure the static k-value at site: Load test using the steel load plate, 30-50 cm square; calculating back to the results of load test by means of the Chang's method; horizontal load test utilizing boring hole. Among these methods, the horizontal load test utilizing boring hole is used most frequently, because of the ease of performance.

The load test using boring holes as presently performed in this country, consists of two methods i.e., examining the difference in load and the displacement control. The first, the uniform load method, measures the mechanical constant and shearing strength of the ground around the boring walls obtained from the load-displacement correlation as obtained by applying equal direct pressure to the whole circumference of the test wall. The other method, uniform displacement, has similar measurements but controlling the uniform displacement of the wall of the boring hole in a specified direction.

The preciometer shown in Fig. 1, and L.L.T shown in Fig. 2 is the tester for the uniform load method. K.K.T. shown in Fig. 3 is a tester for the uniform displacement method.

As shown in Fig. 3, the body of the loading part of the tester, K.K.T. for the uniform displacement method, is a small-sized special jack. Two high-pressure hoses from this body are connected to the high-pressure hydraulic pump on the ground. The cylinder of the loading body has 2 holes, one for sending oil to push out the piston and the other for sending oil to push the piston back into the cylinder after the load test. When pressed from one direction during the measurement, the piston is pushed out to give pressure to the load plate. Then, the oil filled around the piston in the cylinder flows backward to the ground passing through the other hose. The amount of the oil flowing back is proportional to the displacement of the load plate. Utilizing this phenomenon, the flow taken into the small-bore stand pipe and the displacement of the load plate is measured.

The method of the load test in the hole, using the K.K.T. tester, is called the uniform displacement method because the steel load plate outstretches the hole wall horizontally by the force of the jack to give rise to a uniform displacement. In short, the displacement is similar to the horizontal displacement of a pile which occurs in

the load plate during the test.

Aside from the merits and demerits of the testers, it has been clarified by past test results by the authors, that there are no great differences in the measured values among the testers, if the hole walls and ground are under the same conditions. (Literature 1-2).

That the condition of the hole wall during the test, is the greatest factor which gives rise to errors on the results of load test in holes, has been confirmed. It has been noted that differences in measured values, caused by the testers, is so small in comparison with the difference in the degree of irregularity of the boring wall surface.

Basic problems of the bore hole field test, in addition to the measuring of the static k-value, lie in the fact that the boring technique and the measuring technique are difficult.

If the boring wall surface became irregular or uneven in the boring process or collapses during the load test, the data obtained therefore will be erroneous and unusable, even though the test may be conducted carefully. Because no excellent boring technique can be expected at all times, a device is required to develop favorable boring wall conditions at all the times during the test. This is achieved by attaching a boring trimmer to the tester in order to obtain the accurate data during measurements.

Fig. 7 shows the dynamic k-value measuring tester. As just described the trimmer is required and is fitted at the edge of the tester of the bore hole not only for the dynamic load test but for the static load test.

The testing method of the K.K.T. tester with attached trimmer, is to dig a hole whose bore is a little smaller than the load plate of the tester. Then enlarge the hole by cutting with the trimmer until the load plate comes in close contact with the boring hole, and then insert the load plate. Because of the trimming, the test can be performed with a boring wall which has no irregularities.

The irregularity of the boring wall creates an underestimation of static lateral k-value. In this regard, Nishigaki (Literature-5) compared the modulus of deformation obtained from various tests of viscous soils and pointed out that the modulus of deformation obtained from the load test in the boring hole varies greatly under the effect of irregularity of the boring wall.

Fig. 4 compares the results of the measurement of the static k-value for the alluvial clay of Osaka (W_L = 89%, W = 63%, q_u = 0.67 kg/cm^2) for the cases when trimming was made and was not made.

Fig. 5 shows the results of similar comparative test for the diluvial clay (W_L = 100%, W = 50%, q_u = 5.6 kg/cm^2) called Ma-3 that is found in hills of Osaka region.

These figures show that when the boring hole is trimmed, the load displacement curve shows a sharp start and accordingly a high k-value.

The load displacement curve, in the conventional case where no trimmer is used, shows no sharp curve at the initial stage and measuring starts at a point on the secondary ine for the case in which trimming is made.

Fig. 6 shows the measurement results made for the purpose of ascertaining the effects in the use of trimmer in a single boring hole in diluvial clay of Osaka. This indicates

how great the difference of k-values may be dependent on whether the trimmer is or is not used in hard clay soils, where irregular boring is generally believed not to occur.

4. Dynamic k-Value Tester

The dynamic k-value tester, shown in Fig. 7, is a tester in which the K.K.T.'s principles have been applied with inclusion of some new devices in its construction. As shown portions 5, 6, and 7 consist of the same construction of the loading body of the K.K.T. The load plate 5 is loaded with the boring wall when oil pressure acts on piston 6. Movement of the load plate can not be simple, as in the case of measuring the static k-value. As mentioned already, the working stress, amplitude and number of vibrations must be interchanged. For instance, when the load plate is charged with sine-wave type load, the oil pressure on the piston must be varied.

When using the K.K.T. for static tests, the oil pressure is given to the piston from the hydraulic pump on the ground through the high-pressure hoses (refer. to Fig. 3). If the wave type load is applied by attaching a servo-valve etc. to the hydraulic pump, attenuation of pressure occurs in the process of transmitting pressure to the loading body in the boring hole through a slender high-pressure hose, and thereby makes it impossibil to transmit the desired load change. This is always the case, when a pressure control is conducted on the ground, even if any other tester (for instance, a rubber tube) is used.

In this dynamic k-value tester, the mechanism corresponding to the hydraulic pump on the ground is replaced with the portions given as 10, 11 and 13, and the pressure control is devised to go directly above the test place. The piston of the hydraulic pump on the ground is substituted by the piston 10. The cylinder shown by the thick black lines in the diagram is filled sufficiently with oil to actuate freely the piston 8. Free performance of the piston 10 under principles that will be mentioned later, causes the required orderly wave-form oil pressure load to act on the piston 6. Then the load plate 5 gives the required load change to the ground around the boring wall.

The operative power of piston 10 is given from the micro air cylinder 13 through the coupler 11. The high-pressure air required for the operation of 13 is supplied from the high pressure tank of the air compressor on the ground through the air hose and the regulator 16.

The regulator is capable of regulating the pressure from zero to a maximum pressure by moving up-and-down the pin projected from the upper part of the regulator.

The pin projected from the regulator 16 moves up-and-down in conformity to the rotation of the cam circular plate 18, to the height of the cam connected directly to the DC motor 20 with a reduction gear. The air pressure in the air cylinder can be changed by adjusting the shape of the cam circular plate to regulate its rotation. Next, the air pressure in the air cylinder and the movement of piston 10 and finally the load on the load plate can be changed freely to meet the test conditions.

The stress that acts on the load plate causes a complicated displacement to the ground around the boring wall. Displacement is measured indirectly by the linear motion

potentiometer 12 directly connected to the coupler 11 and then registered.

The change in oil pressure in the body, which acts on the piston 6, is measured by the pressure transducer 4 inserted at the edge of the hydraulic cylinder of the body and then registered together with the displacement of the load plate.

The notable feature of the dynamic k-value tester lies in the fact that installations on the ground are successfully housed in the body of the tester, which was considered difficult for conventional type of testers. Thanks to completion of this tester, accurate dynamic load tests can now be performed easily.

The development of a superior tester can be obtained by remodeling this tester as determined from field experiments.

5. Results of Measurement of Dynamic k-Value

Shown is an example of the analysis made using the results of the measured stress-displacement from the tester, when a sine-wave type load is given to the load plate. (Experiment at Urayasu in Chiba Pre).

Experimental results of the dynamic k-value tester are sent to a data recorder as shown in Fig. 8. Fig. 9 shows the results of the stress-displacement measurement. The wave form shown on the upper part, represents the stress and that on the lower part represents the displacement.

As shown in this Fig., similar strains occur in the ground around the boring wall in response to the sine-wave type stress. With the increase in number of repetitions of the load, the displacement of the boring wall gradually increases.

The results of the vibration test of the linear elastic body are shown in Fig. 10. When a sine-wave type vibration stress is given to the linear elastic body and a stationary state is reached, the strain phase of the elastic body lags by δ from that of the stress. This is because the stress energy is consumed in the elastic body.

Fig. 11 shows the above phenomenon by a hysteresis loop. In this Fig., the loop area, ΔW, shows the loss of energy consumed in one cycle of the steady vibration. The energy given, W, is indicated by the area of ΔABC.

The damping factor (Loss $\tan\delta$) indicated the ratio of ΔW to W is defined by the following equation.

$$\tan\delta = \frac{2}{\pi} \cdot \frac{\Delta W}{W} = \frac{c \cdot d}{a \cdot b} \qquad \text{(When } \delta \text{ is extremely small)}$$

From the hysteresis loop, the dynamic elastic constant is obtained as follows.

$$E_d = \frac{\sigma_1 - \sigma_2}{\varepsilon_1 - \varepsilon_2} = \frac{b}{a}$$

If the dynamic elastic constant is equal to the static elastic constant, the following formula is obtained.

$$E = \frac{\sigma_1}{\varepsilon_1} = \frac{\sigma_2}{\varepsilon_2} = \frac{\sigma_1 - \sigma_2}{\varepsilon_1 - \varepsilon_2}$$

Generally, in the case of vibration under the initial stress, σ_o, the A.B axis increases as compared to the O.A axis, as shown in Fig. 12. As a result:

$$E_1 = \frac{\sigma_1}{\varepsilon_1} \qquad E_2 = \frac{\sigma_2}{\varepsilon_2}$$

$$E_3 = \frac{\sigma_1 - \sigma_2}{\varepsilon_1 - \varepsilon_2}$$

Accordingly, Ed > E_1 > E_2.

The k-value, can be found by substracting the above mentioned strain quantity, ε, by the displacement of the ground, X, and all other elements may be assumed the same, viz. P_1, corresponds to stress σ_1 and P_2 to σ_2 as given in Fig. 9 and the corresponding displacements are X_1 and X_2. The E-values are obtained from Fig. 12, therefore three k-values are given as follows:

$$k_{dh-1} = \frac{P_1}{X_1} \quad \text{(max. stress/max. displacement)}$$

$$k_{dh-2} = \frac{P_2}{X_2} \quad \text{(min. stress/min. displacement)}$$

$$k_{dh-3} = \frac{P_1 - P_2}{X_1 - X_2} = \text{dynamic k-value } (k_{dh} \text{ value})$$

The dynamic k-value, given as the value of the k_{dh-3}, is obtained from the inclination of the line A-B.

For reference, the dynamic k-value is calculated as follows, using the experimental record of Urayasu in Chiba Pre., GL - 17.5 m.

Stress $P_1 = 0.367 kg/cm^2$

$P_2 = 0.231 kg/cm^2$

$P_3 = 0.136 kg/cm^2$

Displacement $X_1 = 0.0239 cm$

$X_2 = 0.0186 cm$

$$X_3 = 0.0053\text{cm}$$

$$k_{dh-1} = \frac{P_1}{X_1} = \frac{0.367}{0.0239} \fallingdotseq 1.54\text{kg/cm}^3$$

$$k_{dh-2} = \frac{P_2}{X_2} = \frac{0.231}{0.0186} \fallingdotseq 12.84\text{kg/cm}^3$$

$$k_{dh-3}\ (\text{dynamic k-value}) = \frac{P_3}{X_3} = \frac{0.136}{0.0053} \fallingdotseq 25.7\text{kg/cm}^3$$

Fig. 13 shows a trend of the gradual decrease in the dynamic k-value with a small change in the absolute quantities of the stress and displacement as the result of the repetitions of the sine-wave type loading.

Fig. 14 shows the results of experiments conducted at Urayasu in Chiba Pre., for a study of the problems concerned with the k-value. The dynamic k-values, plotted in Fig. 14, show the values for ten repetitions of the load.

The E-value was converted, using the following equation, using k-values measured by the tester;

$$E = K \cdot I_p \cdot D(1 - \mu^2)$$

D : Diameter in terms of load plate

I_p : Form factor (0.79 in the case of circular plate)

μ : Poisson's ratio

The load plate used in this experiment was 8.5 cm x 12 cm. Substituting the above values in to the following equation, 9.95 cm is obtained as the reduced diameter D.

$$\frac{L}{A} = \pi D \times \frac{4}{\pi D^2} \qquad \therefore D = \frac{4A}{L} = 9.95\text{cm}$$

Area of circle : $A = \frac{1}{4}\pi D^2$

Peripheral length : $L = \pi D$

Therefore, the E-value can be obtained from k-values using the following equation.

$$E = 6.60k$$

The results of a comparative study where all the test values are converted into E-values, are shown on the right column of Fig. 14.

Correlation between the static k-value and the dynamic k-value indicates that no clear answer can be given unless more data is collected. This correlation is shown as based on the following field test results.

When the k-value measured by the conventional method is assumed 1, the static k-value measured by K.K.T., using trimmer 3-4 and the dynamic k-value 6-7. The correlation may of course differ according to the conditions of the ground and the test. In any case, however, it is true that the dynamic k-value is higher than the static k-value. The static k-value, measured with the tester inserted in the hole without trimming by means of the conventional method, is low compared with the dynamic k-value. Whether or not to use such a value in the earthquake-proof design has become questionable, and it has been made known that there is need to make further studies.

6. k-Value and Foundation Design

A series of experiments, conducted by the authors, have revealed that various k-values are obtainable by changing the test conditions even in the same soil. The question is then in selecting the k-value for use in foundation design. This is a great problem which still remains unsolved at present.

The pending problem lies in how to solve the questions arising from the assumed conditions for Chang's formula, that is generally used in this kind of calculation. Chang has assumed a constant k-value, which is not consistent with the test conditions, and utterly disregards the depth and bending. In the Chang's method the tolerable quantity of displacement is determined first, from which the allowable bearing power is calculated. No clear view, however, has been established in the determination of the tolerable displacement. This poses another important problem which must be solved.

Reasonable determination of the tolerable displacement is as important as the exact measurement of the k-values, that suit the design conditions. This fact is demonstrated as follows;

The bearing power, by Chang's formula, while the pile head is set free will be:

$$\beta = \sqrt[4]{\frac{kD}{4EI}} \qquad \delta = \frac{2\beta H}{kD} \qquad H = \frac{\delta kD}{2\beta}$$

Therefore,

$$H = \delta \cdot k^{\frac{3}{4}} \cdot \sqrt[4]{\frac{EID^3}{4}}$$

In short, the horizontal force of a pile is proportional to the displacement with the k-value raised to the 3/4th power. To clarify this, tolerable displacement is

doubled and the k-value is multiplied by 2, or;

$$H = 2\delta \cdot \left(\frac{k}{2} \right)^{\frac{3}{4}} \cdot T = 1.19\delta \cdot k^{\frac{3}{4}} \cdot T \quad \left(T = \sqrt[4]{\frac{EID^3}{4}} \right)$$

The horizontal yield strength of the pile increases by 20%, despite having the k-value multiplied by 1/2. When the displacement is multiplied by 1/2 and the k-value is doubled, H becomes;

$$H = 0.84\delta \cdot k^{\frac{3}{4}} \cdot T$$

The horizontal yield strength decreases by about 20% despite having the k-value doubled.

In designs, reasonable determination of the tolerable displacement, together with reasonable and exact k-values that suits the design conditions, are required. The amount of the elastic strain of the ground is very small and the allowable horizontal yield certainly becomes larger, if a large amount of tolerable displacement is incorporated into the calculation. Should the tolerable displacement exceed the amount of the elastic strain of the ground, the calculation of the k-value using the modulus of reaction force of the ground, becomes utterly meaningless. In such a case, introduction of the concept of passive earth pressure becomes necessary. The behavior of piles in the ground varies widely, even under the same horizontal load; these variations are due to construction materials of the foundation, the ratio of the diameter of pile to its length, method of treating the pile head; number and space of piles. Therefore, in using k-values, examination of the conditions of the design for the foundation is also required.

In performing this kind of calculation, attention should be given as to whether the load received by the foundation structure is transitory, constant or repetitious in nature.

Needless to say, if the stratum is subjected to long hours of horizontal pressure that exceeds the preloading value hold by the stratum, a phenomenon of consolidation takes place which causes vacant space to occur between the structure wall or piles and the ground.

If a horizontal load is applied again after the occurrence of the vacant space, such a load must be resisted by the stratum located deeper than the initial one, as the resistance value at the vacant space is zero. As a result, stability of the foundation of such a structure will be reduced, and sometimes it becomes necessary to make further detailed calculations on the stability, even if safety was assured in the calculations using k-values.

In order to make a rational foundation design, there are many problems to be dealt, besides the question of the k-value. It has been revealed that there is a k-value, the basic value in calculation, that is more than 6 times higher than others, according to the selection of the measuring method. It is necessary to reflect on such facts in the foundation design. The k-value measuring method, using conventional boring holes which have been proved to afford too small k-value because of large errors, must be corrected.

If the tolerable displacement of the foundation caused by the horizontal load is within the elastic region of the ground and such a load doesn't work constantly, the k-values measured by use of trimming method should be used in the calculation. When conditions of the foundation and ground are clearly known, and dynamic k-value is well adaptable and can be measured with reliable results, such dynamic k-value should be used in the calculation.

As regard to the amount of the soil elastic strain caused by each structure, it is considered necessary to elucidate it theoretically through repetitious experiments in the future. The authors suggest the following, based on the results of experiments, is a tolerable displacement for which dynamic k-value is applicable in the case of comparatively tight sand stratum ($N > 10 - 15$) or clay ($N > 3 - 5$) and the pile diameter is smaller than 100 cm.

$$\text{Tolerable displacement} = \text{Pile diameter} \times 0.1 \times 0.25$$

The breaking strain of the pile, whose diameter is not large, is about 10% of the pile diameter. It may not be a great error to consider the elastic region to be about 25% of the diameter.

At present there are many problems associated with the dynamic k-value and the design of the foundation.

7. Postscript

Despite difficulties in construction work due to the lack of suitable ground in the narrow land of this country, there are many cases in which important structures must be built. In addition, there is an unfavorable condition of frequent occurrence of earthquake which makes it quite difficult to design a safe and rational foundation.

The authors wish to continue the study of the dynamic k-value problems, because we believe that many problems may be solved in the course of this study which in turn would contribute to the improvement of design techniques for foundations used in this country.

References

1. Yoshiharu Arie, Tetsuo Okada, Kaname Yahagi (1970), Horizontal Resistance to Steel Piles in the Arakawa Canal, (1) Difference in k-Value in Boring Holes Resulting from Difference in Boring Measuring Instruments, Soil and Foundation, Vol. 18, No. 9.

2. Yoshiharu Arie, Tetsuo Okada, Kaname Yahagi (1970), Horizontal resistance to steel piles in the Arakawa Canal (2) Study on k-Value Obtained in the Horizontal Load Test

3. Harumitsu Tamano, Kaname Yahagi, Kozo Miki (1974), Basic Study of Dynamic k-Value, Soil and Foundation, Vol. 22, No. 3

4. Kozo Miki, Hideo Yugami, Matsuo Amamiya (1973), Measurement by Superhigh-Pressure K.K.T. tester of strength of Rock Bed, Soil and Foundation, Vol. 21, No. 2.

5. Yoshihiko Nishigaki, Yoichi Okajima (1972), Modulus of Deformation of Viscous Soil, Lectures to the 27th Annual Meeting of the Civil Engineering Society.

6. Yoshihiko Nishigaki, Tadayuki Hirobe (1973), Hysteresis Characteristic of Osaka Diluvial Clay Announcement at the 8th Meeting of Geotechnique Society.

7. Report for Tokyo Expressway Public Corporation Geological Survey at BC-282 Engineering Zone.

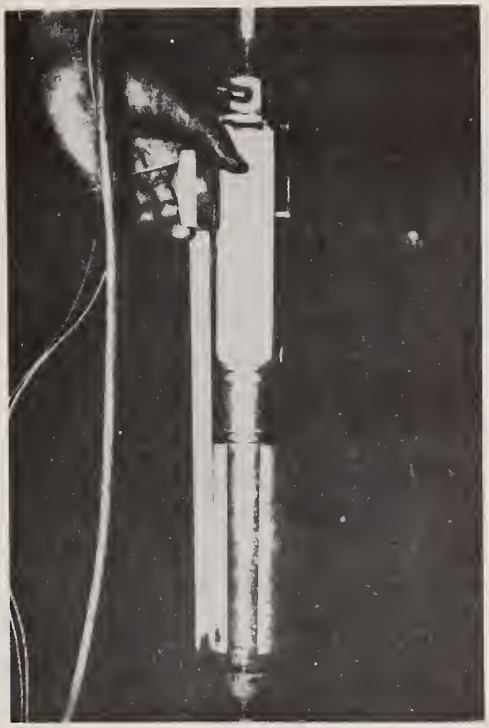

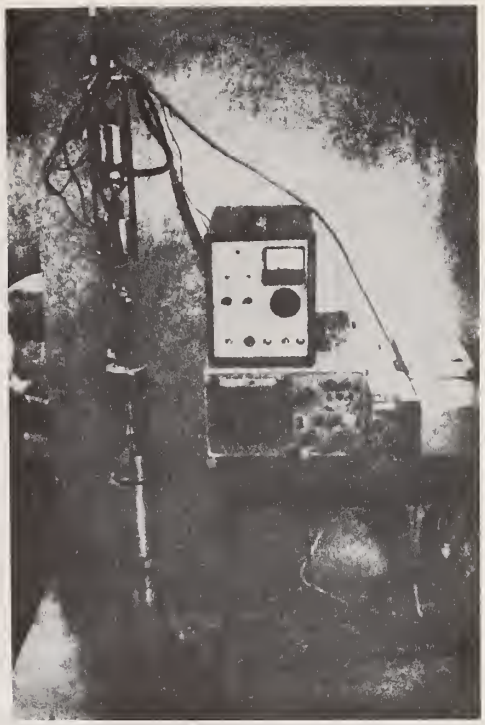

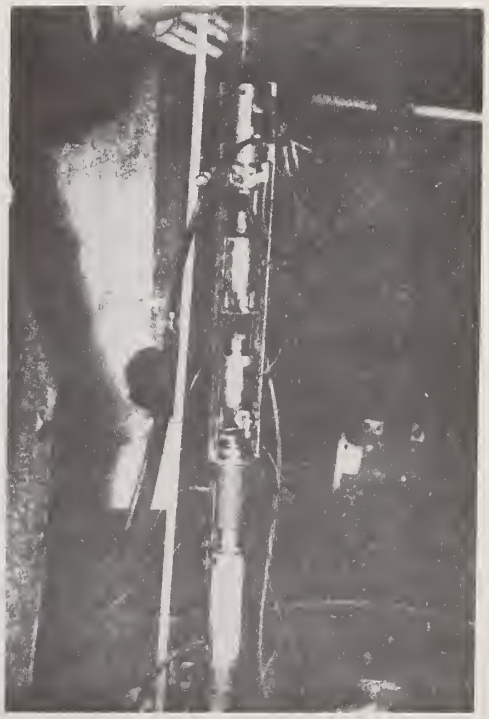

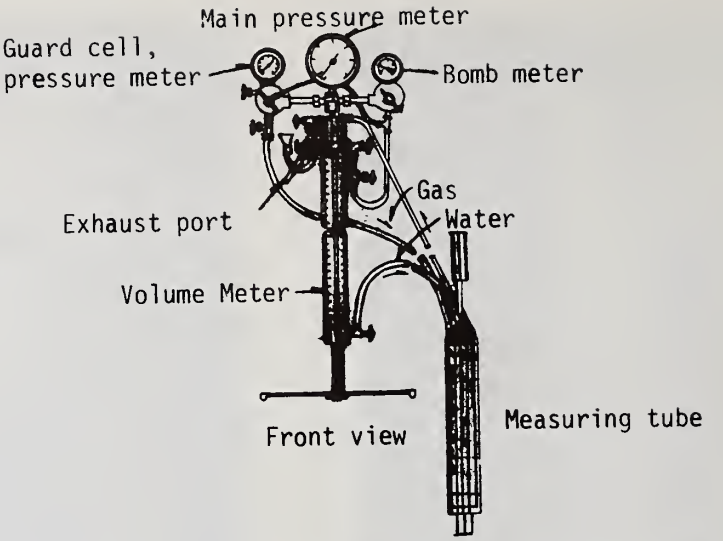

Fig. 1 Block Diagram of Preciometer

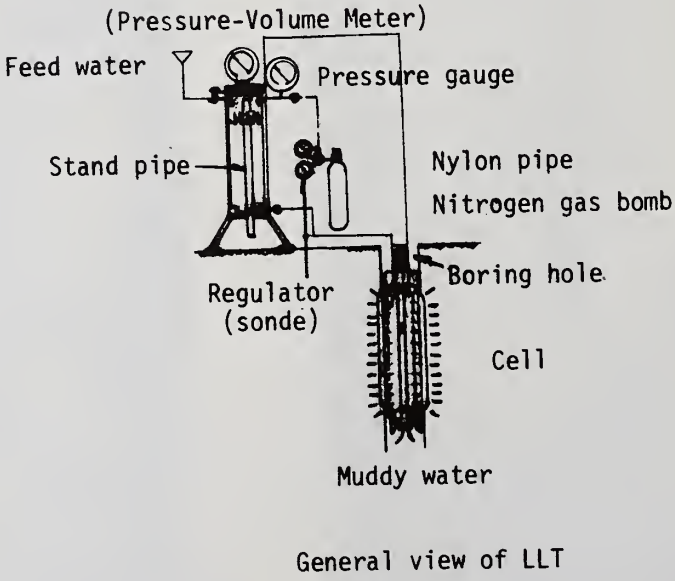

Fig. 2 Block Diagram of LLT

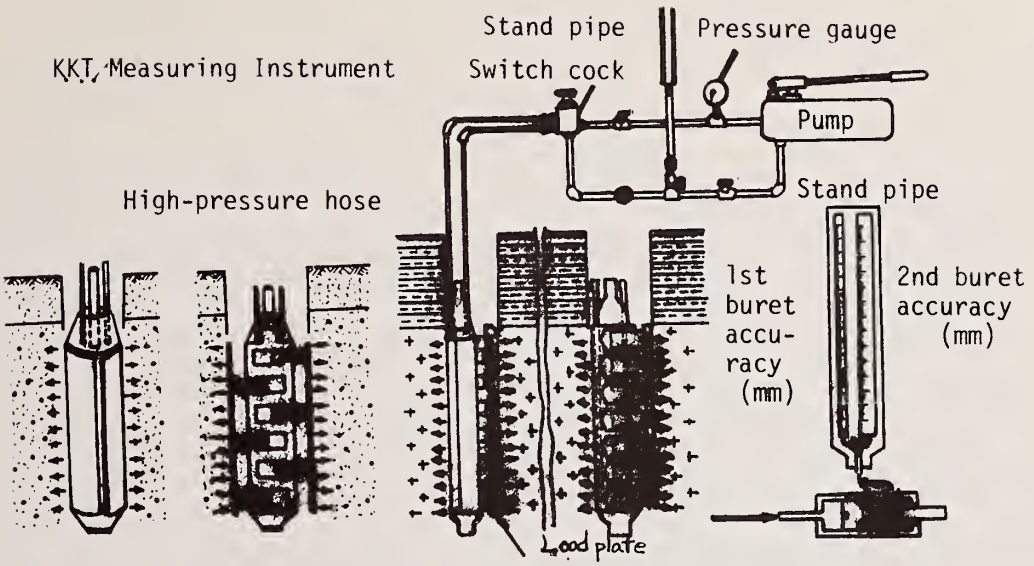

Fig. 3 Block Diagram of KKT

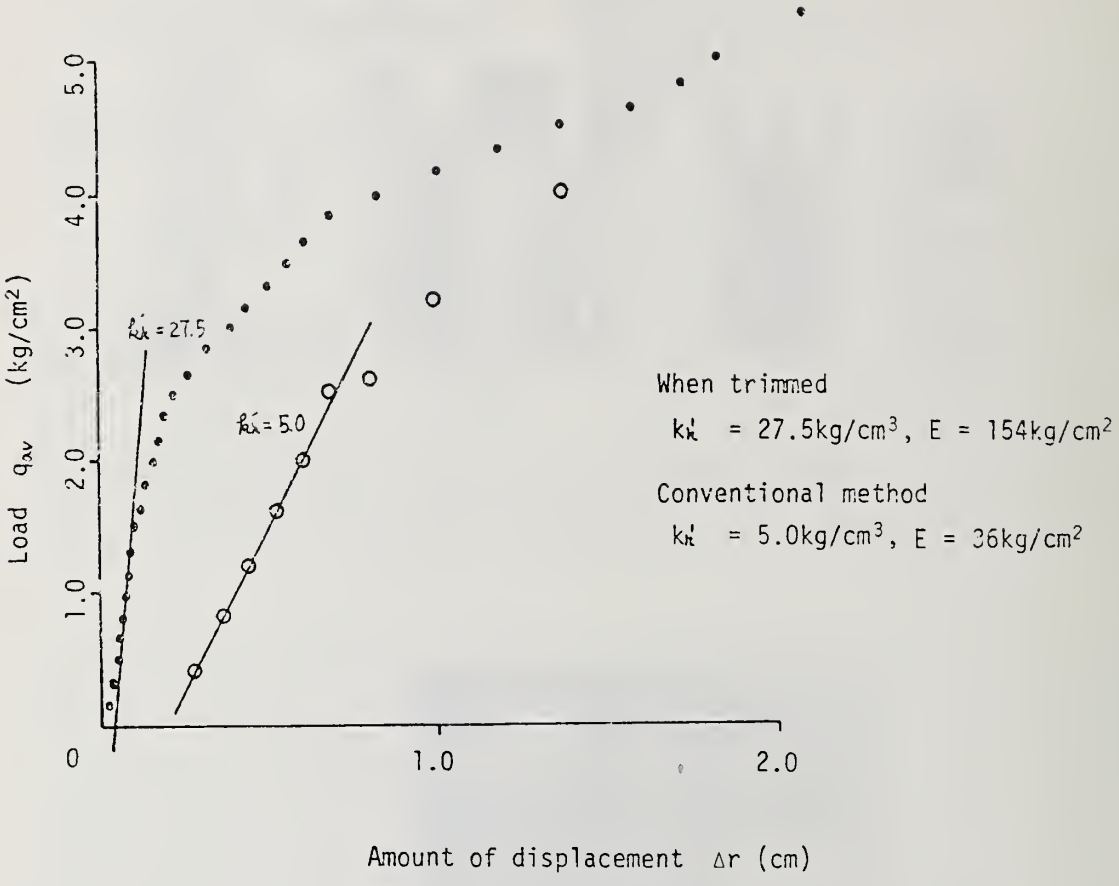

Fig. 4 Effects of Trimming on k-Value (Osaka diluvial clay)

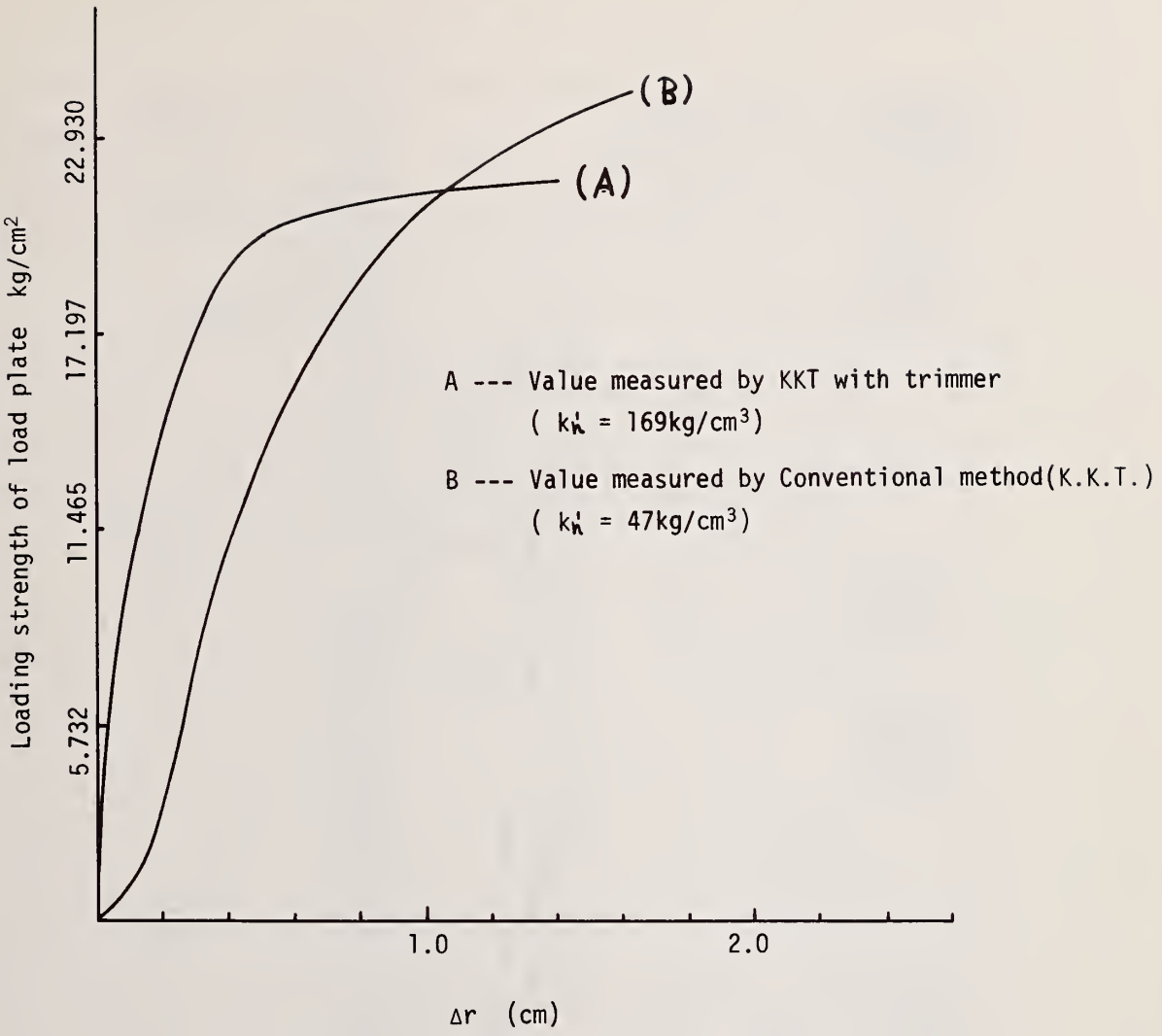

Fig. 5 Effects of Trimming on k-Value (Osaka diluvial clay)

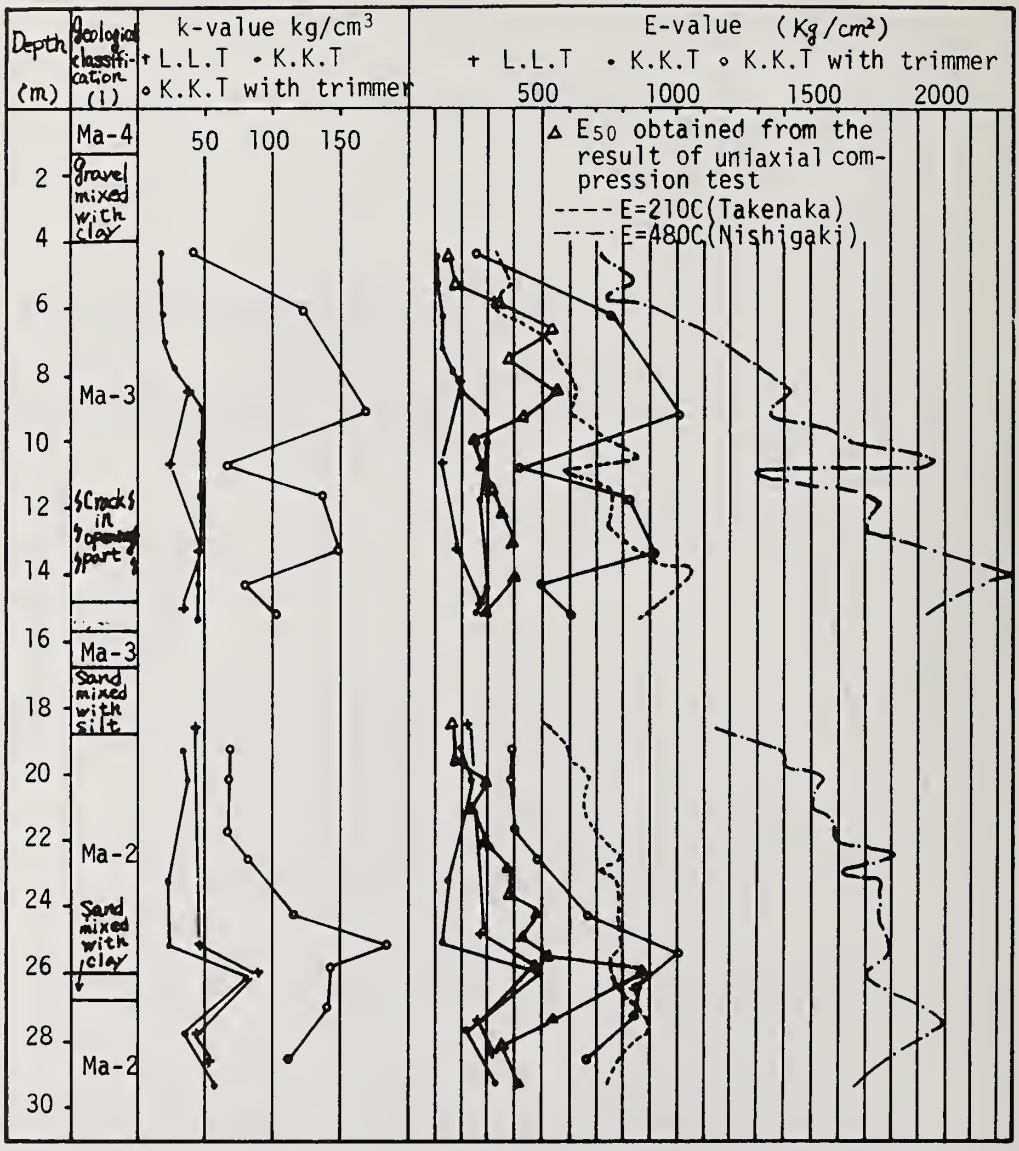

Fig. 6 Comparative Test of Static k-Value

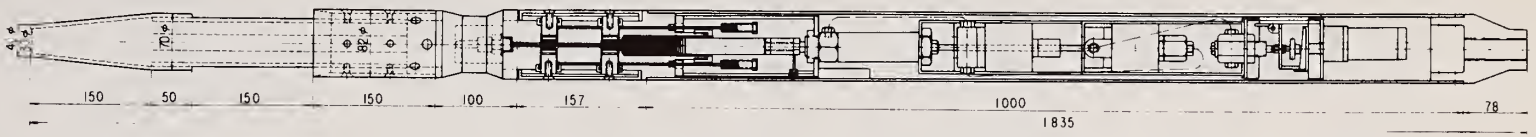

Figure 7 Diagram of Dynamic k-Value Measuring Instrument

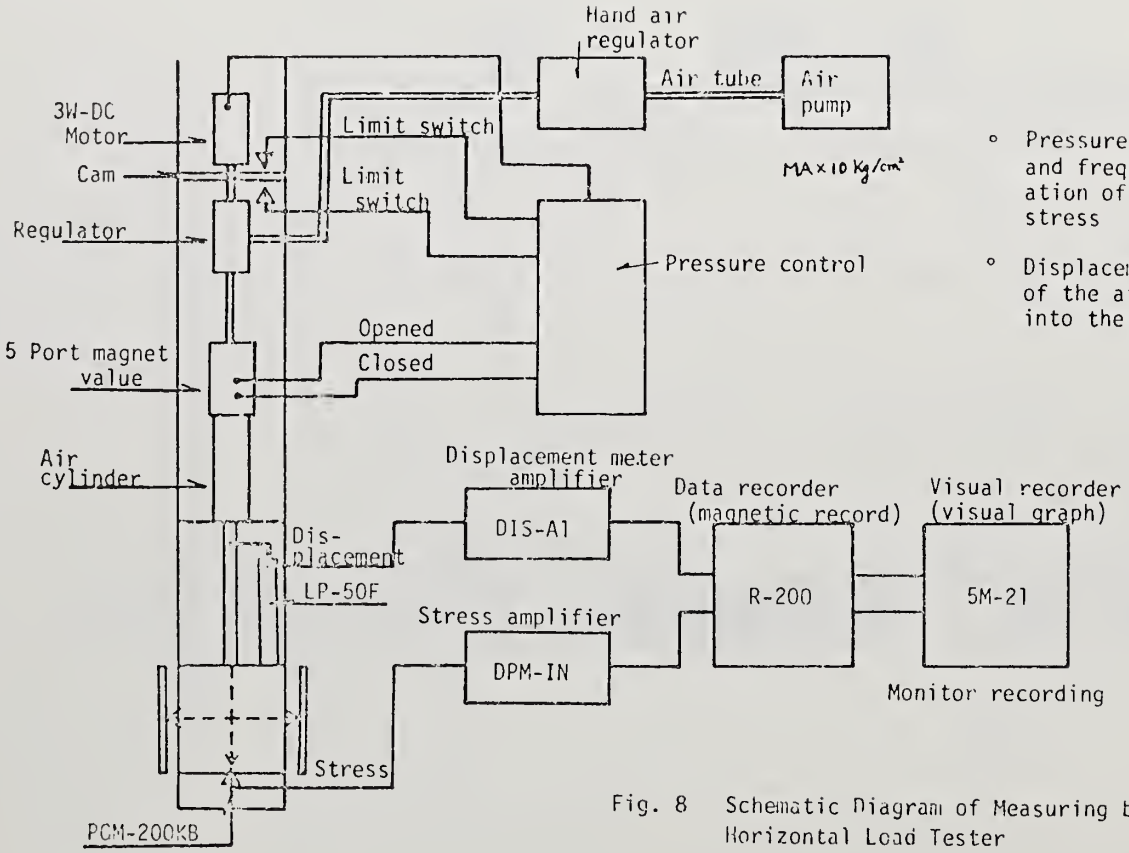

- Pressure control works to control the mode and frequency of sine wave for the generation of stress and the maximum value of stress
- Displacement meter measures the displacement of the air cylinder and later converts it into the displacement of the load plate

Fig. 8 Schematic Diagram of Measuring by Dynamic Horizontal Load Tester

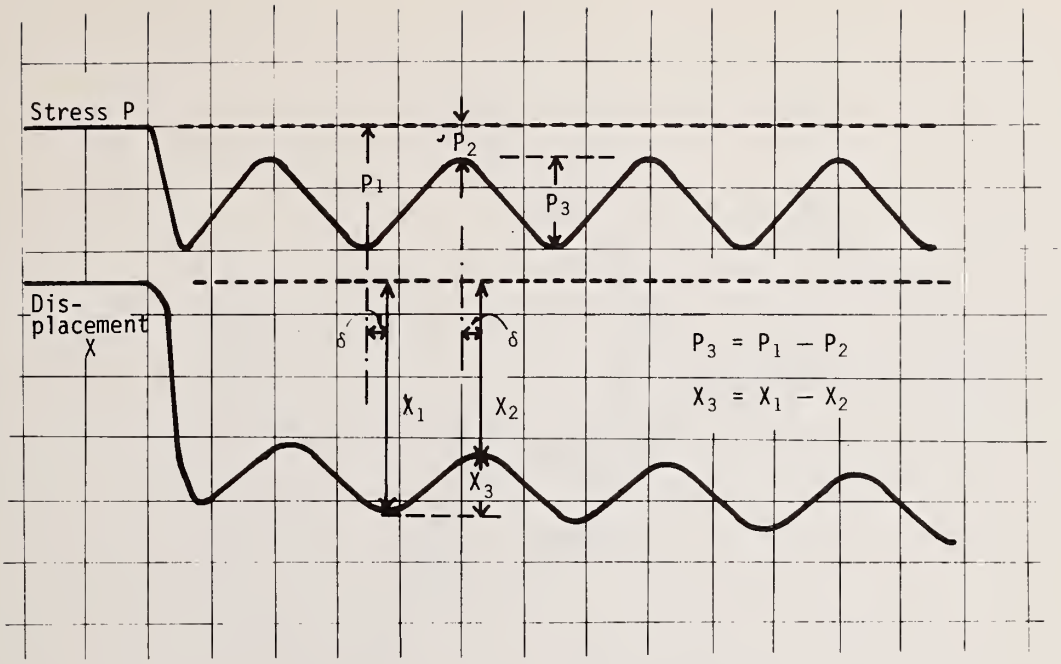

Fig. 9 An Example of Dynamic k-Value Measuring by Sine-Wave Stress Method

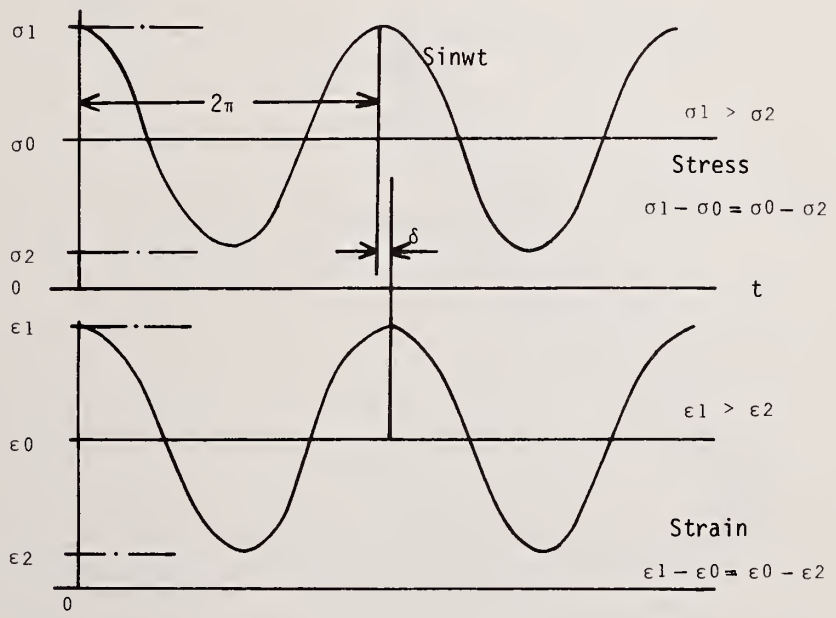

Fig. 10 Diagram Showing Results of Vibration Test on Linear Elastic Body

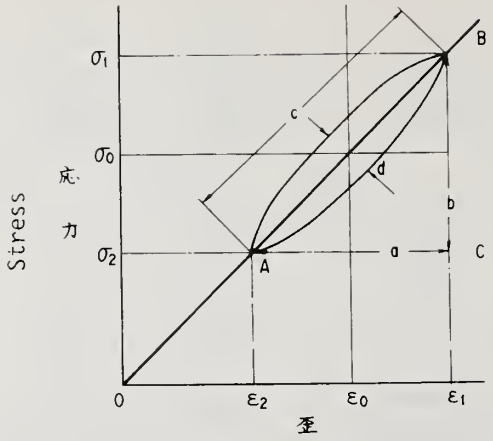

Fig. 11 Hysteresis Loop of Linear Elastic Body Vibration Test

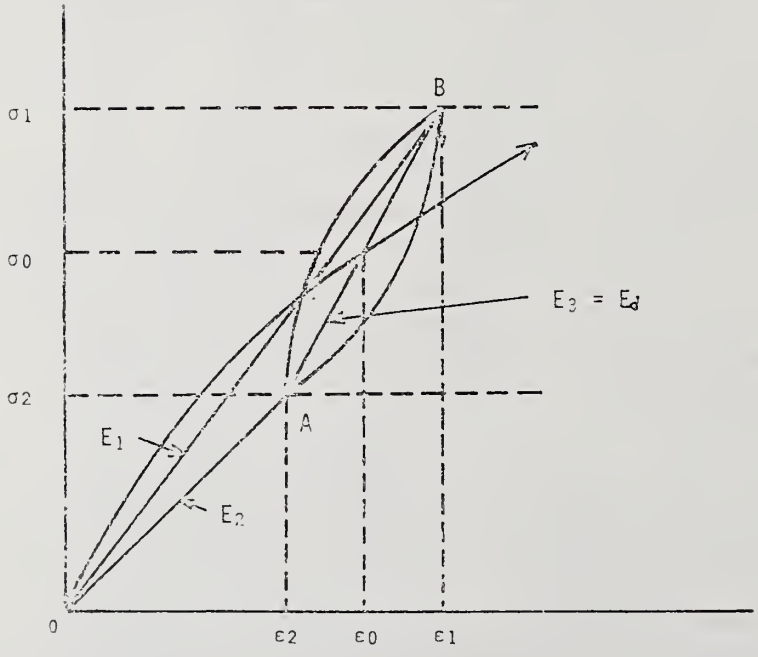

Fig. 12 Comparison of Elastic Constant ($E_d > E_1 > E_2$)

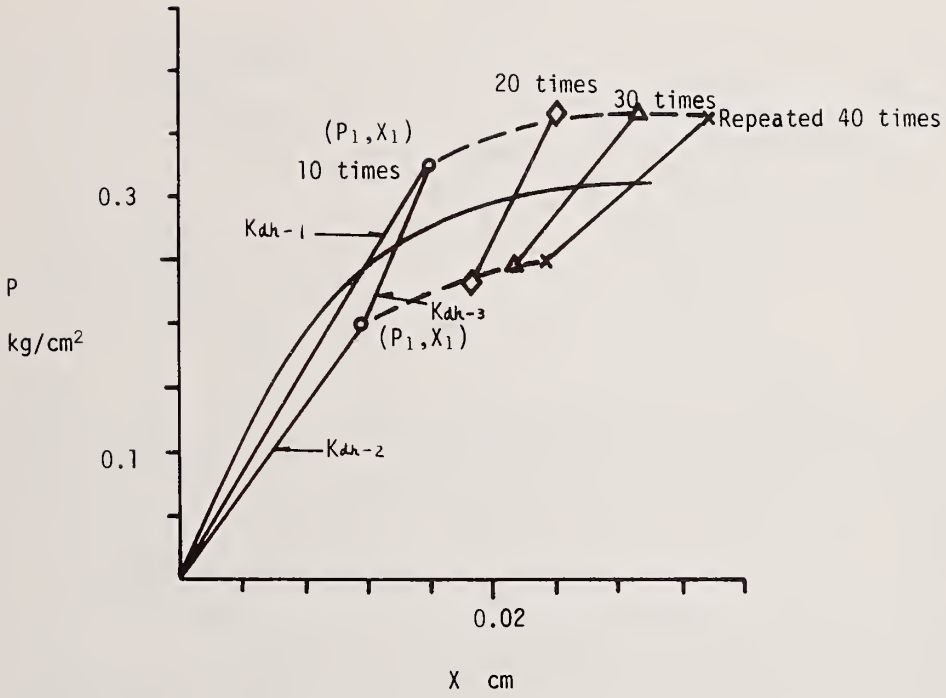

Fig. 13 Decrease of Dynamic k-Value Resulting from Increase in Number of Repetition

Fig. 14 Results of Soil Test at Urayasu in Chiba Pre.

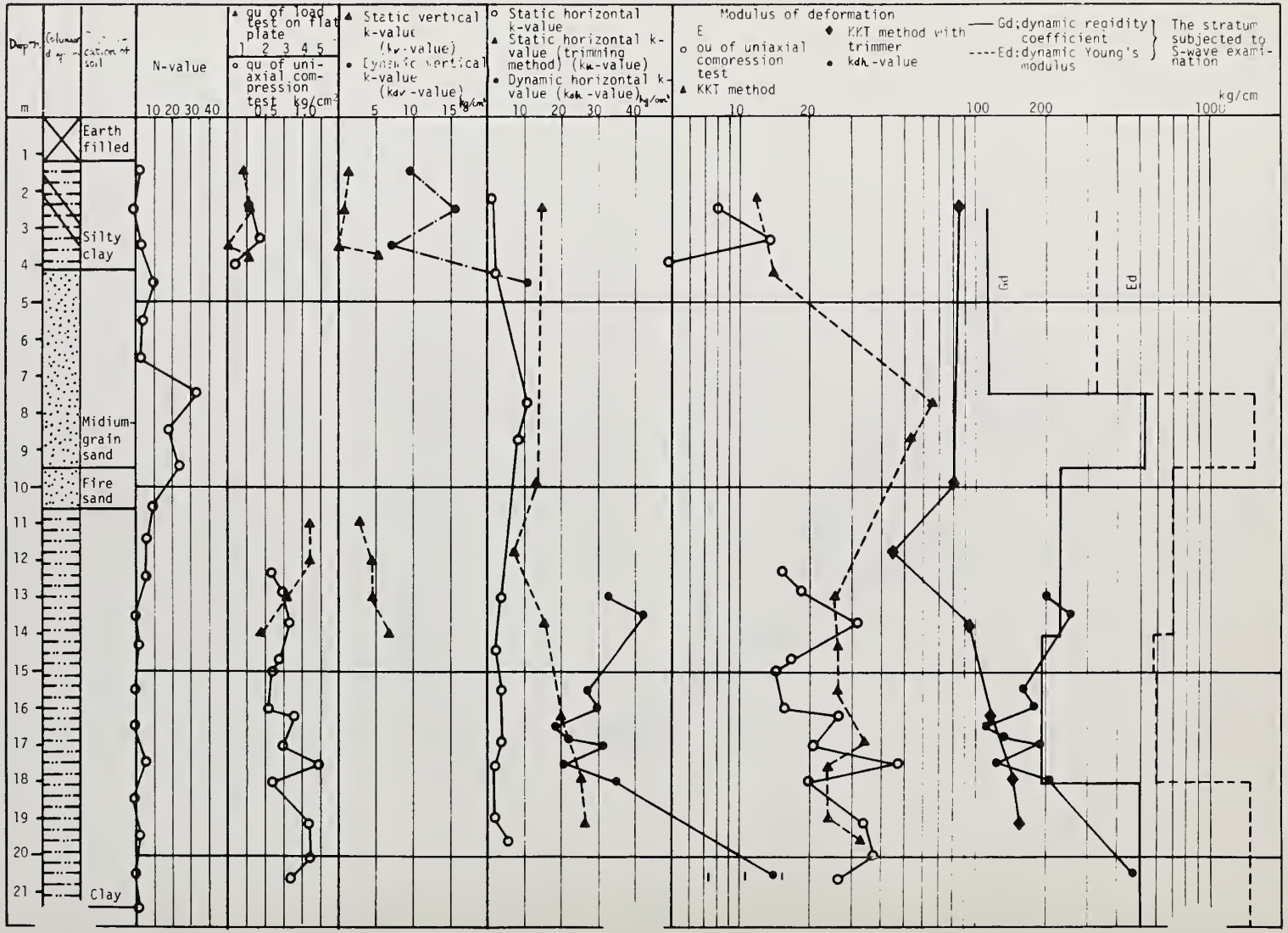

LABORATORY INVESTIGATION OF UNDISTURBED SAMPLING AND STANDARD PENETRATION TESTS ON FINE SANDS

W.F. MARCUSON, III
S.S. COOPER
M.A. BIEGANOUSKY

ABSTRACT

Determination of density of sand is presented. Densities determined from using undisturbed samples and from the standard penetration tests are compared. It is shown that the standard penetration test is not sufficiently accurate to be recommended for final evaluation of the density at a site unless site specific correlations are developed.

Key Words: Density; Liquefaction; Sand; Soils; Tests; Undisturbed Sampling.

1. Introduction

a) Reliable determinations of in situ density of sands below the water table are essential to assess the engineering properties of such materials particularly when liquefaction may be a problem. This problem has become more critical in recent years because more and more structures are being constructed which would cause catastrophic damage and loss of life if they failed as the result of stresses attributed to earthquakes. This is particularly true in the case of nuclear power plants and large dams. The critical nature of this problem, and the difficulties encountered in actually determining the in situ density has led the Corps of Engineers to extend previous work (1,2,3). The earlier work was conducted at the Waterways Experiment Station (WES) and resulted in the development of an undisturbed sand sampler, which incorporated a fixed piston and drilling mud to obtain representative samples in situ (1).

b) Less direct methods of determining the in situ density have also been developed for use in the field. The most common technique for estimating the in situ density of a deposit is the Standard Penetration Test (SPT) (4-8). This method is based on correlations between penetration resistance, overburden pressure, and relative density. The SPT is widely used because it is expedient and economical. However, the empiricism of the technique has led many engineers to doubt the validity of the correlations. WES has evaluated the SPT procedure in the laboratory, the results of which will be presented in the literature (9), and are summarized here.

c) In conjunction with the SPT investigation, WES also studied the undisturbed fixed piston sampler. This was accomplished by comparing sampled densities obtained under laboratory conditions, to the actual density of the sampled medium. Results of the comparisons are also presented. If desired, more detailed documentation will be available in the literature (10).

2. Test Facility

a) The major components of the test facility consist of a 4-ft-(1.22 m) diameter ring soil container, a massive reinforced concrete foundation, and loading equipment for applying pressure to the top of the soil specimen (9-11). Figure 1 shows the circular stacked ring soil container in which 4-ft- (1.22 m) diam by 6 ft (1.83 m) high specimens were constructed. A schematic of the test facility is shown in Fig. 2.

3. Sampling Equipment

a) The drilling rig used in this study is a commercially available skid mounted Acker Teredo Mark II Soil Sampling Drill. Low overhead clearance in the laboratory precluded the use of a mast, so lifting tackle for the drill rods was secured to rafters in the ceiling. For sampling and drilling operations the rig was elevated on a platform built level with the top of loader support pedestals. Mud circulation during reaming operations was accomplished with a portable mud pump which was supplied with mud from a pump atop the loading head.

b) Undisturbed samples were taken with a Hvorslev (12) 3 in. (7.62 cm) ID thin wall fixed piston sampler. Nominal dimensions for the 16-gage sample tube included a 2.97 in (7.54 cm) ID cutting edge, a taper angle of 10 degrees on the cutting edge, and an area ratio of 11 percent (13). A schematic of this sampler is shown in Fig. 3. The drill rod used in the sampling operation was 2 in. (5.08 cm) OD "N" size. Reaming was accomplished with the WES-modified fishtail bit. The bit itself is commercially available, however, special baffles were added at WES to direct the flow of drilling mud in an upward direction, away from the bottom of the borehole. Thus, disturbance of the underlying material by circulating mud is minimized when reaming or drilling to the sampling depth.

c) The split-spoon sampler was driven by a hydraulically operated 140 lb (63.42 kg) hammer, contained in a perforated cylinder, which was designed by the Vicksburg District, Corps of Engineers, Fig. 4. This hammer was designed to deliver an identical impulse for each blow, eliminating the undesirable effects of impulse variations on blow counts. The hammer is mechanically lifted to a 30 in. (76.2 cm) drop height by two lugs positioned on a continuous chain. The chain is driven by a hydraulic motor connected to the hydraulic system of the drill rig.

d) The split-spoon sampler used in the conduct of the test conforms to the specifications outlined in ASTM D1586-67, Penetration Test and Split Barrel Sampling of Soils (14).

4. Test Program

a) The test program consisted of undisturbed sampling and standard penetration testing on twenty-six 4 ft (1.22 m) diam by 6 ft (1.83 m) high sand specimens built to various relative densities and subjected to a range of overburden pressures. These specimens were incrementally constructed in lifts as will be discussed subsequently. Table 1 summarized the test program, and includes information of a general nature regarding the preparation and testing of the specimens.

b) Two uniform fine sands (SP) were tested during the program. The first sand tested was Reid-Bedford Model sand, a locally procured material with a coefficient of uniformity of 1.6. The D_{50} for Reid-Bedford Model sand is 0.25 mm, and the grain shape is subangular to subrounded. The second sand tested was Ottawa sand which has a uniformity coefficient of 1.5, a D_{50} of 0.21 mm, and a subrounded to rounded grain shape. Fig. 5 depicts typical grain size distributions for Reid-Bedford Model and Ottawa sands.

c) The maximum and minimum dry densities of the respective sands were determined by procedures contained in Engineer Manual 1110-2-1906, entitled "Laboratory Soil Manual" (15). The values of maximum and minimum density for Reid-Bedford Model and Ottawa sand are shown in Fig. 5.

d) The samples were constructed in approximately 6 in (15.24 cm) thick using various raining procedures (9,10,16). Beginning with Test No. 4, density control of the indivi-ual lifts was monitored using the WES developed box density device (17). This device is a 4 in (10.16 cm) by 12 in (30.48 cm) metal form which, including the cutting edges, is 3 in (7.62 cm) deep. A box-shaped scoop and a scraper-type cleanout tool, corresponding to the desired depth of cleanout, are used to remove the soil sample from within the box.

e) Overburden pressure was applied to every specialty in increments according to a pre-scribed test schedule. The usual pressures were 10, 40, and 80 psi (69, 276, and 552 kN/m^2, respectively). There were some departures from the foregoing sequence since some speci-mens were tested at only one pressure, while others were staged at two or more pressures. The application of the overburden pressure caused consolidation within the specimen, densi-fication being significant for loose specimens and minimal for dense specimens. A density correction for overburden pressure was derived from the results on one dimensional con-solidation tests performed on submerged, 3 in (7.62 cm) diam specimens at the same testing pressures used in the full-scale laboratory test program (9). The one-dimensional consolidation test was assumed to be reasonably analogous to conditions in the stacked ring soil container.

f) As previously mentioned, undisturbed sampling was conducted in conjunction with standard penetration testing. The sampling was accomplished in stages to conform with the penetration tests planned (see Table 1), and all of the undisturbed samples were taken through the center hole in the loading head, i.e., along the cylindrical axis of the specimen. Sampling was originally planned at overburden pressures of 10, 40, and 80 psi (69, 276, and 552 kN/m^2, respectively), however, this could not be accomplished in many instances, because the drill rig employed did not develop sufficient force to drive the sampler at pressures greater than 10 psi (69 kN/m^2). Consequently, most of the undisturbed 3 in (7.62 cm) QD samples were taken with 10 psi (69 kN/m^2) applied to the specimen. After each sampling operation the center, or sampling, hole was stemmed with pipe before penetration tests were conducted in the peripheral holes. This practice was adopted to prevent hole closure and concomitant reductions in lateral pressure.

g) The test sequences was generally as follows;

1. With 10-psi (69-kN/m^2) pressure applied, the first tube was driven 2 ft (0.61 m) into the specimen through the center hole in the loading head. After withdrawal,

the center hole was stemmed with pipe 2 ft (0.61 m) in depth.

2. Split-spoon tests were conducted in a peripheral hole to a total depth of 6 ft (1.83 m), after which the peripheral hole was stemmed.

3. The stemming pipe was withdrawn from the center hole and the overburden pressure raised to 40 psi (276 kN/m^2). Next, the hole was reamed to a depth of 2 ft (0.61 m) and the second undisturbed sample was taken from 2 to 4 ft (0.61 m to 1.22 m) in depth (by temporarily reducing the overburden applied, if necessary). Afterwards, the hole was stemmed to 4 ft (1.22 m) in depth.

4. Penetration tests were conducted in the second peripheral hole as in b, above.

5. The last undisturbed sample was taken from 4 to 6 ft (1.22 m to 1.83 m) in depth as described in c except that, conditions permitting, the last sample was driven with 80 psi (552 kN/m^2) overburden pressure applied to the specimen.

6. Penetration tests were conducted in the third peripheral hole, concluding the test.

h) Sampling and incremental density determinations were carried out in accordance with procedures outlined in Ref. 12 and 13. The undisturbed samples were sealed with end packers and stored overnight in a vertical position. The following day, the tubes were placed in a horizontal position in a wooden carrying rack built for the purpose. The top surface of each tube was marked so that this orientation could be maintained throughout the density determinations. Each tube was then tapped 50 blows with a rubber hammer along its top surface to consolidate the sand (25 blows in one direction and 25 blows in the opposite direction along the tube). The tubes were later cut into 6 in (15.24 cm) increments for density determinations. Density determinations were also made on shorter sections if enough additional material remained after the tube was cut into 6 in (15.24 cm) increments

5. Analyses and Presentation of Results

a) Undisturbed Sampling: It is obvious that an assessment of sampling accuracy is no better than the accuracy with which the specimen conditions can be determined at the time of sampling. Given the nature of soil materials and the current state-of-the-art of soil measurements, it is equally obvious that the test results will be accurate only to within certain limits. Accordingly, it is necessary to evaluate, by the most practical means, any variables which are believed to influence the tests results significantly. Considering the test procedures employed in this investigation, the most significant variables to be evaluated were as follows;

Variables	Probable Range of Variation, pcf
Box density measurement error	$\pm$0.2 ($\pm$3.20 kg/m^3)
Specimen nonuniformity	$\pm$2.0 ($\pm$32.04 kg/m^3)
Density change due to overburden pressure	+0.7 (+11.21 kg/m^3) (average)

This table if formulated from data in Ref. 10. accumulated upper bounds for all three variables would thus be ± 2.9 pcf (46.45 kg/m^3) and the corresponding lower bound would be -1.5 pcf (-24.03 kg/m^3). The positive (+) bias is assumed to represent overburden pressure affects.

b) During the course of this study, data such as shown in Fig. 6 were typically obtained. The best quality data available from the study was plotted in Fig. 7 as sampled dry density versus placed dry density. A linear regression analysis was performed on the data shown and the derived linear fit is indicated by the dashed line on the plot. The equation of the line is:

$$Y = 0.81X + 19.5$$

where: Y = sampled density, pcf

X = placed density, pcf

The correlation coefficient for the linear fit to the data is $r_{sy} = 0.83$.

c) The placed dry density can be corrected for applied overburden pressure (9,10). Fig. 8 shows the data plotted as sampled dry density versus corrected placed dry density. A statistical analysis was also performed on this data and the results are shown in Fig. 3.

d) The corrections for density changes due to overburden pressure are apparently very significant to the test results as shown by the difference in the regression fits in Fig. 7 and 8. The random variables associated with placed density determinations are much less susceptable to evaluation and cause some degree of uncertainty in an assessment of sampling accuracy. However, an assessment can be made from Plots 7 and 8. Assuming a normal frequency distribution, 95 percent of the sampling data falls within the range of $\pm 2\sigma$, where σ is the standard deviation. Within this range, sampling accuracy is indicated to be ±3.4 pcf (54.46 kg/m^3) for the density samples taken at relative densities D_r ranging from 20 to 60 percent. The linear regression fits, to the data presented in Fig. 7 and 8, indicate that sampling slightly densifies the sand at low relative densities and tends to loosen denser sand.

e) Standard Penetration Tests: Details of this analysis are presented elsewhere (9, 11). A summary plot of these data are shown in Fig. 9.superimposed on this plot are the scatter bands for 10, 40, and 80 psi (69, 276, and 552 kN/m^2) data. A regression analysis was conducted on these data and the following equation derived:

$$D_r = 8.6 + 0.83 \left[\left| \frac{N + 10.4 - 3.2(OCR) - 0.24(\sigma_v)}{0.0045} \right| \right]^{1/2}$$

where: D_r = relative density, percent

N = standard penetration N values, blows/ft

OCR = overconsolidation ratio

σ_v = vertical overburden stress, psi

This equation fits the data with a coefficient of determination (r^2) of 0.78 and has a standard deviation of ±7.6 percent. The maximum difference between relative density predicted by Equation 5 and that observed in the laboratory was +18.9 percent (10).

f) The study by Gibbs and Holtz (4) resulted in a recommended family of curves. These recommended curves are superimposed on the WES data spreads in Fig. 10. Good agreement exists at the 10-psi (69 kN/m^2) testing pressure. The Gibbs and Holtz correlation curves were derived from testing two sands, a coarse well graded sand and a fine well graded sand with 14 percent passing the No. 200 sieve (4). Reid-Bedford Model and Ottawa sands are appreciably different with respect to the grain size distributions of the Gibbs and Holtz sands. Ignoring all other factors, one might conclude that soil type exerts a significant influence on the penetration results, which is in agreement with Kolbuszewski (18). WES has extended the SPT study using Platte River sand (the WES Platte River sand is very similar to the Gibbs and Holtz coarse sand), and early results display some agreement with the findings of Gibbs and Holtz.

g) Along with the recommended curves, Gibbs and Holtz also published the family of curves which resulted from testing submerged sands. These curves are also superimposed on Fig. 10. In this instance, there appears to be better agreement at the 40-psi (276 kN/m^2) testing pressure, but overall poor agreement. These curves were not considered reliable, and were not recommended for use by the authors (5).

h) The correlation curves based on the study performed by Bazaraa (6) are also superimposed on the WES data in Fig. 10. These curves are based on actual field data and take into account many different types of sands derived from many sources. The curves predict lower values of relative density for a given N-value than either the Gibbs and Holtz or WES curves.

6. Conclusions

a) The conclusions drawn from this study directly apply to only the two sands tested. The equation and data presented herein are not intended for use in predicting the penetration resistance or relative density of sands in general but are presented to describe the empirical behavior of these two sands under the stipulated laboratory conditions.

b) Undisturbed Sampling: Considerable attention was given to the test variable which can influence test results (10), and it was noted that placed density at the time of sampling probably varied from +2.9 to -1.5 pcf (+46.45 to -24.03 kg/m^3) from measured values due to the combined effects of the test variables.

c) The sampled versus placed density comparisons presented suggest that sampling accuracy using the techniques described is within ±3.4 pcf (±54.46 kg/m^3) for 95 percent of the sampling conducted at relative densities D_r ranging from 20 to 60 percent.

However, it can also be concluded that a more meaningful assessment of sampling accuracy could have been made had it been possible to exercise better placed density control during the study; it is probable that in this event the apparent accuracy of sampling would have shown a corresponding improvement.

d) Despite the uncertainties cited, results of this and earlier work exhibit generally similar trends. For instance, this and the preceding work indicate that sampling tends to slightly densify loose sand (D_r < 40 percent) and tends to slightly loosen denser sand (D_r > 50 percent). The plots presenting linear regression fits to selected data also lead to the conclusion that overburdened pressure corrections can significantly influence the density determinations made with the sampling techniques described. More definitive conclusions regarding sampling accuracy cannot be advanced because of the uncertainty associated with the placed density results obtained in this study.

e) Standard Penetration Tests: The penetration resistance (N-value) was observed to be sensitive to changes in density, overburden pressure, and overconsolidation ratio.

f) The SPT as performed was fairly repeatable in a nearly homogeneous deposit ($\pm$2 or $\pm$3 pcf ($\pm$32.03 or $\pm$48.06 kg/m^3)); however, variations in the testing medium produced scattered N-values. The results obtained do not permit more than a gross estimate of relative density from N-values. A single value of penetration resistance can represent a 30 percent spread ($\pm$15 percent) in relative density. The heterogeneous conditions of the field would seem to make the task of estimating relative density even more difficult; hence correlations between N-values and relative density should be used cautiously and mainly in a qualitative sense.

g) It has been recently established that different structures and different lateral stresses are associated with various sand placement techniques (19). The results of this testing program (9) showed that the penetration resistance was sensitive to the various placement techniques. It is concluded from this that the results reflect variations in the structure and lateral stress conditions of a deposit. In practice, this sensitivity would tend to obscure the actual density condition.

h) The tests performed on specimens having an overconsolidation ratio of 3 produced N-values which consistently fell near the top of the scatter band for their respective pressures. This also indicates that the SPT is sensitive to lateral stress conditions.

i) Multiple regression analyses were conducted and relationships, in terms of the standard penetration N-value and relative density, were developed. These relationships appear quite good from a statistical point of view, having a coefficient of correlation, r, of approximately 0.9. The relationship for relative density as a function of N, σ_v, OCR has a standard deviation of about $\pm$7.5 percent. Caution should be exercised in the use of this equation to predict relative density because it was developed from a limited data bank and is only applicable to results on Reid-Bedford Model sand.

j) Based on a comparison between the correlations presented by Gibbs and Holtz, and WES, it is concluded that the SPT is not sufficiently accurate to be recommended for final evaluation of the density or relative density at a site unless site specific correlations are developed. However, the SPT does have value in planning the undisturbed

sampling phase of the subsurface investigation and for purposes of qualitative comparisons.

Acknowledgement

Grateful appreciation is expressed to those colleagues at WES who assisted in the data acquisition phase of this undertaking and to those who offered constructive criticism as well as moral support during the development and documentation stages. In addition, the support of the Office, Chief of Engineers, who funded this project, is gratefully acknowledged.

References

1. Goode, T.B., "Undisturbed Sand Sampling Below the Water Table," Bulletin No. 35, Jun 1950, U.S. Army Engineer Waterways Experiment Station, CE, Vicksburg, MS.

2. "Density Changes of Sand Caused by Sampling and Testing," WES Potamology Investigations, Report 12-1, June 1952.

3. Potamology Report 18-1, "Rotary Cone Penetrometer Investigations," Jun 1962, U.S. Army Engineer Waterways Experiment Station, CE, Vicksburg, MS.

4. Gibbs, H.J. and Holtz, W.G., "Progress Report of Research on the Penetration Resistance Method of Subsurface Exploration," EM 314, Sep 1952, United States Department of the Interior. Bureau of Reclamation, Denver, CO.

5. Gibbs, H.J. and Holtz, W.G., "Research on Determining the Density of Sands by Spoon Penetration Testing," Proceedings, Fourth International Conference on Soil Mechanics and Foundation Engineering, London, Vol. 1, 1957, pp 35-39.

6. Bazaraa, A.R.S.S., "Use of the Standard Penetration Test for Estimating Settlements of Shallow Foundations on Sands," Ph.D. Thesis, Sep 1967, University of Illinois at Urbana, University Microfilms, Inc., Ann Arbor, MI.

7. De Mello, V.F.B., "The Standard Penetration Test", Fourth Pan-American Conference on Soil Mechanics and Foundation Engineering, Vol. 1, 1971, pp 1-86.

8. Peck, R.B., et al., "The Standard Penetration Test, Discussion," Fourth Pan-American Conference on Soil Mechanics and Foundation Engineering, Vol. 3, 1971, pp 59-60, 80-84, 89-103.

9. Bieganousky, W.A. and Marcuson, W.F., III, "Laboratory Standard Penetration Tests on Reid-Bedford Model and Ottawa Sand," Research Report in publication, U.S. Army Engineer Waterways Experiment Station, CE, Vicksburg, MS.

10. Cooper, S.S., "Laboratory Investigation of Undisturbed Sampling of Cohesionless Material Below the Water Table," Research Report (in publication), 1976, U.S. Army Engineer Waterways Experiment Station, CE, Vicksburg, MS.

11. Marcuson, W.F., III, and Bieganousky, W.A., "Laboratory Standard Penetration Tests on Fine Sands," to be presented at the Annual American Society of Civil Engineers, meeting in Philadelphia, PA, 1 Oct 1976.

12. Hvorslev, M. Jull, "Subsurface Exploration and Sampling of Soils for Civil Engineering Purposes," Bulletin No. 35, June 1950, U.S. Army Engineers Waterways Experiment Station, CE, Vicksburg, MS.

13. Office of the Chief of Engineers, "Soil Sampling," EM 1110-2-1907, 31 Mar 1972, Department of the Army, Washington, D.C.

14. "Penetration Test and Split-Barrel Sampling of Soils," ASTM D1586-67, American Society of Testing and Materials, 1916 Race Street, Philadelphia, PA.

15. Office of the Chief of Engineers, "Laboratory Soils Testing," EM 1110-2-1906, 30 Nov 1970, Department of the Army, Washington, D.C.

16. Bieganousky, W.A. and Marcuson, W.F., III, "Uniform Placement of Sand", Journal of the Geotechnical Engineering Division. American Society of Civil Engineers.

17. Sloan, R.C., "Dynamic Bearing Capacity of Soils; Dynamic Loading Machine and Preliminary Small-Scale Footing Tests," Technical Report No. 3-599, Jun 1962, U.S. Army Engineer Waterways Experiment Station, CE, Vicksburg, MS.

18. Kolbuszewski, J., Discussions, Fourth International Conference on Soil Mechanics and Foundation Engineering, London, Vol. III, 1957, p 126.

19. Mulilis, J.P., "The Effects of Method of Sample Preparation on the Cyclic Stress-Strain Behavior of Sands," 1970, submitted in partial fulfillment of the requirements for the degree of Doctor of Philosophy, Graduate Division, University of California, Berkeley.

Table 1

Summary Table of Tests

Test No.	Material	γ_d Placed (pcf)*	D_r Placed (Percent)	Preparation Method	Overburden Pressure Sequence (psi)**	OCR	Undisturbed Sample	Water Table Condition	Remarks
1	RBMS†	95.4	40.9	Rotating Rainer (RR)	40	1	None	Submerged	Data considered Unreliable
2	RBMS	95.4	40.9	RR	10-40-80	1	Center Hole	Submerged	--
3	RBMS	94.4	35.1	RR	5-40-80	1	Center Hole	Drained	--
4	RBMS	91.6	18.3	RR	10-40-80	1	Center Hole	Submerged	--
5	RBMS	98.5	57.6	RR	10-40	1	Center Hole	Submerged	No data at 80 psi Water bag ruptured
6	RBMS	97.7	53.4	RR	10-40-80	3	Center Hole	Submerged	--
7	RBMS	94.4	35.2	RR	10-40-80	3	Center Hole	Submerged	--
8	RBMS	95.5	41.3	RR	40	1	None	Submerged	Check test for Test No. 1
9	RBMS	93.3	28.9	RR	40	1	None	Submerged	Rained into water
10	RBMS	99.9	65.1	RR Rodded	40	1	None	Submerged	Rained into water Rodded
11	RBMS	93.2	28.2	RR	40	1	None	Submerged	--
12	RBMS	100.9	70.5	RR	40	1	None	Submerged	--
13	RBMS	96.0	44.3	RR	40	1	None	Submerged	--
14	RBMS	100.4	67.7	RR Rodded	40	1	None	Submerged	Rained into water Rodded
15	RBMS	98.9	60.2	RR Rodded	40	1	None	Submerged	Rained into water Rodded
16	RBMS	92.2	21.9	RR	10	1	None	Submerged	--
17	RBMS	101.4	72.8	RR Tamped	10	1	None	Submerged	Manual tamping with 1 ft square plate
18	RBMS	101.5	73.5	RR Tamped	80	1	None	Submerged	Manual tamping with 1 ft square plate
19	RBMS	101.3	72.5	Single Hose Rainer	40	1	None	Submerged	--
20	RBMS	95.4	40.8	Circular Rainer (CR)	40	1	None	Submerged	--
21	RBMS	93.7	30.8	CR	40	1	None	Submerged	--
22	RBMS	97.0	49.7	CR	80	1	Center Hole	Submerged	--
23	RBMS	90.5	11.6	CR	80	1	Center Hole	Submerged	--
24	RBMS	101.5	73.3	CR	80	1	Center Hole	Submerged	--
25	Ottawa	100.9	53.1	CR	10-40	1	Center Hole	Submerged	--
26	Ottawa	101.5	56.8	CR	10-40	1	Center Hole	Submerged	--

* Pounds per cubic foot (16.02 kg/m^3).
** Pounds per square inch (6.9 kN/m^2).
† Reid-Bedford Model Sand.

FIG. 1.--STACKED RING SOIL CONTAINER

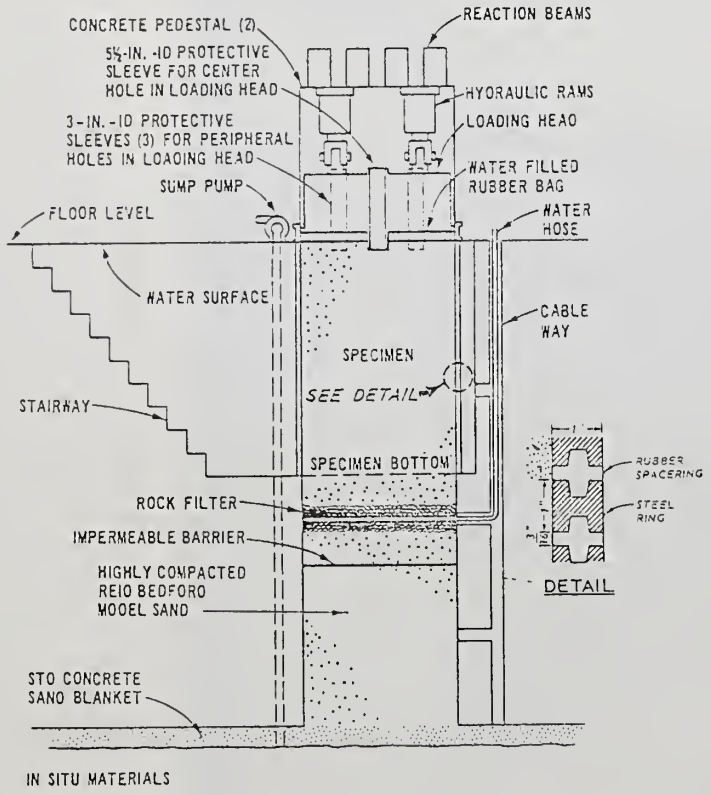

FIG. 2.--SECTIONAL VIEW OF TEST APPARATUS

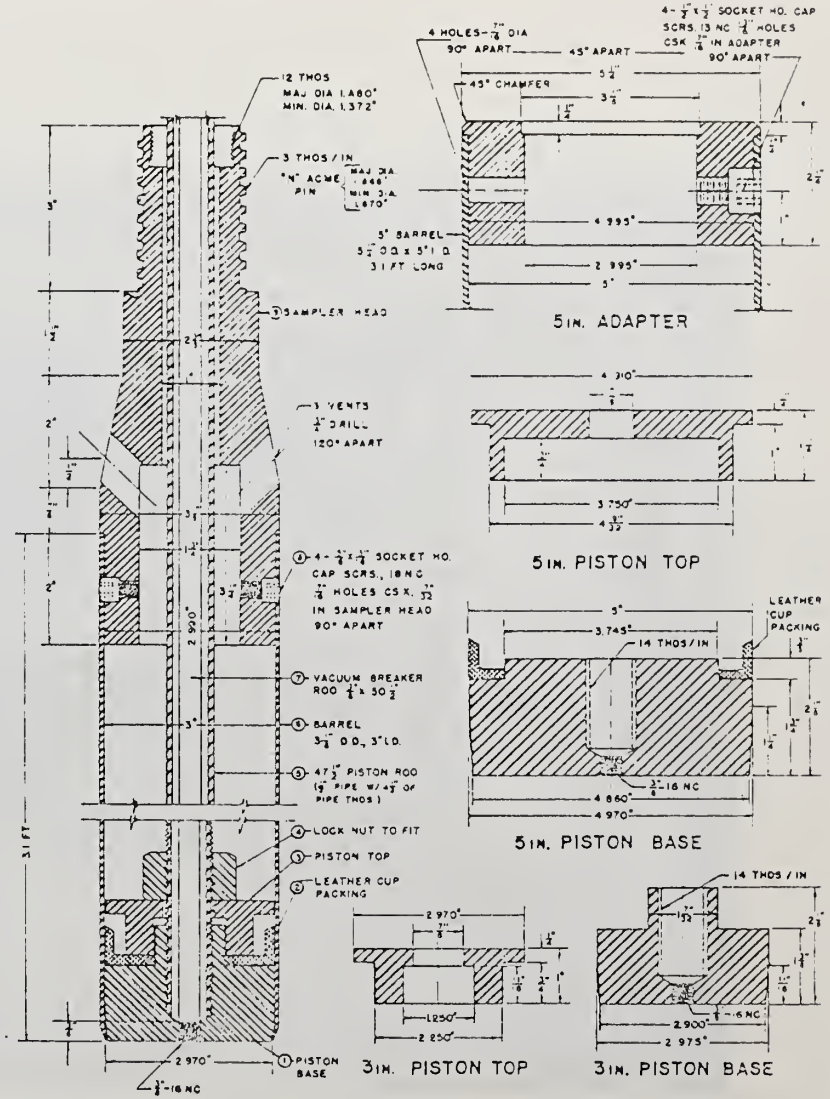

FIG. 3.--HVORSLEV-TYPE 3-IN.-DIAM FIXED-PISTON SAMPLER WITH 5-IN. ADAPTOR. (U. S. ARMY ENGINEER WATERWAYS EXPERIMENT STATION DRAWING NO. 1295-3, REVISED 9 OCT 53)

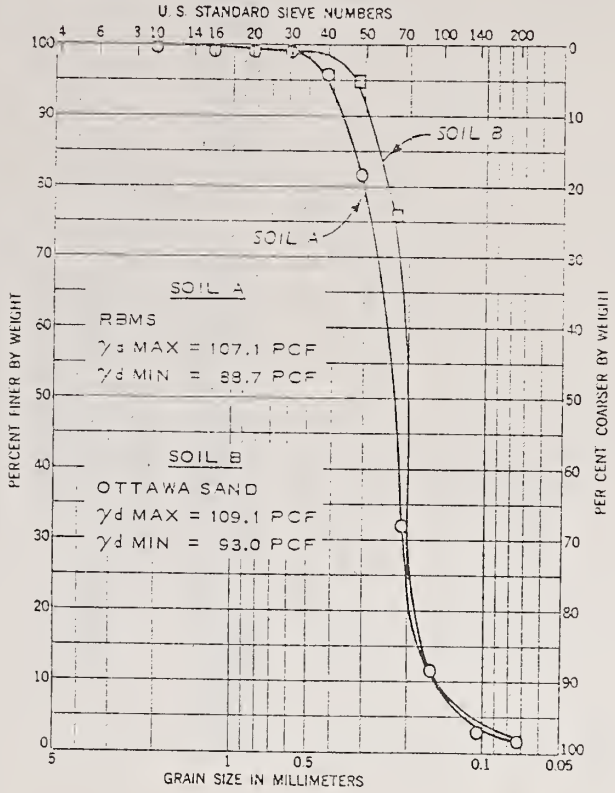

FIG. 5.--REID-BEDFORD MODEL SAND AND OTTAWA SAND GRAIN SIZE DISTRIBUTION CURVES

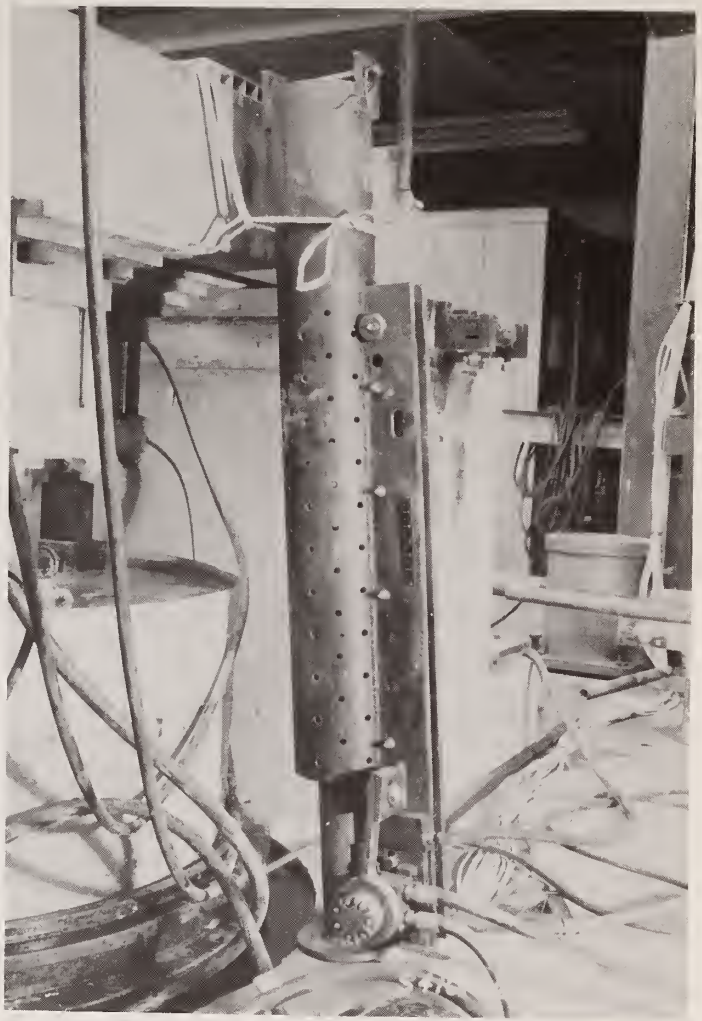

FIG. 4.--HYDRAULICALLY OPERATED TRIP HAMMER

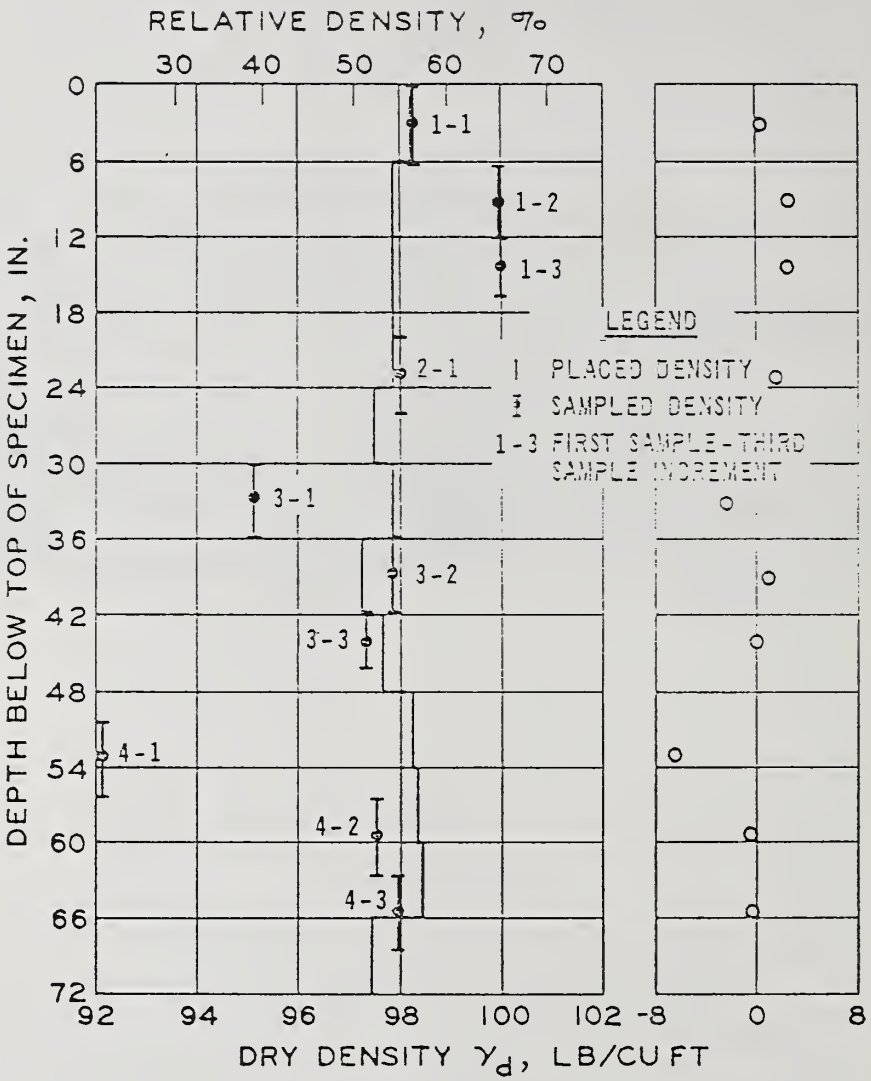

REID-BEDFORD SAND

NOMINAL RELATIVE DENSITY, D_R = 55 %

(SPECIMEN 7)

FIG. 6.--TEST RESULTS

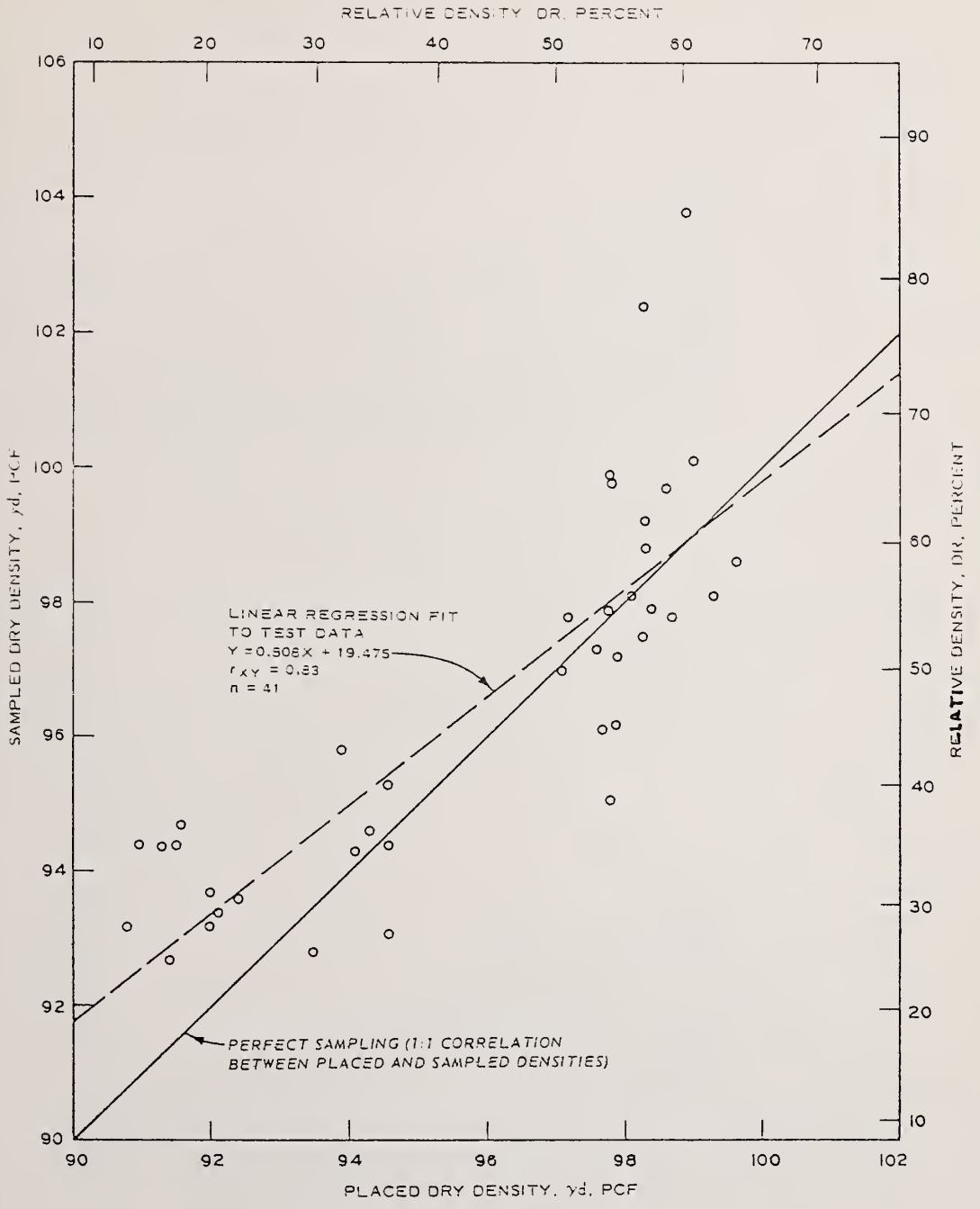

FIG. 7.--LINEAR REGRESSION FIT TO SELECTED DATA

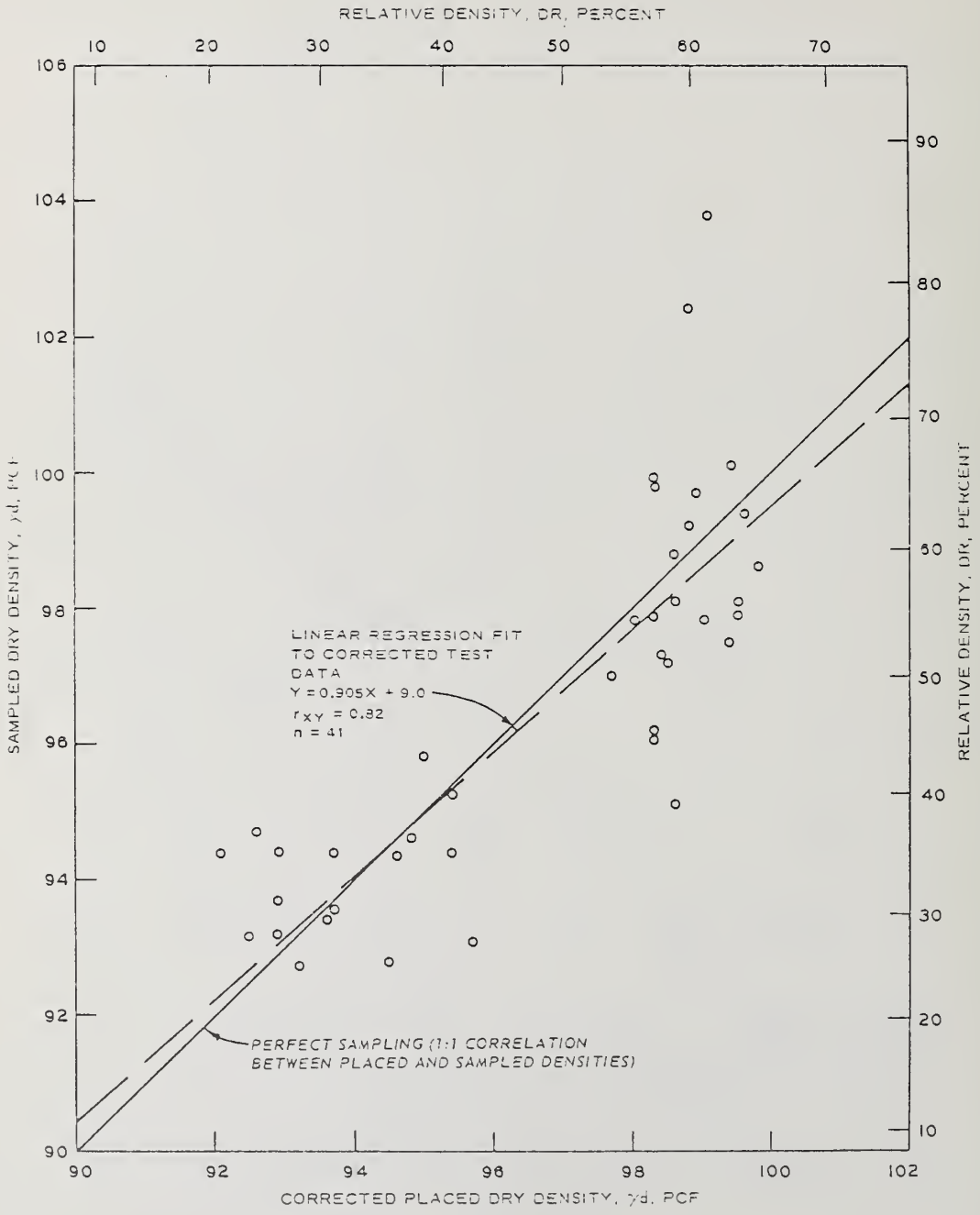

FIG. 8.--LINEAR REGRESSION FIT TO DATA CORRECTED FOR CONSOLIDATION EFFECT

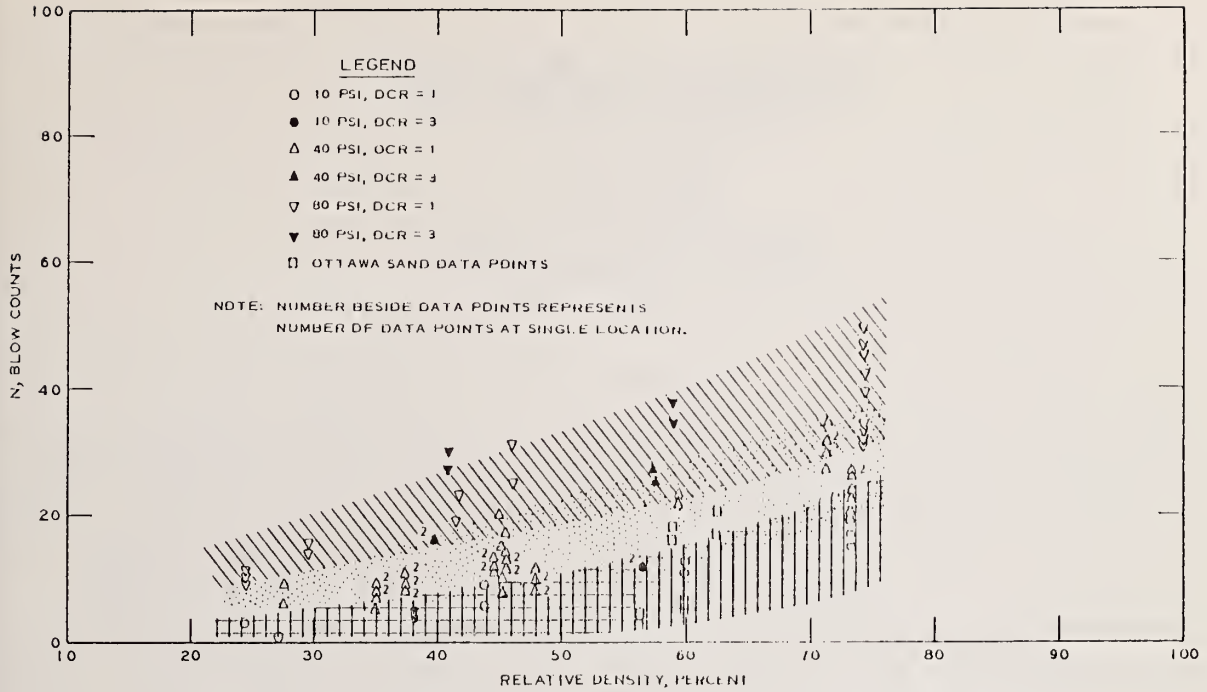

FIG. 9.--A DEPICTION OF THE SPREAD OF WES DATA FOR THE THREE OVERBURDEN PRESSURES

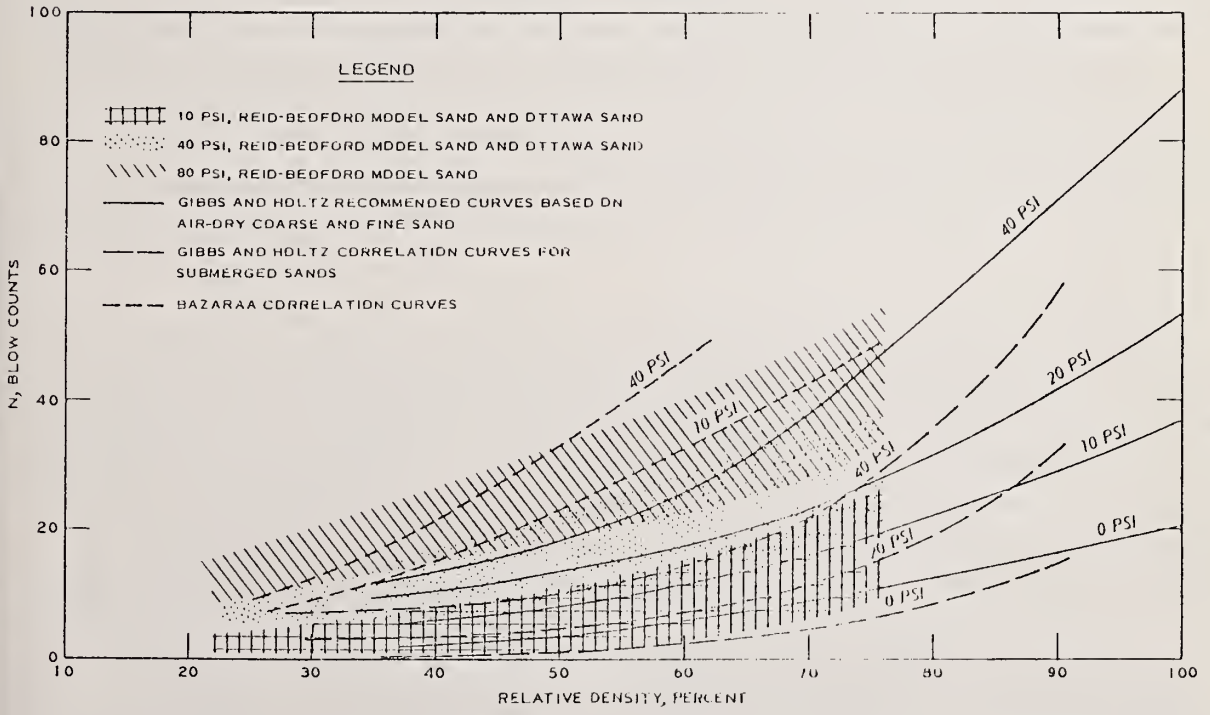

FIG. 10.--COMPARISON OF WES DATA, GIBBS AND HOLTZ CORRELATION CURVES, AND BAZARAA CORRELATION CURVES

DYNAMIC SOIL PROPERTIES WITH EMPHASIS ON COMPARISON OF LABORATORY TESTS AND FIELD MEASUREMENTS

TOSHIO IWASAKI
FUMIO TATSUOKA
Ground Vibration Section
Public Works Research Institute
Ministry of Construction
Japan

ABSTRACT

In order to evaluate analytically the motion of the ground during earthquakes, it becomes necessary to obtain the dynamic deformation properties of the soil deposits, expecially the strain amplitude-dependent shear moduli and the damping coefficients. At two sites, Iruma, Minami-Isu-cho and Ohgi-shima, Kawasaki-shi, insitu seismic surveys were performed. At the former site, a sand embankment was damaged during the Off-Izu-peninsula earthquake on May 9, 1974 and at the latter is located reclaimed land where borehole accelerometers are installed. Furthermore, sand sampled from these sites were tested with the resonant-column apparatus of the Drnevich type in order to obtain the shear moduli and damping capacities at small strains. Laboratory test results showed that the two natural sands, which are well-graded and include fine particles, have smaller shear moduli than does uniform clean sands such as Toyoura-sand and Ottawa-sand.

A comparison of the shear moduli from shear wave velocities and those from resonant column tests was performed, giving excellent correlation for sands from both sites.

Key Words: Dynamics ; Field Tests; Laboratory Tests ; Relationships ; Soil Properties.

1. Introduction

In order to analyze the earthquake response of a ground, it becomes necessary to obtain the dynamic deformation properties of the soil for each layer at the site. For engineering application, the earthquake response analyses for horizontally layered sites have been performed. In these analyses, only the horizontal displacements of the layers are taken into account and therefore only the density $\rho = (\gamma_t/g)$, shear modulus G, and damping factor η of each layer is needed. In this paper comparisons of shear moduli G obtained from laboratory tests and those obtained from insitu seismic surveys is presented.

2. Shear Modulus G by Resonant-Column Method

The shear moduli G of sands were obtained by performing dynamic tests using a resonant-column apparatus developed at the Public Works Research Institute. A schematic diagram of the apparatus is shown in Fig. 1. This resonant-column apparatus is the Drnevich-type (1) with a hollow cylindrical sample, as shown in Fig. 2. The sample is

25 cm in height, 10 cm in outside diameter and 6 cm in inside diameter and is fixed at the bottom. A pair of oscillators, which supply the system with a torsional vibratory force, are fastened to the rigid mass on top of the specimen. The confining pressure, equally applied to the outside and to the hollow of the specimen, is supplied by air pressure. The axial load can be applied independently of the confining pressure. The quantities measured during a steady state vibration test are the resonant frequency of the oscillator-specimen system, the vibration amplitudes at the top of the specimen, the changes of length and volume in the specimen, the confining pressures and the axial load. Furthermore, amplitude time decay curves are recorded after shutting off the driving power at resonance. From these measurements, the shear strain amplitudes, the shear moduli and the logarithmic decrements can be evaluated for the materials examined. Typical test results are shown in Fig. 10, where the shear moduli in the range of shear strain of 2×10^{-6} to 5×10^{-4} are presented. Details of the principle and testing procedures have been presented in previous papers (2,3).

Listed in Table 1 are details of the sands tested in this study. These sands can be divided into two groups: (1) Clean sands which do not include fine particles smaller than 0.074 mm in diameter, are poorly graded, and are made by sieving several natural sands, (2) Natural sands, Irumasand and Ohgi-shima-sand, which are well graded and include finer particles. Shown in Fig. 2 are gradations of the sands tested, where TO, OS,... and the abbreviations of the names of sands, listed in Table 1. All of the tests were conducted on air-dry or saturated isotropically consolidated ($\sigma_1/\sigma_3 = 1.0$) samples.

The shear moduli of clean sands, at a single shear strain amplitude (γ) of 10^{-6}, 10^{-5} and 10^{-4}, are shown in Fig. 4, Fig. 5 and Fig. 6, respectively. The factor p represents the mean principal stress denoted by $(\sigma_a + 2\sigma_r)/3$ where σ_a is the axial stress and σ_r is the radial stress. These figures show that the shear moduli G of clean sands can be represented by the following empirical equations, irrespective of the type of sands;

$$(\gamma = 10^{-6}) \quad G = 900 \frac{(2.17 - e)^2}{1 + e} p^{0.38} \tag{1}$$

$$(\gamma = 10^{-5}) \quad G = 850 \frac{(2.17 - e)^2}{1 + e} p^{0.44} \tag{2}$$

$$(\gamma = 10^{-4}) \quad G = 700 \frac{(2.17 - e)^2}{1 + e} p^{0.50} \tag{3}$$

where G is the shear modulus in kg/cm^2, p is the mean principal stress in kg/cm^2 and e is the void ratio. Eq. (3) is identical to the empirical equation for round Ottawa-sand as proposed by Hardin, et al (4).

However, natural sands are generally well graded and to some extent include silty or clay particles. Test results, for all natural sands, have shown that their shear moduli are less than those expressed by eqs. (1) through (3). Therefore, it is apparent

that shear moduli of various sands can not be predicted by eqs. (1) through (3).

In the following section, it will be shown that the shear moduli predicted by eqs. (1) through (3) is larger than those measured during in situseismic surveys. Also, it will be shown that the shear moduli measured by resonant-column tests, for sand samples taken from the sites, are almost the same as those obtained during field measurements.

3. Comparison of Laboratory Tests and Field Measurements

Insitu borehole seismic surveys and samplings were conducted at two sites: Iruma, Minami-Izu-cho and Ohgi-shima, Kawasaki-shi (see Fig. 7). At the former site, a sandy embankment was damaged by the Off-Izu-peninsula earthquake in 1974. The surrounding slopes of the embankment slipped down and wooden houses on the embankment were severely damaged. The latter site is reclaimed land, where borehole accelerometers were installed down to the depth of about 120 m below the ground surface.

At iruma, the borehole seismic surveys were carried out at three locations. The soil properties are shown in Fig. 8 and Fig. 14, where the soil profile, N-value, wave velocity Vs and density are presented. The shear wave velocity measurements were performed at 2 m depth intervals. Shown in Fig. 9 are the relationship between the N values and the shear moduli G_o, obtained from the following equation.

$$G_0 = \frac{\gamma t}{g} Vs^2 \qquad (4)$$

where G_o is the shear modulus, γ_t is the total unit weight, g is the acceleration of gravity and vs is the shear wave velocity. Also shown in this figure are three lines, which represent the empirical relationship between G_o and N-values proposed by three different groups, Ohsaki, et al.(5), Kajima (6) and Ohyo-chishitsu (7). As seen in Fig. 9 the data is scattered, therefore, empirical relations can not be obtained in predicting G_o from N-value. This is due to the fact that the sand deposit of Iruma includes some gravel, which make the N-value much larger in comparison with sands without gravel. It has also been determined that for the Ohgi-shima site, the shear moduli at very small strain levels can not be predicted by empirical relationships between G_o and the N-value.

Resonant-column tests were performed on sands sampled from the Iruma site. Sands were taken from the deposit just below the ground surface. As the sand deposit is almost uniform to a depth of about 10 through 20 m, the sand near the ground surface could represent properties of the entire sand deposit. Tests were carried out on dense air-dry and saturated samples which were completely disturbed. Samples were made by placing air-dry sand through air into a split mold or by placing saturated sand into a mold filled with de-aired water. Densification was performed by tamping the split mold with a wooden hammer. Consolidation time was about 1 hr. Considering that the sand deposit is young and the plasticityindex of the sand is almost zero, the effect of cementation and delayed consolidation is negligible (8). Therefore, the shear modulus of the sand deposit can be estimated from the test results on completely disturbed specimens. Fig. 10 shows some

test results on the Iruma sand. Fig. 11 gives the shear moduli at $\gamma = 10^{-6}$, 10^{-5} and 10^{-4} of the Iruma sand. As seen from Fig. 11, the shear modulus of the Iruma sand does not depend on wet conditions, and is smaller than those represented by eqs. (1) through (3). It should also be noted that the shear moduli of Iruma sand A, Iruma sand C and Iruma sand Z3, which were made by sieving Original Iruma Sand are identical to those represented by eqs. (1) through (3) as shown in Fig 4 through 6. This means that the shear moduli of sands are not affected by the properties of the particles but are affected by the grading or content of fine particles. To obtain the shear moduli of the sand deposit of the Iruma sand from empirical equations, it is necessary to estimate the effective mean principal stress p' and the void ratio e in the ground. First, the relative density of every layer 1 m thick, was estimated from the relationship of the effective overburden pressure σ'_v and N-value, (Fig. 12), as proposed by Gibbs and Holtz (9). In this estimation extremely high N-values, due to the existence of gravels, was omitted. Second, both values of the maximum and minimum void ratios were obtained by the method proposed by Yoshimi and Tohno (10). In this method, the maximum void ratio is obtained by pouring air-dry sand into a steel mold with an inner diameter of 6 cm and an inner height of 5.3 cm. The minimum void ratio is obtained by pouring air-dry sand into a mold and by tamping horizontally the mold with a wooden hammer. Thirdly with the information on saturation rate of sand and the underground water table, the unit weight of sand γ_t was estimated. Then, the effective mean principal stress p' was calculated by using the values of γ_t, the groundwater table supposing the earthpressure coefficient at rest to be 0.5. Last, the shear moduli at $\gamma = 10^{-6}$ and $\gamma = 10^{-4}$ were obtained by the empirical equations for the shear moduli of the Iruma sand shown in Fig. 11, using the estimated p' and e values. Shown in Fig. 13 are the shear moduli, at extreme small strains, obtained from the shear wave velocities Vs as denoted by solid vertical lines the values of the shear moduli at $\gamma = 10^{-6}$ and $\gamma = 10^{-4}$, obtained from the laboratory tests, are represented by the black circles (G at $\gamma = 10^{-6}$) and black triangles (G at $\gamma = 10^{-4}$). The solid curve given in Fig. 13 indicates that the shear moduli, estimated from these two laboratory-test, has values of G at $\gamma = 10^{-6}$ and $\gamma = 10^{-4}$, these shear strain amplitudes occurred in the ground during borehole seismic survey decrease with depth on the order of about 10^{-7} to 10^{-5}. Examination of this curve indicates that there is agreement between the values of the shear moduli predicted by the laboratory tests and those values obtained by shear wave velocities. Similar results have been obtained for other location points at Iruma site, as shown in Fig. 15. On the other hand, the shear moduli obtained from empirical equations for "clean" sands, eqs. (1) through (3), using estimated values of p' and e are also plotted in Figs. 13 and 15 designated by the white circles (G at $\gamma = 10^{-6}$) and white triangles (G at $\gamma = 10^{-4}$). As seen by Figs. 13 and 15, the predicted values of eqs. (1) through (3) are much larger than the values from the shear wave velocities.

A similar survey was also conducted at the Ohgi-shima site, the soil profile of which is shown in Fig. 16. As the reclaimed sand deposit at this site is also almost uniform to a depth of about 25 m, resonant-column tests were performed on samples taken just

below the ground surface, these results were then used to determine the shear moduli in the ground. The shear moduli at $\gamma = 10^{-6}$, 10^{-5} and 10^{-4} are shown in Fig. 17, from which it can be seen that well-graded Ohgi-shima sand including fine particles, has a smaller shear moduli than those estimated by eqs. (1) through (3). It can be seen that the shear moduli of both air-dry and saturated sands can be represented by the same equations.

Ohgi-shima was reclaimed recently with sands from Sengenyama, located in Chiba-prefecture. It should also be noted that Sengenyama sands A,B, and C, which have properties as shown in Fig. 3 and Table 1, have shear moduli expressed by eqs. (1) through (3) as illustrated in Figs. 4 through 6. This means that the shear moduli of natural sands are lower than those of clean sands, because the properties of natural sands contain fine particles. Shown in Fig. 18 is a comparison of the shear modulus estimated from laboratory tests and those obtained from the shear wave velocity Vs. From this figure it can be seen that the shear moduli predicted by the laboratory tests are almost identical to those obtained from field measurements, and that the shear moduli estimated by empirical equations of clean sands are over estimated.

Another important point to be noted is that shear moduli, estimated from resonant column tests, vary smoothly with respect to depth, but similar variations can not be obtained by the field seismic survey. Therefore, when conducting earthquake response analyses of soil deposits, it would be better to determine shear moduli of soil by considering results from both field seismic surveys and laboratory tests.

4. Conclusions

The paper presented the results of a study in which shear moduli were at very small strain. The principal conclusions drawn from this study are as follows:

1. With a resonant-column apparatus, the shear moduli of sands were obtained for the range of strain of $\gamma = 10^{-6}$ to $\gamma = 10^{-4}$,
2. The shear moduli at each shear strain level of clean sands can be expressed by an identical empirical equation irrespective of the sand tested,
3. The shear moduli of natural sands, which are well-graded and contain silty and clay particles, are smaller than those for clean sands.
4. The shear moduli obtained from laboratory tests is almost identical to those obtained from borehole seismic surveys.
5. The shear moduli in ground, estimated by laboratory tests varies more with respect to depth, when comparing with the variation of the shear moduli obtained by seismic surveys.

Acknowledgements

This research was strongly supported by Mr. E. Kurbayashi, Chief of Earthquake Engineering Section, Public Works Research Institute. Comprehensive tests were conducted with an assistance of Mr. S. Yoshida, engineer of Ground Vibration Section, Public Works Research Institute. The authors wish to acknowledge his cooperation.

References

1. Drnevich, V.P., Effects of Strain History on the Dynamic Properties of Sand, Ph.D. Dissertation, University of Michigan, 1967.

2. Kuribayashi, E., T. Iwasaki and F. Tatsuoka, Effects of Stress-Strain Conditions on Dynamic Properties of Sands, Proc. of JSCE, No. 242, Oct. 1975. pp. 105-114.

3. Kuribayshi, E., T. Iwasaki and F. Tatsuoka, Effects of Particle Characteristics on Dynamic Deformational Properties of Soils, Proc. of 5th Asian Regional Conf., Bangalore, India, Dec. 1975.

4. Hardin, B.O. and W.L. Black, Sand Stiffness Under Various Triaxial Stresses, Jour. of ASCE, Vol. 92, No. SM2, 1966.

5. Ohsaki, Y. and R. Iwasaki, On Dynamic Shear Moduli and Poissons Ratios of Soil Deposits, Soils and Foundations, Vol. 13, No. 4, Dec., 1973.

6. Hara, A. et al.,Shear Modulus and Shear Strength of Cohesive Soils, Soils and Foundations, Vol. 14, No. 3, Sept. 1974.

7. Imai, T., H. Fumoto and K. Yokota, The Relation of Mechanical Properties of Soils to P- and S-wave Velocities in Japan, Proc. of 4th Japanese Symposium of Earthquake Engineering, Tokyo, Nov. 1975.

8. Afifi, S.S. and F.E. Richart, Jr., Stress-history Effects on Shear Modulus of Soils, Soils and Foundations, Vol. 13, No. 1, Mar. 1973.

9. Gibbs, H.J. and W.G. Holtz, Research on Determining the Density of Sand by Spoon Penetration Test, Proc. of 4th Int. Conf. on Soil Mech. and Found. Eng., Vol. I, 1957.

10. Yoshimi, Y. and I. Tohno, Statistical Significance of the Relative Density, ASTM, STP, No. 523, 1972.

11. Drnevich, V.P. and F.E. Richart, Dynamic Prestraining of Dry Sand, J. of ASCE, Vol. 96, No SM2, Mar., 1970.

Table 1 List of Materials

Material	G_s	D_{10} (mm)	D_{60} (mm)	U_c	$e_{max.}$ [b]	$e_{min.}$ [b]
Toyoura-sand (TO)[c] sub-angular, uniform	2.64	0.12	0.175	1.46	0.96	0.64
Sengenyama-sand A (SA) uniform	2.65	0.85 ∿ 2.0[d]		-	0.82	0.61
" B (SB) "	2.72	0.40 ∿ 0.85[d]		-	0.92	0.67
" C (SC) "	2.68	0.25 ∿ 0.40[d]		-	0.98	0.65
Crushed sand-stone (CS) angular, uniform	2.73	2.0 ∿ 5.0[d]		-	1.09	0.80
Crushed lime-stone (CL) sub-angular, uniform	2.74	2.0 ∿ 5.0[d]		-	0.93	0.64
30-50 Ottawa-sand (OS) round, e) uniform	2.66	0.3	0.54	1.8	0.80	0.48
Ohgi-shima-sand (OG) sub-angular, well-graded	2.69	0.2	0.45	2.25	0.72	0.49
Iruma-sand (IR) angular, well-graded	2.75	0.28	0.56	2.0	0.84	0.57
Iruma-sand A (IRA) angular, uniform	2.67	2.0 ∿ 5.0[d]		-	1.06	0.79
Iruma-sand C (IRC) angular, uniform	2.83	0.4 ∿ 0.85[d]		-	0.98	0.66
Iruma-sand Z3 (IRZ3) angular, uniform	2.79	0.5	0.74	1.48	0.94	0.68

a) All tests were conducted under $\sigma_1/\sigma_3=1.0$ - condition.

b) $e_{max.}$ and $e_{min.}$ were obtained on air-dry condition.

c) TO, SA, CS, ... are abbreviation for materials tested.

d) Range of diameter.

e) After Drnevich and Richart (1970).[11]

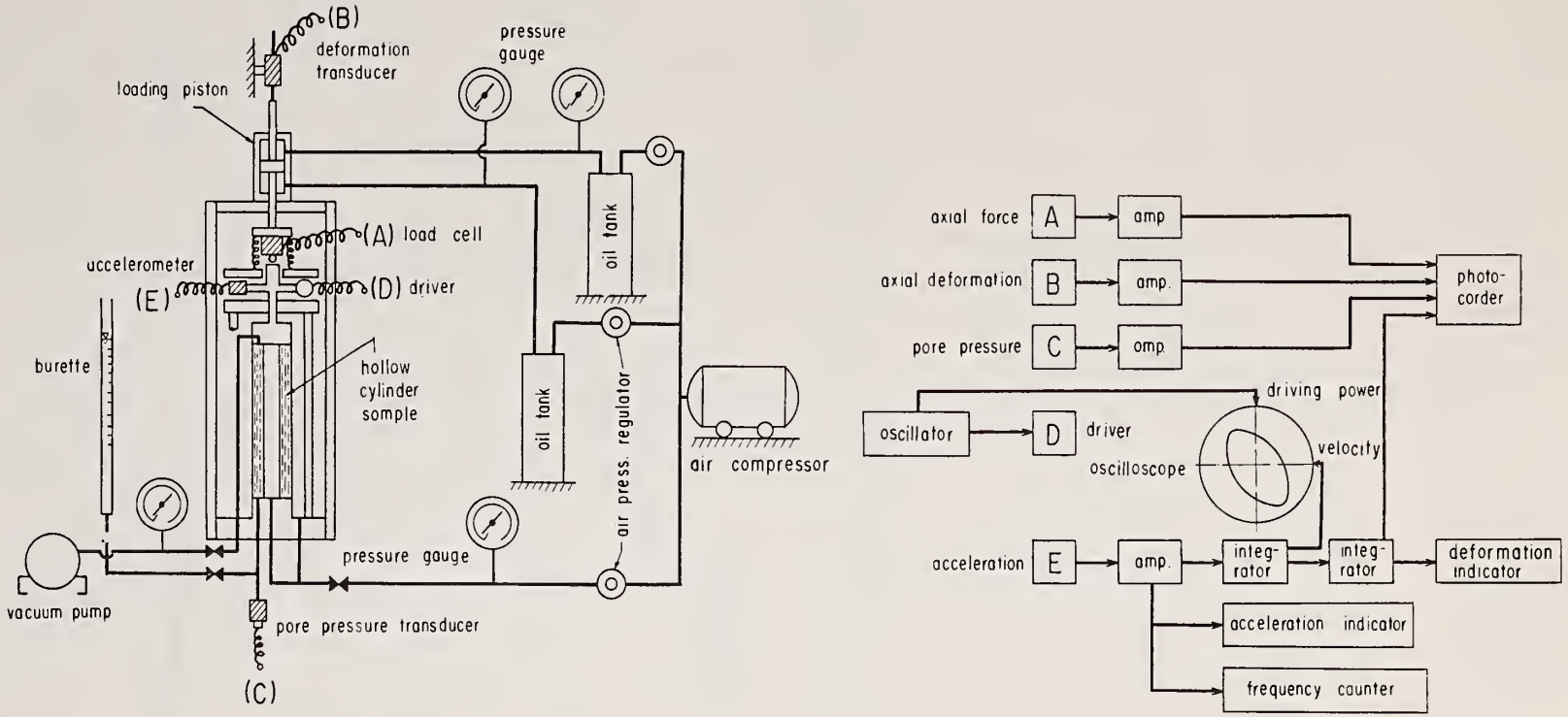

Fig. 1 Schematic Diagram of Resonant-column Apparatus

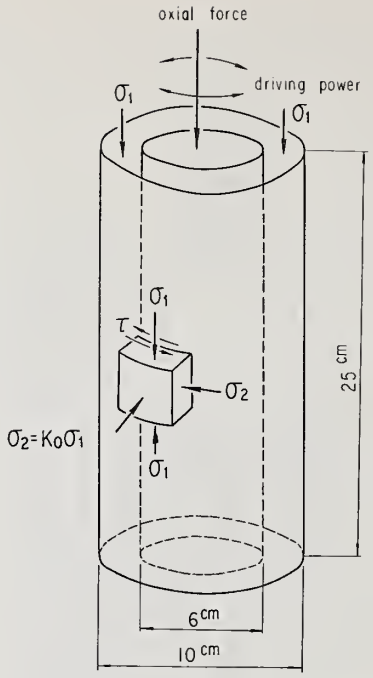

Fig. 2 A Hollow Cylindrical Sample and its' Stress Condition

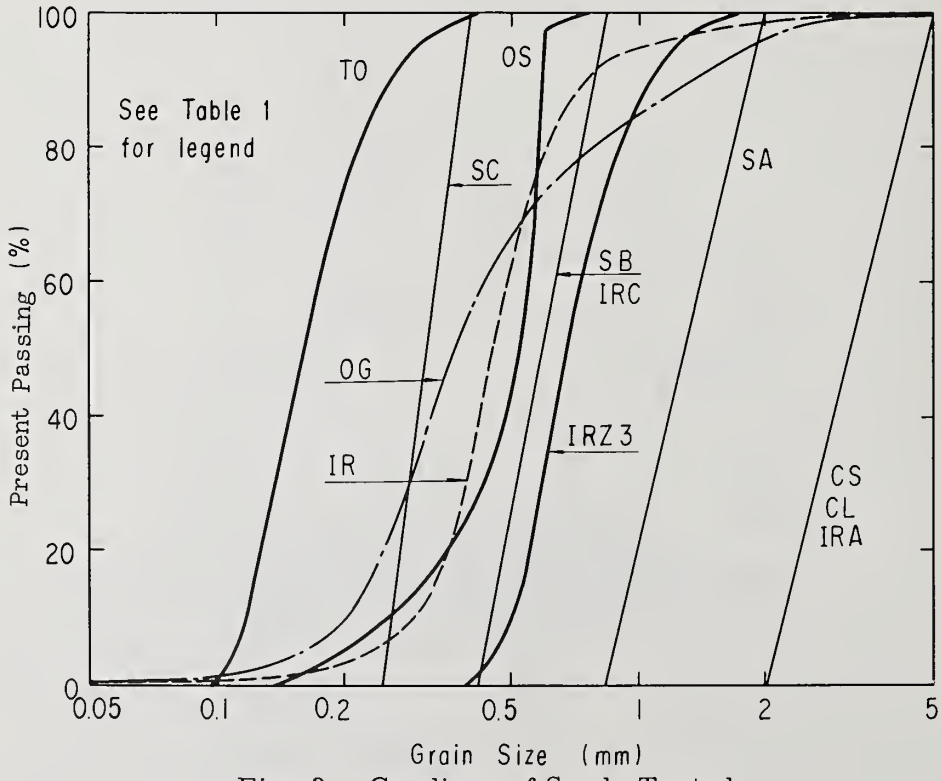

Fig. 3 Gradings of Sands Tested

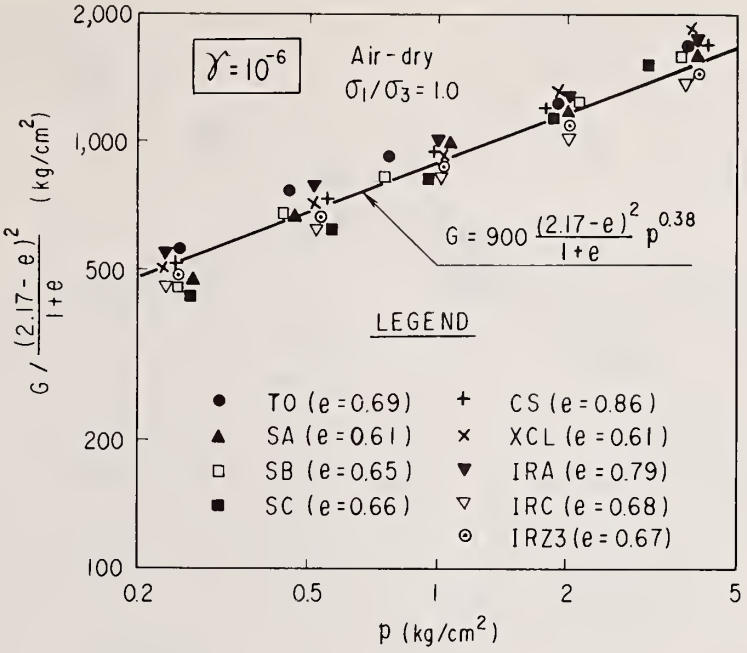

Fig. 4 Shear Moduli at $\gamma = 10^{-6}$ of Clean Sands

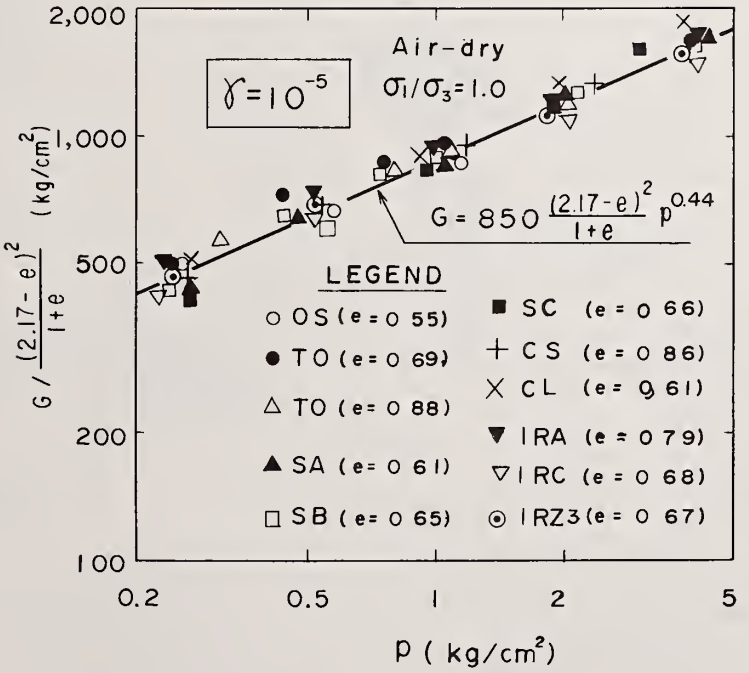

Fig. 5 Shear Moduli at $\gamma = 10^{-5}$ of Clean Sands

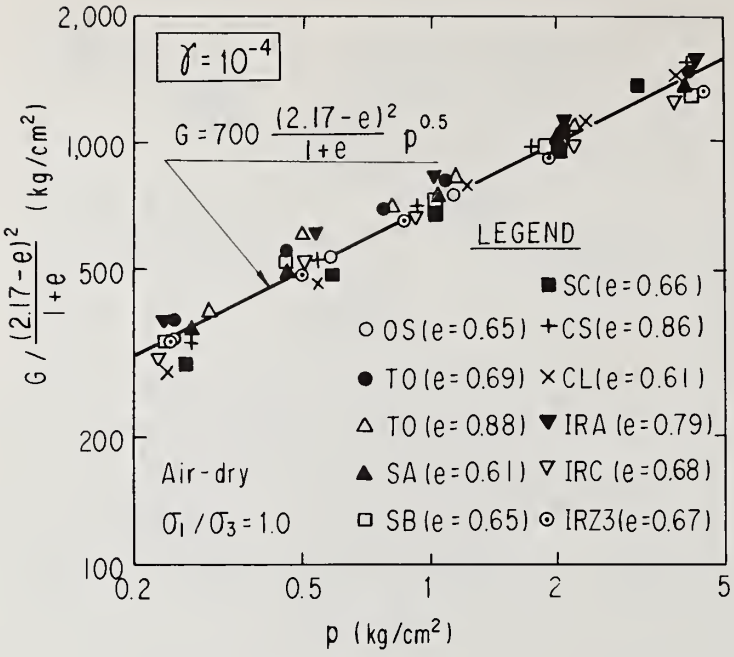

Fig. 6 Shear Moduli at $\gamma = 10^{-4}$ of Clean Sands

Fig. 7 Locations of Iruma and Ohgi-shima

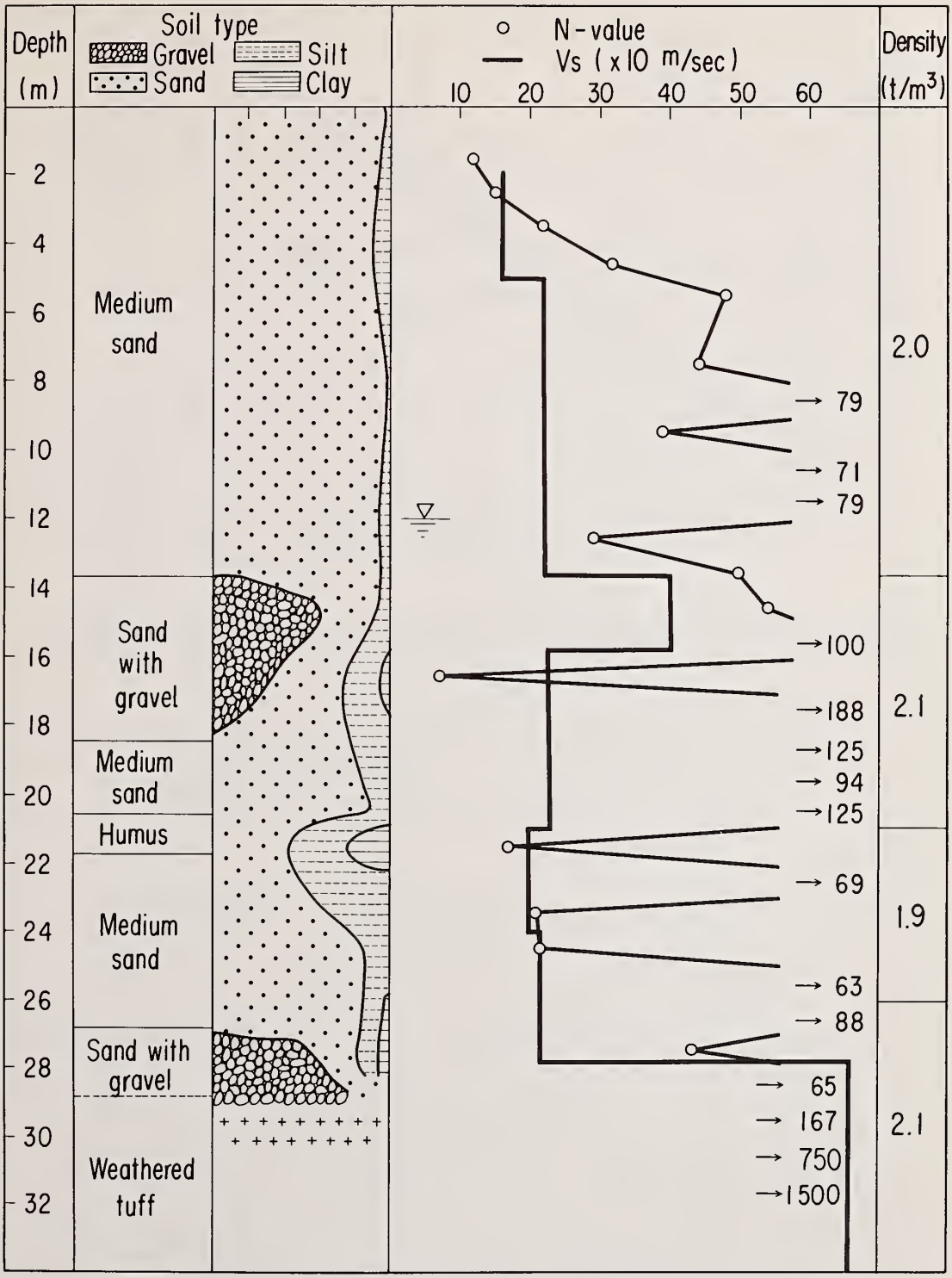

Fig. 8 Soil Profile of Point No. 1 at Iruma

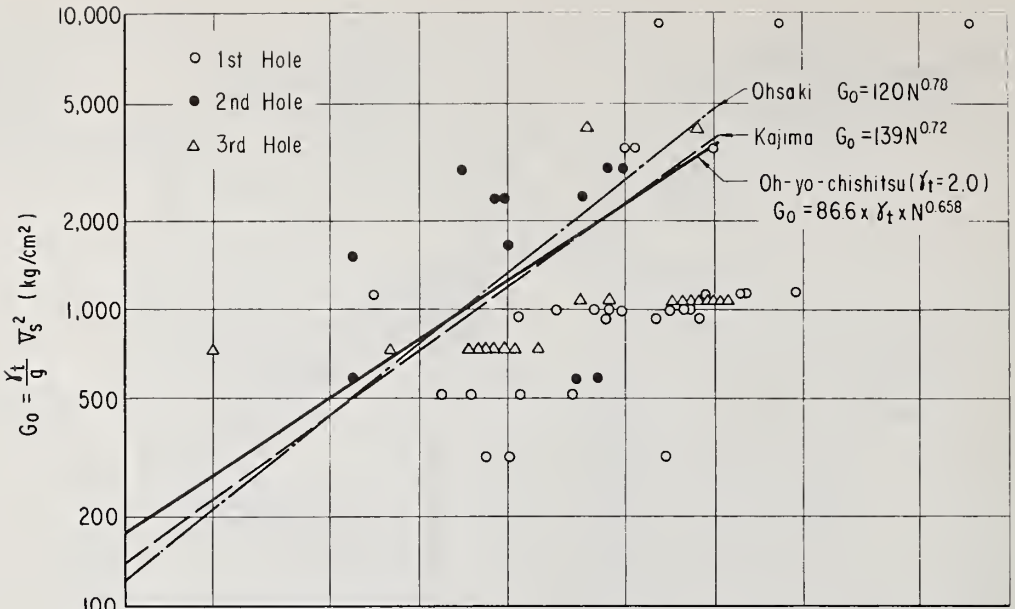

Fig. 9 Relationship between G_0 from Seismic Survey and N-values

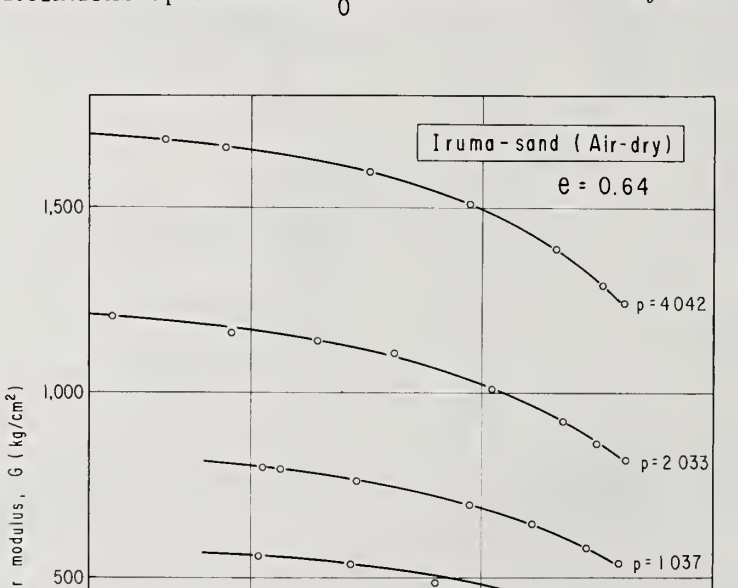

Fig. 10 Typical Test Result on Iruma Sand

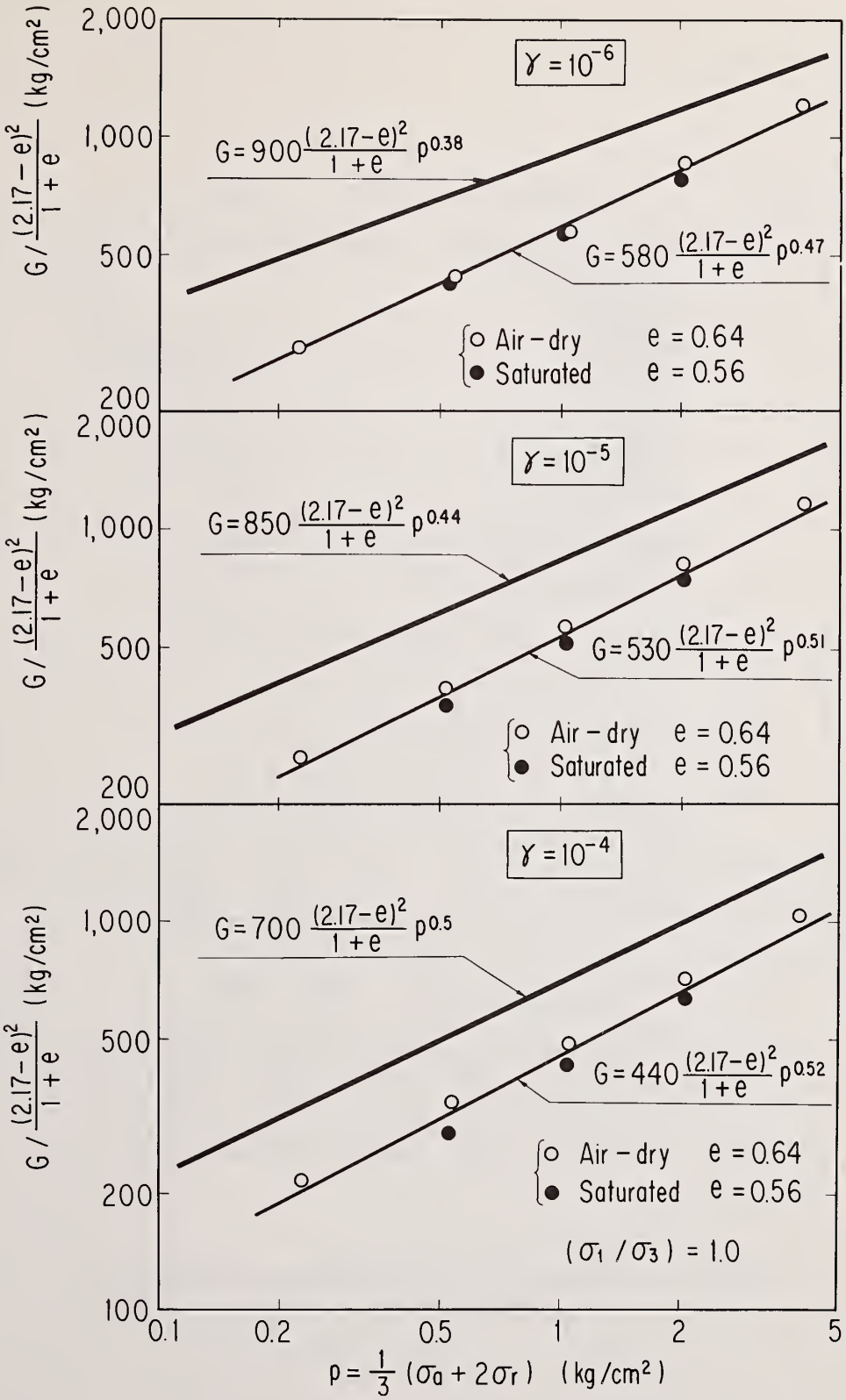

Fig. 11 Shear Moduli at $\gamma = 10^{-6}$, 10^{-5} and 10^{-4} of Iruma Sand

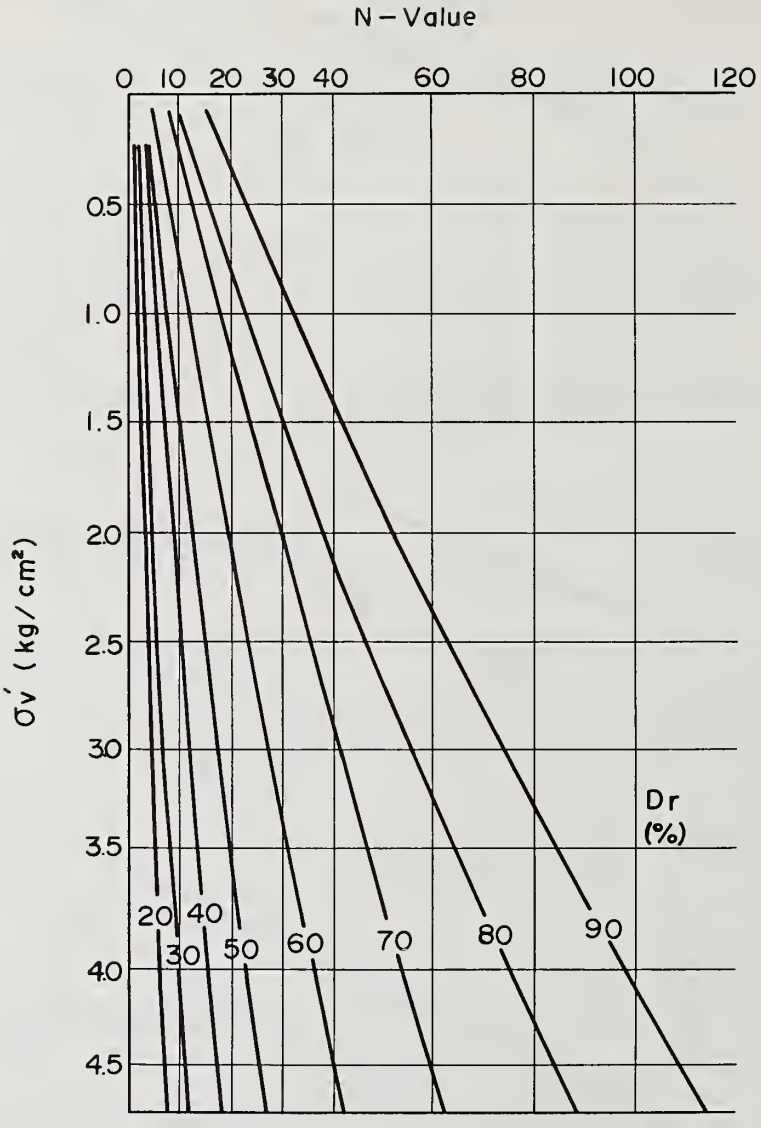

Fig. 12 Relationship between Effective Overburden Pressure σ_v' and N-values

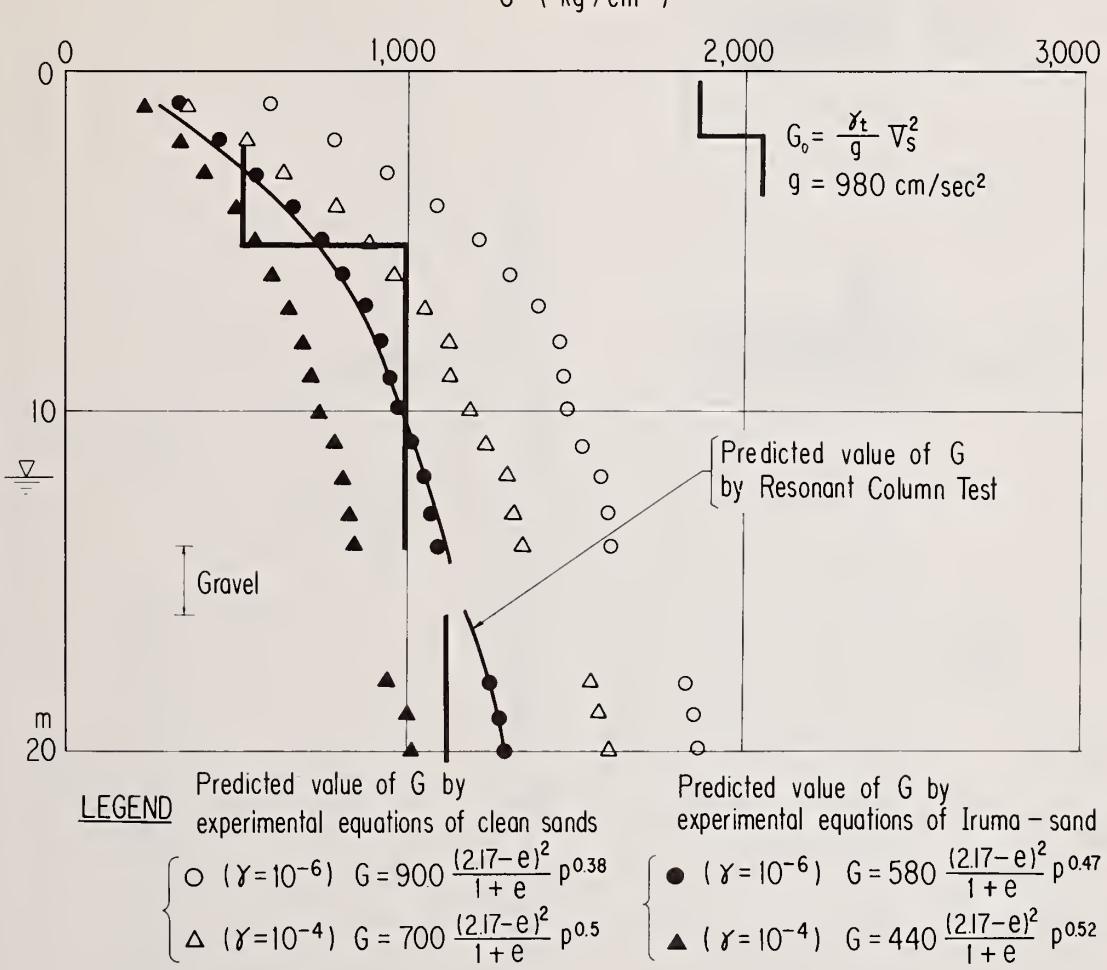

LEGEND

Predicted value of G by experimental equations of clean sands

○ ($\gamma = 10^{-6}$) $G = 900 \frac{(2.17-e)^2}{1+e} p^{0.38}$

△ ($\gamma = 10^{-4}$) $G = 700 \frac{(2.17-e)^2}{1+e} p^{0.5}$

Predicted value of G by experimental equations of Iruma – sand

● ($\gamma = 10^{-6}$) $G = 580 \frac{(2.17-e)^2}{1+e} p^{0.47}$

▲ ($\gamma = 10^{-4}$) $G = 440 \frac{(2.17-e)^2}{1+e} p^{0.52}$

Fig. 13 Comparison of Shear Modulus by Laboratory Tests and Field Measurements at Point No. 1 at Iruma

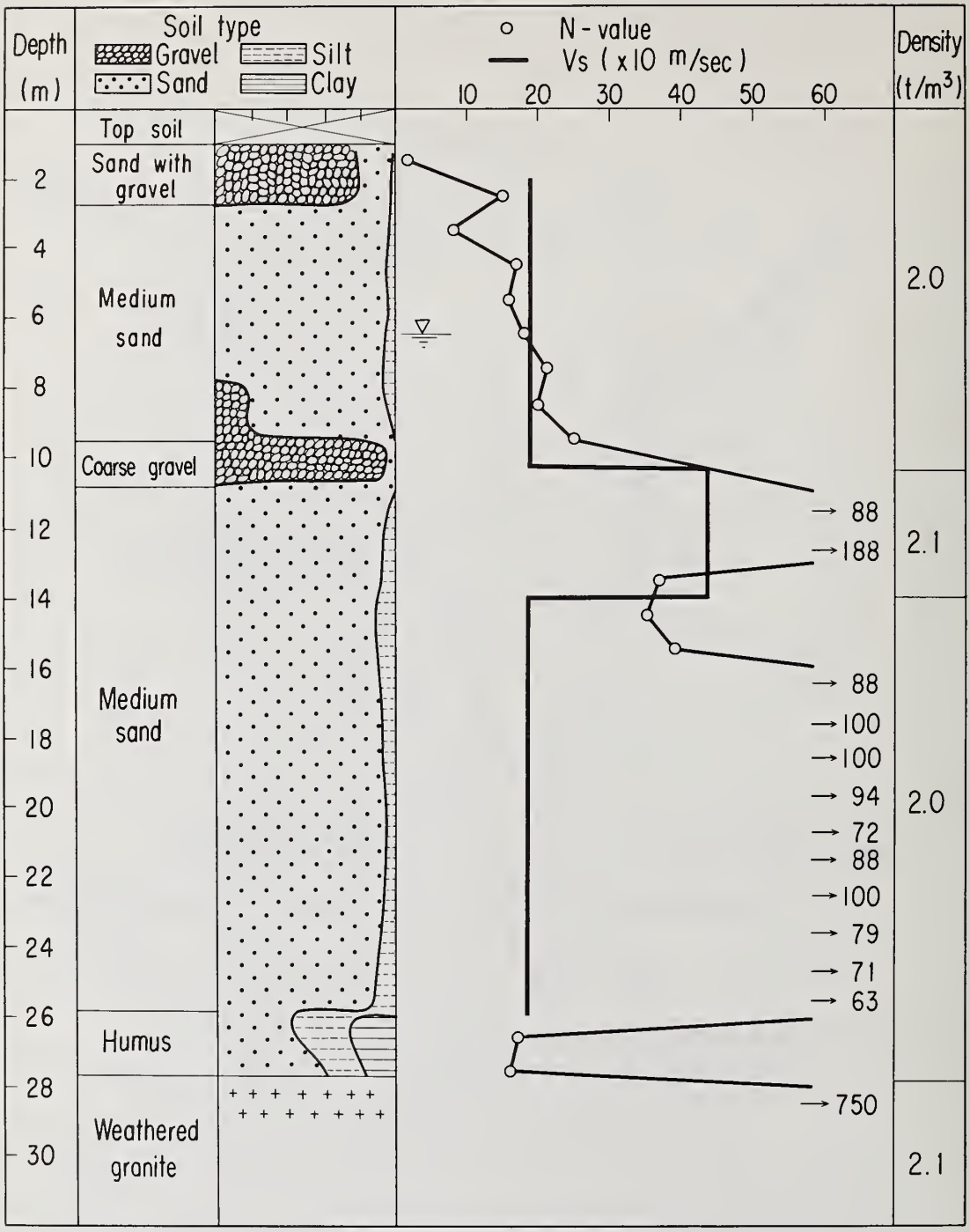

Fig. 14 Soil Profile of Point No. 3 at Iruma

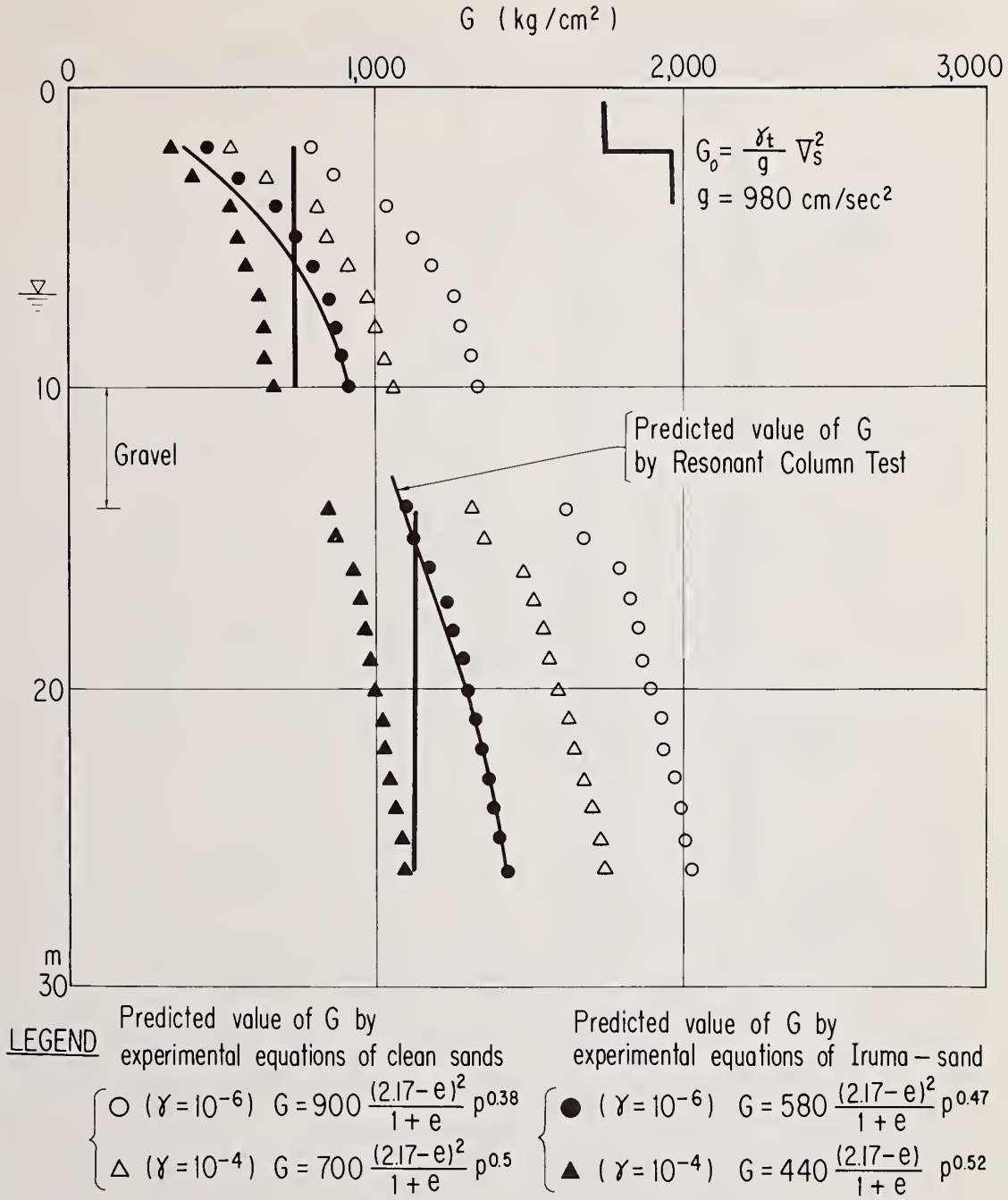

Fig. 15 Comparison of Shear Moduli by Laboratory Tests and Field Measurements at Point No. 3 at Iruma

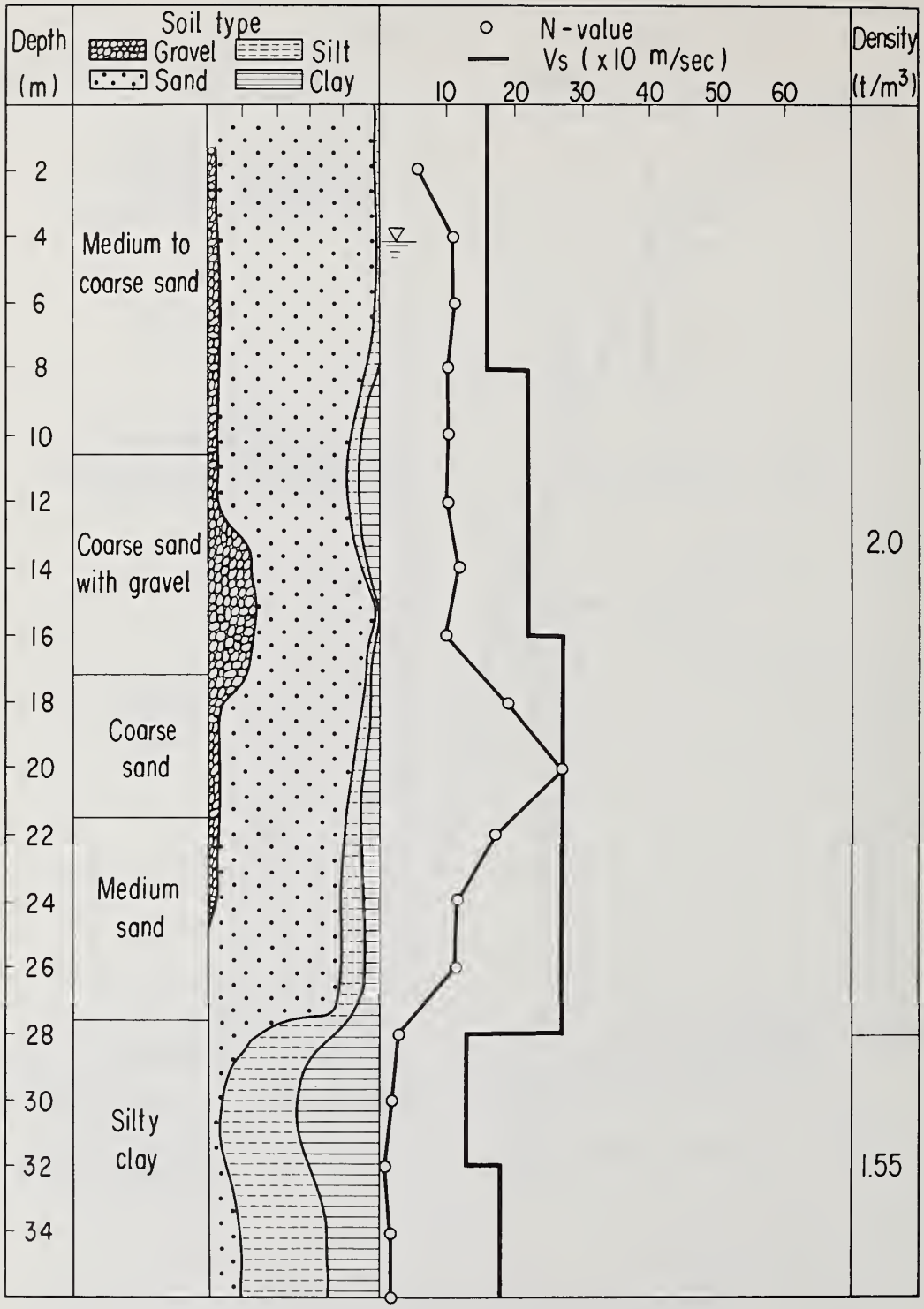

Fig. 16 Soil Profile of Ohgi-shima

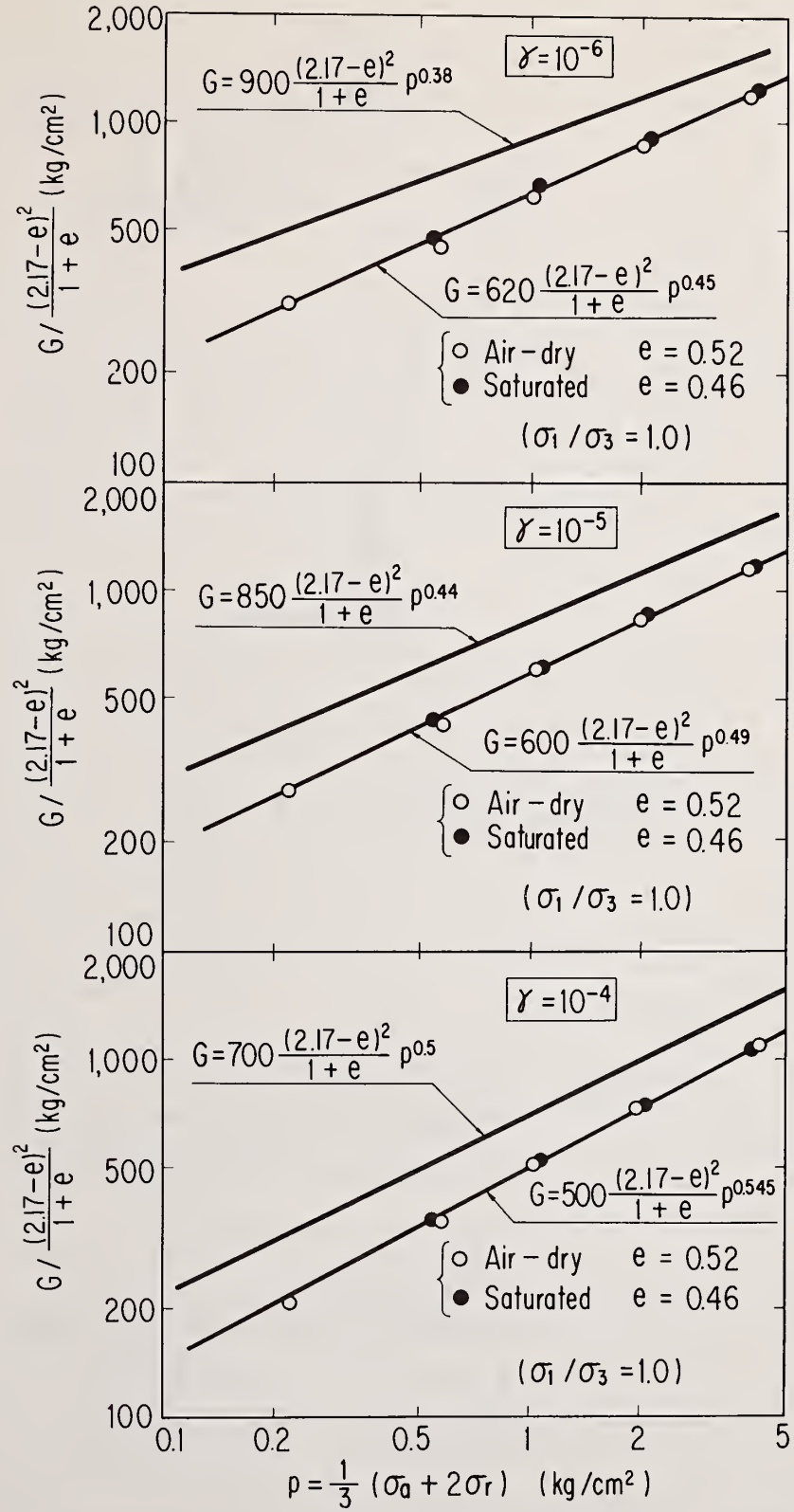

Fig. 17 Shear Moduli at $\gamma = 10^{-6}$, 10^{-5} and 10^{-4} of Ohgi-shima Sand

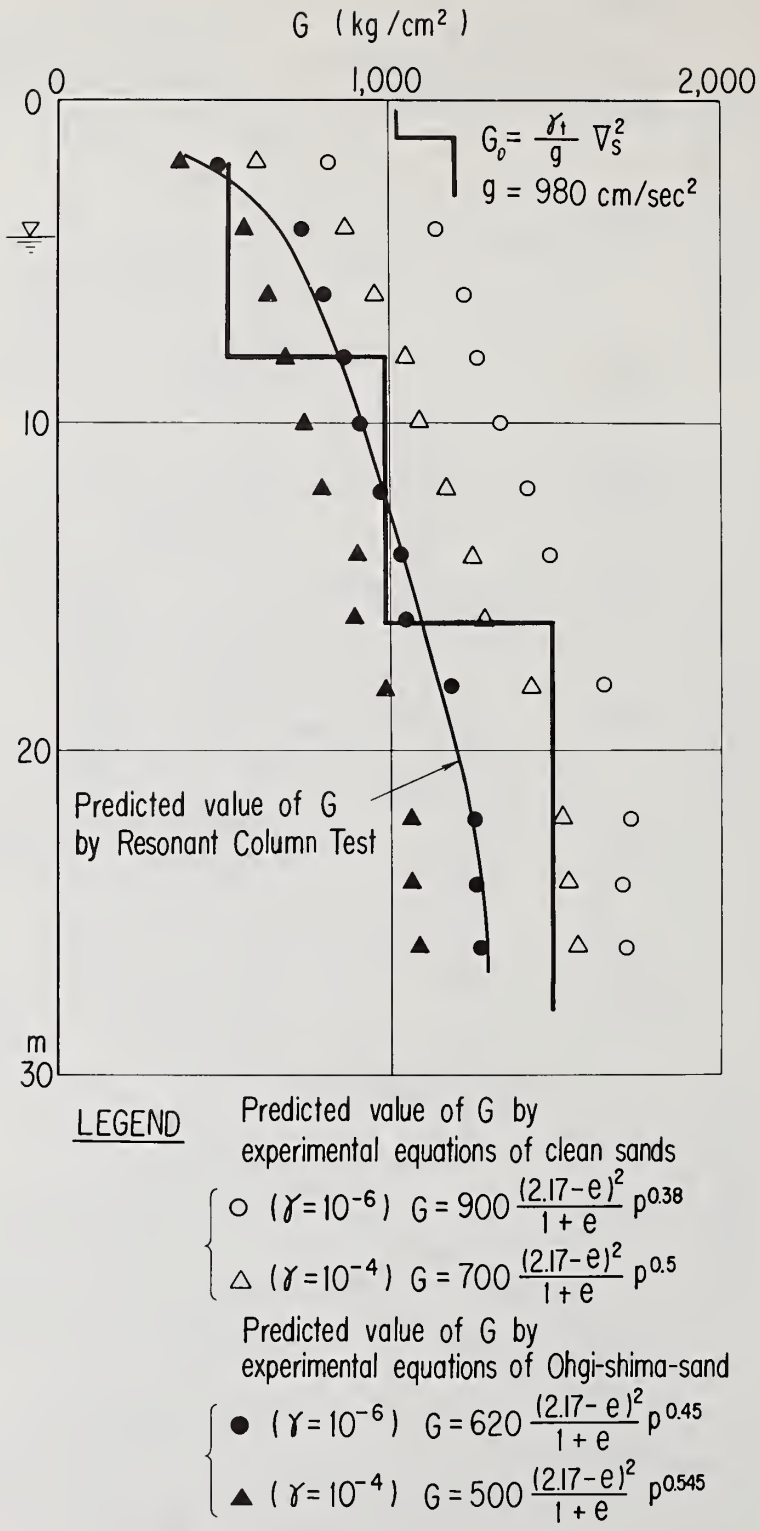

Fig. 18 Comparison of Shear Modulus by Laboratory Tests and Field Measurements at Ohgi-shima

DESIGN EARTHQUAKES

E.L. KRINITZSKY and FRANK K. CHANG
Corps of Engineers
Waterways Experiment Station
Vicksburg, Mississippi 39180

ABSTRACT

Relationships between earthquake intensity and epicentral distance are presented. Peak motion results, from 187 field records, are also given for examination. Also presented is data on displacements, velocities and intensities.

Key Words: Data; Displacements; Intensity; Seismic Records; Velocity.

1. Summary

a) A design earthquake is the bedrock ground motion which is specified for a dynamic analysis. It is based on motions assigned to the maximum credible earthquake (the largest that is reasonably expected) and attenuated to the site. Given several sources for maximum credible earthquakes, there are several design earthquakes.

b) The size of a maximum credible earthquake and the area in which it occurs is determined by geological and seismological studies. Attenuation from source to site is based on seismological interpretation.

c) Since most earthquake data is available only as intensity, it is necessary to specify peak motions in terms of intensity. Fig. 1 relates magnitude to Modified Mercalli (MM) intensity and to epicentral distance so that instrumentally recorded data can be related to areas in which there are only observations of intensity.

d) The dispersion of values for acceleration, velocity, and displacement for any given level of intensity is so large that average or mean lines are meaningless for the purposes of engineering design. For any important project, peak motions are needed. Lesser levels of shaking are appropriate if they are accepted in terms of lower levels of safety.

e) Peak motions, particularly for acceleration, differ greatly in the near to far field for the same level of intensity. Near field limits for different magnitudes and epicentral intensities of earthquakes are shown in Table 1. Accelerations, based on 187 strong-motion records uniformly processed at the California Institute of Technology, are shown in Figures 2 and 3 for near and far fields, respectively. Ground conditions, whether soil or rock, are not specified as large overlapping variations were found among them. Figs. 4 and 5 show corresponding curves for velocity and Figs. 6 and 7 for displacement. The peak curves are reduced by 10 percent increments to a 50 percent level of the spread of data. Thus, these curves may be used to select appropriate parameters for peak or lesser motions. The lesser motions can be related to cost-risk analyses based

on calculated recurrence rates of earthquakes.

f) These parameters may thus be used to rescale appropriate earthquake records, those taken from comparable geological settings, for comparable types of faults and recorded at similar distance from the causative faults. Also, synthetic records can be rescaled using these values.

g) Durations must also be specified. Figs. 8 and 9 show upper boundaries for durations in terms of intensity for the near and far fields, respectively. The boundaries are shown separately for soil and rock. Significantly, durations for soil are double those for rock. Fig. 10 shows the relation of peak values for a magnitude 6.6 earthquake (San Fernando) in terms of duration and epicentral distance. General statements of magnitude versus epicentral distance and duration for rock and for soil are shown on Figs. 11 and 12, respectively. These values may be used to rescale the time functions for the earthquake records that are selected.

h) Because of uncertainties in the appropriateness for rescaling of any single earthquake record, several records should be used.

Table 1

Limits of the Near Field,

Western United States

Magnitude	Maximum Intensity	Radius of Near Field (km)
5.0	VI	5
5.5	VII	15
6.0	VIII	25
6.5	IX	35
7.0	X	40
7.5	XI	45

Table 1. Boundaries for field conditions.

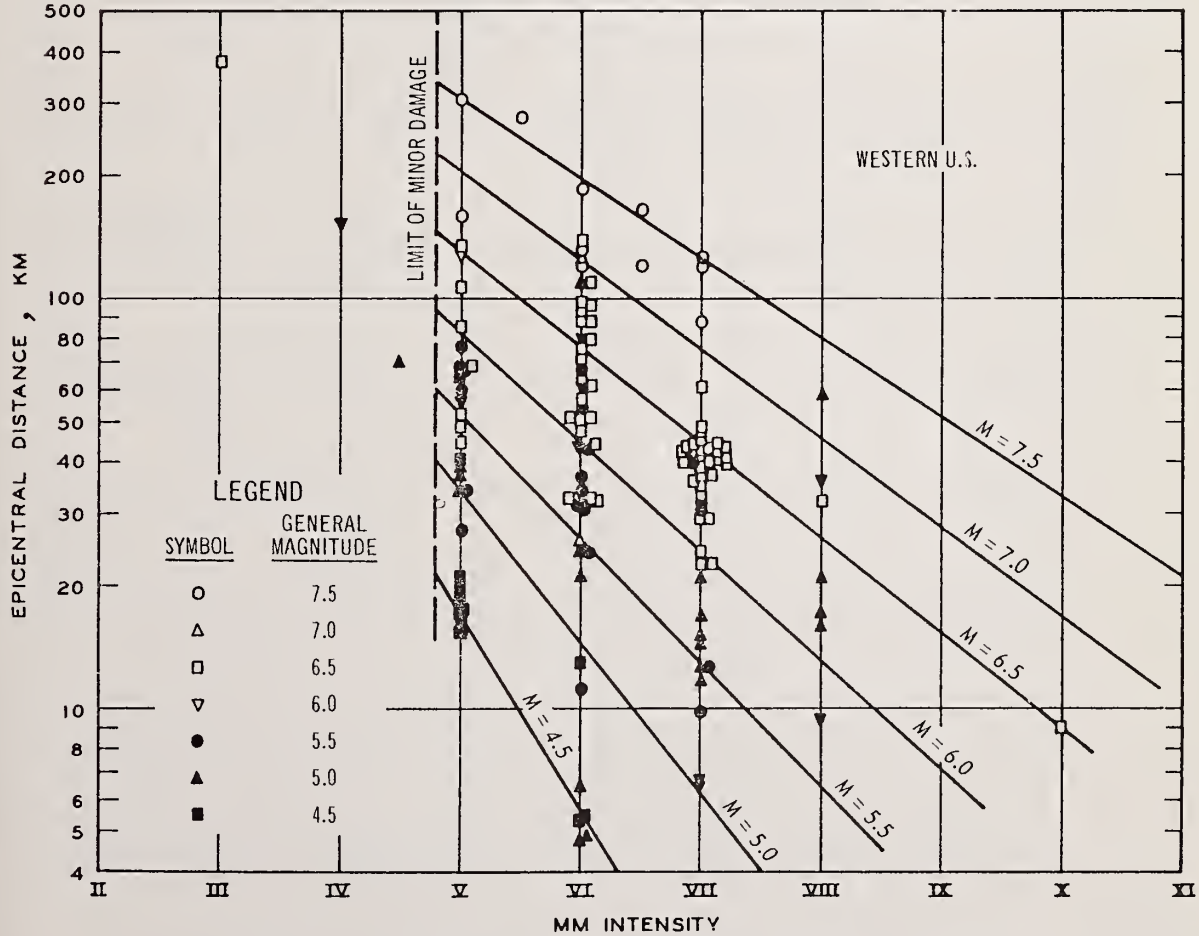

Figure 1. Relation of magnitude to MM intensity and epicentral distance.

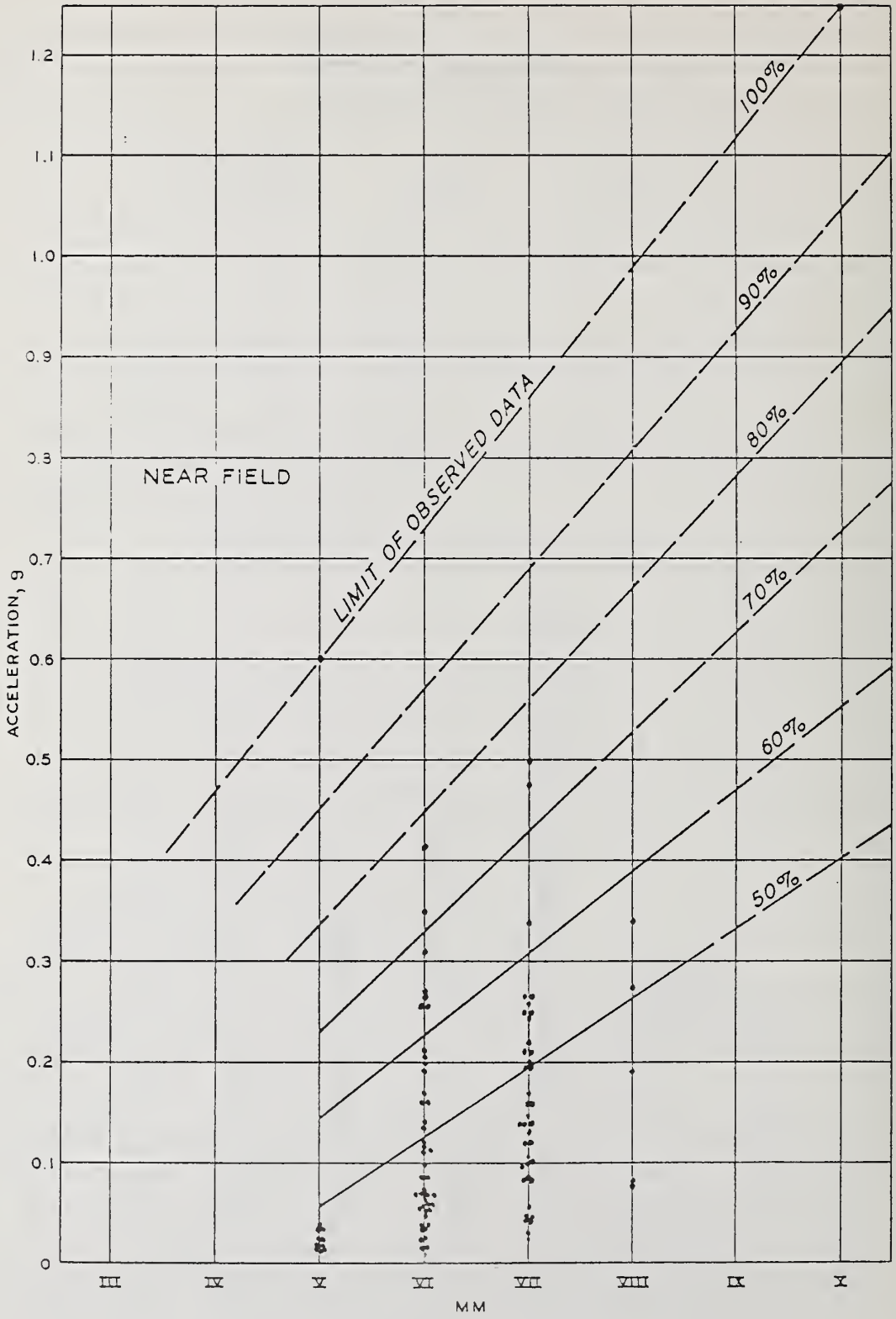

Figure 2. Acceleration values for MM intensity in the near field.

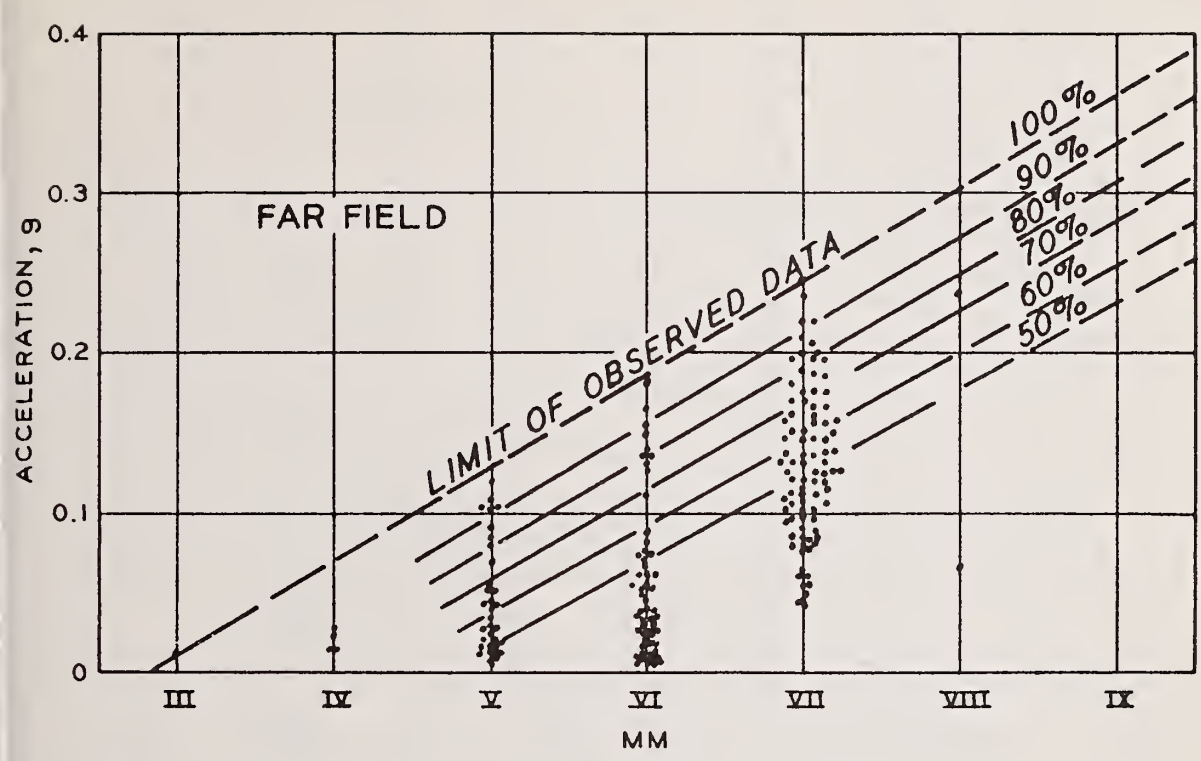

Figure 3. Acceleration values for MM intensity in the far field.

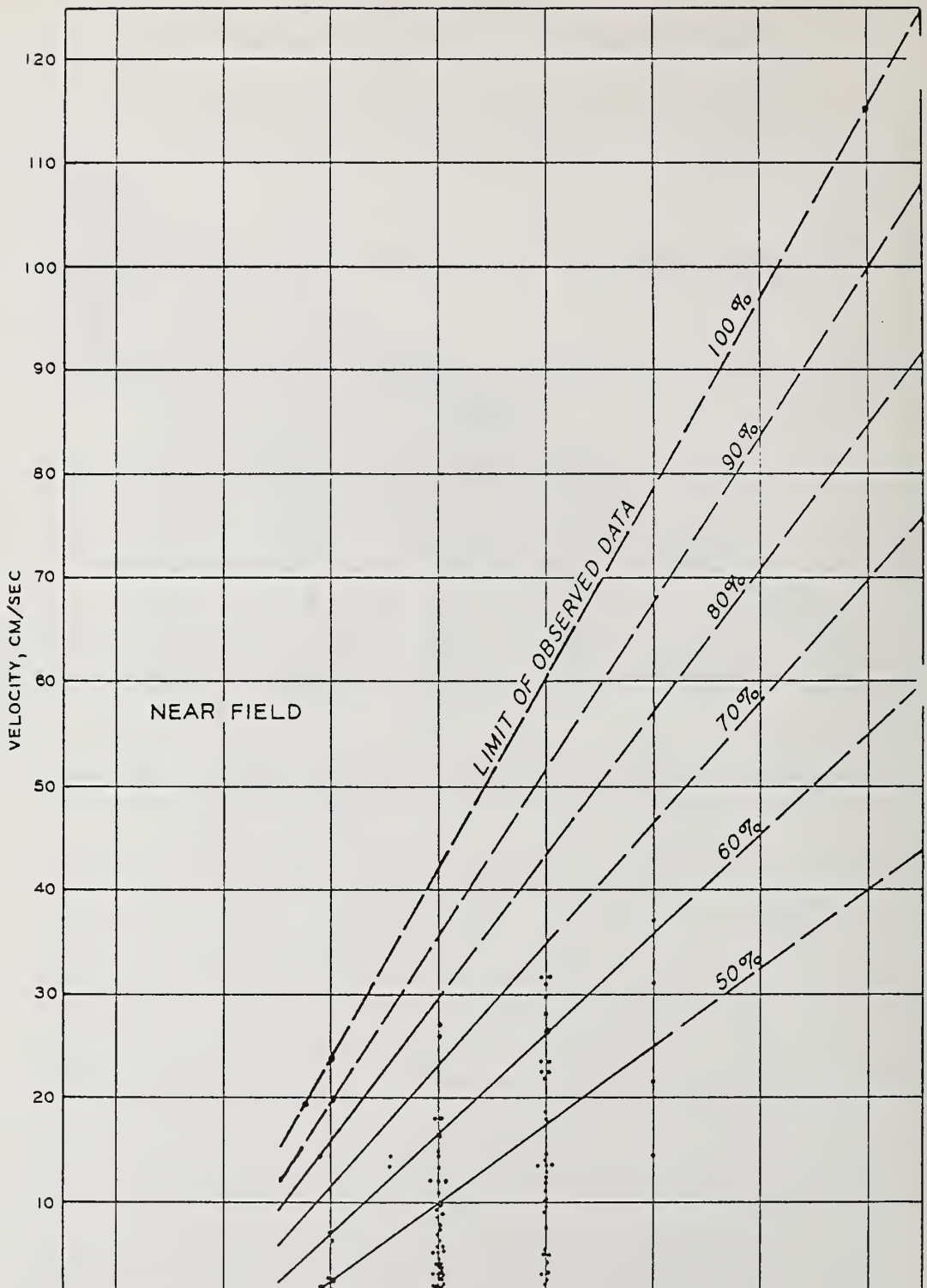

Figure 4. Velocity values for MM intensity in the near field.

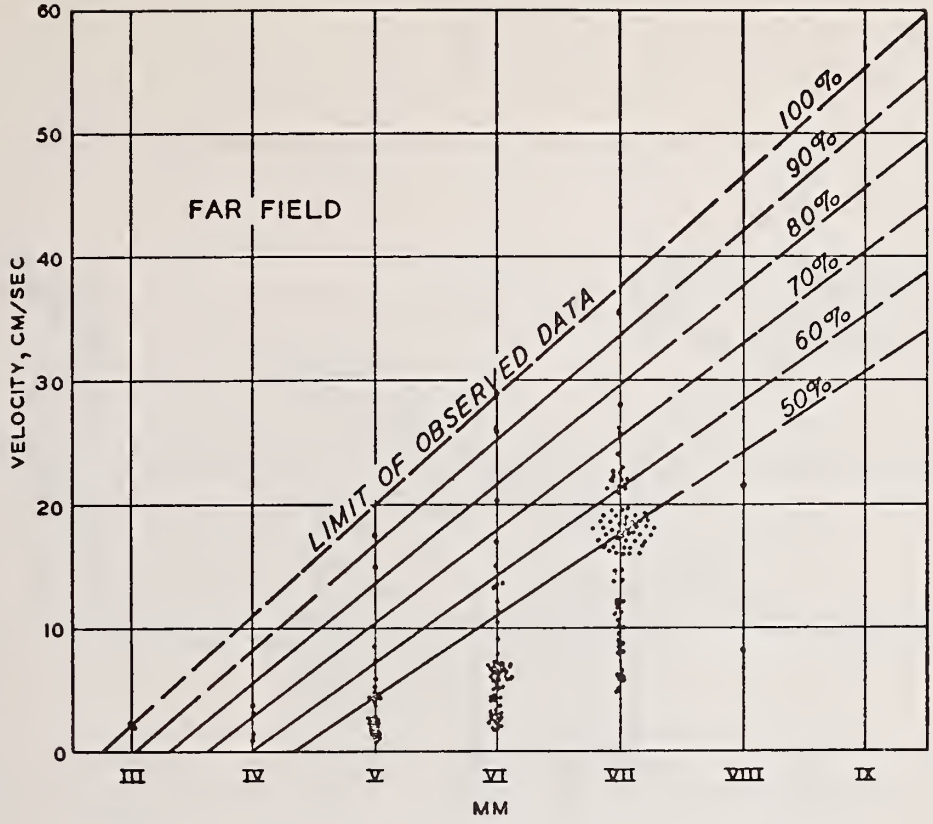

Figure 5. Velocity values for MM intensity in the far field.

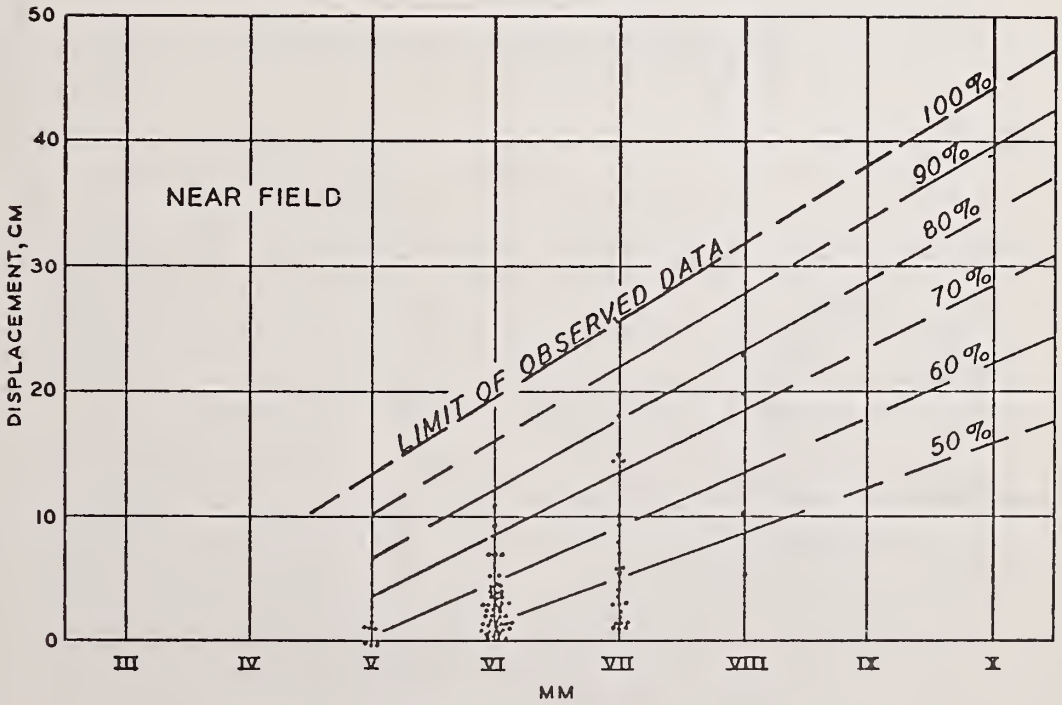

Figure 6. Displacement values for MM intensity in the near field.

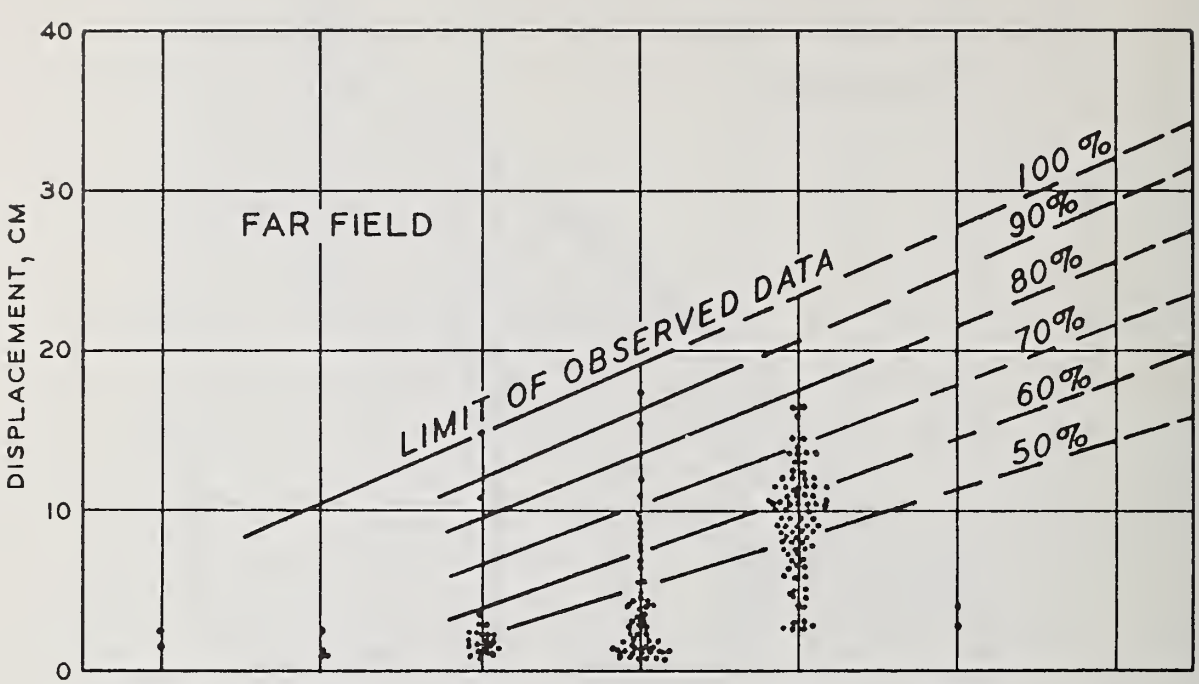

Figure 7. Displacement values for MM intensity in the far field.

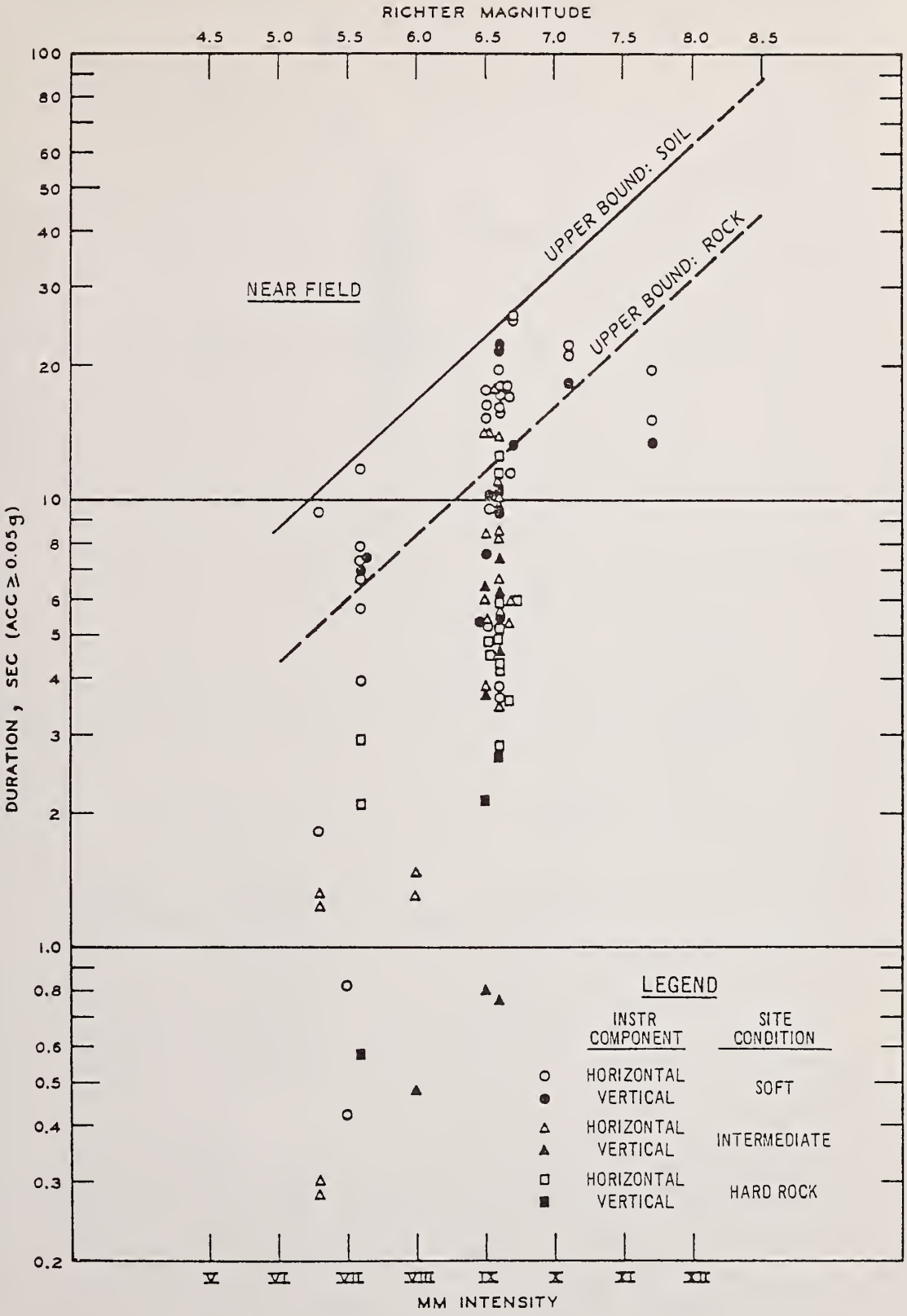

3

Figure 8. Durations for MM intensity in the near field.

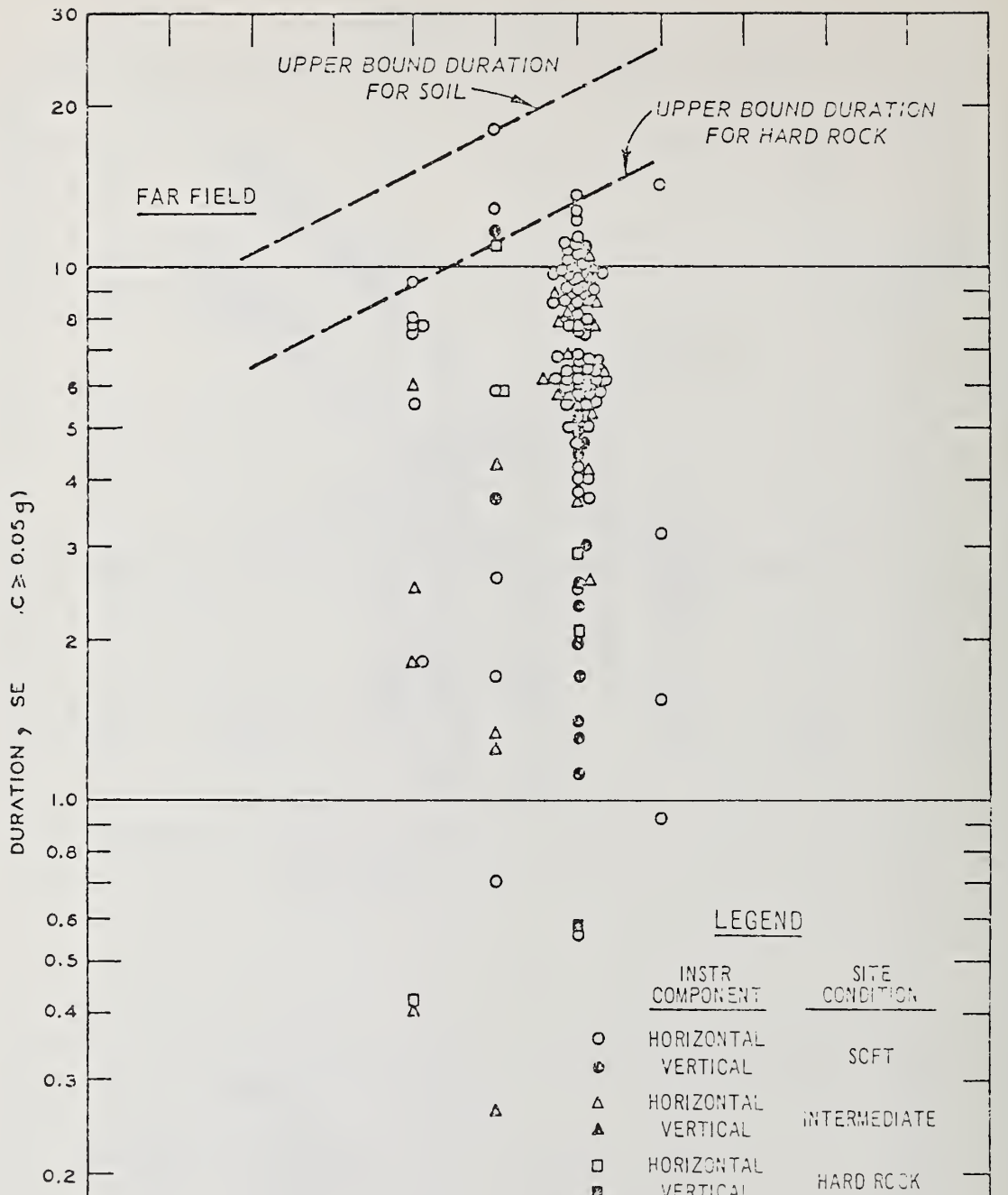

Figure 9. Durations for MM intensity in the far field.

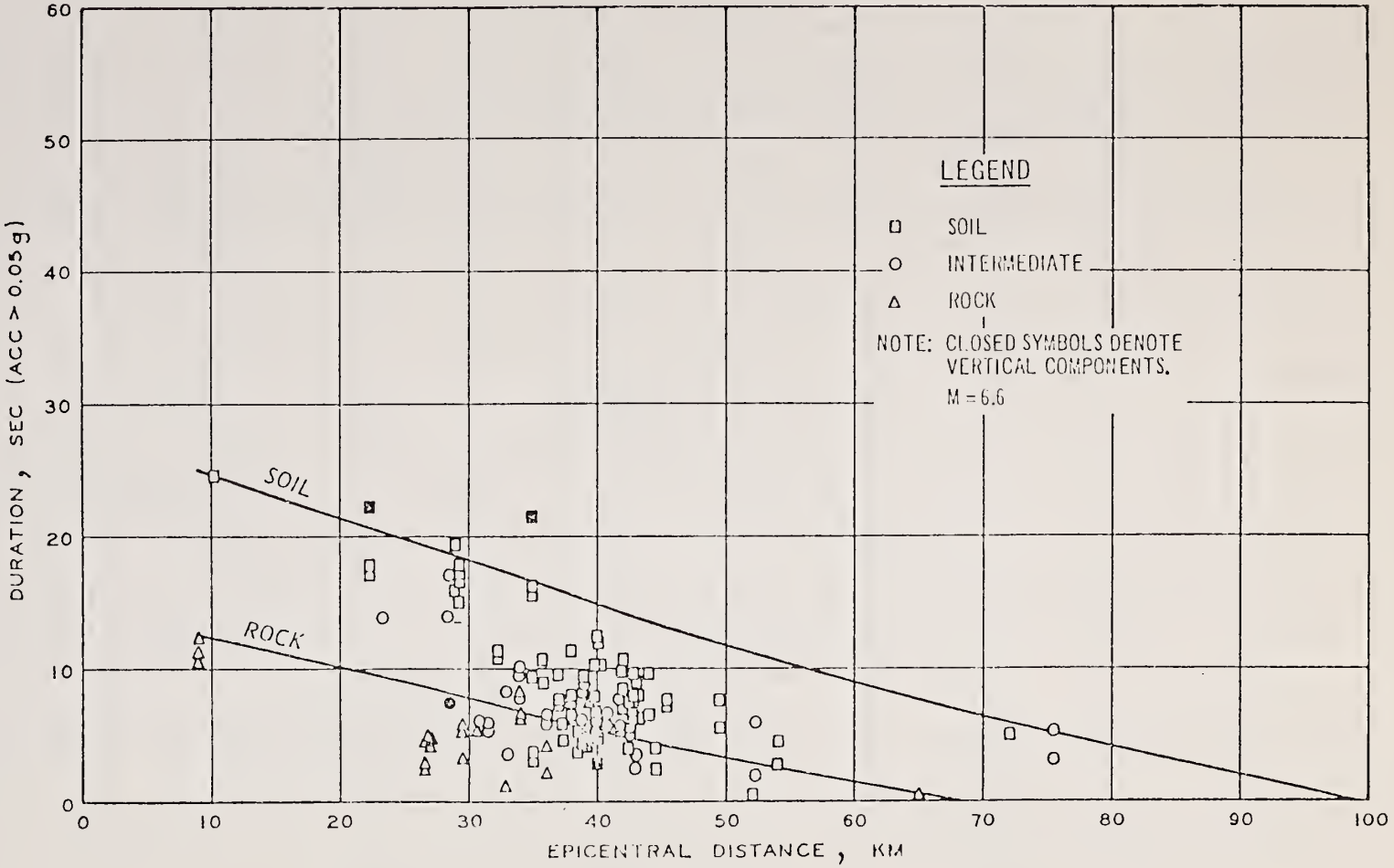

Figure 10. Epicentral distance and duration for soil and rock for a magnitude 6.6 earthquake.

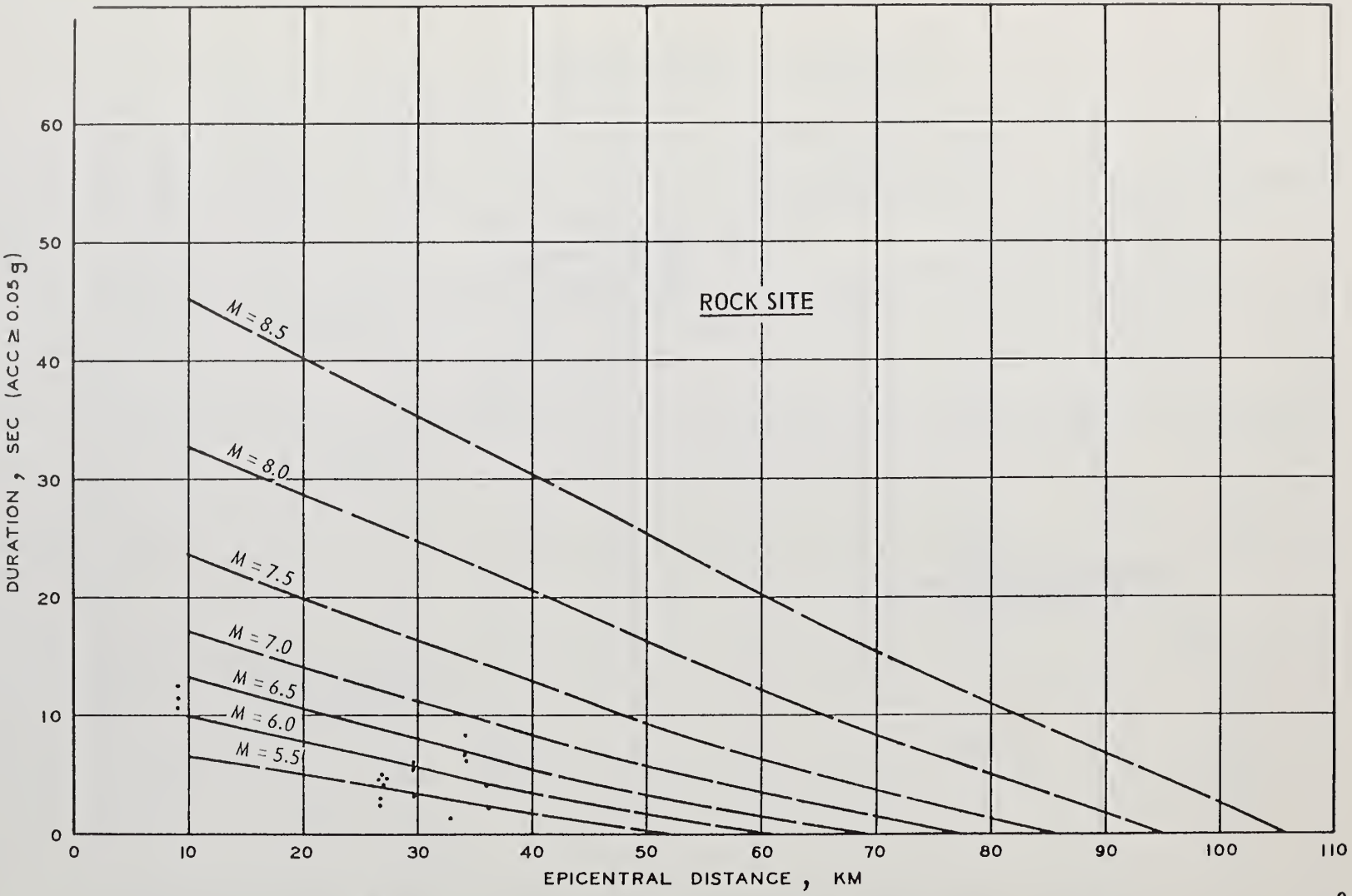

Figure 11. Epicentral distance versus magnitude and duration for rock.

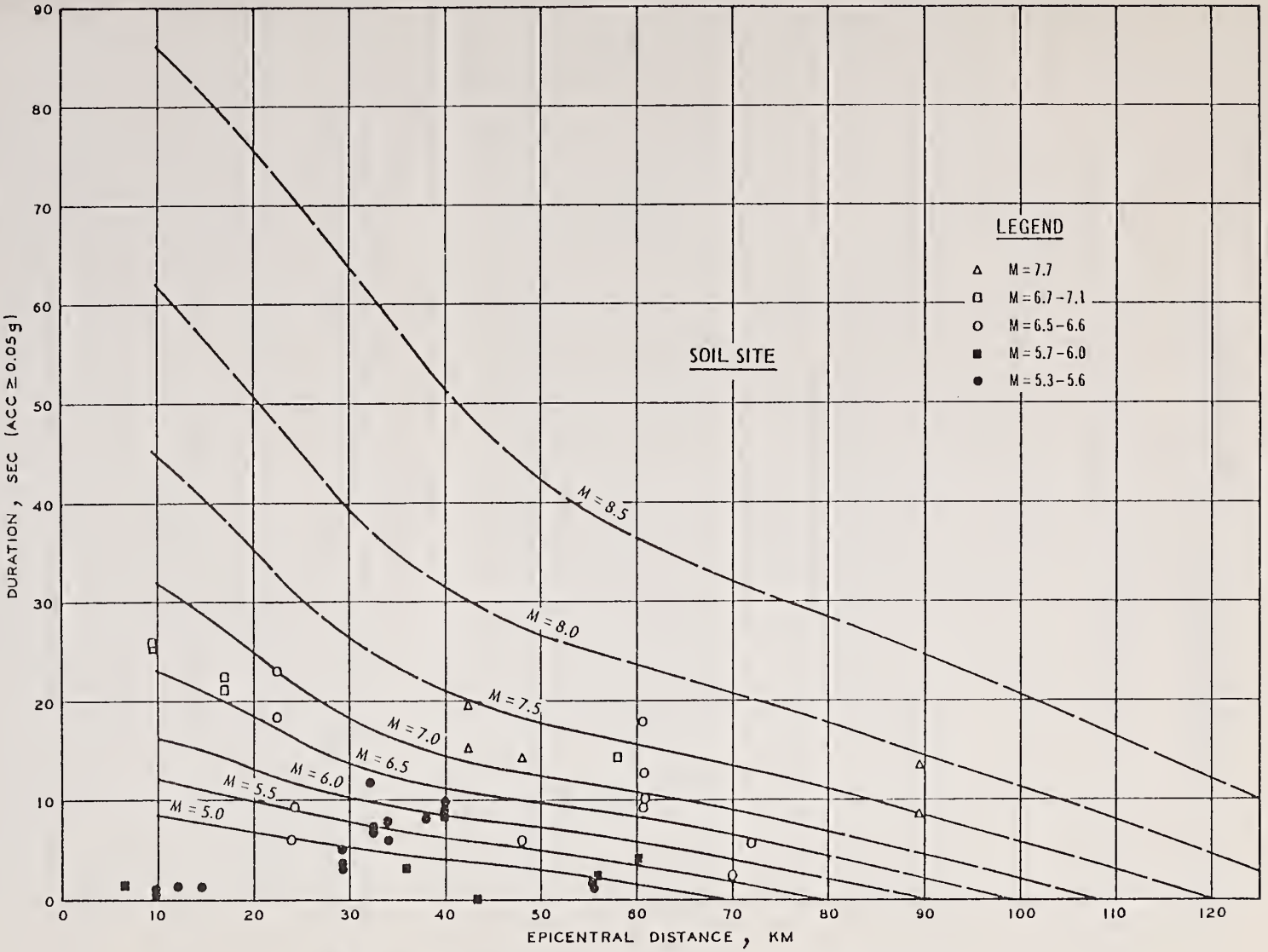

Figure 12. Epicentral distance versus magnitude and duration for soil.

RELATION BETWEEN SEISMIC COEFFICIENT AND GROUND ACCELERATION FOR GRAVITY QUAYWALL

SATOSHI HAYASHI
Head, Structures Division
Port and Harbour Research Institute
Ministry of Transport

SETSUO NODA
Chief, Subaqueous Tunnels and Pipe Lines Laboratory
Structures Division
Port and Harbour Research Institute
Ministry of Transport

TATSUO UWABE
Earthquake Resistant Structures Laboratory
Structures Division
Port and Harbour Research Institute
Ministry of Transport

ABSTRACT

The present design standard for port and harbor structures, utilizes seismic coefficients which were obtained from records of 129 gravity quaywalls in 49 ports damaged by 12 earthquakes. The maximum ground accelerations in the ports were estimated by calculating the ground response during the earthquake with reference to the attenuation curves of the base rock acceleration based on the accelerograms in port area.

The seismic coefficients in past earthquakes had upper values of 0.25, and this upper limit can be related between the coefficient and the maximum ground acceleration by the following equation.

$$e_A = \frac{1}{3}\left(\frac{\alpha}{g}\right)^{\frac{1}{3}}$$

where e_A: seismic coefficient
α: maximum ground acceleration (gal)
g: acceleration of gravity (gal)

Key Words: Acceleration; Accelerogram; Gravity Quaywall; Rock Motion; Seismic Coefficient.

1. Introduction

The present earthquake resistant design for the port and harbor structures is based on the static theory, so called the seismic coefficient method (1).

The seismic effect on a structure varies with and the stability of the structure will depend on such factors as the predominant period, amplitude and duration of the earthquake motion. Therefore, dynamic design can only become an effective method for the port facilities through the use of computers. However, the seismic coefficient method is still an accepted procedure for common structures, because this method is based on experiments and

requires simple calculations for a stability analysis.

Many authors have made an attempt to improve the reliance of the seismic coefficient method. The gravity quaywalls, damaged by earthquakes, were analyzed by the present design procedure, and the seismic coefficients corresponding to the severity of the seismic effect were obtained. The maximum ground accelerations in the ports were also estimated by calculating the ground response during the earthquake. These results were investigated from the aforementioned point of view.

2. Seismic Coefficient

A list of earthquakes and the damaged ports discussed in this paper are shown in Table 1. The locations of the ports are indicated in Fig. 1. Examples of the damaged quaywalls are shown in Figs. 2 through 4. In Fig. 5* a flowchard of the estimated seismic coefficients (represented by e_Δ in this paper) is explained. As it is seen in this figure, the stability against sliding, overturning and the bearing capacity at the base of a structure for each port facility are analyzed. The seismic coefficients, for a safety factor equal to 1, has been obtained. Judging from the characteristics of damage on quaywalls, the cause of damage has been estimated and the ranges of the seismic coefficients were deduced for each facility. Finally, only one seismic coefficient or the range of the coefficient, in the particular port, was determined from these ranges (2). Although there are various problems in estimating seismic coefficient e_A, use of this coefficient was consistent with results obtained from the harbor structures due to the 1968-Tokachi-oki Earthquake and 1973-Nemuro-hanto-oki Earthquake (3). Therefore, in this report the estimation of the seismic coefficient was based on the procedure as shown in Fig. 5.

3. Base Rock Motion

The rock motion at any particular site will depend in large measure on the magnitude of the earthquake and the distance of the site from the zone of energy release. In general, the amplitude of motion decrease with increasing distance from the zone of energy release. Methods of determining the maximum accelerations in rock have been proposed by several investigators. As shown in Fig. 6, the site distance differs for each investigator. The distance from the zone of energy release, causative fault or the epicenter of the principal shock may be more reasonable than the epicentral or hypocentral distance. But it is difficult to determine this distance from the past earthquakes because the developing process of the source region for a great earthquake is very complicated. Considering these matters, Mr. Katsumata has proposed the distance from the edge of source region (the effective distance) which was taken as a sphere of radius r. The following empirical formula is therefore introduced in this paper (4).

$$\log_{10} r = 0.5\,M - 2.25$$

*Please note that Fig. 5 appears after Fig. 6.

where, r: radius of source region (km)

M: magnitude of earthquake

As discussed by Mr. Katsumata, the ground acceleration of the average ground condition in Japan, is related to the base rock acceleration, the magnitude of the earthquake and the effective distance using strong motion accelerograms.

Source Region: The fault parameters of some past earthquakes were determined by seismologists. In this study, it was assumed that the source region was equal to the fault plane. When the fault parameters are unknown, the region is taken as a sphere which is equal to the aftershock area. If the aftershock area is unknown as in the case of a small earthquake, the region is calculated by the aforementioned equation. According to reference (4), it is assumed that the maximum base rock acceleration at an edge of the source region is 400 gals, regardless of the magnitude of the earthquake.

Strong Motion Accelerogram: The Earthquake Resistant Structures Laboratory of the Port and Harbour Research Institute has been observing strong motion earthquakes in port areas of Japan for 14 years. The observation network consists of 65 stations at 44 ports, and at the end of 1975 more than 1058 accelerograms have been obtained (5). 106 accelerograms from 21 stations were selected based on the condition that the maximum acceleration exceeded 20 gals and the magnitude of the earthquake is known.

Calculation of Base Rock Motion: In order to develop the attenuation curves, the base rock motions were calculated by the method based on the multiple reflection theory. The computer program SHAKE developed by Dr. Schnabel and et al. was used, in which the shear modulus and the damping of soil changed with the strain level. The source regions were determined from past earthquakes in which the accelerograms were obtained. For example,the fault plane and the aftershock area during the 1968-Tokachi-oki earthquake is as shown in Fig. 7. The relations between the effective distances that were determined from the source region and the base rock accelerations that were calculated, by the aforementioned method, are shown in Fig. 8.

Using the attenuation curves, the base rock accelerations in the damaged ports were obtained. The source regions of the earthquake, relative to damage of the facilities, were determined in the same manner as described above. For example, the fault plane and the aftershock area during the Nankai earthquake are shown in Fig. 9. As shown in this figure, the fault plane agrees with the aftershock area. Additionally, a 63 km radius of source region, for M = 8.1, is given by the equation previously described.

4. Ground Acceleration

The maximum ground acceleration at the ports damaged by earthquakes were estimated by calculating the ground response during the earthquake. The incident wave used as an input for the ground response calculation was obtained from the accelerograms at the nearest station to the damaged port. The ground motions were calculated by the aforementioned computer program.

5. Result and Discussion

The severity of ground motion during past earthquakes was estimated, in the form of a seismic coefficient, on the basis of the stability analysis on the gravity quaywalls by current design procedure. Using the attenuation curves of the base rock acceleration, the maximum ground acceleration was also estimated by calculating the earthquake response of the subsoil layer. The results are shown in Fig. 10. The expression $\dagger$ indicates that the seismic coefficient exists within the range, and $\downarrow$ or $\uparrow$ means the upper or lower limit of the range.

According to Fig. 10, 0.25 represents the maximum seismic coefficient during the past great earthquakes. This fact may be very informative in the re-examination on the aseismicity of the port facilities.

As shown in Fig. 10, the upper limit of the relation between the seismic coefficient and the maximum ground acceleration was determined as shown by the solid line. Consequently it can be concluded that the gravity quaywall, for which the design seismic coefficient exists over the line, may have sufficient aseismicity against an earthquake with the corresponding maximum ground acceleration.

In this figure the seismic coefficient is not proportioned to the ground acceleration. If the seismic force acting on the structure is considered to be equivalent to the product of the mass of the structure and maximum ground acceleration α, the coefficient must be equal to α/g. Experimental studies on the model, using a shaking table, indicates that the earthpressure under the sinusoidal excitation up to 500 gals is the same as the results from the current design procedure and the coefficient is in proportion to the acceleration. Therefore, this fact does not explain the solid line curve shown in Fig. 10.

Although the gravity quaywall is generally a simple earth structure, its behavior during the earthquake is not clear. It is supposed from the results that one of the major reasons the solid line curve exists is the dynamic response effect of the wall and the backfill, this suggests that seismic force as the earthpressure is not always increased proportionally with an increase in the ground acceleration during an earthquake.

6. Conclusion

Judging from the stability analysis of gravity quaywalls, by the current design standard, 0.25 is the maximum value of the seismic coefficient e_A corresponding to the severity of the ground motions in the ports during the past earthquakes.

The maximum ground accelerations α in the ports was estimated by calculating the ground response during the earthquakes with reference to the attenuation curves of the base rock accelerations based on the accelerograms in the port area.

The upper limit of the relation between e_A and α is expressed by the following equation:

$$e_A = \frac{1}{3}\left(\frac{\alpha}{g}\right)^{\frac{1}{3}}$$

where e_A: seismic coefficient

α: maximum ground acceleration (gal)

s: gravitational acceleration (gal)

Reference

1. Design Manual of Harbour Structures in Japan, The Japan Port and Harbour Association, April 1967.

2. S. Noda and T. Uwabe; Seismic Disasters of Gravity Quaywalls, Technical Note of the Port and Harbour Research Institute, No. 227, 1975.

3. I. Mitsuhashi and T. Nakayama; Analysis of the damage to Harbour Structures by the 1973 Nemuro-Hanto-oki Earthquake, the same as the above, No. 184, 1974.

4. M. Katsumata; Note on Maximum Amplitude of Acceleration of Earthquake Motion, Quarterly Journal of Seismology, Vol. 37, No. 3, 1972.

5. E. Kurata, S. Iai and H. Tsuchida; Annual Report of Strong-motion Earthquake Records in Japanese Ports (1975), Technical Note of Port and Harbour Research Institute, No. 236, 1975.

6. P.B. Schnable, J. Lysmer and H.B. Seen; SHAKE-A Computer Program for Earthquake Response Analysis of Horizontally Layered Sites, Report No. EERC 72-12, Col. of Eng., Univ. of Calif. Berkeley, 1972.

Name of Earthquakes	Location of Epicenter	Damaged Harbours
Kanto Sep. 1, 1923 M = 8.16	WESTERN KANTO (35.4°, 139.2°) DEPTH 0~20km	TOKYO YOKOHAMA YOKOSUKA KAMAKURA
Kitoizu Nov. 26, 1930 M = 7.0	E. SHIZUOKA PREF. (35.1°, 139.0°) DEPTH 0~5km	SHIMIZU
SHIZUOKA Jul. 11, 1935 M = 6.3	MIDDLE OF SHIZUOKA PREF (35.0°, 138.4°) DEPTH 10 km	SHIMIZU
OGAHANTO Apr. 1, 1939 M = 7.0	W. AKITA PREF. (39.95°, 139.8°) DEPTH 0	AKITA FUNAKAWA
NANKAI Dec. 21, 1946 M = 8.1	OFF NANKAIDO (33.0°, 135.6°) DEPTH 30km	UNO SAKAIOE KOMATSUJIMA TAMASHIMA TAKAMATSU WAKAYAMA UWAJIMA KOCHI
1952-TOKACHIOKI Mar. 4, 1952 M = 8.1	OFF TOKACHI (42.20°, 148.9°) DEPTH 45km	AKKESHI KUSHIRO TOKACHI HOROIZUMI URAKAWA MURORAN
HYUGANAOA Feb. 27, 1961 M = 7.0	OFF MIYAZAKI PREF. (31.6°, 131.85°) DEPTH 40 km	HOSOJIMA MIYAZAKI AOSHIMA UCHIUMI ABURATSU TONOURA
NIIGATA Jun. 16, 1964 M = 7.5	SW. AWASHIMA (38.35°, 139.18°) DEPTH 40km	NIIGATA IWAFUNE SAKATA AKITA
1968-TOKACHIOKI May 16, 1968 M = 7.9	OFF TOKACHI (40.98°, 142.33°) DEPTH 20km	URAKAWA MURORAN HAKOOATE AOMORI NOHEJI KAWAUCHI HACHINOHE MIYAKO
1973-NEMUROHANTOOKI Jun. 17, 1973 M = 7.4	OFF NEMURO PEN. (42.97°, 145.93°) DEPTH 40 km	HANASAKI KIRITAPPU NEMURO AKKESHI KUSHIRO
1974-IZUHANTOOKI May 9, 1974 M = 6.9	OFF IZU PEN. (34.57°, 138.8°) DEPTH 10 km	SHIMODA INATORI MERA
CHIRE May. 23, 1960 M = 8.5	OFF CHIRE (37.5°, 73.5°) (39.5°, 74.5°)	Pt. Montt Talcahuano

Table-1 Earthquakes and Harbors

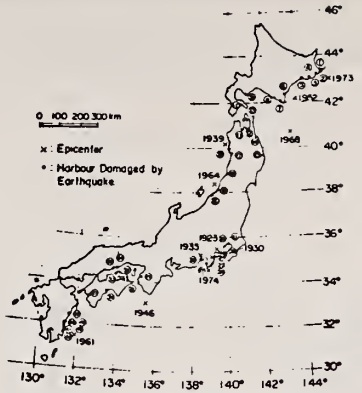

Fig.1 Harbors damaged by earthquakes

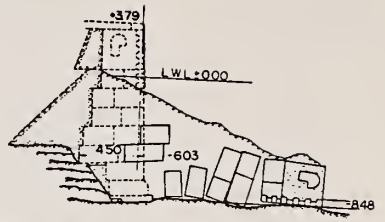

Fig.2 Damage to block quaywall at Yokohama port (Kanto earthquake)

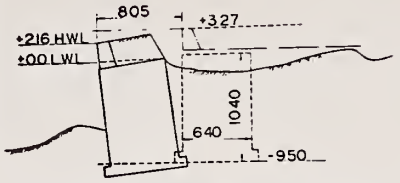

Fig.3 Sliding of caisson quaywall at Shimizu port (Kitaizu earthquake)

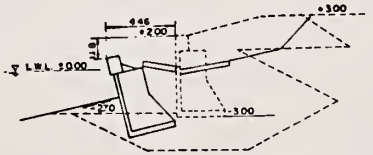

Fig.4 Damage to L-shaped block quaywall at Shimizu port (Kitaizu earthquake)

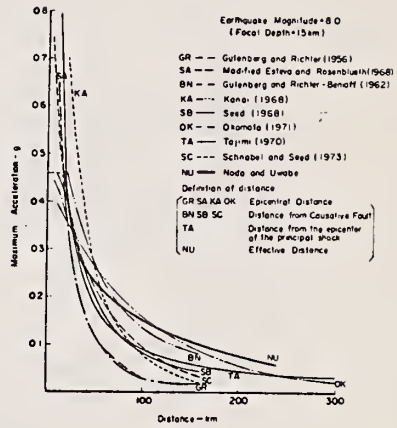

Fig.6 Comparison of maximum accelerations at bed rock

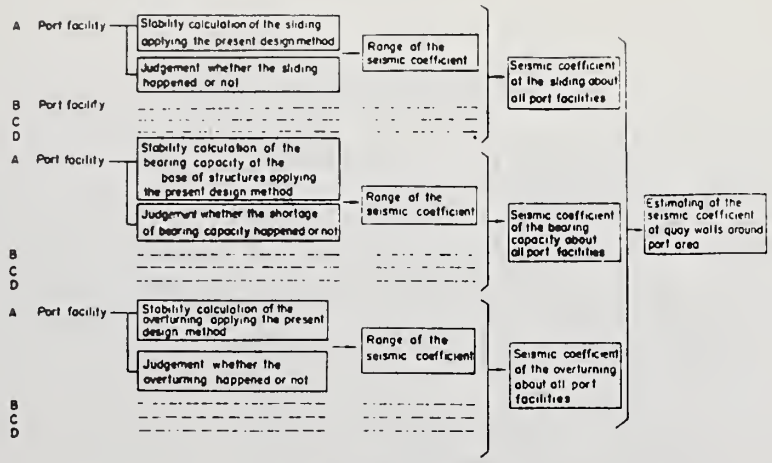

Fig.5 Flow chart for estimation of seismic coefficient

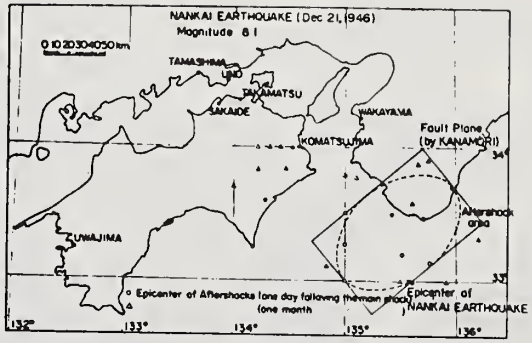

Fig.9 Distribution of epicenters of aftershocks (Nankai earthquake)

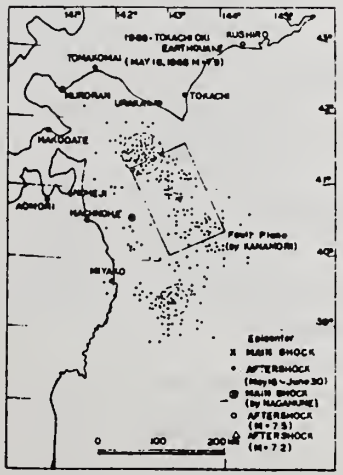

Fig.7 Distribution of epicenters of aftershocks(1968 Tokachi-oki earthquake)

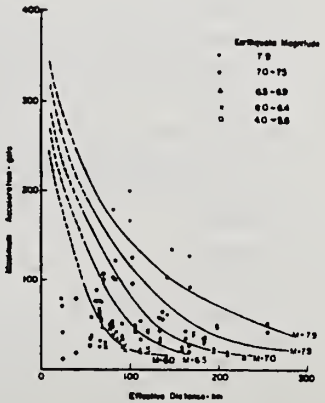

Fig.8 Proposed attenuation curves of bed rock acceleration

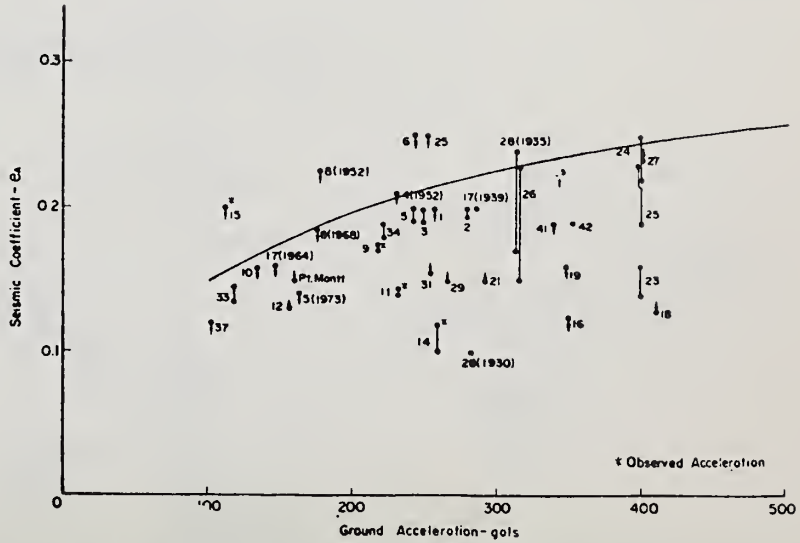

Fig.10 Relation between seismic coefficient and ground acceleration

Investigation of
Earthquake Resistance of Structural (Shear) Wall Buildings
Carried out at Portland Cement Association

Reported by

Mark Fintel

Portland Cement Association, Skokie, Illinois

In July of 1974, PCA started (with NSF-RANN sponsorship) a comprehensive analytical and experimental study to investigate the response to earthquake excitation of reinforced concrete structures containing structural (shear) walls. The aim of the study is to develop design procedures and reinforcing details for earthquake resistant multistory reinforced concrete structures containing structural walls.

ANALYTICAL INVESTIGATION

The objective of the analytical study is to investigate (through inelastic dynamic response) the effects of the following parameters:

1. Fundamental period of vibration

2. Yield level
3. Post yield stiffness
4. Viscous tamping
5. Character of moment-rotation hysteretic loop
6. Stiffness table
7. Strength table
8. Degree of fixity at base
9. Number of stories or height of building
10. Ground motion intensity
11. Ground motion frequency characteristics
12. Duration of ground motion

In addition to the major effort of undertaking the dynamic analysis associated with the parametric studies, preliminary studies of input motion data were undertaken to determine a suitable basis for normalizing accelerograms with respect to intensity, and also to characterize accelerograms approximately in terms of their frequency content. Also, an initial effort was made to carry out a parametric study of typical structural wall sections under combined flexure and axial load.

The analytical work of the initial 18 months has been concentrated on the evaluation of the results of the dynamic analysis, as well as the experimental data, with the aim of (1) arriving at guidelines for the design of earthquake-resistant structural walls, with particular reference to force (moment and shear) levels and deformation demands (ductility and energy dissipation) which may reasonably be expected under particular ranges of values of both structural and ground motion parameters. This information, together with data obtained from laboratory tests, will serve as the basis for the design procedure to be developed as the ultimate result of the project; (2) synthesizing a "representative" loading history which can be used in the laboratory testing of isolated wall specimens on the basis of the results of the dynamic analysis;

and (3) studying the measured force-deformation curves from the experimental program for the purpose of determining the influence of shear and examining the range of values of the forces (moment and shear) as well as the specimen properties when the primary (monotonic) curve can be adequately predicted on the basis of flexural considerations alone.

A brief discussion of the work carried out during the last six months, and some of the results obtained is given below:

(A) Force levels and deformation demands corresponding to various ranges of major structural and ground motion parameters

To determine the range of forces (mainly moments and shears) as well as the deformation requirements which can be reasonably expected for practical cases, a number of building configurations using structural walls which could properly be classified as isolated walls were studied. Sample configurations are shown in Fig. 1. The variations in plan shown in Fig. 1 reflect an effort to vary the fundamental period of vibration of the structure by varying the stiffness-to-mass relationship. Two types of wall sections were considered, i.e., the plane rectangular section and a flanged section.

Tests have indicated that the behavior (i.e., stiffness, strength and ductility) of walls subjected to reversed cycles of inelastic deformation can be significantly affected by the magnitude of the shear stresses in the critical (hinging) region. For this reason, particular attention was given to the levels of shear stresses which can be expected in practical cases. This information will also serve to guide the experimental program in the choice of shear stress levels to use in tests.

On the basis of the curves shown in Fig. 2, and the assumed plan configurations shown in Fig. 1, the variation of the maximum shear stress with the width (i.e., the horizontal dimension

in the plane of the wall) of the wall, ℓ_w, was determined for particular values of f_c and ρ corresponding to the different plan configurations considered. A typical plot of the results is shown in Fig. 3. Also indicated in Fig. 3 are the corresponding rotational ductility requirements and interstory displacements.

Among others, Fig. 3 indicates that for a particular plan configuration or fundamental period there is an optimum width of wall with respect to the magnitude of the shear stress below which a rapid increase in expected shear stress occurs with a decrease in the width of the wall for the same thickness.

The information typified by Fig. 3, together with the results of the evaluation of the critical shear/moment ratios expected in isolated walls, as obtained from graphs such as shown in Fig. 4 and the associated rotational ductility requirements at the bases of walls as indicated by analyses, will provide the basis for recommendations of force levels and deformation requirements to guide the design of structural walls. When considered together with the experimental data on strength and deformation capacity of walls of typical sections, this information will form the basis for the rational design of isolated structural walls for earthquake resistance.

(B) Loading history study

The major aim in undertaking this study is to determine a representative range of earthquake induced deformations in terms of the amplitude of the maximum response and the number of cycles of significant amplitude which can be expected in isolated walls under a range of structure and ground motion parameter combinations. The study was motivated by the belief that the behavior of laboratory specimens, or actual structures for that matter, can be influenced significantly by the type of loading (magnitude, number of cycles and sequence) imposed on the structure.

Most, if not all, of the quasi-static reversed loading tests conducted to date have used more or less arbitrary loading sequences. The type of loading generally used in laboratory tests is one characterized by progressively increasing amplitudes of load, sometimes with smaller intermediate load cycles used just before an increment in the maximum load is applied.

Figures 5(a), (b) and (c), for example, show the histories of rotation of a section at the first floor level (indicative of the total rotation occurring in the first story) of the lumped-mass model shown in Fig. 6. The ordinates in Fig. 5 have been normalized in each case with respect to the corresponding yield rotation.

In trying to characterize the response history, as depicted in Fig. 5, the maximum amplitude as well as the number of "fully reversed cycles", "partially reversed cycles", and the total number of inelastic cycles of significant amplitude, were noted in each of the cases covered in the parametric study. Except for two cases in which a 20-second duration of the input motion were used, all of the cases in the parametric study used 10 seconds of input motion.

A major observation which can be made in relation to Fig.7 is that for a wide range of values of structural and ground motion parameters, the number of "fully reversed inelastic cycles" of response (or loading) is not likely to exceed 5 or 6, under a 10-second duration of strong ground motion. Of significant interest is the fact that in many cases the maximum amplitude of response occurs rather early with no significant inelastic cycles preceding it.

EXPERIMENTAL INVESTIGATION

The experimental program is divided into three parts. In Part I, reversing loads are applied to isolated walls. In Part II, reversing loads are applied to wall-systems. In Part III, elements of systems are to be tested. Part III is primarily an investigation of the behavior of confined concrete.

Highlights of the program to date

Part I - Isolated Walls. The isolated walls represent an element of a structural wall system. They are being tested to determine their strength, ductility, and energy dissipation capacity.

The test specimens are approximately 1/3-scale models of actual walls. The model walls are 15-ft. high and have a horizontal length of 6 ft. 3 in. The web thicknesses are 4 in. All test specimens are subjected to in-plane horizontal reversing loads. The loads are applied alternately on one side and then on the other. A specimen and the testing apparatus are shown in Fig. 8.

Controlled variables covered in the program to date include the shape of the wall cross section, the amount of main flexural reinforcement, and the amount of hoop reinforcement around the main flexural reinforcement.

A summary of results of the entire isolated wall test series through March 1976 is shown in Table 1.

Part II - Systems. Systems containing connecting elements with various proportions will be constructed and tested at reduced scale. The systems specimens are being designed with the intent of providing proof tests of structures having proportions and details representative of typical structures. The process of selecting representative elements for the first systems specimen is in progress.

Plans have been made to cast the specimens vertically with construction joints at each floor level. Lateral loads will be introduced into the systems through stubs representing floor

slabs. The walls will be constructed with flanges to increase the lateral stability of the systems. An individual wall of the system will be tested prior to the test of the coupled wall system.

Part III - Elements. Tests have been performed on specimens representing the compression zones of structural walls. These tests are being performed to evaluate the effect of confinement reinforcement and to determine the effective stress-strain curve of confined concrete.

Figure 9 shows a specimen being tested. The controlled variables in the test program include spacing and size of the confinement reinforcement, concrete strength, amount of longitudinal reinforcement, and size of test specimen.

Fourteen of the 17 tests planned have been completed. Table 2 summarizes the entire program.

In addition, a series of tests of coupling beam elements for coupled walls is being carried out. To date, three specimens have been tested to failure under slow load reversals. All coupling beams had a cross section of 4 x 6-2/3 in. and an overall length of 16-2/3 in., giving an aspect ratio of 2.5.

TABLE 1 TEST RESULTS

Specimen	Reinforcement[1]				Conc.	ACI Design Strength				Observed Loads			
						Flexural		Shear		Yield		Maximum	
	ρ_f (%)	ρ_h (%)	ρ_n (%)	ρ_s (%)	f'_c (psi)	kips	$\sqrt{f'_c}$	kips	$\sqrt{f'_c}$	kips	$\sqrt{f'_c}$	kips	$\sqrt{f'_c}$
F1	3.89	0.71	0.30	-	5575	145	8.1	140	7.8	150.6	8.4	187.9	10.5
B1	1.11	0.31	0.29	-	7685	46	2.2	82*	3.9	45.1	2.1	61.0	2.9
B2	3.67	0.63	0.29	-	7775	129	6.1	127	6.0	119.7	5.7	152.8	7.2
R1	1.47	0.31	0.25	-	6490	18	0.9	82*	4.2	20.1	1.0	26.6	1.4
B3	1.11	0.31	0.25	1.28	6860	46	2.3	82*	4.1	45.2	2.3	62.0	3.1
R2	4.00	0.31	0.25	2.07	6740	35	1.8	82*	4.2	33.2	1.7	48.7	2.5
B4[2]	1.11	0.31	0.25	1.28	6530	46	2.4	82*	4.2	45.3	2.3	75.3	3.9
B5	3.67	0.63	0.29	1.35	6570	129	6.6	127	6.5	112.2	5.8	171.3	8.8
B5R[3]	3.67	0.63	0.29	1.35	6170	129	6.8	127	6.7	-	-	167.8	8.9

(1) ρ_f = Ratio of main flexural reinforcement area to gross concrete area of boundary element

ρ_h = Ratio of horizontal shear reinforcement area to gross concrete area of a vertical section of wall web

ρ_n = Ratio of vertical web reinforcement area to the gross concrete area of a horizontal section of the wall web

ρ_s = Ratio of effective volume of confinement reinforcement to the volume of core in accordance with Eq. (A-4) of ACI 318-71

(2) Monotonic Loading

(3) Repaired Specimen

* Shear reinforcement governed by maximum bar spacing requirements

TABLE 2 DETAILS OF TEST SPECIMENS

Group	Dimensions of Crossection in.	Concrete Comp. Str. ksi	Long. Reinf. Ratio ρ'	Hoop Size Bar No.	Hoop Reinf. Ratio ρ_s	Specimen No. and Hoop Spacing				Comments
						2-in.	4-in.	8-in.	∞	
10x16-in. Specimens										
1	10x16	3	0		0				1P*	Plain Concrete
				3	0.010		7			
				4	0.037	2				Meets ACI Hoop Req.
2	10x16	3	0.005	4	0.019		3P*			Meets ACI Hoop Req.
				4	0.009			4		
				5	0.029		6P			Meets ACI Hoop Req.
				3	0.010		13P			
				4	0.037	8				Meets ACI Hoop Req.
3	10x16	3	0.039	4	0.019		9*			Meets ACI Hoop Req.
				4	0.009			10		
				5	0.029		12			Meets ACI Hoop Req.
5x8-in. Specimens										
4	5x8	3	0		0				20	Plain Concrete
5	5x8	3	0.005	2	0.019	16				
6	5x8	3	0.044	2	0.019	19				
7	5x8	6	0		0				17	Plain Concrete
8	5x8	6	0.005	2	0.019	18				
9	5x8	6	0.044	2	0.019	15				

Notes: Groups 4, 5 and 6 are repetitions, in half scale, of the specimens marked with asterisk* in Groups 1, 2 and 3, respectively. Groups 7, 8 and 9 are repetitions in 6 ksi concrete, of Groups 4, 5 and 6, respectively.

1 in. = 25.4 mm 1 ksi = 70.3 kg/cm^2

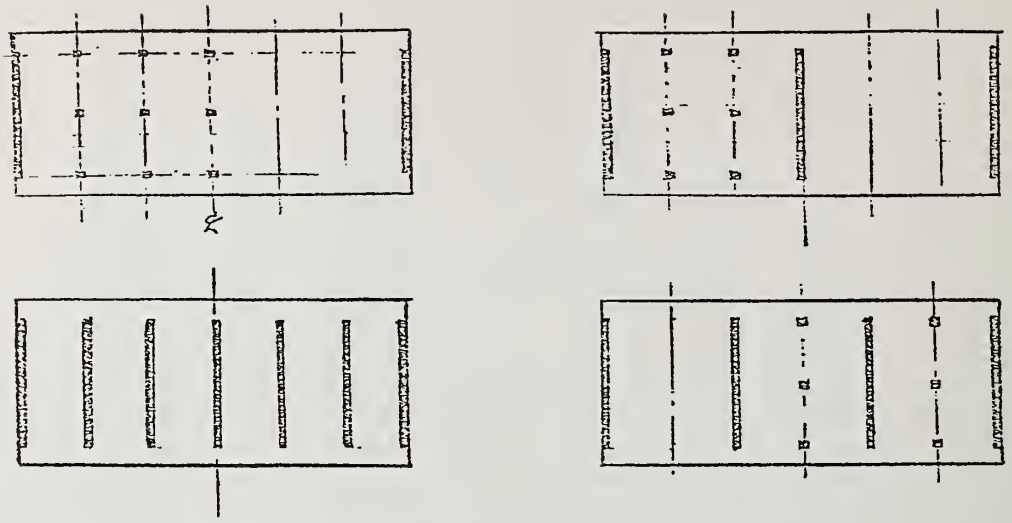

Figure 1(a) - Building Configurations Considered

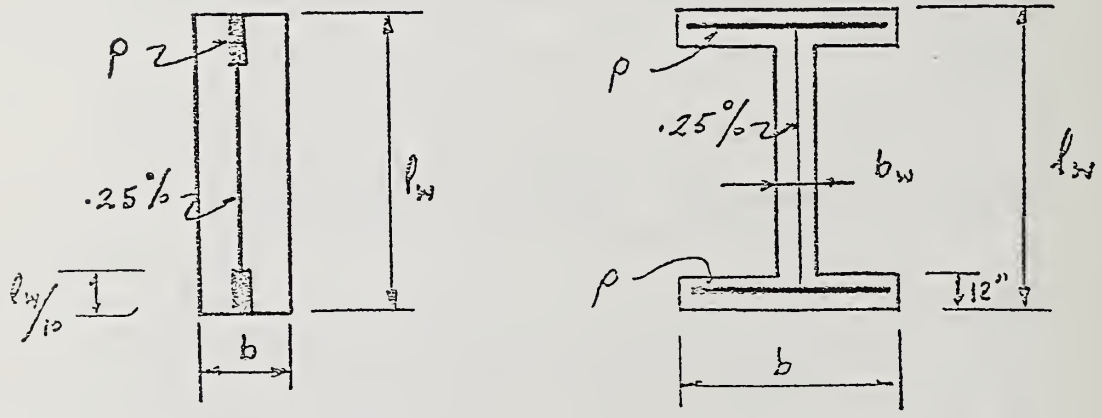

Rectangular Section

Flanged Section

Figure 1(b)- Typical Wall Cross Sections

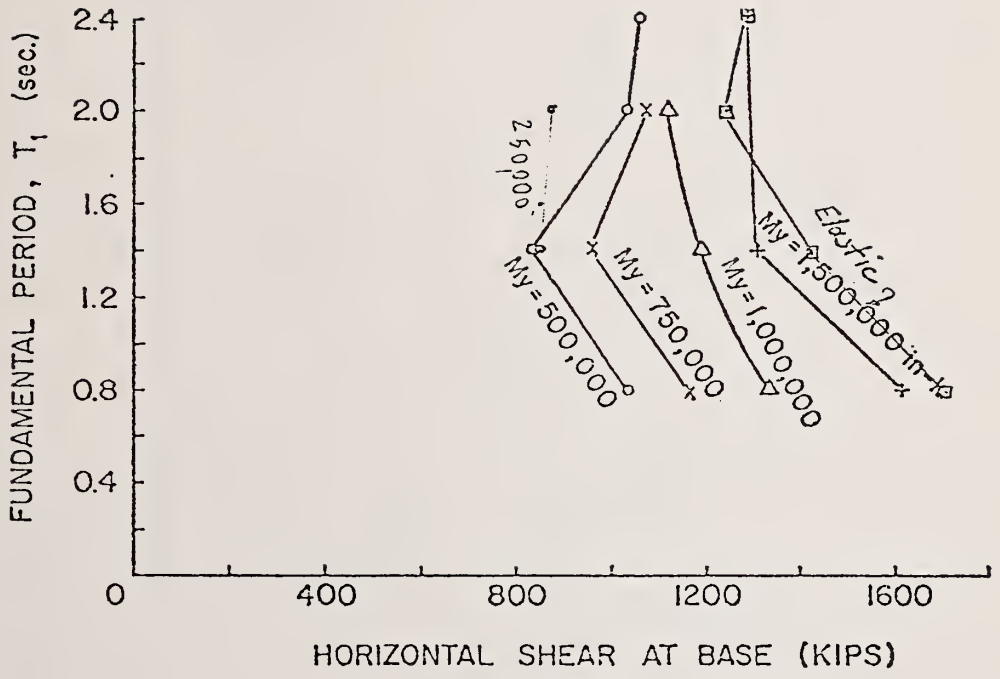

Figure 2 - Variation of Base Shear with Fundamental Period, T_1, and Yield Level, M_y

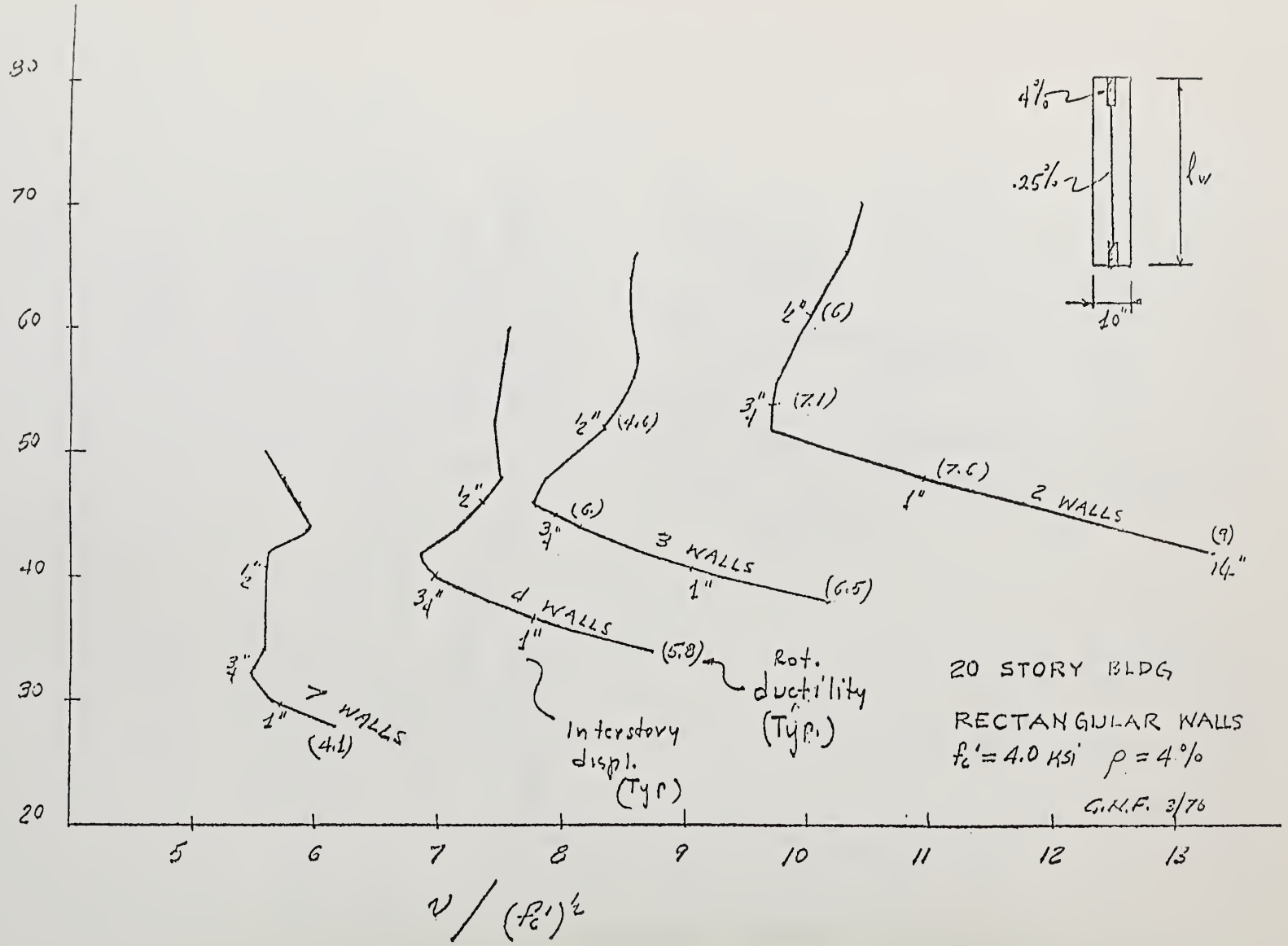

Figure 3 - Variation of Shear Stress at Base of Rectangular Walls with Width of Wall for Different Plan Configurations

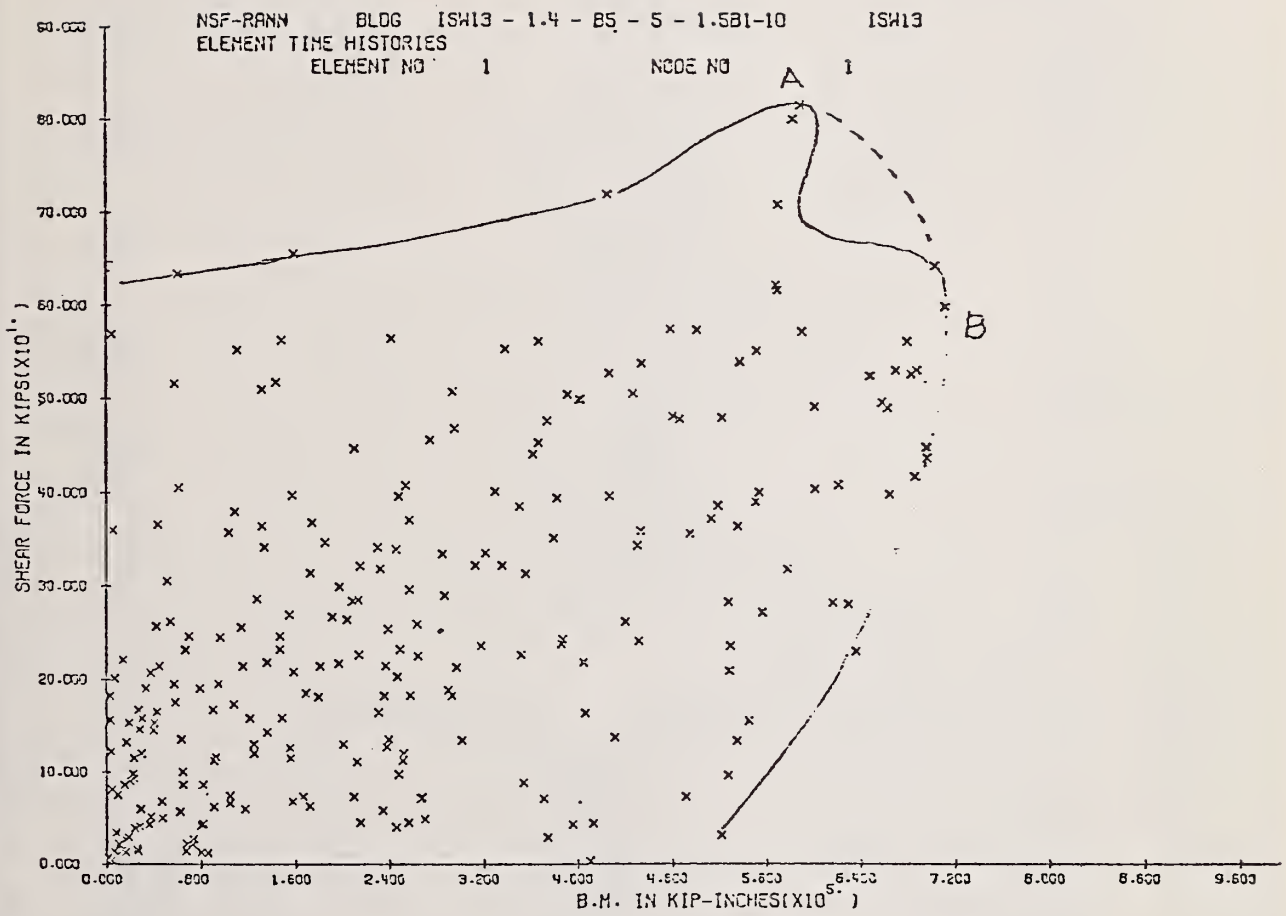

Figure 4 - Envelope of Critical M/V Combinations

Parameter: FUNDAMENTAL PERIOD, T_1

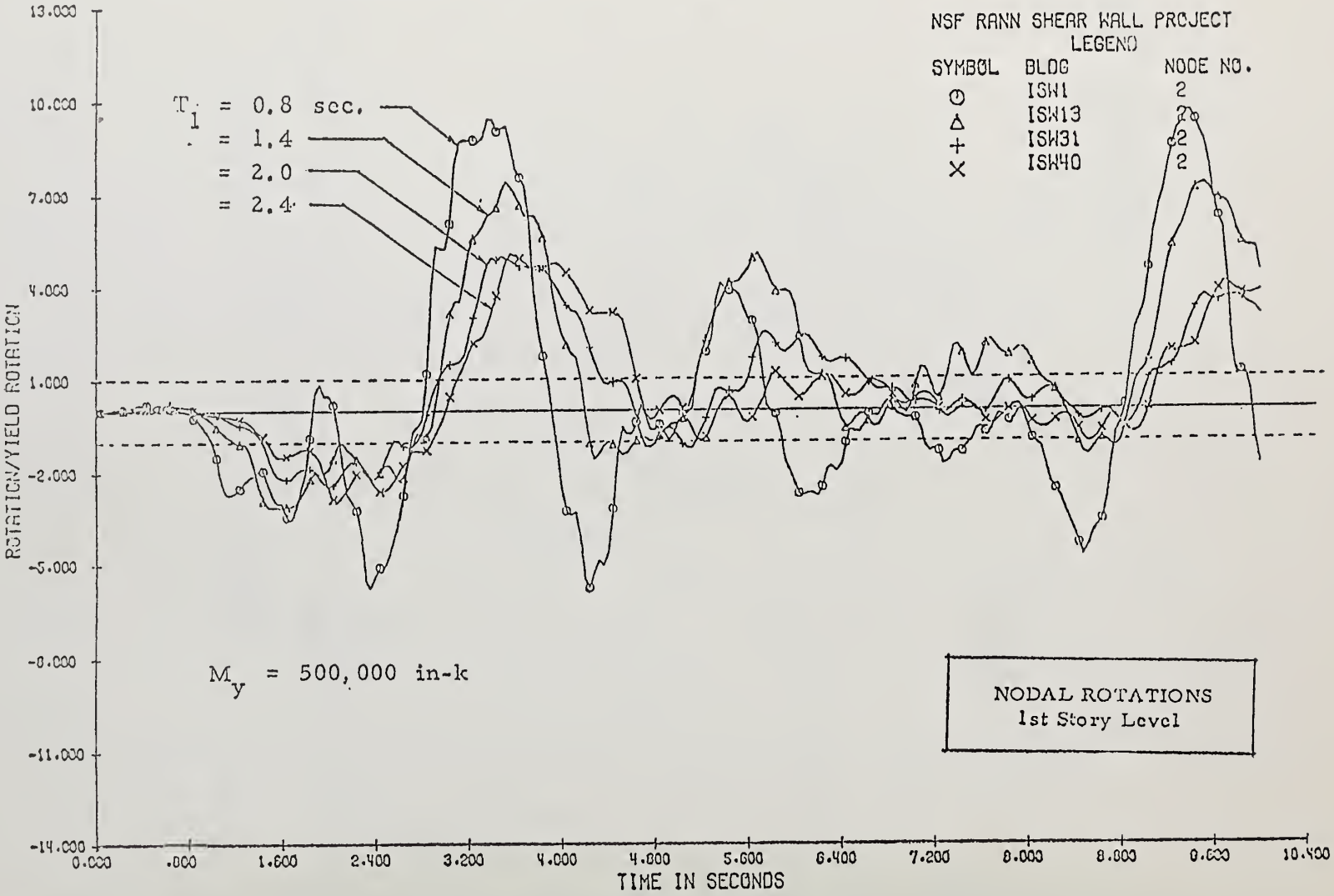

Figure 5(a)

Parameter: YIELD LEVEL, M_y

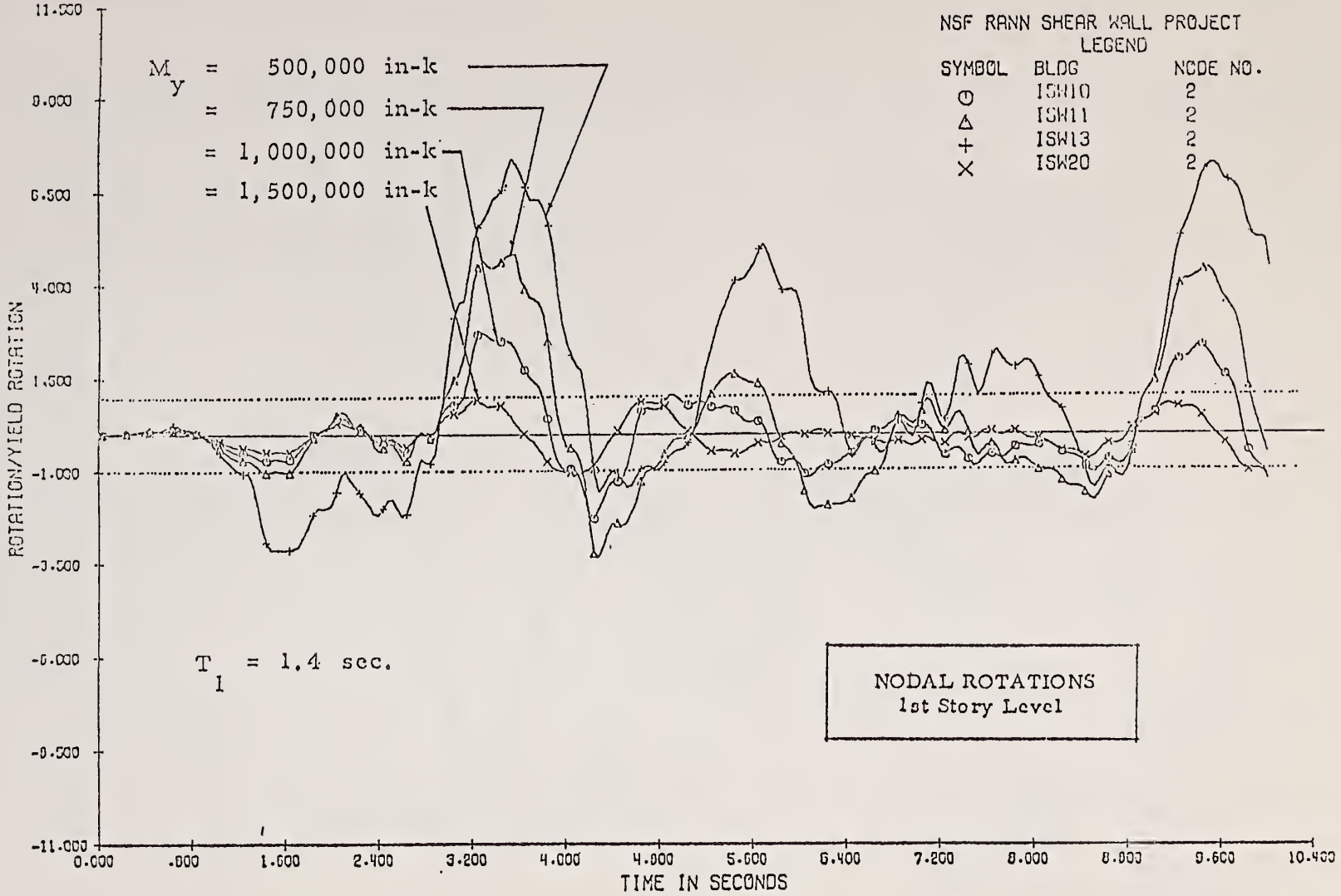

Figure 5(b)

Parameter: TAKEDA MODEL PARAMETER β

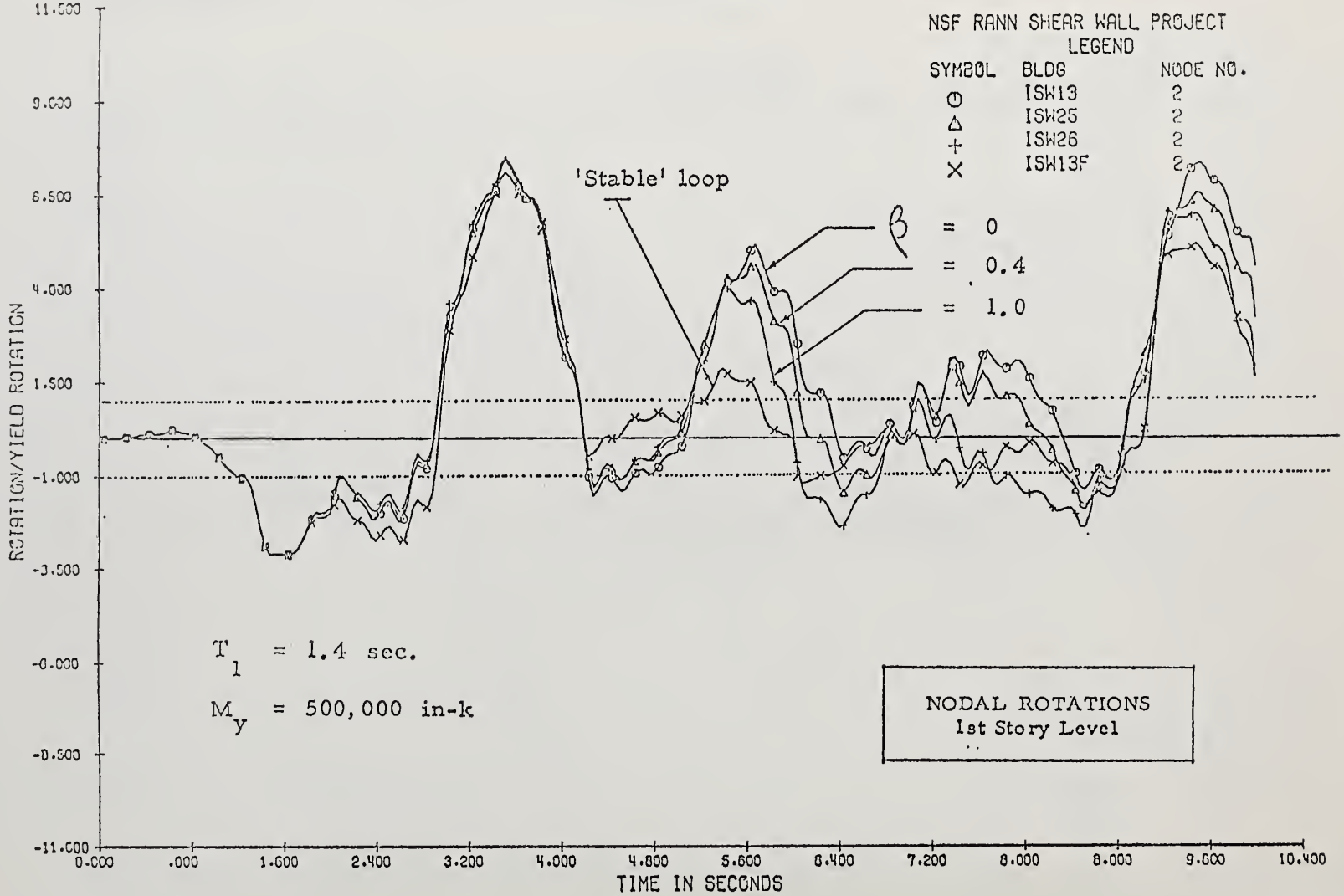

Figure 5(c)

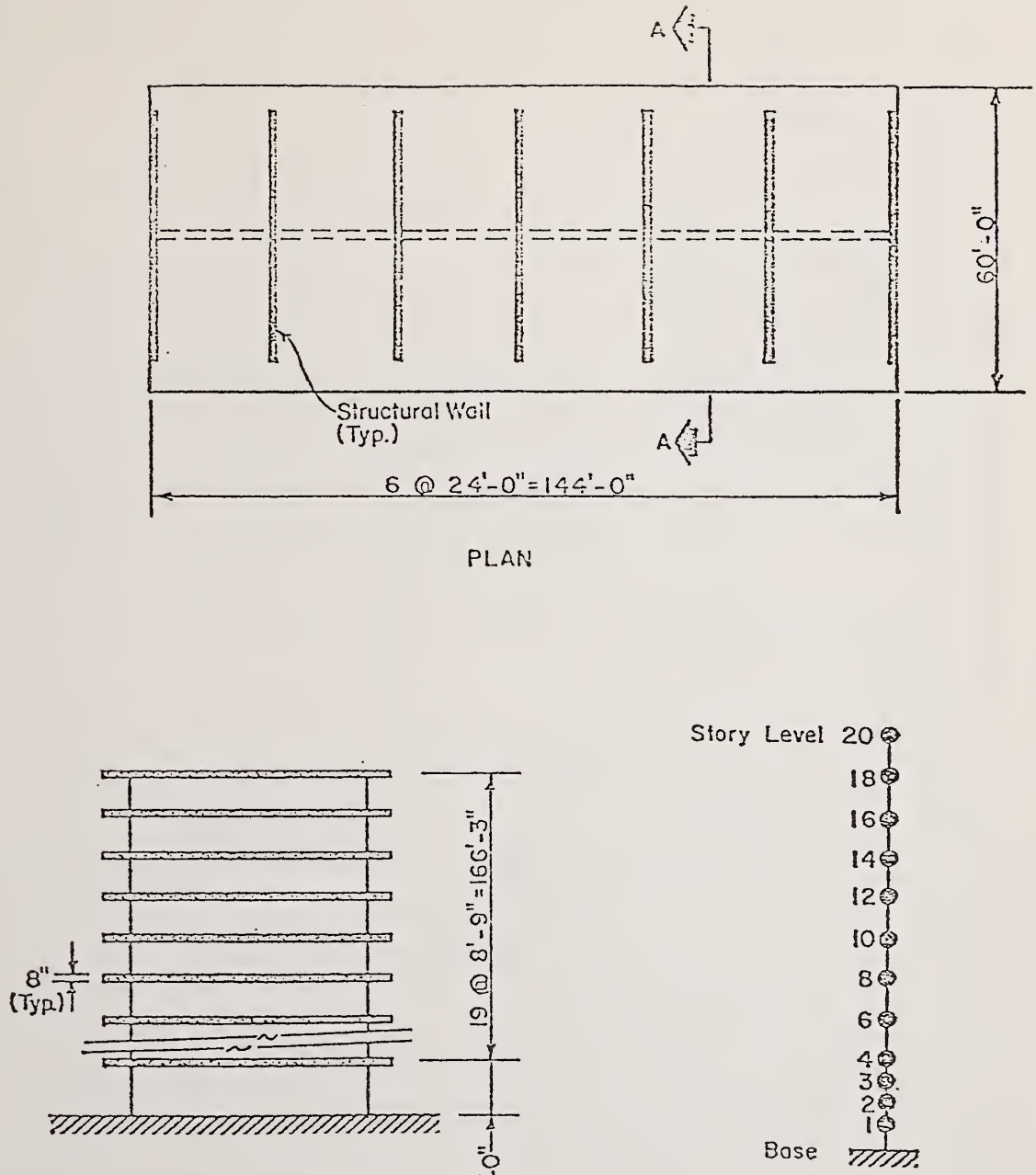

Figure 6 - TWENTY STORY BUILDING WITH ISOLATED STRUCTURAL WALLS

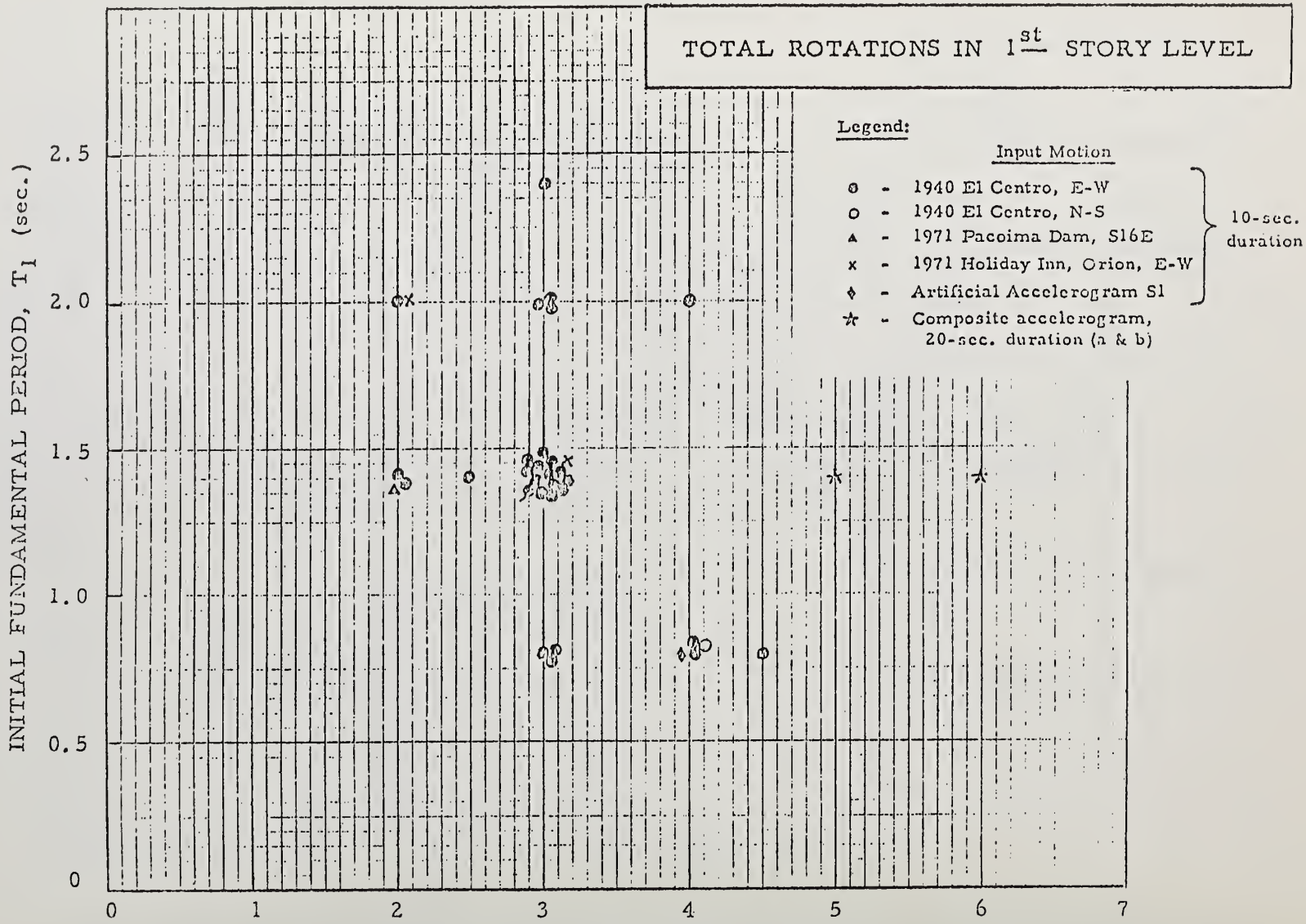

Figure 7(c). TOTAL NO. OF INELASTIC CYCLES

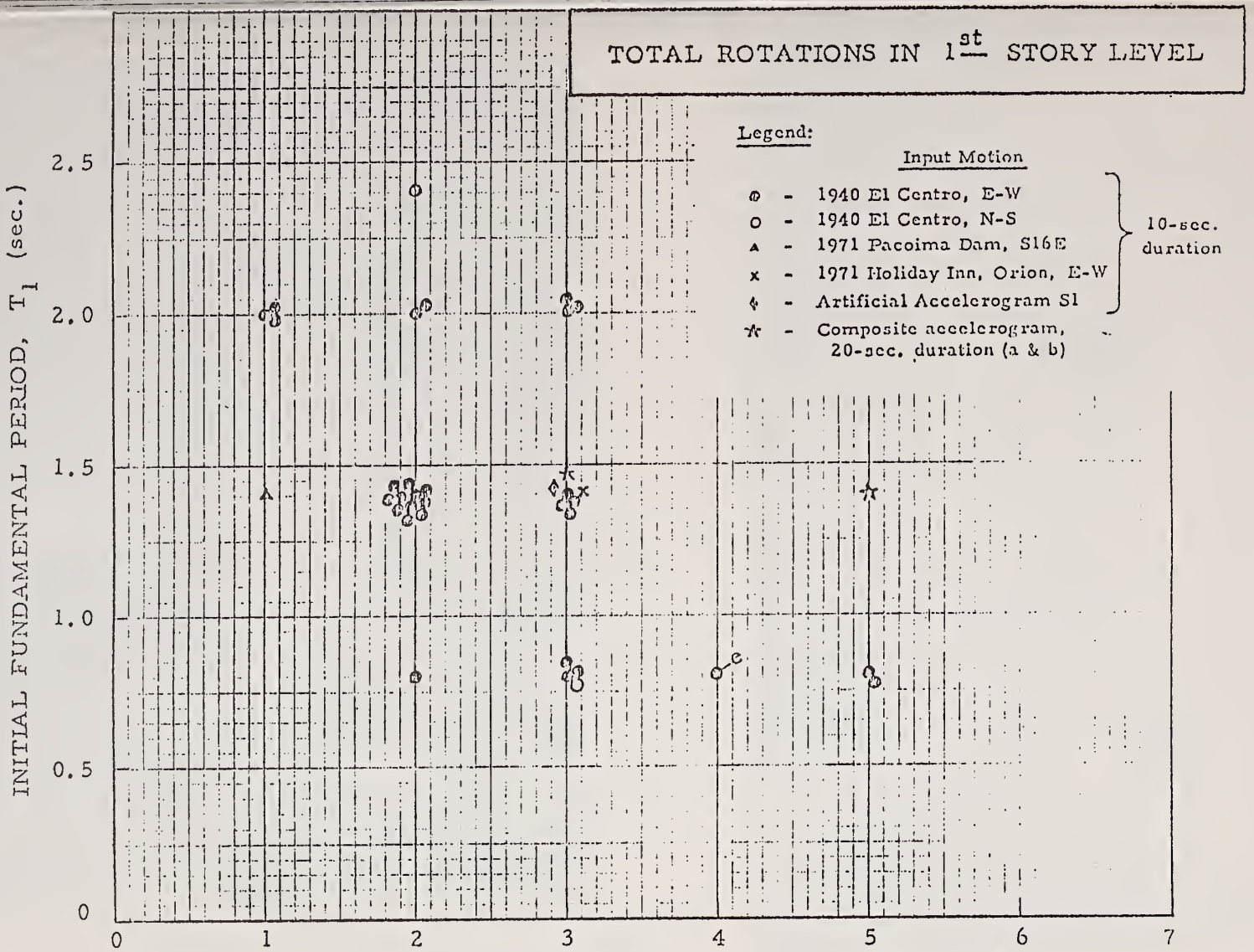

Figure 7(a).

- 'Large' amplitudes are those inelastic deformations between 0.75-1.0 of the corresponding maximum amplitude

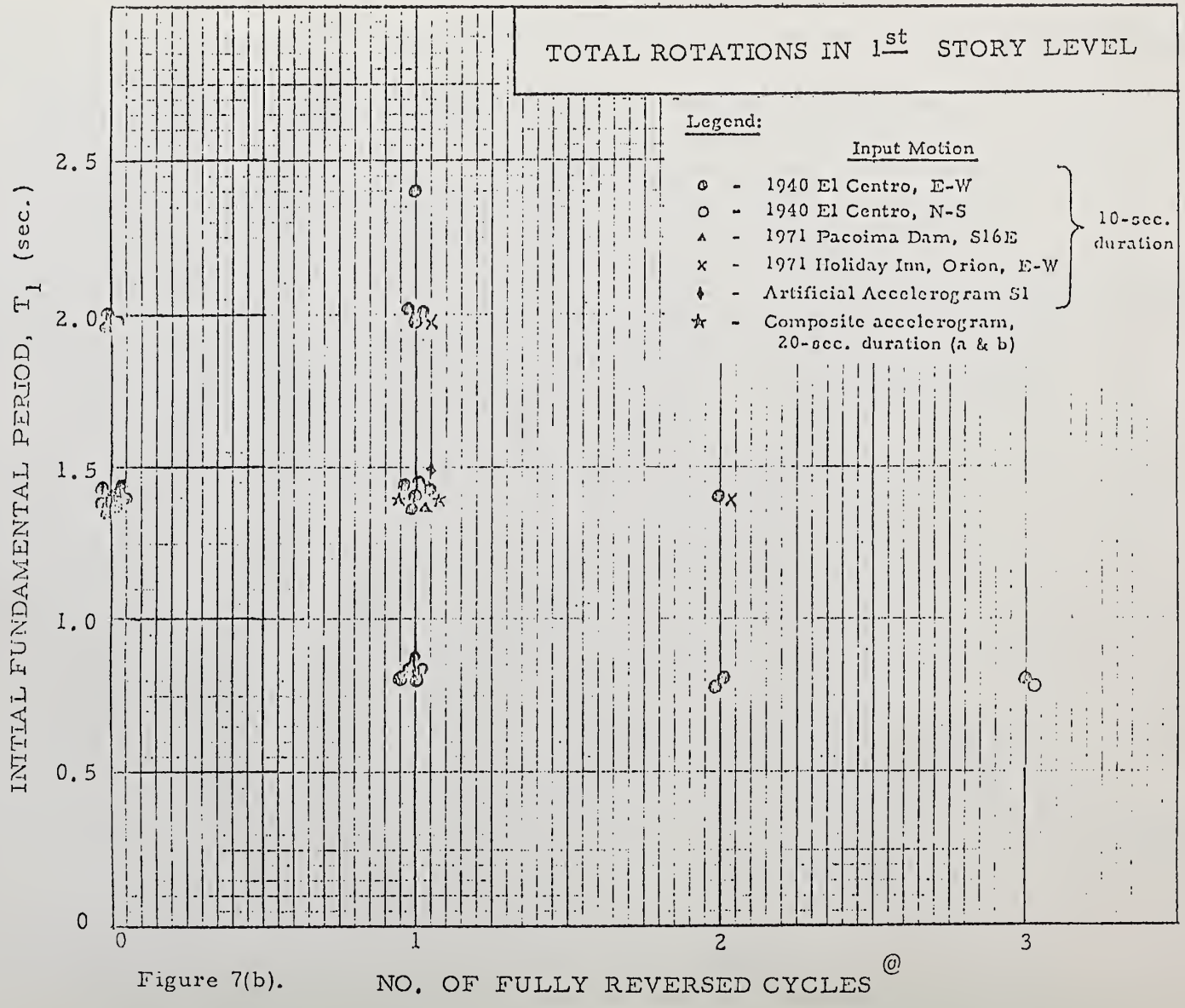

Figure 7(b).

@ - 'Fully reversed cycles' are complete cycles with at least one peak amplitude between 0.75-1.0 of the maximum amplitude of response and the other - on reversal - between 0.50-1.0 of the maximum.

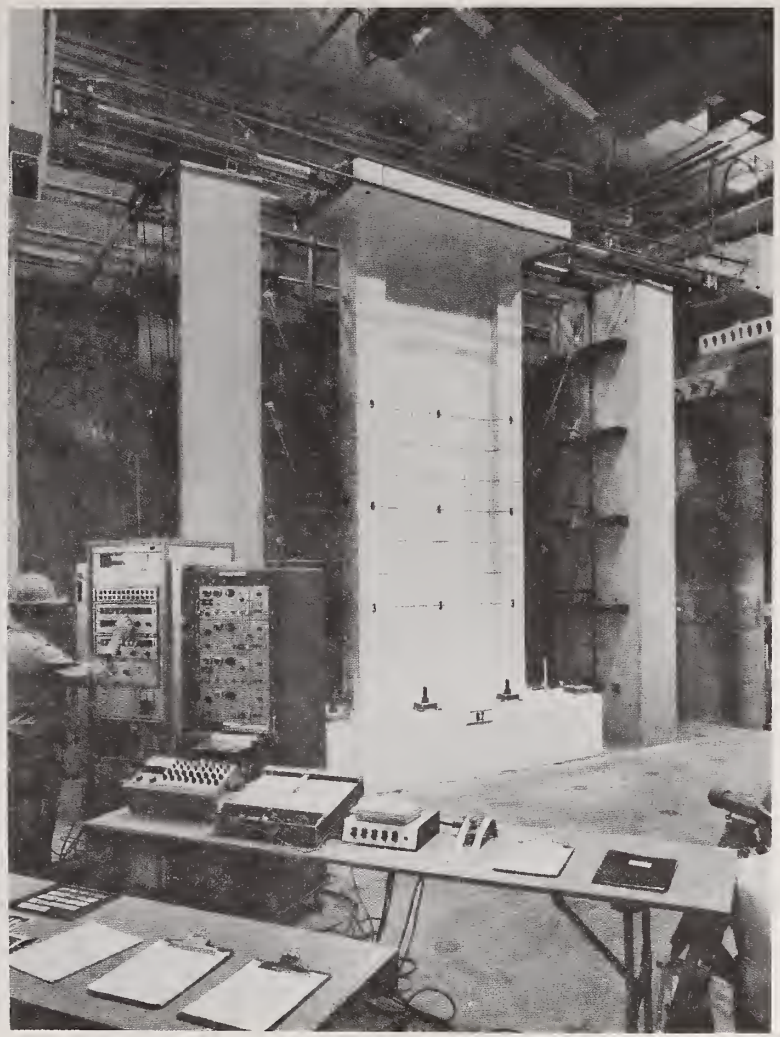

Fig. 8 Test Specimen and Test Apparatus

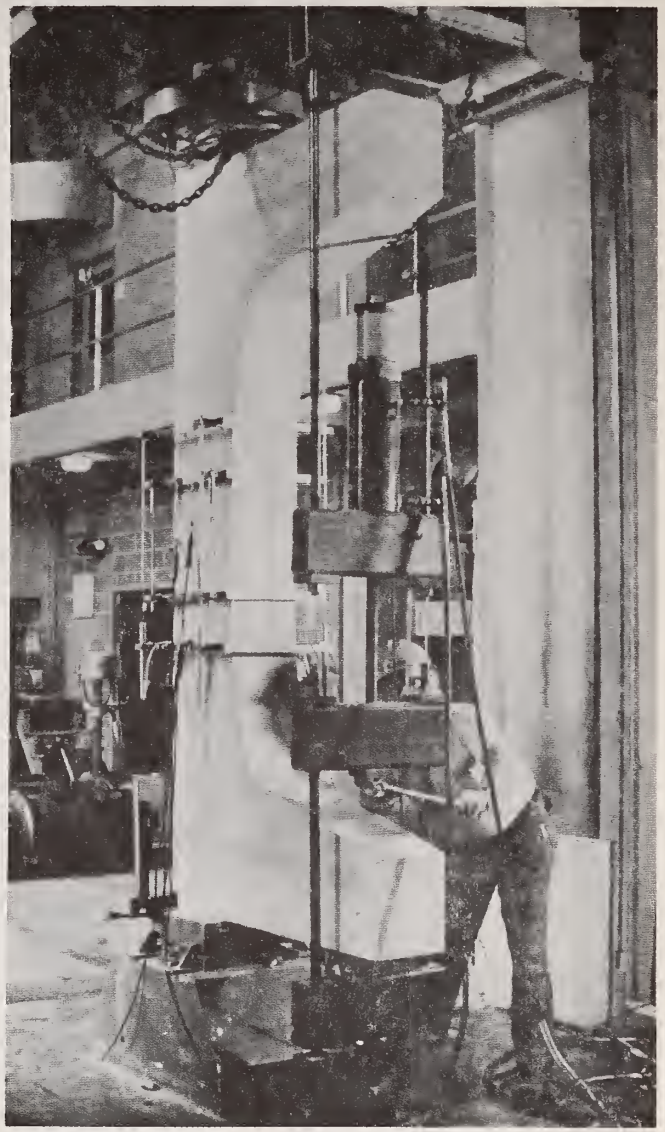

Fig. 9 Element Test Specimen

A PHILOSOPHY FOR STRUCTURAL INTEGRITY OF LARGE PANEL BUILDINGS

MARK FINTEL
Director
Engineering Services Department
Portland Cement Association
Skokie, Illinois

DONALD M. SCHULTZ
Senior Structural Engineer
Engineering Services Department
Portland Cement Association
Skokie, Illinois

ABSTRACT

The paper reviews the various methods to reduce risk from abnormal loads. To limit the occurrence of progressive collapse in large panel residential structures, a philosophy for establishing General Structural Integrity is developed to assure bridging of local damage while maintaining overall stability, thus eliminating the need to design for any particular abnormal load. In this approach, tensile continuity and ductility of the elements, and their connections as well as of the overall structure, is stressed. The rationale for a minimum tie system consisting of transversal, longitudinal, vertical and peripheral ties to establish this General Structural Integrity is developed.

The objective of this approach is not to afford absolute safety in regard to any exceptional event in any part of every building; rather, the intention is to limit and substantially reduce the general risk of collapse, as compared to that existing if no such measures were taken.

Key Words: Buildings; Collapse; Concrete; Panels; Structural Integrity.

1. Introduction

When a local failure is not confined to the area of initial distress, but spreads either horizontally or vertically through the structure, it is termed a progressive collapse. More accurately, it may be defined as a phenomenon in which the spread of a local failure, eventually results in the collapse of a whole building, or a disproportionately large part of it. Abnormal loading conditions and effects which can be structurally significant (1-3) include:

- service system (gas) explosions,
- explosive bombings,
- external explosions from accidents involving transportation of hazardous materials,
- ground vehicular collisions with buildings,
- aircraft collisions with buildings,

- tornados,
- flooding,
- foundation settlements, and
- errors in design and construction.

Traditionally, it was assumed by the profession that if one followed established practice and codes, the resulting building would automatically have a degree of structural integrity which would assure an alternate path for the load when a load-carrying element failed (Fig. 1). This belief was justified for some traditional forms of construction which have continuity and ductility, however, it was not valid for every form of construction (4-12).

In 1968, attention of the engineering community was focused on the problem of lack of structural integrity in certain precast structures in a tragic way. In May of that year a progressive collapse of an apartment building occurred at Ronan Point in London (Figs. 2, 3). A gas explosion in an apartment on the 18th floor caused an exterior panel to be blown out (Fig. 4a); this initiated a progressive collapse upwards to the roof, and then almost down to the ground, as debris fell on succeeding floors (Fig. 4b). In terms of hazard, the initial damage was of minor consequence. The progressive collapse which occurred, however, was the result of the inability of the structure to bridge over the local failure, that is, its lack of integrity. Therefore, it is not merely the hazard of abnormal loading --- it is also the susceptibility of a structure to progressive collapse which presents the real risk.

2. Reducing the Risk of Progressive Collapse

Three alternative approaches, widely varying in concept, can be employed to reduce the risk of progressive collapse (13):

1. Eliminate the hazards which cause local failures (e.g., elimination of gas installations in multistory buildings, as has been done in France);

2. Design the structure so that the hazard does not cause any local failure (e.g. 5 psi gas explosion load requirement initiated in Great Britain);

3. Allow the local failure to occur but design the structure so that progressive collapse does not occur (ensure an alternate path for the load).

a) Elimination of Hazards. Regarding the first approach, it can be assumed that certain abnormal loadings could actually be eliminated: gas installations could be disallowed in large panel buildings; barriers could make vehicular collision avoidable; and construction in flood zones could be regulated. However, with the above exceptions, abnormal loads can hardly be eliminated, and also most of them defy quantitative determination. Since any realistic solution must deal with all abnormal loading conditions to some extent, this method of eliminating the hazards cannot be deemed an overall solution.

b) Local Resistance. In the second approach, providing local resistance, explicit loading requirements are established in an effort to provide sufficient strength to resist any local failure. In lieu of a probabilistic approach, it has been suggested that a minimum design load of 5 psi for gas explosions be used. However, the approach of

providing resistance to one specific abnormal load has been challenged on a number of grounds. It is not reasonable to assume that adequate resistance for one abnormal loading condition will necessarily provide sufficient strength to resist all other abnormal loading conditions. From an economic viewpoint, additional costs to provide a certain safety against local failure may not be justifiable in light of the small number of cases where progressive collapse of large panel structures has occurred

c) Alternate Path through Structural Integrity. Since the nature and magnitude of most abnormal loads are unpredictable, the third approach of allowing local failure to occur but providing an alternate path within the structure to avoid an overall collapse appears to be a sound concept. In this approach, a local failure is accepted as an inevitable consequence.

When a structure has the ability to bridge over local failure it has what will be termed in this article General Structural Integrity (GSI), the principal elements of which are continuity and ductility of members and connections and of the structure as a whole.

The General Structural Integrity approach can be implemented in two distance manners: the design engineer can be required to apply a rational procedure to establish the necessary integrity; or, alternatively, code writers can develop the necessary minimum detailing practice (as has been done for other forms of construction) to establish a degree of continuity and ductility. In either case it is necessary to identify the special sensitivity to abnormal loadings that the particular structural form possesses (4-10).

Minimum detailing as code requirements is recommended as the most viable alternate.* Although it is sometimes more complex, and by its nature, more general, it has a number of advantages:

1. Code writers and researchers have a general responsibility to evaluate details to assure the safety of structures.

2. Design engineers should not be required to directly consider the effects of abnormal loads for one form of construction and not for another.

3. Experience in other building forms has shown that minimum detailing requirements based on good engineering judgment can establish an adequate degree of structural integrity.

While, by its very nature, LP construction does not lend itself easily to a design with moment continuity, it is possible to develop force continuity and ductility of the connections as well as of the overall system through minimum details specified as recommended practice. Since such minimum requirements cannot possibly encompass all situations, substantial reduction in the risk of progressive collapse in all future designs could be achieved if the detailing requirements are supplemented with an educational program for the engineering profession.

*Most recently this approach has been adopted by the PCI Committee on Precast Bearing Wall Buildings (Ref. 14).

3. Prototype Structure

The cross wall and spine wall type of large panel residential structures (Fig. 5) have been selected as the representative prototypes for this study since they are the most popular types used in the United States. The reasons for their popularity are the economic advantages of a low wall-to-slab ratio, resulting from the comparatively large slab spans of up to 42 feet utilized until now. The large distance between the concrete bearing walls permits an open, flexible architectural layout using light partitions. An added advantage of the cross wall type is the architectural freedom in handling the longitudinal elevations. With individual variety for each building made possible, the uniformity inherent in industrial production can be avoided.

4. Rationale for General Structural Integrity

Connections between the precast elements of LP structures are recognized as the weak link in this structural system. This weakness is attributable to the lack of continuity through the connections, and to their brittle nature. Friction-type connections can theoretically provide sufficient stability for gravity loads within an LP structure; however, such connections offer little resistance to the effects of abnormal loadings. Recent studies and discussions (7-12, 15-25) on the performance of structures under normal and abnormal loads have concluded that the integrity of a structure, regardless of the type of construction, depends on its connection characteristics; and that the strength of the elements cannot be utilized if the strength of the connections is insufficient. Therefore, as stated earlier, a degree of continuity <u>across</u> the connections and ductility <u>within</u> the connections should be ensured to achieve General Structural Integrity.

Continuity is essential to develop the bridging capabilities needed for transmission and redistribution of loading (alternate paths). Ductility is necessary, not only to sustain the deformations that may be associated with conditions of partial stability (stability of the structure in the damaged state), but also to establish some measure of energy absorption under the dynamic effects of both normal and abnormal conditions.

The magnitude of required continuity can be determined by assessing the forces acting within the connections under various conditions of local failure. Because of the nature of LP structures, these forces occur only as compression, tension, and shear.* Adequate compression and shear capacity in LP connections will usually be provided by design under normal loads. Little tensile capacity, however, is found between elements in LP structures, and therefore, tensile capacity between elements across the connections (both horizontally and vertically) must be provided. This required tensile continuity across and within the connections can be effectively achieved by providing the ties schematically shown in Fig. 6.

The rationale for GSI should encompass the following: 1)Extent of damage--an assessment of the nature and extent of local damage that is likely to occur under abnormal loadings; 2)Alternate paths--evaluation of alternate structural actions which can develop as a consequence of a local failure to re-establish load flow in the remaining undamaged

*Development of significant moment continuity between individual elements is not considered essential technically nor easily attainable economically in the usual American-type LP systems.

structure--stability analysis of the partially damaged structure; and

3. Tie requirements--quantitative determination of requirements for transversal, longitudinal, vertical and peripheral ties to bridge local failures and to assure stability of the partially damaged structure.

5. Extent of Damage

The extent of local damage which the structure must be capable of bridging affects the amount of ties needed to establish alternate structural action. Code writing bodies in the United Kingdom (26) and Sweden (27) have directly acknowledged that a certain amount of local structural damage is considered inevitable and acceptable by specifying the extent of local failure which the structure must be able to bridge. The specified amount of damaged load-bearing wall is to be assumed as "notionally removed" from the structure at any location within a given building.

The main premise when using the "notional removal" approach is that an element or portion of the structure has been totally removed. In LP buildings with brittle joints which depend primarily on friction and bond under compressive loadings, the "notional removal" concept may be a realistic representation of their response to abnormal loadings. However, as vertical and horizontal ties are introduced within and between the wall elements and floor components, it becomes less likely that the elements can be literally removed. Therefore, with ductility and continuity in the form of ties between structural elements specified as recommended practice in American LP construction, the "notional removal" approach becomes somewhat questionable.

With LP structures tied together horizontally and vertically it is reasonable to assume that in most instances wall panels become "ineffective" as a result of abnormal loadings. They will no longer function as load-bearing members as originally intended, but will remain in place in their damaged condition. Whether wall panels become ineffective or are notionally removed is actually of minor consequence, since in either case the original load flow is interrupted and an alternate path must be available. In fact, differentiation between the two concepts is not required at all with regard to the main alternate paths available, that of cantilever and beam action.

The concept of ineffective behavior is introduced here primarily because of its effect on debris loading and slab behavior in the damaged state. Specifically, the requirements for the slabs to "hang together" over the damaged (buckled) wall vary from the requirement of developing full catenary action over double span when the supporting wall is notionally removed. As a result, the tie requirements for the slabs using the "ineffective member" rationale will be different from those required if the "notional removal" approach is adopted.

When estimating damage extent, the following should be taken into account:

1) probability of occurrence of an abnormal load for each element of the structure,
2) the consequence of failure of a particular element within the structure, and
3) the influence of a particular structural configuration and layout of the walls.

6. Element Vulnerability

Since the probable damage caused by abnormal loads differs in various parts of a building (1), damage criteria which do not delineate the damage location, if applicable in one area, may not apply in other portions of the building. As a result, it is appropriate to define an element's vulnerability by its location within the structure, considering the consequence of its failure.

a) Exterior (Flank) Wall Panel. The wall panels along the perimeter of an LP building are the most susceptible elements to abnormal loadings. Although the sizes of typical flank wall elements range from 25 to 45 ft. in length, it is reasonable to assume that, as an outside limit, an entire unit of a flank wall assembly can become ineffective (Fig. 7). This assumption can be somewhat relaxed, however, if measures are taken in the design to ensure that only a part of the wall panel becomes ineffective. Such measures may include "weak planes", or additional stiffening elements in the form of bracing walls or integral columns (Fig. 8).

Under the above conditions, "ineffective" indicates that the wall, although physically damaged and possibly buckled, is still "strung" in place, not allowing the slab units to drop to the level below to create impact loading.

b) Interior Wall Panel. Interior wall panels, being farther removed from the periphery of the structure than flank wall elements, are subjected to a somewhat lesser degree of risk of specific abnormal loadings. However, it is assumed as an outside limit that an entire wall panel can become ineffective as shown in Fig. 7. As in the case of flank wall assemblies, this assumption can be relaxed if similar measures are taken in the design to ensure that the entire wall panel cannot become ineffective (Fig. 8).

c) Floor/Roof Panel. Floor/roof systems typically consist of side-by-side members (planks) up to 8 ft. wide. As a result, full continuity of the system perpendicular to the span is interrupted at each joint. It is reasonable to assume, therefore, that in case of an abnormal loading, only a few floor/roof planks would become ineffective for a full span length. As the floor slab consists of individual planks, there is little tendency for the failure to spread beyond the planks affected by the abnormal loading. For floor/roof elements, "ineffective' suggests that they are physically damaged and substantially weakened, and no longer capable of providing lateral support of wall units or of participating in the required diaphragm action. However, they are still strung together and capable of supporting their own dead loads within their original spans.

The most critical condition for floor/roof panels occurs when they lose their stability due to partial loss of one of their end supports, i.e., a wall panel. The loss of such support would be due to the ineffectiveness of the wall element below, resulting in large displacements at the original support. Such conditions require adequate tensile continuity between adjacent slab spans for the slab elements to hang together in their deflected shape.

7. Tie Functions and Alternate Paths

Structural design for "normal" loadings (those specified in codes) begins with an assessment of the loads on the building. These loads should be safely transferred from the point of application to the final resisting point through a logical load flow. If a panel becomes ineffective as a consequence of an abnormal loading, a new load flow must be established in the remaining undamaged structure, i.e., an alternate path must be created.

To avoid progressive collapse which may occur if the structure is unable to bridge local damage, alternate load paths should be available for any load-bearing wall or portion thereof that might become ineffective. For the slab elements such alternate paths are not essential. However, to avoid uncontrollable debris loading, provisions should be made to effectively tie (or string) the floor/roof elements together.

Tying the large panel structure together horizontally and vertically makes it possible to utilize the following structural mechanisms to bridge local failures:

1. cantilever action of wall panels,
2. beam action of wall panels,
3. partial membrane action of successive spans of floor planks,
4. vertical suspension of wall panels, and
5. diaphragm action of the floor planks.

a) Transverse Ties and Cantilever Action. When, at a given floor level, a wall panel or portion thereof becomes ineffective, the wall panels above that level have lost their support. The most effective method of transferring the loads is through cantilever action of the remaining panels above. However, to obtain cantilever action, the means to transfer the vertical load at the supported end of the cantilever must exist. Vertical support at the cantilever root can be provided by:

1. a vertical connection designed to carry the shear in each story in a wall assembly consisting of two or more adjacent vertical stacks (Fig. 9);
2. a vertically continuous return wall or a vertically continuous integral column at the interior edge of the wall assembly consisting of a single vertical stack (Fig. 10); or
3. the remaining portion of the wall (Fig. 11); special detailing should ensure that only a portion of the wall becomes ineffective.

Although cantilever support can be assured through proper panel design and layout, the cantilever moment can be developed only if adequate tensile continuity in the form of a reinforcing tie exists in the transverse horizontal connection between the wall panels. To assess these tie force requirements the behavioral mode must be determined.

Depending on the horizontal connection properties, two modes of cantilever action can be defined as giving upper and lower bounds to the transverse tie force requirements. In the cantilever action shown in Fig. 12a, no horizontal shear is transmitted between story-high cantilevers. The strength of this builtup cantilever is equal to the sum of the strengths of the individual cantilever panels. In practice, this type of action is unlikely, since the joint is filled with drypack or grout, and some vertical reinforcement

(in the form of vertical ties) is used to interconnect successive wall panels. Both the concrete and the vertical ties act to provide shear resistance across the connection by shear friction, and consequently, enhance the cantilever strength. This behavioral mode provides a lower bound in predicting cantilever strength.

If adequate shear capacity can be achieved between successive stories, the entire wall panel assembly will act as a monolithic cantilever as shown in Fig. 12b. This behavior can be achieved when there is no relative slip between stories. Such an idealized condition is questionable as some slip will most likely occur within the vertical tie connection details. Therefore, this behavioral mode should be considered an upper bound in predicting the cantilever strength.

In practice, the behavior will be somewhere between the two modes described above, and the tensile force requirements for the transverse tie in a multistory cantilever will depend primarily on the details affecting shear characteristics of the horizontal connections.

The transverse tie within the connection can be in the form of mild steel or unstressed prestressing strand. To ensure its effectiveness, the tie should extend the full width of the structure, and be adequately secured to the peripheral tie system (Fig. 13).

b) Transverse Ties and Beam Action. Although cantilever action through the use of transverse ties is the single most important element in establishing alternate paths in LP buildings, in some instances of local damage the transverse ties can also be very effective in developing "beam" action of the wall panels. However, to develop beam action, a capacity to transfer the vertical load to each of the supported ends must exist. Such supports are available in the cases shown in Fig. 14.

As in the case of cantilever action, the vertical supports for beam action are provided through proper panel design and layout. The beam's flexural resistance can be developed only if adequate tensile capacity in the form of reinforcing ties exists in the transverse horizontal connection or within the wall panels themselves. The factors affecting the overall behavior of this alternate load flow are similar to those examined under cantilever action. Vertical load-carrying capacity at each end must be assured and, as before, the shear characteristics of the horizontal connection between successive wall panels substantially influence the behavior.

The necessary ties to resist the tensile forces from the bending moment will be less than those required under similar span cantilever action; however, this structural behavior will usually require more return walls or integral columns to assure vertical supports. The transverse ties to effect beam action can be either of mild steel reinforcing or unstressed prestressing strand. The ties should be continuous the full width of the building and anchored to the peripheral tie system (Fig. 13).

c) Longitudinal Ties and Partial Membrane Action (Large Deflections of Slabs). Cantenary action of the continuous slab spans due to loss of supports has been investigated in Europe (28). Although full catenary action is accepted as an appropriate and functional means of reestablishing the load flow in European LP structures, it is not considered in this study a suitable method for American LP construction for the following:

1. The typical slabs for European systems span from 10 to 18 ft., are cast for a particular building, and are joined together by interlacing loops protruding from the slabs. LP systems used in the United States have floor spans which range from 20 to 40 plus feet. The U.S. slab systems are generally prestressed hollow core slabs produced in long beds and cut to shorter lengths according to the required span. In this fabrication technique, reinforcement protrusions at the ends are not feasible, and tensile continuity between adjacent spans must be developed by other means. Since the span of the necessary catenary in U.S. construction (double the slab span) is about twice that of its European counterpart, the problems related to physical development of the necessary longitudinal tensile forces are greatly magnified.

2. To develop the necessary catenary action, the floor systems must undergo large deflections. With 40 to 80 foot catenary spans in U.S. construction, the necessary deflection may approach a total story height. Such large deflections can be accommodated only when the panel below is totally removed; this is, in turn, contrary to the concept of walls becoming ineffective.

The major element of resistance and stability in the damaged wall-type structure is provided by cantilever and beam action. The function of the slab is to ensure an adequate degree of partial catenary action to effect a stringing of the elements to inhibit progressive collapse from debris loading should an interior wall become ineffective. The wall's ineffectiveness is suggested as a limited displacement (Fig. 15), say up to 24 inches. Thus, to string the slab elements together in this deflected shape, adequate tensile continuity must exist between them, above the ineffective wall. Ductility of the connection must be ensured to permit the large deformations and to resist any dynamic effects that may occur.

Continuity can be developed with reinforcing placed in the longitudinal horizontal keyways between floor panels, or in the topping slab if one is employed. These ties must provide tensile continuity between adjacent spans and, to ensure integral behavior, the ties of the end span should be anchored into the peripheral tie system. Since floor elements are well reinforced, the ties need not be continuous for the full length; the tie force should be transferred by bond or mechanically from an element in one span to the one in the next span (Fig. 16).

d) Vertical Ties and Suspension Action. The primary functions of vertical ties between wall elements in the damaged structure are:

1. to provide vertical suspension of ineffective wall panels and thus avoid debris loading;

2. to provide resistance against "kicking out" of the walls sideways, thus fostering "ineffective" behavior of wall elements, rather than total removal under abnormal loading; and

3. to assure clamping and dowel action in the horizontal connections for shear friction to resist horizontal shear and thus develop cantilever and beam action.

If an alternate path for the load transfer around an ineffective wall panel has been established either through cantilever or beam action, the damaged panel should be suspended from the alternate supporting mechanism. To ensure this suspending action, vertical continuity in the form of tensile ties must exist between and through all wall panels. Tensile continuity from foundation to the roof can be assured by providing vertical ties proportioned to resist (within each story) the dead loads of the wall plus those loads superimposed by the floor panels. In addition, the vertical tie must resist the stresses from shear friction clamping in the horizontal connection.

Because of the increased vulnerability of exterior wall panels (as compared to interior wall panels) with regard to abnormal loadings, greater vertical continuity is desirable in flank wall assemblies in order to afford them increased protection against removal from the structure. The vertical tie of the flank walls should be placed within the peripheral tie system to improve its integral connection with the slab system.

The vertical ties may take the form of mild steel, prestressing rods, or prestressing strand, stresses or unstressed. They should be continuous for the full height of the panel assembly (Fig. 17). The ties can also function as reinforcement required for service and erection loads.

e) Peripheral Ties and Diaphragm Action. The main functions of peripheral ties in the damaged buildings are:

1. to establish the necessary diaphragm action to resist the effects of wind, torsion and unequal load distribution throughout the structure;

2. to anchor the longitudinal and transverse tie forces at the periphery; and

3. to help create membrane action in corner slabs when the corner support becomes ineffective.

These functions can be accomplished by employing a ring beam at the periphery of the structure at each floor and roof level.

To assess the force level required in such a ring beam in a structure is a difficult, if not impossible, task. In the damaged state the entire slab or roof may act as a membrane, with its periphery subject to large ring beam forces. It is suggested that the peripheral tie forces be based on the diaphragm action necessary to resist normal lateral loads, assuming the customary load factors and capacity reduction factors. However, for purposes of continuity and anchorage requirements in the damaged state, the transversal tie forces required in the flank wall assemblies should be continued in the longitudinal faces (if larger than those required for diaphragm action) for the design of the complete periphery (Fig. 18). These continuous ties, which should be located as close to the actual periphery as possible, may be of mild steel or prestressing strand or mechanical connectors between ends of planks in adjacent spans.

8. Loads and Safety Factors in the Damaged Structure

To determine the quantity of ties needed for stability of the damaged structure, the necessary loads to be resisted must be established. Consideration should be given only to those loads likely to occur before temporary or permanent measures are taken to repair the

damaged area. Included in this category are the full deal load and part of the design wind and live loads. It is sufficient to assume 1/3 of the design live load and 1/3 the design wind load. Reduced live load is based on the assumption that a building will be evacuated after an abnormal incident has caused local damage. The reduced wind loading is based on the supposition that the building will have partial stability for a limited period of time.

Since the rate of occurrence of local damage due to abnormal loadings is relatively low, and since the intent is to assure the stability of partially damaged structures, it is assumed that the above loads are resisted at a level close to the ultimate strength of the sections, say 90% of ultimate capacity. Therefore, for the determination of minimum tie forces, liberal load factors, γ, are appropriate. However, the capacity reduction factors, ϕ, which account for variations in material strengths, workmanship and dimensional errors combining to result in undercapacity, must still be used. Since the ties are utilized to resist axial tension and tension due to bending, a ϕ factor of 0.9 can be used.

Combining the loads (D, L, W) and load factor, γ, the required strength equation may be expressed as:

$$U = 1.10\ (D + L/3 + W/3)$$

Incorporating the capacity reduction factor, ϕ, the safety factor of the damaged structure becomes:

$$S.F. = \frac{\gamma}{\varphi} = \frac{1.10}{0.9} = 1.22$$

9. Specifying Tie Forces - Unstressed Strand

Specifying tie requirements, in terms of forces rather than amounts of steel permits flexibility in the choice of tie type, while fostering a better understanding of the issues involved. Specifying forces allows the use of unstressed prestressing strand, which has the advantage of large tensile capacity with a relatively small diameter. Flexible strand also offers the advantage of easy placement in misaligned connections where a normal mild steel bar cannot be placed due to its rigidity. While unstressed prestressing strand cannot be used for resistance at service load levels, since it would result in unacceptable crack widths, the large strains of the strand are not objectionable under catastrophic conditions.

10. Planform

Proper structural planform, i.e., the layout of the structural walls, improves the overall rigidity and stability of the structure, thereby increasing its structural integrity. Effective planform is best accomplished by arranging walls in both orthogonal directions of the building.

Since current connection details make frame action between adjacent slab spans and between slabs and walls almost impossible, lateral resistance of LP buildings is provided economically only by cantilever action of the stacks of wall panels in their own planes. Therefore, where possible, longitudinal spine walls or segments should be used to enhance the stability of the longitudinal direction. They will also improve the stability of individual transversal walls, while decreasing the length of wall likely to be affected by an abnormal load.

For exterior walls, returns or integral columns are desirable to enhance their resistance to abnormal loadings. If vertical stabilizing cores are the only elements for lateral stability, it is desirable to distribute them throughout the building (Fig. 10) so that if one is damaged, total stability of the structure under lateral loads is not forfeited. Shrinkage, temperature and distribution steel placed in the topping can also be used to enable the slab to span in a perpendicular direction and prevent collapse where a support configuration is favorable for two-way action (Fig. 20).

11. Building Protection

Protecting the structure from abnormal effects is one of the basic methods to avoid progressive collapse. When an abnormal load can be controlled, such control is recommeded; e.g., provision of venting to relieve explosions, use of shock absorbers for crash barriers against vehicular collision, prohibiting construction in flood plains, etc. In this way, the forces and their effects due to certain abnormal events can be reduced or eliminated, thus lowering the overall risk from abnormal events.

12. Concluding Remarks

It is technically very difficult and economically prohibitive to design residential-type buildings for absolute safety. On the other hand, there is no justification for constructing buildings which do not afford a certain degree of safety with regard to abnormal loads.

To reduce the risk of progressive collapse of large panel residential buildings, a philosophy is developed to assure bridging of local damage while maintaining stability of the partially damaged structure by tying the components of large panel structures together horizontally and vertically. Based on this philosophy, explicit requirements for a minimum tie system of transversal, longitudinal, vertical and peripheral ties will be developed. It is intended that these requirements establish a General Structural Integrity for the building to minimize the effects of abnormal loadings.

The provision of General Structural Integrity eliminates the need to design for any particular abnormal load, since the ability to bridge local damage is provided.

In establishing structural integrity, the need for tensile continuity and ductility of the elements, as well as of the overall structure, is recognized. This will be accomplished through a rational arrangement of tensile ties and through connection details which will assure alternate structural behavior of the damaged building. This combination of system continuity and ductility should enable the structure to either absorb the

abnormal loads with minimal damage, or bridge localized damage as a result of the abnormal load. The provision of General Structural Integrity will bring the safety of LP structures closer to that of the traditional cast-in-place reinforced concrete buildings.

The objective of this approach is not to afford absolute safety in regard to any exceptional event in any part of every building; rather, the intention is to limit and substantially reduce the general risk of collapse, as compared to that existing if no such measures were taken. Based on experimental results performed thus far, it appears that the amount of ties required to achieve the desired level of General Structural Integrity will have a minimal effect on the economics of LP structures. With the philosophy established, subsequent experimental tests and analytical studies will focus on development of purposeful details to optimize the effectiveness of the ties in the structure.

Acknowledgement

The material in this paper is excerpted from a larger publication entitled: "Structural Response of Large Panel Buildings to Normal and Abnormal Loads". It is the second in a series of reports prepared at the Portland Cement Association for the Department of Housing and Urban Development under Contract H-2131 (Development of Criteria for the Design and Construction of Large Panel Concrete Structures).

References

1. Schultz, D.M. and Fintel, M., "Report 1: Loading Conditions," Design and Construction of Large Panel Concrete Structures, Office of Policy Development and Research, Department of Housing and Urban Development, Washington, D.C., April 1975.

2. Somes, N.F., Abnormal Loading on Buildings and Progressive Collapse, NTIS Com-73-1113, prepared for the Office of Policy Development and Research, Department of Housing and Urban Development, Washington, D.C., May 1973.

3. Burnett, E.F.P., "Abnormal Loading and Building Safety," Industrialization in Concrete Building Construction, SP-48, American Concrete Institute, Detroit, Michigan, 1975.

4. Ferahian, R.H., Design Against Progressive Collapse, Technical Paper 332, Ottawa, Canada, National Research Council of Canada, Division of Building Research, July 1971.

5. Ferahian, R.H., "Buildings: Design for Prevention of Progressive Collapse," Civil Engineering, American Society of Civil Engineers, New York, February 1972.

6. Creasy, L.R., "Partial Stability," Design Circular, Directorate of Civil Engineering Development, Department of the Environment, London, England, August 1971.

7. Creasy, L.R., "Stability of Modern Buildings," The Structural Engineer, Vol. 50, No. 1, London, England, January 1972.

8. Discussion of the Stability of Modern Buildings, The Structural Engineer, Vol. 50, No. 7, London, England, July 1972.

9. Creasy, L.R., "The Art of the Possible," A Presidential Address given before the Institution of Structural Engineers, London, England, October 4, 1973.

10. Stability of Modern Buildings, The Institution of Structural Engineers, London, England, September 1971.

11. Popoff, A., "State-of-the-Art Report No. 3 - Stability of Precast Concrete Systems Buildings," Planning and Design of Tall Buildings, Vol. III, American Society of Civil Engineers, New York, 1973.

12. Popoff, A., "Design Against Progressive Collapse," Journal of the Prestressed Concrete Institute, Vol. 20, No. 2, March-April 1975.

13. Burnett, E.F.P., The Avoidance of Progressive Collapse: Regulatory Approaches to the Problem, prepared for Center for Building Technology, National Bureau of Standards, Washington, D.C., October 1975.

14. PCI Committee on Precast Bearing Wall Buildings, "Considerations for the Design of Precast Beaming Wall Buildings to Withstand Abnormal Loads," Journal of the Prestressed Concrete Institute, Vol. 21, No. 2, March/April 1976.

15. Granstrom, S., and Carlsson, M., Building Design for Avoidance of Progressive Collapse, Part II: Survey of Some Recent Collapses, Library Translation No. 1670, Building Research Station, Watford, England, April 1972.

16. "Aims of Structural Design", The Institution of Structural Engineers, London, England, August 1969.

17. Granstrom, S., "Byggnaders Stabilitet Efter Katastrofskador. Drafter i Elementfogar-Modellforsok," (Stability of Building After Accidental Damage. Forces in Element Joints-Model Tests), Statens Institut for Byggnadsforskning, Report R20:1971, Sweden Symposium at University College of Cardiff, December 1970.

18. The Stability of Precast Concrete Structures, (Proceedings of the discussion periods following the morning and afternoon sessions at a Seminar at the Europa Hotel, London, March 27, 1973), Building Research Establishment, Department of the Environment Garston, Watford, England, December 1973.

19. "Stability of Buildings and Their Design for Prevention of Progressive Collapse Due to Local Damage," Report of Subcommittee on Large Concrete Panels, Nordic Concrete Association Committee on Regulations, Sweden, January 29, 1970.

20. Allen, D.E. and Schriever, W.R., "Progressive Collapse, Abnormal Loads, and Building Codes," Structural Failure: Modes, Causes, Responsibilities, American Society of Civil Engineers, New York, 1973.

21. Smith, B.S. and Rahman, K.M.K., "A Theoretical Study of the Sequences of Failure in Precast Panel Shear Walls," Proceedings of the Institution of Civil Engineers, Vol. 55, Part 2, London, England, September 1973.

22. Armer, G.S.T. and Kumar, S., Tests on Assemblies of Large Precast Panels, Current Paper CP 20/72, Building Research Station, Department of the Environment, Garston, Watford, England, 1972.

23. The Behavior of Large Panel Structures, CIRIA Report No. 45, Construction Industry Research and Information Association, London, England, 1973.

24. Granstrom, S.A., "The Scandinavian Approach to Structural Safety," Buildings and the Hazards of Explosion , Proceedings of the Symposium at BRE, Garston, October 18, 1972, Building Research Establishment, Department of the Environment, Garston, Watford, England, 1974.

25. "Symposium on Progressive Collapse," ACI Annual Convention, sponsored by the ad hoc committee on progressive collapse, Technical Activities Committee, American Concrete Institute, Boston, Massachusetts, April 1975.

26. British Standards Institution, "Part I - Design Materials and Workmanship," The Structural Use of Concrete, CP110: Part 1, BSI, London, England, 1972.

27. Swedish Building Standards, "Swedish Regulations for Prevention of Progressive Collapse," SBN 22:35, Stockholm, Sweden, 1973.

28. Wilford, M.J. and Yu, C.W., Catenary Action in Damaged Structures-Tests on R.C. Beams and Slabs, Building Research Establishment, Ref. 391/73, Watford, England.

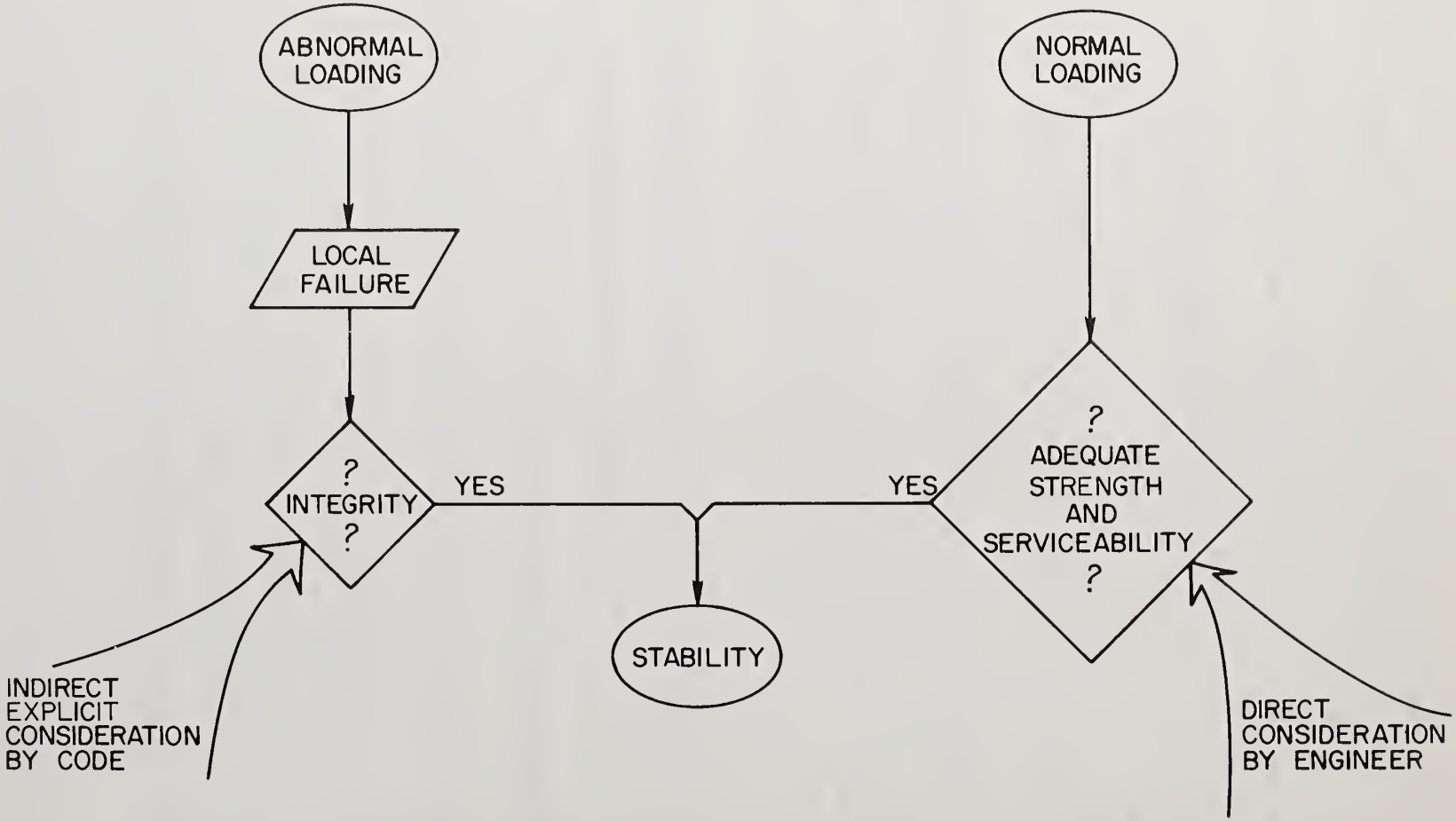

Figure 1 Schematic Diagram of Design Process with Adequate Detailing Standards

Figure 2 Collapse at Ronant Point

Figure 3 Collapse at Ronant Point

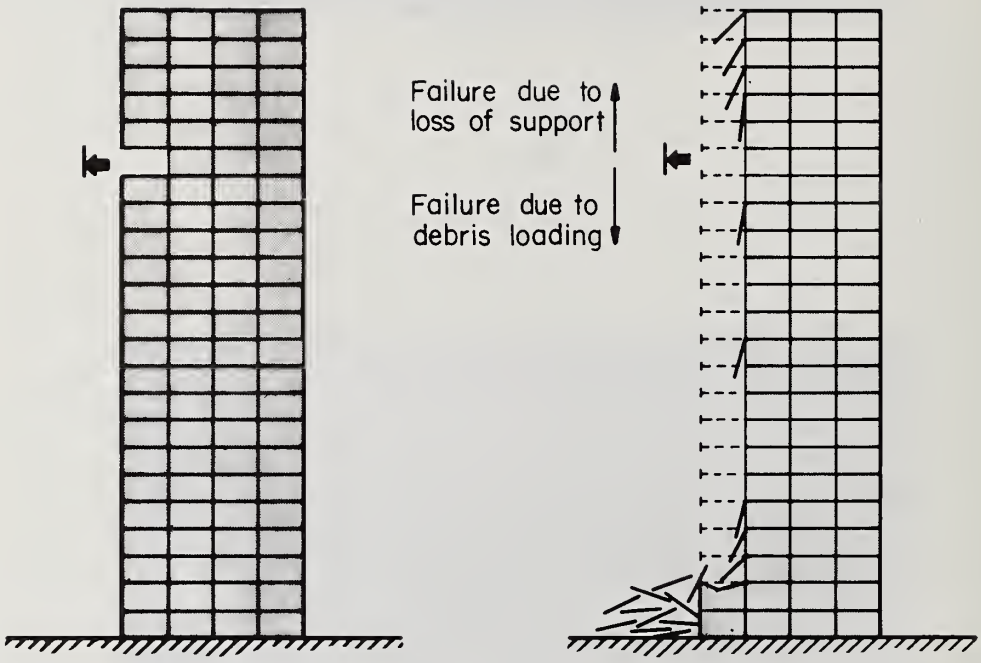

(a) Immediate Local Damage

(b) Progressive Collapse

Figure 4 Failure Modes of Ronant Point Collapse

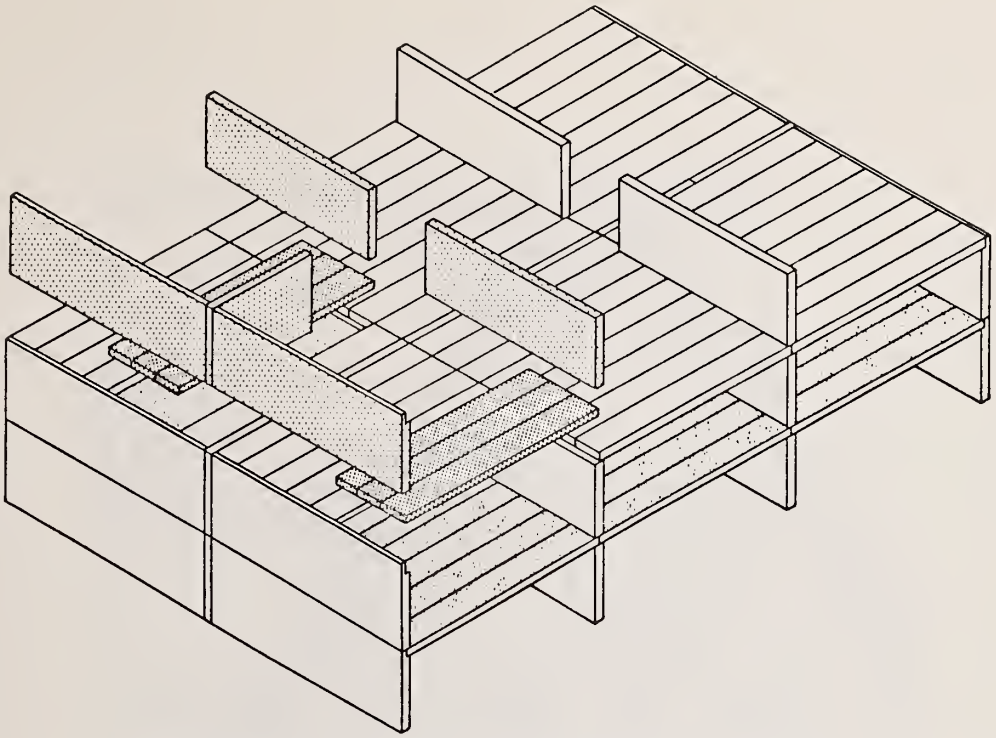

Isometric View of Typical Large Panel Concrete Structure

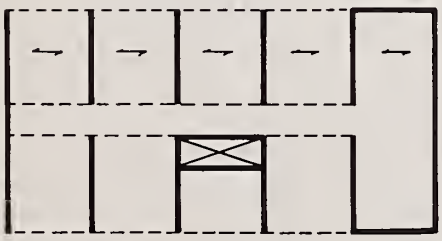

Cross Wall System

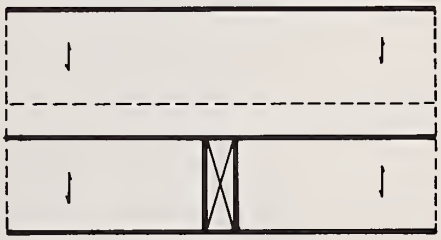

Spine Wall System

Figure 5 Typical Large Panel Structures

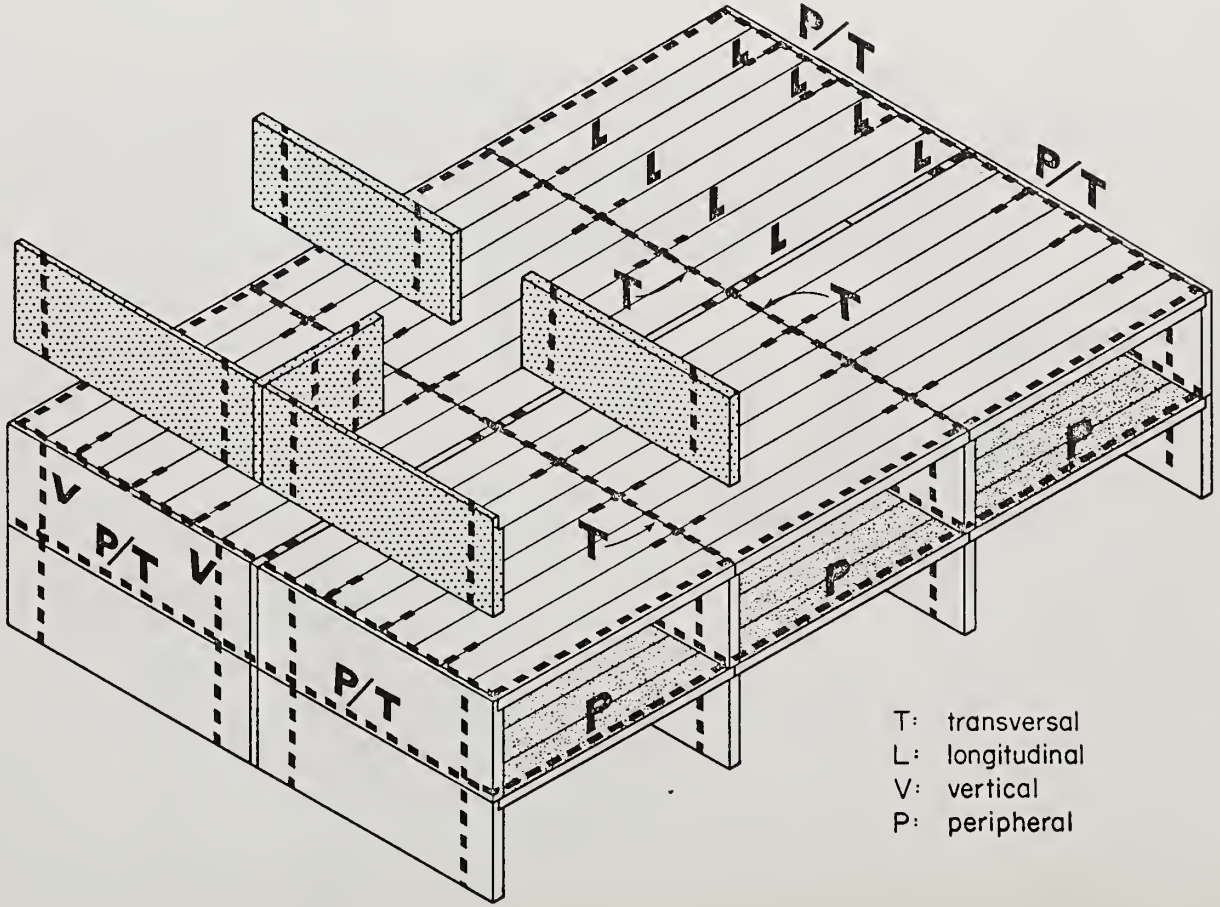

Figure 6. Suggested Systems of Tensile Tiers in Large Panel Structures

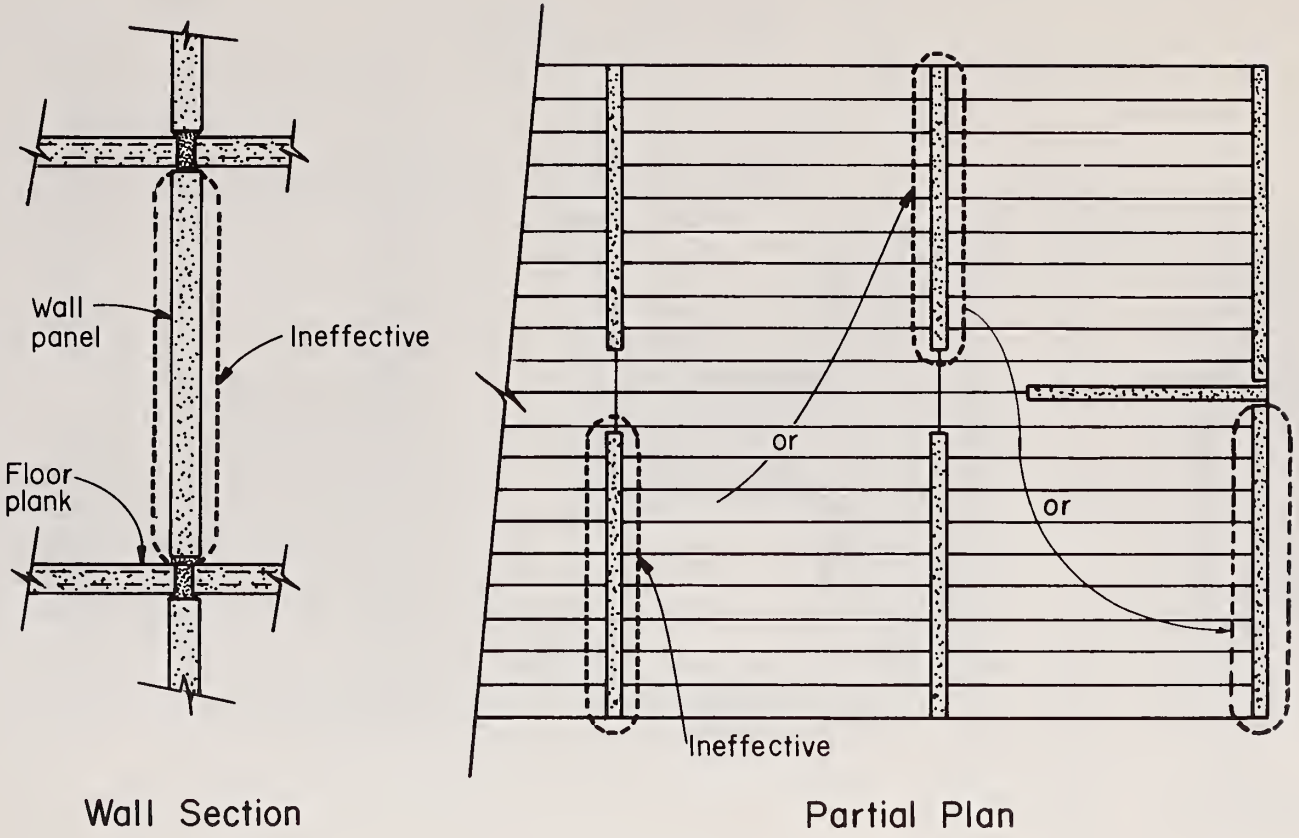

Figure 7 Extent of Assumed Maximum Wall Damage under Abnormal Loads

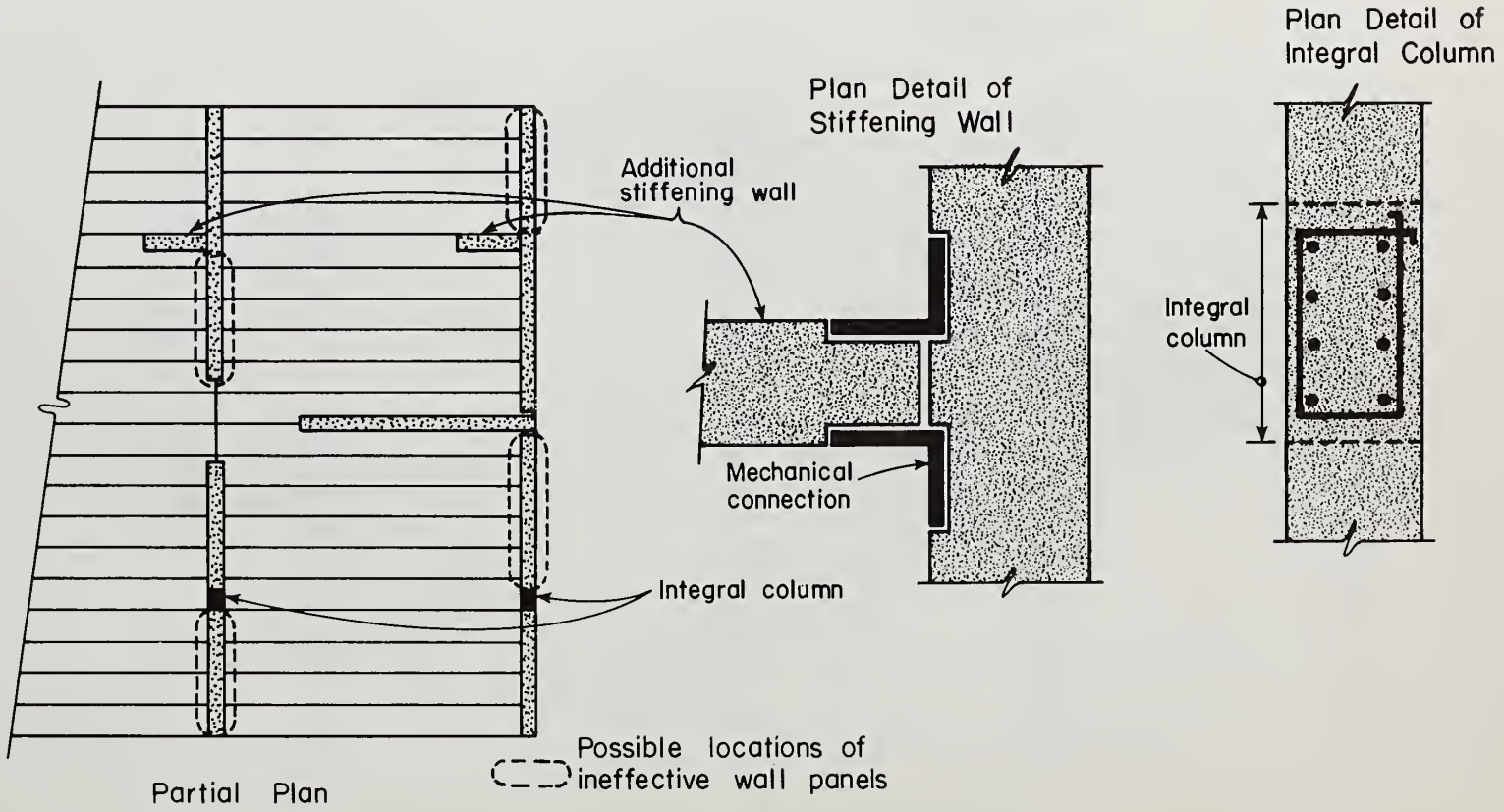

Figure 8. Extent of Assumed Wall Damage Under Abnormal Loads with Limiting Measures Taken

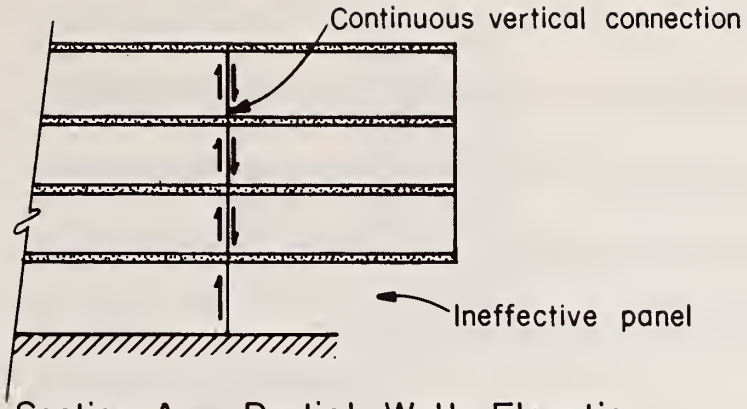

Section A - Partial Wall Elevation

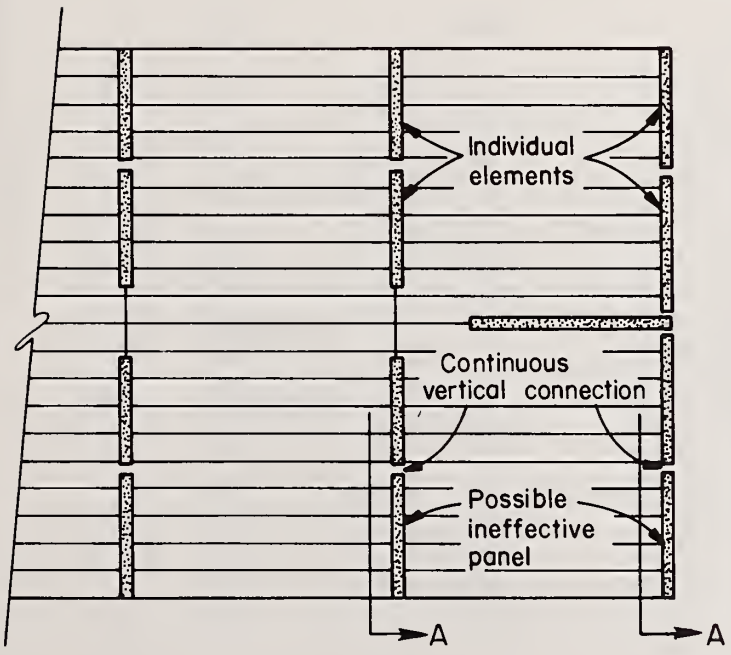

Partial Plan

Figure 9 Cantilever Mode--Two Adjacent Wall Panel Stacks

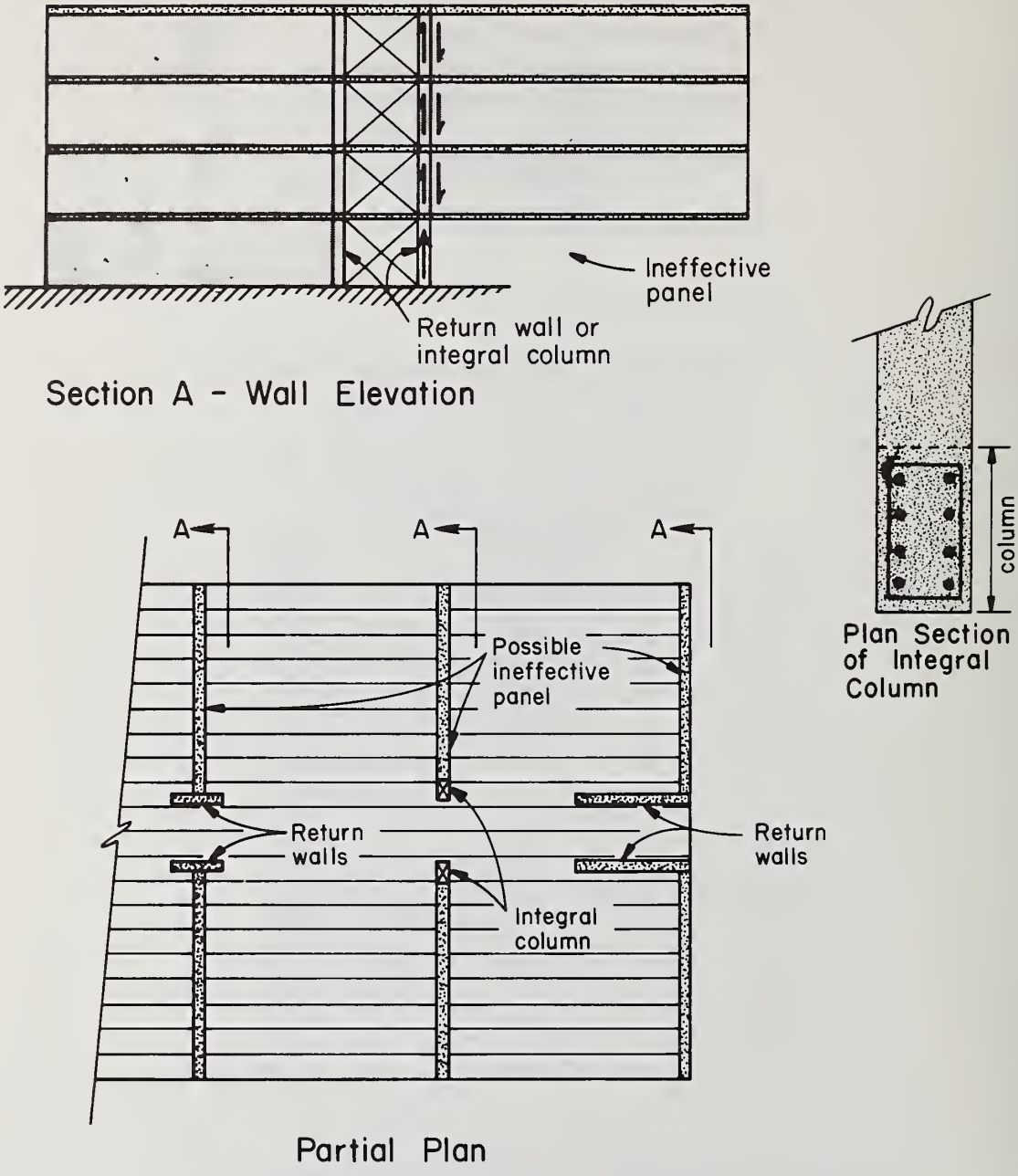

Figure 10 Cantilever Mode--Single Vertical Wall Panel Stack

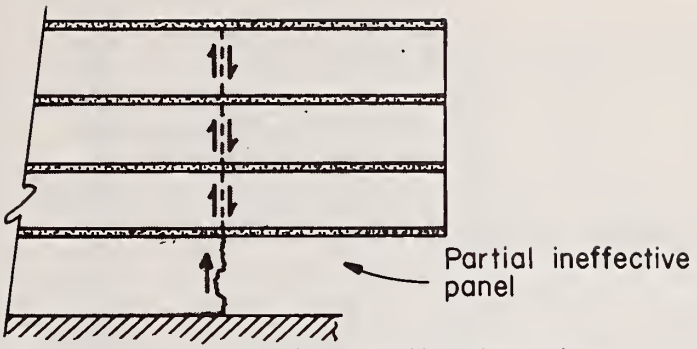

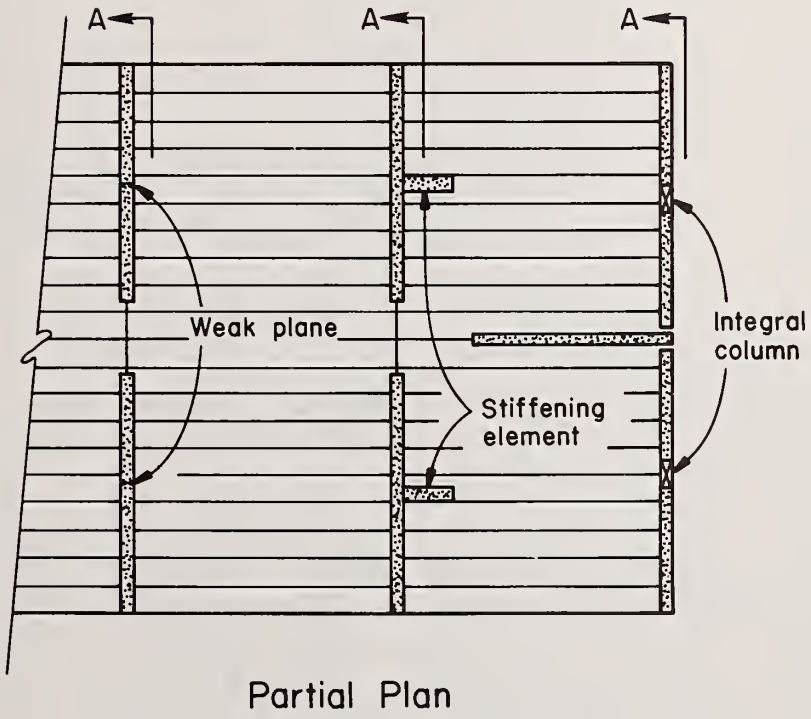

Figure 11 Cantilever Mode--Partial Element Ineffectiveness

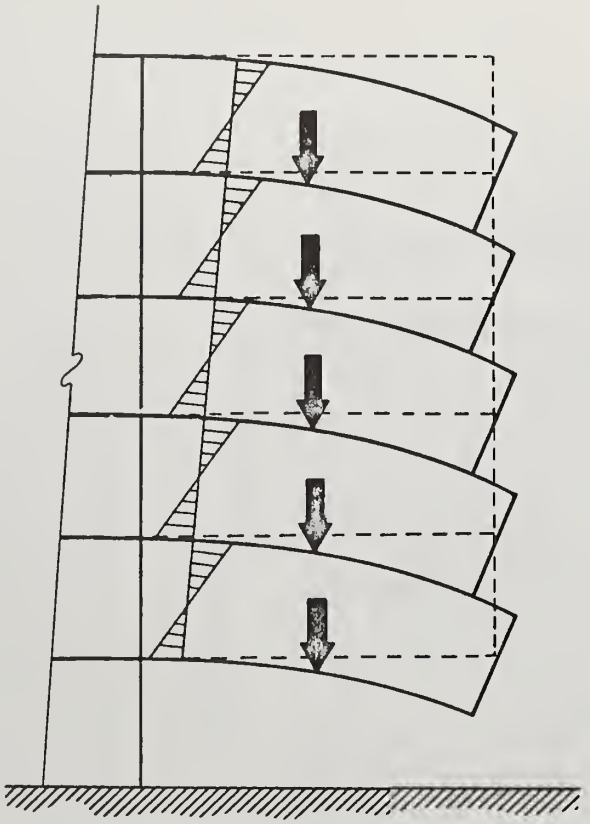

(a) No Shear Capacity in Horizontal Joints

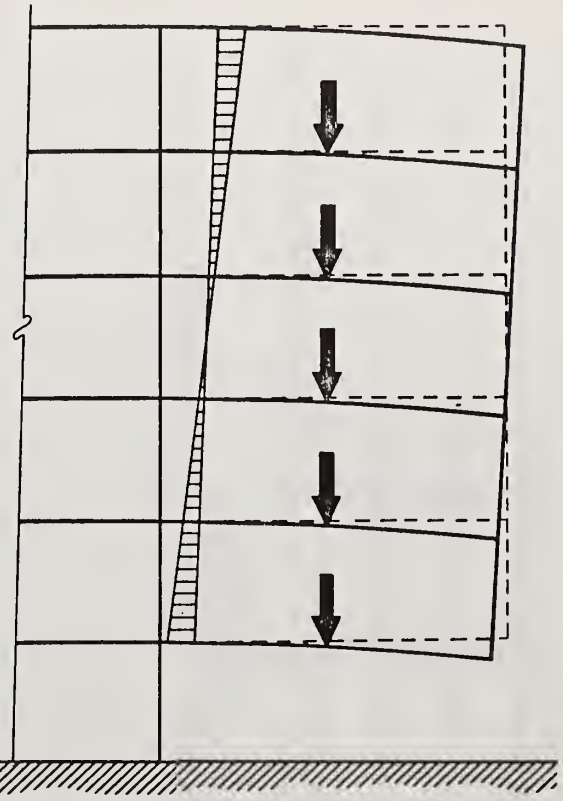

(b) Adequate Shear Capacity in Horizontal Joints

Figure 12. Modes of Cantilever Action

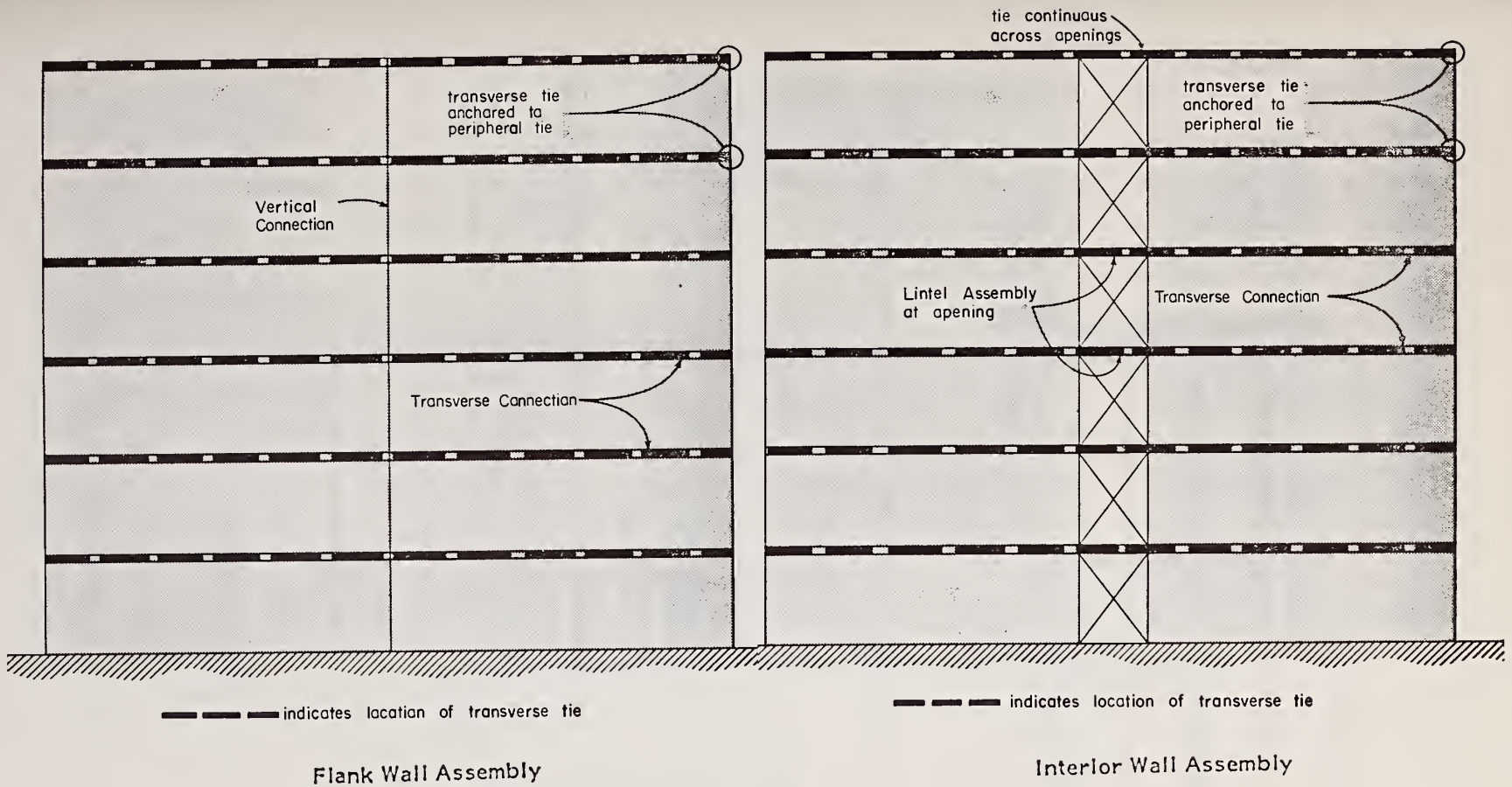

Figure 13. Suggested Extent and Location of Transverse Ties

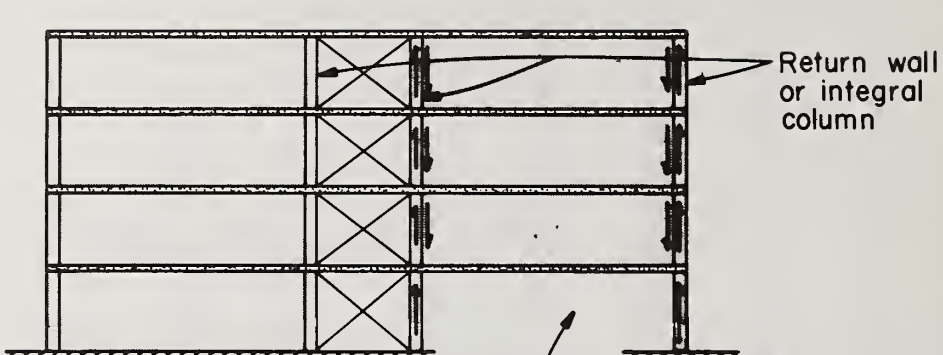

Section A - Wall Elevation

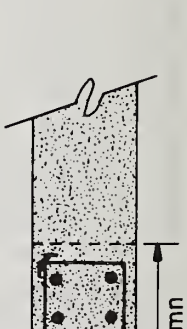

Plan Section
of Integral
Column

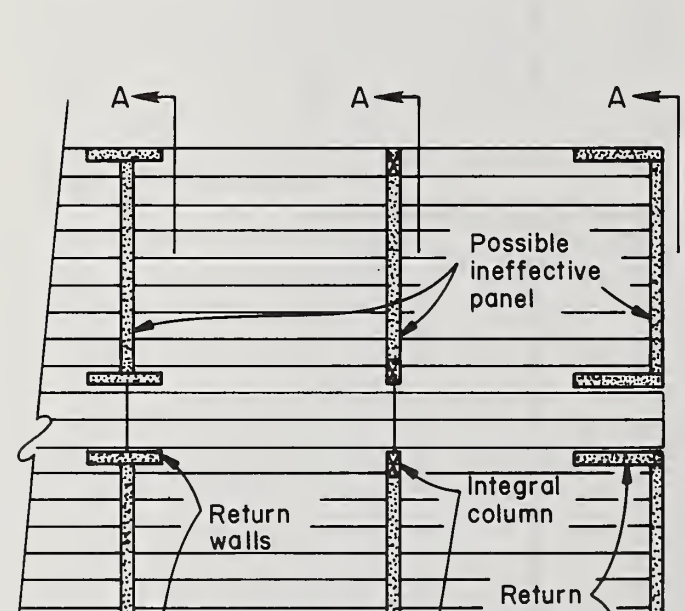

Partial Plan

Figure 14 Beam Mode--Single Vertical Wall Panel Stack

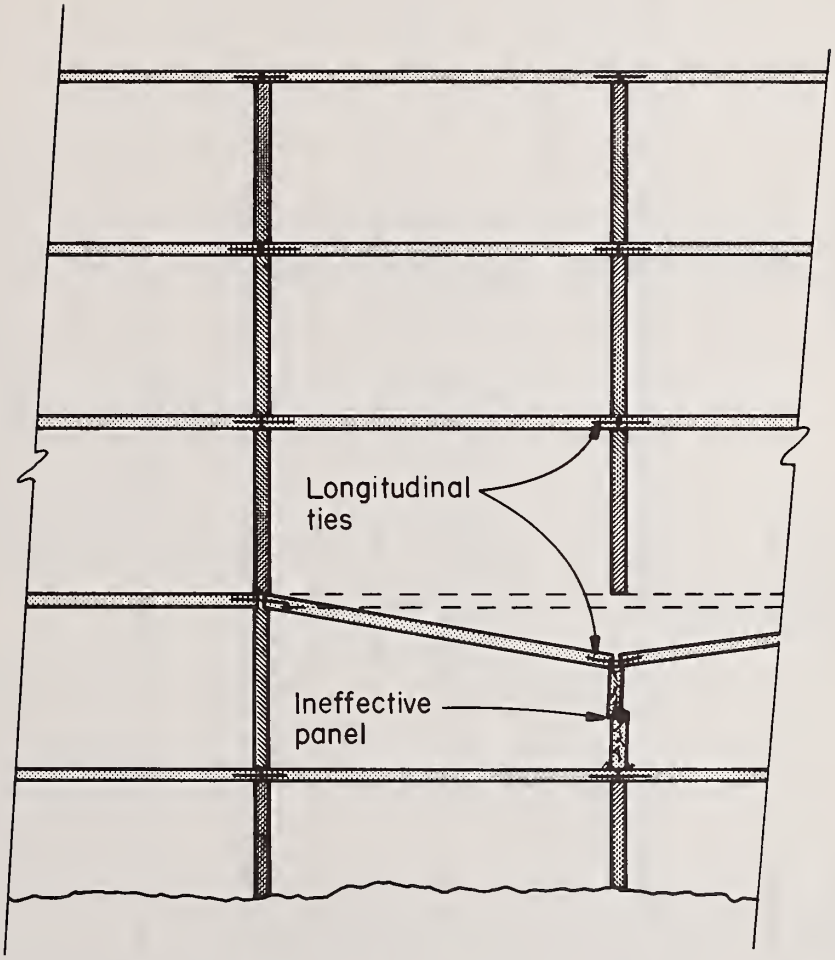

Figure 15 Partial Membrane Action of Floor Elements at Ineffective Wall Panel

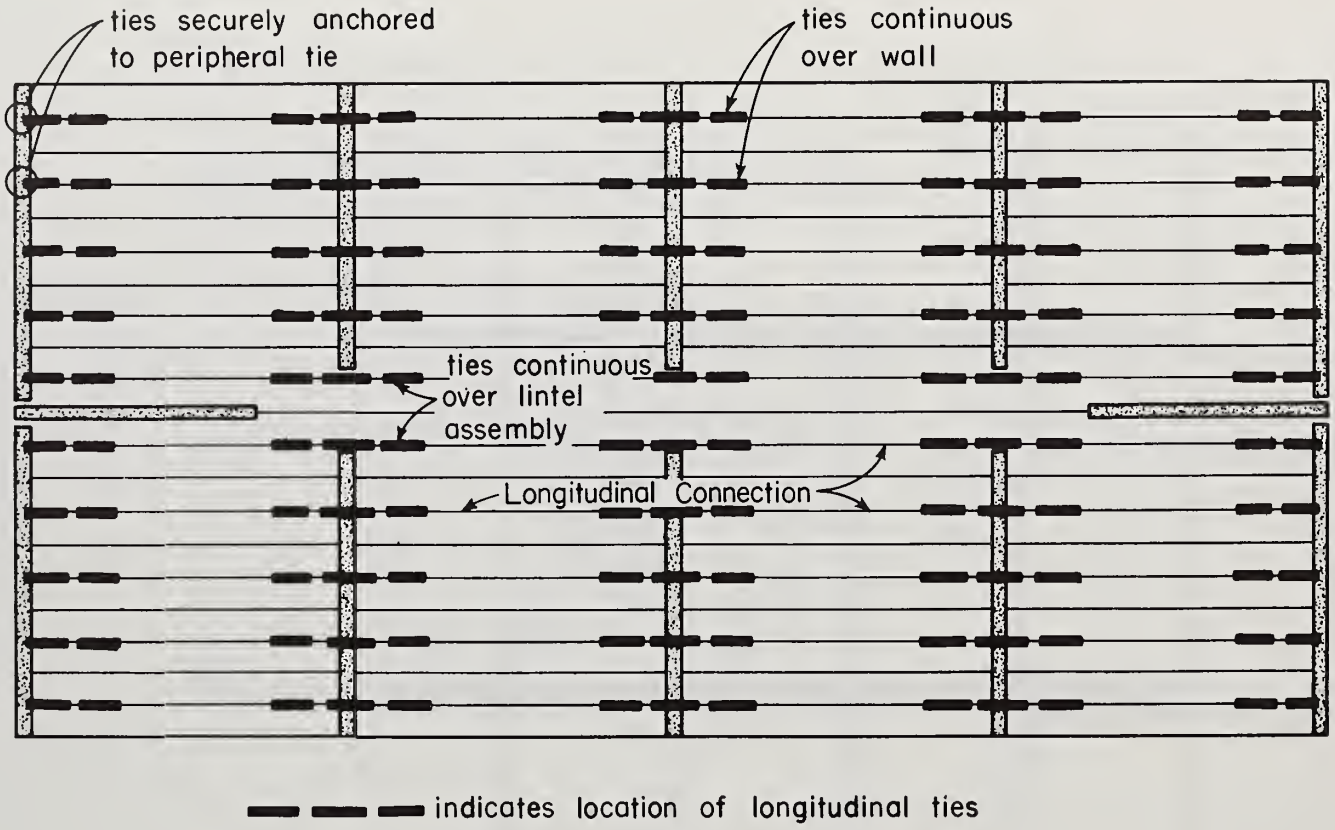

Typical Floor/Roof Panel Assembly

Figure 16 Suggested Extent and Location of Longitudinal Ties

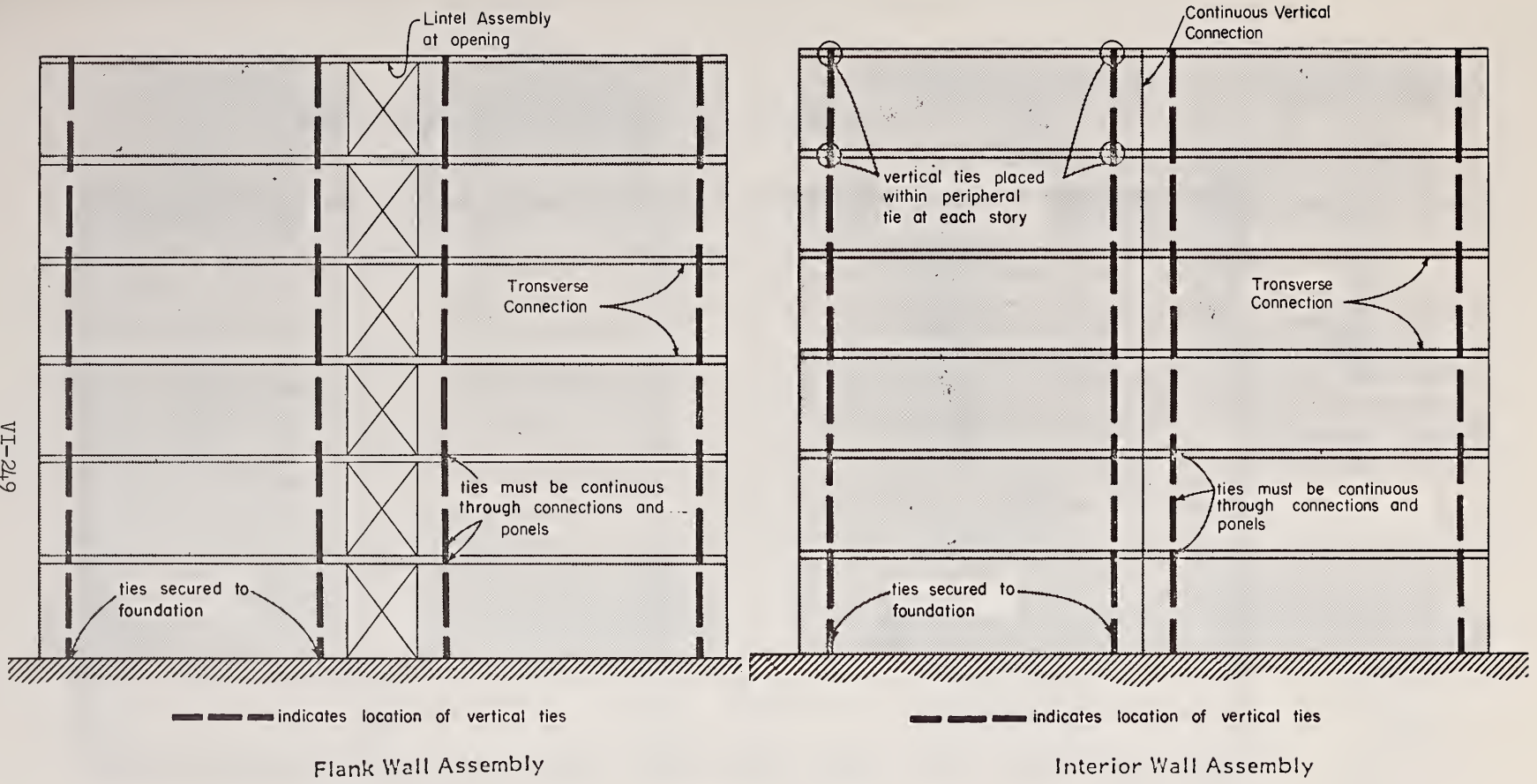

Figure 17. Suggested Bent and Location of Vertical Ties

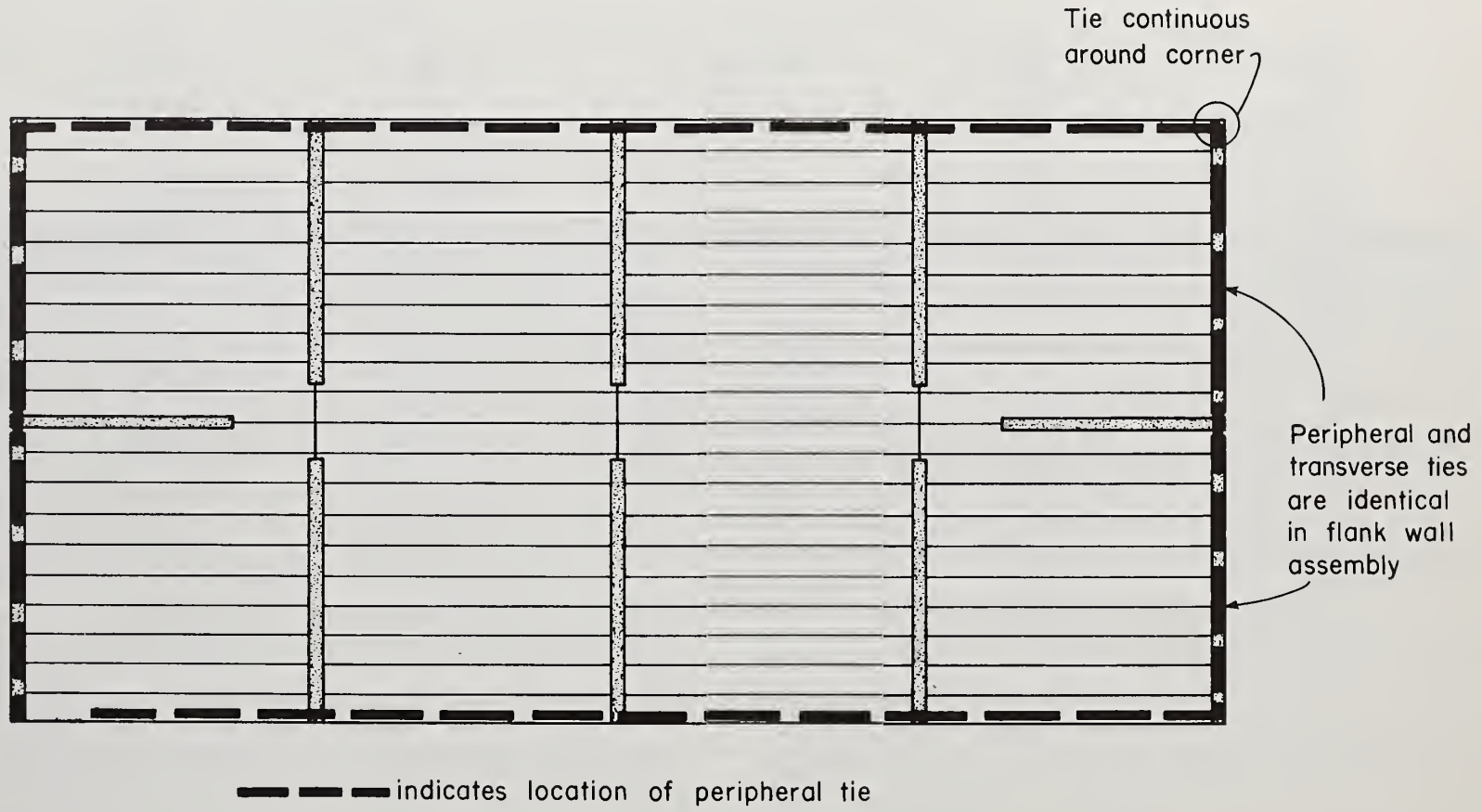

Figure 18. Suggested Peripheral Tie in Typical Roof/Floor Panel Assembly

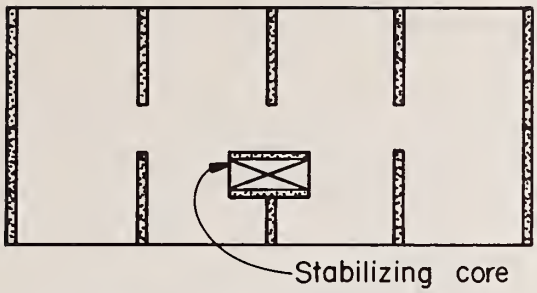

Longitudinal stabilizing core centrally located within building

(a) Undesirable Core Layout

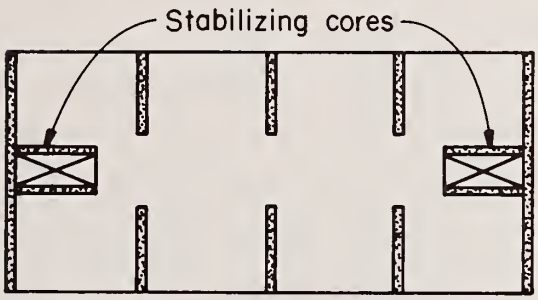

Longitudinal stabilizing cores distributed throughout building

(b) Desirable Core Layout

Figure 19 Possible Core Layouts in Typical Cross Wall Structure

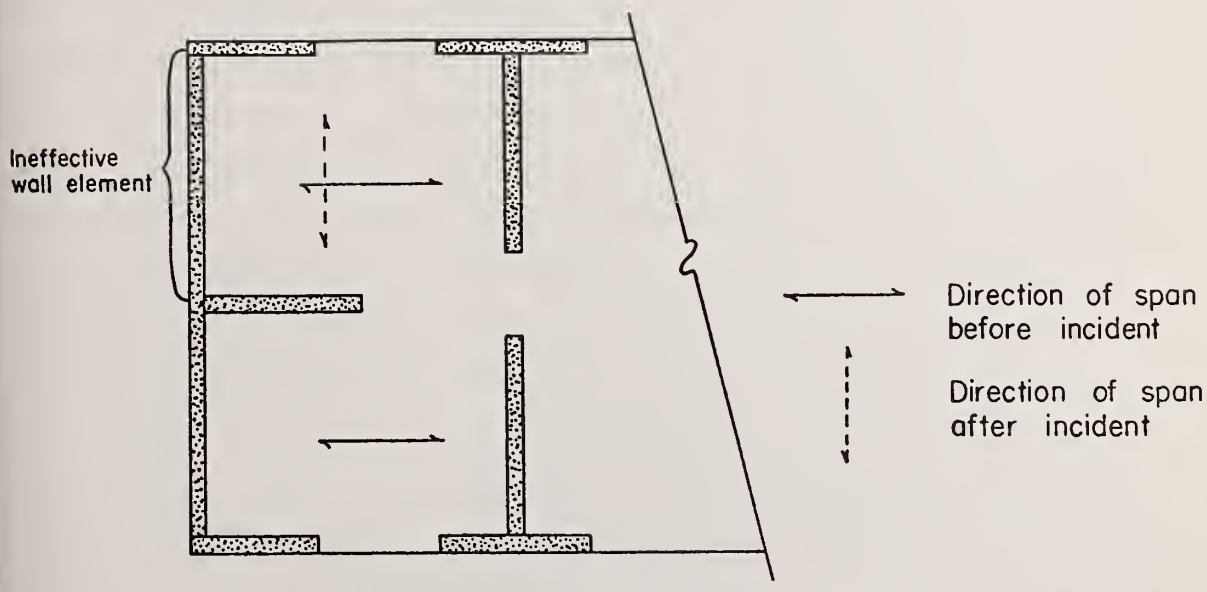

Figure 20 Change of Slab Span Direction under the Effects of Abnormal Loadings

Wind And Seismic Design of United States Nuclear Power Plants

LAWRENCE C. SHAO, RICHARD J. STUART and CHARLES H. HOFMAYER

Nuclear Regulatory Commission, Bethesda, Maryland

ABSTRACT

All U.S. Nuclear Power Plants are currently designed to resist the effects of severe and extreme environmental loads in combination with operating and accident loads (tornado and accident loads are not combined). This affords two levels of resistance to wind and seismic loads i.e., the plant can remain operational during and following the operating basis earthquake or the design wind, and shall be able to safely shut down following the design basis tornado or safe shutdown earthquake. The design wind parameters are normally selected based upon a one hundred year recurrence interval. These parameters (wind velocity, velocity vertical profiles, and applicable gust factors) are transformed into applied pressures on exposed surfaces of safety related structures considering the effects of ground exposure, shape coefficients and pressure profiles at discontinuities. The design basis tornado is selected as the most severe tornado that can reasonably be predicted at a site based on the geographical distribution of the frequency of tornado occurrence. The continental United States is divided into three tornado regions and for each region the following tornado characteristics are specified: the rotational wind speed, the translational wind speed, the pressure drop across the tornado, the rate of pressure drop and the radius of maximum rotational wind speed. The conversion of these parameters to design pressures must consider the orientation of the tornado relative to the structure as well as the other factors considered for the design wind. Various design tornado missiles and corresponding velocities are specified for each plant. Safety related structures are designed to resist both local damage (penetration and spalling) and overall structural response due to these missiles. The SSE*is chosen as the maximum earthquake expected to occur at the site and normally has a probability of occurrence of

KEY WORDS: Seismic effects; Wind; Tornado; Nuclear Power Plant

* Safe Shotdown Earthquake

less than 10^{-5}. The OBE is chosen as the earthquake which could reasonably be expected to affect the plant during its operating life; however, its magnitude cannot be less than one half that of the SSE. Vertical and horizontal ground acceleration values and broad band ground response spectra are specified for each plant site. A detailed dynamic analysis is required for each plant, including the consideration of the effects of damping, soil-structure interaction, three components of earthquake motion, combination of modal responses, etc. These considerations are detailed in recently published U.S. Nuclear Regulatory Commission's Standard Review Plans 3.7.1 Seismic Input, 3.7.2 Seismic System Analysis, 3.7.3 Seismic Subsystem Analysis and 3.7.4 Seismic Instrumentation.

INTRODUCTION

The regulations which govern the wind and seismic design of U.S. nuclear power plants are 10 CFR, Part 50, Appendix A - "General Design Criteria" and 10 CFR, Part 100, Appendix A - "Seismic and Geologic Siting Criteria". From these regulations the U.S. Nuclear Regulatory Commission has developed positions and Standard Review Plans[1] which detail approved techniques for satisfying 10 CFR requirements. The appropriate sections of the Standard Review Plans which cover wind, tornado and seismic design are listed in Table I.

Before discussing the details of wind and seismic design, it is helpful to review several cross sections through a reactor containment building. Figures 1 and 2 depict the containments for a typical Boiling Water Reactor (BWR) and a typical Pressurized Water Reactor (PWR), respectively. The reactor vessel is located in the center of both figures. In both of these cases the containment boundary is protected by a layer of reinforced concrete which is between two and one half (2-1/2') and five feet (5') thick. Between the reactor vessel and the containment are concrete walls which function in part, as both radiation and

---

[1] Standard Review Plan for the Review of Safety Analysis Reports for Nuclear Power Plants (NUREG-75/087), September 1975, U.S. Nuclear Regulatory Commission, Office of Nuclear Reactor Regulation, Washington, D. C. 20555

missile shields. Typical containment dimensions are 220 feet high by 140 feet in diameter with a 10 foot basemat. The plant embedment varies from thirty (30') to ninety feet (90') below grade. Although the bearing pressure is extremely high, power plants are founded on both soil and rock sites. Support buildings and control buildings are located adjacent to the containment and are more similar to conventional rectilinear buildings constructed of steel and concrete. However, the design of all safety related nuclear power plant structures far surpasses conventional structures in the severity of the design loads and in the precision of the analysis and design techniques. For example, there are two levels of both wind and seismic design. During the less severe events the plants are designed to remain fully operational and during the more severe events the plants are designed to safely insert control rods and shut the reactor down.

REQUIREMENTS FOR WIND LOADINGS

Design Wind

The design wind parameters are normally selected based on a one hundred (100) year recurrence interval. Figure 3 is a plot of the one hundred (100) year basic wind speed at thirty feet (30') above the ground for the continental United States.

Having the basic wind speed for a general location one must determine the vertical velocity profiles and applicable gust factors. These parameters are dependent upon the site, terrain, and surrounding structures and are generally determined from site specific meteorological data. These parameters are transformed into design pressures on the structures using ASCE Paper No. 3269[2] or ANSI A58.1-1972[3]. This transformation procedure considers the ground exposure, structural shape coefficients, gust factors and pressure profiles at discontinuities.

---

[2] ASCE Paper No. 3269, "Wind Forces On Structures," Transactions of the American Society of Civil Engrs., Vol. 126, Part II, (1961)

[3] ANSI A58.1-1972, "Building Code Requirements for Minimum Design Loads in Building and Other Structures," Committee A58.1, American National Standards Institute (1972)

As an example of the transformation considerations, Figure 4 illustrates a qualitative depiction of the pressure profiles of wind impinging on a rectangular structure.

Tornado Loads

Tornado design considerations constitute the second level of wind design of U.S. Nuclear Power Plants. The continental United States is divided into three tornado intensity regions as depicted in Figure 5. The most severe tornado effects occur in Region I. The Design Basis Tornado characteristics differ for each region and are summarized in Table II.

The qualitative distribution of the rotational wind speed and the pressure drop relative to the centerline of the tornado is shown in Figure 6. It is apparent from this distribution, that several tornado attitudes and locations must be investigated in order to determine the worst possible effects upon the structure.

Tables III and IV list typical missiles, missile parameters and corresponding velocities used in the design of nuclear safety related structures. These missiles vary slightly from plant to plant, but are intended to encompass the range of credible missiles which might affect plant operation during a tornado. The missiles listed in Table III are considered to be capable of striking in all directions. Missiles A, B, C, D, and E are to be considered at all elevations and missiles F and G at elevations up to thirty (30) feet above all grade levels within one half (1/2) mile of the facility structures. The "no-tumbling" horizontal missile velocities presented in the Topical Report TVA-TR74-1[4] are also acceptable provided that a four thousand pound (4000#) automobile at seventy (70) mph and elevations up to thirty (30) feet above grade level is added. These velocities are listed in Table IV. Vertical velocities equal to eighty percent (80%) of the TVA horizontal velocities listed in Table IV are also acceptable on an interim basis.

---

4 "The Generation of Missiles by Tornadoes," TVA-TR74-1, Tennessee Valley Authority (1974)

Given the tornado design parameters listed in Tables II, III and IV, one must consider the following items in the tornado design of each plant:

1. Transformation Procedures
    a. Wind Velocity to Pressure
    b. Missile Effective Loads
2. Failure of Non-Safety Related Structures Onto Category I Structures
3. Venting of Structures
4. Combinations of Tornado Design Parameters.

The transformation procedures to convert wind velocity to pressure and to account for building shape factors, are identical to those outlined under wind loading. The conversion of the missile parameters to structural effective loads is done by calculating the kinetic energy of the missile and subsequently converting that energy to structural reactions. Another consideration in tornado design is to insure that non-safety related structures will not collapse or generate missiles which might impact upon safety related (Category I) equipment or structures. Such structures must be designed to mitigate these failures although significant deformation may be permitted.

As depicted in Figure 7, venting of structures to reduce the consequences of the tornado negative pressure may reverse the normal pressure distribution due to wind. This process becomes even more complex when there are many vented cells within a structure and detailed air flow computer programs are necessary to solve such problems.

In order to determine the total tornado load (W_T) to be combined with dead loads, live loads, temperature loads, accident loads, etc, the wind, pressure and missile loads are combined as follows:

$$W_T = W_W$$

$$W_T = W_P$$

$$W_T = W_M$$

$$W_T = W_W + 0.5\ W_P$$

$$W_T = W_W + W_M$$

$$W_T = W_W + 0.5\ W_P + W_M$$

where: W_T = Total Tornado Load

W_W = Tornado Wind Load

W_P = Tornado Differential Pressure Load

W_M = Tornado Missile Load

It should be noted that fifty percent of the negative pressure load is combined with the wind load as depicted in Figure 6.

In order to mitigate the effects of missile impact, building walls are strengthened to function as missile barriers, or walls are constructed in the paths of potential missiles to function solely as missile barriers. These barriers could be constructed of concrete, steel, or composite construction and multiple barriers may also be employed. Acceptable methods to determine the depth of penetration for each barrier type are:

1. Concrete - depth of penetration by modified Petry as given by Amirikian[5] - prevent perforation, limit spalling and scabbing
2. Steel - depth of penetration by Stanford Research Institute Formula[6]
3. Composite and multiple barriers - by Recht and Ipson[7]

The overall structural damage of a barrier is normally determined by equating the kinetic energy of the missile to the elasto-plastic strain energy of the structural component during the impact. The acceptable deformation is limited by restricting the allowable ductility to a small percentage of the ultimate failure ductility for a particular component and failure mode. Moments, forces, and shears are

---

[5] A. Amirikian, "Design of Protective Structures," Bureau of Yards and Docks, Publication No. NAVDOCKS P-51, Department of the Navy, Washington, D. C. (August 1950).

[6] W. B. Cottrell and A. W. Savolainen, "U.S. Reactor Containment Technology," ORNL-NSIC-5, Vol. 1, Chapter 6, Oak Ridge National Laboratory.

[7] R. F. Recht and T. W. Ipson, "Ballistic Perforation Dynamics," Journal of Applied Mechanics, Transactions of the ASME, Vol. 30, Series E, No. 3, September 1963.

calculated by developing plastic hinges and using standard formulation for determining their magnitudes. An alternate acceptable method to determine missile loads on structures is an equivalent static load technique developed by Williamson and Alvy[8].

REQUIREMENTS FOR EARTHQUAKE LOADINGS

The design wind and tornado loads are classified, respectively as severe and extreme environmental conditions. In addition to these loads there is another set of severe and extreme environmental loads which must also be considered. They are the Operating Basis Earthquake (OBE), and the Safe Shutdown Earthquake (SSE), respectively. As with the design wind and the tornado, a nuclear power plant must remain operational during an OBE and must be capable of safely shutting down during an SSE.

Seismic Input

The design parameters for both design events are the ground acceleration values determined from site investigations of geology, proximity to faults and the surrounding tectonic provinces, and the design response spectra specified in Regulatory Guide (R.G.) 1.60[9]. A typical R.G. 1.60 spectra is depicted in Figure 8. This response spectra was determined by subjecting a series of linear oscillators of varying frequencies to all available earthquake time histories recorded in the U.S. and enveloping those results. Given the design parameters, the procedure to determine the building floor response spectra considering soil structure interaction, damping values and the analytical model will be discussed in more detail.

Variation of soil properties is considered in the analysis procedure as illustrated in Figure 8. The resulting basemat response is then enveloped for use in determining the floor response.

---

[8] R. A. Williamson and R. R. Alvy, "Impact Effect of Fragments Striking Structural Elements," Holmes and Narver, Inc., Revised November 1973.

[9] Regulatory Guide 1.60, "Design Response Spectra for Nuclear Power Plants," USNRC, Washington, D. C. 20555

The method of analysis for soil supported sites utilizes a finite element grid as depicted in Figure 9. Having developed a synthetic time history at the rock layer which envelops the Regulatory Guide 1.60 spectra in the free field, this input motion is used to determine the response of the basemat and other major structural elements. On rock sites a simpler model, depicted in Figure 10, is acceptable. The spring constants and damping coefficients are normally determined by using an infinite half space model. The acceptable analytical tools for soil-structure interaction are listed in Table V as a function of the supporting geological medium.

Seismic System Analysis

Given the basemat response, a more detailed model is developed for the remainder of the structure and major systems and components. These models are normally three dimensional or axisymmetric. In the development of these models, in the analysis procedure and in the evaluation of the results, the following considerations must be made:

1. Seismic Analysis Methods
2. Natural Frequencies and Response Loads
3. Procedures Used for Analytical Modeling
4. Soil-Structure Interaction
5. Development of Floor Response Spectra
6. Three Components of Earthquake Motion
7. Combination of Modal Responses
8. Interaction of Non-Category I Structures with Category I Structures
9. Effects of Parameter Variations on Floor Responses
10. Use of Constant Vertical Static Factors
11. Methods Used to Account for Torsional Effects
12. Comparison of Responses
13. Methods for Seismic Analysis of Category I Dams
14. Determination of Category I Structure's Overturning Moments
15. Analysis Procedure for Damping

These items are discussed in great detail in the NRC Standard Review Plan 3.7.2 (and

the reader is referred to that document). Table VI and Figure 11 depict two of these considerations. Table VI is a list of acceptable damping values from Regulatory Guide 1.61[10]. Using these values with the appropriate analytical tools one can develop floor response spectra for use in equipment design and qualification. As depicted in Figure 11, the design peak is broadened fifteen percent (15%) on either side of the predicted peak in order to account for possible variations in the analytical technique and the input parameters.

Seismic Subsystem Analysis

Smaller components and piping systems are analyzed in a similar manner. They are classified as subsystems. In the analysis of such systems, the following items are considered:

1. Seismic Analysis Methods
2. Determination of Number of Earthquake Cycles
3. Procedures Used for Analytical Modeling
4. Basis for Selection of Frequencies
5. Use of Equivalent Static Load Method of Analysis
6. Three Components of Earthquake Motion
7. Combination of Modal Responses
8. Analytical Procedures for Piping Systems
9. Multiply-Supported Equipment and Components With Distinct Inputs
10. Use of Constant Vertical Static Factors
11. Torsional Effects of Eccentric Masses
12. Category I Buried Piping Systems and Tunnels
13. Interaction of Other Piping with Category I Piping
14. Seismic Analyses for Reactor Internals
15. Analysis Procedure for Damping

---

[10] Regulatory Guide 1.61, "Damping Values for Seismic Analysis for Nuclear Power Plants," USNRC, Washington, D. C. 20555

Seismic Instrumentation

In order to monitor the ground acceleration and response spectra during a seismic event, the NRC requires the following seismic instrumentation requirements[11]:

1. Triaxial Time History Accelerograph
2. Triaxial Response Spectrum Recorder
3. Seismic Switch

Such instrumentation is not only used to provide an historical record of the structural response, but it is also used to provide operator notification for shut down of the plant when the OBE ground acceleration is exceeded.

The number and location of typical seismic instrumentation is depicted in Table VII. The recorded data from such instrumentation is used to compare the predicted response of structures, systems and components with the response measured during a seismic event. To date, the predicted response has always enveloped the measured response.

CONCLUSION

A brief discussion of wind and seismic design of U.S. nuclear power plants has been presented. All plants are currently designed to resist the effects of severe and extreme environmental loads in combination with operating and accident loads (tornado and accident loads are not combined). This affords two levels of resistance to wind and seismic loads, i.e. the plant can remain operational during and following the operating basis earthquake or the design wind, and shall be able to safely shut down following the design basis tornado or safe shutdown earthquake. More detailed information with regard to any of the items discussed can be obtained from the documents referenced in this discussion.

---

[11] Regulatory Guide 1.12, "Instrumentation for Earthquakes," USNRC, Washington, D. C. 20555

TABLE I — U.S. NUCLEAR REGULATORY COMMISSION STANDARD REVIEW PLANS

Section	Topic
3.3.1	Wind Loadings
3.3.2	Tornado Loadings
3.5.3	Barrier Design Procedures
3.7.1	Seismic Input
3.7.2	Seismic System Analysis
3.7.3	Seismic Subsystem Analysis
3.7.4	Seismic Instrumentation

TABLE II — DESIGN BASIS TORNADO CHARACTERISTICS

REGION	MAXIMUM WIND SPEED[a] (mph)	ROTATIONAL SPEED (mph)	TRANSLATIONAL SPEED (mph)		RADIUS OF MAXIMUM ROTATIONAL SPEED (feet)	PRESSURE DROP (psi)	RATE OF PRESSURE DROP (psi/sec)
			MAXIMUM	MINIMUM[b]			
I	360	290	70	5	150	3.0	2.0
II	300	240	60	5	150	2.25	1.2
III	240	190	50	5	150	1.5	0.6

[a]THE MAXIMUM WIND SPEED IS THE SUM OF THE ROTATIONAL SPEED COMPONENT AND THE MAXIMUM TRANSLATIONAL SPEED COMPONENT.

[b]THE MINIMUM TRANSLATIONAL SPEED, WHICH ALLOWS MAXIMUM TRANSIT TIME OF THE TORNADO ACROSS EXPOSED PLANT FEATURES, IS TO BE USED WHENEVER LOW TRAVEL SPEEDS (MAXIMUM TRANSIT TIME) ARE A LIMITING FACTOR IN DESIGN OF THE ULTIMATE HEAT SINK. THE ULTIMATE HEAT SINK IS THAT COMPLEX OF WATER SOURCES, INCLUDING ASSOCIATED RETAINING STRUCTURES, AND ANY CANALS OR CONDUITS CONNECTING THE SOURCES WITH; BUT NOT INCLUDING, THE INTAKE STRUCTURES OF NUCLEAR REACTOR UNITS, REGULATORY GUIDE 1.27 (SAFETY GUIDE 27), "ULTIMATE HEAT SINK." DESCRIBES A BASIS THAT MAY BE USED TO IMPLEMENT GENERAL DESIGN CRITERION 44 OF APPENDIX A TO 10 CFR PART 50 WITH REGARD TO THE ULTIMATE HEAT SINK.

TABLE III — TYPICAL TORNADO MISSILES USED IN THE DESIGN OF NUCLEAR SAFETY RELATED STRUCTURES

		Fraction of Total Tornado Velocity
A.	Wood Plank, 4 In. x 12 In. x 12 Ft., Weight 200 Lb.	0.8
B.	Steel Pipe, 3 In. Diameter, Schedule 40, 10 Ft. Long, Weight 78 Lb.	0.4
C.	Steel Rod, 1 In. Diameter x 3 Ft. Long, Weight 8 Lb.	0.6
D.	Steel Pipe, 6 In. Diameter, Schedule 40, 15 Ft. Long, Weight 285 Lb.	0.4
E.	Steel Pipe, 12 In. Diameter, Schedule 40, 15 Ft. Long, Weight 743 Lb.	0.4
F.	Utility Pole, 13½ In. Diameter, 35 Ft. Long, Weight 1490 Lb.	0.4
G.	Automobile, Frontal Area 20 $Ft.^2$, Weight 4000 Lb.	0.2

TABLE IV — TYPICAL TORNADO MISSILES BASED ON TVA TOPICAL REPORT

		Horizontal Velocity Ft./Sec.
A.	Wood Plank, 4 In. x 12 In. x 12 Ft., Weight 200 Lb.	368
B.	Steel Pipe, 3 In. Diameter, Schedule 40, 15 Ft. Long, Weight 115 Lb.	268
C.	Steel Rod, 1 In. Diameter x 3 Ft. Long, Weight 8 Lb.	259
D.	Steel Pipe, 6 In. Diameter, Schedule 40, 15 Ft. Long, Weight 285 Lb.	230
E.	Steel Pipe, 12 In. Diameter, Schedule 40, 30 Ft. Long, Weight 1500 Lb.	205
F.	Utility Pole, 14 In. Diameter, 35 Ft. Long, Weight 1500 Lb.	241
G.	Automobile, Frontal Area 20 $Ft.^2$, Weight 4000 Lb.	100

TABLE V — ACCEPTABLE METHODS FOR SOIL-STRUCTURE INTERACTION ANALYSIS

METHOD OF SOIL-STRUCTURE INTERACTION ANALYSIS	ROCK * * FOUNDATION	DEEPLY EMBEDDED CASE †	SOIL FOUNDATION * SHALLOWLY EMBEDDED CASE		
			DEEP SOIL FOUNDATION W/UNIFORM PROPERTIES	DEEP SOIL FOUNDATION W/LAYERED PROPERTIES	SHALLOW SOIL FOUNDATION
SINGLE LUMPED MASS-SPRING APPROACH	X		X		
MULTIPLE LUMPED MASS-SPRING APPROACH ††	X		X	X	X
FINITE ELEMENT APPROACH ††	X	X	X	X	X

* SOIL FOUNDATION MEANS THE DEPTH OF SOIL BETWEEN THE BOTTOM OF THE FOUNDATION SLAB AND THE BASE ROCK.

** A MEDIUM FOR WHICH THE SOIL-STRUCTURE INTERACTION EFFECT IS NEGLIGIBLE OR ALTERNATELY, A MEDIUM WITH A SHEAR WAVE VELOCITY GREATER THAN OR EQUAL TO 3500 fps.

† DEEP EMBEDMENT: ACTUAL EMBEDDED DEPTH $>$15% OF THE LEAST BASE WIDTH OR OTHER APPROPRIATE VALUE TO BE JUSTIFIED.

†† OR EQUIVALENT.

TABLE VI — DAMPING VALUES
(PERCENT OF CRITICAL DAMPING)

STRUCTURE OR COMPONENT	OPERATING BASIS EARTHQUAKE OR ½ SAFE SHUTDOWN EARTHQUAKE[1]	SAFE SHUTDOWN EARTHQUAKE
Equipment and Large-Diameter Piping Systems[2]		
Pipe Diameter Greater Than 12 Inches	2	3
Small-Diameter Piping Systems, Diameter Equal to or Less Than 12 Inches	1	2
Welded Steel Structures	2	4
Bolted Steel Structures	4	7
Prestressed Concrete Structures	2	5
Reinforced Concrete Structures	4	7

1. In the dynamic analysis of active components as defined in Regulatory Guide 1.48, these values should also be used for SSE.

2. Includes both material and structural damping. If the piping system consists of only one or two spans with little structural damping, use values for small diameter piping.

TABLE VII — SEISMIC INSTRUMENTATION REQUIREMENTS

INSTRUMENTATION		TRIAXIAL TIME-HISTORY ACCELEROGRAPH		TRIAXIAL RESPONSE SPECTRUM RECORDER		TRIAXIAL PEAK ACCELEROGRAPH		SEISMIC SWITCH	
LOCATION	SSE	0.3G Or LESS	OVER 0.3G	0.3G Or LESS	OVER 0.3G	0.3G Or LESS	OVER 0.3G	0.3G Or LESS	OVER 0.3G
I. Free Field		1	1						
II. Inside Containment									
Basement		1* **	1* **	1*	1*			1*	1*
At Elevation		1	1						
Reactor Equipment Sup.				1***	1***				1***
Reactor Piping Sup.									
Reactor Equipment						1	1		
Reactor Piping						1	1		
III. Outside Containment									
Cat. I Structure			1	1	1				
Cat. I Equip. Sup.					1				
Cat. I Piping Sup.				1***	1				
Cat. I Equipment							1		
Cat. I Piping						1***	1		

* Control Room Readout
** May be Omitted if Soil-Structure Interaction is Negligible.
*** Denotes Either of the Two Locations.

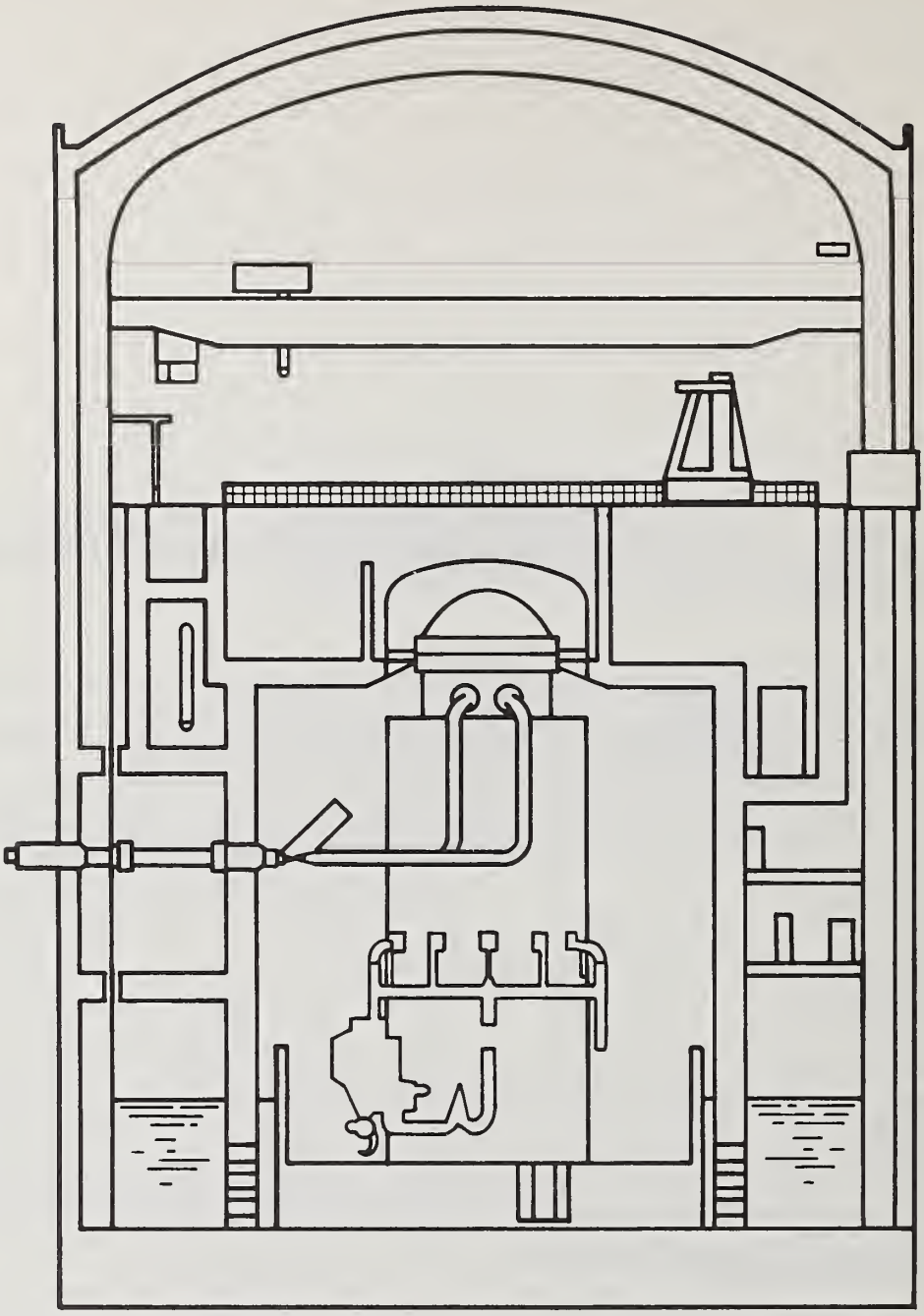

FIGURE 1 — CONTAINMENT FOR TYPICAL BOILING WATER REACTOR

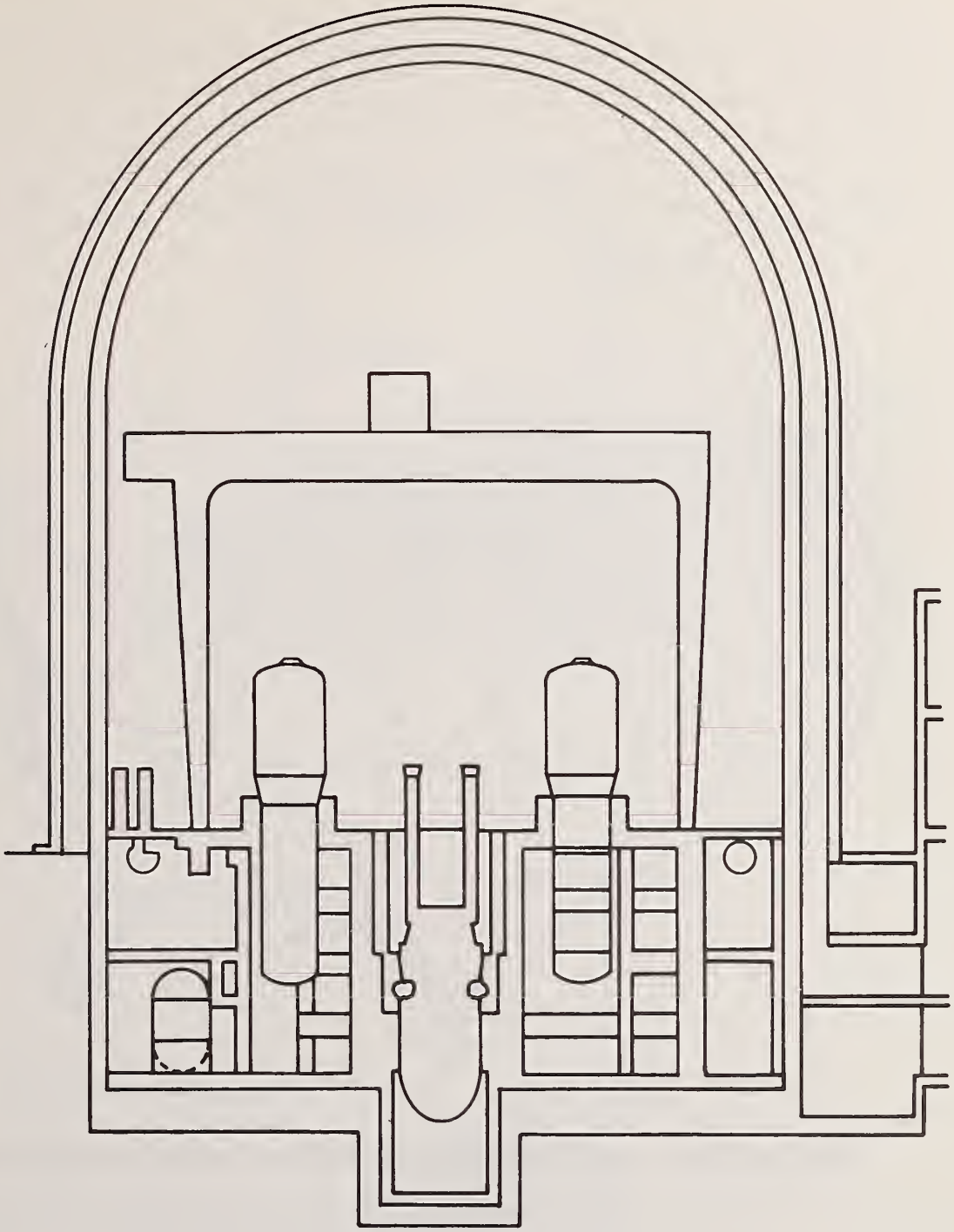

FIGURE 2 — CONTAINMENT FOR TYPICAL PRESSURIZED WATER REACTOR

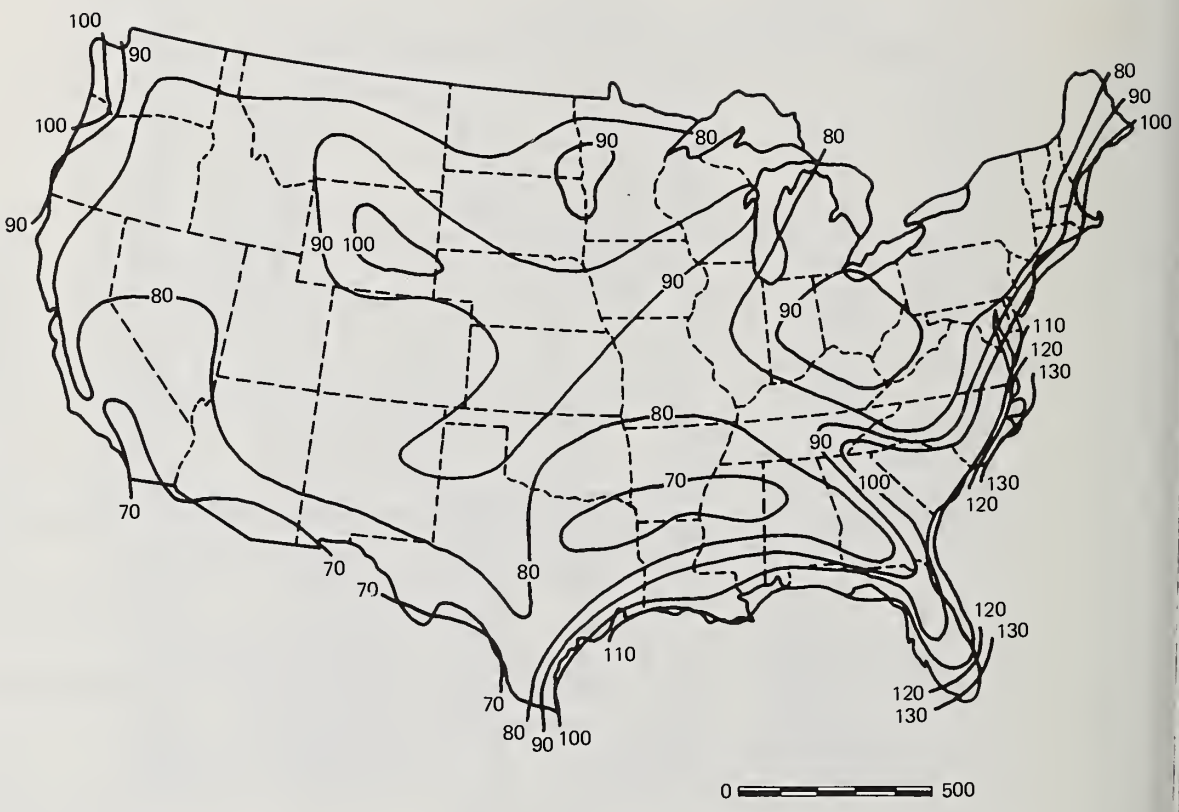

FIGURE 3 — BASIC WIND SPEED IN MILES PER HOUR 100 YEAR MEAN RECURRENCE INTERVAL

(ANNUAL EXTREME FASTEST - MILE SPEED 30 FEET ABOVE GROUND)

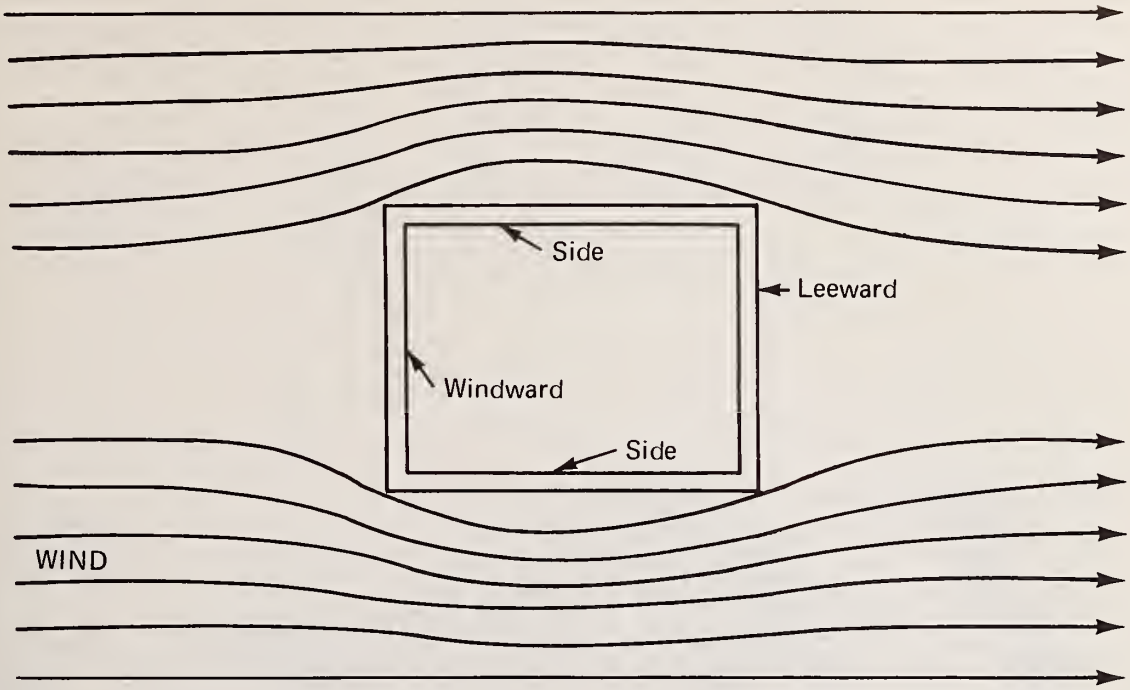

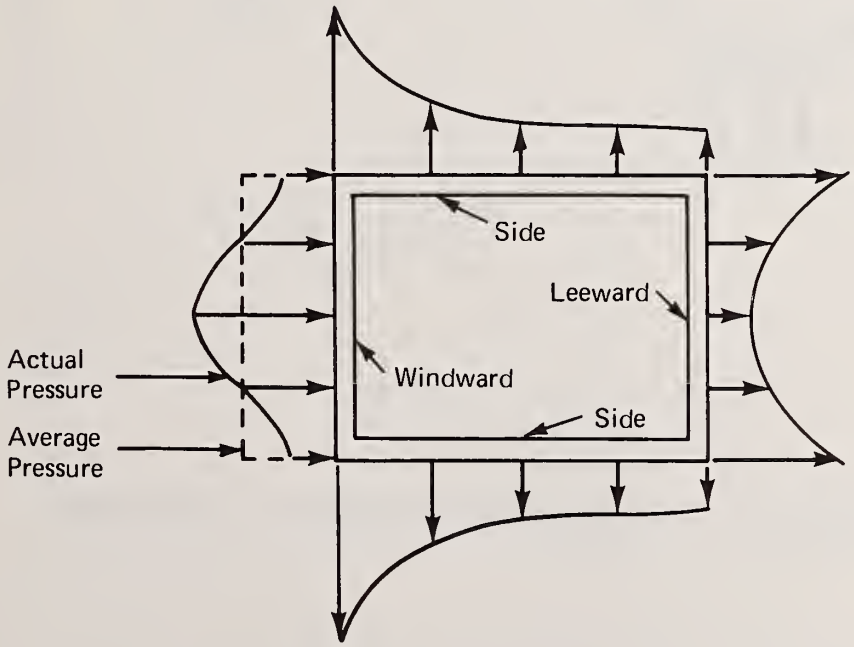

FIGURE 4 — WIND PRESSURE DISTRIBUTION ON WALLS

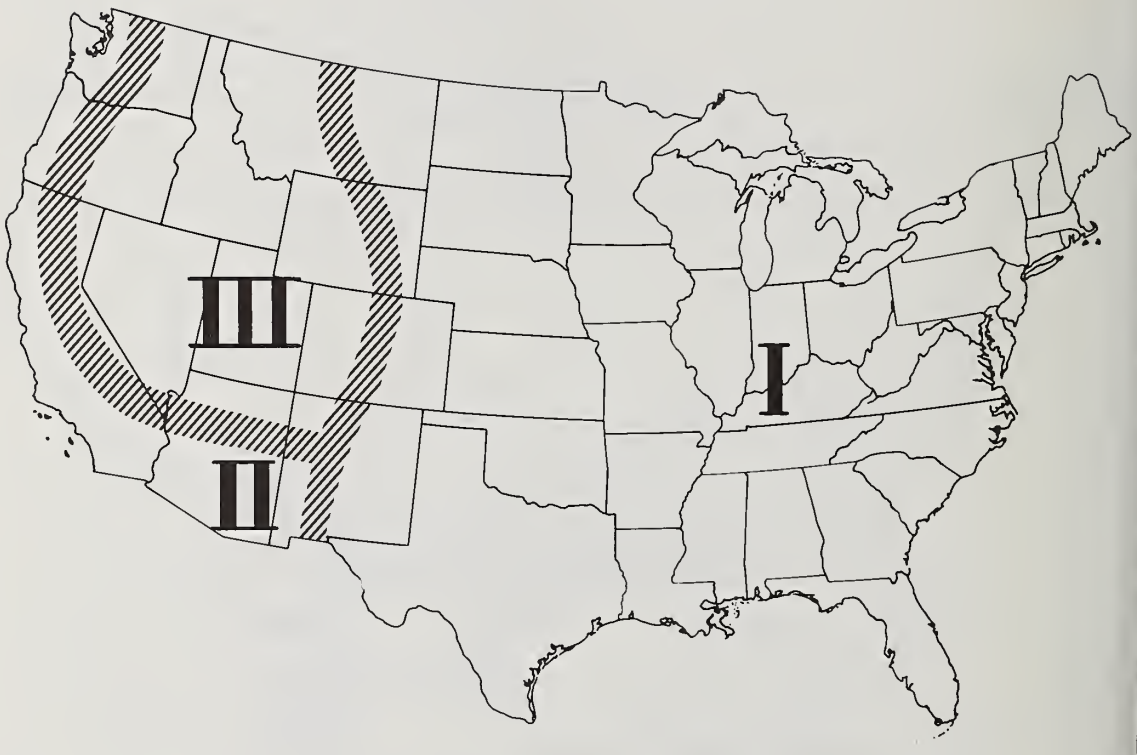

FIGURE 5 — TORNADO INTENSITY REGIONS

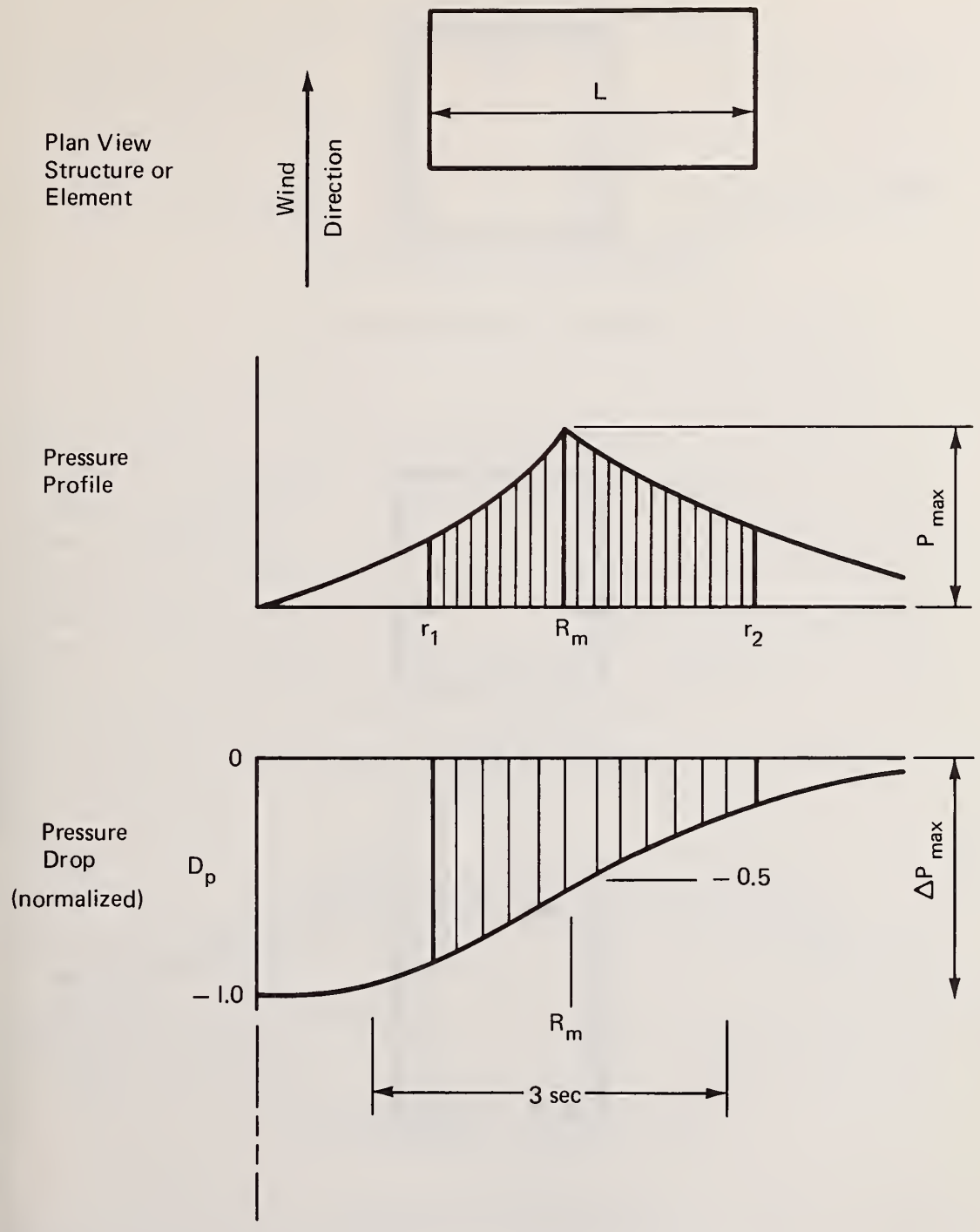

FIGURE 6 — DISTRIBUTION OF ROTATIONAL WIND SPEED AND PRESSURE DROP RELATIVE TO THE CENTERLINE OF THE TORNADO

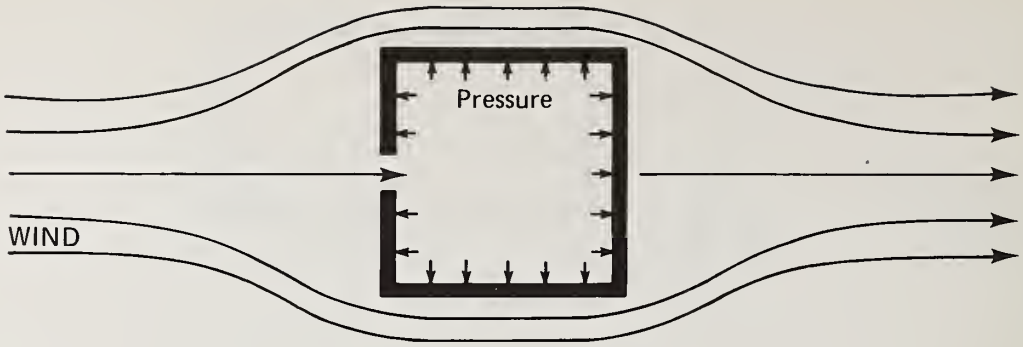

OPENING IN WINDWARD WALL

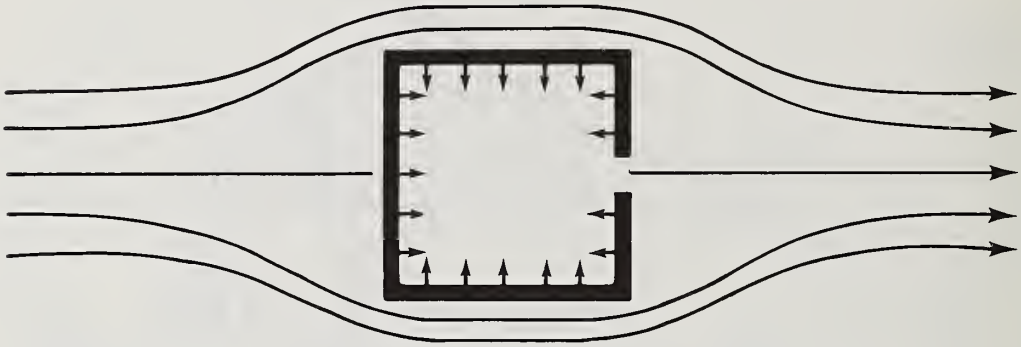

OPENING IN LEEWARD WALL

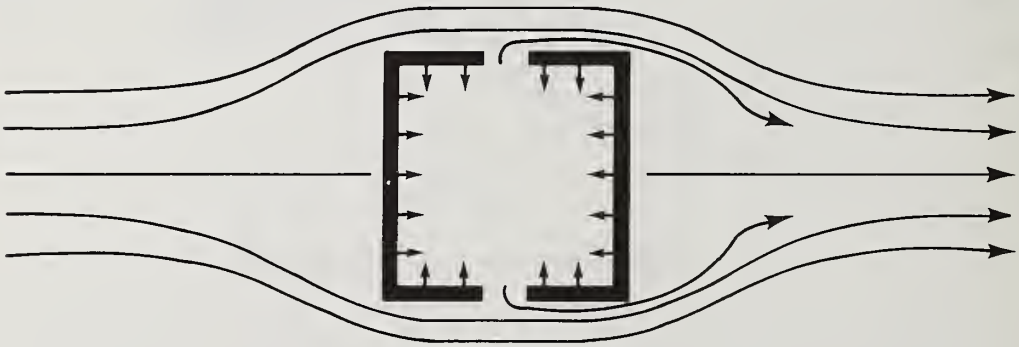

OPENING IN SIDE WALLS

Note: Pressures shown are due to effects of openings only.

FIGURE 7 — WIND PRESSURE DISTRIBUTION DUE TO OPENINGS IN THE STRUCTURE

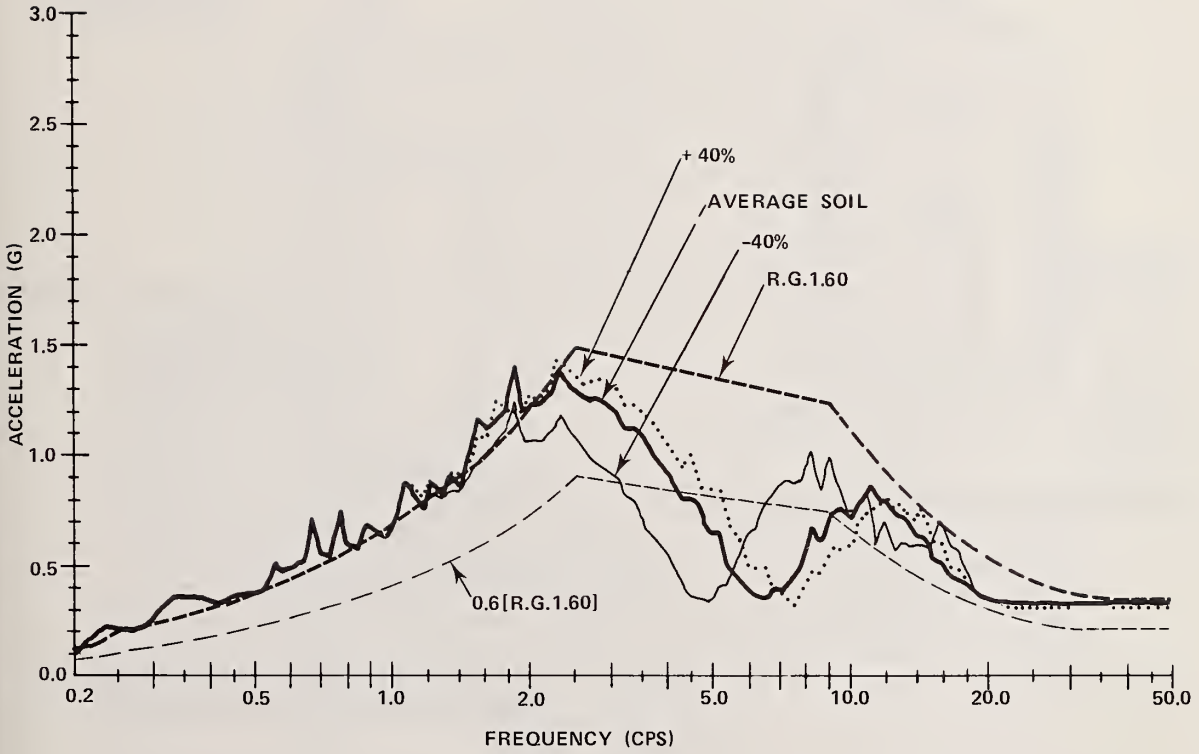

FIGURE 8 — FREE FIELD R.G.I.60 AND 60% OF R.G.I.60 COMPARED TO BASEMAT RESPONSE AFTER DECONVOLUTION WITH ± 40 PERCENT VARIATION OF SOIL PROPERTIES

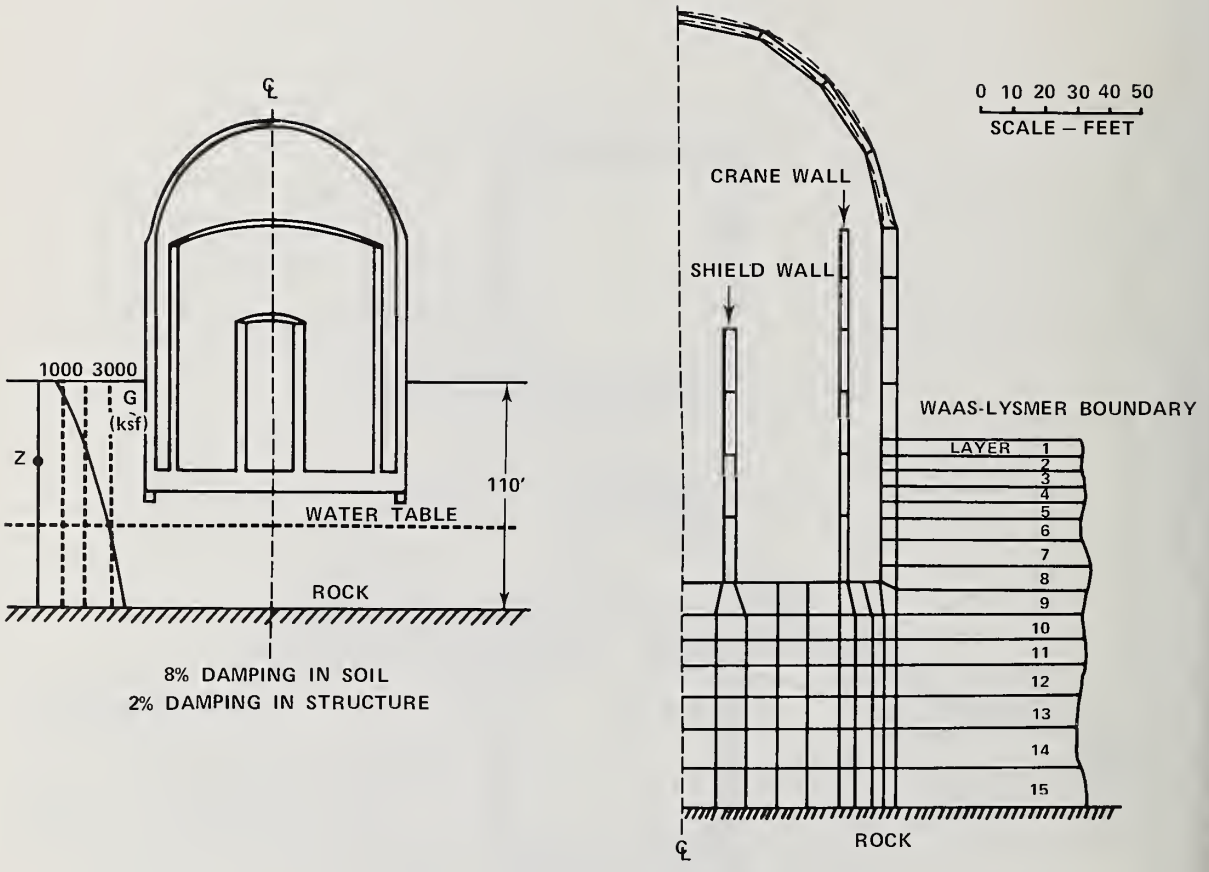

FIGURE 9 — SOIL-STRUCTURE SYSTEM REPRESENTED BY AXI-SYMMETRIC FINITE ELEMENTS

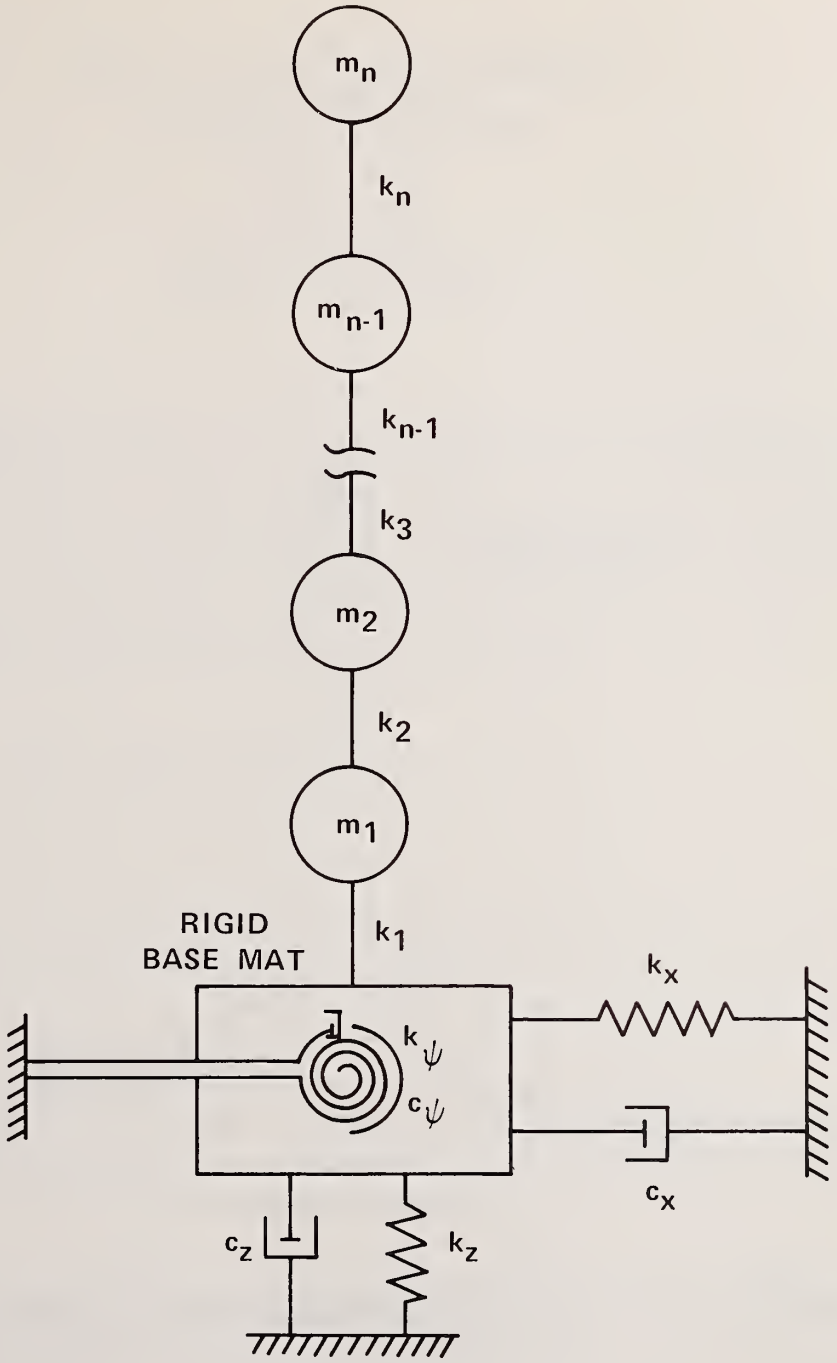

FIGURE 10 — A LUMPED MASS MODEL OF STRUCTURE-FOUNDATION SYSTEM

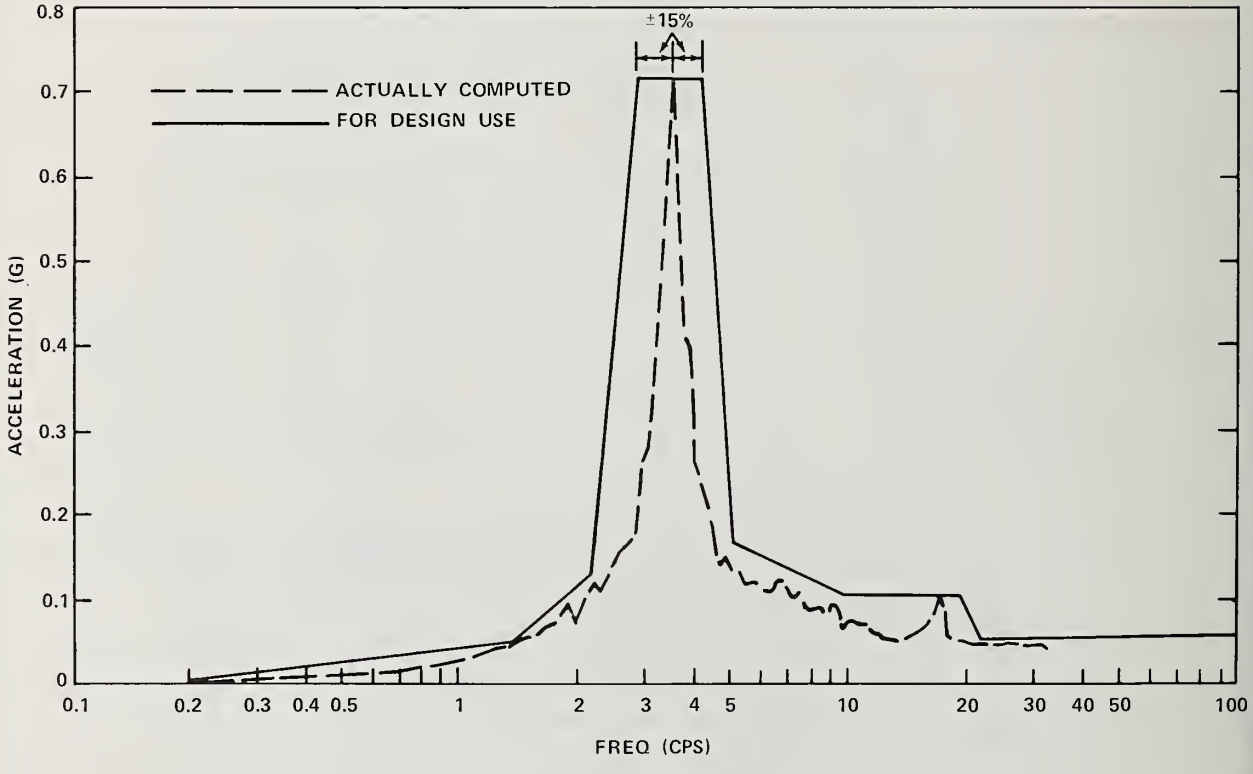

FIGURE 11 — FLOOR RESPONSE SPECTRUM CURVE

OUTLINE OF BASIC PHILOSOPHY AND PRACTICES OF ASEISMATIC DESIGN FOR NUCLEAR FACILITIES IN JAPAN

MAKOTO WATABE
YORIHIKO OHSAKI
Chief, IISEE
Building Research Institute
Ministry of Construction
Japan

ABSTRACT

In Japan, consistent standard specifications or guide lines for the aseismatic design of nuclear facilities has not officially been established. Only recently, in March 1975, has the Regulatory Guide of Design Earthquake Ground Motions for Nuclear Power Facilities been proposed. The proposed Regulatory Guide has already had an effect in a practical sense in spite of its interim nature. It is the purpose of this paper to briefly summarize the design philosophies and procedures of this aseismatic design currently being used in practice in Japan.

Key Words: Design Guides, Nuclear Facilities.

1. Foreward

The Aseismic Design Committee was established on September 25, 1974, at the 129th meeting of the Examination Committee on Reactor Safeguards for the purpose of reviewing the fundamental concept underlying the articles related to aseismic design of nuclear power facilities in "the Regulatory Guide for Safety Design of Light Water Reactors", of the Japan Atomic Energy Commission, which has been in effect since April, 1970.

Since the first meeting on October 30, 1974, five meetings have since been held, and a tentative conclusion has been arrived at recently on the regulatory guide of earthquake ground motions for aseismic design of nuclear power facilities as is shown in this Interim Report.

The Aseismic Design Committee is presently continuing to investigate matters to be attended to in the practical application of this regulatory guide, and the results will be appended as a commentary to the regulatory guide afterwards.

Further, "Aseismic Design Classification of Nuclear Power Facilities" and "Load Combinations and Evaluation of Stresses" will be investigated and, upon completion, the final report will be published as "Regulatory Guide for Aseismic Design of Nuclear Power Facilities" (tentative title) including the "Regulatory Guide of Design Earthquake Ground Motions for Nuclear Power Facilities".

The design earthquake ground motions [1] for aseismatic design of nuclear power facilities shall be determined based on earthquake motions at the surface of the base

stratum (1,2) in the proposed site. Where the surface of the base stratum remarkably undulates, is excavated, or is overlain by surface layers (1,3), the effects thereof shall be taken separately into account.

The design earthquake ground motions at the free surface (1,4) of the base stratum (hereinafter referred to as "the basic design earthquake ground motions") in the proposed site shall be determined in accordance with fundamental concepts as described in the following items:

1. The basic design earthquake ground motions are classified into S1 and S2 depending upon the intensity.

(a) The basic design earthquake ground motions S1 are such ground motions as considered to be caused at the free surface of the base stratum in the proposed site by the maximum design earthquakes.

The maximum design earthquake is referred to that which causes the free surface of the base stratum, in the proposed site, the most unfavorable ground motions among earthquakes which are expected to occur.

(b) The basic design earthquake ground motions S2 are such ground motions as considered to be caused at the free surface of the base stratum in the proposed site by the extreme design earthquakes.

The extreme design earthquakes, is referred to that which causes the free surface of the base stratum, in the proposed site, the most unfavorable ground motions among earthquakes which are expected to occur.

2. The earthquakes causing the basic design earthquake motions, near to distant earthquakes shall be considered.

3. The basic design earthquake ground motions shall be specified in terms of the following items:

(a) Maximum velocity amplitude

(b) Wave shape

(c) Duration

4. The maximum velocity amplitude (5), the wave shape (6), and the duration (7) of the basic design earthquake ground motions shall be evaluated taking the following items into consideration:

(a) Magnitudes, epicenters, hypocenters, after-shock areas, after-shock volumes (8), the highest intensities (or estimated values thereof) of ground motions, and situations of damage (including damage to structures, overturning of tombstones, etc.) of historic earthquakes which have affected the proposed site and neighboring areas.

(b) Statistical expectation (9) of the intensity of ground motion based on the past destructive earthquakes' data.

(c) Magnitudes and distances from the centers of energy release to the proposed site of the design earthquakes.

i) The magnitude of the maximum design earthquakes shall be determined primarily upon activities of past earthquakes which have influenced the proposed site, also considering the state (10,11) of active faults (12) existing nearby and the seismo-

tectonical structures (13).

The magnitudes of the extreme design earthquakes shall be determined based upon maximum values (13) potentially pertaining to the seismo-tectonical structures and the maximum scales of active faults existing nearby.

ii) The distance from the centers of energy release of the maximum or extreme design earthquakes shall be determined in consideration of the locations of nearby active faults, the centers of energy release of past earthquakes, and the seismo-tectonical structures.

(d) Data from instrumental observations during past earthquakes, and the results of instrumental observations at the proposed site and lithological surveys of strata underlying the proposed site.

5. The basic design earthquake motions (14,15) shall be expressed as time histories and/or smoothed design response spectra, collectively considering the above paragraphs a, b, c, and d. As the design time histories,

(a) records of past earthquake ground motions at the proposed site or adequate modifications therof,

(b) records of past strong-motion earthquakes under similar conditions or adequate modifications therof, or

(c) simulated (artifically synthesized) ground motions may be used. In any case, however, careful attention should be paid to the compatibility (16) between the design time histories and the design response spectra.

2. Definitions and Reference Data

a) Fig. 1

DEFINITIONS AND REFERENCE DATA

Fig.1

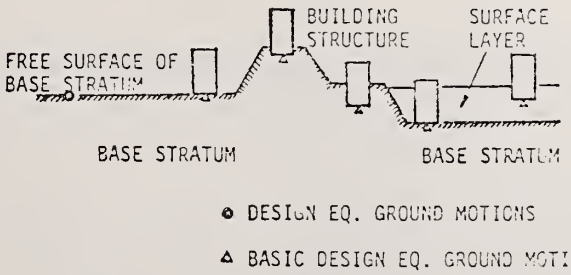

b) Base Stratum: a firm, intact (not significantly fissured nor weathered) rock which was formed in general in the Tertiary or earlier era.

c) Surface Layer: geologically newer soil layer or formation, or weathered rock overlying the base stratum

d) Free Surface of Base Stratum: a horizontal, flat surface of the base stratum extending over a considerable area, above which neither surface layers nor structures

are assumed to be present. Where such surface cannot really be identified within or around the proposed site, it should reasonably be assumed.

e) The maximum velocity amplitude of the basic design earthquake ground motions may be evaluated by

$$v_{max} = 10^{0.61M-P\log_{10}X-Q} \quad (1)$$

where v_{max}: max. velocity amplitude (cm/sec.) at the free surface of the base stratum

M: magnitude in Gutenberg-Richter scale

P: 1.66 + 3.60/X

Q: 0.631 + 1.83/X

X: hypocentral distance (Km)

f) Envelope function defining the wave shape may be assumed as shown in Fig. 2

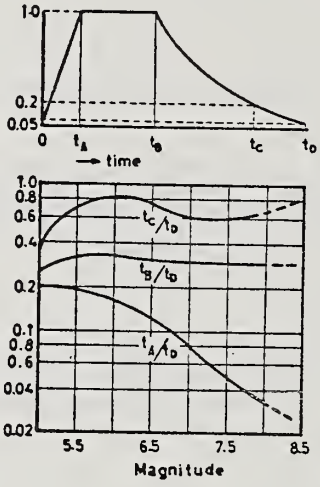

Fig.2

g) The duration of the basic design earthquake ground motions may be estimated by

$$t_D = 10^{(M-2.5)/3.23} \quad (2)$$

where t_D: duration (sec.)

M: magnitude in Gutenberg-Richter scale

h) When the after-shock volume is approximately assumed as a sphere, its radius may be estimated by

$$D = 10^{0.353M-1.134} \quad (3)$$

where D: radius of spherical after-shock volume (km)

M: magnitude in Gutenberg-Richter scale

i) Knowing the magnitude M and the epicentral distance R or the hypocentral distance X from a site with respect to an earthquake, it is possible to approximately estimate the intensity scale I, for instance, by an empirical formula

$$\text{for} \quad \begin{cases} I = 2(M-\ln R)-0.00183R-0.307 & R \geq 100 \text{ km} \\ I = 2M-0.86861\ln X-0.01668X-3.9916 & R \leq 100 \text{ km} \end{cases} \qquad (4)$$

Therefore, from earthquakes' data for the past T years, the probability distribution

$$f(I) = F(I)/T \qquad T = 0,1,2,\ldots\ldots\ldots,7 \qquad (5)$$

may be evaluated, where F(I) represents the number that the site experienced the earthquakes of intensity scale I. Usually, as shown in Fig. 3 (a), the probability distribution F(I) approximately takes an exponential form. Thus, the integral

$$\int_I^{\infty} f(I)dI$$

represents the probability per one year that the site will be influenced by an earthquake of intensity scale larger than I. From Fig. 3(b), where the integral values are plotted against I, the statistical expectancy of the intensity scale, I_r, can be found corresponding to any return period of r years. Since the relation between intensity scale I and acceleration α on the surface of medium-staff soil deposit may be expressed approximately by

$$\alpha = 0.45 \times 10^{I/2} \quad \text{gal} \qquad (6)$$

the statistical expectancy of the acceleration can be obtained by substituting I_r for I in eq. (6). In a similar way, the statistical expectancy of the velocity of ground motions can be determined based on the same past earthquakes' data by using eq. (1) instead of eqs. (4) and (6).

j) Status of Active Fault: 1) length, 2) activity (average displacement velocity), 3) pattern of movement and displacement at earthquake occurrence, and 4) the year of the last movement (blank period) of the active fault

k) If, with respect to an active fault,

S: average displacement velocity (m/year)

D: displacement at earthquake occurrence (m)

L: length (km)

M: magnitude of caused earthquake

R: period of earthquake occurrence (year)

there are the relations

$$\log D = 0.60M - 3.91 \quad (7)$$

$$\log L = 0.60M - 2.91 \quad (8)$$

$$R = D/S \quad (9)$$

Eqs. (7) and (8) have been obtained from the experience of Japanese island earthquakes, while from world-wide data they become

$$\log D = (0.55 \pm 0.07)M - (5.71 \pm 0.50) \quad (10)$$

$$\log L = 1.32M - 7.99 \quad (11)$$

It is frequently recognized that there is the specific magnitude M_c pertaining to a specific active fault or its localized segment.

1) Active Fault: a fault which evidently moved in the Quarternary era (within last 1,000,000 years) and also is capable of causing earthquake in the future.

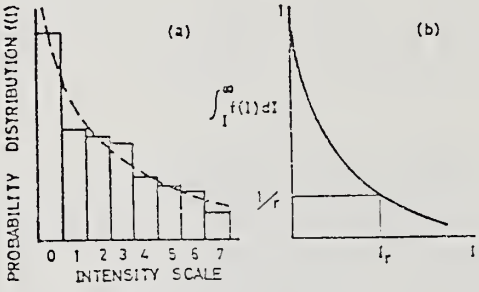

Fig.3

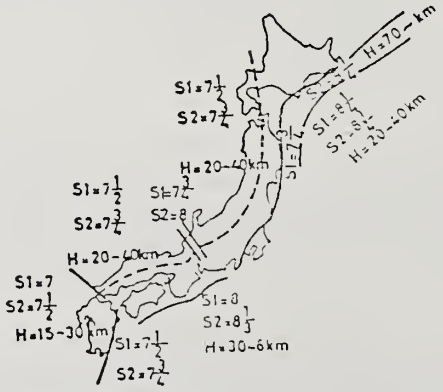

Fig.4

EXAMPLE OF FLOW CHART FOR ESTIMATION OF S1 AND S2

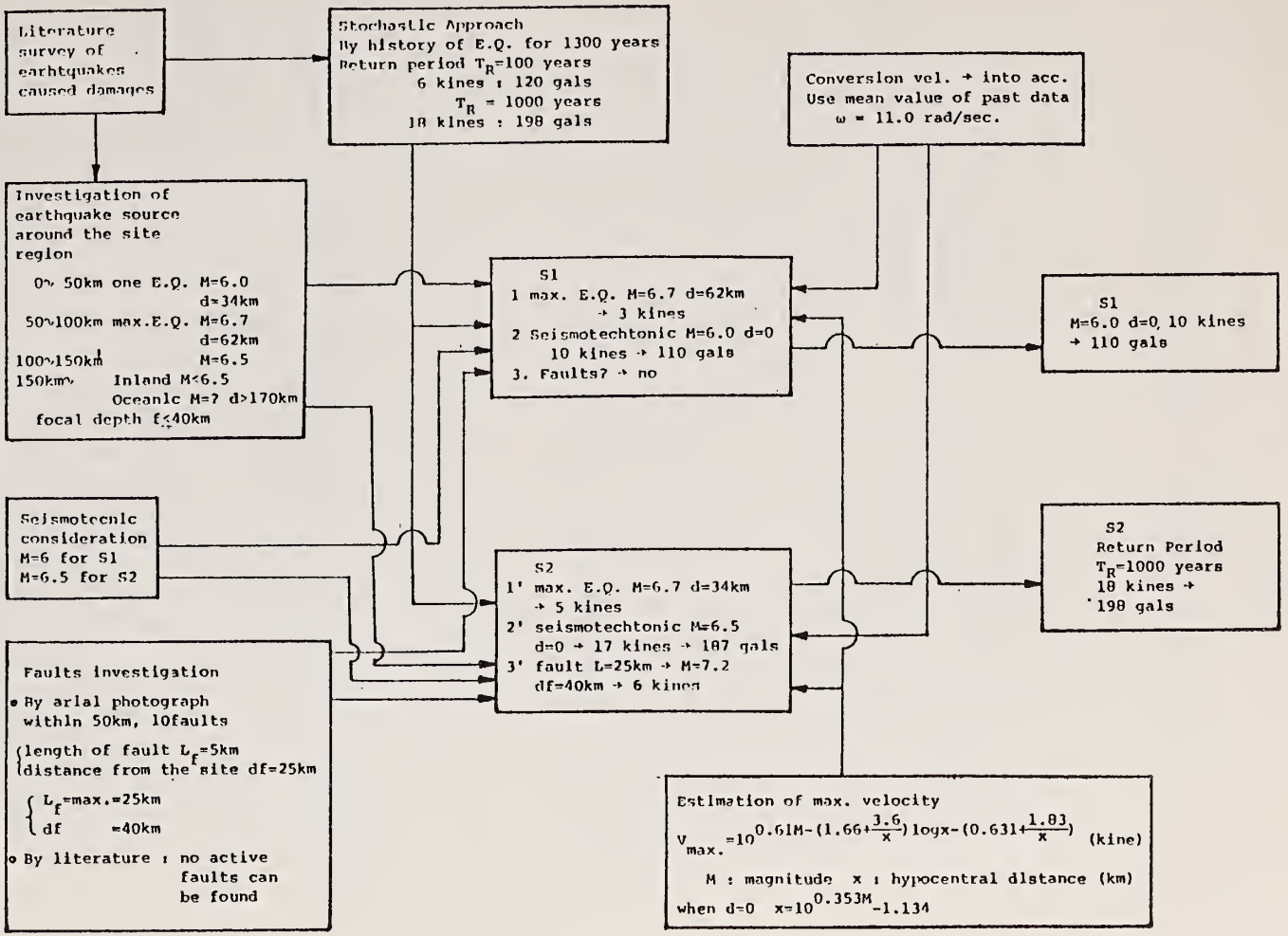

TORNADO-BORNE MISSILES

by

James F. Costello
U.S. Nuclear Regulatory Commission, Washington, D.C.

ABSTRACT: Nuclear power plants are designed to withstand the effects of severe environmental events, including tornadoes, without endangering public health and safety. Along with high wind velocities and drops in pressure, an effect which must be considered is the fact that objects of varying sizes are displaced by tornadoes. Predictions of what objects are likely to fly and at what velocities are difficult. Knowledge of the actual windfields present in a tornado is sketchy as is information about the aerodynamics of bluff bodies. This paper outlines methods which have been developed in order to make conservative estimates of the effects of tornado-generated missiles.

KEY WORDS: Structural Engineering; Dynamics; Tornadoes; Missiles; Trajectories; Power Plants.

INTRODUCTION

To ensure the safety of nuclear power plants in the event of a tornado strike it is required that, in addition to the direct action of the wind and of the moving ambient pressure field, the designer consider the impact of tornado-borne missiles, i.e., of objects moving under the action of aerodynamic forces induced by the tornado wind. It is, therefore, necessary that estimates be made of the speeds attained by potential missiles under tornado wind conditions specified for the design of nuclear power plants.

In order to make these estimates, some assumptions are necessary. These assumptions include:

a) the initial conditions of the problem, i.e., the initial position of the object with respect to the ground and to the tornado center, and the initial velocity of the object, b) the detailed features of the wind flow field, and c) the aerodynamic characteristics of the object (which, in most cases of practical interest, is a bluff body).

Differences between the various sets of basic assumptions used in estimating tornado-borne missile velocities may be ascribed, in part, to the probabilistic nature of the problem. For any given tornado wind field, the initial conditions constitute a set of random variables. More importantly, however, such differences are a consequence of serious uncertainties regarding both the structure of the tornado flow and the aerodynamic behavior of the potential missile.

MODEL FOR THE TORNADO-BORNE MISSILE MOTION

The motion of an object may be described in general by solving a system consisting of three equations of balance of momenta and three equations of balance of moments of momenta. In the case of a bluff body, one major difficulty in writing these six equations is that the aerodynamic forcing functions are not known.

It is possible to measure in the wind tunnel aerodynamic forces and moments acting on a bluff body under static conditions for a sufficient number of positions of the body with respect to the mean direction of the flow. On the basis of such measurements, the dependence of the forces and moments on position, and corresponding aerodynamic derivatives, can be obtained. Aerodynamic forces and moments can then be calculated following the well-known pattern used in airfoil theory; for example, if an airfoil has a time-dependent vertical motion h(t) in a uniform flow with velocity U, and if the angle of attack is α = const, the lift coefficient is

$$C_L = \frac{dC_L}{d\alpha} \left(\alpha + \frac{1}{U}\frac{dh}{dt}\right) \qquad (1)$$

This procedure for calculating aerodynamic forces and moments is valid if the quasi-steady assumption is acceptable and if the body concerned behaves aerodynamically like an airfoil - i.e., if the body is streamlined and if no flow separation occurs. However, in the case of unconstrained bluff bodies moving in a wind flow the validity of such a procedure remains to be demonstrated.

In the absence of a satisfactory model for the aerodynamic description of the missile as a rigid (six-degrees-of-freedom) body, it is customary

to resort to the alternative of describing the missile as a material point acted upon a drag force

$$\overline{D} = 1/2\ \rho\ C_D A\ |\ \overline{v}_w - \overline{v}_M\ |\ (\overline{v}_w - \overline{v}_M) \qquad (2)$$

where ρ = air density, $\overline{v}_w$ = wind velocity, $\overline{v}_M$ = missile velocity, A is a suitably chosen area and C_D is the corresponding drag coefficient.

This model is reasonable if, during its motion, the missile either (a) maintains a constant or almost constant attitude with respect to the relative velocity vector $\overline{v}_w - \overline{v}_M$, or (b) has a tumbling motion such that, with no significant errors, some mean value of the quantity $C_D A$ can be used in the expression for the drag $\overline{D}$. The assumption of a constant body attitude with respect to the flow would be credible if the aerodynamic force were applied at all times exactly at the center of mass of the body--which is highly unlikely in the case of a bluff body in a tornado flow--, or if the body rotation induced by a non-zero aerodynamic moment with respect to the center of mass were inhibited by aerodynamic damping forces intrinsic in the body--fluid system.

Wind tunnel test results suggest that no stabilizing effect by the flow can generally be expected to inhibit the rotation of bluff bodies. The assumption that potential tornado-borne missiles will tumble during their motion appears therefore to be reasonable.

Assuming that Eq. 2 is valid and that the average lift force vanishes under tumbling conditions, the motion of the missile viewed as a one-degree-of-freedom system is governed by the relation:

$$\frac{d\bar{v}_M}{dt} = -1/2\,\rho\,\frac{C_D A}{m}\,|\,\bar{v}_M - \bar{v}_w\,|\,(\bar{v}_M - \bar{v}_w) - g\bar{k} \qquad (3)$$

where g = acceleration of gravity, $\bar{k}$ = unit vector along the vertical axis and m = mass of missile. It follows from Eq. 3 that for a given flow field and initial conditions, the motion depends only upon the value of the parameter $C_D A/m$. Experimental studies aimed at finding reasonable ways to estimate an "effective" $C_D A$ value are now being carried out at Colorado State University.

The subject of tornado-borne missiles is still under active investigation by the U.S. Nuclear Regulatory Commission and the Electric Power Research Institute as well as by a number of architectural and engineering firms. The following section gives a list of references. The list is by no means exhaustive. But it includes, as well as some more recent work, some papers of historical interest.

REFERENCES

F. C. Bates, A. E. Swanson (1967), "Tornado Considerations for Nuclear Power Plants," Transactions, American Nuclear Society, Vol. 10, pp. 712-713.

A. K. Bhattacharyya, R. C. Boritz and P. K. Niyogi (1975), "A Consistent Method of Determining Effects of Tornado Missiles on Nuclear Power Plant Design," Proceedings, Second ASCE Conference on Structural Design of Nuclear Plant Facilities.

J. R. Eagleman, V. U. Muirhead, and N. Willems (1975) Thunderstorms, Tornadoes and Building Damage, Lexington Books, Lexington, Mass.

W. H. Hoecker, "Wind Speed and Air Flow in the Dallas Tornado of April 2, 1975," Monthly Weather Review, Vol. 88, No. 5.

W. Huang and J. M McLaughlin (1975), "Tornado Generated Missiles," Proceedings, Second ASCE Conference on Structural Design of Nuclear Plant Facilities.

R. A. James, E. G. Burdette, and C. N. Sun (1975), "Generation of Missiles by Tornadoes," Proceedings, Second ASCE Conference on Structural Design of Nuclear Plant Facilities.

A.J.H. Lee (1975), "Trajectory of Tornado Missiles and Their Design Parameters" Proceedings, Second ASCE Conference on Structural Design of Nuclear Plant Facilities.

E. H. Markee, J. G. Beckerley, and K. E. Sanders (1974), Technical Basis for Interim Regional Tornado Criteria, WASH-1300 (UC-11), U.S. Atomic Energy Commission, Office of Regulation.

J. R. McDonald, R. C. Mehta, and J. E. Minor (1974), "Tornado-Resistant Design of Nuclear Power-Plant Structures," Nuclear Safety, Vol. 15, No. 4.

D. F. Paddleford (1969) Characteristics of Tornado Generated Missiles, Report WCAP - 6897, Westinghouse Electric Corp., Pittsburgh, Pennsylvania.

G. H. Redman (1976), "Wind Field and Trajectory Models for Tornado-Propelled Objects," EPRI-308, Electric Power Research Institute, Palo Alto, CA.

E. Simiu and M. R. Cordes (1976), "Tornado-Borne Missile Speeds," NBS ID-1050, National Bureau of Standards, Washington, D.C.

Structural Damage to Bridges Resulting From the Guatemala Earthquake

James D. Cooper

Federal Highway Administration, Washington, D. C.

ABSTRACT

The Guatemala earthquakes of February 4 and 6, 1976, caused severe economic hardships because of highway bridge failures and damage. The damage to three major bridges, Agua Caliente, LaAsuncion, and Incienso is described. A general discussion of damage to bridges and the roadway along a major highway, the Atlantic Highway, (Route CA9), is also presented.

KEYWORDS: Earthquake damage; Bridges; Guatemala earthquake

INTRODUCTION

The Guatemala earthquakes of February 4 and 6, 1976, caused extensive damage to two major highway bridges, LaAsuncion located in the northeast part of Guatemala City, and Agua Caliente located approximately 17 miles (27 km) northeast of Guatemala City on Route CA9. A third major bridge, Incienso, located in the northwest section of Guatemala City suffered some damage. Bridges within Guatemala City, with the exception of LaAsuncion and Incienso, performed well, suffering little or no damage. Some evidence of displaced bearing pads, settled aprons on abutment slopes and minor impacting at abutments was evident on a few of these structures. Bridge damage outside Guatemala City was generally confined to the area of approximate surface faulting, Figure 1, along the Motagua River northeast of the city. Eleven bridges along the 184 miles (297 km) of Route CA9 between Guatemala City and Puerto Barrios on the east coast experienced varying degrees of damage, mostly to bearings.

The earthquake caused additional extensive damage to mostly non-engineered structures situated along the Motagua River Valley. The approximate location of surface faulting (left lateral), the shaded area shown in Figure 1, follows the Motagua River and Route CA9, and extends approximately 149 miles (240 km) from just east of Gualan, to northwest of Guatemala City. A maximum 55 inches (140 cm) of fault displacement was reported north of Guatemala City.

The National Earthquake Information Service reported the February 4 earthquake as being 7.5 on the Richter scale with the epicenter at latitude 15.27°N, longitude 89.25°W, 99 miles (160 km) northeast of Guatemala City between the towns of Gualan and Los Amates. Reportedly, ground shaking in Guatemala City lasted between 20 and 30 seconds. Two seismoscope records were obtained and no strong-motion accelerograph records were recorded. The February 6 earthquake is reported as being a 5-3/4 to 6 magnitude event with a preliminary epicentral location of 14.3°N, 90.5°W. Most damage was caused by the February 4 event.

Specific discussion of damage to the Agua Caliente, LaAsuncion, and Incienso bridges is presented, followed by a brief general discussion of damage to the bridges and roadway along Route CA9, the Atlantic Highway. The bridge inspections were made in cooperation with the second reconnaissance team fielded by the Earthquake Engineering Research Institute March 1 - 6, 1976, one month following the earthquakes.

RIO AGUA CALIENTE BRIDGE

The most severely damaged bridge was the important Rio Agua Caliente Bridge, located approximately 17 miles (27 km) northeast of Guatemala City on Route CA9, the Atlantic Highway. This highway serves as the major transportation link between Guatemala City and the economically strategic port facility at Puerto Barrios, on the east coast of Guatemala.

A simple plan and elevation view of the five-span, simply supported steel plate girder bridge is shown in Figure 2. The bridge was designed in accordance with the 1953 AASHO "Standard Specification for Highway Bridges" using an earthquake factor of 10% dead load. The span lengths from the west abutment are 148 feet (45 m), 98 feet (30 m), 148 feet (45 m), 98 feet (30 m), 98 feet (30 m).

The straight steel superstructure spans were designed using two 8-foot (2.4 m) deep, built-up exterior plate girders, two interior 18 WF 50 stringers with spirals for composite deck action, 30 WF 108 floor beams, and bottom lateral bracing. The concrete deck slab, curved in plan with 8.5% superelevation, is 6.5 inch (16.5 cm) thick with a 2 inch (5.1 cm) asphalt concrete overlay. Total deck width, including parapets, is 33.7 feet (10.25 m).

The superstructure sits on four reinforced concrete pier bents which vary in height between 72 feet (21.9 m) and 76 feet (23.2 m) above maximum high water level. The pier bents are tied into pedestals which sit on spread footings. Total depth of pedestals and spread footings vary between 10 feet (3.1 m) and 33 feet (10 m) below maximum high water level. The end spans sit on abutment walls on spread footings.

Figure 3 shows a general view of the bridge looking south. The earthquake caused the three center spans to fall off the bearing supports. Pier bents and abutments appeared to be undamaged with the exception of minor spalling where the falling girders had impacted against the columns and tie beams. Extremely minor hairline cracks were noted around the base of the columns of pier #2.

The fallen second and fourth spans appear to have initially lost support on the south side of the bent; i.e., along the outside radius of the deck curvature. As the south side of the superstructure fell, the bearings on the north side of the bent gave way, thus allowing the spans to rotate down to their final resting position.

Significant longitudinal pier motion occurred, propelling the girder of span #2 approximately 7 feet (2 m) beyond the centerline of pier bent #2, as seen in Figure 4.

Additional evidence of pier rocking can be seen in Figure 5. Note the soil at the base of pier #2 which has been compressed leaving approximately 1/2 inch (1.2 cm) void between soil and foundation. This could account for approximately 1.5 inches (3.8 cm) of longitudinal displacement about the centerline at the top of the pier bent, assuming simple rocking about the base of the foundation. Figure 6 shows the collapsed center span and roadway which slid straight down pier #3. Note the only visible damage to pier #3 is in the form of spalled concrete from girder impact above the lower tie beam on the left column and on the upper right side of the lower tie beam.

A view looking east from the base of pier #3 through twisted girders, stringers, floor beams, and lateral bracing is shown in Figure 7.

The bridge collapsed, principally because of the bearing details used and the lack of longitudinal and transverse superstructure restraint at the supports. Figure 8 shows a fallen expansion rocker at the base of pier #3. The rocker, which supported a 148 foot (45 m) span, is 11 inches (28 cm) by 17 inches (43 cm) at the base and 13.5 inches (34 cm) high. Figure 9 shows the fixed bearings in place atop the free standing piers. An expansion rocker can be seen resting on the tie beam in the foreground. The north girder appears to have walked approximately 5 inches (13 cm) to the south on the expansion bearing. It is speculated that had appropriate hinge restrainers been in place, thus tying the structure together, collapse probably could have been avoided.

Figure 10 shows the north girder and fixed bearing detail at the east abutment. Minor extension of anchor bolts was noted, otherwise no significant damage was visible at the east abutment. There was no indication of loose soil or stones having been expelled from weep holes in the abutment or stone wall and no cracking was observed in the stone wall.

Figure 11 shows the north girder fixed bearing detail at the west abutment. The bearing support is inclined approximately 8°. Note the anchor bolt extension and the space between the abutment bearing ledge and bearing plate. Figure 12 shows the north girder resting on the expansion bearing which is inclined at approximately 30°. A recommendation was made to place temporary shoring under the girders at the west abutment and pier #1 in view of the extremely unstable position of the span.

The pier bents and abutments appear to be structurally undamaged and plans are being made to reuse them when the superstructure is rebuilt. Particular attention will be devoted

to the bearings in the design of the replacement structure.

Immediately following the inspection of the collapsed Agua Caliente Bridge, the U. S. Army Corps of Engineers moved in to clear the site and start construction of a temporary Bailey Bridge.

It is interesting to note that a curved railroad steel truss bridge located approximately 1 mile (1.6 km) north of the Agua Caliente, oriented in the same direction as Agua Caliente, suffered no apparent damage. Although the railroad structure was inaccessible at the time of the Agua Caliente inspection, it was operational as evidenced by the passage of a freight train. It is believed that the rails probably provided adequate structural continuity to resist the earthquake motions.

LA ASUNCION BRIDGE

The LaAsuncion Bridge, located in the northeast section of Guatemala City, is a three-span, continuous plate girder bridge that was severely damaged during the earthquake. The bridge is under the jurisdiction of the local city government. No plans are available; however, personnel from the Guatemala Department of Roads, Ministry of Communications and Public Works provided the general plan and elevation views of the bridge, shown in Figure 13. The span lengths are 148 feet (45.1 m), 196 feet (59.9 m), and 148 feet (45.1 m). The deck is 48 feet (14.6 m) wide. The piers are single, reinforced concrete columns with cap beams. The west pier is 86 feet (26 m) above grade while the east pier is 82 feet (25 m) above grade. Foundation type is unknown.

During the earthquake, the superstructure rotated, in plan, about the east pier causing the bearing supports to dislodge. The west end of the bridge deck displaced 39 inches (100 cm) laterally to the south while the east end displaced 20.5 inches (52 cm) laterally to the north, as shown by the dashed line in the plan view of Figure 13. The lateral offset at the west abutment is shown in Figure 14 between the once continuous median delineator on the approach roadway and deck.

The approach roadway itself was badly cracked, Figure 15, and damage to the west abutment and wing walls indicated the presence of extremely high backfill forces. Figure 16 shows abutment wall failure. The pipe in the foreground is a drain scupper. Figure 17

shows a lateral foundation offset of 2.5 inches (6.4 cm) relative to the south wing wall. The view looks down along the south wing wall which is shown at the right of the photograph. The evidence indicates the complete failure of the west abutment. There was, however, no evidence of foundation failure at the east abutment, and the piers, as viewed from both abutments, appeared undamaged.

The bridge deck dropped 8.3 inches (21 cm) as it displaced and dislodged from the rocker bars at the west abutment, Figure 18. Figure 19 shows the bottom chord of the end diaphragm at the west abutment resting on a bearing plate with shear key and a dislodged rocker bar to the right. A view of a failed bearing detail at the east abutment ledge is shown in Figure 20.

Figure 21 shows a general view of the bridge. Note a missing bearing plate under the north (right) girder at the east pier in the foreground. The only noticeable damage to the steel superstructure was at the west abutment, as shown in Figure 22. The bottom lateral bracing and end diaphragm were slightly buckled. Figure 23 shows the elbow of a 10-inch (25 dm) water pipe at the southeast corner of the bridge with no apparent damage. The pipe could not be traced and there was no evidence of seeping water along the embankment or apron at the east abutment.

The LaAsuncion Bridge appears to be structurally sound and can be jacked back into place once the damage to the west abutment has been corrected.

INCIENSO BRIDGE

The Incienso Bridge, Figure 24, located in the northwest section of Guatemala City, was constructed in 1972. The bridge is of interest because it incorporates seismic hinge and abutment restrainers and although minor damage occurred, remained in service following the earthquake. The performance of the eight-span concrete bridge provided an indication that the incorporation of new seismic design techniques in new construction can provide adequate structural resistance against major earthquakes.

The three main spans were twin segmental, precast, prestressed concrete box girders, 203 feet (62 m), 400 feet (122 m), 203 feet (62 m) in length constructed by the balanced cantilever method. The main span is supported on reinforced concrete piers 262 feet (80 m) and 230 feet (70 m) in height. The five side spans, each 92 feet (28 m) in length, are

constructed with seven prestressed concrete I-beams supported on reinforced concrete pier bents. The total deck width is 82 feet (25 m).

The main three spans suffered no visible damage. Figure 25 shows evidence of compressional failure of the pavement at the west abutment due to impacting. Although not quite as visible in the photograph, there is evidence of a 1 inch (2.5 cm) vertical displacement of the deck. There is also evidence of minor deck impacting between the prestressed I girder spans.

The generally good performance of the bridge is attributed to the use of seismic restraint mechanisms ; i.e., hinge restrainers, which tied the prestressed I girders together, Figure 26. The restrainer caps, which pass through the concrete end diaphragms of the girders, can be seen in Figure 27. A total of 12 restrainers are placed across each joint. Each restrainer cable is prestressed to 45 metric tons and has a 63 metric ton tensile strength. The only restrainer failure occurred across the west abutment, where all 12 cables failed. Figure 28 shows a "seismic block" i.e., a concrete block tied to an abutment or pier through which the restrainer cable passes, at the west abutment between the end diaphragm on the left and abutment wall on the right. The restrainer cable failed in tension and shear at the point which is flush against the girder end diaphragm. (The cable in the photograph is not the restrainer cable.)

The failure of the restrainer cables at the west abutment resulted in the walking of bearing pads including the dislodging of one pad, shown in Figure 29. The temporarily blocked girder on the concrete bearing plate where the bearing pad was removed is shown in Figure 30.

Additional restraint was provided through the use of abutment tie back cables, shown in Figure 31. It was reported that there are seven tie back cables across each abutment, although only five cable caps were noted across the abutment wall. Each cable is reported to have a tensile strength of 180 metric tons. There was no evidence of abutment tie back cable failure.

THE ATLANTIC HIGHWAY - CA9

The Atlantic Highway is one of the most economically strategic highways in Guatemala, extending from Guatemala City to the port facility at Puerto Barrios, 184 miles (297 km) to

the north east. The road was closed following the earthquake due to severe landslides, damaged bridges and road sloughing, thus interrupting the flow of commercial traffic.

Bridges

There are approximately 42 bridges along the Atlantic Highway, including the Agua Caliente. Eleven suffered varying degrees of damage. Typical types of structures include deck, through, and pony trusses; steel girders with composite acting decks; and prestressed and reinforced concrete girder bridges. The predominant types are simple span trusses supported on rocker bearings. Excluding the Agua Caliente bridge, most damage included lateral displacement of the decks, impacting of deck against abutment walls causing cracking and spalling, and tipping or falling of rocker bearings.

Figure 32 shows the damaged Guastatoya Bridge, 44 miles (71 km) northeast of Guatemala City. The structure, a three-span deck truss with approximately 120-foot (37 m) spans, was closed to traffic. Rocker bearings tipped, note the differential vertical displacement at the right pier, and the right span at the abutment displaced laterally, almost falling off its bearing.

Figure 33 shows the Teculutan Bridge, which is typical of many that experienced damage along the Atlantic Highway. Minor abutment pounding was noted at this site. Typical damage to truss-structures is shown in Figure 34. Keeper plates on flange bearing shoes provided little lateral resistance to earthquake forces, as evidenced in the photograph. In spite of the widespread damage, all bridges along the highway were open to traffic except the Agua Caliente and Guastatoya structures.

Roads

The Atlantic Highway is a two-lane asphalt road 22 feet (6.6 m) wide. Significant road sloughing occurred between Guatemala City and the Agua Caliente Bridge site, typically on fill areas across steep erosional cuts. Figures 35 and 36 show typical sloughing along the route. Damage was held to a minimum where retaining walls were constructed at the sides of the road, Figure 37.

The most severe landslides, which closed the highway, occurred approximately 31 miles (50 km) northeast of Guatemala City and extended over a distance of approximately 6 miles

(10 km), Figures 38 and 39. The U. S. Army Corps of Engineers was in the process of clearing the roads and allowed limited passage over the tops of the slides. Future earthquakes can be expected to cause similar traffic disruption along CA9 because of the unfavorable terrain.

Figure 40 shows the Motagua Fault Zone passing across the Atlantic Highway approximately 2 miles (3 km) northeast of El Progresso. The roadway across the fault zone was totally pulverized. Note the 39.4 inch (100 cm) left lateral displacement at the fault as measured from the projection of the white centerline in the background to white centerline in the foreground. Figure 41 shows the fault zone passing through the cut slope at the side of the road. There was no indication of vertical fault displacement at this site.

CONCLUSIONS

The Guatemala earthquakes vividly demonstrated the vulnerability of bearing assemblies commonly used to support typical highway bridges, not only in Guatemala, but also in the United States. The types of bearings which failed have not been designed to withstand the large dynamic forces and motions imposed by earthquake. Lessons learned from this and previous earthquakes will preclude the use of this type detail in future construction. Thus, the critical issue is what can or will be done to improve the seismic resistance of existing bridges which have this vulnerable detail. Retrofitting techniques have been identified which can reduce susceptibility to damage. The most difficult problem, however, is to convince appropriate responsible authorities that for a relatively small investment, future major damage can be averted.

The Guatemala earthquakes provided the first full-scale test of a structure whose design had apparently been modified to incorporate some of the lessons learned from bridge damage in the 1971 San Fernando, California, earthquake. The performance of the Incienso Bridge demonstrated that bridges which are properly designed, and, in particular, tied together can withstand major earthquakes.

An attempt should be made to identify the multitude of existing bridges which are located in seismically vulnerable areas of the United States. Importance and seismic vulnerability factors can be developed for each so that as funding becomes available, the structures can be retrofitted.

It is obviously impossible to totally prevent landslides from occurring in areas of unfavorable terrain. However, critically important routes in rough terrain should be identified and plans made to provide either quick opening or alternate emergency routes following an earthquake.

REFERENCES

1. Newsletter of the Earthquake Engineering Research Institute, David J. Leeds, Ed., "The Guatemala Earthquake of February 4, 1976 - A Preliminary Report by the EERI Reconnaissance Team," Volume 10, No. 2B, March 1976.

2. M. A. Sozen and J. Roesset, "Preliminary Notes on Structural Damage Caused by Guatemala Earthquakes of 4 and 6 February 1976." A report to the Panel on Earthquakes, Committee on National Disasters of the Commission on Sociotechnical Systems, National Research Council, February 15, 1976.

Acknowledgements

The author wishes to express his appreciation and sincere thanks to Ing. Ernesto Argueta Pineda and his staff at the Guatemala Departmento da Puentes, Direccion General de Caminos, who provided valuable technical data and assistance during the inspection of damaged bridges. Official transportation, provided by Ing. Argueta, assured prompt access to points of interest along the Atlantic Highway.

The author is also greatly indebted to the Earthquake Engineering Research Institute (EERI) and Mr. Henry J. Degenkolb for providing names of key contact persons while in Guatemala.

FIGURE 1

GUATEMALA - LOCATION MAP

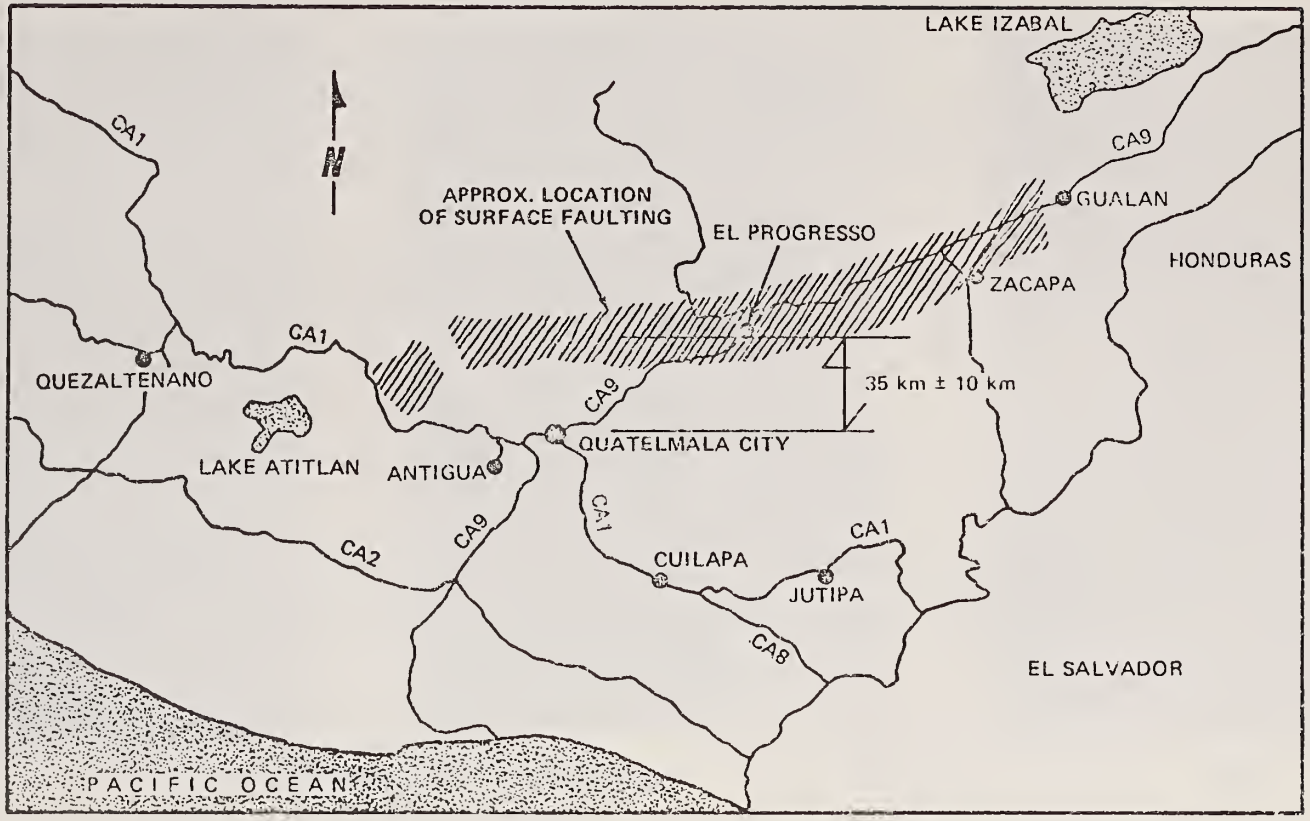

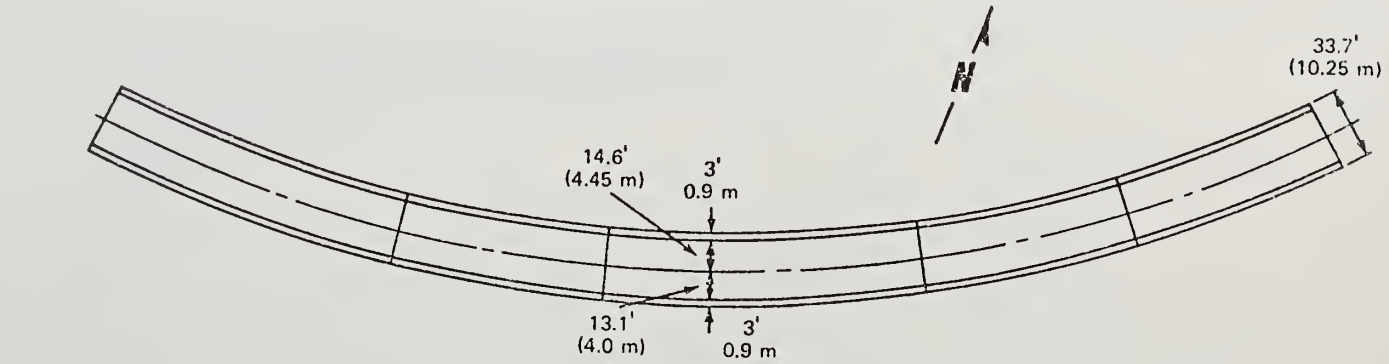

GENERAL PLAN

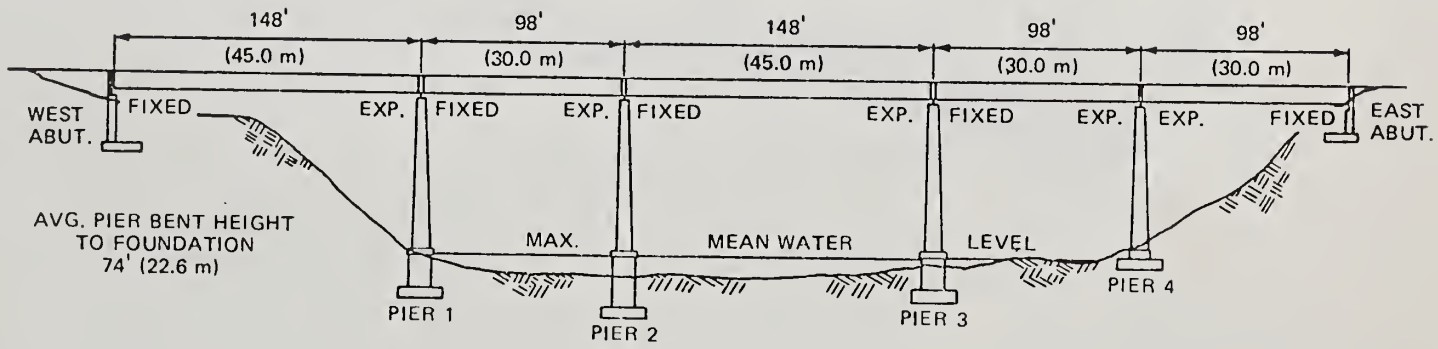

GENERAL ELEVATION

AGUA CALIENTE BRIDGE

FIGURE 2

Figure 3 Agua Caliente - General View

Figure 4 Agua Caliente - Longitudinal Girder Displacement, Base of Pier 2

Figure 5 Agua Caliente - Foundation, Base of Pier 2

Figure 6 Agua Caliente

Collapsed Center Span and Roadway

Figure 8 Agua Caliente

Fallen Expansion Rocker, Base of Pier 3

Figure 7 Agua Caliente - Detail of Collapsed Span at Base of Pier 3

Figure 9 Agua Caliente - View from East Abutment

Figure 10 Agua Caliente
East Abutment, North Girder and Bearing

Figure 11 Agua Caliente
Bearing Detail, West Abutment, North Girder

Figure 12 Agua Caliente - Tipped Rocker, Pier 1

Figure 14 LaAsuncion - Lateral Offset at West Abutment

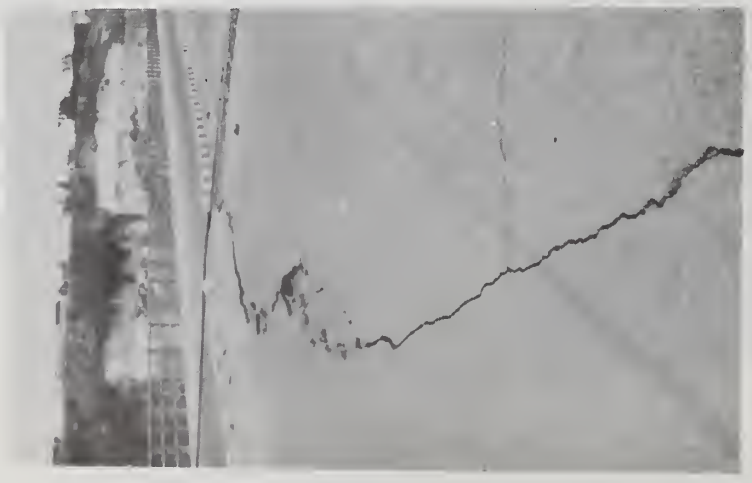

Figure 15 LaAsuncion - Cracked Approach at West Abutment

FIGURE 13

LA ASUNCION BRIDGE GEOMETRY

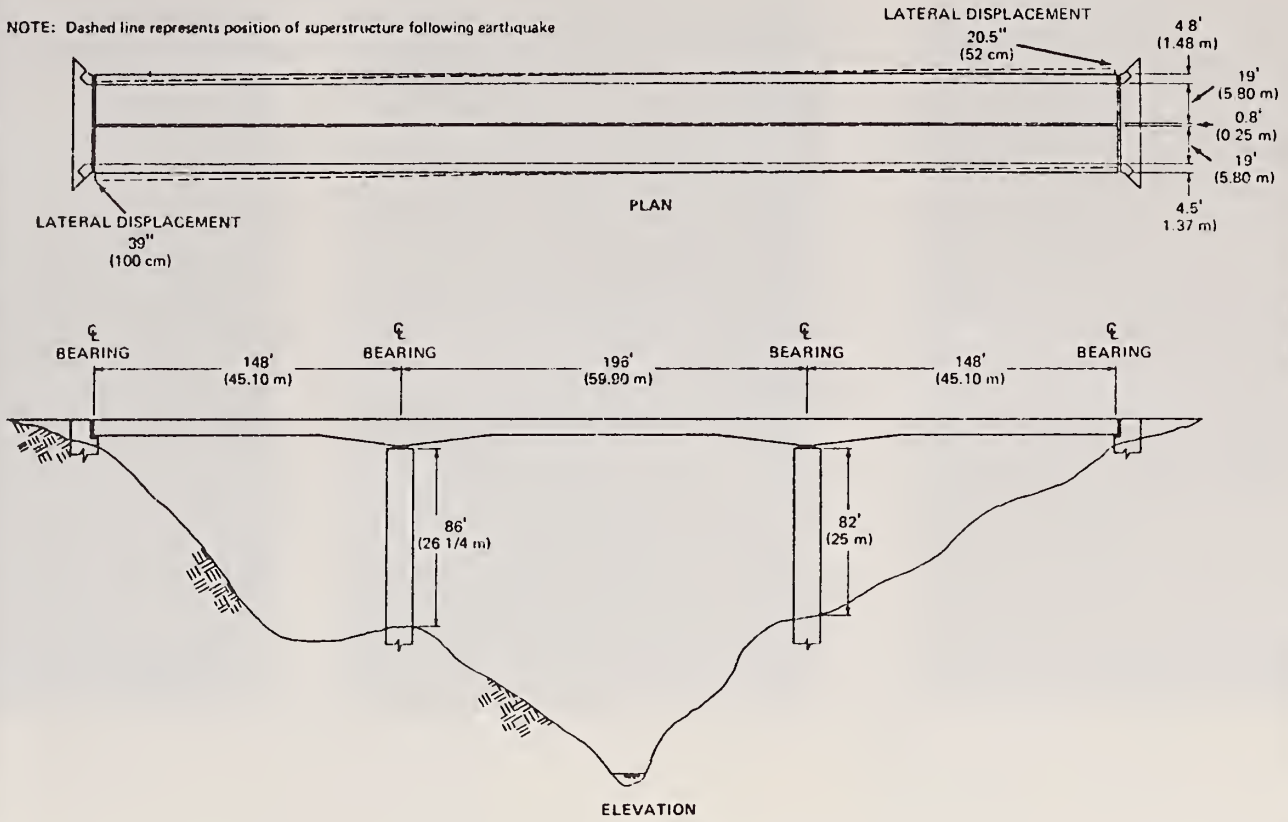

Figure 16 LaAsuncion - West Abutment Wall Damage

Figure 17 LaAsuncion - West Abutment Foundation Damage

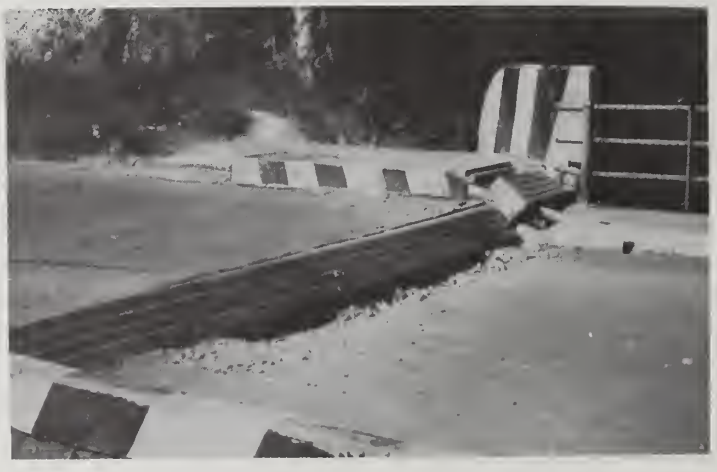

Figure 18 LaAsuncion - Vertical Deck Displacement at West Abutment

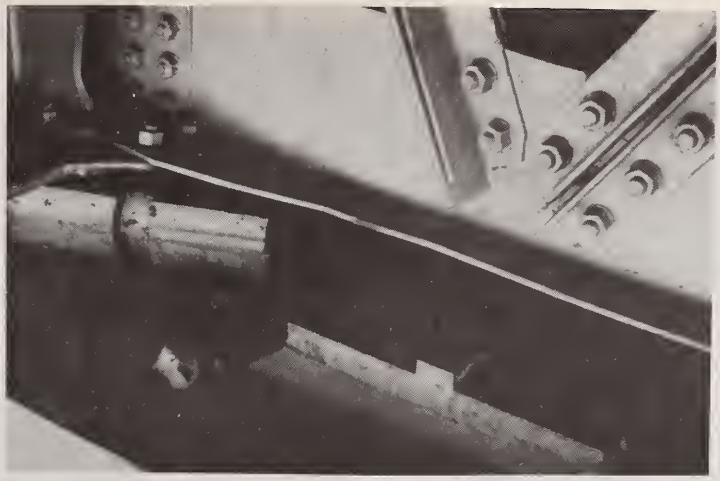

Figure 19 LaAsuncion - Displaced Rocker Bar at West Abutment

Figure 20 LaAsuncion - Displaced Girder, East Abutment

Figure 21 LaAsuncion - Missing Bearing, East Pier

Figure 22 LaAsuncion - Bottom Lateral Bracing and End Diaphragm Damage

Figure 23 LaAsuncion - Undamaged Water Pipe at East Approach

Figure 24 Incienso - General View of Bridge

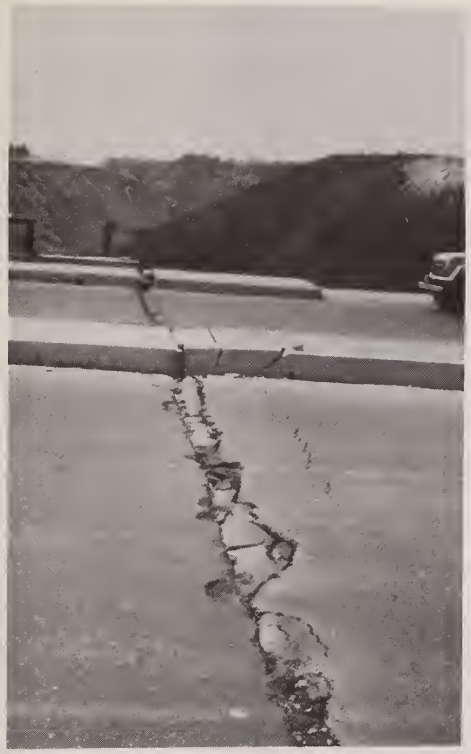

Figure 25 Incienso - Pavement Cracking at West Abutment

Figure 27 Incienso - Hinge Restraint, West Pier Bent

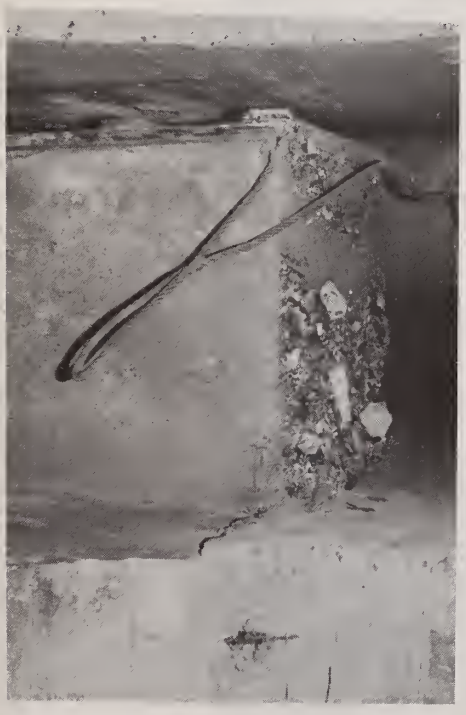

Figure 28 Incienso - Seismic Block, West Abutment

Figure 29 Incienso
Dislodged Neoprene Bearing Pad

FIGURE 26

INCIENSO BRIDGE SEISMIC RESTRAINT

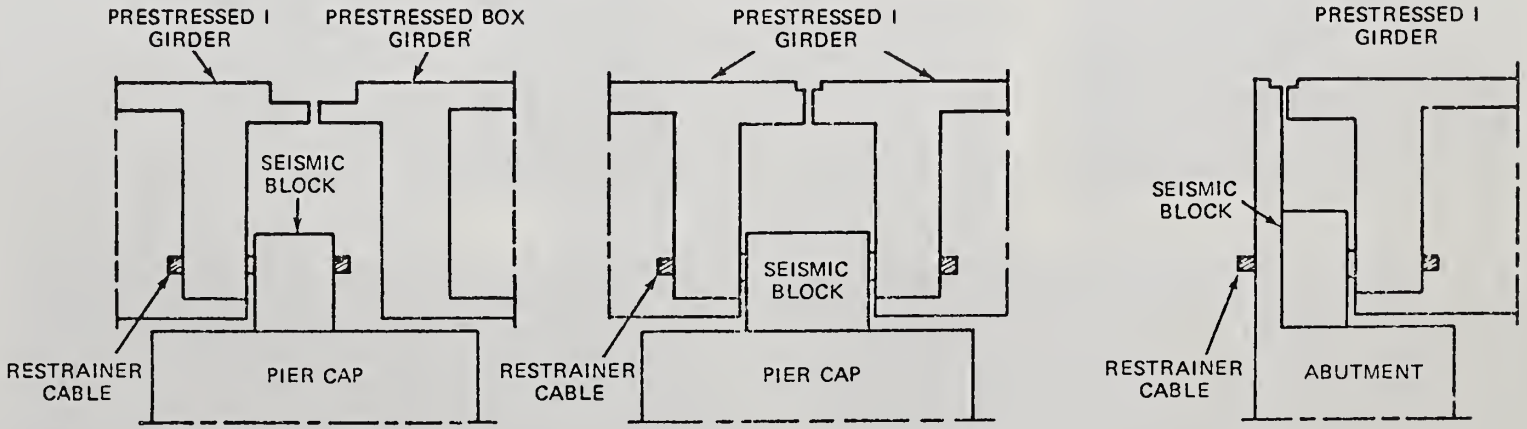

Figure 30 Incienso - Missing Neoprene Bearing Pad at South Girder, West Abutment

Figure 32 CA9-Guastatoya - Deck Truss

Figure 33 CA9-Teculutan - Typical Through Truss

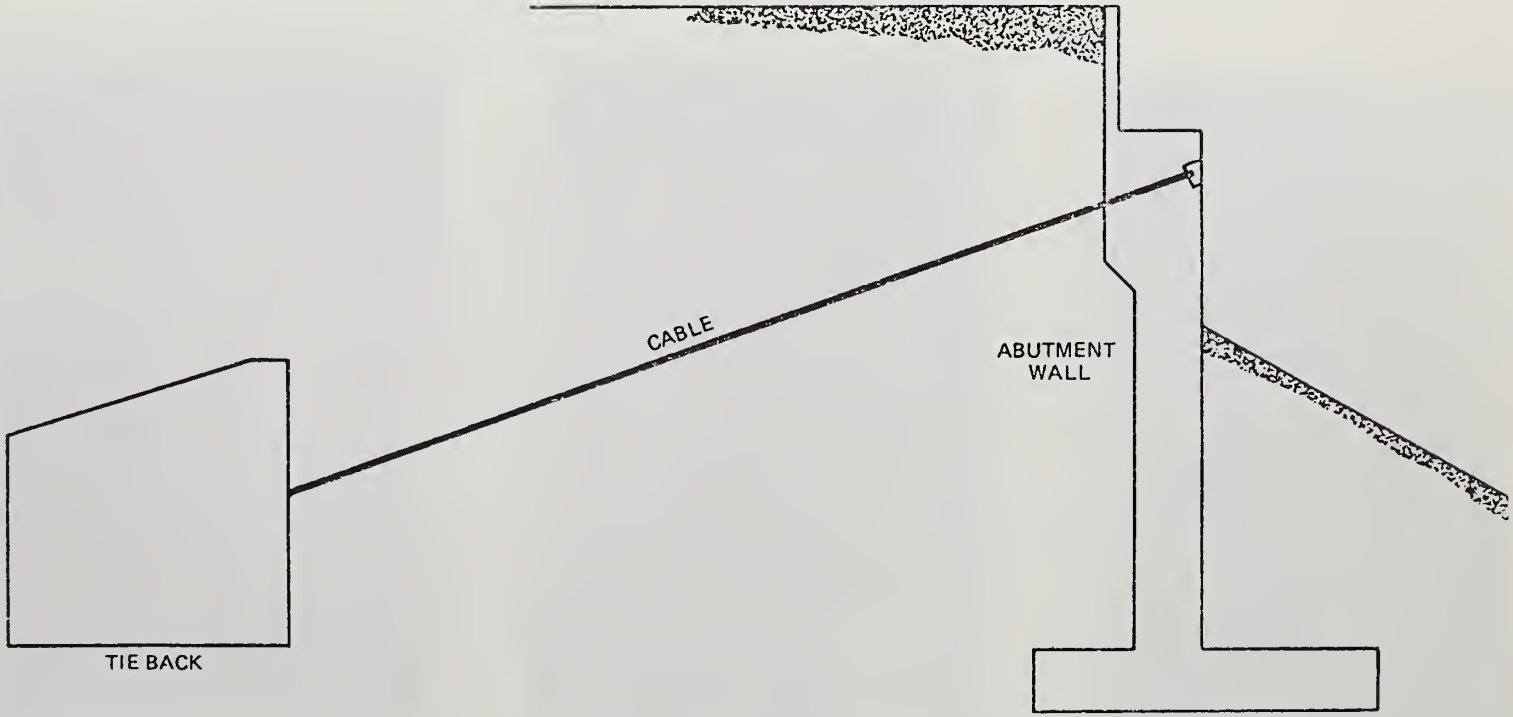

INCIENSO BRIDGE ABUTMENT RESTRAINT

FIGURE 31

Figure 34 CA9-Typical Damaged Fixed Bearing Detail

Figure 35 CA9-Typical Road Failure

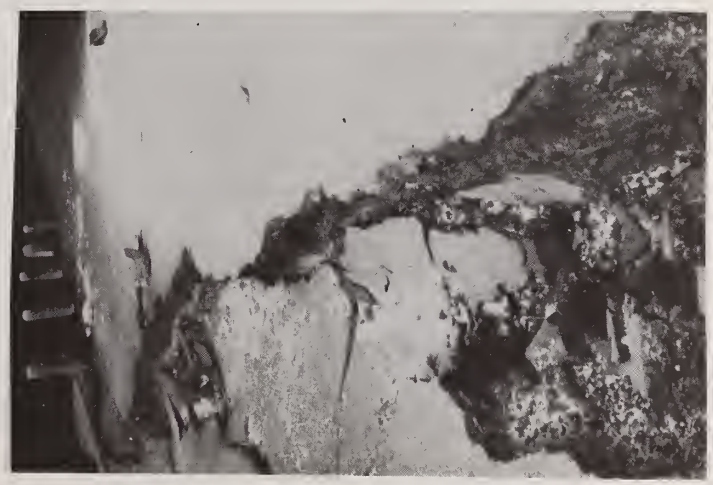

Figure 36 CA9-Typical Road Sloughing

Figure 37 CA9-Roadway Retaining Wall

Figure 38 CA9-Landslides

Figure 39 CA9-Landslides

Figure 40 CA9-The Motagua Fault

Figure 41 CA9-The Motagua Fault

NBS-114A (REV. 7-73)

U.S. DEPT. OF COMM. BIBLIOGRAPHIC DATA SHEET	1. PUBLICATION OR REPORT NO. NBS SP-477	2. Gov't Accession No.	3. Recipient's Accession No.

4. TITLE AND SUBTITLE

WIND AND SEISMIC EFFECTS

Proceedings of the Eighth Joint Panel Conference of the U.S. - Japan Cooperative Program in Natural Resources, May 18-21, 1976, National Bureau of Standards, Gaithersburg, Maryland

5. Publication Date: May 1977

6. Performing Organization Code

7. AUTHOR(S)

H. S. Lew, Editor

8. Performing Organ. Report No.

9. PERFORMING ORGANIZATION NAME AND ADDRESS

NATIONAL BUREAU OF STANDARDS
DEPARTMENT OF COMMERCE
WASHINGTON, D.C. 20234

10. Project/Task/Work Unit No.

11. Contract/Grant No.

12. Sponsoring Organization Name and Complete Address *(Street, City, State, ZIP)*

Same as Item 9

13. Type of Report & Period Covered: Final

14. Sponsoring Agency Code

15. SUPPLEMENTARY NOTES

Library of Congress Catalog Card Number: 77-600015

16. ABSTRACT *(A 200-word or less factual summary of most significant information. If document includes a significant bibliography or literature survey, mention it here.)*

The Eighth Joint Meeting of the U.S.-Japan Panel on Wind and Seismic Effects was held in Gaithersburg, Maryland on May 18-21, 1976. The proceedings of the Joint Meeting include the program, the formal resolutions, and the technical papers. The subject matter covered in the papers includes wind effects on structures and design criteria; extreme winds for structural design; earthquake ground motions and instrumentation; seismicity and earthquake risk; seismic effects on structures and design criteria; lessons learned from recent natural disasters; design of nuclear reactor facilities.

17. KEY WORDS *(six to twelve entries; alphabetical order, capitalize only the first letter of the first key word unless a proper name; separated by semicolons)*

Accelerograph; Bridges; Buildings; Codes; Disaster; Dynamic Analysis; Earthquakes; Ground Failures; Nuclear Facilities; Seismicity; Soils; Standards; Structural Response; and Winds

18. AVAILABILITY

[x] Unlimited

[ ] For Official Distribution. Do Not Release to NTIS

[x] Order From Sup. of Doc., U.S. Government Printing Office Washington, D.C. 20402, SD Cat. No. C13 • 10:477

[ ] Order From National Technical Information Service (NTIS) Springfield, Virginia 22151

19. SECURITY CLASS (THIS REPORT)	21. NO. OF PAGES
UNCLASSIFIED	626
20. SECURITY CLASS (THIS PAGE)	22. Price
UNCLASSIFIED	

USCOMM-DC 29042-P74

☆U.S. GOVERNMENT PRINTING OFFICE: 1977 O-234-396/6268

NBS TECHNICAL PUBLICATIONS

PERIODICALS

JOURNAL OF RESEARCH reports National Bureau of Standards research and development in physics, mathematics, and chemistry. It is published in two sections, available separately:

• **Physics and Chemistry (Section A)**
Papers of interest primarily to scientists working in these fields. This section covers a broad range of physical and chemical research, with major emphasis on standards of physical measurement, fundamental constants, and properties of matter. Issued six times a year. Annual subscription: Domestic, $17.00; Foreign, $21.25.

• **Mathematical Sciences (Section B)**
Studies and compilations designed mainly for the mathematician and theoretical physicist. Topics in mathematical statistics, theory of experiment design, numerical analysis, theoretical physics and chemistry, logical design, programming of computers and computer systems. Short numerical tables. Issued quarterly. Annual subscription: Domestic, $9.00; Foreign, $11.25.

July-August, 1977 To begin publication as a single journal.

DIMENSIONS/NBS (formerly Technical News Bulletin)—This monthly magazine is published to inform scientists, engineers, businessmen, industry, teachers, students, and consumers of the latest advances in science and technology, with primary emphasis on the work at NBS. The magazine highlights and reviews such issues as energy research, fire protection, building technology, metric conversion, pollution abatement, health and safety, and consumer product performance. In addition, it reports the results of Bureau programs in measurement standards and techniques, properties of matter and materials, engineering standards and services, instrumentation, and automatic data processing.

Annual subscription: Domestic, $12.50; Foreign, $15.65.

NONPERIODICALS

Monographs—Major contributions to the technical literature on various subjects related to the Bureau's scientific and technical activities.

Handbooks—Recommended codes of engineering and industrial practice (including safety codes) developed in cooperation with interested industries, professional organizations, and regulatory bodies.

Special Publications—Include proceedings of conferences sponsored by NBS, NBS annual reports, and other special publications appropriate to this grouping such as wall charts, pocket cards, and bibliographies.

Applied Mathematics Series—Mathematical tables, manuals, and studies of special interest to physicists, engineers, chemists, biologists, mathematicians, computer programmers, and others engaged in scientific and technical work.

National Standard Reference Data Series—Provides quantitative data on the physical and chemical properties of materials, compiled from the world's literature and critically evaluated. Developed under a world-wide program coordinated by NBS. Program under authority of National Standard Data Act (Public Law 90-396).

NOTE: At present the principal publication outlet for these data is the Journal of Physical and Chemical Reference Data (JPCRD) published quarterly for NBS by the American Chemical Society (ACS) and the American Institute of Physics (AIP). Subscriptions, reprints, and supplements available from ACS, 1155 Sixteenth St. N.W., Wash. D. C. 20056.

Building Science Series—Disseminates technical information developed at the Bureau on building materials, components, systems, and whole structures. The series presents research results, test methods, and performance criteria related to the structural and environmental functions and the durability and safety characteristics of building elements and systems.

Technical Notes—Studies or reports which are complete in themselves but restrictive in their treatment of a subject. Analogous to monographs but not so comprehensive in scope or definitive in treatment of the subject area. Often serve as a vehicle for final reports of work performed at NBS under the sponsorship of other government agencies.

Voluntary Product Standards—Developed under procedures published by the Department of Commerce in Part 10, Title 15, of the Code of Federal Regulations. The purpose of the standards is to establish nationally recognized requirements for products, and to provide all concerned interests with a basis for common understanding of the characteristics of the products. NBS administers this program as a supplement to the activities of the private sector standardizing organizations.

Consumer Information Series—Practical information, based on NBS research and experience, covering areas of interest to the consumer. Easily understandable language and illustrations provide useful background knowledge for shopping in today's technological marketplace.

Order **above** *NBS publications from: Superintendent of Documents, Government Printing Office, Washington, D.C. 20402.*

Order **following** *NBS publications—NBSIR's and FIPS from the National Technical Information Services, Springfield, Va. 22161.*

Federal Information Processing Standards Publications (FIPS PUBS)—Publications in this series collectively constitute the Federal Information Processing Standards Register. Register serves as the official source of information in the Federal Government regarding standards issued by NBS pursuant to the Federal Property and Administrative Services Act of 1949 as amended, Public Law 89-306 (79 Stat. 1127), and as implemented by Executive Order 11717 (38 FR 12315, dated May 11, 1973) and Part 6 of Title 15 CFR (Code of Federal Regulations).

NBS Interagency Reports (NBSIR)—A special series of interim or final reports on work performed by NBS for outside sponsors (both government and non-government). In general, initial distribution is handled by the sponsor; public distribution is by the National Technical Information Services (Springfield, Va. 22161) in paper copy or microfiche form.

BIBLIOGRAPHIC SUBSCRIPTION SERVICES

The following current-awareness and literature-survey bibliographies are issued periodically by the Bureau:

Cryogenic Data Center Current Awareness Service. A literature survey issued biweekly. Annual subscription: Domestic, $25.00; Foreign, $30.00.

Liquified Natural Gas. A literature survey issued quarterly. Annual subscription: $20.00.

Superconducting Devices and Materials. A literature survey issued quarterly. Annual subscription: $30.00.

Send subscription orders and remittances for the preceding bibliographic services to National Bureau of Standards, Cryogenic Data Center (275.02) Boulder, Colorado 80302.

U.S. DEPARTMENT OF COMMERCE
National Bureau of Standards
Washington, D.C. 20234

OFFICIAL BUSINESS

Penalty for Private Use, $300

POSTAGE AND FEES PAID
U.S. DEPARTMENT OF COMMERCE
COM-215

U.S.MAIL

SPECIAL FOURTH-CLASS RATE
BOOK